

Nagra

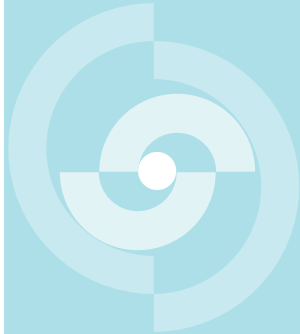
Nationale
Genossenschaft
für die Lagerung
radioaktiver Abfälle

Cédra

Société coopérative
nationale
pour l'entreposage
de déchets radioactifs

Cisra

Società cooperativa
nazionale
per l'immagazzinamento
di scorie radioattive



TECHNICAL REPORT 87-40/1

3-D MIGRATION EXPERIMENT-Report 3,
Part I: Performed Experiments, Results and
Evaluation.

Harald Abelin
Lars Birgersson
Jard Gidlund
Luis Moreno
Ivars Neretnieks
Hans Widén
Thomas Agren

November 1987

Royal Institute of Technology, Stockholm

Nagra

Nationale
Genossenschaft
für die Lagerung
radioaktiver Abfälle

Cédra

Société coopérative
nationale
pour l'entreposage
de déchets radioactifs

Cisra

Società cooperativa
nazionale
per l'immagazzinamento
di scorie radioattive

TECHNICAL REPORT 87-40/1

3-D MIGRATION EXPERIMENT-Report 3,
Part I: Performed Experiments, Results and
Evaluation.

Harald Abelin
Lars Birgersson
Jard Gidlund
Luis Moreno
Ivars Neretnieks
Hans Widén
Thomas Agren

November 1987

Royal Institute of Technology, Stockholm

Der vorliegende Bericht betrifft eine Studie, die für das Stripa-Projekt ausgeführt wurde. Die Autoren haben ihre eigenen Ansichten und Schlussfolgerungen dargestellt. Diese müssen nicht unbedingt mit denjenigen des Auftraggebers übereinstimmen.

Le présent rapport a été préparé pour le projet de Stripa. Les opinions et conclusions présentées sont celles des auteurs et ne correspondent pas nécessairement à ceux du client.

This report concerns a study which was conducted for the Stripa Project. The conclusions and viewpoints presented in the report are those of the authors and do not necessarily coincide with those of the client.

Das Stripa-Projekt ist ein Projekt der Nuklearagentur der OECD. Unter internationaler Beteiligung werden von 1980-86 Forschungsarbeiten in einem unterirdischen Felslabor in Schweden durchgeführt. Diese sollen die Kenntnisse auf folgenden Gebieten erweitern:

- hydrogeologische und geochemische Messungen in Bohrlöchern
- Ausbreitung des Grundwassers und Transport von Radionukliden durch Klüfte im Gestein
- Verhalten von Materialien, welche zur Verfüllung und Versiegelung von Endlagern eingesetzt werden sollen
- Methoden zur zerstörungsfreien Ortung von Störzonen im Fels

Seitens der Schweiz beteiligt sich die Nagra an diesen Untersuchungen. Die technischen Berichte aus dem Stripa-Projekt erscheinen gleichzeitig in der NTB-Serie der Nagra.

The Stripa Project is organised as an autonomous project of the Nuclear Energy Agency of the OECD. In the period from 1980-86, an international cooperative programme of investigations is being carried out in an underground rock laboratory in Sweden. The aim of the work is to improve our knowledge in the following areas:

- hydrogeological and geochemical measurement methods in boreholes
- flow of groundwater and transport of radionuclides in fissured rock
- behaviour of backfilling and sealing materials in a real geological environment
- non-destructive methods for location of disturbed zones in the rock

Switzerland is represented in the Stripa Project by Nagra and the Stripa Project technical reports appear in the Nagra NTB series.

Le projet Stripa est un projet autonome de l'Agence de l'OCDE pour l'Energie Nucléaire. Il s'agit d'un programme de recherche avec participation internationale, qui sera réalisé entre 1980 et 1986 dans un laboratoire souterrain, en Suède. Le but de ces travaux est d'améliorer et d'étendre les connaissances dans les domaines suivants:

- mesures hydrogéologiques et géochimiques dans les puits de forage
- chimie des eaux souterraines à grande profondeur
- écoulement des eaux souterraines et transport des radionucléides dans les roches fracturées
- comportement des matériaux de colmatage et de scellement des dépôts finals
- méthodes de localisation non destructive des zones de perturbation de la roche

La Suisse est représentée dans le projet Stripa par la Cédra. Les rapports techniques du projet Stripa sont publiés dans la série des rapports techniques de la Cédra (NTB).

ABSTRACT

This report is one of the four reports describing the Stripa 3D experiment where water and tracer flow has been monitored in a specially excavated drift in the Stripa mine. The experiment was performed in a specially excavated drift at the 360 m level in granite. The whole ceiling and upper part of the walls were covered with more than 350 individual plastic sheets where the water flow into the drift could be collected. 11 different tracers were injected at distances between 11 and 50 m from the ceiling of the drift. The flowrate and tracer monitoring was kept up for more than two years. The tracer breakthrough curves and flowrate distributions were used to study the flow paths, velocities, hydraulic conductivities, dispersivities and channeling effects in the rock.

The present report describes the structure of the observations, fracture mapping the flowrate measurements and how these were used to estimate the hydraulic conductivities. The main part of this report addresses the interpretation of the tracer movement in the rock outside the drift. The tracer movement as measured by the more than 160 individual tracer curves has been analyzed with the traditional advection-dispersion model, but also with more recent models which include the effects of channeling and the diffusion of tracers into stagnant waters in the rock matrix and in stagnant waters in the fractures themselves. The tracer experiments have permitted the flow porosity and dispersion to be studied.

RESUME

Ce rapport est l'un des quatre rapports décrivant l'essai 3D de Stripa où les circulations d'eau et de traceurs ont été enregistrées dans une galerie spécialement excavée dans le granite au niveau 360 m dans la mine. Tout le plafond et la partie supérieure des parois de la galerie ont été recouverts par plus de 350 feuilles individuelles en plastique permettant de recueillir les entrées d'eaux dans la galerie. 11 traceurs différents ont été injectés à des distances se situant entre 11 et 50 m du plafond de la galerie. Les mesures de débit et la détection des traceurs ont été maintenues durant plus de deux années. L'irruption des traceurs et la distribution des débits ont permis d'étudier les cheminements d'eau, les vitesses d'écoulement, les conductivités hydrauliques, les dispersivités et les effets de "channeling" dans la roche.

Le présent rapport décrit la structure des observations, le lever des fractures, les mesures de débits et comment ces éléments ont été utilisés pour estimer les conductivités hydrauliques. La partie principale du rapport concerne l'interprétation du mouvement des traceurs dans la roche entourant la galerie. Le mouvement des traceurs, relevé par plus de 160 courbes spécifiques de traceurs, a été analysé à l'aide du traditionnel modèle "advection-dispersion" ainsi qu'avec des modèles plus récents qui tiennent compte des effets de "channeling" et de diffusion des traceurs dans les eaux stagnantes de la matrice rocheuse et des fractures elles-mêmes. Les essais avec traceurs ont permis d'étudier les porosités concernant les écoulements et la dispersion.

ZUSAMMENFASSUNG

Dieser "Report" ist einer von gesamthaft vier Berichten, die das 3D-Experiment in der Stripa-Mine beschreiben. In einem neu erstellten Stollen auf der 360 m-Sohle wurden Wasser- und Tracerfluss im Granitgestein beobachtet. Die ganze Stollendecke und der obere Teil der Stollenwände wurden mit über 350 einzelnen Abdeckfolien ausgerüstet, um den gesamten Wassereintrag in den Stollen zu ermitteln. 11 verschiedene Tracers wurden in Abständen von 11 bis 50 m von der Stollendecke ins Gestein injiziert. Die Fliesszeiten des markierten Wassers wurden über einen Zeitraum von mehr als zwei Jahren registriert. Die Tracer-Durchbruchskurven und die Fliessratenverteilungen ergaben Daten über Fliesswege, Wassergeschwindigkeiten, hydraulische Leitfähigkeiten, Dispersivitäten und Kanaleffekte im Gestein.

Dieser Bericht beschreibt den Aufbau und die Durchführung des Versuchs. Die Erkennung und die Kartierung der Klüfte sowie die Schüttungsmessungen ermöglichten die Abschätzung der hydraulischen Leitfähigkeiten. Der Hauptteil des Berichts ist der Interpretation von Tracerbewegung im Gestein gewidmet. Die Tracerbewegung wurde mit über 160 Tracerkurven dokumentiert und wurde sowohl mit dem traditionellen Advektions-Dispersionsmodell als auch mit neueren Modellen analysiert; die letzteren beinhalten auch die Kanaleffekte und die Tracerdiffusion in stagnierendem Wasser in der Gesteinsmatrix sowie in den Klüften. Die Studie der Tracerexperiment-Resultate haben Aussagen über die Fliessporosität und Dispersion ermöglicht.

TABLE OF CONTENTS

	Page
ABSTRACT	ii
SUMMARY	ix
1 STRUCTURE OF REPORT	1
2 INTRODUCTION	2
2.1 Background	2
2.2 Some features of the present investigation	3
2.3 Aims	3
3 EXPERIMENTAL DESIGN	5
3.1 Overview	5
3.2 Selection of injection points	7
4 STRUCTURE OF OBSERVATIONS	11
4.1 Overview	11
4.2 Water flowrates	11
4.3 Tracer concentration in water to drift	12
4.4 Rock characteristics and fracture data	12
4.5 Water chemistry	12
4.6 Injection pressures and flowrates	12
4.7 Hydrostatic pressures	12
4.8 Daily logs	13
4.9 Summary of performed measurements referring to location	13
5 FRACTURE MAPPING	15
5.1 Overview	15
5.2 Results from the visual fracture mapping of the test site	15
5.3 Results from the stereo photography of the test site	21
6 FLOWRATE MEASUREMENTS	23
6.1 Overview	23
6.2 Pilot hole	23
6.3 Test site	24
6.4 Injection holes	30
6.5 Access drift	30
6.6 Ventilation experiment	31
6.7 Summary of the water inflow measurements	33
7 TRACER INJECTION AND BREAKTHROUGH CURVES	34
7.1 Overview	34
7.2 Tracer injection	36
7.3 Water collection	37
7.4 Compiled tracer breakthrough data	38
7.5 Detailed breakthrough curves for one sampling area	43
7.6 Tritium as a tracer	46

	Page	
7.6.1	Overview	46
7.6.2	Results of the tritium measurements	46
8	DIFFUSION MEASUREMENTS IN THE LABORATORY	49
8.1	Overview	49
8.2	Experimental method	49
8.3	Theory	51
8.4	Experimental results	53
9	SOME CONCEPTS OF WATER FLOW AND TRACER TRANSPORT IN FRACTURED ROCK	57
9.1	Overview	57
9.2	Channeling	58
9.3	Dispersion	59
9.4	Diffusion into the porous matrix	60
9.5	Sorption and other interactions	61
9.6	Mathematical modelling	62
9.6.1	Advection-Dispersion model	62
9.6.2	Channeling model	64
9.6.3	Matrix diffusion	68
10	CORRELATION BETWEEN FRACTURE CHARACTERISTICS, WATER FLOWRATES AND TRACER MOVEMENT	72
10.1	Overview	72
10.2	Discussion	74
11	OUTER DISTURBANCES AND THEIR EFFECTS ON WATER INFLOW AND TRACER MOVEMENT	79
11.1	Overview	79
11.2	Variation in water inflow rates	80
11.3	Injection pressures and injection flowrates	84
11.4	Tracer movement	88
12	EVALUATION AND INTERPRETATION OF EXPERIMENTAL RESULTS	90
12.1	Models used for fitting tracer curves	90
12.1.1	Overview	90
12.1.2	Advection-Dispersion model AD	90
12.1.3	Advection-Channeling model AC	91
12.1.4	Advection-Dispersion-Diffusion model ADD	92
12.1.5	Advection-Channeling-Diffusion model ACD	93
12.1.6	Accounting for dilution and variable injection	94
12.2	The fitting process	96
12.2.1	Overview	96
12.2.2	Treatment of injection curves	96
12.3	Results of the model fitting of breakthrough curves	97
12.3.1	Advection-Dispersion model: Individual curves	97
12.3.2	Advection-Dispersion-Matrix diffusion model: Individual curves	105
12.3.3	Advection-Channeling model: Individual curves	107
12.3.4	Fitting of breakthrough curves collected in groups	108
12.3.5	Discussion	110

	Page	
12.4	Determination of flow porosity	111
12.4.1	Method and results	111
12.4.2	Discussion	114
12.5	Interpretation of recovery of tracer	116
12.5.1	Determination of recovery of tracers	116
12.5.2	Matrix diffusion effects	118
12.5.3	Diffusion into stagnant pools of water in the fracture	126
12.5.4	Discussion	129
12.6	Determination of hydraulic conductivity	129
12.6.1	Overview	129
12.6.2	Flowrate measurements	132
12.6.3	Results	135
12.6.4	Discussion	136
12.7	Flowrate and tracer distribution	137
12.7.1	Overview	137
12.7.2	Flowrate distribution	137
12.7.3	Tracer distribution	140
12.7.4	Discussion	145
12.8	Some other indications and observations	145
13	SUMMARY OF MAIN RESULTS, DISCUSSION AND CONCLUSIONS	148
13.1	Development of techniques for tracer tests	148
13.2	Flow porosity	149
13.3	Longitudinal and transverse dispersion and channeling	150
13.4	Observations to modify concepts and models	153
14	NOTATION	154
15	LITERATURE	156
16	ACKNOWLEDGEMENT	160
	LIST OF ILLUSTRATIONS	161

APPENDICES

1	Storage medium for the obtained data
2	Injection flowrates compared with injection pressures
3	Monitored pressures as a function of time
4	Compilation of fracture characteristics
5	Flow variations with time at selected locations on the test site
6	Ventilation test
7	Injection curves real and idealized
8	Diffusion measurements
9	Comparison between fracture characteristics and water flowrates (Plot on fracture characteristics and water inflow rates)
10	AD-model fits to all curves
11	Fits of all selected curves
12	Recovery of tracers
13	Results from fit with truncated injection curves for Uranine
14	Table over numbering of sheets

STAND ALONE APPENDICES

- 15 Tracer breakthrough curves
- 16 Fitted breakthrough curves
- 17 Flowrate curves and tracer breakthrough curves for individual sheets—smoothed data

SUMMARY

In the Stripa experimental mine a drift was excavated at the 360 m level below the ground in order to study water flow and tracer migration in low permeability fractured granite. The broader aim is to understand and quantify transport processes relevant to the safety of a final repository for high level radioactive waste.

The drift, which is located in water saturated rock, has a natural inflow of water. The water flowrate to the totally 100 m long drift was monitored by collecting the water in about 375 plastic sheets which were glued onto the ceiling and upper part of the walls. More than 700 m² of the drift was covered. In addition the water inflow to the lower part of the drift was measured by a ventilation test. The 140 m long access tunnel, which was excavated in order to ensure that the drift was far away from other tunnels and galleries in the old mine, was also used for a ventilation experiment. Hydraulic heads were measured in three vertical 70 m long holes extending upwards from the drift. Water flows were monitored for more than 2 years.

The water flowrates varied very much between the different sheets. One sheet carried 10 % of the total water flow to all the sheets. 50 % of the water came to about 10 of the sheets, 90 % of the water came to 42 of the sheets or about 10 % of the covered area.

The average hydraulic conductivity of the covered area was found to be between $0.4 \cdot 10^{-11}$ – $0.8 \cdot 10^{-11}$ m/s. The floor and lower sides have a conductivity of $2 \cdot 10^{-11}$ – $4 \cdot 10^{-11}$ m/s and the average of the access drift was $0.5 \cdot 10^{-11}$ – $1 \cdot 10^{-11}$ m/s.

The variations along the experimental drift were so large that it is doubtful if the 100 m long drift was long enough to make up a "Representative Elementary Volume" (REV) of an equivalent porous medium.

The three vertical holes were sealed off except in a total of nine 2 m long sections at distances varying from 10 to 55 m from the drift. Nine different tracers were injected for nearly two years into these sections. Later two more tracers were injected in one of the previous locations.

The tracers were monitored in all sheets carrying water and in some locations in the floor of the drift where water was seeping out. Many of the tracers were strongly colored dyes and were looked for in other drifts and galleries as well as in waters sampled in other places in the mine. The tracer concentration curves for 6 of the tracers which arrived in measurable concentrations, in all 167 curves, were analyzed by fitting them to several different models which describe tracer transport. 25 of the curves representing most of tracer flowrate were analyzed in more detail. The models were the Advection–Dispersion model, the Advection–Channeling model and two models based on the previous two, to which is added the further mechanism of molecular diffusion of the tracers into and out of stagnant pools of water. The

fitting of the models to the experimental concentration curves gave values of the mean travel time of water from the different injection points and also information on dispersion. Matrix diffusivities for the tracers were measured in the laboratory and the second set of models were used in an attempt to determine values of the frequency of water conducting fractures and the average amount of fracture surface in the rock which was in contact with the mobile water.

The travel times were found to vary between 2000 and 7000 hours as averages for the tracers, but considerably shorter as well as longer times were found in some of the sheets.

The flow porosity determined from these data was $15.5 \cdot 10^{-5}$ for the tracer injected nearest to the drift. The porosity decreased with increasing distance and was $2 \cdot 10^{-5}$ – $3 \cdot 10^{-5}$ at the farthest injection points. The higher porosity near the drift was interpreted to be caused by the change of rock stresses induced by the presence of the drift.

The dispersivity was found to be very high for all except one tracer. Peclet values of less than 4 were obtained for two of the tracers. For two of the tracers, values around 5 were typical and for one of the tracers values around 30 were found. The low and very low values are deemed to be caused by other mechanisms than what is usually included in the term hydrodynamic dispersion. The main cause seems to be channeling, i.e. the transport of the tracer in a few channels with different transport properties. The presence of "channels" or some preferential pathways was also noted by the presence of tritium in some of the holes. The tritium must have been carried from surface waters in a time period less than 30 years.

The recovery of the tracers varied between 2.8 % and 65 % for 5 of the tracers. One of the tracers had a recovery of 0.002 %, four were not found at all, and one was recovered in a considerable but unknown quantity. The tracers which were not found were, as a rule, injected at the farthest distances.

The recovery data were used to analyze the possibility of matrix diffusion and diffusion into stagnant pools of water as a cause for the loss of tracer. The analyses show that both mechanisms are probably active and will cause the loss of tracer to some extent. It can not be ruled out, however, that there are also other causes for the loss of tracer. One tracer which was injected 18 m above the drift was found to have traveled more than 150 m to a newly excavated gallery in a considerable quantity.

It cannot be ruled out that also some of the loss of the other tracers may be due to transport to some other location, although with the exception of one tracer no traces of the tracers have been found in the water samples taken in many other parts of the mine.

The conventional models used in the evaluation of this experiment cannot be used without modification to accurately and in detail describe the movement of water or tracers in the Stripa rock. The variability of rock properties is very large and results will be strongly influenced by local variations of the properties.

The variability in the data obtained in this investigation may, however, be useful in stochastic models which then may also indicate not only expected average properties but also the expected variability in the properties.

STRUCTURE OF REPORT

The present report sets out to describe the performed experiments, the results obtained, and how the results have been evaluated and interpreted.

A very large amount of information has been gathered. The site has been characterized in various ways. This is described in detail in the report "Site preparation and documentation." Several new techniques have been developed to perform the investigations and tracers previously not used in hydrology have been tested and new tracers have been synthesized. This is described in the report "Instrumentation and tracers."

Extracts of the information from those reports is included for background in the present report but the reader is referred to these reports for more detailed information.

Supporting investigations have been performed by measuring the diffusivity in the rock matrix of the tracers used. Ventilation tests in the experimental drift and the access drift have also been performed. The details of these investigations are given in separate appendices in this report.

About 200 different tracer breakthrough curves have been obtained. Each curve is based on typically more than 1000 individual measurements. These data are available on 5 1/4 inch magnetic discs and on magnetic tape. All the curves have been plotted and are available in the separate stand alone appendix "Tracer breakthrough curves."

Most of the curves have been analyzed by comparing them with model results by a least square fitting using several different models. These results are shown in tables. For each of the five tracers five tracer curves have been selected. These curves have been analyzed in more detail using various models. The experimental curves together with the fitted model results are compiled in the separate stand alone appendix "Fitted tracer curves." A selection of these curves is included in this report.

INTRODUCTION

This report is one of the four reports and three stand alone appendices which make up the final report of the Stripa 3-D project. The series consists of the following reports:

1. *Site preparation and documentation*
2. *Instrumentation and tracers*
3. *Performed experiments, results and evaluation*
4. *Fracture network modelling of the Stripa 3-D site.*

"Stand alone" appendices:

- *Tracer breakthrough curves*
- *Fitted tracer curves*
- *Flowrate curves and tracer breakthrough curves for individual sheets - smoothed data.*

2.1

BACKGROUND

In many countries the final repositories for high level radioactive waste are planned to be located at large depths in crystalline rock formations. The only known means for the radionuclides to migrate to the accessible environment is by flow with mobile water in the fractures in the rock and by molecular diffusion. The latter process can be neglected as an escape mechanism for the depths considered. It is known that the rock is fractured and that practically all water movement is confined to the fractures. The rock matrix is porous and may be accessed by diffusing species but due to the low hydraulic conductivity of the matrix, flow is negligible under repository conditions.

To assess the potential release and transport of the radionuclides, information on the flowrates, velocities and on the pathways of the water is needed. The nuclides which are dissolved in water will be able to diffuse into the micropores of the porous rock matrix and so be withdrawn from the flowing water in the fractures. Sorbing nuclides will sorb on the surfaces of the fractures and also on the inner surfaces of the rock matrix which are accessed by diffusion. The rate of uptake into the rock matrix will thus be directly influenced by the size of the fracture surfaces that are wetted by the mobile water.

Only a small fraction of the fractures in the rock is open to flow. In the Stripa 2-D experiments it was also observed that the water flow was unevenly distributed in the fractures (Abelin et al., 1985). Such channeling effects may give rise to preferential fast pathways and limit the wetted area.

The velocity variations between fractures or channels may cause dispersion of the migrating radionuclides both in the longitudinal direction and in the transverse direction. Longitudinal dispersion may cause dilution but may also allow some part of the nuclides to arrive earlier than the main portion and thus allow less time for decay. Transverse dispersion may also give dilution.

2.2 SOME FEATURES OF THE PRESENT INVESTIGATION

Very few investigations have been made regarding flow and transport properties in deep lying crystalline rocks. There are no well developed techniques available to investigate the properties of interest. The flow patterns and mechanisms are not well known and the investigative techniques must be developed so that many conceivable results can be accommodated with the experiments.

The flowrates, velocities, channeling frequencies and geometry of pathways were not known before the experiment to within several orders of magnitude. Nor were the possible variations in the properties known or could be reasonably assessed.

To accommodate possible large variations of these properties some special techniques were developed. The basis for the whole experiment was the development of the plastic sheeting technique which permitted a very detailed monitoring of the water flowrate and tracer path distribution. Another special aspect of the experiment was to use as many different tracers as possible, 9 tracers, in order to investigate variations in the transport properties of the rock. The choice of different injection distances was made with dual purposes. First, because of the a priori unknown water velocity a large difference in the migration distance would ensure that at least some of the tracers would arrive during the duration of the experiment. Second, different migration distances along essentially the same flow path may give information on how the dispersivity is influenced by the migration distance. This is an open question of some importance.

The size of the wetted surfaces is unknown. If it is large, small molecular weight tracers might diffuse into the micropores of the matrix and to a large extent be withdrawn from the mobile water. This might cause the tracers to be retarded and diluted to such an extent that detection in the collected water in the drift may be difficult. Tracers of different molecular weight were used and a high molecular weight tracer was synthesized especially for this purpose.

2.3 AIMS

The broader aims of the investigation have been discussed above. The detailed aims are summarized below:

- * Develop techniques for large scale tracer experiments in low permeability fractured rock
- * Determine flow porosity
- * Obtain information on longitudinal and transverse dispersion

- * Obtain information on channeling
- * Obtain data and other information for validation and/or modification of models.

3 EXPERIMENTAL DESIGN

3.1 OVERVIEW

The Stripa experimental mine is located in mid Sweden. Adjacent to a disused old iron mine there is a body of granite. In the old mining area there are several mine galleries at depths down to 410 m. The main experimental activities were performed in a nearby granite body at the 360 m level. The granite extends to the surface and the water table is a few meters below the surface of the ground. The water head measured at the 360 m level was several MPa, which ensured natural water flow into drifts.

An experimental drift was excavated starting about 100 m from the nearest drifts and extending 75 m due north further into the undisturbed granite. Figure 3-1 shows an overview of the mine adjacent to the experimental drift.

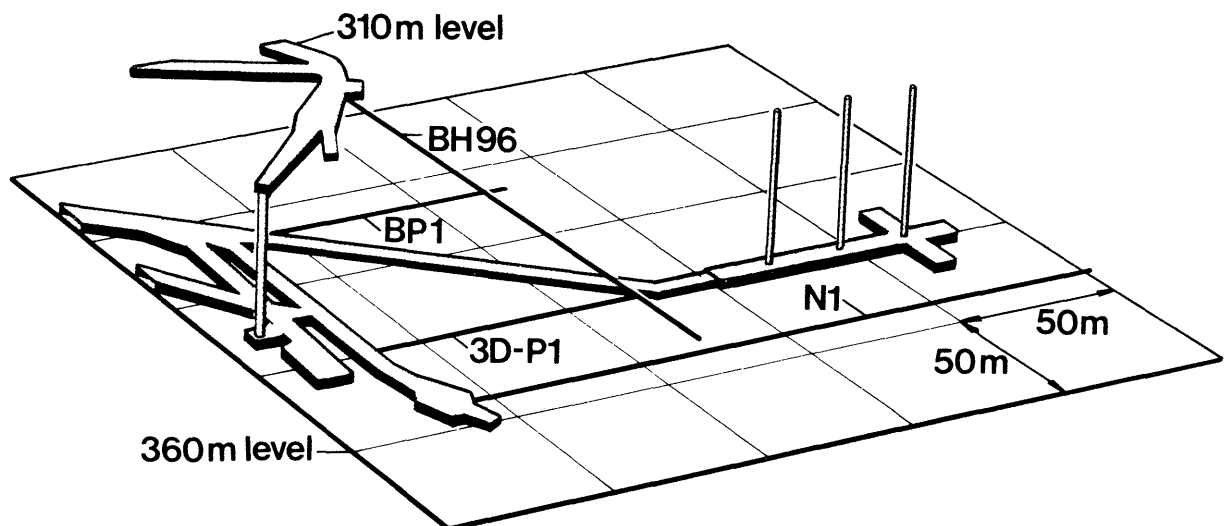


Figure 3-1. Overview of the mine adjacent to the 3-D test site.

The test site consists of a 75 m long main drift and a crossing arm 25 m in length as shown in Figure 3-2.

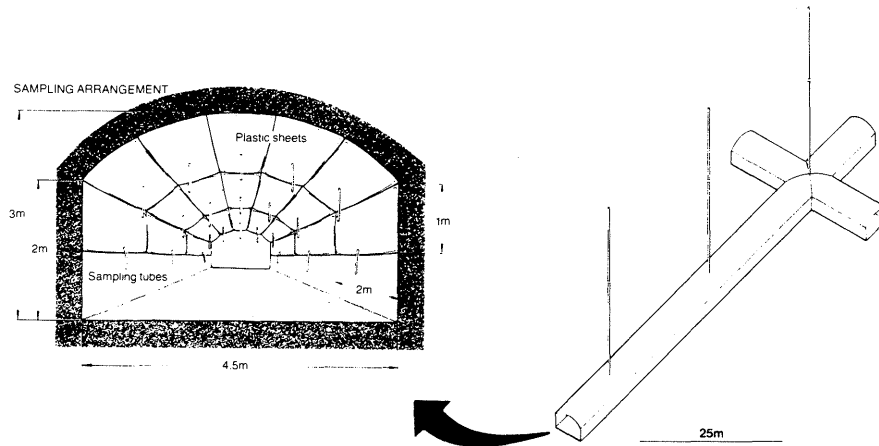


Figure 3-2. Dimensions of the 3-D test site.

The whole ceiling and the upper part of the walls were covered with about 375 plastic sheets which were used to collect the water seeping in from the rock.

The water flowrates were monitored for several weeks after the excavation of the drift and before the 70 m vertical injection holes for the tracers were drilled. The injection holes were fitted with a packer system which sealed the holes efficiently except for the selected 2.5 m zones selected for the tracer injections. Nine different injection zones, each with a different tracer were used. Figure 3-3 indicates the location of the injection holes and the location of the 9 injection zones.

The tracers were continuously injected for more than one and a half year. The collection of water was continued for more than two years. The total injection flowrate, approximately 50 ml/h, was about 10 % of what was monitored in the plastic sheets.

A detailed description of the site preparation and its documentation is given in Report 1, "Site Preparation and Documentation." A full description of instruments and tracers is given in Report 2, "Instrumentation and Tracers."

Below is a short description of the reasons for choosing the injection points and tracers used, and the considerations underlying the injection of a certain tracer in a specific location.

3.2

SELECTION OF INJECTION POINTS

After drilling the three injection holes, each hole was hydraulically tested in 2 meter sections by inflow measurements. In addition core loggings and TV inspections were made. Radar measurements were also made to detect any larger features which might have hydraulic significance near the test site. Enough conductive zones were found in the injection holes for the injection of 9 tracers at distances varying between 10 m and 56 m. The largest distance of 56 m was deemed to be the farthest possible distance from which tracers could arrive at the test site within the duration of the experiment.

A detailed description of the investigations preceding the choice of the injection points is given in Report 1, "Site Preparation and Documentation."

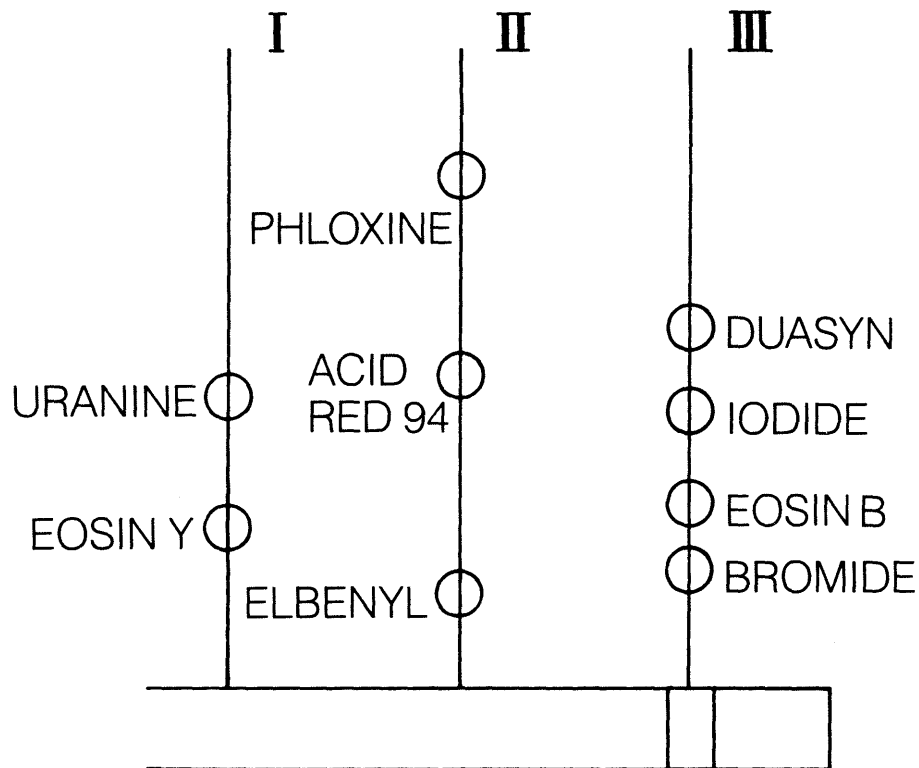


Figure 3-3. Location of the injection points and the tracer injected at each point.

Choice of injection points for the different tracers

The following considerations were made when deciding where to inject the 9 different nonsorbing tracers:

- Earlier experiences with the tracer
- Solubility versus detection limit
- Distance from injection point to test site
- Interference between different tracers during analysis
- Diffusivity of the tracers and possible loss due to uptake in matrix
- Ease of detection at the site.

The main considerations for the decision where to inject the different tracers are given below.

The tracers injected in the Stripa mine are as follows:

Acid red 94 (Rose Bengal)
 Bromide
 Duasyn Acid green V (DP AF 605)
 Elbenyl Brilliant Flavine A-FF
 Eosin Bluish
 Eosin Yellowish
 Iodide
 Phloxine B
 Uranine

Of the 9 different tracers, Elbenyl, Eosin Y, Iodide, and Uranine have been used earlier at the Stripa mine. The five remaining tracers were chosen from among some 100 dyes and salts that were tested in the laboratory. For further information on these tests see Report 2, "Instrumentation and Tracers." There are three main drawbacks using the two salts, Bromide and Iodide, as tracers: (1) the salts are not visible, (2) the analysis with Ion-selective electrodes are time consuming, and (3) Bromide analyses are sensitive to high Iodide concentrations.

The tracers not previously used in the Stripa mine were either injected close to the test site or at the injection points where there was a lower possibility that these tracers would reach the test site within the time frame of the experiment. Due to the effect of matrix diffusion on the migration of tracers, it is desirable to have the large molecular tracers at the furthest injection points. Therefore in this case all the dyes were larger than the two salts, Bromide and Iodide.

Bromide (Hole III: 12-14 m)

Bromide has the smallest molecular weight and thereby the largest diffusivity of all the tracers used. It was decided that Bromide should be injected in a point with a short residence time i.e. close to the drift, thereby reducing the effects of the matrix diffusion on the breakthrough. The selection of the short residence time was also deemed suitable for a tracer for which we had no earlier experience. The short travel distance was also suspected to give a small spreading.

The choice of the injection point for Bromide depended on the location of the injection point for Iodide due to the interference by Iodide on the analysis of Bromide.

Duasyne (Hole III: 36–38 m)

Based on radar and water inflow measurements, it was suspected that the possibility of a tracer to reach the test site from this injection point would be low. If the tracer should reach the test site, it would probably be highly diluted and must therefore have a high detectability. Duasyne has an absorbance peak at 640 nm which is well separated from all the other tracers, thus making it unique. There was a second benefit in using a dye at this injection point since the uncertainty was large, adjacent drifts and boreholes could easily be checked for the presence of this tracer.

Elbenyl (Hole II: 9–11 m)

Due to the poor uniqueness in light absorbance and poor detectability of Elbenyl, it was decided that it should be injected close to the site to prevent a high dilution.

Eosin B (Hole III: 18–20 m)

Due to the similarity of Eosin B to Eosin Y it was desirable to reduce the possibility of these two tracers mixing. This could be done by injecting the tracers far from each other and close to the test site.

Eosin Y (Hole I: 17–19 m)

Injection point for Eosin Y was based on the decision of where Eosin B was injected, see Eosin B above.

Iodide (Hole III: 28–30 m)

This injection zone was suspected to be in contact with the right arm of the drift which was the major area of water inflow and therefore a potential area for high dilution. Iodide has a high uniqueness and high detectability which, in this case where the flowrates were high, were essential. A second advantage of using a salt at this injection point was that the spreading of the tracer was assumed to be small.

Phloxine B (Hole II: 55–57 m)

The decision to use Phloxine at this distant injection point was based on the general considerations given above for Duasyne.

Uranine (Hole I: 31–33 m)

It was suspected that the tracer, Uranine, injected at this point would not only reach the test site but might also reach the pilot hole and the access drift. Then Uranine was chosen since it was a well tested tracer from several tracer experiments in the Stripa mine. Uranine has a high detectability and uniqueness which makes it suitable for large migration distances where much dilution could occur.

Acid Red 94 (Hole II: 33–35 m)

The only remaining tracer to inject at this injection point was Acid Red 94 which has never been used in the Stripa mine.

Effect of molecular size on travel time

If the rock in contact with the flowing water is porous, tracers will diffuse into the pores and thereby be retarded. The magnitude of this retardation will depend, among other things, on the diffusivity of the tracer. Because a large molecule has a lower diffusivity than a smaller molecule, it was decided to test tracers with a large difference in molecular size. The small molecular weight tracer was F^- and the large molecule tracer was synthesized by the Department of Organic Chemistry at the Royal Institute of Technology, Stockholm. For further information on the tracers see Report 2, "Instrumentation and Tracers."

The effect of matrix diffusion is larger at long contact times and a long travel time will increase the possibility to detect matrix diffusion. The injection of the additional tracers started 5000 h after the beginning of the injection of the other nine tracers. At this time there was some information available on the early breakthrough of some of the tracers. Since the detectability of the large molecular tracer was low, it was desirable to have a low mixing of the other tracers. At this time the injection point for Uranine fulfilled the requirements of a long travel time as well as low mixing with other tracers. The injection of the additional tracers was superimposed on the continuous injection of Uranine.

Summary of experimental design

- Test site location in undisturbed granitic rock 360 below ground level.
- Total water sampling area 750 m² divided into 375 separate sampling areas.
- Nine different injection zones were used.
- Eleven different conservative tracers were injected.
- Closest injection zone was at ten m from the drift.
- Farthest injection zone was at 56 m from the drift.
- Continuous injection was maintained for 20 months.
- Water sampling was conducted for 20 months and for additional 6 more months after the completion of injection.

4 STRUCTURE OF OBSERVATIONS

4.1 OVERVIEW

The data obtained from the experiment can be grouped as follows:

- Water flowrates
- Tracer concentration in water to test site
- Rock characteristics and fracture data
- Water chemistry
- Injection pressures and flowrates
- Hydrostatic pressures
- Daily logs

These groups of data will be presented under separate headings below. Appendix 1 contains references to where and how these data are stored.

4.2 WATER FLOWRATES

Monitoring of water flowrates was performed at different locations and during different time periods.

In the pilot hole, drilled prior to the excavation of the test site, water inflow rates were measured over 7.5 m intervals. These data are presented in Report 1, "Site Preparation and Characterization."

As soon as the site had been characterized, the upper part was covered with plastic sheets which allowed a high resolution in water inflow and tracer monitoring. The water inflow monitoring continued for 26 months. During this time period the injection holes were drilled, measured, sealed, and the injection of tracers was completed. For data on water flowrates see Chapter 6, "Flowrate Measurements."

The water inflow rates to the three vertical injection holes were measured in 2 m sections. The results are given in Report 1, "Site Preparation and Characterization."

In addition to the detailed inflow rate in each sheet the total water inflow rate has been monitored by a "ventilation experiment." In this experiment the total inflow rate to the access drift was also monitored, see Chapter 6, "Flowrate Measurements."

4.3 TRACER CONCENTRATION IN WATER TO DRIFT

Water samples were collected in test tubes every 16 hour from all sampling sheets with a high enough water flowrate. Selected test tubes were sampled for tracer content and if any tracers were found, all the samples from that area were analyzed. In the case of I^- and Br^- the minimum time interval between analyzed samples was increased to 160 hours because the analysis was time consuming. Data exist on the breakthrough from 7 of the 11 injected tracers that were found in about 65 different sampling sheets. The results are presented in Chapter 7, "Tracer Injection and Breakthrough Curves."

4.4 ROCK CHARACTERISTICS AND FRACTURE DATA

All cores from the pilot hole drilling and 3 injection holes drilling, a total of 400 m, have been logged for: (1) rock type, (2) fracture frequency, (3) fracture direction relative to the core, (4) fracture infilling and coating, and (5) signs of water flow. Radar measurements and TV logs have been performed in both the pilot hole and in the 3 injection holes. The TV logs were of poor quality and could not be used for orientating the cores. Deviation measurements have been performed in all 4 boreholes. This information is given in Report 1, "Site Preparation and Characterization."

The test site has been mapped for fractures both visually and by photographing. The data from the visual mapping are presented in compiled form in Chapter 5, "Fracture mapping." A more detailed presentation of both the visual and photographic results are given in Report 1, "Site Preparation and Characterization."

4.5 WATER CHEMISTRY

Water samples have been taken from both sampling sheets and injection holes, from a total of 12 different locations at two different times. Tritium analysis has been performed on water samples from both the site and from the injection holes. The results of these analyses are given in Report 1, "Site Preparation and Characterization."

4.6 INJECTION PRESSURES AND FLOWRATES

The tracers were injected with a "constant" overpressure. The injection pressures were logged on the average every 2 h and injected volumes were measured every work day. The injection pressures and flowrates are given in Appendix 2.

4.7 HYDROSTATIC PRESSURES

The hydrostatic pressure in each of the top zones in the injection holes, about 70 m from the site, has been monitored over the whole experimental period. The natural pressures at the injection points were monitored for a period of 3 weeks before the start of injection. The monitoring of the pressures both at the top zones and the injection zones were continued for 5 months after completing the injection of tracers. These data are given in Appendix 3.

4.8 DAILY LOGS

Daily logs contain the daily status such as: (1) injection pressures, (2) injected volumes, (3) condition of plastic sheets and tubings, (4) status of fractional collectors and flow switches, (5) ambient temperature, and (6) other activities in the mine that could effect the conditions at our test site.

4.9 SUMMARY OF PERFORMED MEASUREMENTS REFERRING TO LOCATION

Pilot hole 3D-P1	:	Deviation measurements Core logging TV logging Water inflow measurements Radar measurements Tracer occurrence
Access drift	:	Limited water inflow measurements Ventilation experiment Tracer occurrence Water chemistry Tritium measurements
Test site	:	Fracture mapping Water inflow monitoring Water chemistry Tracer occurrence Ventilation test Tritium measurements
Injection holes	:	Deviation measurements Core logging TV logging Water inflow measurements Radar measurements Pressure monitoring Tritium measurements
N1,310 m level, BP1, BMT area, extensometer drift, N2,N3,N4,W1,W2		In some cases water flow measurements and in all cases tracer occurrence, see Figure 4-1 for the location of some of the sampling points.

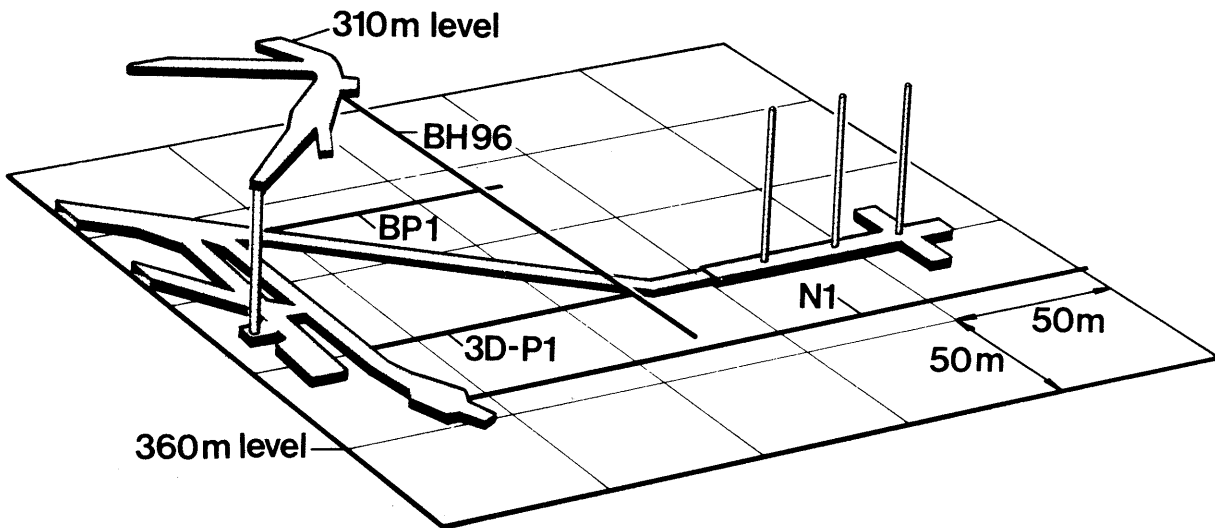


Figure 4-1. 3-D test site with surroundings.

5 FRACTURE MAPPING

5.1 OVERVIEW

All the fracture mapping in the test site has been performed by VIAK AB, Falun, Sweden. The test site has been fracture mapped both visually and by stereo photography. The purpose of the visual fracture mapping was to map the most prominent fractures in the test site, excluding the floor. After the fracture mapping the drift was stereo photographed to enable the determination of fracture directions and dips.

For each of the mapped fractures in the drift the following has been noted: (1) location and extension, (2) direction and dip, (3) infilling and coating materials, (4) surface characterization, and (5) signs of water flow.

All the drill cores obtained during the preparation of the experiment have also been mapped for fractures. The results from this mapping are given in Report 1, "Site Preparation and Documentation." An attempt to orient the cores by TV logging of the injection holes was also performed but was not successful.

5.2 RESULTS FROM VISUAL FRACTURE MAPPING OF THE TEST SITE

Figure 5-1 gives fracture orientations in the form of a lower hemisphere diagram. The fracture map is shown in Figure 5-2.

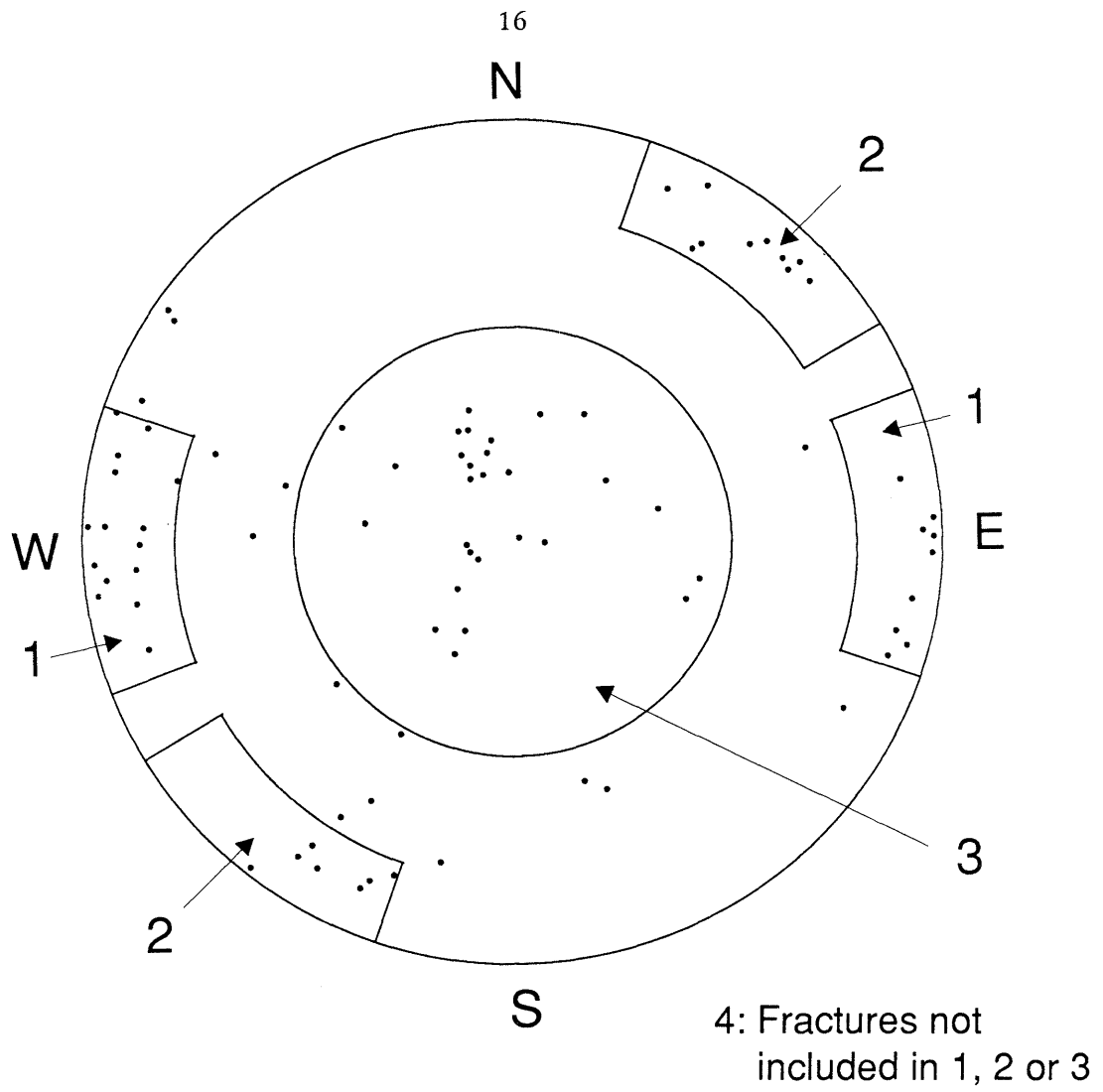


Figure 5-1. Orientation of the 100 most prominent fractures.

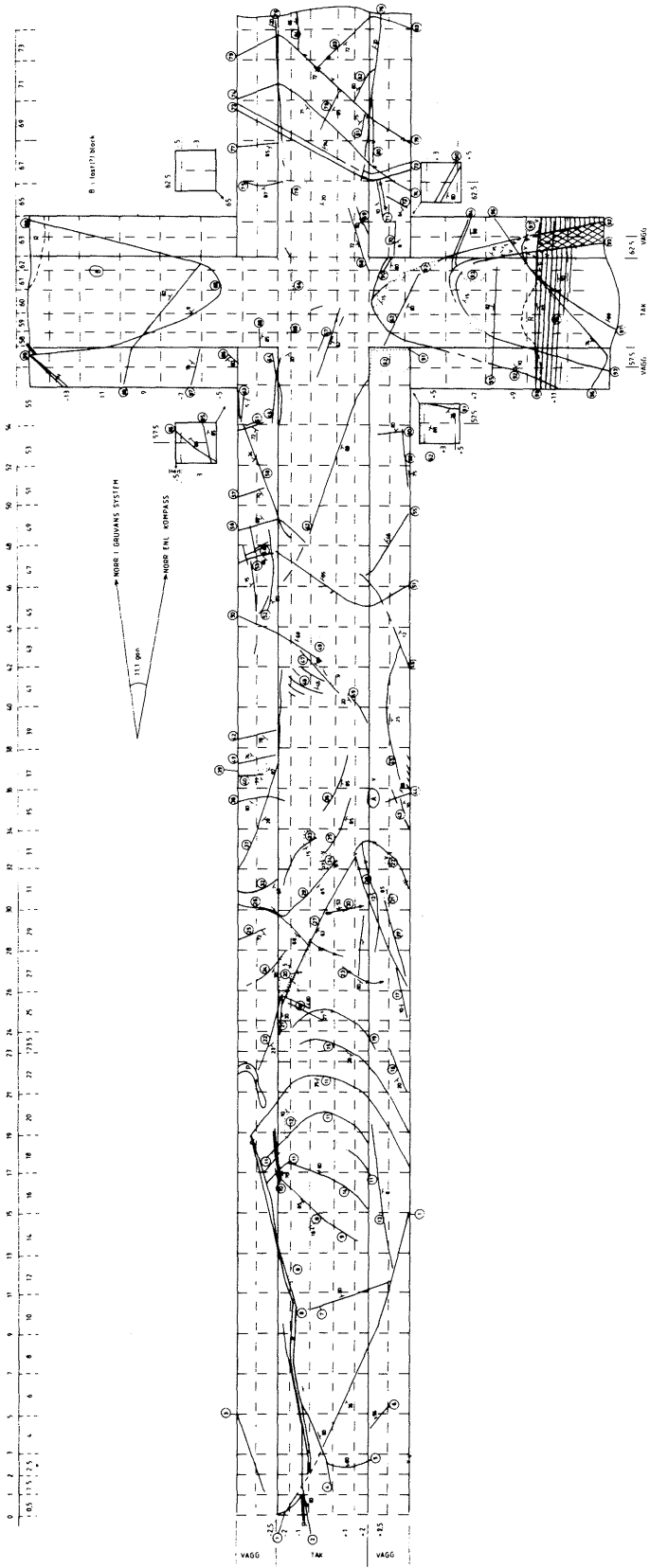


Figure 5-2. Actual fracture map over 3-D migration test site.

Based on the results shown in Figure 5-1 all the mapped fractures have been grouped into 4 sets, the last set containing those fractures that could not be included in the three other sets.

The fractures have also been divided into two other groups, namely individual fractures and fracture zones. A fracture zone is defined here as a set of at least five more or less parallel fractures which are close to each other. The definition for fracture length in this report is the whole visible length of the fracture over the mapped area. The number of individual fractures and zones in the different fracture sets are given in Figure 5-3.

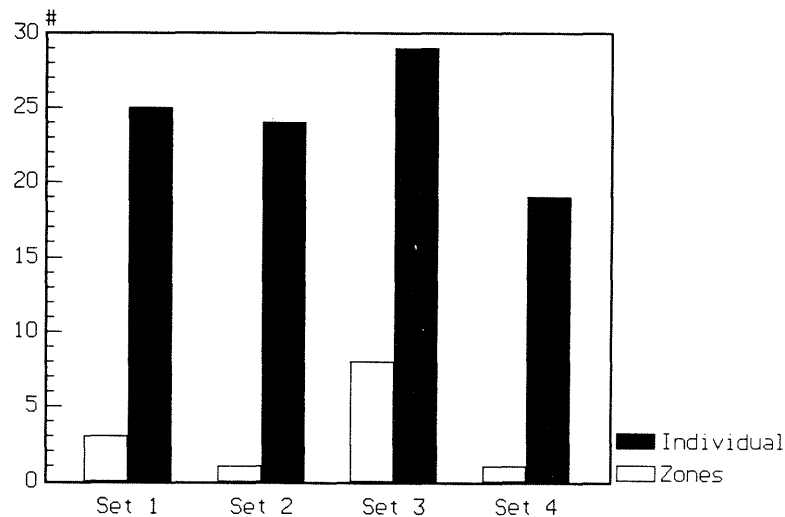


Figure 5-3. Number of individual fractures and zones in the different fracture sets.

The number of individual fractures seems to be evenly distributed between the different sets. This is not the case for the fracture zones where fracture set 3, nearly horizontal, has as many fracture zones as the three remaining sets together. All the fractures and zones add up to more than 100 fractures. This is because very similar fractures running more or less parallel have been mapped as "one" fracture but is here presented with the actual number of fractures. The 99 fractures which have been mapped make up the majority of all fractures in the drift.

It is impossible from Figure 5-1 to see if there are any differences between the individual fractures and fracture zones concerning dip and direction, so the same data are presented in Figure 5-4 but separated for individual fractures and zones.

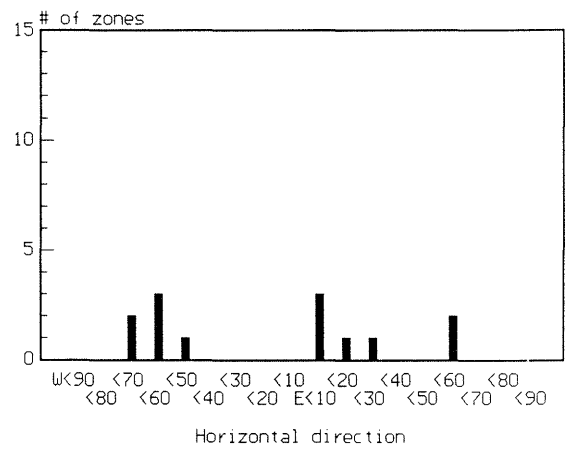
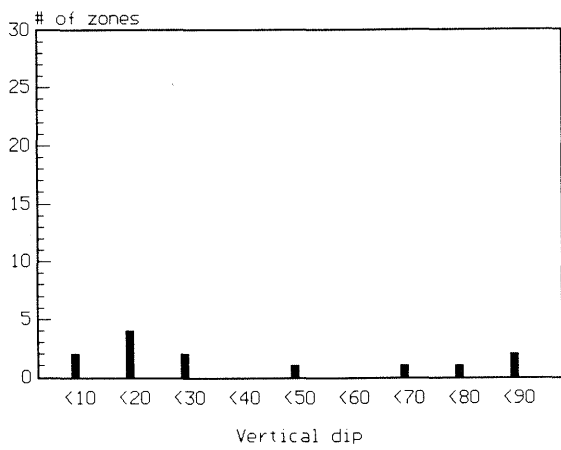
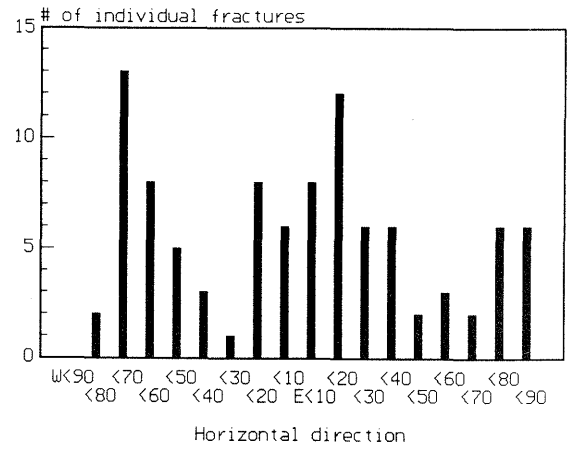
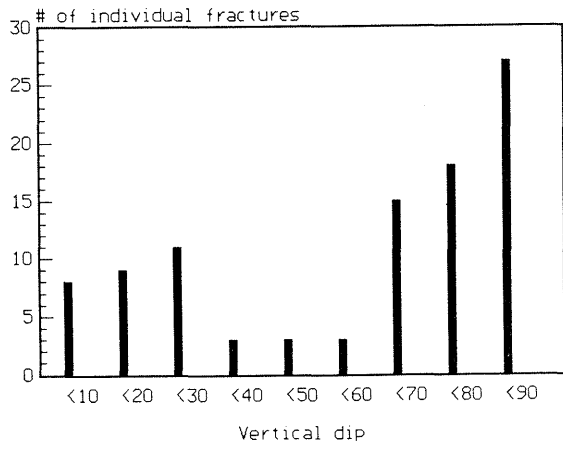


Figure 5-4. Dip and directions for individual fractures and fracture zones.

The fractures have also been mapped for fracture coating and filling materials, Chlorite (CL), Calcite (CA), Epidote (EP), Feltspar (FP), Quartz (QZ), and Mica (MI), and the compiled results are given in Figure 5-5. Comparing the mineral content for individual fractures with fracture zones it is obvious that Chlorite is more common in the individual fractures. For more detailed information on fracture characteristics see Appendix 4.

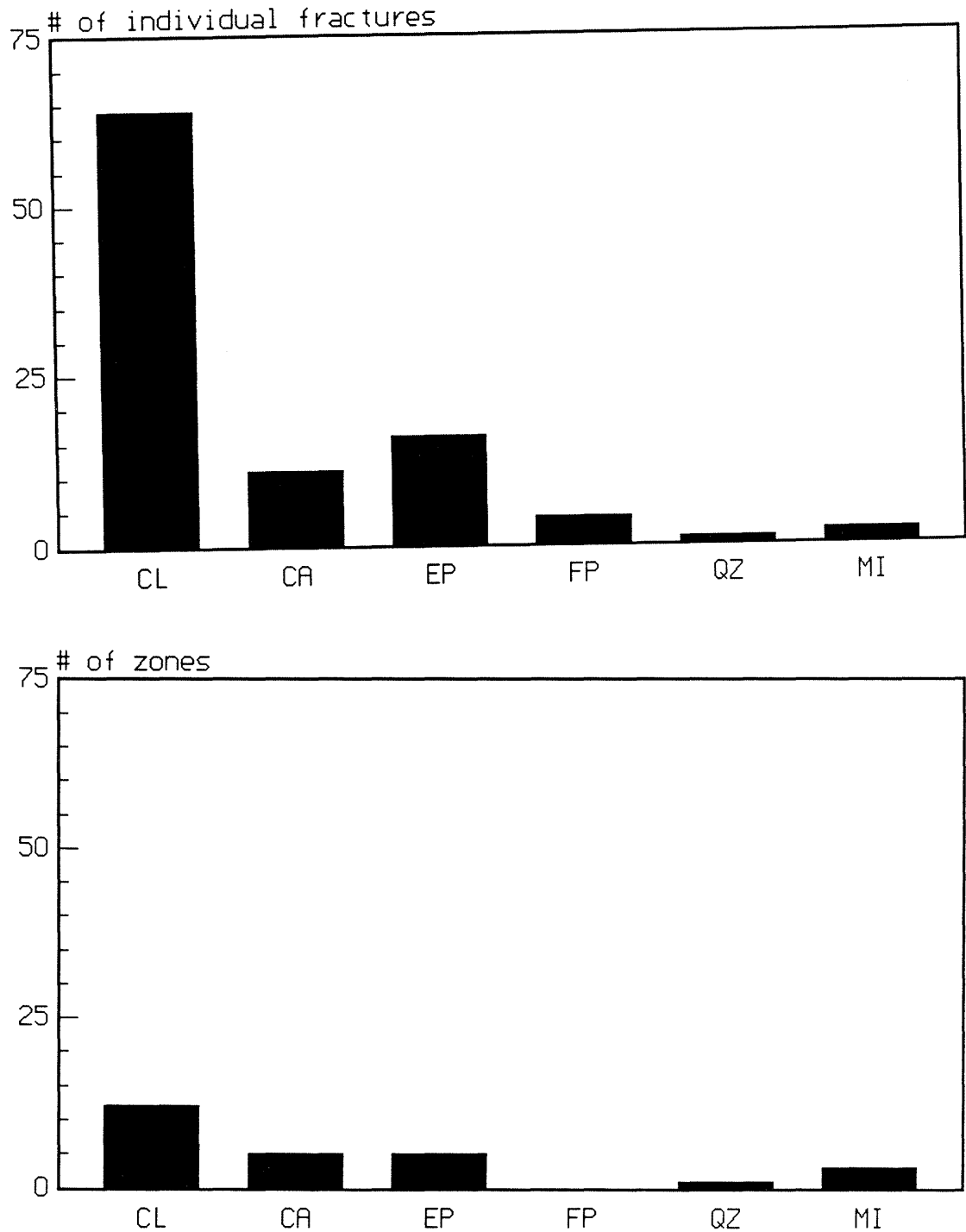


Figure 5-5. Fracture coating and filling materials for individual fractures and fracture zones.

5.3

RESULTS FROM THE STEREO PHOTOGRAPHY OF THE TEST SITE

When compiling the results from the stereo photography of the test site only those fractures that were mapped as water bearing were extrapolated into the unknown rock volume. Based on previous field experience on fracture directions it is seldom possible to extrapolate individual fractures over longer distances than a few meters at most. The results in Figures 5-5 and 5-6 should more be seen as a general tendency than the actual directions of the individual fractures.

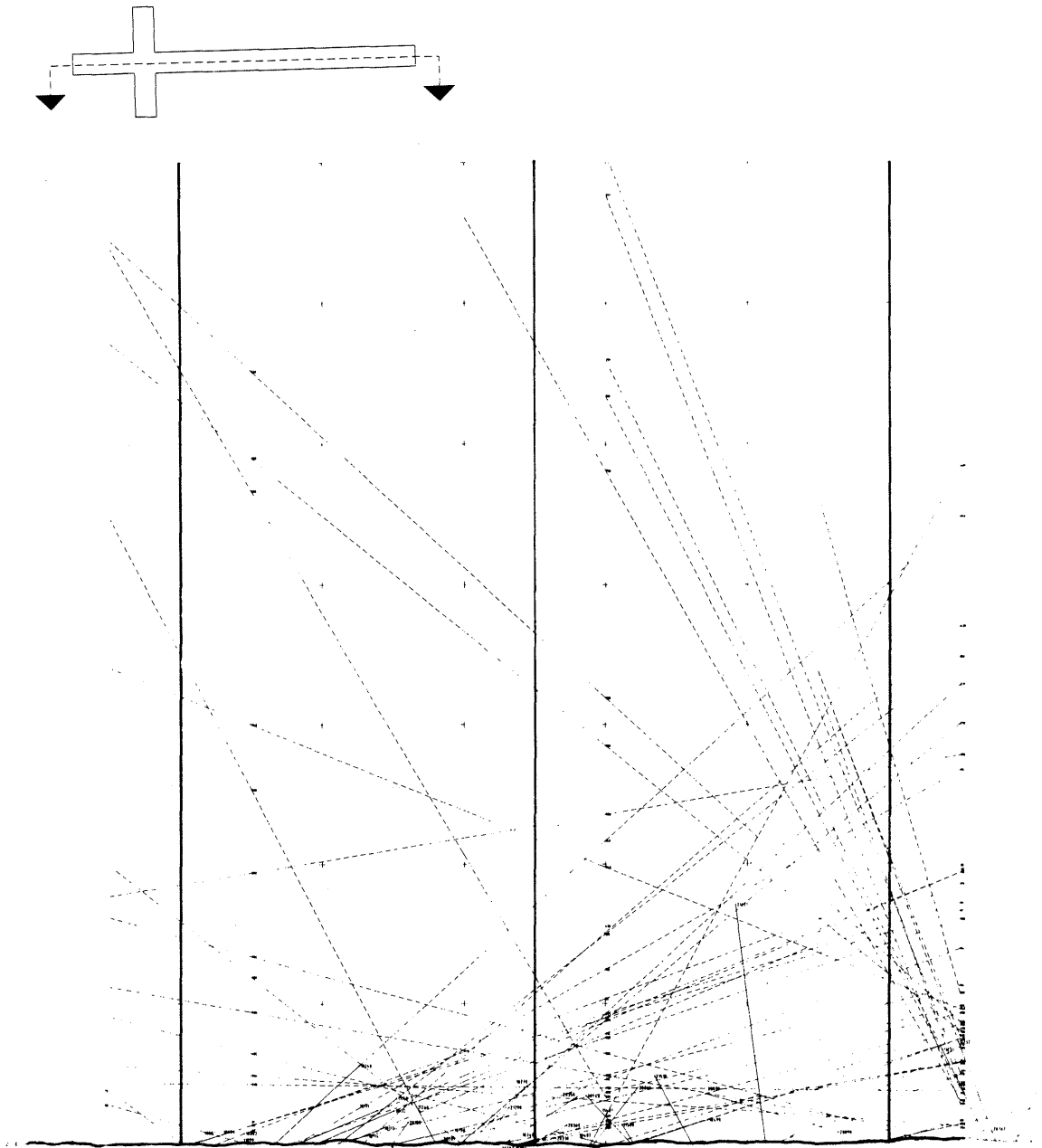


Figure 5-6.

Extrapolation of "wet" fractures based on stereo photos.

6 FLOWRATE MEASUREMENTS

6.1 OVERVIEW

Water inflow rates have been measured at the following locations:

- Pilot hole
- Test site
- Injection holes
- Access drift

Water inflow rates were measured in the pilot hole which was drilled prior to the excavation of the test site.

As soon as the test site had been characterized the upper part was covered with plastic sheets. The water inflow rates into these sheets were monitored continuously for 26 months. During this time period the injection holes were drilled, measured, sealed and the injection of the tracers was performed.

The water inflow rates into the three 70 m long vertical injection holes were measured in 2 m sections.

In addition to the flowrate monitoring in the plastic sheets, a "ventilation" test was performed to measure the water flowrate into the uncovered portion of the test site and into the access drift.

6.2 PILOT HOLE

The water inflow measurements were performed with 7.5 m intervals in that section of the pilot hole where later the test site would be excavated. In the rest of the pilot hole an interval of 15 m was used. A compilation of the results from the inflow measurements is given in Figure 6-1.

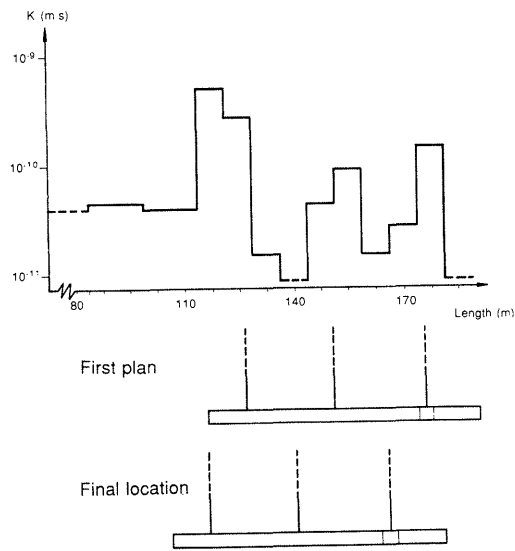


Figure 6-1. Results from inflow measurements in the pilot hole.

The highest water inflow rate was found at around 115 m depth, while at the innermost part of the pilot hole there was no or low water inflow. Due to this it was decided to move the location of the test site so that the high water inflow rates would be located between two of the injection holes to make certain that this zone would be tested. A second advantage of this new location was that the dry part was left outside the test site. The planned and actual location of the test site is given in Figure 6-1. The total inflow to the 190 m long pilot hole was 6.5 l/h and in the part of the pilot hole that coincides with the test site there was an inflow of 3.0 l/h. The calculated conductivities ranged from less than 10^{-11} to 5×10^{-10} m/s with an arithmetic mean close to 10^{-10} m/s. The measuring limit was set to 10^{-11} m/s. The first 90 meters of the pilot hole that remained after the excavation of the test site was monitored for water flow during the whole duration of the experiment. This part of the hole had a water inflow rate of approximately 3 l/h before the excavations but did not give any water during the experiment, until the preparation for the Phase III started when the inflow reached 0.7 l/h.

6.3 TEST SITE

The water flow monitoring at the test site can be divided into 3 periods: (1) before drilling of the injection holes, (2) during the period when the injection holes were left open, (3) after sealing of the injection holes and during injection.

The upper part of the test site, approximately 700 m^2 (which is half the surface area of the test site) was divided into about 350 sampling areas each with an area of 2 m^2 . As more sheets were added during the experiment at potential points of interest there were approximately

375 sheets at the end of the experiment. Each sampling area was covered with a plastic sheet. The method of covering the upper part of the test site with plastic sheets is described in detail in Report 2, "Instrumentation and Tracers." The total water inflow to the covered area was 0.7 l/h.

Of the 375 sampling sheets 145 gave measurable amounts of water, 50 % of the total inflow came from approximately 10 % of the covered area. The wettest sheet carried about 10 % of the total inflow.

Before drilling of the injection holes

The water inflow rate distribution from the "undisturbed" rock (prior to the drilling of the three injection holes) was monitored for 6 weeks. The results from these measurements are presented in Figure 6-2 below where it can be seen that the water inflow is concentrated in a few areas with large dry areas in between. Figure 6-3 shows the inflow rates plotted along the main axis of the test site as well as along the crossing arm.

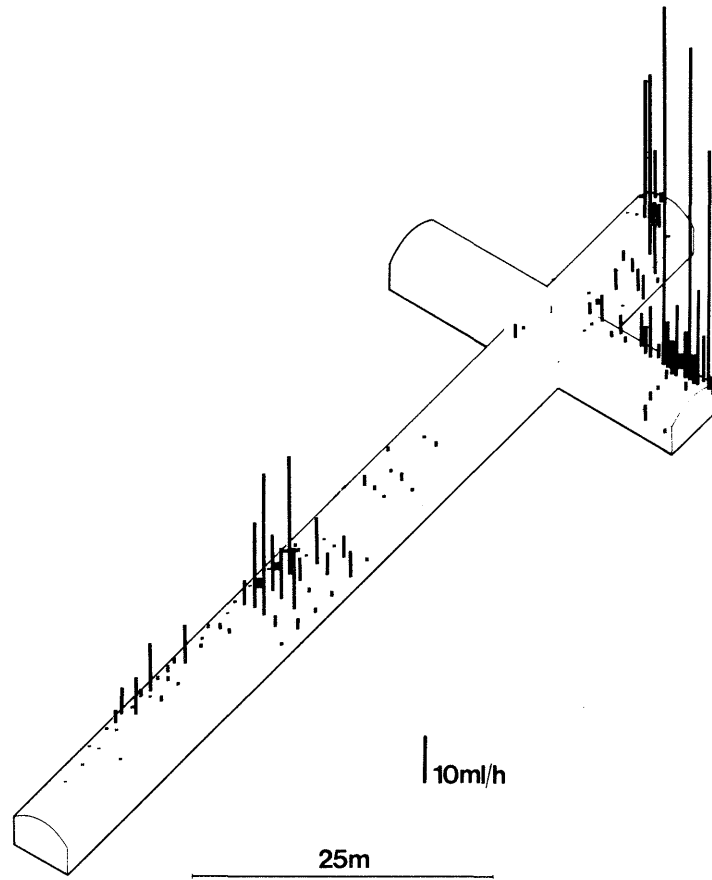


Figure 6-2. Water inflow rates into the test site before drilling of the injection holes.

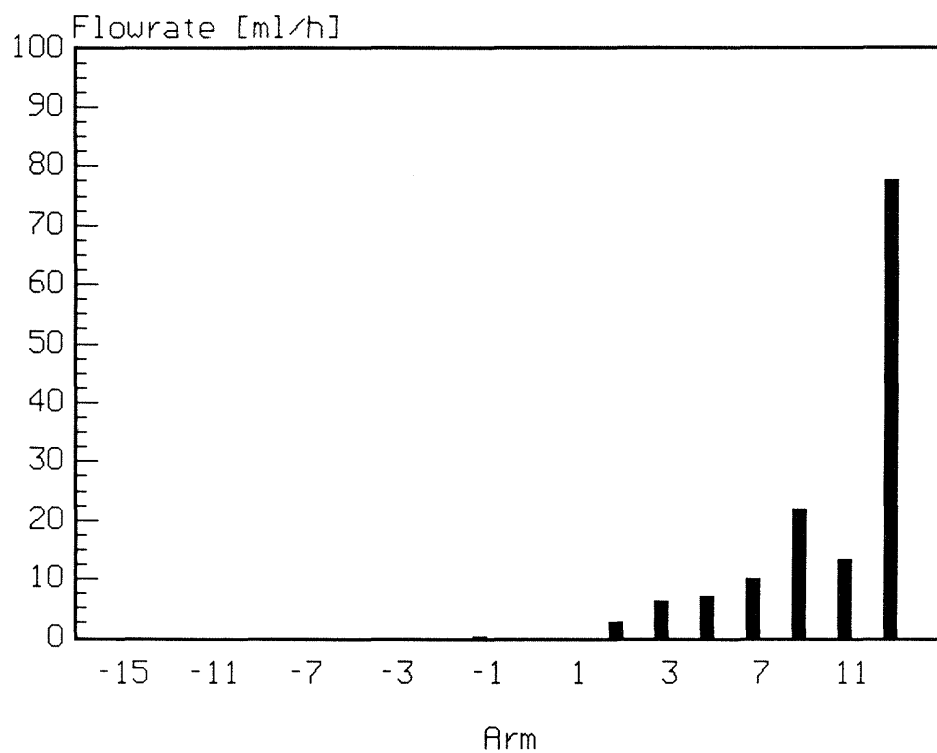
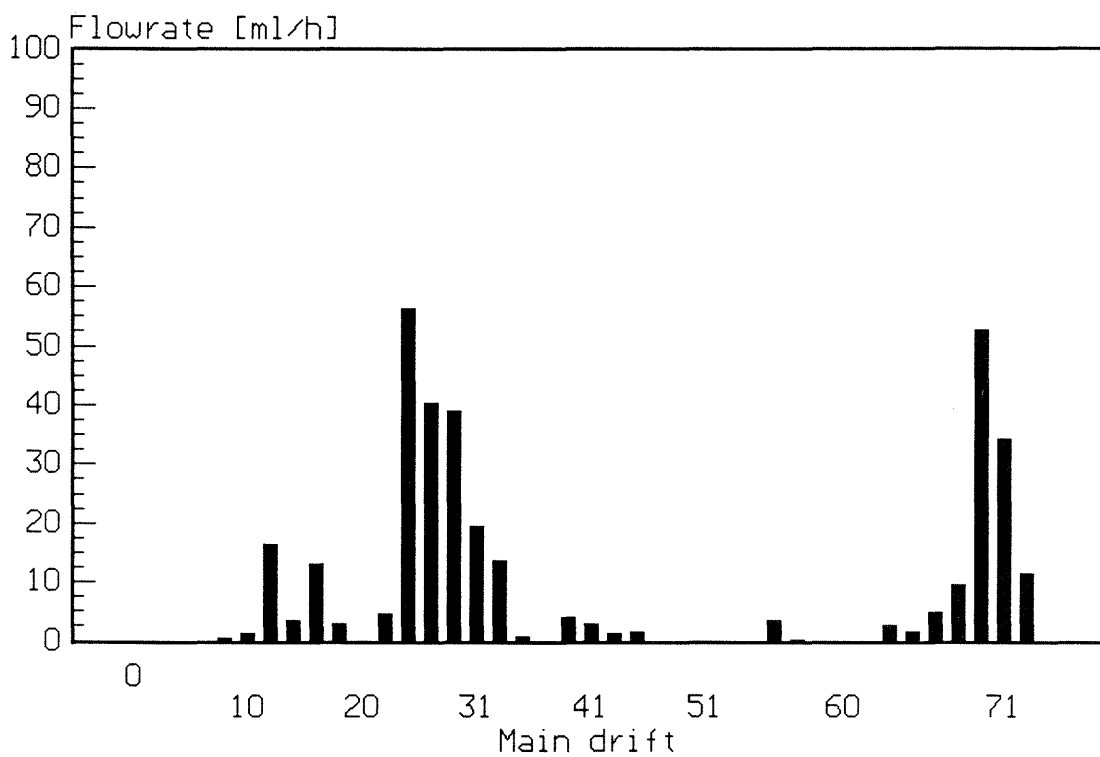


Figure 6-3. Water inflow rates along the two main axes of the test site.

A comparison of the results on the inflow into the pilot hole, in that part which coincided with the test site, and the inflow monitored to the plastic sheets is given in Figure 6-4. To facilitate the comparison with the results from the pilot hole, the results from the inflow measurements into the plastic sheets have been recalculated from 2 m sections to 8 m sections. It should, however, be kept in mind that only half of the circumference of test site was covered with plastic sheets. The "high" water flowrate into the pilot hole at 8 to 23 m (local coordinates of the test site) is not found in the corresponding plastic sheets. However, at this location in the test site water is entering through the floor.

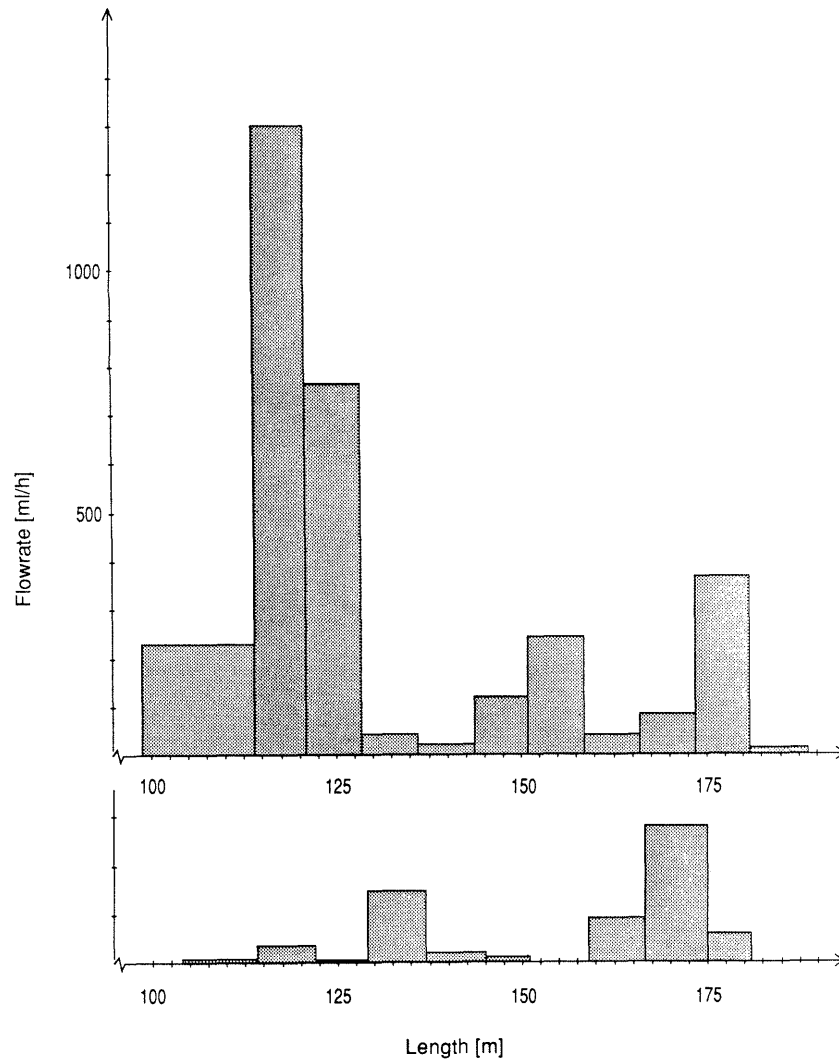


Figure 6-4. Comparison of the water inflow rates to the pilot hole and later measurements at the test site.

During the time period when the injection holes were kept open

The injection holes were kept open for about 6 months to perform different measurements. The total water inflow rate into the test site decreased after the injection holes had been drilled and were kept open. See Figure 6-5 -6000 h to -1000 h.

After sealing of the injection holes

After sealing of the injection holes with compacted bentonite the total water inflow rate into the test site increased to approximately the same value as before the drilling of the injection holes, see Chapter 11 "Outer Disturbances and Their Effects on Water Inflow and Tracer Movement," see also Figure 6-5 -1000 h to 18500 h.

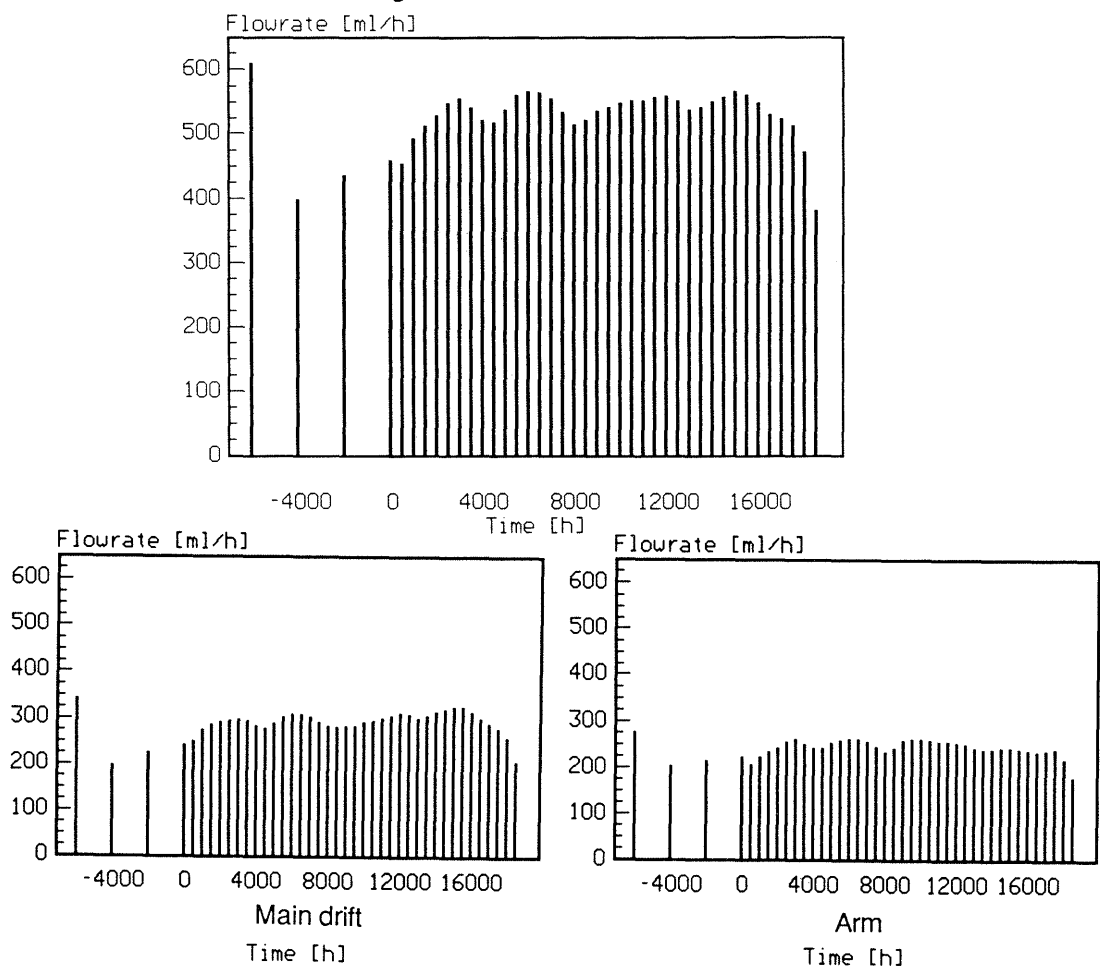


Figure 6-5. Total flowrate as function of time. Integral over whole test site (main drift, and arm). Time zero is when the injection started.

Areas on the floor where water was found were covered with plastic sheets to prevent evaporation. The total size of these areas were approximately 25 m² and had a total inflow rate of about 0.4 l/h. For more detailed information on the variation of water inflow rates with time at different sections of the test site, see Appendix 5. Individual flowrates for each sheet as function of time is given in Appendix 7, "Flowrate Curves and Tracer Breakthrough Curves for Individual Sheets - Smoothed Data" (Stand alone appendix).

6.4 INJECTION HOLES

The information obtained from the inflow measurements in the injection holes (2 m zones) were used when deciding where to inject the tracers. Figure 6-6 shows the water inflow rates into the injection holes when open.

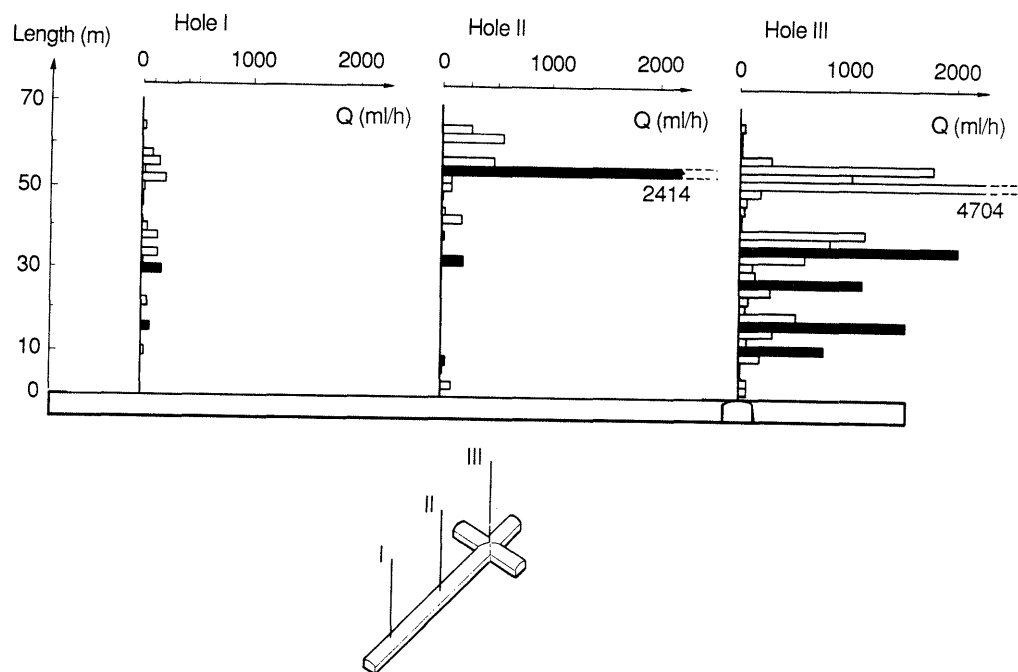


Figure 6-6. Water inflow rates into 2 m sections of the injection holes.

As can be seen in Figure 6-6, the water inflow rates into the holes were very uneven distributed. The total inflow rates into the holes were:

Hole I	:	≈	1 l/h
II	:	≈	4 l/h
III	:	≈	17 l/h

6.5 ACCESS DRIFT

In the access drift only areas with visible water flow were covered by plastic sheets. The covered area was about 20 m² out of about 750 m² of wall and ceiling. The water flowrate in the covered part was on an average 0.2 l/h with fluctuations of ± 0.05 l/h. The total water inflow to the access drift has also been monitored by a "ventilation" experiment, see separate heading below.

6.6 VENTILATION EXPERIMENT

The water inflow rates obtained in the pilot hole (part that was located within the test site) were a factor 4 higher than those monitored in the plastic sheets.

The estimated total inflow to the test site (including ceiling, roof and wall) was a factor 2 less than the actually measured inflow into the corresponding part of the pilot hole. Therefore it was assumed that the inflow into the lower part of the test site (uncovered) was larger than the inflow into the upper part. To determine the total inflow into the test site, a ventilation experiment was performed. For this purpose one extra wall was constructed at the start of the access drift.

Including the already existing wall at the entrance of the test site mass transport of water due to ventilation could be monitored at two places, see Figure 6-7.

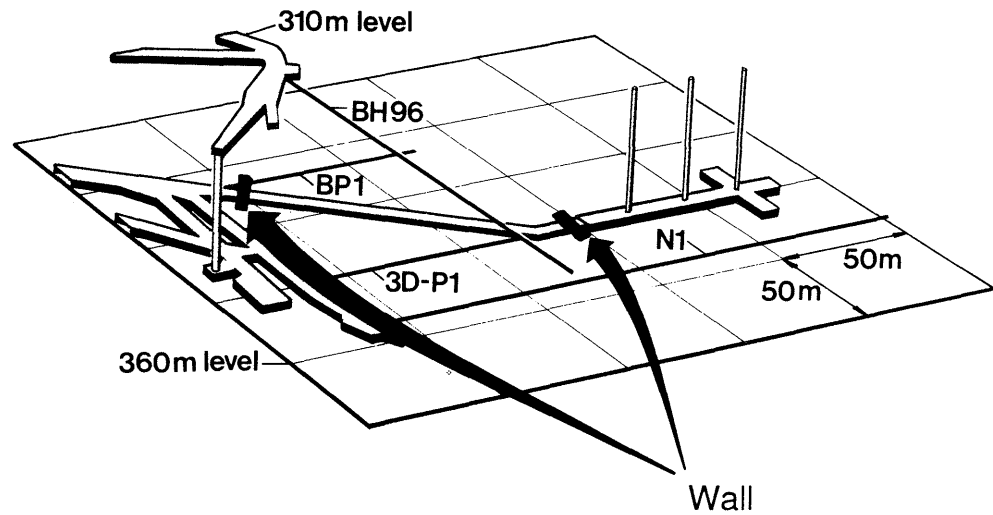


Figure 6-7. Location of the two walls used for the ventilation experiment.

The duration of the ventilation experiment was half a year. The total water inflow rate into the uncovered part of the test site and access drift was found to be 4 l/h. Of this measured total water inflow 2 l/h came from the uncovered part of the test site. Summing up all the measured inflow into the test site ($0.7+0.4+2.0$ l/h, 0.4 refers to covered areas on the floor of the test site) gives a total measured inflow of 3.1 l/h, which compares well with the water inflow rate into the corresponding part of the pilot hole, 3 l/h. For information on the equipment used in this experiment, see Appendix 6.

6.7 SUMMARY OF WATER INFLOW MEASUREMENTS

The water inflow rates into the sheets were monitored for more than 2 years. During this period only two major decreases in the inflow rates occurred; (1) when drilling the injection holes, between -6000 h to -1000 h; (2) when the preparations for Stripa Project Phase III started, at 14500 h. What seems to be seasonal changes also occurred but were within $\pm 10\%$. For further discussion on disturbances see Chapter 11, "Outer Disturbances and Their Effects on Water Inflow and Tracer Movement". Table 6.1 gives a compilation of the water inflow rates and the conditions under which they were obtained.

Table 6-1. Compilation of water inflow rates.

Location	Length	Duration	Total flow	Flowrate/ meter
Pilot hole	190 m	Hours	6.5 l/h	0.03 l/h
Test site	100 m	Years	3.1 l/h	0.03 l/h
Access drift	115 m	Months	2.2 l/h	0.02 l/h
Inj hole I	70 m	Days	1.0 l/h	0.01 l/h
Inj hole II	70 m	Days	4.0 l/h	0.06 l/h
Inj hole III	70 m	Days	17.5 l/h	0.26 l/h

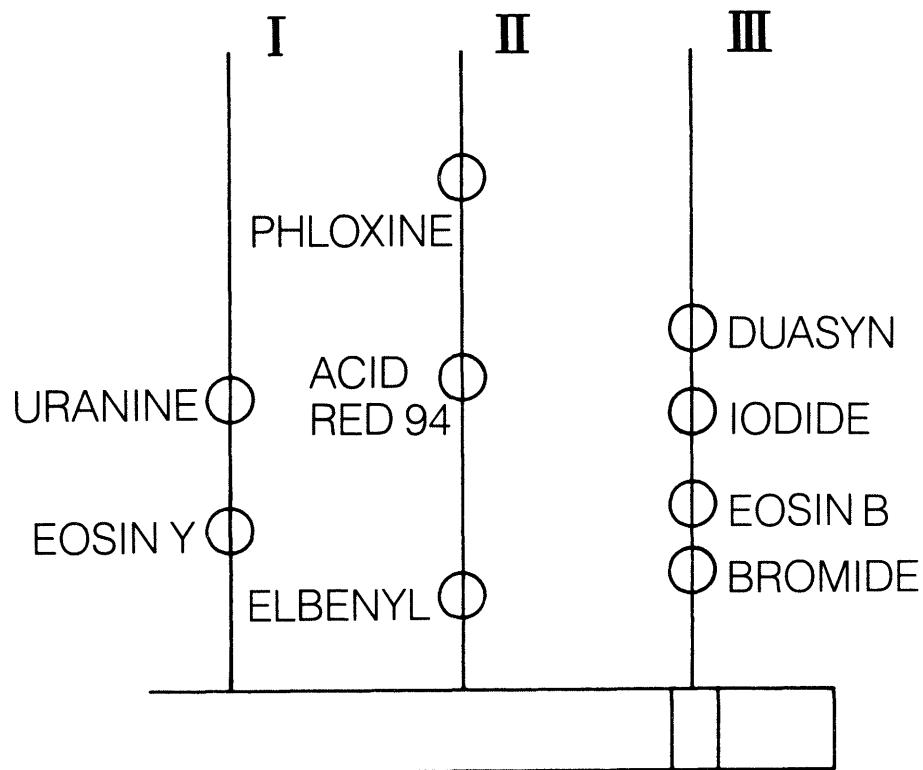
It may be noted that in one of the drilled injection holes (III) the water inflow rate per meter is nearly one order of magnitude larger than for the rest of the monitored locations.

7

TRACER INJECTION AND BREAKTHROUGH CURVES

7.1 OVERVIEW

Tracers were injected from 9 different 2.5 m long zones located between 10 and 56 m above the test site. The locations of the injection zones are shown in Figure 7-1. The tracers were injected continuously for more than 20 months except for STR-7, a large molecular weight tracer, and Fluoride. These two tracers were added to the Uranine injection after 5000 h. Water entering the test site was sampled for tracers during the time of injection plus an extra 6 months after the end of injection. Figure 7-2 shows the time schedule for injection and sampling.



I	II	III
:1 31-33 Uranine*	:1 55-57 Phloxine B	:1 36-38 Duasyn
:2 17-19 Eosin Y	:2 33-35 Acid red 94	:2 28-30 Iodide
	:3 9-11 Elbenyl	:3 18-20 Eosin B
		:4 12-14 Bromide

* Uranine, STR-7, Fluoride after 5000 h.

Figure 7-1. Location of the injection zones and injected tracers.

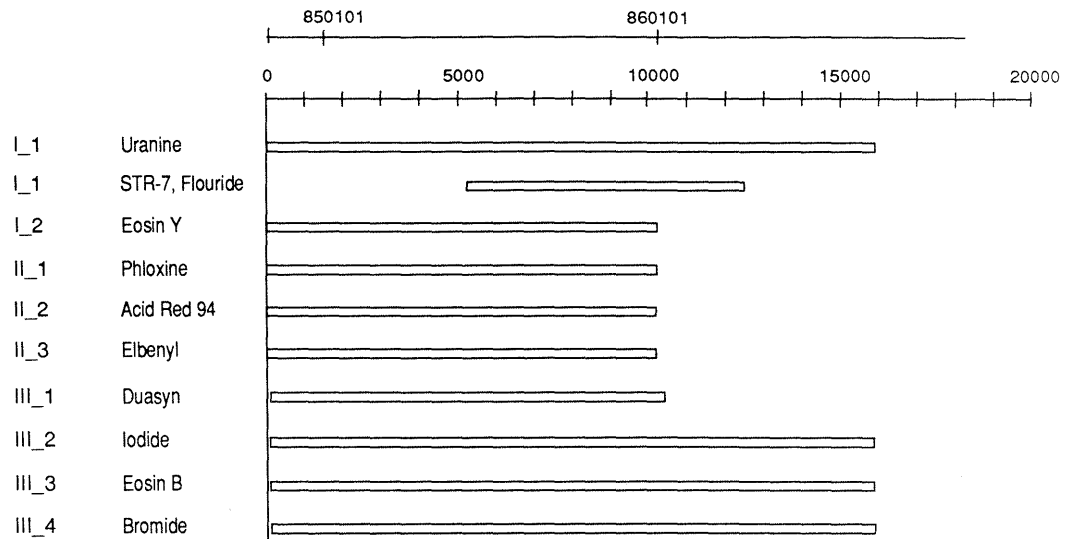


Figure 7-2. Time schedule for tracer injection.

Figure 7-3 illustrates the different types of breakthrough curves that were obtained: (1) those having a continuously rising concentration, I⁻ - dashed line; (2) those reaching a plateau within the time of injection, Uranine - dot-dashed line; (3) those rising and then falling off e.g due to decrease in injection flowrates or redirection of flow paths, Eosin Y - dot-dot-dashed line; (4) those that were blurred by high concentrations of other tracers, Elbenyl - solid line and Eosin B - dotted line; and (5) those where only the very first part of the breakthrough curves have been obtained, Duasyne - vertical dashed line.

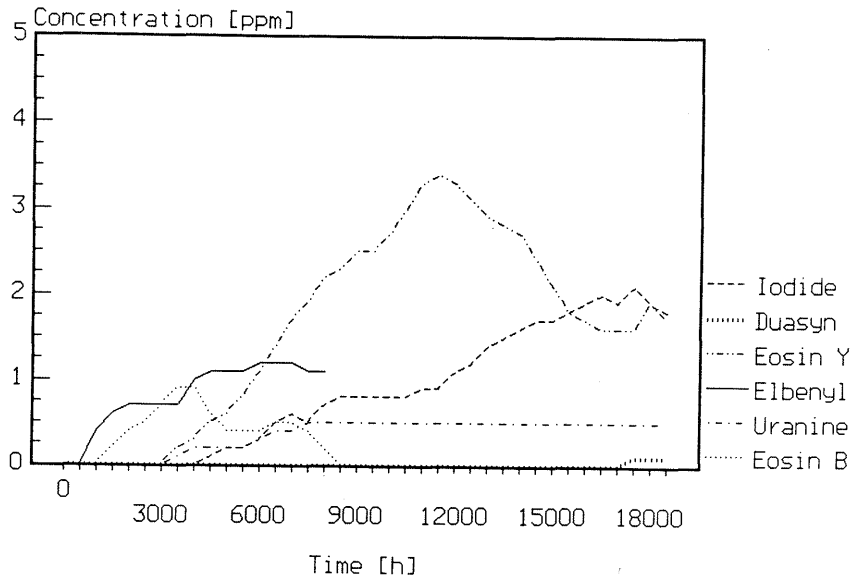


Figure 7-3. Example of different breakthrough curves.

7.2 TRACER INJECTION

The tracers were injected continuously for about 20 months with a "constant" overpressure, about 10 % above the natural pressure. The injection pressures ranged between 1.3 and 2.3 MPa, see Table 7-1 for the injection pressures. These injection pressures gave injection flowrates between 1 and 20 ml/h.

Table 7-1. Location of injection zones and injection pressures.

Hole	Zone location (m)	Injection pressure (MPa)	Flowrates	
			natural ¹	injection ² (ml/h)
I	31-33	1.9	181	5
I	17-19	1.4	75	2.5
II	55-57	2.1	2414	8
II	33-35	1.8	95	2
II	9-11	1.2	20	0.4
III	36-38	2.0	1966	15
III	28-30	2.2	1102	10
III	18-20	2.1	1489	2
III 12-14	2.1	734	3	

¹ Inflow to injection zone, monitored before start of injection.

² Average injection flowrate

One effect of injecting with a "constant" overpressure is that the injection flowrates will decrease with time due to pressure build up in the adjacent rock. A second effect is that any opening of adjacent boreholes that lowers the pressure at the injection point will increase the injection flowrates.

Figure 7-4 shows the injection flowrate for injection zone II:2, the rest of the injection flowrates are given in Appendix 7.

It can be seen in Figure 7-4 that the injection flowrate varied during the time of the experiment. The decrease in the injection flowrate at the start of injection was not only caused by the natural pressure build-up, but also due to the closing of the adjacent bore hole N1. For further discussions on outer disturbances see Chapter 11, "Outer Disturbances and Its Effects on Water Inflow and Tracer Movement." If the injection flowrate decreased below a certain level, the injection pressure was increased to get an acceptable mass inflow rate of tracers.

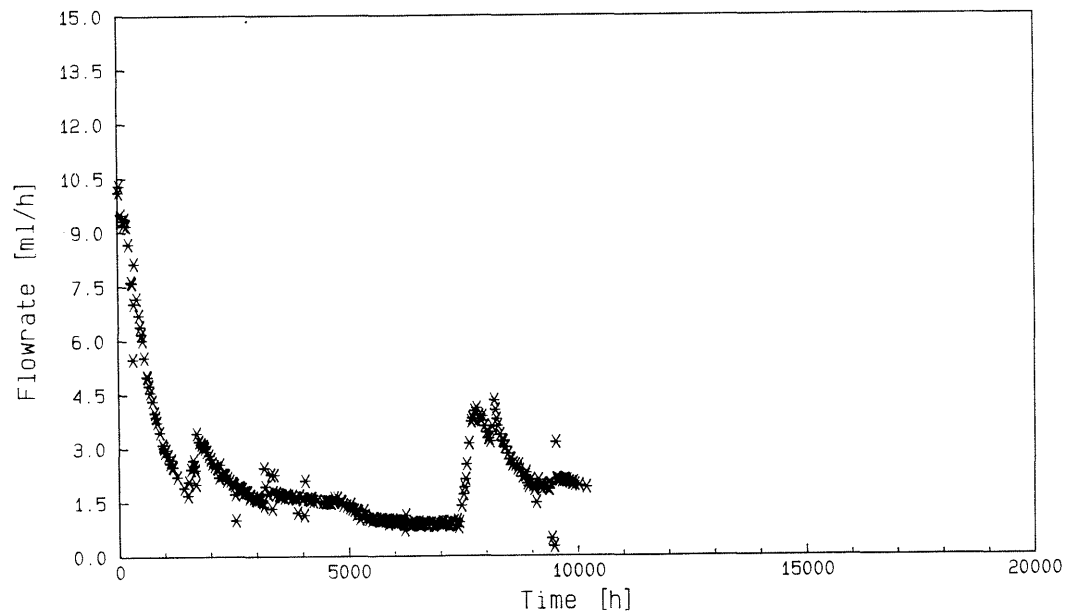


Figure 7-4. The injection flowrate at injection point II:2 (Eosin B).

7.3

WATER COLLECTION

Water entering the drift was sampled for tracers during the injection time of 20 months and an additional 6 months after the end of injection. Water samples were taken every 16 hours from all sampling areas with a high enough water flowrate. Test tube racks were changed every 3 weeks. Each rack contained water samples from up to five different sampling areas and each sampling area had a maximum

content and if tracers were found, then all the test tubes from that area were analyzed for tracers.

In the case of I^- and Br^- the minimum time interval between analyzed samples was increased to 160 hours, i.e. every tenth test tube, due to the time consuming analyzing method.

Water sampling during the last 6 months was performed at a reduced scale. Samples were only taken once a month at locations of interest.

7.4

COMPILED TRACER BREAKTHROUGH DATA

An overview of tracer breakthrough is given in the following figures. For detailed information of the breakthrough curves for each plastic sheet, see the Stand alone appendices 15 "Tracer Breakthrough Curves," and 17 "Flowrate Curves and Tracer Breakthrough Curves for Individual Sheets - Smoothed Data." Figure 7-5 shows the test site from the side and to which parts of the test site the different tracers have migrated.

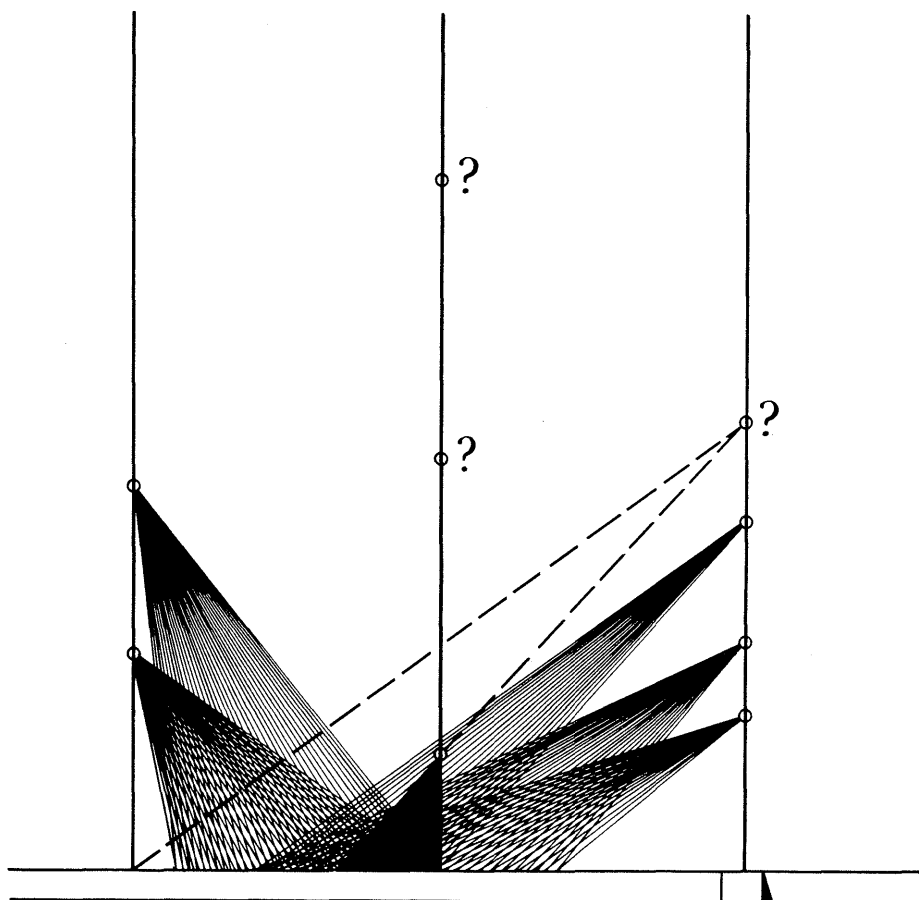


Figure 7-5.

Areas in the test site where the different tracers have emerged.

It can be seen in Figure 7-5 that tracers from 6 of the 9 zones have emerged into the test site. During the time of reduced sampling a seventh tracer was found which is illustrated with dashed lines in Figure 7-5. This occurrence might be due to the preparations for STRIPA Project Phase III, i.e. excavations of drifts and drilling of new holes that started just before the seventh tracer was found.

All 7 tracers were present in the water samples taken around injection hole II. No tracers were been found in the right part of the arm which is the area with the highest water inflow rates. The right arm is also closest to the injection zones in hole III, but the tracers injected at these zones emerged at the central part of the main drift.

The same data are also presented in Figure 7-6. Only those sampling areas with "high" water flowrates i.e. connected to fractional collectors, are included in the figure.

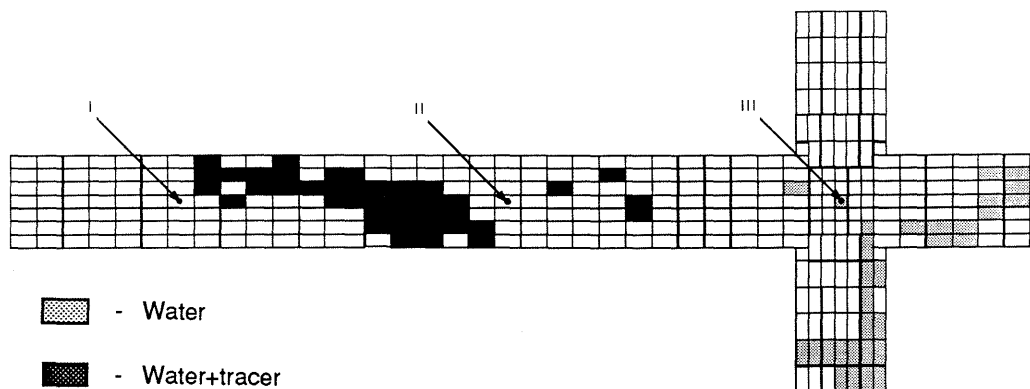


Figure 7-6. Areas where tracers have been found in the test site.

Figure 7-7 shows the locations where the individual tracer emerged. The concentrations are presented in three different intervals: (1) low, (2) medium, and (3) high. The concentrations utilized were the maximum concentrations obtained during the whole experiment which means that the different concentration peaks could have emerged at different times.

As can be seen in Figure 7-7 all tracers emerge in the central part of the main drift over a length of 35 meters. The areas of high concentrations for the different tracers were not located at the same spot but seem to depend on from which injection hole and at which depth the tracer was injected. There seems to be a tendency that

tracers injected further away from the drift have only one area of high concentration but those injected closer to the drift have two areas of high concentration. This was, however, not the case for Elbenyl, injected only 9 - 11 m from the drift, which had a narrow area of high concentration. This might be due to the very short distance from the injection point to the drift which would not allow for a large spreading sideways.

The same type of diagrams are given in Chapter 13, "Summary of Main Results, Discussion and Conclusions" where the total recovery is plotted instead of concentration.

Figure 7-8 shows the number of sampling areas in which an individual tracer has emerged as a function of time. The time of first arrival depended on the detection limit of the individual tracer. Elbenyl seemed to appear in all the sampling sheets within a short time period. The opposite can be said about Uranine, where its appearances were evenly spread out over a longer time period. For the rest of the tracers the appearances were unevenly distributed over time. If a large scale channelling exists, these are the types of curves that would be expected.

Bromide, one of the tracers that was found in the test site, can only be used to a limited extent due to severe disturbances in analysis which gave recoveries of over 100 %.

To experimentally investigate the matrix diffusion effect, two tracers were used. The tracers were STR-7 which has a large molecular weight, and Fluoride which has a small molecular weight. These tracers never arrived at the test site in detectable concentration. For further discussion on this see Chapter 13.3, "Longitudinal and Transverse Dispersion and Channelling."

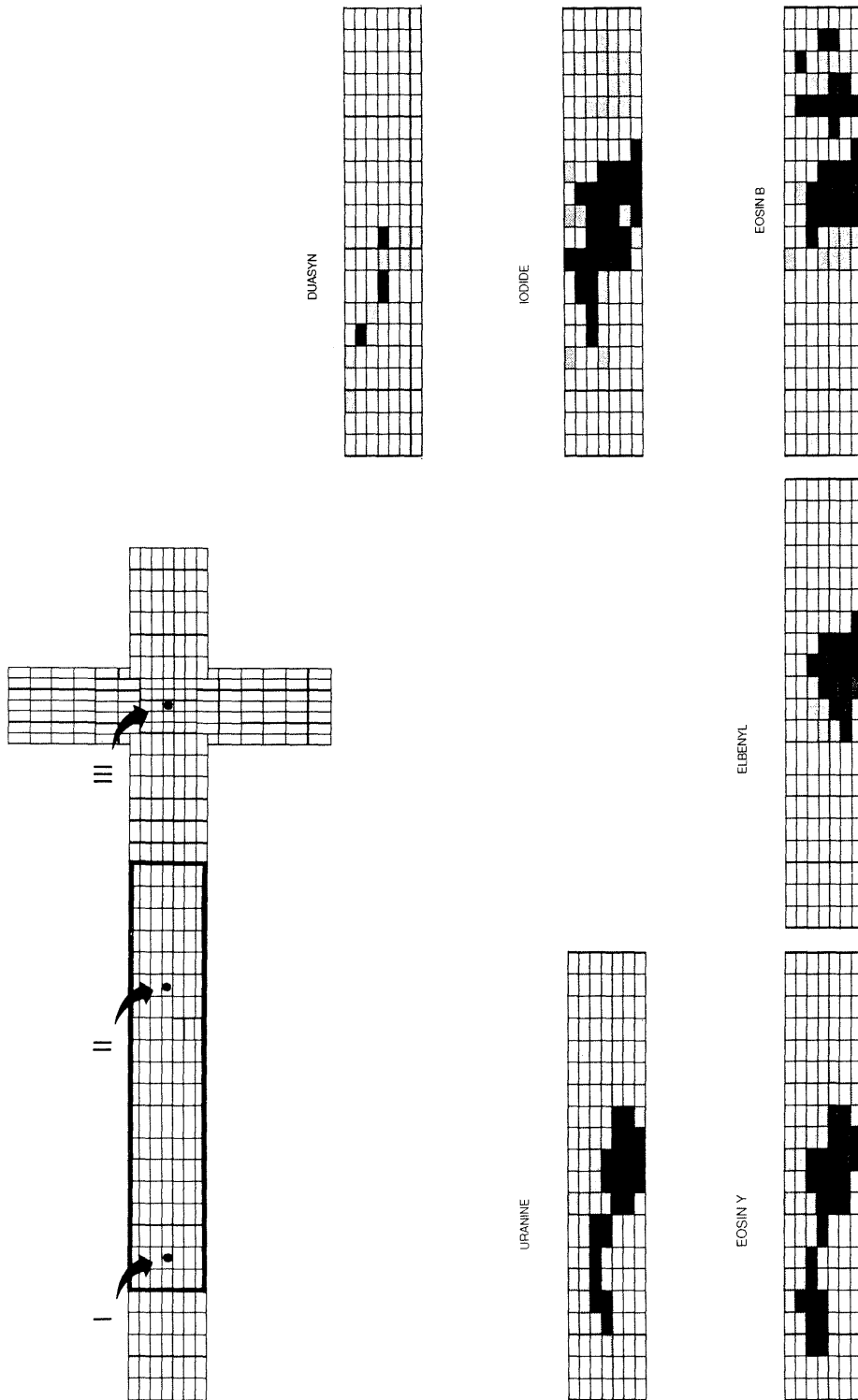


Figure 7-7.

Tracer occurrence in the main drift for the individual tracers.

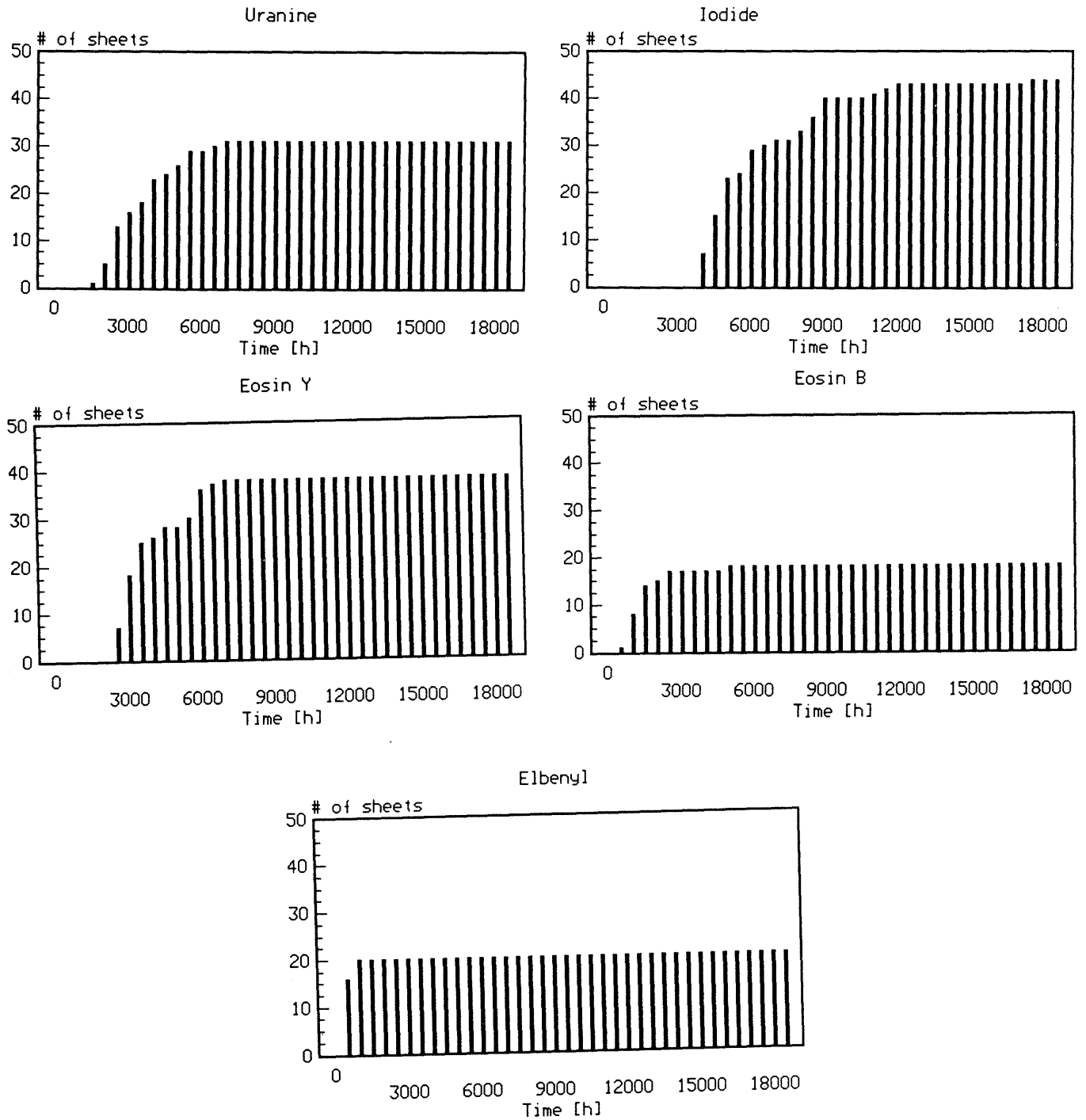


Figure 7-8.

Number of sampling areas into which individual tracers have emerged as function of time. Time of appearance is the first arrival of the tracer with a concentration above the detection limit.

7.5 DETAILED BREAKTHROUGH CURVES FOR ONE SAMPLING AREA

The detailed breakthrough curves for one of the sampling areas in the central part of the test site are shown in Figure 7-9. Detailed breakthrough curves for other sampling areas are given in Stand alone appendix 15, "Tracer Breakthrough Curves."

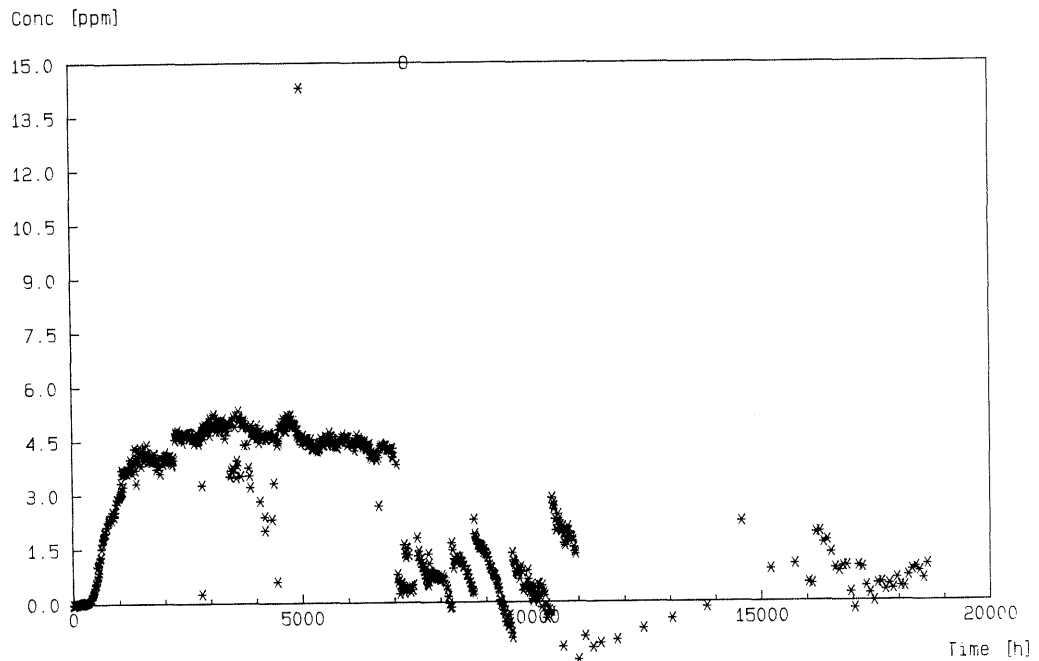


Figure 7-9. Detailed breakthrough curve for one sampling before data processing.

The small scale variations in the breakthrough curves were due to both physical and analytical variations, among these one can mention: (1) variation in the injection flowrates, (2) natural variations in the water inflow rates into the sampling areas, (3) redirections of water flow pathways due to outer disturbances, (4) different sampling times i.e. a long sampling time will average the tracer concentration, (5) degradation of tracer due to light exposure, and (6) multicomponent analysis sensitivity to relative tracer concentrations i.e. high concentration of one tracer will increase the analysis error for the low concentration tracers and in some instances even make the analysis impossible. This effect is illustrated in Figure 7-10 where it can be seen that when the concentration of Eosin Y rises above a certain level it is not possible to determine the concentrations of Eosin B and Elbenyl with any accuracy.

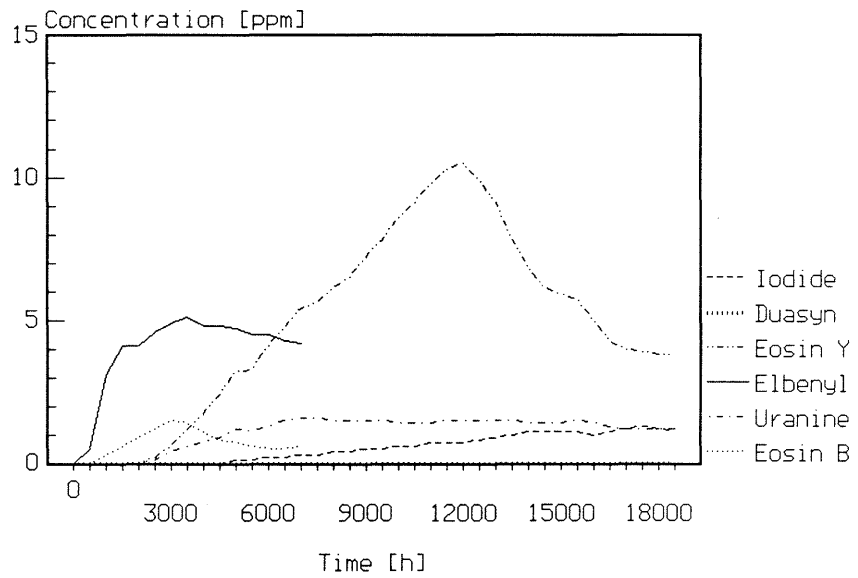


Figure 7-10. An example of how a high Eosin Y concentration blur the analysis of Elbenyl and Eosin B.

The first step in the pretreatment of the breakthrough curves was to eliminate points which had obvious analysis errors. The processed breakthrough curve after this sorting out is given in Figure 7-11.

27+1 C=f (t) Distance (inj-sampl) ~ 12 [m]

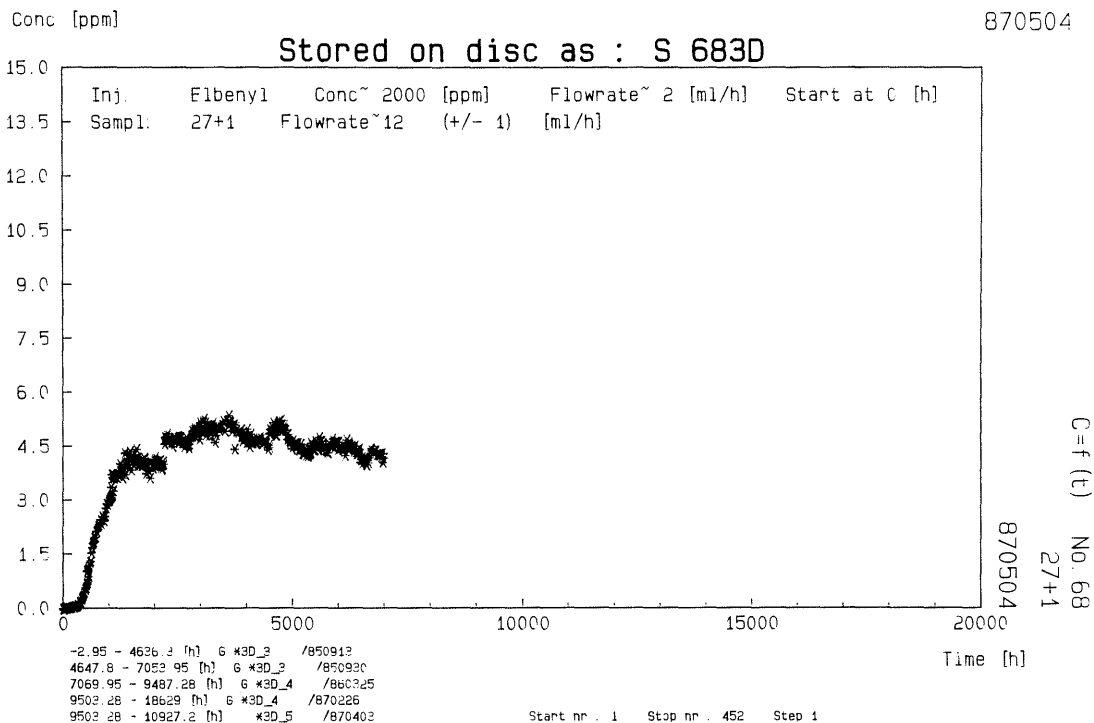


Figure 7-11. Breakthrough curve after sorting out analysis errors.

For a second smoothing of the curves both numerical and manual methods were tested. It was found that the best procedure was to actually fit a curve by hand. This curve was then digitized with a digitizer and then transferred to the main computer where the modelling was done. The same data as in Figure 7-11 are shown in Figure 7-12 after the second smoothing.

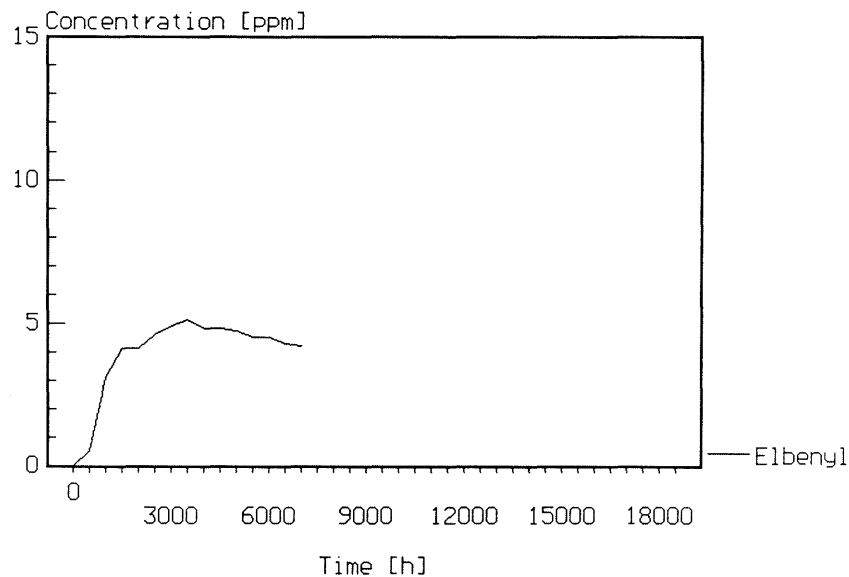


Figure 7-12. Breakthrough curve after second smoothing.

7.6 TRITIUM AS A TRACER

7.6.1 Overview

Tritium is often used as an environmental tracer. Infiltrating rain water contains about 10–20 TU (Tritium Units), at present. During the nuclear bomb tests in the 1950's and 1960's considerable amounts of Tritium were released to the atmosphere. The Tritium content of the rain was increased considerably and peak values of more than 500 TU were measured in the period 1963–1967. The Tritium content of water before the bomb tests was on the order of 5 TU. Tritium has a half-life of 12.3 years. Therefore "pre-bomb" tritium should have decayed to about a tenth of the initial concentration of those times i.e. to values below 1 TU. If values higher than this are found, then it is an indication that the surface water has reached the sampling points in less than about 30 years.

7.6.2 Results of tritium measurements

Tritium samples were taken in May 1985 and in June 1986 at several locations in the drifts and in two of the injection zones in hole III. Table 7-2 shows the results of the analyses.

Table 7-2. Tritium content of water samples expressed in Tritium units (TU).

Location	May 85	June 86
Sheet 12-1	<3	(2.9)
Sheet 25-0	*	(2.7)
Sheet 33+2	*	(1.8)
Sheet 39-1	5±1	5.7±1
Sheet 45+1	*	7.3±2
Sheet 62.75+11	<3	(0.8)
Access drift	<3	(1.4)
Hole III:3	*	(1.0)
Hole III:4	*	(1.8)

* Indicate that no samples were taken in 1985. The measurement limit is 3 TU, figures below 3 are not significant.

The location of the sheets where the samples were taken is shown in Figure 7-13. An inspection of the location of the sheets which have significant increases in Tritium show that the water to these sheets contains a "high" concentration of the tracer Eosin B, but none of the other tracers except a very low concentration of Iodide. Eosin B was injected in Hole III:3. No tritium was found in the samples taken from the tracer solutions used in Hole III:3 and III:4.

There are two possibilities; either the samples in the two Tritium-containing sheets have been contaminated or there is some channel which carries the tritium from some source near the surface. It may be excluded that tritium containing water in the mine can infiltrate the rock because the hydraulic heads in the rock are always higher than in the drifts. Tritium has also been found in Hole E1 with a concentration of 17-43 TU (Nordström et al., 1985). Considering also that samples taken at different times give very similar results it can be ruled out that the samples have been contaminated.

The result indicate that in at least two sheets, the surface water has had a residence time of less than 30 years.

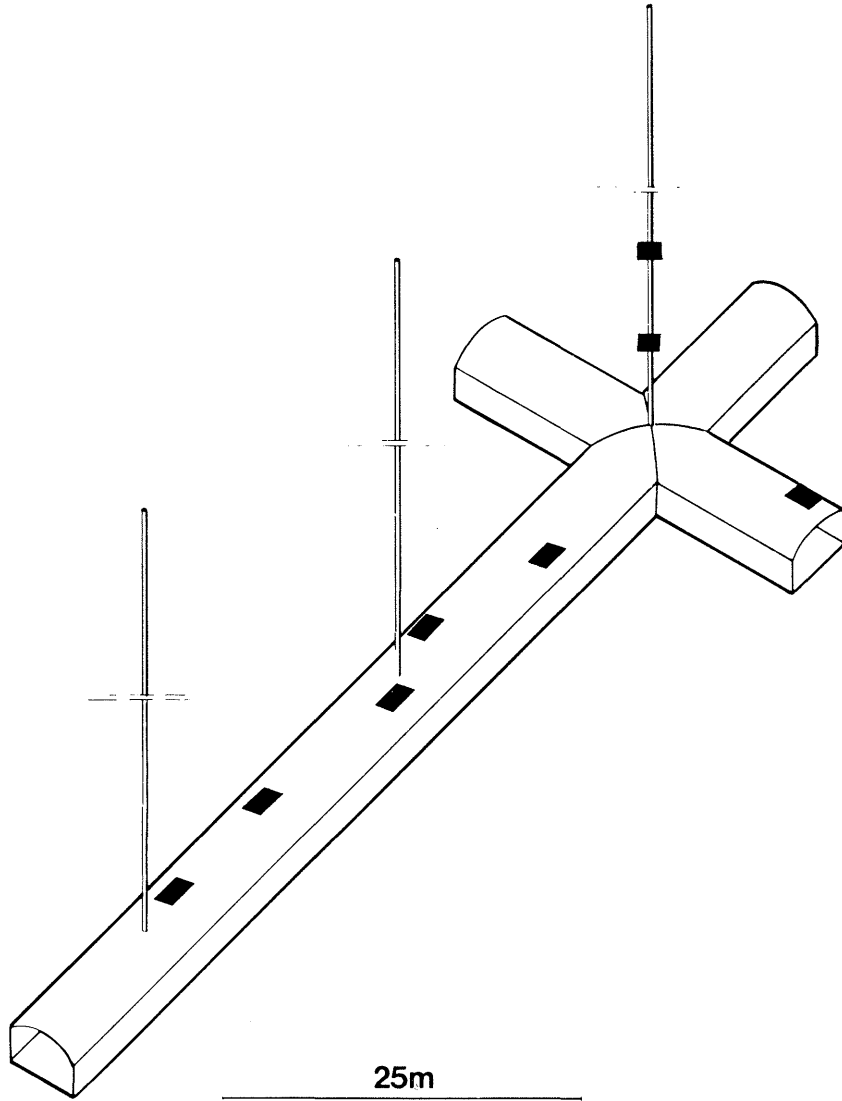


Figure 7-13. Location of Tritium sampling.

8 DIFFUSION MEASUREMENTS IN THE LABORATORY

8.1 OVERVIEW

The matrix in crystalline rocks has been found to be porous with a connected porosity in the range 0.1 to 0.5 % typically. Skagius and Neretnieks (1985, 1986a, 1986b) and Birgersson and Neretnieks (1982, 1984) found in laboratory and in in-situ experiments in Stripa that tritiated water, Iodide, Uranine, and Chrome-EDTA readily diffused into the pore system.

One phenomenon that may occur is the penetration of tracers into the stagnant waters in the matrix which may withdraw the tracer from the cause a noticeable part of the tracers to disappear from the mobile water and may, in the extreme, cause the mobile water which arrives to the plastic sheets to have tracer concentrations that are below the detection limit.

For most of the tracers used in the present experiment there were no previously measured matrix diffusion data available. A series of measurements of all tracers found in the sheets were performed on tablets taken from a core in the extensometer drift.

8.2 EXPERIMENTAL METHOD

A "through diffusion" technique used by Skagius was used. A machined tablet 8-10 mm thick and 42 mm in diameter was placed between two vessels filled with water. One vessel contained a known high concentration of the tracer or a tracer mixture. The other vessel contained no tracer originally but the ionic strength was maintained the same by adding Sodium Nitrate in those experiments where inorganic salts were the diffusing substances. Figure 8-1 shows the principle layout of the diffusion cell used in the measurements.

Diffusion cell

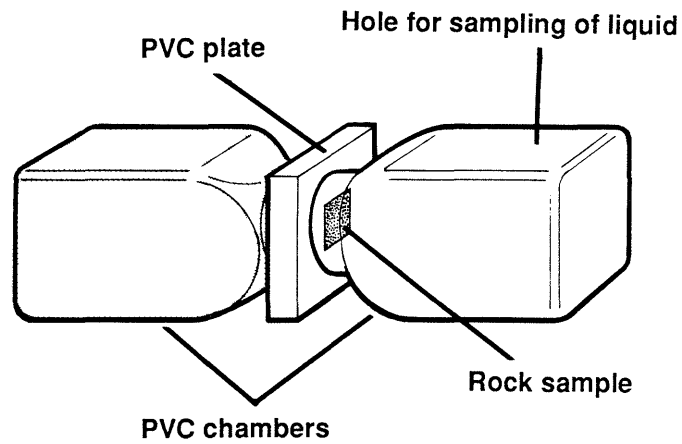


Figure 8-1. Principle layout of diffusion cell used in matrix diffusion measurements.

The rock tablets were glued into the hole in the 10 mm thick PVC plate. The vessels were glued onto both sides of the PVC plate to ensure that there was no contact between the two vessels except via the rock tablet. In the present experiments the size of the vessels were 500 ml.

When the tracers started to diffuse into and eventually through the porous rock tablet, the tracer concentration in the receiving vessel was monitored at regular intervals. A typical concentration-time curve is shown in Figure 8-2.

The porosity of the rock samples was measured by weighing the samples both dry and wet. Another method available to assess the porosity and also to determine possible sorption effects is by utilizing the time lag for the arrival of the tracer to the low concentration side.

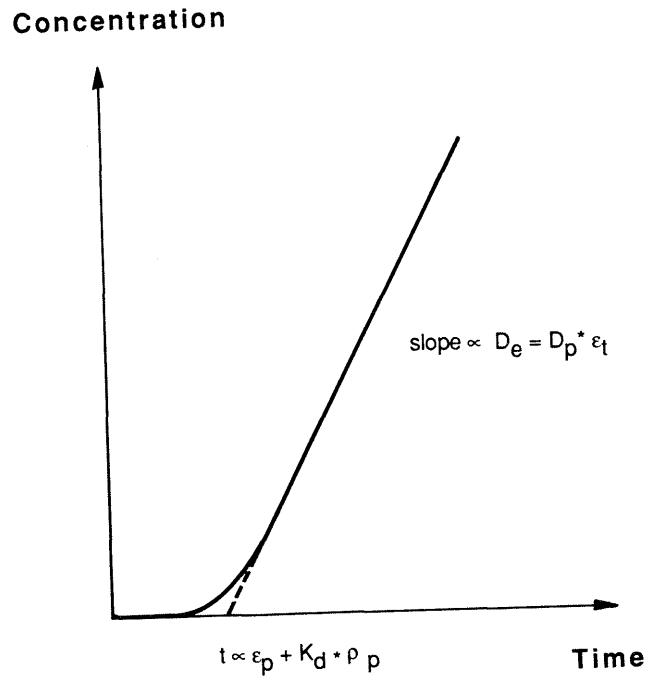


Figure 8-2. Typical concentration – time curve from a matrix diffusion experiment.

It was observed that the concentration increased proportionally to time after an initial period. This increase occurred as long as the concentration in the receiving vessel was very low compared to that on the "high concentration side" and as long as the concentration on this side was constant. This was always the case in the present experiments.

In Figure 8-2 the slope of the straight part of the curve gives the rate of transport through the rock tablet and is used to determine the diffusivity using Fick's first law. The lag time (intercept with the time axis) is due to the filling up of water in the pores with tracer and can be used to estimate the amount of water in the matrix (porosity).

The theory for these calculations is given below.

8.3

THEORY

Fick's second law gives the rate of change of concentration in a homogeneous medium. For one dimensional transport, the diffusion equation can be written

$$\frac{\partial C}{\partial t} = D \frac{\partial^2 C}{\partial x^2} \quad (8.1)$$

The diffusion coefficient, D , is assumed to be constant. In a porous medium the effects of the pores must be accounted for. The total porosity is the sum of "transport" porosity and "storage" porosity. By transport porosity is meant those pores which aid in transporting species from one side to the other side of the sample. The pores with a dead end are denoted by "storage" porosity. These pores will

contribute to the capacity of the pore system to hold the dissolved species, but will contribute nothing or very little to the transport. Equation (8.1) can be written

$$(\epsilon_p + K_d \rho_p) \frac{\partial C}{\partial t} = D_p \epsilon_t \frac{\partial^2 C}{\partial x^2} \quad (8.2)$$

ϵ_p = total porosity

ϵ_t = "transport porosity"

K_d = sorption coefficient

ρ_p = density of the solid material

D_p = pore diffusion coefficient

Assuming that the porous system may be approximated by a homogeneous one, a combination of Equation (8.1) and (8.2) gives

$$D = \frac{D_p \epsilon_t}{\epsilon_p + K_d \rho_p} = \frac{D_e}{\alpha} \quad (8.3)$$

where $\alpha = \epsilon_p + K_d \rho_p$ is the rock capacity factor and $D_e = D_p \epsilon_t$ is the effective diffusion coefficient.

Crank (1975) gives a solution to Equation (8.2) for the case of diffusion through a porous slab initially at zero concentration. The inlet concentration is constant C_1 and the outlet concentration is C_2 ($C_2 \ll C_1$) at $x = L$

$$\frac{C(x, t)}{C_1} = 1 - \frac{x}{L} - \frac{2}{\pi} \sum_{n=1}^{\infty} \frac{1}{n} \sin \frac{n\pi x}{L} \exp\left(-\frac{D_e n^2 \pi^2 t}{L^2 \alpha}\right) \quad (8.4)$$

By differentiating Equation (8.4) to obtain the gradient at $x=L$, the rate of transport, N , out from the slab at $x=L$ is obtained. N is the flux at $x=L$

$$N = - D_e \left. \frac{\partial C}{\partial x} \right|_{x=L} \quad (8.5)$$

By integrating Equation (8.5) with respect to the time t , the total amount of diffusing substance M which had passed through the slab at time t is obtained

$$\frac{M}{LC_1} = \frac{D_e t}{L^2} - \frac{\alpha}{6} - \frac{2\alpha}{\pi^2} \sum_{n=1}^{\infty} \frac{(-1)^n}{n^2} \exp\left(-\frac{D_e n^2 \pi^2 t}{L^2 \alpha}\right) \quad (8.6)$$

As $t \rightarrow \infty$, Equation (8.6) approaches the linear relation

$$M = \frac{C_1 D_e}{L} t - \frac{C_1 L \alpha}{6} \quad (8.7)$$

with the slope $C_1 D_e/L$ and an intercept on the time axis

$$t = \frac{L^2 \alpha}{6 D_e}$$

where $\alpha = \epsilon_p + K_d \rho_p$, but if there is no sorption then $\alpha = \epsilon_p$. The intercept on the time axis gives the total porosity of the material.

8.4

EXPERIMENTAL RESULTS

Table 8-1 and Table 8-2 summarize the 11 diffusion experiments which were performed. Experiments 1-7 were made using mixtures of three tracers in such a way that every tracer was mixed with every other in at least one experiment. Experiment 8 was a blind where the rock tablet was exchanged for a PVC tablet of the same size. In experiments 9-11 Iodide was used in mixtures with two other tracers. For more detailed information about the experiments and results see Appendix 8.

Table 8-1. Composition of tracers on the high concentration side in the different cells.

Experiment No.	Tracers	Concentration
1	Uranine Elbenyl Br. Flavine Br ⁻	10 000 ppm 5 000 ppm 0.1 M
2	Eosin blueish Elbenyl Br. Flavine I ⁻	10 000 ppm 5 000 ppm 0.1 M
3	Eosin yellowish Elbenyl Br. Flavine F ⁻	10 000 ppm 5 000 ppm 0.1 M
4	Uranine F ⁻ I ⁻	10 000 ppm 0.1 M 0.1 M
5	Uranine Eosin blueish Eosin yellowish	10 000 ppm 10 000 ppm 10 000 ppm
6	Eosin yellowish Br ⁻ I ⁻	10 000 ppm 0.1 M 0.1 M
7	Eosin blueish Br ⁻ F ⁻	10 000 ppm 0.1 M 0.1 M
8	Same tracers as in cell No. 1, but the granite piece was replaced by a PVC plate.	
9	Elbenyl Br. Flavine I ⁻	5 000 ppm 0.1 M
10	STR-7 I ⁻	20 000 ppm 0.1 M
11	Elbenyl Br. Flavine I ⁻	5 000 ppm 0.1 M

Table 8-2. Obtained results on the effective diffusivity and porosity.

Diffusion- No.	Tracers	$D_e * 10^{+14}$	ϵ_p weighing	ϵ_p time lag
1	Uranine	0.9	0.59	0.01
	Elbenyl	1.2		
	Br ⁻	31		
2	Eosin B	2	0.51	0.04
	Elbenyl	2.3		
	I ⁻	26		
3	Eosin Y	1.5	0.70	0.02
	Elbenyl	1.2		
	F ⁻	<5		
4	Uranine	1.6	0.63	0.03
	F ⁻	<5		
	I ⁻	11		
5	Uranine	1.7	0.55	0.03
	Eosin B	1.2		0.02
	Eosin Y	2.3		0.04
6	Eosin Y	2.9	0.50	0.06
	Br ⁻	Interference by I ⁻		
	I ⁻	29		
7	Eosin B	0.3	0.69	0.05
	Br ⁻	-		
	F ⁻	<5		
8	Same tracers as in cell No. 1, but the granite piece was replaced by a PVC plate. No tracers were found in this experiment.			
9	Elbenyl	7.8	0.63	0.03
	I ⁻	14		
10	STR-7	<0.01	0.49	0.05
	I ⁻	22		
11	Elbenyl	3.3	0.48	0.06
	I ⁻	27		

The results are summarized in Table 8-3.

Table 8-3. Summary of diffusion and porosity measurements.

	Effective diffusivity $D_e \cdot 10^{14} \text{ m}^2/\text{s}$	Porosity (Weight) %	Porosity (Time lag) %	Pore diffusivity $D_e \cdot 10^{10} \text{ m}^2/\text{s}$ col.1/col.3
Column	1	2	3	4
Tracer				
Eosin B	0.3-2	0.51-0.69	0.02-0.05	0.2-0.4
Uranine	0.9-1.7	0.55-0.63	0.01-0.03	0.5-0.9
Elbenyl	1.2-7.8	0.48-0.70	-	-
Eosin Y	1.5-2.9	0.50-0.70	0.02-0.06	0.5-0.8
Iodide	11-29	0.48-0.63	0.03-0.13	2-4
Bromide	31		-	-
Fluoride	<5		-	-
STR-7	<0.01		-	-

Discussion

The results obtained in the present measurements are similar to those obtained by Skagius and Neretnieks (1985, 1986a, 1986b). The dyes, which are larger and bulkier molecules, have a smaller diffusivity than Iodide and Bromide. The results are somewhat contradictory to those obtained in the in-situ experiments in Stripa. In these experiments Iodide and Uranine were found to have migrated equal distances. Also the porosity values were somewhat lower, 0.25-0.45 %, than those obtained here. There is a surprisingly large difference between the porosity measured by weighing and that obtained from the time lag. Skagius (1986a) made measurements on fracture coating materials and on rock tablets taken immediately adjacent to a fracture. The porosity in some samples was found to be as high as 4 % and the effective diffusivity measured with Iodide was as high as $2 \cdot 10^{-11} \text{ m}^2/\text{s}$. This is nearly two orders of magnitude higher than for rock not immediately adjacent to a fracture. Skagius also found a considerable variability in the porosity and diffusivity between samples taken quite close to each other from the same core.

It cannot be ruled out or may even be probable that quite often the rock nearest to a water carrying channel has a higher diffusivity and porosity than the rock located further away.

9 SOME CONCEPTS OF WATER FLOW AND TRANSPORT IN FRACTURED ROCK

9.1 **OVERVIEW**

It is usually implicitly assumed that the fractured rock, even at depth, is sufficiently fractured to allow for an averaging to be performed of the properties in a volume of rock such that it is meaningful to assign an average value of the properties to a "point" in the rock. The properties of interest for flow are the hydraulic conductivity and the porosity. The size of the volume over which the averaging is performed is called a "Representative Elementary Volume" - REV. It is implicitly assumed that the REV is considerably smaller than the rock volume studied. To calculate the flowrate in the rock volume, Darcy's law is used together with the appropriate boundary conditions to calculate the flowrate and flow directions in "all" points in the rock mass of interest.

Solutes which are dissolved in water will be carried by the moving water but will also move independently by various mechanisms such as diffusion and will be retarded by interactions with the solids. Molecules or ions diffuse in a concentration gradient and can move from one "stream tube" to another. Different water volumes move with different velocities and may mix at more or less regular intervals. A regular type of mixing may be described as a process of the same type as molecular diffusion and is often described as such by what is called Fickian dispersion.

With only advection and dispersion active, the classical advection-dispersion description results. It has been used extensively to describe tracer movement in porous media. It has also been used to model transport in individual fractures and channels. It is possible to modify the equations to account for an instantaneous chemical reaction with linear or nonlinear equilibria and can also accommodate reaction rates if the reactions cannot be approximated as instantaneous.

Ideally, hydrologic tracers are not supposed to react chemically or physically with the solid material, but some naturally occurring tracers, e.g. C-14 and H-3, do and the problem cannot be neglected especially for long travel times. Also in cases where it is of interest to describe the movement (and retardation) of reactive species, e.g. chemical waste and many radionuclides, the chemical reactions are an integral part of the problem. In many instances, laboratory experiments are designed so that kinetic effects are eliminated. But in the field cases the kinetic effects often cannot be eliminated.

The dissolved species may also experience kinetic effects due to physical processes. One such process which has a very large impact for flow in fractured rock is the diffusion in and out of zones with so very slowly moving water that it can for practical purposes be assumed to be stagnant. Such stagnant zones can be expected in fractures with uneven surfaces.

In rocks with a connected matrix porosity, the accessible pore volume of the matrix can be very much larger than the mobile water volume in the fracture. The species which have access to the pore water will then have a residence volume and residence time determined by the sum of the water volume in the fractures with flow and the water volume accessed in the stagnant areas. As the stagnant zones are reached by diffusion, the volume of stagnant water accessed is dependent on the time that the rock is in contact with the water containing the diffusing species. Stagnant zones of water may also exist in fractures with channeling where the water volumes between the channels do not participate in the flow.

Rock fractures often have preferential channels where the water flows. Channels in the same fracture may not meet and mix their water over considerable distances. The mixing required for the process to become one of hydrodynamic dispersion, in the sense that it may be modelled as a Fickian process, may not be sufficient over the distances of interest. The situation may then be better described as stratified flow or channeling. It may be expected that the mixing will eventually be sufficient to obtain Fickian dispersion. This may not happen in media where even larger features are encountered when the distance increases. The larger pathways may always dominate the flow.

The properties of the medium can vary considerably in crystalline fractured rock. Fracture openings and thus the transport capacity of the individual fractures are known to span many orders of magnitude. Fractures are only open in places where the blocks are not in contact. The open areas may be much smaller than the closed areas. The porosity of and diffusivity in the rock matrix have similar variability. Fracture coating and filling materials also may vary considerably as to the type and amount. In fracture zones the block sizes vary from very small particles up to blocks of considerable size. The size of the blocks will strongly influence the amount of stagnant volume accessible at a given contact time.

9.2

CHANNELING

In the so called 2-D experiment in the Stripa mine it has been noted that the flow in individual fractures takes place in channels (Abelin et al., 1985). Figure 9-1 shows how the natural water flow emerges from two fractures as they intersect the face of the drift. The white arrows are proportional to the flow and the figures beside the arrows indicate the magnitude of the flow. Subsequent injection of small amounts of water with nonsorbing tracers showed that the tracers arrived at two of the collection points in the fracture used for the tracer experiment. The collection was made by drilling 1 m long holes in the plane of the fracture with a spacing varying between 0.5 and 0.7 m. This means that every hole collected water from about this width of fracture. These results indicate that about 5-20 % of the fracture plane carries more than 90 % of water. The actual width of the channels is less than 1 m and could be considerably smaller.

description is found in the paper by de Josselin de Jong (1958). The common basis for practically all these treatments is that the spreading is described by one parameter — the variance σ^2 of a pulse as it spreads with distance. The variance increases with traveled distance. Gelhar and Axness (1983) show that for certain media there is a theoretical basis for this observation.

For a random process such as molecular diffusion, a dispersion coefficient D_L analogous to the diffusion coefficient could be determined from $D_L = \sigma_z^2/2t$. For a porous media with fairly uniform particle size, this has been verified experimentally in the laboratory by many different investigators.

The dispersion coefficient is found to be proportional to the velocity and the particle size: $D_L \propto v d_p$. This also implies that the variance is proportional to the distance:

$$\sigma_z^2 \propto 2 t v d_p = 2 d_p z$$

In some investigations (Neretnieks, 1985), the dispersion coefficient increases considerably with distance. The explanation for this is usually summarized in the words "channeling" or "uneven distribution". Schwartz (1977), by computer simulation, has shown that the uneven distribution of resistances in a porous medium may not lead to a variance which increases proportionally to the distance traveled. Mercado (1967) and Neretnieks (1983) by a different method showed that in a medium where stratification occurs — where there are parallel unconnected strata with transmissivity differences between channels, $\sigma_z \propto z$ instead of $\sigma_z^2 \propto z$ as in the diffusion—dispersion case above.

Matheron and de Marsily (1980) arrived at the same conclusion and also concluded that the common "convection diffusion equation" cannot in general be applied even for large distances.

Neretnieks (1983) discussed several dispersion mechanisms including stratification and derived a model which includes these effects as well as the effects of physical interaction by diffusion into stagnant zones of water in the matrix of the rock. It was shown that matrix diffusion effects can have a dominating influence on the pulse spreading when the accessed stagnant water volume is large in comparison to the mobile water.

9.4

DIFFUSION INTO THE POROUS MATRIX

Crystalline rocks, such as granites and gneisses, have microscopically small fractures between the crystals. These microfissures comprise an interconnected pore system containing water. The dissolved species are much smaller than the microfissures and can diffuse into this pore system. The inner surfaces in the rock matrix are many times (thousands and more) larger than the surfaces in the fractures in which the water flows. Penetration into and sorption on the inner crystal surfaces may retard the species far beyond the retardation caused by sorption on the fracture faces. Even nonsorbing species will move slower than the flowing water, since they diffuse into the stagnant water in the pores.

Gneisses and granites in Swedish Precambrian rock have been found to have a continuous pore system consisting of the microfissures between the crystals in the rock matrix. The porosity in this pore system varies between 0.06 % and 1 % for the rock matrix (Skagius and Neretnieks, 1986a). Similar results have been obtained by other investigators (Brace, 1965 and Bradbury, 1982). Fracture minerals and rock in crushed zones have higher porosities. Values between 1 and 9 % have been measured (Skagius, 1986). Substances dissolved in the water can diffuse into this pore system and sorb on the inner surfaces.

The penetration depth increases with time. Nonsorbing species penetrate far into the matrix, while sorbing species are retarded since they also have to fill up the sorption sites before migrating further.

The penetration depth can be calculated using Fick's law for diffusion, if the diffusivity is known and by taking the retardation due to sorption into account.

9.5

SORPTION AND OTHER INTERACTIONS

The minerals of crystalline rocks have a considerable cation exchange capacity. The minerals also exhibit a capacity to form surface complexes with anions as well as cations. The capacity to bind different ions to the surface depends on the pH, the concentration of many of the other ions, and on the form the species have in the solution. Many cations form complexes with the anions and other complexing agents in the water. The complexed metal ions may be positively charged species, neutral species or even negatively charged species, depending on the composition of the water.

The component may be bound, by adsorption or ion exchange, to the surface of the minerals of the rock or it may form its own minerals by precipitation. It may also react irreversibly by mineralization into some very stable solids.

The different complexes will of course have different affinities to the mineral surfaces. Because of the complexity of the situation it is often convenient to summarize all the effects into a term "sorption coefficient" (K_d). This expresses how much of a component, e.g. Ca^{2+} , is bound to the surfaces of the rock and how much is in the water at equilibrium. One neglects which form, complexed or noncomplexed, the various species containing the component have in the solution as well as in the bound state. K_d is the ratio of concentrations of the component in the two phases.

$$K_d = q/C$$

where q denotes the concentration on (in) the minerals and C is the concentration in the water.

The component may simultaneously be one part of several species (complexes) which are sorbed in different ratios. K_d often varies very much with changes in the composition of the groundwater (pH, Eh, concentration of complexing agents etc.). It is therefore not a very

precise entity, but because of its simplicity it has been found to be very useful in mathematical modeling and in transferring information from the chemists to the modelers.

Adsorption and ion exchange are often summarily called sorption by which is meant a fast reversible reaction of the dissolved components with the surfaces of the rock. These processes are treated by the K_d -concept. Processes such as precipitation and irreversible mineralization are usually not included in the K_d -concept.

9.6 MATHEMATICAL MODELING

The description of the mathematical models will be limited to one dimension. The concepts and models may be extended to 2 or 3 dimensions in a straightforward way. There are, however, very few analytical solutions available for more than one dimension problems and usually numerical solutions are used.

The simplest models are based on the concept of advective flow with a known velocity. A tracer pulse transported by the flow will be dispersed around the mean due to random velocity components. The dispersion is assumed to behave similarly to molecular diffusion.

9.6.1 Advection - Dispersion description

The advection-dispersion equation for a nonreactive tracer for linear flow can be written:

$$\frac{\partial C}{\partial t} + v \frac{\partial C}{\partial z} = D_L \frac{\partial^2 C}{\partial z^2} \quad (9.1)$$

A very common case of interest is where the medium is of infinite length and a tracer is suddenly injected at a point $z = 0$. The injection is continued forever and is made in such a way that the concentration always is C_0 at the injection point. This is not a very realistic assumption but the case has been extensively treated in the literature. Other more realistic cases are treated in a comprehensive way by Maloszewski and Zuber (1984). The initial and boundary conditions can be written:

$$\text{IC} \quad C = 0 \quad z > 0 \quad t = 0 \quad (9.2a)$$

$$\text{BC1} \quad C = C_0 \quad z = 0 \quad t \geq 0 \quad (9.2b)$$

$$\text{BC2} \quad C = 0 \quad z \rightarrow \infty \quad t \geq 0 \quad (9.2c)$$

The classical solution to this is given by Lapidus and Amundsen (1952). It is given in Chapter 12, Equation (12.2) but can be written in a shortened way as:

$$C/C_0 = f(t, \{t_w, Pe\}) \quad (9.3)$$

thus indicating that the concentration is a function of time t and that the two parameters t_w , water residence time, and Pe , measure of dispersivity, suffice to fully define the solution. The parameters include

the velocity, distance, and dispersion coefficient and could have been combined in other ways. However, two groups suffice to define the solution.

Extension to the case where instantaneous equilibration of the tracer with the solid material takes place and where the equilibrium is linear is also straightforward. With the following expression:

$$R_d = 1 + K_d \rho_p \frac{1 - \epsilon_p}{\epsilon_p} \quad (9.4a)$$

for instantaneous volume reaction and

$$R_a = 1 + K_a a \quad (9.4b)$$

for instantaneous surface reaction, Equation (9.3) is changed only by exchanging t_w for $t_0 = t_w/R$, where R is either R_a or R_d .

Equation (9.1) can easily be made to include reaction rates between the liquid and solid and to accommodate other initial and boundary conditions. A common boundary condition is that the inlet concentration varies with time

$$C = C(z = 0, t) \quad (9.5)$$

The convolution integral may be used to relate the output concentration to the input concentration.

$$C(t) = \int_0^t C(0, t') g'(t-t', t_w R, Pe) dt' \quad (9.6)$$

where g' is the response to an instantaneous pulse.

In the chemical engineering literature and hydrology literature many other inlet and outlet boundary conditions have been discussed. Very often the simple solutions are not sufficient to explain the curve forms of an experiment. Recently Landström et al. (1982) in an experiment using nonreacting tracers over 11.8 m in fractured crystalline rock in Studsvik obtained a very long tail which could not be fitted with the above model. A similar result was obtained in another field experiment over 30 m in Finnsjön by Gustafsson and Klockars (1981). In both cases it was concluded that this could be caused by the presence of at least three different independent channels through which the water flows. The slower channels will contribute to the tailing. Other mechanisms may also cause such tailing. Several such mechanisms will be treated later.

9.6.2 Channeling model

Fractured rock, especially at larger depths, may have considerable distances between water bearing fractures. Data from deep holes, down to 800 m, in the Swedish rock indicate that at depths below a few 100 m the spacing of conducting fractures is on the order of 1 fracture per 5 to 10 m (Carlsson et al., 1983). Other observations in individual fractures by Abelin et al. (1985) and Neretnieks et al. (1982) indicate that even in well defined fractures in crystalline rock there is considerable channeling. Abelin et al. (1985) found that in 3 well visible fractures in the Stripa deep (360 m) rock laboratory, less than 20 % of the fracture widths carried more than 70 % of the flow.

Observations in several tunnels in Sweden show that water flows very unevenly distributed in the fractured crystalline rocks. The water flows into the drifts in distinct channels or spots and the flowrates of the different spots vary considerably (Neretnieks, 1987).

A model had been tested where all "dispersion" is assumed to be caused by channeling (Neretnieks, 1983). It was tested on some laboratory experiments using a natural fracture (Neretnieks et al., 1982) and several field experiments (Moreno et al. 1983, 1985).

The model is based on the assumption that all channels conduct the flow from the inlet to outlet without mixing between channels underway. At the outlet, however, the fluid from all channels is instantaneously mixed. This would simulate a very common way of sampling for tracers. It is assumed that the channels can be uniquely described by their apertures in regard to the flowrate and concentration response.

For the case with a discrete distribution $F(\delta_i)$ of channel openings δ_i , the effluent concentration in each channel is denoted by $C(t, \delta_i)$. The flow in each channel is $Q(\delta_i)$. Both $C(t, \delta_i)$ and $Q(\delta_i)$ are assumed to be functions totally defined for every class of channel opening δ_i . The effluent concentration $C(t, \delta_i)$ may be obtained from the advection-dispersion equation when applicable or if other mechanisms are active then the appropriate function must be used. The underlying assumption is that the time and some characteristic of the channel, e.g. δ_i , are sufficient to characterize the effluent. Other effects, such as dispersion in the channel or reactions with the walls of the channel, must be known functions of δ_i . For a discrete distribution $F(\delta_i)$ the mixed effluent from all channels has the concentration

$$\frac{C(t)}{C_o} = \frac{\sum_{i=1}^N F(\delta_i) Q(\delta_i) C(\delta_i, t)}{\sum_{i=1}^N F(\delta_i) Q(\delta_i)} \quad (9.7a)$$

For a continuous distribution of channel openings $f(\delta)$ the concentration is

$$\frac{C(t)}{C_0} = \frac{\int_0^{\infty} f(\delta) Q(\delta) C(\delta, t) d\delta}{\int_0^{\infty} f(\delta) Q(\delta) d\delta} \quad (9.7b)$$

A flow system with channeling will spread a tracer pulse along its pathways and the pulse will also be spread at the observation (mixing) point, even if there is no spreading in the individual channels.

Figure 9-2 shows the response of a stratified system to a Dirac pulse at the inlet. The channel apertures in this case are taken to be log normally distributed and the cubic law for flowrate,

$$Q = \text{const}_1 \cdot \delta^3 \quad (9.8)$$

is assumed to apply. The velocity in such a system is

$$v = \text{const}_2 \cdot \delta^2 \quad (9.9)$$

For the distribution $F(\delta_i)$ of $f(\delta)$, which is described entirely by a mean μ_1 and variance σ_{ρ}^2 , the mean transit time \bar{t} can be determined from the first moment. A Dirac pulse at the inlet is

$$\bar{t} = \int_0^{\infty} C(t) t dt / \int_0^{\infty} C_0 dt \quad (9.10)$$

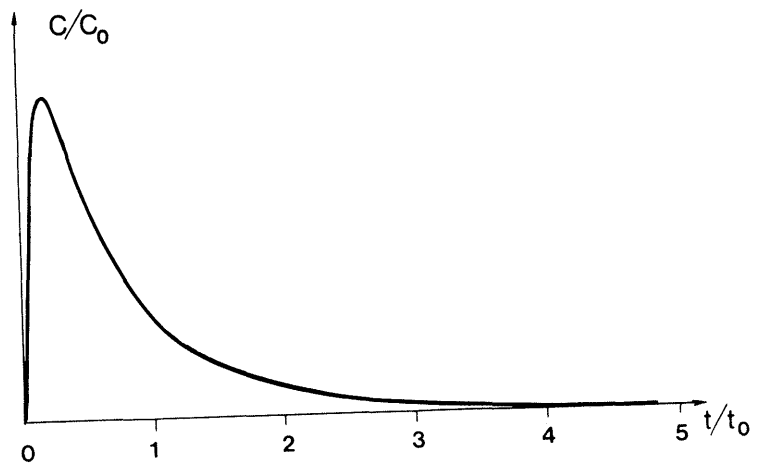


Figure 9-2.

Concentration at the outlet of a medium with parallel fractures which has been injected with a tracer pulse.

From the second moment the variance σ_t^2 can be determined,

$$\sigma_t^2 = \frac{\int_0^{\infty} C(t) (t - \bar{t})^2 dt}{\int_0^{\infty} C_0 dt} \quad (9.11)$$

From the latter the equivalent of the dispersion coefficient for this experiment can be determined,

$$D_L = \frac{\sigma_t^2}{\bar{t}^2} \cdot \frac{1}{2} \bar{v}z \quad (9.12)$$

From Equations (9.10) and (9.11) the following simple expression for the variance is obtained,

$$\left(\frac{\sigma_t}{\bar{t}}\right)^2 = e^{4(\ln 10 \sigma_\rho)^2} - 1 \quad (9.13)$$

where σ_ρ is the standard deviation in the log normal distribution. From Equation (9.13) it is seen that $(\sigma_t/\bar{t})^2$ is a constant for a given σ_ρ . In fact it has been shown that for an arbitrary distribution, $f(\delta)$, this applies (Neretnieks, 1983).

From Equation (9.12) it is found that

$$D_L = \text{const} \cdot \bar{v}z \quad (9.14)$$

It then may be concluded that if there is pure channeling in a flow region then an apparent hydrodynamic dispersion coefficient will increase with distance between the injection and observation (mixing) points. Equations (9.12) and (9.13) give a direct and simple relation between D_L and σ_ρ .

The consequences of using the wrong mechanism in predicting the tracer behaviour over longer distances are shown in Figure 9-3.

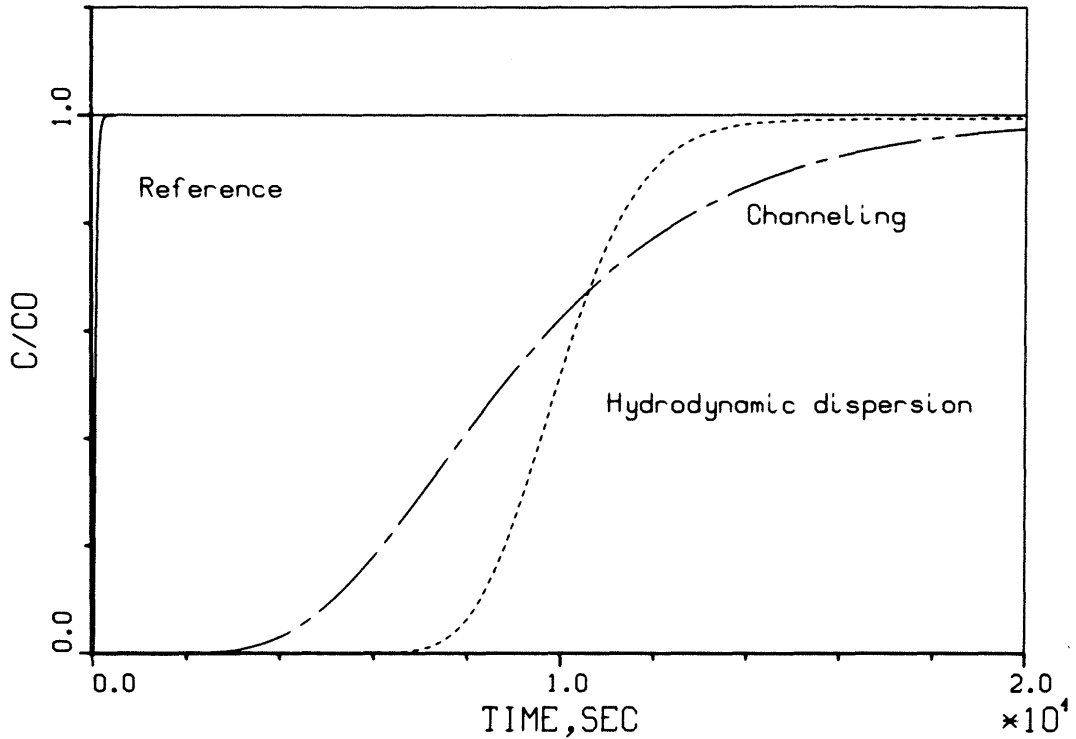


Figure 9-3. Predicted curves using the hydrodynamic dispersion model and the channeling dispersion model. For nonsorbing tracer for a longer distance (10 times) and a lower flow ($Pe = 100$, $\sigma = 0.208$).

This figure shows a reference case breakthrough curve for a step injection (the "experimental" results obtained from the channeling model with $\sigma_\rho = 0.208$). From this a Pe value of 10 was obtained by fitting with the advection-dispersion model. The predicted curves are for a 10 times longer distance. It can be seen that the two models predict very different breakthrough curves. Figure 9-4 shows some results on dispersion coefficients obtained from experiments in fractured crystalline rock (Neretnieks, 1985). The few data available indicate an increase of D_L with distance.

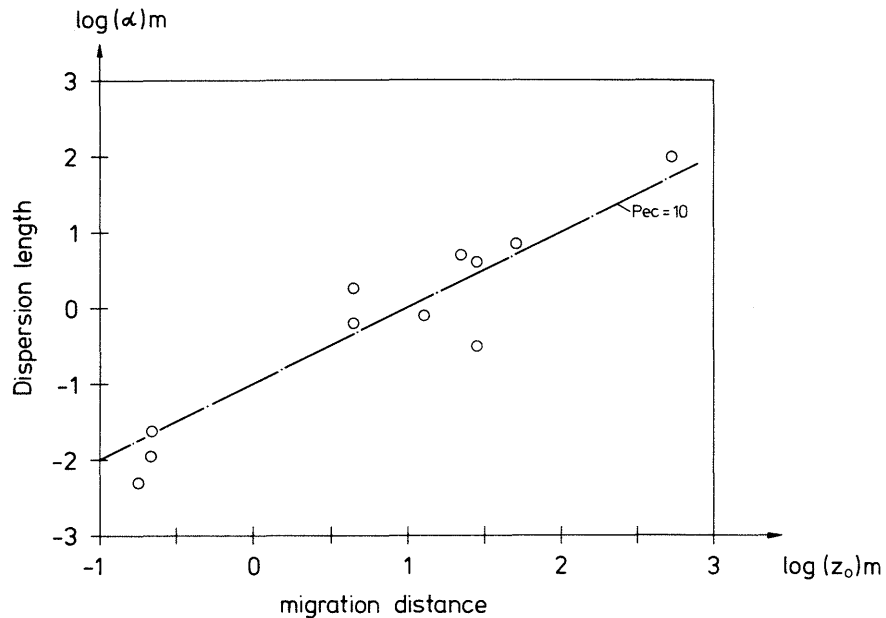


Figure 9-4. Experimentally determined dispersion lengths in fractured crystalline rock.

Hydrodynamic dispersion will take place in every channel in addition to the channeling. Equations (9.7a) and (9.7b) are quite general and can be used also for such cases. It can be seen from Figure 9-3 that the influence of hydrodynamic dispersion will have a diminishing influence over longer distances if channeling is in effect.

If the frequency of mixing between the various channels between the inlet and outlet is known, it is possible to modify the model to account for this (Rasmuson, 1985).

9.6.3 Matrix diffusion

There is considerable experimental evidence on crystalline rock porosities and diffusivities from the laboratory (Skagius and Neretnieks, 1985, 1986a, 1986b; Bradbury, 1982), and from the field (Birgersson and Neretnieks 1982, 1984) in undisturbed rock. Porosities in unaltered rock range from 0.06 to over 1 % and the effective diffusivities, $D_e = D_p \epsilon_p$, for small ions and molecules range from $1 \cdot 10^{-14}$ – $70 \cdot 10^{-14}$ m²/s.

Dissolved species in the water in a fracture will diffuse in and out of the porous rock matrix. The process can be described by the diffusion equation (including here the effects of sorption with linear equilibrium), and if there is no flow in the matrix,

$$K \frac{\partial C_p}{\partial t} = D_e \frac{\partial^2 C_p}{\partial x^2} \quad (9.15)$$

where

$$K = \epsilon_p + K_d \rho_p (1 - \epsilon_p) \quad (9.16)$$

With the low hydraulic conductivities of crystalline rock less than 10^{-12} m²/s (Brace et al., 1968) and low natural hydraulic gradients, transport by advection is negligible compared to that by diffusion.

For short contact times the penetration depths are short and may not deplete the water in the fracture to any large extent. For long contact time the influence can be considerable. Figure 9-5 shows the penetration depth from a plane surface versus time for nonsorbing species as well as for species with different sorption coefficients. The penetration depth $\eta_{0.01}$ is defined here as the distance from the surface at which the concentration in the pore water is 1 % of that at the surface. It is obtained by solving Equation (9.15) and using the appropriate boundary and initial conditions. These describe that a body initially with $C_p = 0$ is at time 0 exposed to a concentration at the surface which is then kept constant. The result is

$$\eta_{0.01} \approx 4 \sqrt{\frac{D_e t}{K}} \quad (9.17)$$

To describe the coupled processes of advection–dispersion and matrix diffusion an additional term is added to Equation (9.1) to account for rate of tracer uptake into the matrix. Equation (9.1) becomes

$$R_a \frac{\partial C}{\partial t} + v \frac{\partial C}{\partial z} = D_L \frac{\partial^2 C}{\partial z^2} + a D_e \frac{\partial C_p}{\partial x} \Big|_{x=0} \quad (9.18)$$

Equations (9.15) and (9.18) are coupled by $C = C_p$ at the fracture surface $x = 0$. There are some analytical solutions to Equations (9.15) and (9.18) available for different boundary conditions. The solutions all apply to cases with regular bodies: infinite slabs, cylinders, or spheres.

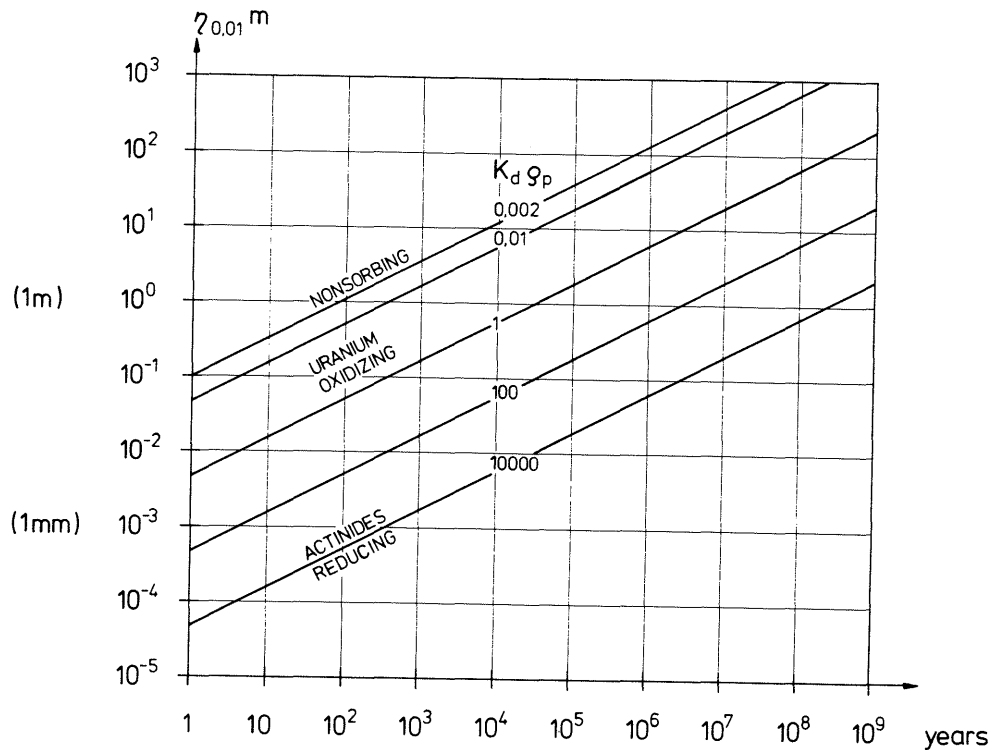


Figure 9-5. The penetration depth $\eta_{0.01}$ versus time for nonsorbing $K = \epsilon_p$ and sorbing $K > \epsilon_p$ species.

The inlet boundary condition for a sudden increase in the inlet concentration is $C = C_0$ at $z = 0$ for $t > 0$.

For the case when there is no hydrodynamic dispersion and when the solution is (Neretnieks, 1980)

$$C/C_0 = \operatorname{erfc} \left\{ \frac{t_w}{\delta} \sqrt{\frac{D_e K}{(t - R_a t_w)}} \right\} \quad (9.19)$$

for $t > R_a t_w$, else C/C_0 is equal to zero.

A criterion for when the matrix diffusion becomes important may be constructed in the following manner. When the time for the breakthrough given by Equation (9.19) to reach a value of C/C_0 equal to 0.5 is twice as long as for plug flow, i.e. $t = 2t_w \cdot R_a$, then matrix diffusion becomes important. From Equation (9.19) it is obtained that the $\operatorname{erfc}(\arg)$ is equal to 0.5 which then gives

$$\arg = \frac{t_w}{\delta} \sqrt{\frac{D_e K}{t - R_a t_w}} = 0.477 \quad (9.20)$$

and with $t = 2 R_a t_w$, the following for t_w is obtained:

$$t_w > 0.23 \frac{\delta^2 R_a}{D K_e} \quad (9.21)$$

The matrix diffusion considerably influences the transport of a dissolved species (note the square dependence on fracture aperture). For a nonsorbing species $K = \epsilon_p$ and $R_a = 1$, and as an example it is obtained for $\epsilon_p = 0.002$ and $D_e = 5 \cdot 10^{-14} \text{ m}^2/\text{s}$ that $t_w > 0.23 \cdot 10^{16} \cdot \delta^2 \text{ s}$. For a $100 \mu\text{m}$ fracture t_w must be larger than 0.7 year to feel the influence of matrix diffusion, whereas for δ equal to $10 \mu\text{m}$, t_w must be greater than 2.7 days.

The criterion could of course be chosen differently. If the time is chosen where the 50 % concentration point has traveled a time $1.1 \cdot R_a t_w$ instead of $2 R_a t_w$, the criterion is sharpened by a factor of 100. This would give t_w equal to 2.7 days in the $100 \mu\text{m}$ fracture and t_w being 40 minutes in the $10 \mu\text{m}$ fracture.

Even the second criterion gives a clearly noticeable influence on the shape of a breakthrough curve especially in the tail. The values of D_e and ϵ_p were taken from data on fresh, unaltered crystalline rocks. For fractures where the surfaces are altered, the few available data (Skagius and Neretnieks, 1986a) indicate that the values can be considerably higher.

It may thus be expected that the effect of matrix diffusion will be noticeable in many field experiments and even may become the dominant effect in small fractures and for long water transit time. Maloszewski and Zuber (1984) recently discussed the impact of matrix diffusion in field experiments and also concluded that it may have a considerable impact. In short the solutions to the matrix diffusion case Equations (9.15) and (9.18) can be written:

$$C/C_o = f(t, \{Pe, t_w R_a, \frac{D_e K}{\delta^2}, S\}) \quad (9.22)$$

If channeling also must be accounted for, at least an additional parameter describing the channeling distribution, e.g. σ_ℓ , must be introduced (Moreno et al., 1985) have chosen to use either σ_ℓ or Pe in their models). If the penetration depth $\eta_{0.01}$ is comparable to the block sizes S , the solution is also dependent on this as shown in Equation (9.22).

10

CORRELATION BETWEEN FRACTURE CHARACTERISTICS, WATER FLOWRATES, AND TRACER MOVEMENT

10.1

OVERVIEW

In order to compare the fracture characteristics with the results of water flowrates and tracer occurrences, only the fracture data from those areas where water was collected is presented in the following diagrams. For the correlation between the water flowrates and fracture characteristic for the pilot hole and injection holes see Report 1, "Site Preparation and Documentation."

Because of the geometry of the test site it is easier to present the data if the test site is divided into two separate drifts: (1) the 75 m long main drift, and (2) the 30 m long arm crossing west to east, see Figure 10-1.

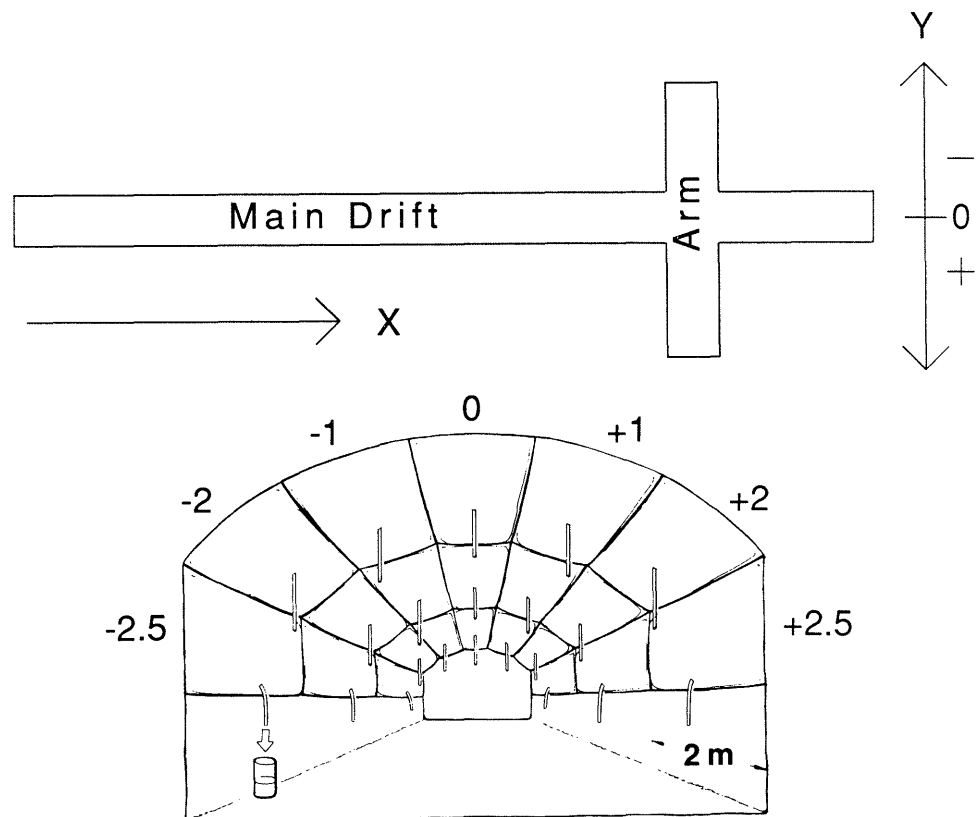


Figure 10-1.

Division of test site into two different drifts, and the cross-section of the drifts showing the parts used in the compilation of fracture data.

The term fracture zone is defined here as a set of at least five parallel fractures, that are close to each other. Out of the 99 mapped fractures, 86 were classified as individual fractures and 13 as fracture zones. Fracture length is defined here as the whole visible length of the fracture over the mapped area.

It has been of interest to compare the water flowrates and tracer occurrences along the two drifts with the following fracture characteristics per surface area within thin sections, about 2 m, along the two drifts:

- Total fracture lengths
- Total zone lengths
- Number of fracture intersections
- Presence of different fracture filling materials
- Fracture length within the 4 fracture sets.

The first three fracture characteristics for both the individual fractures and fracture zones are given in Figure 10-2 and can be compared with the water flowrates for the main drift and the arm given in Figure 10-3. In the histograms for the number of intersections only the intersections concerning individual fractures are included, i.e. zones are excluded from these compilations. The flowrates given in Figure 10-3 are measured before the drilling of the injection holes. These flowrates were chosen since they represent, as close as possible, the flow within the undisturbed rock volume. Comparisons between the flowrates and histograms for individual fractures and fracture zones for the four fracture sets and fracture fillings are given in Appendix 9. No obvious correlation between these fracture characteristics and the measured water flowrates is evident.

In Figures 10-4 and 10-5 tracer mass flowrates at 6000 h can be compared with water flowrates at 6000 h. Comparing the general outlook of the histograms it seems that the tracers injected at injection hole I, Uranine and Eosin Y, have mass flowrates that resemble the water flowrates around 25 m.

10.2

DISCUSSION

The average single fracture length was just above 0.5 m/m^2 for both the main drift and the arm. In the main drift the variation in the fracture lengths occurred along the whole drift, but in the arm the longer fracture lengths were observed only in the right part.

Fracture zones were found at a few distinct areas both in the main drift and in the arm. In the right part of the arm, zone lengths were equal to or greater than the lengths of the individual fractures. The zone illustrated in Figure 10-2 located at the left part of the arm is related to a very narrow zone crossing several of the sampling areas.

In Figure 10-2, the number of fracture intersections is higher in two areas in the main drift, 25-33, and 65-73 m, and in the arm in the area between +7 to +11 m. The areas which have a higher number of fracture intersections also exhibit an increased fracture length per m^2 and have higher water flowrates.

Based on this fracture mapping and water flow monitoring, one can not conclude that there is any correlation between the fracture trace length per area and water flowrates. Even if the fractures were split up into four fracture sets and mineral composition no such correlation can be developed, see Appendix 9. Water flowrates tend to be more related to the number of fracture intersections per area than to fracture trace length per area.

Figures 10-4 and 10-5 seem to indicate that the location of high water flowrates and high tracer mass flowrates do not have to coincide with each other.

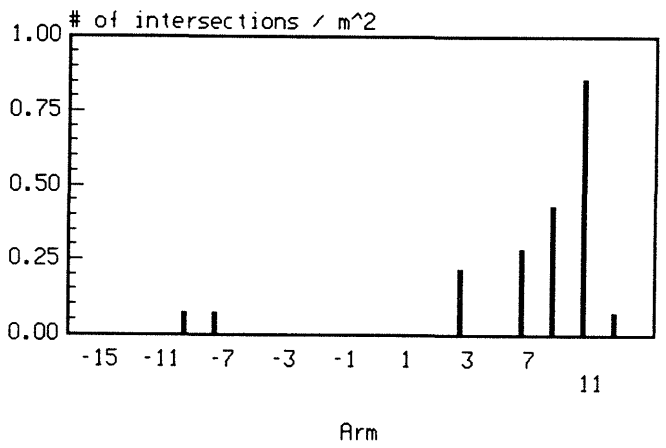
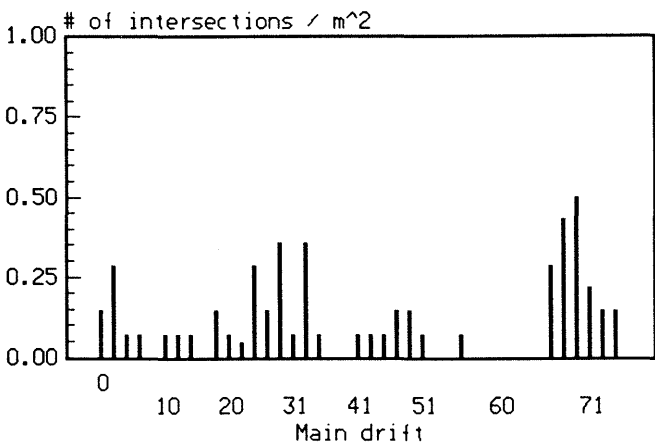
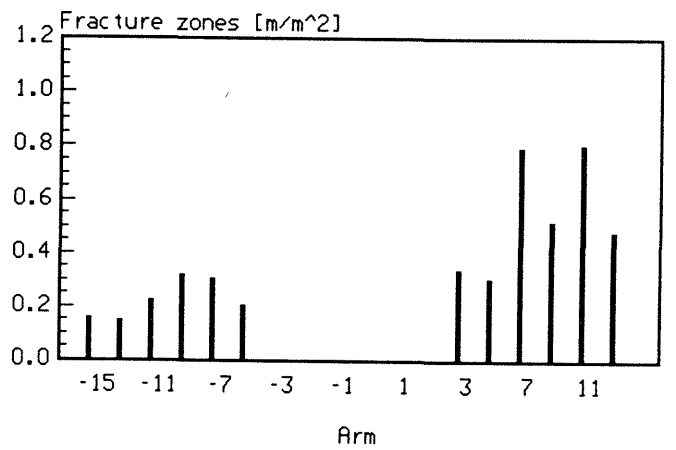
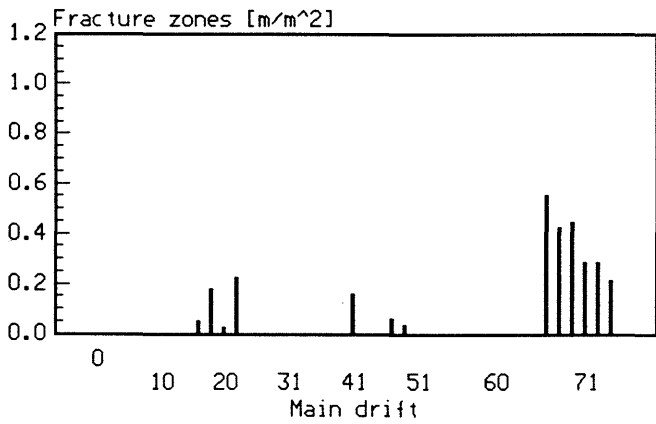
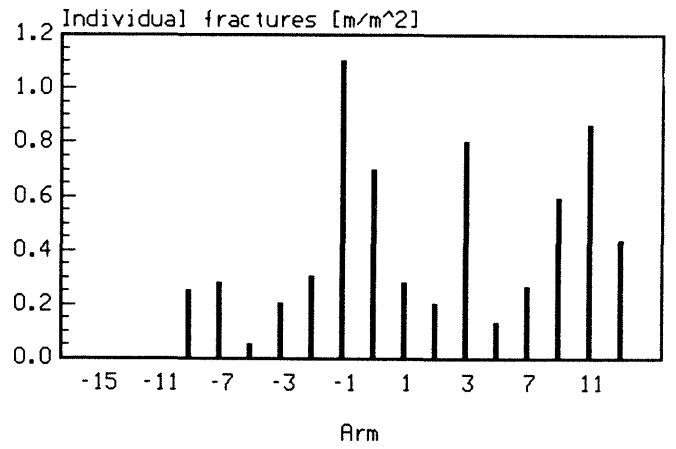
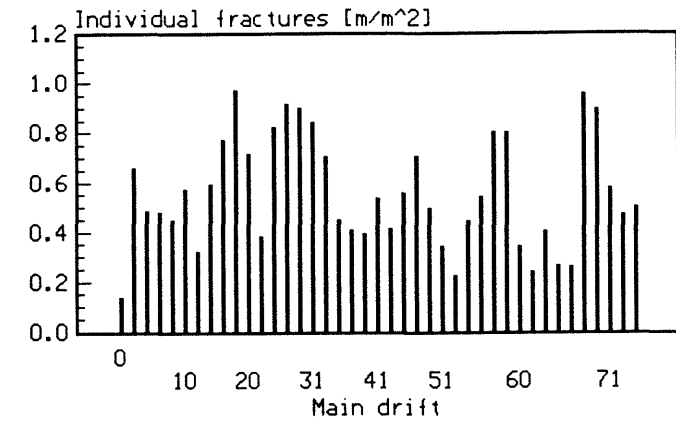
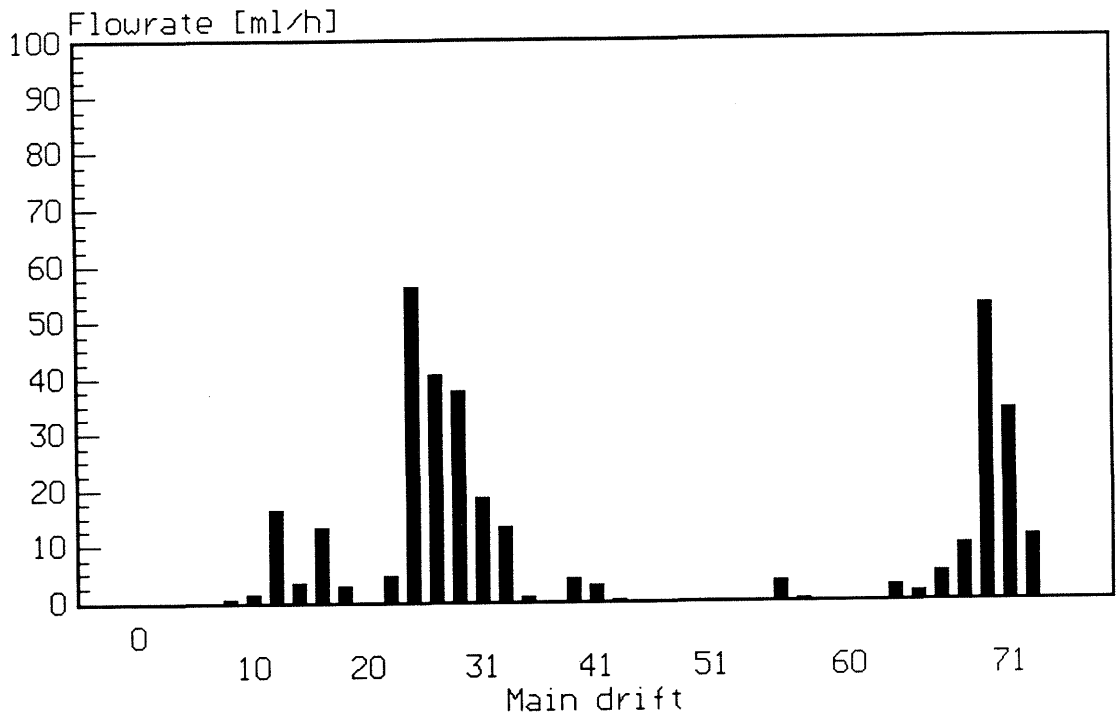


Figure 10-2.

Fracture length, fracture zone length, and number of single fracture intersections per m² for main drift and arm.

-6000 h



-6000 h

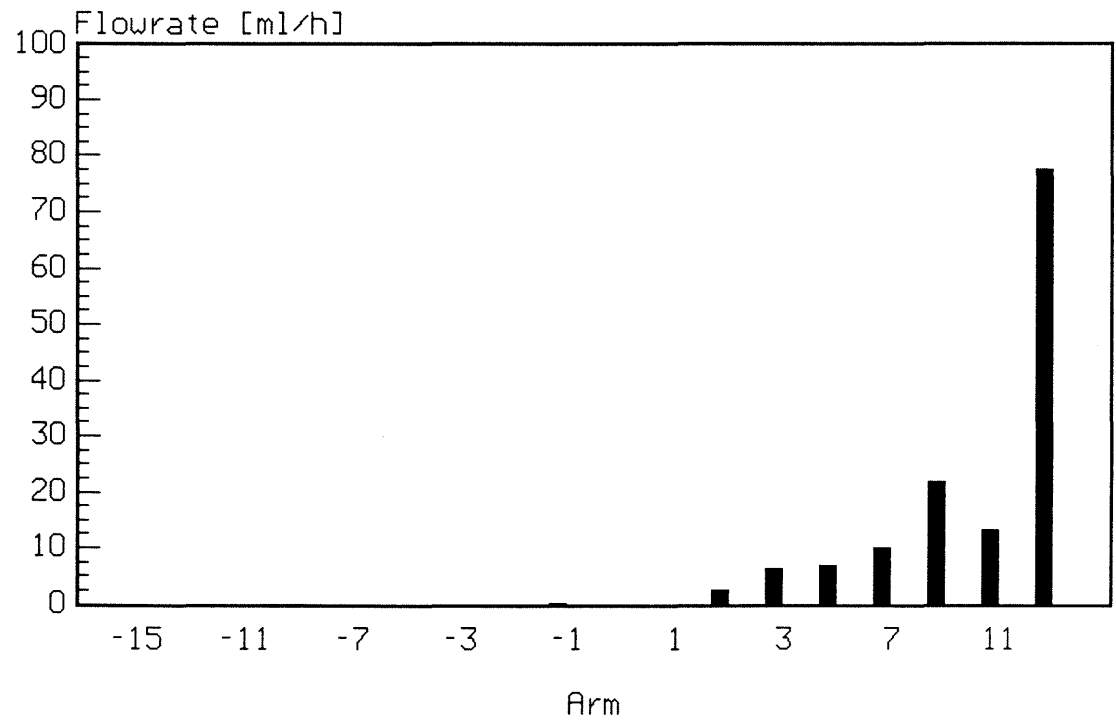
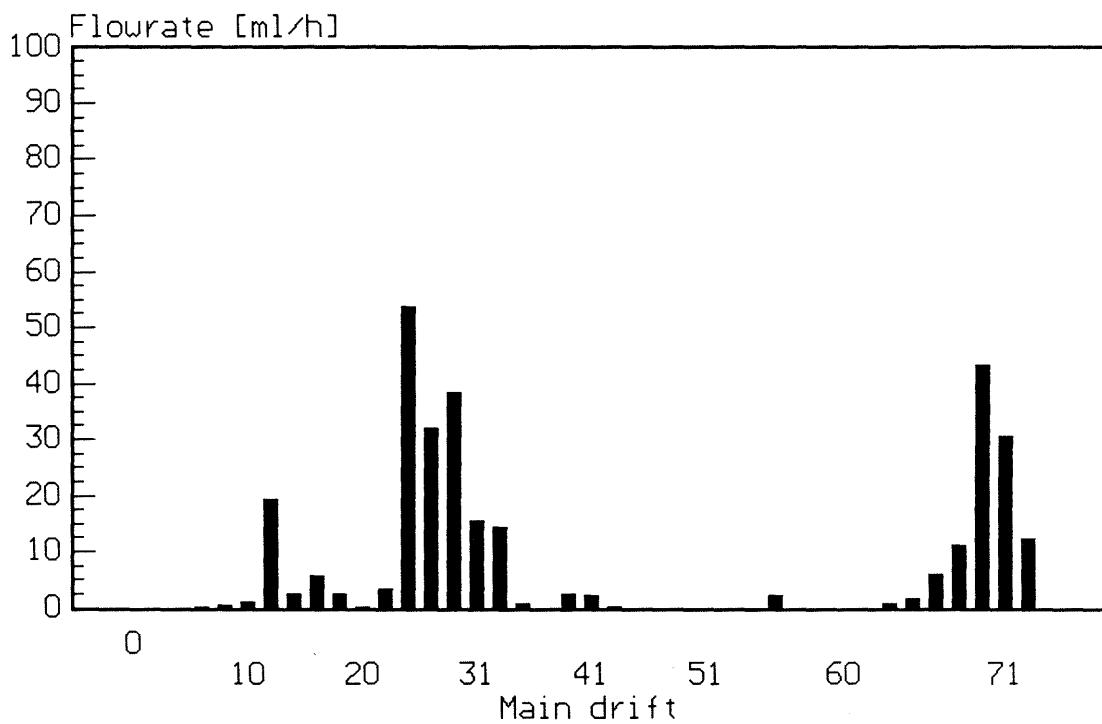


Figure 10-3. Water flowrates for main drift and arm before drilling of the injection holes.

6000 h



6000 h

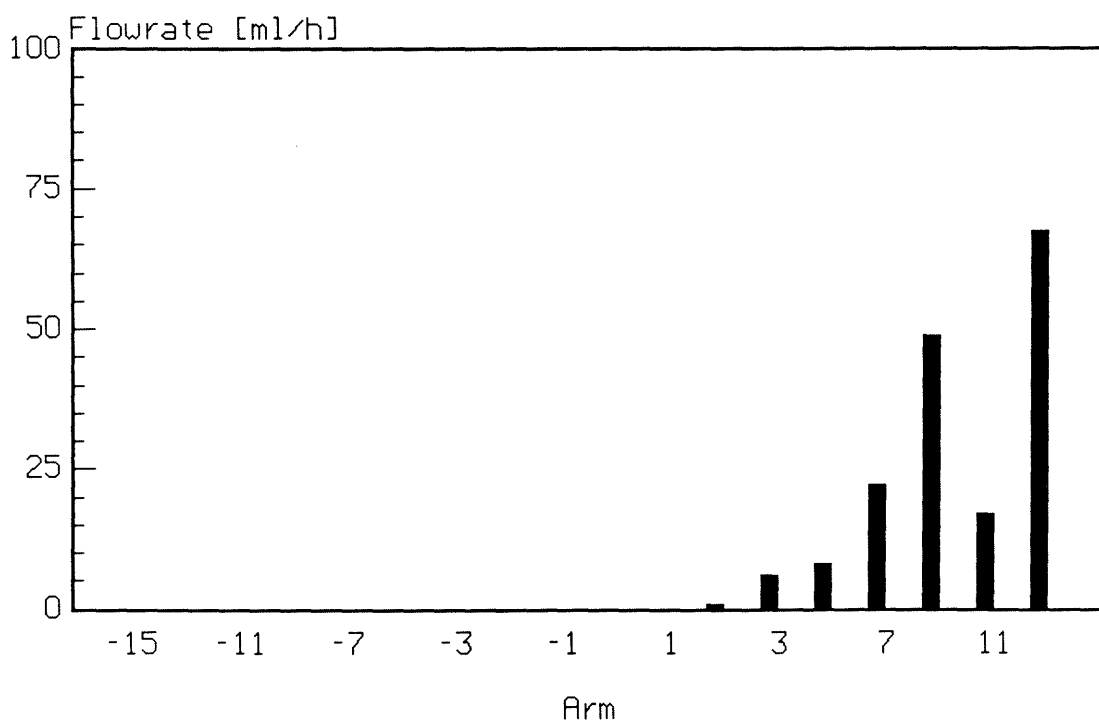


Figure 10-4.

Water flowrates in main drift and arm at 6000 h after start of tracer injection.

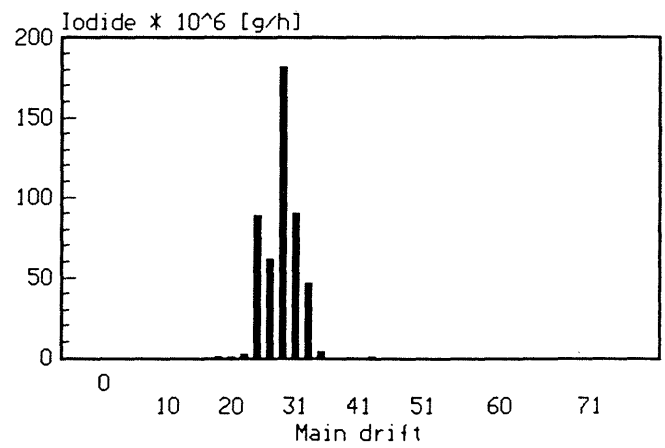
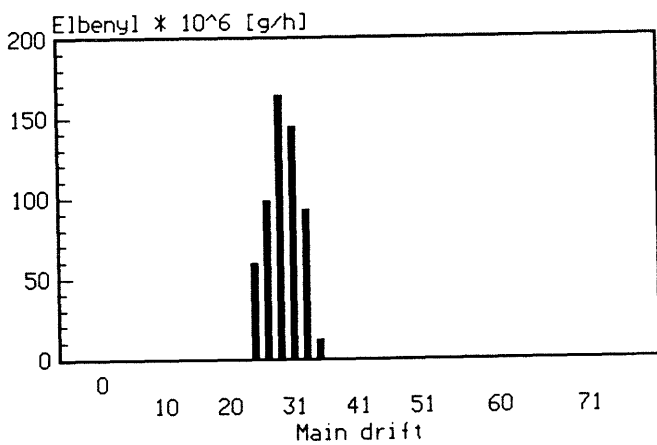
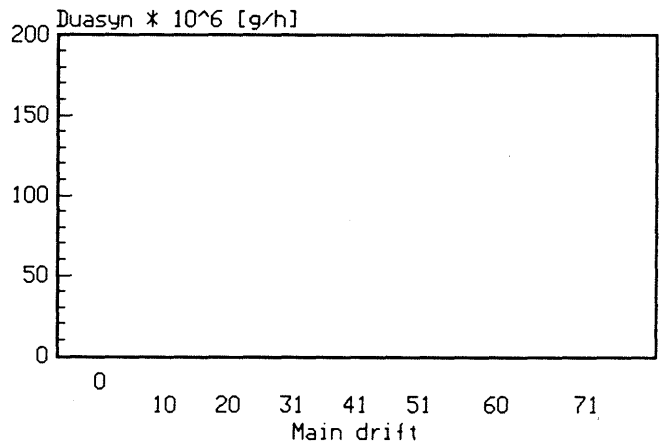
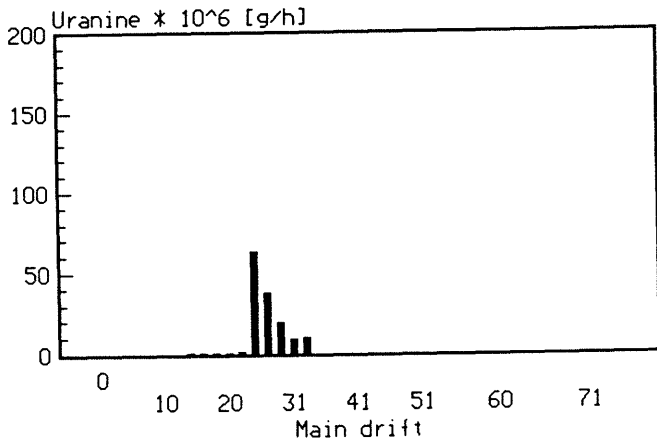
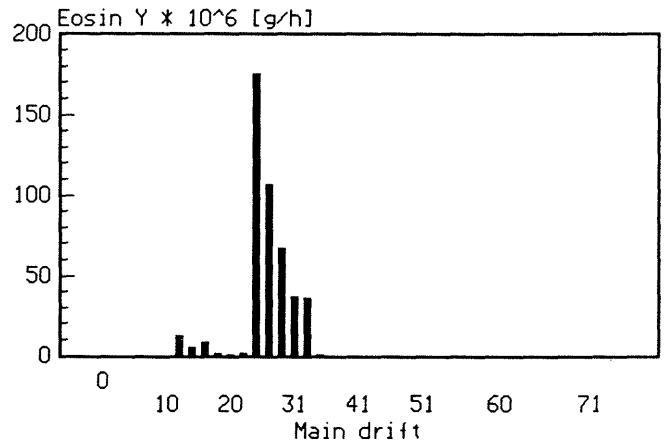
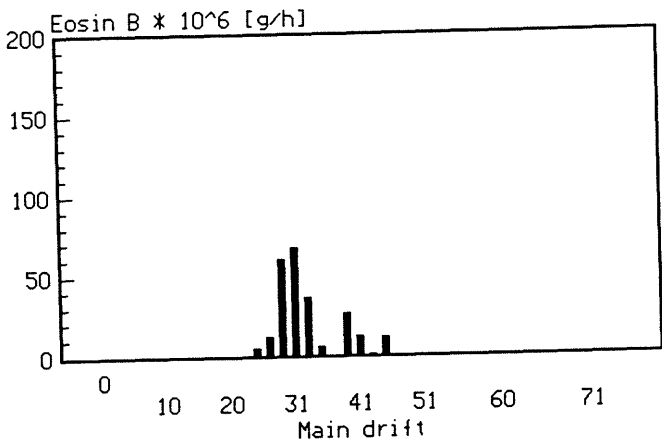


Figure 10-5. Tracer mass flowrates at 6000 h after start of injection.

11

OUTER DISTURBANCES AND THEIR EFFECTS ON WATER INFLOW AND TRACER MOVEMENT

11.1

OVERVIEW

Outer disturbances can be related to activities in the mine such as excavations and drillings, opening and closing of existing holes, and seasonal changes.

Figure 11-1 shows the 360 m level around the 3-D test site and locations for the major areas where disturbances occurred during the time of the 3-D experiment. Figure 11-2 shows when the disturbances occurred and their duration in time.

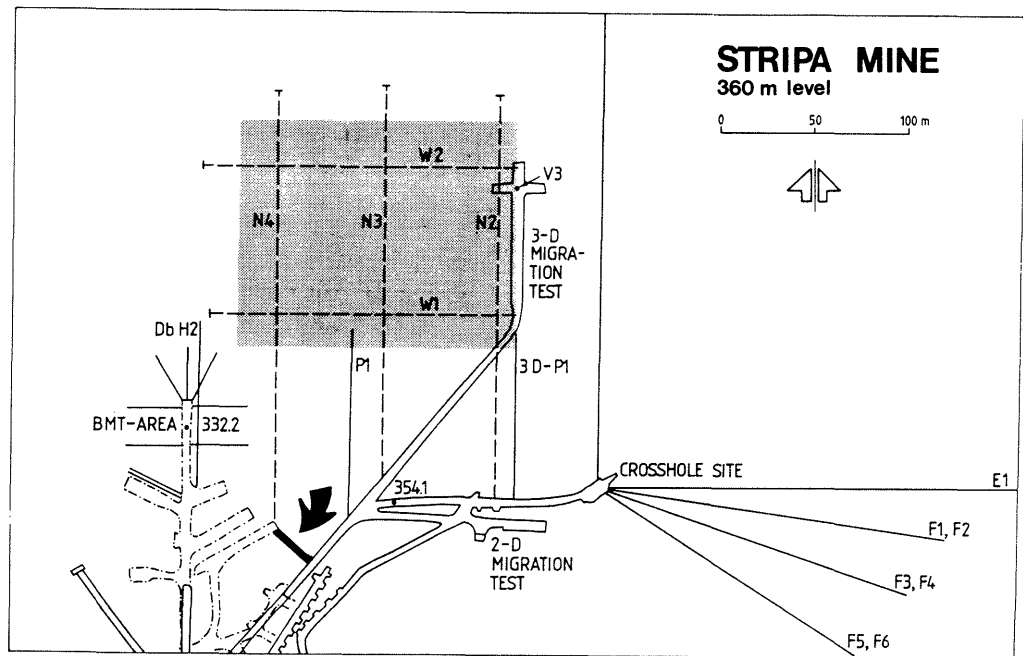


Figure 11-1. The 360 m level around the 3-D test site.

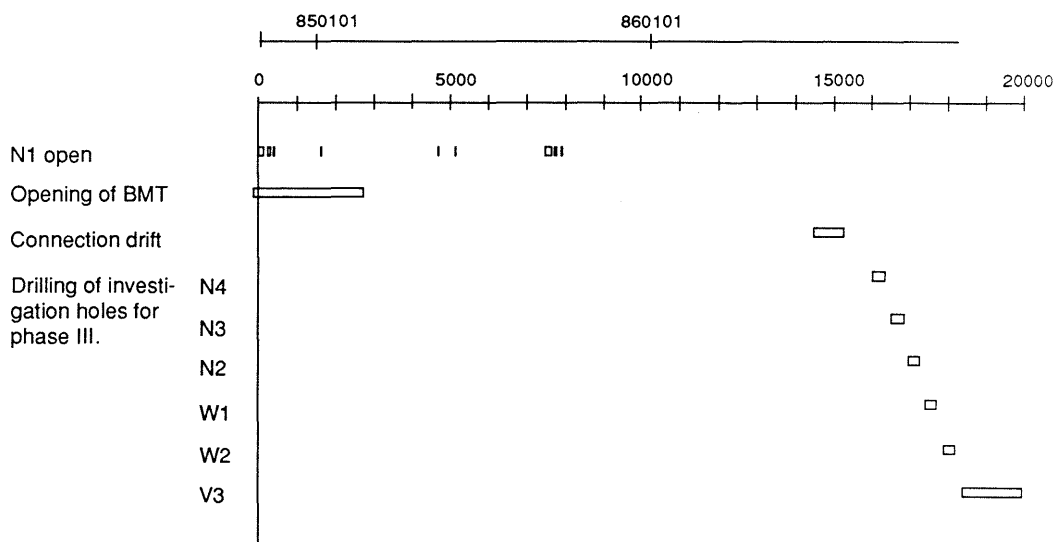


Figure 11-2. Disturbances and their occurrence and duration in time.

11.2 VARIATION IN WATER INFLOW RATES

The total water inflow rate into the upper part of the test site as a function of time is illustrated in Figure 11-3.

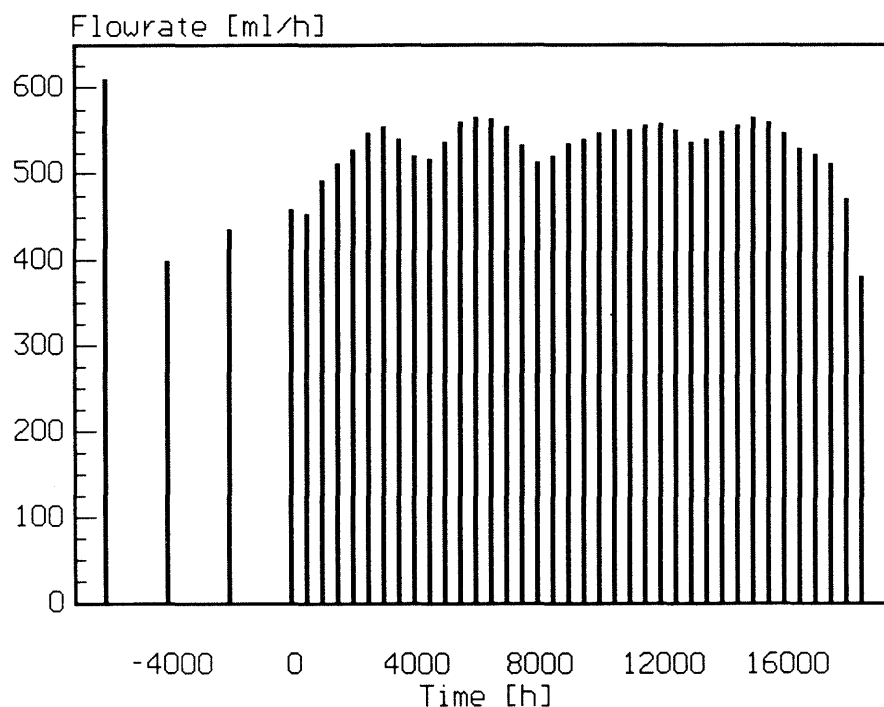


Figure 11-3. Total flowrate as function of time. Integral over whole test site, main drift and arm.

In Figure 11-3, the variation in water inflow rate seemed to occur in a time period of slightly over 4000 h ($\frac{1}{2}$ year). Since time 0 started in late October the first peak of water flow occurred at the end of January. These types of variations were seen both in the main drift and the arm. Unfortunately, the hole N1 was opened and closed at nearly the same time intervals as the observed variations, see Figure 11-2. It is therefore difficult to say what actually causes the periodic variation in the water inflow rates.

It can be seen from Figure 11-3 that there is a decrease in the water inflow rate between -6000 h and -2000 h which is the period when the three vertical injection holes were drilled and kept open for various measurements. After the holes were closed, the water inflow rates increased and reached approximately the original level at 4000 h. See Figure 11-4 for the responses due to the drilling for some of the individual sampling sheets.

Three different types of responses which occurred during the time period when the injection holes were kept open are illustrated in Figure 11-4. The first dashed line represents the start of drilling. The drilling continued for a total of approximately 500 hours for all three injection holes. The second dashed line represents the sealing of the injection holes with compacted bentonite. The injections started at time 0. The most odd response observed was the one represented by sheet 69+2.75 in which the water inflow rate increased when the injection holes were kept open. This could have been caused from the opening of new water flow pathways due to released water pressure in the

adjacent fractures that were intersected by the injection hole or it could have been from the drill fluid (water) that penetrated into the fracture system.

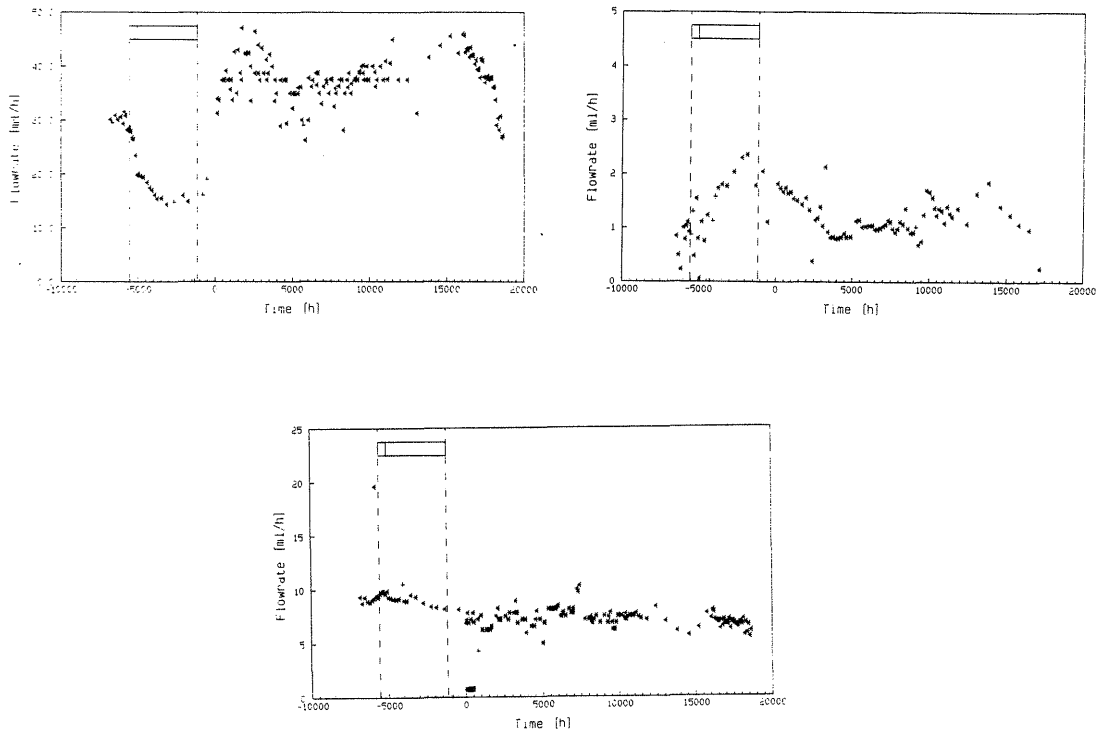


Figure 11-4. Flowrate variations in time for 3 different sampling sheets.

However, in most of the sheets the water inflow rates decreased when the injection holes were kept open and increased when the injection holes were sealed. This is illustrated in Figure 11-4, sheet 25+1. The major part of the sampling sheets that did not show any change in the water inflow rate when the injection holes were kept open were located in the right arm. Due to this difference in responses between the different areas in the test site, it has been of interest to compare the responses in water inflow rates between the sheets where tracers later occurred with those where no tracers occurred. This comparison is given in Figure 11-5.

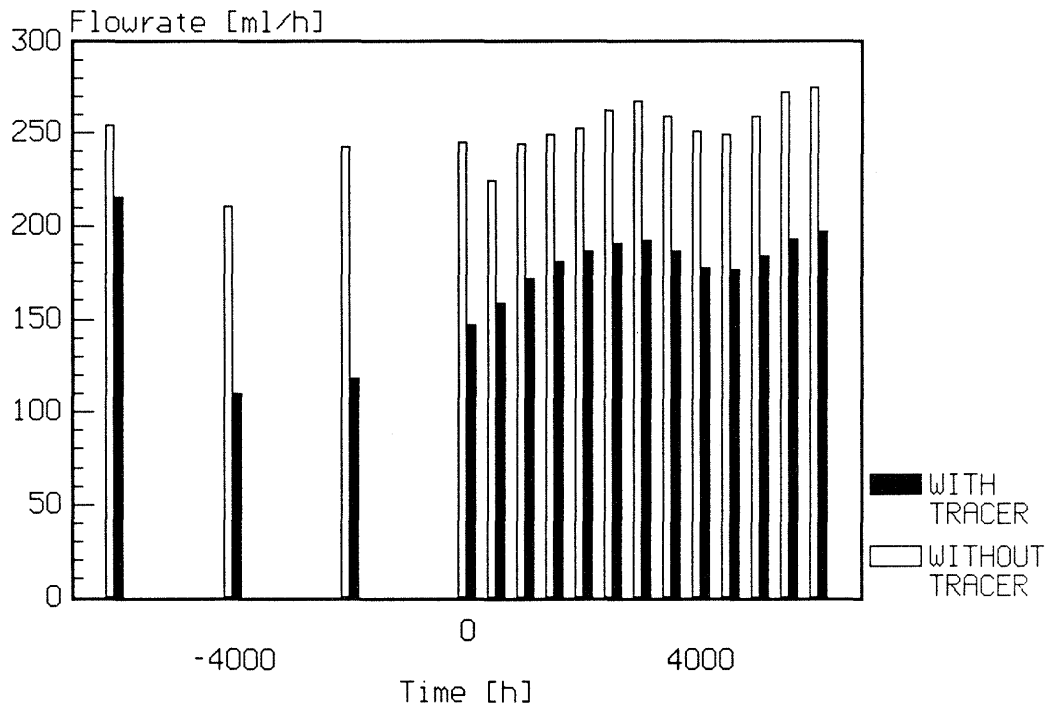


Figure 11-5. Water inflow rates into the test site divided into sheets where tracers were later found and those where no tracers emerged.

The decrease in total water inflow rate, due to the drilling of the injection holes, in those sheets where the tracer arrived was almost 50 % compared with a decrease of less than 20 % for those where no tracer arrived.

A second large outer disturbance was the start of the preparations for the Stripa Project Phase III starting at 14500 h, see Figure 11-2. Observing Figure 11-3, one can clearly see a periodic variation in the water inflow rates during a time period of approximately 4000 h. If one takes into account this variation, one can conclude that there still is a continuous decrease in the water inflow rates from 17000 h. This coincides with the drilling of the investigation holes, N2, N3, N4, W1, W2, and V3, for the Stripa Project Phase III.

The part of the pilot hole which still exists had a water inflow rate of about 3000 ml/h before the excavation of the test site. However, during the whole experiment the pilot hole was dry but at 17250 h the flowrate increased from 0 to 800 ml/h. The investigation hole N2 was drilled parallel to the pilot hole at a distance of approximately 10 m but slightly at a declined angle, see Figure 11-1. The hole N2 was drilled and kept opened during the time period 16900 h to 17250 h.

11.3 INJECTION PRESSURES AND INJECTION FLOWRATES

Injection pressures were monitored every 2 hours during the whole experiment. Not only were the injection zones monitored for pressure but also the top zone in each injection hole. This gave the opportunity to observe the responses in pressure at a large distance where it was not disturbed much by injection as well as the influence on the injection pressures due to outer disturbances. The pressure at the top of injection hole II (70 m depth) as a function of time is given in Figure 11-6. The first graph shows the pressure from -2000 h to 20000 h. The three major irregularities observed are: (1) the initial pressure build up, (2) the pressure decrease around 7500 h, and (3) the pressure decrease at 18000 h.

The initial pressure build up is normal when an open hole is being sealed off and in this case it also coincided with the closing of the hole N1 which was open when the experiment started. The pressure decrease at 7500 h coincided with the opening and closing of the hole N1, see second diagram in Figure 11-2. The distance between the top of injection hole II and hole N1 was at least 100 m. The pressure decrease at the end of the experiment could be explained by the drilling of the investigation holes for Stripa Phase III. The major part of this pressure decrease was likely due to the drilling of hole W2, see third diagram in Figure 11-6 and Figure 11-7 for a higher resolution plot. The same type of diagrams for the other zones are given in Appendix 3.

Compared to the top zones in the injection holes, the pressures in the injection zones were also affected by the actual injection of the tracers. Since the injection flowrates depend on the driving force, i.e. the pressure difference between injection point and surroundings, a change in pressure will also be seen in the injection flowrates.

The injection flowrates were monitored daily. The flowrates from 5000 h to 10000 h are compared with the monitored injection pressure in the same zone in Figure 11-8. It can clearly be seen that the opening of hole N1 greatly affected the injection flowrate which gave a higher flowrate even though the injection pressure at the injection zone was lowered. The same type of diagrams for the rest of the injection zones are given in Appendix 2.

The two diagrams in Figures 11-6 and 11-8 which show the effect of opening hole N1 are from two zones in the same injection hole separated by only 14 m. A general remark on these results is that the response to the opening of hole N1 increases with depth in the injection holes. Of the three injection holes, hole III had the highest response, followed by hole II.

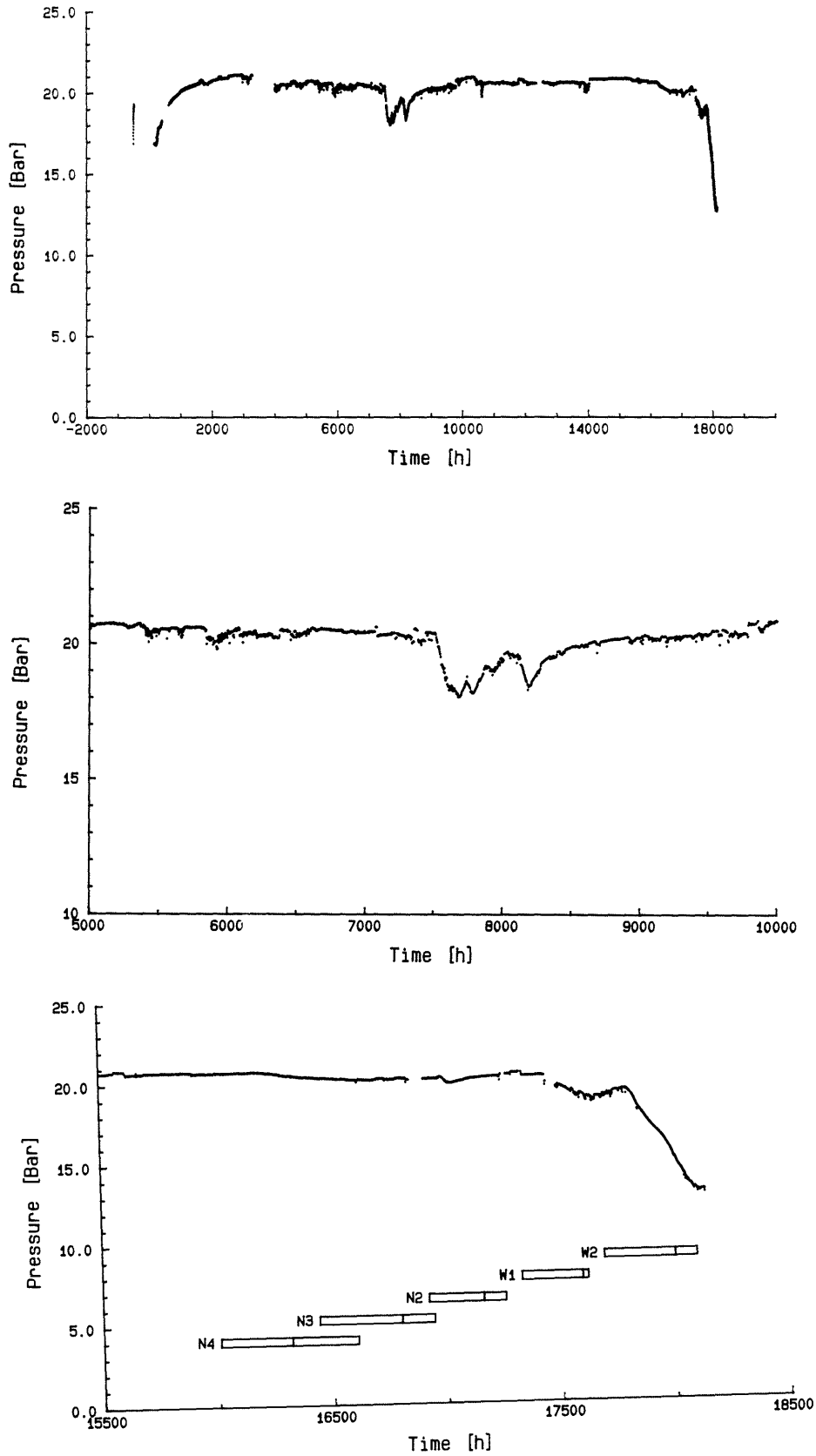


Figure 11-6. Natural water pressure at the top zone in injection hole II (70 m depth). N2,N3,N4,W1, and W2 refer to the drilling of the investigation holes for Stripa Project III.

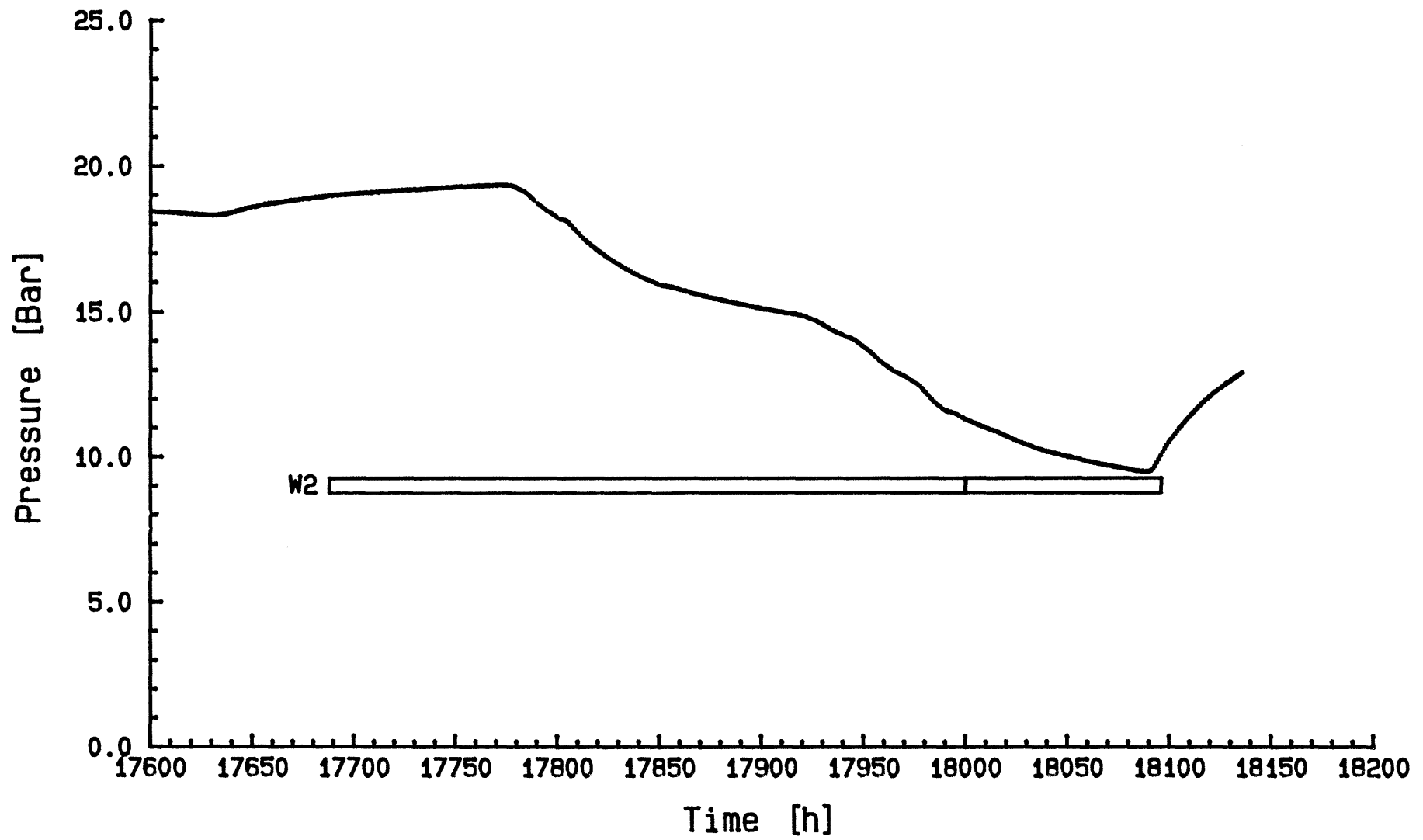


Figure 11-7. Pressure decrease in hole III zone 2 when drilling hole W2 (Stripa Phase III).

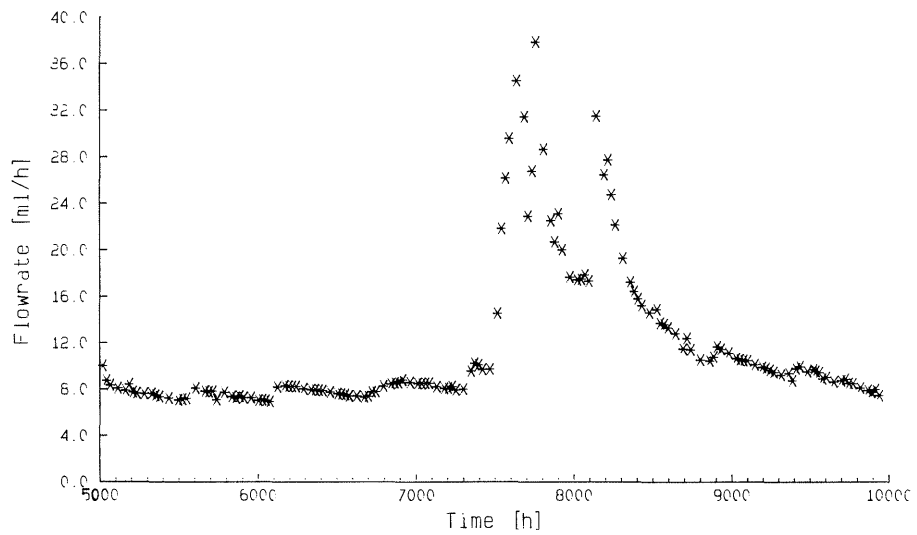
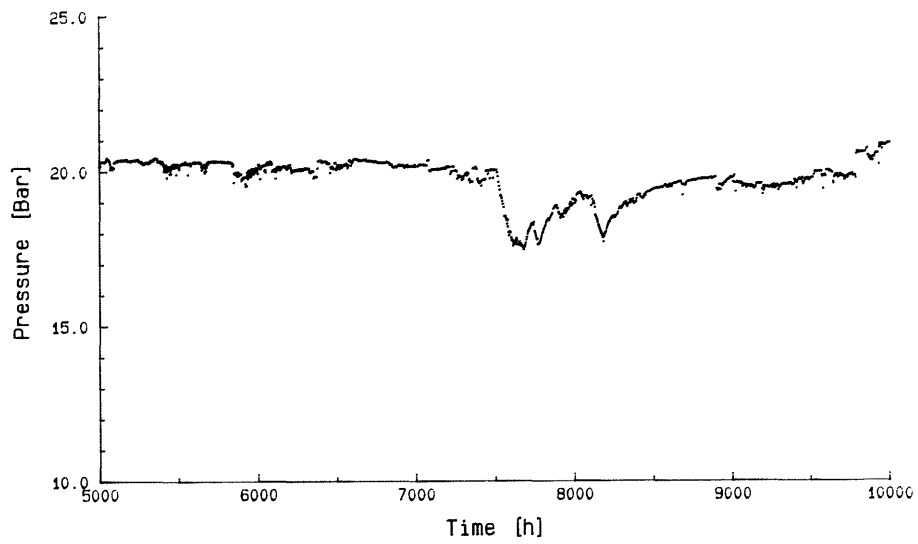


Figure 11-8.

Injection pressure and injection flowrate versus time for zone 1 in injection hole II (56 m depth).

11.4

TRACER MOVEMENT

Duasyn, injected at 37 m depth in injection hole III, did not arrive at any sampling point before the start of the preparations for the Stripa Project Phase III but arrived in some of the sheets between injection hole I and II. This occurred after the excavation of the connecting drift between the BMT (Buffer Mass Test) area and the 360 m level but before the drilling of the investigation holes. Duasyn and Iodide, injected from hole III, have without mixing passed areas where a mixture of all emerging tracers have been found. This indicates that channeling exists even over longer, 50 m, distances.

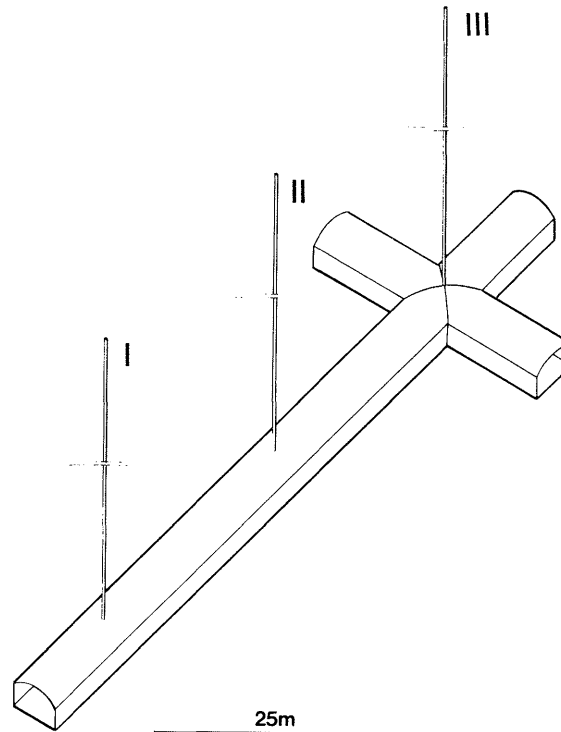


Figure 11-9. 3-D test site with injection holes.

The excavated connection drift between the BMT area and the 360 m level was mapped for fractures by SGAB (Swedish Geological), see Figure 11-1. At the beginning of 1987 a very slight red coloration was observed on the floor of the drift. During the spring 1987 an increase of the coloration occurred which then made it possible to sample the rock surface and analyze for tracers.

It was found that the coloration was due to a mixture of what seemed to be Uranine and Eosin Y. In analyzing the obtained flushing water there were discrepancies between the measured absorbancy spectra and those calculated by the multicomponent analysis. The discrepancy may have been caused by an accident during an earlier experiment in 1983 in the extensometer drift when it was contaminated with high concentrations of Uranine. Since this time, the Uranine had been exposed to light and water which could have degenerated it, thus giving the unknown discrepancy between the real absorbancy spectra and the standard spectra used in the analysis. Both Uranine and Eosin Y were injected from injection hole I at 32 m, respectively 18 m depth. Since Eosin Y had been used in the 3-D experiment, it was decided to estimate the amount of this tracer that had reached the connecting drift and the inner part of the floor in the extensometer

drift. This was accomplished by flushing the areas of interest with water and then pumping the water to a container for which the flushing water volume and tracer concentrations were to be determined.

Based on these analyses it was only possible to obtain a very rough figure on the amount of what seemed to be and very probably was Eosin Y. The amount found could in no way just be explained by Eosin Y used in an earlier experiment but had to include considerable amounts of the Eosin Y injected at the 3-D site.

It is remarkable if Eosin Y, injected only 18 m from the test site, would be able to travel approximately 150 m to the connecting drift without emerging in the water sampled in the access drift or the water sampled in the hole P1 or the BMT area, see Figure 11-1 for locations. During the drilling of the investigation holes for the Stripa Project Phase III and at some later occasions, water was sampled from these holes for tracer content. No tracers were found in the samples.

Uranine was also found in the water emerging into the pilot hole at a concentration of 0.2 ppm. Calculations showed that this was the largest single contributor of Uranine corresponding to 6 % of the injected mass flowrate.

12 EVALUATION AND INTERPRETATION OF EXPERIMENTAL RESULTS

12.1 MODELS USED FOR FITTING TRACER CURVES

12.1.1 Overview

The tracer tests are interpreted with various models. The basis for the models and the mechanisms pertaining to each model have previously been described in detail in Chapter 9.

Listed are some items that are of special interest in evaluating the different models:

- Water travel time (gives flow porosity)
- Dispersion length
- Matrix diffusion effects
- Wetted area
- Channeling characteristics

Models which have more parameters may describe more mechanisms and thus may give better agreement with the experimental results. Of the models used, the simplest models contain only two parameters, e.g. travel time and dispersivity, and the more complex models include three or four independent parameters. By including more parameters, on the other hand, it is easier to obtain better fits without actually increasing the physical meaning of the obtained parameter values. However, a good fit does not imply that the mechanisms which the model is based on actually are active at all. Therefore several models have been analyzed with different mechanisms which may give similar results, e.g. the spreading of a tracer pulse may be caused by hydrodynamic dispersion, channeling, matrix diffusion, or some other causes which are not included in the model. The three mentioned mechanisms will in many circumstances lead to a similar spreading of a pulse and cannot be distinguished from one another by just fitting in a model one or a few experimental curves. In order to separate out the various mechanisms, independent information and/or experimental results of different distances with different residence times are needed.

In this chapter it is described how increasingly more complex models are used to fit the tracer breakthrough curves to obtain the various parameter values which quantify the mechanisms.

12.1.2 Advection-Dispersion model

In the Advection-Dispersion (AD) model it is assumed that the transport of tracers from the injection point to the detection point takes place through a porous medium with constant properties. The tracer is dispersed in the direction of the flow by hydrodynamic dispersion.

The governing equation is given by Equation (9.1) in Chapter 9.

$$\frac{\partial C}{\partial t} + v \frac{\partial C}{\partial z} = D_L \cdot \frac{\partial^2 C}{\partial z^2} \quad (12.1)$$

The initial and boundary conditions are assumed to be a zero initial concentration, a constant concentration at the inlet during the tracer injection, and a medium of very large extension.

The solution to the differential equation with these initial and boundary conditions is given by Lapidus and Amundsen (1952)

$$C = \frac{C_o}{2} \left[\operatorname{erfc} \left[\frac{Pe^{0.5} (1-t_R)}{2 t_R^{0.5}} \right] + e^{Pe} \operatorname{erfc} \left[\frac{Pe^{0.5} (1+t_R)}{2 t_R^{0.5}} \right] \right] \quad (12.2)$$

where

$$t_R = t/t_w \quad (\text{relative residence time})$$

$$Pe = vz/D_L \quad (\text{Peclet number})$$

This is one of the basic models used in the fitting process.

12.1.3 Advection-Channeling model

The Advection-Channeling (AC) model is based on the assumption that dispersion in the direction of the flow is only caused by channeling. Velocity differences in the different channels will carry a tracer different distances over a given time.

The transport of the tracer takes place through a set of channels with different apertures. It is assumed that the channel apertures have a lognormal distribution and the interconnection between the different channels is negligible. Compared to the effects of channeling the hydrodynamic dispersion in each single channel is also assumed to be negligible.

The governing equation for tracer movement through a fracture with negligible longitudinal dispersion is

$$\frac{\partial C}{\partial t} = -v \frac{\partial C}{\partial z} \quad (12.3)$$

the solution to Equation (12.3) with the initial and boundary conditions is

$$C = \begin{cases} 0 & \text{for } t < t_w \\ C_o & \text{for } t \geq t_w \end{cases} \quad (12.4)$$

If separate channels with different apertures, δ , exist, then the water in these channels will have different velocities. By describing the

breakthrough curve for each channel in the actual pathway as $C(\delta, t)$, then the tracer concentration of the mixed effluent from all the channels in the pathway is (Neretnieks et al., 1982)

$$\frac{C(t)}{C_0} = \frac{\int_0^{\infty} f(\delta) Q(\delta) C(\delta, t) d\delta}{\int_0^{\infty} f(\delta) Q(\delta) d\delta} \quad (12.5)$$

In a parallel smooth walled channel of aperture δ and with laminar flow, the flowrate is proportional to the fracture aperture cubed, δ^3 . Snow (1970) studied the fracture frequencies for consolidated rock and found that the fracture apertures have a lognormal distribution. The function $f(\delta)$ is the density distribution function of the fracture aperture.

If the diffusion in the rock matrix is considered, then two models are defined which include diffusion in the matrix. Both models are extensions of the models described above.

12.1.4 Advection-Dispersion-Diffusion model

In the Advection-Dispersion-Diffusion (ADD) model, the tracer transport is assumed to take place through a single fracture or channel. Tracers may penetrate into the porous rock matrix by molecular diffusion. Sorption effects are neglected because test results of tracers have shown no sorption.

The differential equations for the fracture and porous rock matrix stated in Equations (9.17) and (9.15) of Chapter 9, are

$$\frac{\partial C}{\partial t} + v \frac{\partial C}{\partial z} = D_L \frac{\partial^2 C}{\partial z^2} + \frac{2}{\delta} D_e \frac{\partial C_p}{\partial x} \Big|_{x=0} \quad (12.6)$$

$$\frac{\partial C_p}{\partial t} = D_p \frac{\partial^2 C_p}{\partial x^2} \quad (12.7)$$

The initial and boundary conditions for the tracer test experiments allow the concentration in the fracture to be written (Tang et al., 1981) as

$$\frac{C(t)}{C_0} = \frac{2}{\sqrt{\pi}} \exp\left[\frac{Pe}{2}\right] \int_{\ell}^{\infty} \exp\left[-\xi^2 - \frac{Pe^2}{16\xi^2}\right] \cdot \operatorname{erfc}\left[\frac{\frac{Pe_w t}{8 A \xi^2}}{\sqrt{t - \frac{Pe_w t}{4 \xi^2}}}\right] d\xi \quad (12.8)$$

where

$$\ell = \left[\frac{Pe_w t}{4 t}\right]^{1/2}$$

and

$$Pe = \frac{vz}{D_L}$$

and

$$A = \frac{\delta}{2(D_e \epsilon_p)^{1/2}}$$

12.1.5 Advection-Channeling-Diffusion model

In the Advection-Channeling-Diffusion (ACD) model the transport of the tracers takes place through a set of channels with different apertures. The tracers may penetrate into the rock matrix by molecular diffusion.

For a tracer solution traveling through a channel with negligible longitudinal dispersion, the equation for the concentration in the channel is given by the following:

$$\frac{\partial C}{\partial t} + v \frac{\partial C}{\partial z} = \frac{2}{\delta} D_e \frac{\partial C}{\partial x} \Big|_{x=0} \quad (12.9)$$

The diffusion into the rock matrix is described by Equation (12.7). The solution to Equations (12.9) and (12.7) using the initial and boundary conditions from the tracer test experiment is given in the literature (Carslaw and Jaeger, 1959)

$$\frac{C}{C_o} = \text{erfc} \left[\frac{B t_w}{\delta (t - t_w)^{1/2}} \right] \quad (12.10)$$

where

$$B = (D_e \epsilon_p)^{1/2}$$

The tracer concentration of the mixed effluent from all the channels is given by Equation (12.5) where $C(\delta, t)$ is obtained from Equation (12.10).

The flowrate in a channel for laminar flow is proportional to the channel aperture cubed and that the velocity is proportional to the aperture squared. The water residence time over a given distance is determined from

$$t_{wi} = \frac{k_2}{\delta_i^2} = \bar{t}_w \left[\frac{\bar{\delta}}{\delta_i} \right]^2 \quad (12.11)$$

By incorporating Equation (12.11) into Equation (12.10), the tracer concentration at the outlet of a channel with aperture δ_i can be calculated as follows:

$$\frac{C(\delta_i, t)}{C_o} = \text{erfc} \left[\frac{B \bar{t}_w \bar{\delta}^2}{\delta_i^3 [t - \bar{t}_w (\bar{\delta}/\delta_i)^2]^{1/2}} \right] \quad (12.12)$$

12.1.6 Accounting for dilution and variable injection

To illustrate the effects of dilution and tracer injections in the fitting for model parameters, the Advection-Dispersion model is used as an example. In short the solution to this simple model, Equation (12.2), is written as

$$C(t) = C_o \cdot f(t, (t_w, Pe)) \quad (12.13)$$

In the Stripa experiment, an unknown amount of dilution of the injected stream occurred as it moved towards the collection sheets. By the time a portion of the injected stream reached a collection sheet it had been diluted by $1/DF$, where DF is defined as the dilution factor. Incorporating the dilution factor as a coefficient into Equation (12.13), the Advection-Dispersion solution is written as follows:

$$C(t) = C_o/DF \cdot f(t, (t_w, Pe)) \quad (12.14)$$

However, if it is assumed that all the injected tracer move towards the collection sheets and that no stream travels to any unmonitored area, then the dilution of the stream is known from the total amount of effluent concentration collected in all the sheets. The dilution factor can be expressed as the ratio of total flow to the sheets, Q_{tot} , injection flow, Q_{inj} .

$$DF = \frac{Q_{tot}}{Q_{inj}}$$

Inserting this ratio into Equation (12.14) the following is obtained:

$$C(t) = C_o \cdot Q_{inj} / Q_{tot} \cdot f(t, (t_w, Pe)) \quad (12.15)$$

During the experiment the tracer concentration was kept constant but the injection flowrate of the tracers was varied with time. Therefore, to describe this procedure into the model, the product, $C_o \cdot Q_{inj}$, from Equation (12.15) is used to account for the change. Previously it has been assumed that the system is linear. The response for the changing tracer input flowrates is obtained by adding the responses of a series of short consecutive injections. This is done by using the convolution integral in which the response for $C_o \cdot Q_{inj}(t)$ is obtained as

$$C(t) = C_o \int_0^{\infty} Q_{inj}(t-t') g(t') dt' \quad (12.16)$$

where t is the "calender" time, t' is the transit time, and $g(t')$ is the response function to an instantaneous pulse.

In the fitting procedures for the models the injection flowrates have been approximated to be piecewise constant, each constant portion having a duration T_i and injection flowrate $Q_{inj,i}$.

The response to n such constant injections is obtained by adding the responses $C_i(t)$ for each consecutive injection

$$C(t) = \sum_1^n \left[C_i \left(t - \left(\sum_j^{i-1} T_j \right) \right) - C_i \left(t - \left(\sum_j^{i-1} T_j \right) - T_i \right) \right] \quad (12.17)$$

The C_i 's are obtained from Equation (12.15) using the appropriate $Q_{inj,i}$ for the time interval T_i .

12.2 THE FITTING PROCESS

12.2.1 Overview

The theoretical models were fitted to the experimental results by a least squares nonlinear fitting process. The preprocessed concentration-time curves (breakthrough curves) contained thousands of concentration-time data point, but were finally reduced to about 50 data points by the process described in Section 7.5.

First, all the selected individual curves were fitted with the AD model (Advection-Dispersion Model). Of the nearly 170 different curves fitted many had high dilution factors and contain very small amounts of the tracer in comparison to the other curves. This difference was caused by either small flowrates or low tracer concentration or by a combination of both factors. These curves contribute very little to the total transport of the tracer.

After fitting "all" the tracer breakthrough curves, a set of 5 selected curves were chosen for each tracer. The selected curves showed a significant amount of the tracer. These curves were studied in more detail with the ADD model and AC model.

The results from the model fits indicate that the dispersion for many of the breakthrough curves was very high. There are many conceivable reasons for high dispersion values. One is the spreading of the tracer pulse by diffusion of the tracer into and out of stagnant or neary stagnant volumes of water. Such volumes of water are known to exist in the porous matrix of the rock as well as in the fracture itself. They can be accessed by molecular diffusion from the flowing water in the channels. The ADD model (Advection-Dispersion-Diffusion Model) was used to investigate this possible cause of dispersion and also to investigate the matrix diffusion. The matrix diffusion mechanism may be an important cause of withdrawing the tracer from the flowing water and into the rock, thus causing a less than full recovery to be obtained even after very long collecting time periods.

12.2.2 Treatment of injection curves

The injection flow varied with time and for this reason a mean value for the injection flow (or mass of tracer injected in a given time) could not be used. The breakthrough curve of variable injection can be calculated using the convolution theorem which requires an integration over time. To simplify the calculations the injection flow is represented as a function of time as square pulses. The injection curves used in the fitting process are shown in Appendix 7.

The amount of tracer injected and the total injection time are shown in Table 12-1 for the different tracers.

Table 12-1. Mass of injected tracer and injection time.

Tracer	injected volume l	injection concentration	injected mass	total time h
Eosin B	63.98	1 500 ppm	95.98 g	15 662
Uranine	76.96	1 000 ppm	76.96 g	15 819
Elbenyl	4.65	2 000 pm	9.29 g	10 190
Eosin Y	28.06	1 000 ppm	28.06 g	10 190
Duasyn	202.43	1 500 ppm	303.64 g	10 442
Iodide	139.67	0.013 M	1.82 mol	15 662
Bromide	50.84	0.019 M	0.97 mol	15 662

It was found that Bromide had been severely disturbed in the analysis by the presence of Iodide and therefore was only partly used in the subsequent analysis.

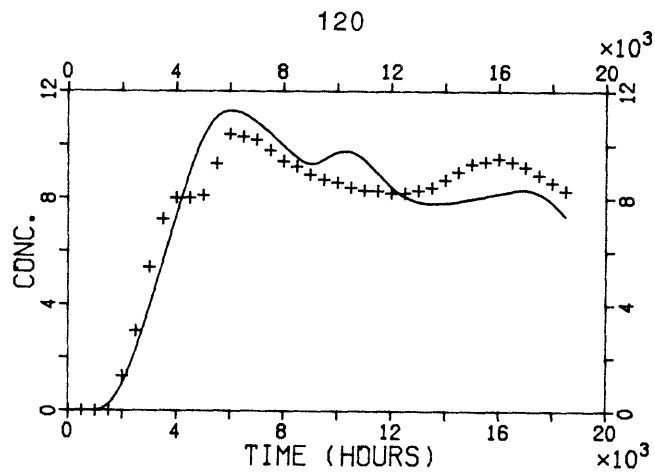
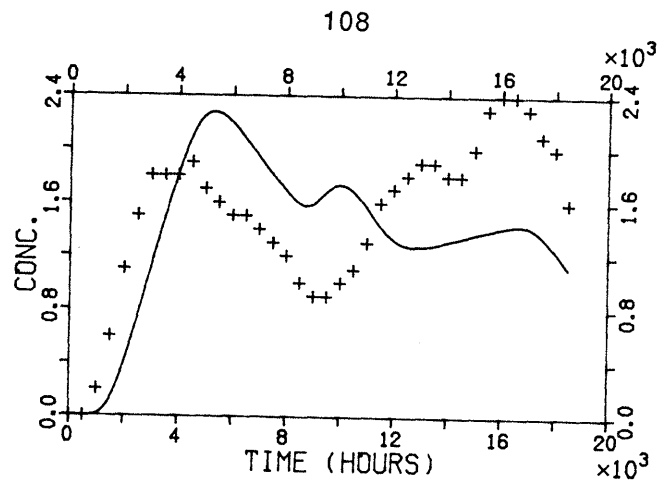
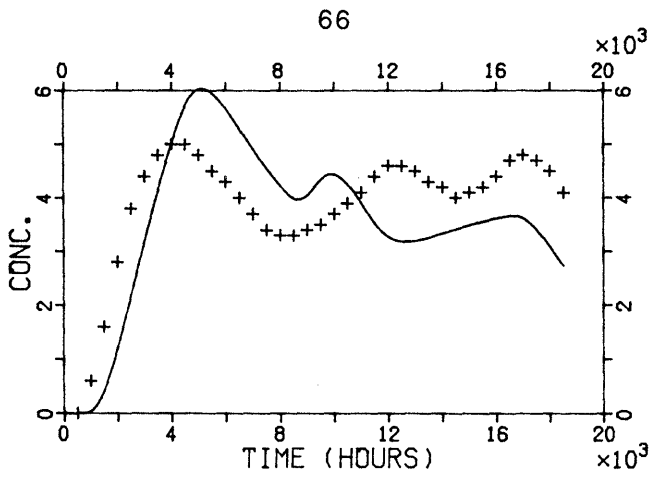
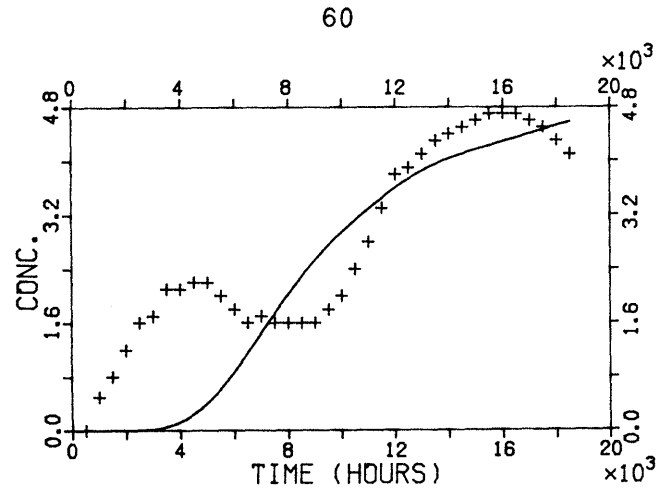
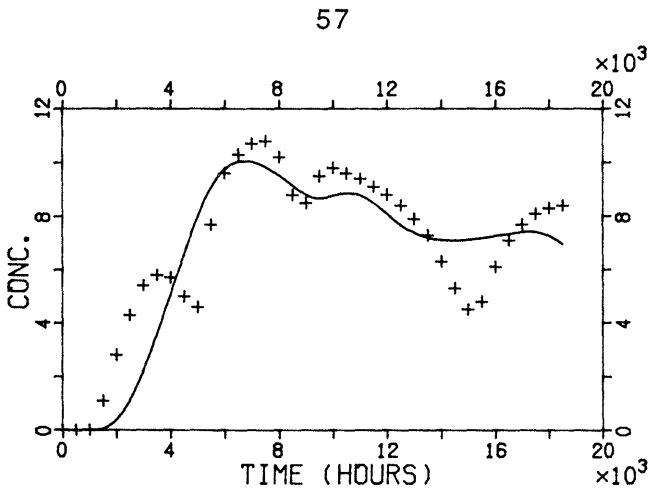
12.3 RESULTS OF MODEL FITTING OF BREAKTHROUGH CURVES

12.3.1 Advection-Dispersion model: Individual curves

The breakthrough curves were first fitted using the Advection-Dispersion Model. The curves which were near the detection limit were often erratic and were not used. Curves in which a plateau was not reached were also not used. In total 167 individual breakthrough curves were fitted. In these nonlinear least square fits three parameters were fitted: the Peclet number, the residence time, and a proportionality factor. The latter is inversely proportional to the dilution factor. In the tables the dilution factor is shown instead of the proportionality factor.

Preliminary results showed that most of the curves have a very low Peclet number. Such low Peclet numbers that were obtained in these preliminary fits are rarely found in in-situ experiments. Furthermore the model used was not valid for Peclet numbers less than three (Sauty, 1980). So for this reason the Peclet number was limited to values greater than 4.0. This was done by introducing a penalty function in the fitting process. The results are shown in Appendix 10, Table A10-1. It was observed that the dispersion was low for the runs with the tracer Iodide. The runs with the tracers Eosin B and Uranine showed high dispersion. The agreement between the fitted curves and the experimental data was good for the runs with the tracers Eosin Y and Iodide. The agreement was very bad for the runs with the tracer Uranine.

Figures 12-1 to 12-5 show some typical results of the fitting.



Figures 12-1 to 12-5.

Eosin B breakthrough curve from sheets 57, 60, 66, 108, and 120. The full line gives a fitted curve by the AD model and the crosses show selected experimental points.

In Figure 12-1 it is shown that the theoretical curve does not reproduce the form of the experimental points very well. There are two distinct dips in the experimental points at 5000 h and at 15000 h which are not seen in the fitted curve. The fit gives a residence time of 7045 h and a Peclet number of 5.1. A visual observation of the experimental points shows that the fitted curve cuts over the two early peaks. Inspection of the other curves for Eosin B shows that the form of the response curves are quite different in some cases. This indicates that there is more than just advection and hydrodynamic dispersion occurring which influences the responses along these pathways.

Figure 12-6 shows a response curve for Uranine.

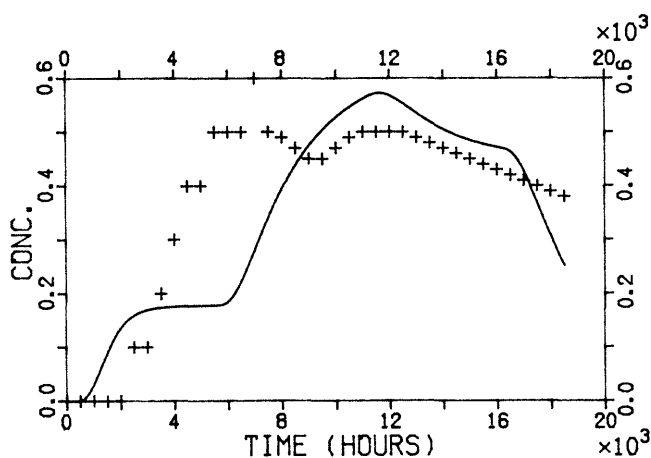
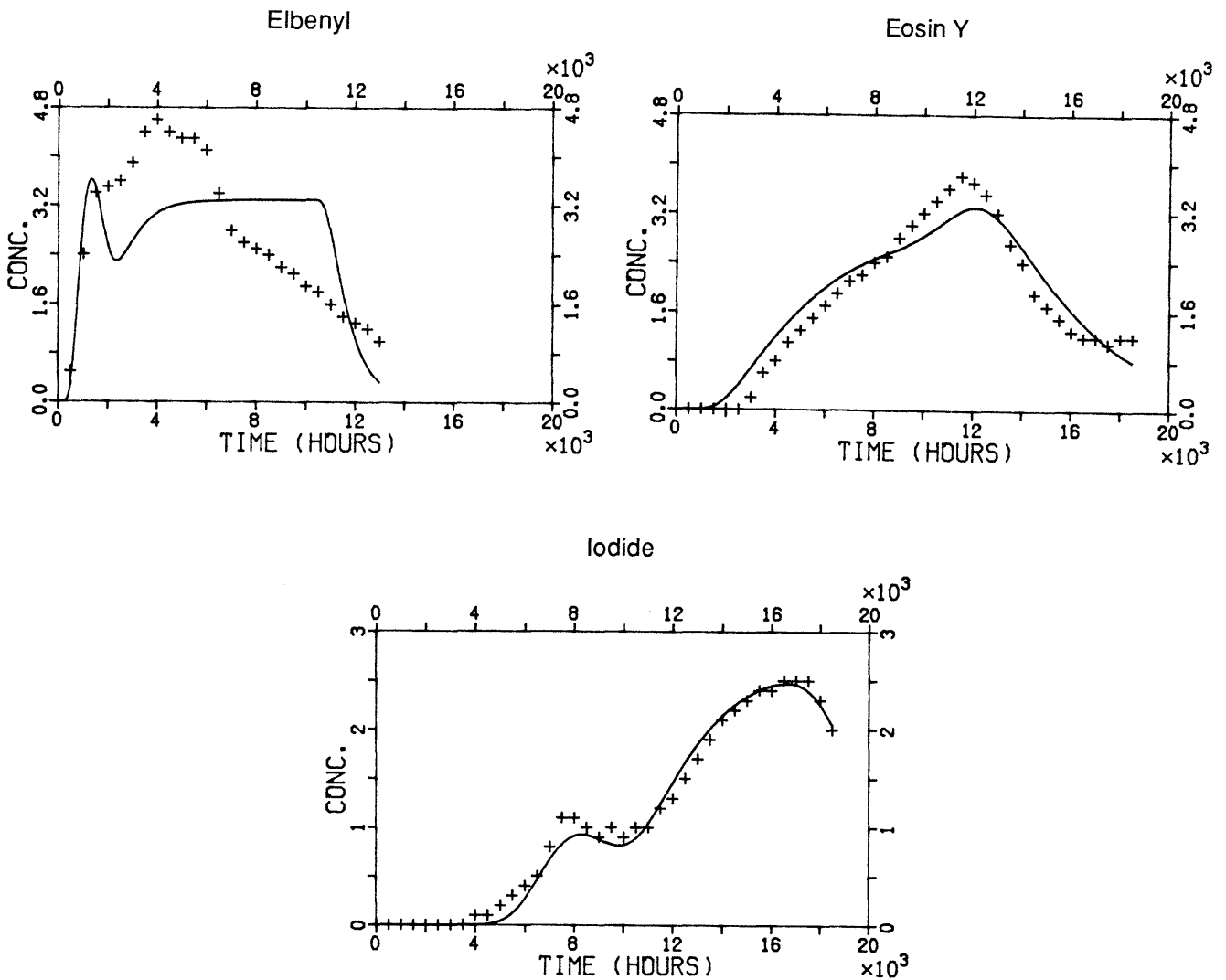


Figure 12-6. Uranine breakthrough curve in sheet 108. The full line gives a fitted curve by the AD model and crosses show selected experimental points.

It is clear that there is little similarity between the expected (fitted) curve and the obtained curve. The other Uranine curves show an equally poor fit, see the stand alone appendix, "Tracer breakthrough curves" and Table 12-2 which summarizes the results of the fitting with the AD model. The right column in the table contains the standard deviation of the fit.

Figures 12-7, 12-8, and 12-9 show some selected response curves and the fitted curves for Elbenyl, Eosin Y, and Iodide.



Figures 12-7, 12-8, 12-9.

Elbenyl, Eosin Y, and Iodide breakthrough curves in sheet 108. The full line gives a fitted curve by the AD model and the crosses show selected experimental points.

From Figure 12-7, the Elbenyl responses deviate more from the model than do the Eosin Y and Iodide results. This is also clearly shown in Table 12-2 where the standard deviation of the fit for these tracers is much less than for the other tracers.

The Bromide curves are given in the stand alone appendix "Tracer Breakthrough Curves." These results could not be used for times longer than about 4000 hours because after this time arriving Iodide interfered with the analysis of the Bromide. It was only possible to approximately evaluate the water residence time by using the early part of the curves. In addition, the dispersion could not be reliably determined from the curves.

For the breakthrough curves with a Peclet number equal to or less than 4.0, a fitting was made with the imposed condition of a Peclet

number greater than 1.0. This is shown in Table A10-2 of Appendix 10. A Peclet number of 1.0 means that transport by dispersion dominates over transport by advection. Such low Peclet values may be explained by the presence of severe channeling, i.e. the tracer is transported in several channels from the injection point. The mixing at the outlet of flows with very different velocities from the channels will cause a seemingly high dispersion.

Because a large number of the curves available contributed to a very small amount of the total recovered tracer, five curves for each tracer were chosen for continued analysis. These curves were chosen because they represented an important part of the tracer recovered during the observation time or because they represented the different zones where the tracer was found.

The results for the Advection-Dispersion model for these 25 chosen curves are shown in Table 12-2a. In these calculations the condition that the Peclet number is greater than 4.0 is imposed.

The injection curves were also divided into 15 parts to determine if the number of divisions was suitable. The resulting fits are shown in Figure 12-b. From the figure it is observed that there is a difference for Iodide but the standard deviation is the same or worse. It was concluded that the division of the injection curves into 5 parts was sufficient.

Table 12-2b shows the result from the fitting with the AD model with injection curves approximated by fifteen different step injections and in Table 12-5b this is also shown for the ADD model.

Table 12-2a. Results obtained using the Advection-Dispersion model. The condition Peclet number greater than 4.0 is imposed.

Number	Peclet number	Residence time hours	Dilution factor	Standard deviation
Tracer: Eosin B				
571	5.1	7045	151.3	.14
601	4.0	20470	181.7	.11
661	4.0	5004	313.3	.22
1081	4.0	5331	797.4	.32
1201	4.0	7077	135.5	.09
Tracer: Uranine				
642	4.7	2273	1152	.38
712	4.0	4223	695	.25
902	4.0	7445	1670	.19
1082	4.0	3634	2194	.29
1342	12.0	11810	190	.03
Tracer: Elbenyl				
603	4.0	2112	285.8	.15
643	6.1	2014	247.7	.22
663	4.0	1969	202.3	.20
683	5.6	1978	382.2	.11
1083	6.3	1636	583.6	.29
Tracer: Eosin Y				
646	6.6	5090	130.7	.10
686	5.5	7320	94.9	.07
716	5.3	7831	93.5	.07
906	4.7	8933	72.4	.03
1086	6.0	6324	277.6	.08
Tracer: Iodide				
618	18.6	7209	126.8	.08
628	4.0	11160	40.3	.05
1038	34.0	7558	98.6	.06
1088	54.5	7113	82.3	.06
1108	34.5	7031	76.2	.06

Table 12-2b. Results obtained using the Advection-Dispersion model. The condition Peclet number greater than 4.0 is imposed. Injection curves approximated by fifteen different step injections.

Number	Peclet number	Residence time hours	Dilution factor	Standard deviation
Tracer: Eosin B				
571	4.6	7421.0	148.22	.14
601	4.0	20470.0	181.77	.11
661	4.0	5005.0	313.28	.22
1081	4.0	5331.0	797.45	.33
1201	4.0	7078.0	135.50	.09
Tracer: Uranine				
642	4.0	2355.0	1143.51	.38
712	4.0	4223.0	695.41	.25
902	4.0	11680.0	1041.02	.17
1082	4.0	3634.0	2194.43	.29
1342	12.3	12030.0	193.01	.03
Tracer: Iodide				
618	14.8	8410.0	112.17	.09
628	5.3	10890.0	40.00	.04
1038	9.8	10260.0	72.46	.07
1088	25.1	8464.0	70.84	.09
1108	19.3	8375.0	65.76	.08

As it can be clearly seen from Tables 12-2a and 12-2b the parameter values for the fits with Eosin B and Uranine with injection curves with fifteen step injections are almost identical to the ones obtained with an injection curve with five step injections. The fits of Iodide show lower values for the Pe number and slightly higher residence times.

From these results representative values for the transport parameters are determined and are shown in Table 12-3. The tracers Eosin B and Uranine show a very high dispersion. The Peclet numbers for the tracer Iodide were about 30.

The water flowrate to each collecting sheet varied throughout the experiment. If it is assumed that an important part of the dilution of the tracer occurs near the drift, then the variation in the water flowrate strongly influences the concentration at the outlet. So for this reason, fittings were made with concentration curves that were modified (corrected) by these flowrate variations. The results are shown in Table 12-4. However, it was observed that the agreement between the fitted curves and the experimental curves did not improve. In the following the concentration curves will be used.

Table 12-3. Representative values for the parameters obtained from the Advection-Dispersion model.

Tracer	Peclet number	Residence time hours	Dist. from injection m
Eosin B	4.0	6 000	31
Uranine	4.0	5 000	35
Elbenyl	5.0	2 000	11
Eosin Y	5.0	7 000	24
Iodide	30	8 000	41

Table 12-4. Results obtained using the Advection-Dispersion model. The concentration is modified by the outlet flow to the respective sheet.

Number	Peclet number	Residence time hours	Dilution factor	Standard deviation
Tracer: Eosin B				
571	6.6	4356	204.8	.38
601	4.0	20470	181.7	.13
661	4.0	5006	317.3	.24
1081	4.0	5331	797.4	.33
1201	4.0	7052	138.5	.15
Tracer: Uranine				
642	4.0	5465	811.0	.33
712	4.0	7173	485.2	.19
902	4.0	11210	1062.9	.17
1082	4.0	6644	1551.8	.24
1342	4.0	19830	68.2	.06
Tracer: Elbenyl				
603	4.0	2104	285.4	.17
643	4.0	2275	243.2	.17
663	4.7	1749	193.2	.28
683	5.7	2208	331.6	.09
1083	7.2	1645	567.1	.30
Tracer: Eosin Y				
646	5.4	5098	115.8	.18
686	7.5	6235	100.6	.07
716	6.9	7698	94.9	.07
906	8.6	7483	78.6	.07
1086	7.4	6006	279.0	.08

Table 12-4. continued.

Tracer:	Iodide				
618	16.5	6566	136.5	.08	
628	14.2	6372	51.1	.17	
1038	35.2	5969	103.8	.15	
1088	54.6	6614	86.2	.09	
1108	41.2	7543	62.3	.09	

12.3.2 Results using the Advection-Dispersion-matrix Diffusion Model: individual curves.

The Advection-Dispersion-matrix Diffusion Model requires the determination of four parameters: the Peclet number, the water residence time, a parameter which takes into account the diffusion into the rock matrix (A-parameter), and the proportionality factor which accounts for the dilution effects. As in the fits with the Advection-Dispersion Model, the Peclet number has also been limited to values larger than or equal to 4.0 by the introduction of a penalty function. The results from the fitting with no modification in the breakthrough curves due to a varying flowrate at the collection points are shown in Table 12-5a.

The A-parameter depends on the fracture geometry and the properties of the rock matrix (porosity and pore diffusivity). Results show that the A-parameter varies by several orders of magnitude. These large variations cannot be explained by the variations in the rock and channel properties. In the fitting procedure, the effects of matrix diffusion and hydrodynamic dispersion are not well distinguished because they influence the breakthrough in a similar way. The noise observed in the experimental results was large, so that in order to distinguish between the different mechanisms additional information was required. To test the influence of dispersion on the fitting process, a fit was made using a high Peclet number to illustrate low dispersion. This models the situation in which practically all the spreading is accounted for by diffusion into the rock matrix. The results are shown in Table 12-6.

Table 12-5a. Results obtained using the Advection-Dispersion-matrix Diffusion model. A Peclet number greater than 4.0 is imposed.

Number	Peclet number	Residence time hours	A-parameter	Dilution factor	Standard deviation
Tracer:	Eosin B				
571	5.1	7035.0	3.10E+05	150.1	.14
601	4.0	20470.0	2.00E+05	181.7	.11
661	4.0	1944.0	1039.0	168.9	.07
1081	4.2	3118.0	1636.0	465.7	.17
1201	4.0	4687.0	2987.0	78.2	.03

Table 12-5a continued.

Tracer: Uranine						
642	19.8	15.1	28.9	946.1	.29	
712	6.5	26.5	22.5	470.4	.15	
902	4.0	11170.0	1.18E+05	1052.2	.16	
1082	4.0	1979.0	2309.0	1645.3	.21	
1342	11.7	12000.0	9.44E+04	173.0	.03	
Tracer: Elbenyl						
603	5.8	1402.0	3632.0	239.9	.11	
643	6.1	2014.0	7.62E+16	247.7	.22	
663	4.0	1941.0	2.00E+05	203.6	.20	
683	5.6	1978.0	1.25E+13	382.2	.11	
1083	6.3	1636.0	4.51E+16	583.6	.29	
Tracer: Eosin Y						
646	6.5	5067.0	1.81E+07	130.4	.10	
686	5.5	7274.0	3.93E+05	94.4	.07	
716	5.4	7758.0	2.82E+05	92.7	.06	
906	34.8	2829.0	1669.0	43.1	.03	
1086	6.0	6325.0	2.02E+05	277.6	.09	
Tracer: Iodide						
618	18.6	7206.0	4.94E+07	126.8	.08	
628	4.0	11090.0	5.00E+05	40.2	.05	
1038	34.0	7557.0	4.49E+06	98.6	.06	
1088	54.5	7113.0	5.28E+08	82.8	.06	
1108	34.5	7030.0	2.50E+07	76.2	.06	

Table 12-5b. Results obtained using the Advection-Dispersion-matrix Diffusion model. A Peclet number greater than 4.0 is imposed. Injection curves are approximated by fifteen different step injections.

Number	Peclet number	Residence time hours	A-parameter	Dilution factor	Standard deviation
Tracer: Iodide					
618	14.8	8410.0	.2273E+16	112.17	.087
628	4.0	11100.0	.3999E+05	27.57	.117
1038	13.9	9017.0	.7725E+06	82.33	.078
1088	25.1	8464.0	.1433E+17	70.84	.091
1108	19.3	8375.0	.2355E+20	65.76	.078

Table 12-6. Results obtained using the Advection-Dispersion-matrix Diffusion model. A Peclet number equal to 100 is imposed (very low dispersion).

Number	Peclet number	Residence time hours	A-parameter	Dilution factor	Standard deviation
Tracer: Eosin B					
571	100.0	1416.0	795.7	83.57	.09
601	100.0	2436.0	563.5	51.60	.04
661	100.0	.0	3.5E-04	166.89	.06
1081	100.0	.0	2.6E-06	400.75	.12
1201	100.0	397.9	200.2	69.57	.03
Tracer: Uranine					
642	100.0	.0	4.0E-04	845.31	.26
712	100.0	18.4	15.7	472.37	.16
902	100.0	6185.0	1.72E+05	1988.86	.28
1082	100.0	.0	2.9E-04	1527.65	.19
1342	100.0	10010.0	75880.0	244.50	.12
Tracer: Elbenyl					
603	100.0	571.1	821.1	213.17	.11
643	100.0	1885.0	5931.0	228.47	.27
663	100.0	675.2	1112.0	159.11	.19
683	100.0	2146.0	2.75E+19	484.50	.51
1083	100.0	1572.0	4.51E+18	686.58	.48
Tracer: Eosin Y					
646	100.0	2163.0	2230.0	92.59	.08
686	100.0	1931.0	1211.0	55.56	.05
716	100.0	2043.0	1222.0	53.88	.04
906	100.0	2151.0	1174.0	41.19	.02
1086	100.0	2242.0	1787.0	180.70	.06
Tracer: Iodide					
618	100.0	4253.0	3513.0	76.07	.06
628	100.0	4185.0	2617.0	29.98	.07
1038	100.0	5642.0	6418.0	66.46	.05
1088	100.0	6462.0	20850.0	71.86	.06
1108	100.0	5484.0	7760.0	55.75	.05

12.3.3 Results using the Advection-Channeling model: individual curves

The Advection-Channeling model requires the determination of three parameters: standard deviation in the lognormal distribution, water residence time for nonsorbing tracer, and the proportionality factor which accounts for the dilution effects. The standard deviation in the lognormal distribution has been limited to values below 0.318 by introducing a penalty function in the same way as for the AD model. This is equivalent to a Peclet number equal to 4.0. The results from the fitting using the AC model are shown in Table 12-7.

Table 12-7. Results obtained using the Advection-Channeling model. The standard deviation was limited to values lower than 0.318.

Number	Standard deviation in model	Residence time hours	Dilution factor	Standard deviation in fit
Tracer: Eosin B				
571	.301	7794	150.0	.14
601	.318	19870	201.6	.12
661	.318	4994	318.8	.23
1081	.318	5191	800.4	.33
1201	.318	7774	135.9	.09
Tracer: Uranine				
642	.318	3039	1162	.39
712	.318	4225	692	.25
902	.318	7445	1666	.19
1082	.320	3555	2325	.31
1342	.194	12080	193	.03
Tracer: Elbenyl				
603	.318	2329	284.9	.14
643	.281	2194	246.6	.22
663	.318	2187	202.2	.20
683	.287	2160	380.2	.11
1083	.273	1762	581.4	.28
Tracer: Eosin Y				
646	.267	5468	130.2	.10
686	.285	7899	95.1	.08
716	.286	8409	94.0	.07
906	.296	9476	73.7	.03
1086	.275	6801	277.8	.09
Tracer: Iodide				
618	.165	7450	126.2	.08
628	.318	11970	41.1	.05
1038	.121	7677	98.5	.06
1088	.096	7180	82.3	.06
1108	.120	7136	76.0	.06

12.3.4 Fitting of breakthrough curves collected in groups

For the tracers Eosin B, Uranine, Elbenyl, Eosin Y, and Iodide, fittings were done for some breakthrough curves that were constructed by adding several (between three and thirty-one) sheets together which seemed to form a group, separated from the other groups by a zone where no tracer were found. The grouping is defined by a section of length of the drift. From the fitting a very large dispersion was observed in the combined breakthrough curves. None of the fits were good except for the Eosin Y curves and one group of Iodide curves. The results of the fitting with the AD model are shown in Tables 12-8a and 12-9. Table 12-8b shows the results from the fitting with the AD model for the tracer Iodide with injection curves approximated

by fifteen different step injections. There is a noticeable difference between the values obtained from the second curve (39-45 m) but since the fits are poor no conclusions can be drawn from them. Results from the fitting with the ADD model are shown in Table 12-10. The breakthrough curves used in the fitting process, were taken from curves obtained by a digitizer from the detailed experimental breakthrough curves. These sampled data contained concentration values at each five hundred hours time period. From each collection sheet the product of the tracer concentration and the water flowrate at the same time was calculated. The mass flows that were obtained in this manner were added together from all the sheets and then divided by the total water flow from all the sheets. The result was a breakthrough curve for each group of sheets and for each tracer. The sheets with a high tracer concentration and a large water flow dominated over those sheets with a small tracer flowrate. From the combining of breakthrough curves from several sheets additional dispersion was introduced to the system because of the different travel distances of the tracer to the different sheets.

In Tables 12-8a and 12-8b the column headed "Section of drift" refers to where the group is located.

Table 12-8a. Results of combined flows from fitting with the AD model with a penalty function for Peclet numbers lower than 4.0.

Tracer	Peclet number	Residence time hours	Dilution factor	Standard deviation	Section of drift m
Eosin B	4.0	6338.0	185.4	.10	39 - 45
Eosin B	4.0	4481.0	1067.6	.46	25 - 35
Uranine	4.0	3583.0	1200.3	.26	25 - 35
Uranine	4.0	4932.0	2895.2	.20	12 - 22
Elbenyl	4.8	1658.0	607.2	.23	25 - 35
Eosin Y	5.9	6938.0	153.4	.07	25 - 35
Eosin Y	4.0	10320.0	234.0	.06	12 - 22
Iodide	32.8	7262.0	118.3	.05	25 - 35
Iodide	4.0	4544.0	760.7	.48	39 - 45

Table 12-8b. Results for combined flows from fitting with the AD model with a penalty function for Peclet numbers lower than 4.0. Injection curves are approximated by fifteen different step injections.

Tracer	Peclet number	Residence time hours	Dilution factor	Standard deviation	Section of drift m
Iodide	19.0	8596	102.0	0.07	25-35
Iodide	4.0	14490	162.5	0.33	39-45

Table 12-9. Results from fitting with the AD model with a penalty function for Peclet numbers lower than 1.0.

Tracer	Peclet number	Residence time hours	Dilution factor	Standard deviation	Section of drift m
Eosin B	4.0	6338	185.4	.10	39 - 45
Eosin B	1.2	10140	608.5	.16	25 - 35
Uranine	1.0	4519	1063.7	.22	25 - 35
Uranine	1.1	14420	1899.7	.11	12 - 22
Elbenyl	4.8	1658	607.2	.23	25 - 35
Eosin Y	5.9	6938	153.4	.07	25 - 35
Eosin Y	1.9	16060	182.7	.04	12 - 22
Iodide	32.8	7262	118.3	.05	25 - 35
Iodide	4.0	4545	760.2	.48	39 - 45

Table 12-10. Results from fitting with the ADD model a with penalty function for Peclet numbers lower than 4.0.

Tracer	Peclet number	Residence time hours	A-para- meter	Dilution factor	Standard deviation	Section of drift m
Eosin B	4.0	6338.0	.9917E+06	185.37	.10	39-45
Eosin B	4.0	96.0	.1518E+02	106.46	.03	25-35
Uranine	4.0	3543.0	.4588E+06	1168.36	.26	25-35
Uranine	4.0	4404.0	.5967E+04	2096.00	.13	12-22
Elbenyl	4.8	1658.0	.4144E+08	607.20	.23	25-35
Eosin Y	5.9	6938.0	.4817E+15	153.44	.07	25-35
Eosin Y	4.0	10270.0	.2303E+07	236.46	.06	12-22
Iodide	32.9	7262.0	.4141E+09	118.29	.05	25-35
Iodide	4.0	1243.0	.5938E+03	379.01	.24	39-45

12.3.5 Discussion

The fitting of the models to the experimental data gave varying results for the different sheets. One of the reasons for the variance is that there exist different travel paths to the different sheets and that these paths exhibit different transport properties. The goodness of the fit expressed as a standard deviation was poor for many of the curves. The different combinations of the parameter values could give nearly as good fits. Therefore, this indicates that there are processes involved which are not included in the models. The incorporation of the mechanism "diffusion into the rock matrix" only produced marginal improvements in the fits. The values resulting from the matrix diffusion parameter fits were very erratic and often outside the range for reasonable values. Although there were independent laboratory measurements performed which showed that this mechanism contributes, the noise in the data did not permit the values to be evaluated.

The injection curves had many changes in the injected tracer flowrate which should have been noticeable in the resulting concentration curves but were seldom observed because they had been evened out. The presence of considerable "noise" was also observed in the results. One of the reasons for the noise was from the mix of different tracers analyzed. As the ratios of the tracer concentrations changed the errors in the analysis were influenced. This was especially noticeable when only one tracer was present in a low concentration and then another tracer arrived in a considerably higher concentration, thus disturbing the first tracer.

One of the possible causes for the deviation from the theoretical curve form was that there were too few (less than tens to hundreds) mixings occurring between channels along the path to even out the random differences between the channels of the path. The models used are based on the assumption that the random variations have been evened out. The deviation from mixing is indicated by the different concentration curve forms in the different sheets.

An attempt was made to combine many curves to a single concentration curve in order to average out the random variations, see Section 12.3.4. This procedure smoother curves, however, the results of the fitting did not improve.

12.4 DETERMINATION OF FLOW POROSITY

12.4.1 Methods and results

When the flowrate, the residence time, and the travel distance are known, the flow porosity may be evaluated. This is done by using the assumption that the flow is radially converging. The residence time of the water along the different flow paths was estimated from the fitting of the models to the breakthrough curves of the different tracers, see Section 12.3. The fits were poor in several cases especially for those curves where the concentration and water flowrate were low. The most reliable results seemed to be those from the "selected" curves (five curves for each tracer) which were selected because the tracer flowrates in those sheets contribute significantly to the total tracer flowrates. In a series of fits, many nearby curves, which seem to form a group were lumped together into one breakthrough curve by adding the tracer flowrates in the sheets. This procedure added together several pathways with different travel times. Table 12-11 summarizes these results.

The flow porosity can be determined by the following expression. It is based on the assumption that the flow is radially convergent in a homogeneous porous medium where Darcy's law applies.

$$\epsilon_f = 2 t_w Q / A_o (r_2^2 / r_1 - r_1) \quad (12.18)$$

where A_o is the collecting area of the drift.

The flowrate to the drift was very unevenly distributed. Tracers were found mainly in the central part of the drift. Other large parts of the drift were dry with the exception of the far end and the right arm where most of the water flow to the drift was located. The question then arises, "At which water flowrate has a tracer been monitored?" Is

it all the water to the drift including that to the uncovered bottom part, is it all the water to the covered part of the drift including the water where no tracers were found, or is it only that water in which tracers were found? In this case the latter assumption is used. The next question then is, "What area of the tunnel is the correct area to use in the above equation?" Is it only the area of those sheets in which the water with tracers were found or should a dry portion of the tunnel near to the tracer carrying sheets also be included? In a case like this where the water is Table 12-11 Residence times t_w estimated by different methods very unevenly distributed there are no established correct ways of choosing the area. Therefore, it has been elected to use a length of drift where the tracers were found, including the area of the dry sheets in that section of the drift.

A further question is, "Which travel distance is correct?" It might be argued that for every sheet there is a correct travel distance, which is the nearest distance between the injection point and the collection sheet. It may also be argued that the nearest distance between the injection point and the drift is more representative because that is where the flow would be in an ideal porous medium, which is the basis for the equation used. It has been elected to use the latter approach. Considering the uncertainties in the basic assumptions the resulting flow porosities are not to be taken as exactly determined experimental values. The porosities will differ by more than a factor of two if the other extreme combinations of the assumptions are used.

The radius r_1 of the drift is taken to be 2.2 m. This would be the radius of a cylinder with the same surface area as the drift. The drift has a covered area of 7 m²/meter of length.

Table 12-12 shows the data used for evaluating the porosities and the obtained porosity values.

Figure 12-10 shows a plot of the porosity as a function of the distance to the injection point. There is a tendency for the porosity to decrease with increasing distance.

Table 12-11. Residence times, t_w , estimated by different methods.

Tracer	AD ¹	ADD ²	ADD ³ high Pe	AC ⁴	AD ⁵ groups	Typical ⁶
Eosin B	5000-20500	1940-20500	0-2400	5190-19900	4480-6340	3000
Uranine	2300-11800	15-1200	0-10000	3040-12100	3580-4930	5500
Elbenyl	1640-2100	1640-2010	570-2150	1760-2330	1660	2000
Eosin Y	5100-8900	2830-7800	1930-2240	5470-9480	6940-10300	6000
Iodide	7000-11200	7030-11100	4190-6460	7140-12000	4540-7260	7000
Bromide	(5200-11800)	(63-11800)	(0-291)	(5890-10700)	-	2500 ⁷

- 1) Fit of the 5 main breakthrough curves using the AD model.
- 2) Fit of the 5 main breakthrough curves using the ADD model.
- 3) Fit of the 5 main breakthrough curves using the ADD model but forcing the fit to use a very low hydrodynamic dispersion (Pe=100).
- 4) Fit of the 5 main breakthrough curves using the AC model.
- 5) Fit of the breakthrough curves collected in groups using the AD model.
- 6) Selected typical values.
- 7) Estimated from early part of curves.
- () Bromide results are not reliable.

Table 12-12. Porosities and basic data used in the calculations.

Tracer	Residence time hours	Flowrate in section ml/h	Length of section m	Distance to injection point m	Porosity $\cdot 10^5$
Eosin B	3000	175	22	19	3.4
Uranine	5500	153	23	32	2.0
Elbenyl	2000	178	10	10	15.5
Eosin Y	6000	198	27	18	6.9
Iodide	7000	200	31	29	3.0
Bromide	2500*	200	31	13	4.5

* The bromide residence times obtained from the fits using the collection time are in error because of interference from Iodide. The residence early time 2500 h was estimated by visually observing the breakthrough curves for the early times when the Iodide has not yet reached the collection sheets in any appreciable concentration. The value is only an approximate.

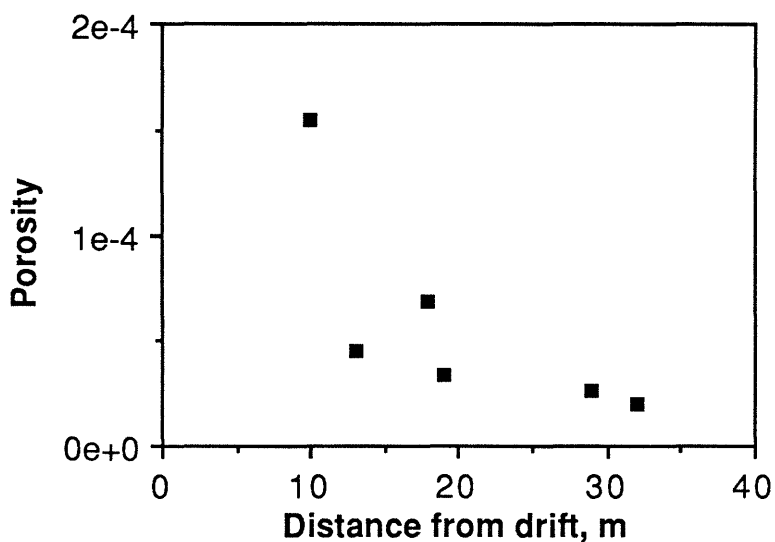


Figure 12-10. Porosity versus distance from drift.

12.4.2 Discussion

In the determination of the porosity there is an underlying assumption that the residence time measured with the tracers represents that of the main flow in which the tracers were subsequently found as they

emerged in the drift. The average individual injection flowrates are in the range 0.45 to 8.94 ml/h for the six tracers in Table 12-12. The sum of the flowrates for these six recovered traces is 24.4 ml/h. This may be compared to the total flowrate to the drift ranging from 600-700 ml/h. The injection flowrates of these tracers made up 3-4 % of the flowrate to the drift. The tracers were recovered in the flow to the central part of the drift where the flow was only about 150-200 ml/h. The dilution of the individual tracers is then between 22 and 396, see Table 12-13.

Table 12-13. Average injection rates and flowrates where the individual tracers were recovered.

Tracer	Average injection rate ml/h	Flowrate in which recovered ml/h	Theoretical dilution factor
Eosin B	4.09	176	43.0
Uranine	4.87	153	31.4
Elbenyl	0.45	178	396
Eosin Y	2.75	190	69.1
Iodide	8.94	200	22.4
Bromide	3.25	200	61.5

The paths for the tracers may not be representative for those waters where the tracers were found if the mixing of the tracer solution and the main water flow has occurred near the drift. In the extreme the porosity of the rock where the tracers have migrated might be smaller by a factor equal to the dilution factor. This gives, however, a meaningless figure for the rock porosity because it includes the assumption that the rock volume for the tracers is the same as that represented by the main water flow.

12.5 INTERPRETATION OF RECOVERY OF TRACERS

12.5.1 Determination of recovery of tracer

The recovery for the different tracers was calculated by integrating the breakthrough curves multiplied by the respective flowrates. The results for each sheet are shown in Appendix 12. The cumulative amount of tracer that reached the drift as a function of time also was calculated, see Figure 12-11. Table 12-14 shows the amount of injected tracer and the mass of tracer recovered during the observation time. The recoveries of the tracer varied from 2.8 % for Uranine to 65.8 % for Elbenyl. The tracers Rose Bengal and Phloxine were not found at all. Only 0.002 % of Duasyn was recovered. The low value for Duasyn was because its first arrival time was about 15,000 hours. Bromide showed a recovery of 153 %. This impossible value for Bromide was caused by errors in the analysis due to the presence of Iodide. Therefore the Bromide data are not used in recovery calculation.

The results do not indicate that the distance from the injection point to the sampling area was the sole factor influencing the recovery. For example, Iodide had a recovery higher than Eosin B even though Eosin B was injected at a shorter distance.

The recovery distribution of the tracers is shown in Figures 12-30 - 12-34 and the injection site and distances are marked in the same figures.

Table 12-14. Mass of injected tracer and tracer recovered during the observation time.

Tracer	Recovered tracer	Injected tracer	Recovery %
Eosin B	4.65 g	95.98 g	4.85
Uranine	2.15 g	76.96 g	2.80
Elbenyl	6.11 g	9.29 g	65.78
Eosin Y	9.58 g	28.06 g	34.15
Duasyn	0.01 g	303.64 g	0.002
Iodide	0.23	1.82 mol	12.39
(Bromide)	1.48	0.97 mol	153.52)

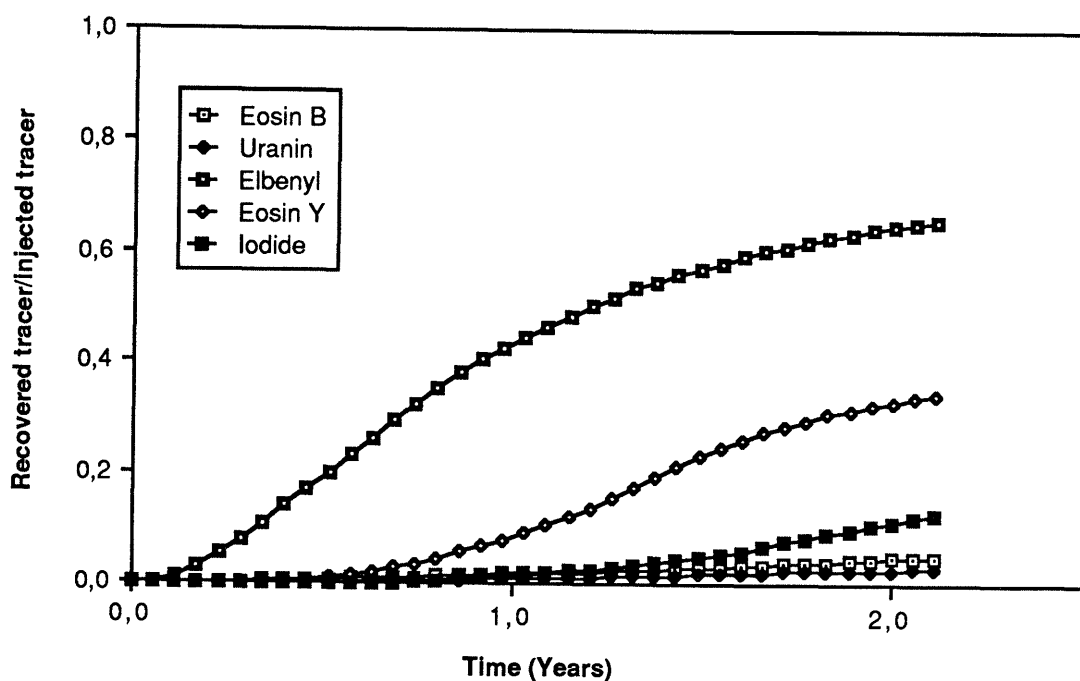


Figure 12-11. Recovered tracer/total injected tracer versus time.

Table 12-15 shows some of the data for the tracers.

Table 12-15. Some data on tracer residence times and recoveries.

Tracer	Injection distance m	Residence time* h	Porosity .10 ^{5**}	Section length m	Recovery %
Elbenyl(II)	9-11	2000	15.5	10	65.8
Bromide(III)	12-14	2500	4.5	31	-
Eosin Y(I)	17-19	6000	6.9	27	34.2
Eosin B(III)	18-20	3000	3.4	22	4.8
Iodide(III)	28-30	7000	3.0	31	12.4
Rose Bengal(II)	33-35	-	-	-	-
Uranine(I)	31-33	5500	2.0	23	2.8
Duasyn(III)	36-38	>15000	-	-	0.002
Phloxine(II)	55-57	-	-	-	0
STR7(I)	31-33	-	-	-	0
Flouride(I)	31-33	-	-	-	0

* Approximate average values estimated from the fits with AD, AC and ADD models.

** Determined from flowrate and residence time.

It is seen in Table 12-15 that there is a trend that the recovery of the tracers decreases with increasing injection distance. There may be several causes for a less than full recovery of the tracers. Some of the causes are listed below:

1. The tracer has partly moved into pathways that do not lead to the experimental drift
2. The tracer is still travelling in the mobile water
3. The tracer has reacted "irreversibly" or been degraded
4. The tracer has moved into stagnant volumes of water by molecular diffusion.

Cause 1 does not seem very probable in general, because although sought for, only one tracer, Eosin Y, has been found in adjacent nearby drifts and holes. Cause 2 is certainly true to some degree. Cause 3 is not probable because extensive sorption tests in the laboratory over long times have not revealed that the tracers react or degrade. Cause 4 is known to take place as diffusion into the stagnant water in the matrix in the rock and is also suspected to take place into the stagnant water in the fractures.

12.5.2

Matrix diffusion effects

In the following the possibility of matrix diffusion as a cause for the low recovery is explored.

It was projected (Neretnieks, 1980) that small readily mobile molecules, dissolved in the water, would migrate into the water in the micropores of the matrix and thereby withdraw the molecules from the moving water. There have been subsequently a series of measurements performed on the porosity and diffusivity of small molecules in granites and gneisses in the laboratory (Skagius and Neretnieks, 1986a, 1986b) and in the field (Birgersson and Neretnieks, 1982, 1984). Typical values of the porosity are 0.1-0.5 % for intact rock. Higher values are often found near fracture surfaces. Effective diffusivities, D_e , are typically in the range 10^{-14} to 10^{-12} m²/s. Pore diffusivities are higher by 2 to three orders of magnitude in comparison to the effective diffusivities ($D_e = D_p \cdot \epsilon_p$, where ϵ_p is the porosity). To illustrate the potential capacity and accessibility of the matrix water to the molecules, it may be noted that the water volume contained in a fracture of thickness 0.05 mm is as large as the water volume in a 100 mm thick slab of rock adjacent to the fracture if the rock has a porosity of 0.05 %. To consider the dilution effect is as follows, if the fracture was filled with a tracer solution with concentration "C" and the solution was given time to equilibrate with the noncontaminated water in the pores of a 50 mm thick rock slab on either side of the fracture (total rock slab on both sides of the fracture is 100 mm), then the concentration in the fracture and in the pores would be 0.5*C. If the fracture was emptied of the water, the recovery would be 50 % and the rest of the tracers would reside in the porous rock matrix.

The time for this process can also be estimated. From the diffusion equation (Bird et al., 1960) it is found that the penetration thickness $\bar{\eta}$ for this case can be determined by

$$\bar{\eta} = \sqrt{D_p t} \quad (12.19)$$

For a pore diffusivity D_p of 10^{-10} m²/s the time to completely penetrate 50 mm is 0.8 years. The duration of the experiment was more than 2 years and the water residence times for the tracers were in the time interval 0.2 to 0.8 years or more. It thus seems reasonable that this effect may be of importance if the fracture apertures are small enough.

The fracture apertures can be estimated if the flow porosity and the fracture frequency are known. The flow porosity was estimated from data on residence times and total flowrates. The porosities ranged between $2 \cdot 10^{-5}$ and $15 \cdot 10^{-5}$. For a given fracture spacing (parallel fractures), the flow porosity ϵ_f is δ/S (the aperture divided by the fracture spacing). For a flow porosity of $5 \cdot 10^{-5}$ and a fracture aperture of 0.05 mm, the spacing is 1 m.

The above data are in the range of possible values. It thus seems worthwhile to explore this possibility further.

Flow in fractures with matrix diffusion

In the above example a case was explored where initially a traced water volume was introduced in a thin fracture and then the water was allowed to reside for a certain time. In the experiment there was a constantly moving water in the fractures or channels in the rock. This may be modeled as flow in a system of fractures with known properties such as aperture, spacing, flowrate, and the matrix properties discussed above.

For flow in a system of fractures where suddenly a tracer pulse is injected in the constantly moving water, the solution to the Advection-Diffusion equation coupled with the Matrix Diffusion equation for the case of negligible dispersion was shown to be:

$$C = C_o \operatorname{erfc} \left[\frac{t_w}{\delta} \left[\frac{D_e \epsilon_p}{t - t_w} \right]^{1/2} \right] \quad (12.10)$$

The equations above have been written for constant water velocity. It was shown by Neretnieks and Rasmuson (1985) that this is not a prerequisite for the validity of the equation. Since the water velocity may vary arbitrarily, only the water residence time will matter as long as the rock properties including the available fracture surface per volume of rock a' is constant.

For radial flow where the water velocity decreases with increasing distance from the drift, the same equation may be used. The fracture aperture δ can, as before, be expressed as a function of the flow porosity and the fracture spacing or the specific surface a' (m² fracture surface/m³ rock).

$$\delta = S \cdot \epsilon_f = 2 \cdot \epsilon_f / a' \quad (12.20)$$

Introducing Equation (12.20) into Equation (12.10) gives

$$C = C_o \cdot \text{erfc} \left[\frac{t_w a'}{2 \epsilon_f} \left(\frac{D_e \epsilon_p}{t - t_w} \right)^{1/2} \right] \quad (12.21)$$

Assuming that the drift can be approximated by a cylinder, the residence time t_w can be determined from the flowrate Q to the collecting area A_o of the drift, the radius r_1 of the drift, and the radial distance r_2 to the injection point. Then t_w becomes

$$t_w = \frac{A_o \epsilon_f}{2Q} \left[\frac{r_2^2}{r_1^2} - r_1 \right] \quad (12.22)$$

Introducing Equation (12.22) into Equation (12.21) gives

$$C = C_o \cdot \text{erfc} \left[\frac{A_o}{2Q} \left[\frac{r_2^2}{r_1^2} - r_1 \right] \frac{a'}{2} \left(\frac{D_e \epsilon_p}{t - t_w} \right)^{1/2} \right] \quad (12.23)$$

For future purposes it is written

$$C = C_o \cdot \text{erfc} \left[G \cdot E \frac{1}{(t - t_w)^{1/2}} \right] \quad (12.24)$$

where

$$G = \frac{A_o}{2Q} \left[\frac{r_2^2}{r_1^2} - r_1 \right] \quad (12.25)$$

and

$$E = \frac{a'}{2} (D_e \epsilon_p)^{1/2} \quad (12.26)$$

G contains only known geometric entities and the flowrate, which is measured, and E contains only the rock properties.

For the experiments at hand estimates of travel times and the flow porosities are available and, in the following the specific surface a' is preferred to be used instead of the fracture aperture. This entity does not give associations of planar fractures. The fractures may in reality vary in aperture and width arbitrarily along the flow path as long as the values of the average flow porosity and average specific area are maintained.

In this section sample calculations are made with the data in Table 12-15 to investigate what values of the specific surface a' would be needed to obtain the recoveries that were measured.

The following values of the matrix porosity and the matrix diffusivity were used

	Dyes	Iodide
$\epsilon_p =$	0.05 %	0.1 %
$D_p =$	$2 \cdot 10^{-14}$	$2 \cdot 10^{-13}$

These values are based on the measurements described in Chapter 8. Figures 12-12 and 12-13 show the calculated recovery curves for Eosin Y and Iodide as a function of time with the specific surface as a parameter.

For Eosin Y the specific surface required to obtain the observed recovery is on the order of $4 \text{ m}^2/\text{m}^3$. For Iodide it is $0.7 \text{ m}^2/\text{m}^3$. The calculations performed here were made for a case with a constant injection in time and do not account for the varying injection rates which took place during the experiments. This is readily introduced and has been accounted for in the evaluations of the experiments described later. It here suffices to note that for the a' values in the above range, the effect of matrix diffusion can account for the seemingly very large losses of the tracers. The above values of a' would imply that 2 and 0.35 fractures per meter, respectively, are needed. These are possible values considering the observation made during the mapping of the drift.

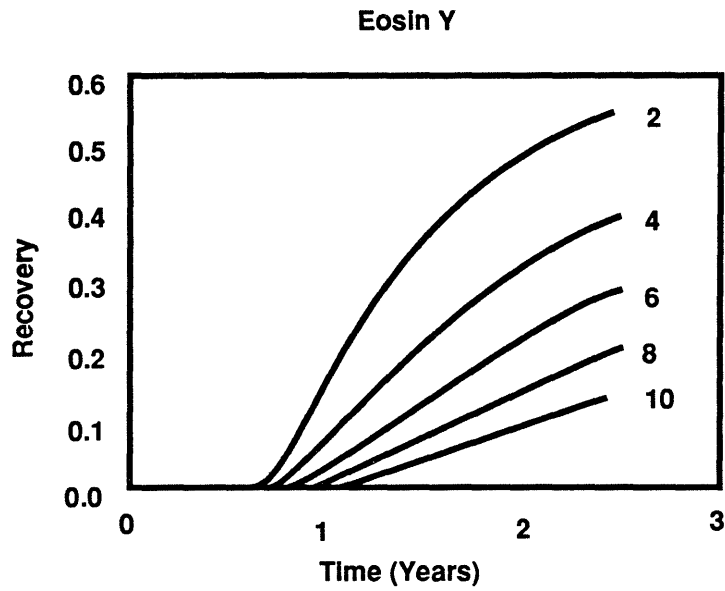


Figure 12-12.

Recovery of Eosin Y as a function of time with the specific surface a' as a parameter.
 $D_e = 2 \cdot 10^{-14}$, $\epsilon_p = 5 \cdot 10^{-4}$, $t_w = 6000$ h,
 $Q = 198$ ml/h, $L = 27$ m, $r_1 = 2.23$, $r_2 = 20.2$ m, $\epsilon_f = 6.9 \cdot 10^{-5}$.

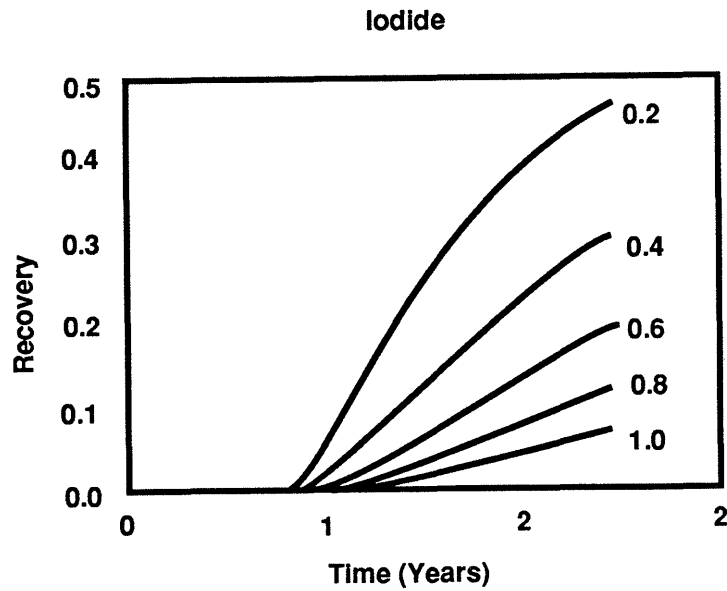


Figure 12-13. Recovery of Iodide as a function of time with the specific surface a' as a parameter.

$$D_e = 2 \cdot 10^{-13}, \quad \epsilon_p = 1 \cdot 10^{-3}, \quad t_w = 7000 \text{ h}, \\ Q = 200 \text{ ml/h}, \quad L = 31 \text{ m}, \quad r_1 = 2.23, \quad r_2 = 31.2, \quad \epsilon_f = 3.0 \cdot 10^{-5}.$$

Determination of specific surface by fitting the recovery curves

In the previous section exploratory calculations of the specific surface were made using a constant injection and assuming no dispersion. In this section the results of a fit made using the actual injection rates for the different tracers is presented. These results are shown in Table 12-16 when the residence time is assumed to be known. Another fit where the residence time is determined in the fit is also presented in the same table.

Table 12-16.

Specific surface determined using a model with diffusion into matrix. No dispersion ($Pe \rightarrow \infty$).

Tracer	Residence time hours ⁽¹⁾	Specific surface a' m ² /m ³ (¹)	Residence time hours ⁽²⁾	Specific surface a' m ² /m ³ (²)
Eosin B	3 000	14	≈ 0	16
Uranine	5 500	5.1	≈ 0	7.0
Elbenyl	2 000	15	≈ 0	19
Eosin Y	6 000	4.7	542	7.7
Iodide	7 000	0.49	≈ 0	0.92

(1) Residence time is given

(2) Residence time is fitted

The fitted residence times are close to zero. In both cases the values of the specific surface are similar. When the residence times are fitted, the specific surface is about 20 % higher. In the fits in which the residence time is given, the agreement with the experimental recovery curve is bad.

From the experimental recovery curves it may be seen that the first arrival of the tracer is less than the residence times given above. For a model without dispersion the time for the first arrival must be greater than or equal to the residence time. These results show that a certain dispersion has to be included in these calculation to determine the specific surface. This is accomplished using a model which includes both dispersion and diffusion into the rock matrix. A Peclet number of 10 was used. Two fits were made, in one fit the values of the residence times were given, in the other fit the residence times and the specific surface were determined. The results are shown in Table 12-17.

Table 12-17.

Specific surface determined using a model with diffusion into the matrix and dispersion. Peclet number of 10 is used.

Tracer	Residence time hours ⁽¹⁾	Specific surface a' m ² /m ³ (¹)	Residence time hours ⁽²⁾	Specific surface a' m ² /m ³ (²)
Eosin B	3 000	20	≈ 0	21
Uranine	5 500	8.2	19.1	9.8
Elbenyl	2 000	15	≈ 0	20
Eosin Y	6 000	5.8	2 868	7.6
Iodide	7 000	0.77	959	1.0

(1) Residence time is given

(2) Residence time is fitted

It is seen that although the fits are not good the obtained specific surface for this model does not change much. The specific surface is found to be the interval 0.8 to 21. The lower figure was obtained for Iodide and the larger for Eosin B.

A fit was also made in which the residence time was given and the Peclet number and the specific surface were fitted. The specific surface obtained is similar to the values obtained in the other fits. The result from this fit is shown in Table 12-18.

Table 12-18. Specific surface determined using a model with diffusion into the matrix and dispersion. Peclet number and specific surface is fitted and residence time is given.

Tracer	Peclet number	Residence time hours	Specific surface a' m^2/m^3
Eosin B	4.1	3000	27
Uranine	4.0	5500	12
Elbenyl	4.0	2000	16
Eosin Y	4.3	6000	7.4
Iodide	4.9	7000	1.1

At first it is surprising that there are only small differences in the values of the specific surfaces obtained because the assumptions used in the different fits are so different. In one fit only one channel was used, the water residence times were assumed to be known and it was assumed that there was no hydrodynamic dispersion. By just comparing the final recoveries for the different tracers the specific areas a' obtained were very near to the values in another fit where dispersion is included. Further, letting the water residence time be a free fitted variable gives values of the residence time orders of magnitude lower than those previously used but essentially the same specific area a' is obtained. During the fitting it was observed that the fitted curve was rather insensitive to the water residence time and to the dispersivity values used. Very different values of these entities gave quite similar results if the standard deviation of the fit is compared. Also visual comparisons of the curves showed no large differences except for the early part of the curves, i.e. for short times.

The matrix diffusion exerts such a large influence on the recovery and on the spreading of a pulse that it, to a large extent, overshadows the influence of the other effects.

This has been foreseen. Neretnieks (1980, 1983) and Rasmuson and Neretnieks (1980) have made theoretical calculations of these effects and have shown that when there is a large uptake in the rock matrix, the water residence time and the hydrodynamic dispersion effect may be totally drowned in the effects of matrix diffusion.

The specific surface is a large value for the tracer Elbenyl, which was injected at a 10 m height. Low values for the specific surface were obtained for tracers that were injected at a greater distance from the drift. Thus, there exists a weak trend that the specific surface decreases with increased injection distance.

Table 12-19 contains the compilation of obtained specific surfaces for some tracers. There is a clear difference between the values obtained for the dyes on the one hand and Iodide on the other hand.

The differences in the a' values obtained from the dyes and those obtained from the Iodide runs indicate that other effects may also play a role. This is explored in the following section.

Table 12-19. Compilation of obtained specific surfaces.

Tracer	Injection distance m	Specific surface m^2/m^3
Eosin B	19	14-27
Uranine	32	5.1-12
Elbenyl	10	15-20
Eosin Y	18	4.7-7.7
Iodide	29	0.49-1.1

12.5.3

Diffusion into stagnant pools of water in the fracture

The large specific surfaces for diffusion into the rock matrix, a' , which were obtained for the dyes are not reasonable because they imply that there should be spacing of conducting fractures $2/a'$ m. For Iodide this would mean spacing of 1-2 meters and for the dyes 0.07-0.4 meters. This contradicts the observations in the drift where, at most, 100 water conducting fractures were observed over a length of 100 m. Since only a fraction of the fractures conduct water this means that the fracture spacing must be larger than 1 m in the rock near the drift.

Another possible cause for the low recovery of tracers is now explored. It is based on the concept that the water flows in channels that are in contact with practically stagnant pools of water. The tracer in the flowing water in the channel may diffuse into the nearby stagnant water and thus be withdrawn from the mobile water. Figure 12-14 illustrates this process.

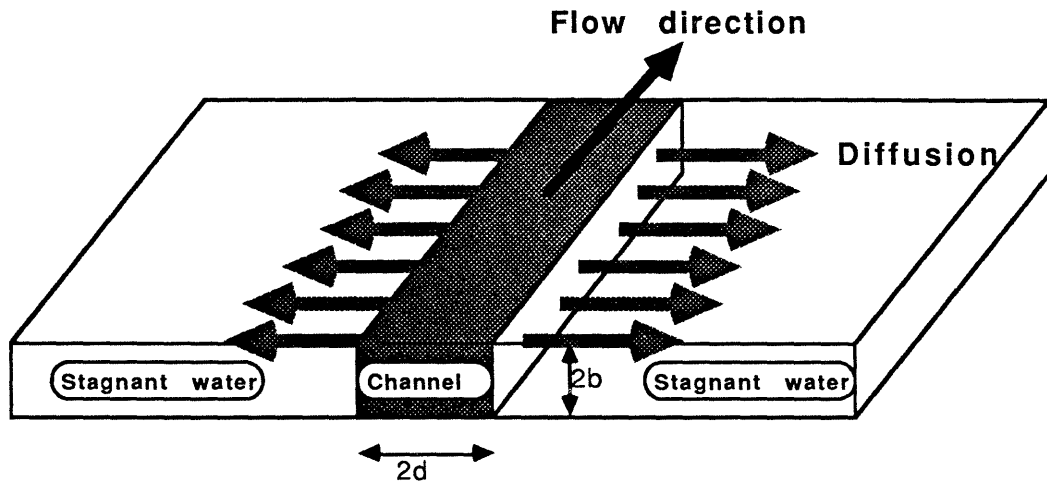


Figure 12-14. A fracture cross section with a channel containing flowing water is shown. In contact with the flowing water are stagnant volumes of water into which the tracer is carried by diffusion.

The aperture of the channel is δ and the width of the channel is $2d$. The species diffuse into the stagnant water. For a long channel with a small width, in comparison to the diffusion distance, it may be assumed that the concentration of the species across the width of the channel is constant. Therefore, the previously obtained equation for diffusion into stagnant water in the rock matrix can also be used to describe this case. The effective diffusivity will then be equal to the diffusivity in unconfined water ($D_e = D_w$) and the equivalent of the matrix porosity is equal to unity. Equation (12.10) then becomes

$$C = C_o \operatorname{erfc} \left[\frac{t_w}{2d} \left(\frac{D_w}{t - t_w} \right)^{1/2} \right] \quad (12.27)$$

Identification of the arguments of Equation (12.21) and Equation (12.27) gives

$$2d = \left[\frac{D_w}{D_e \epsilon_p} \right]^{1/2} \frac{2 \epsilon_f}{a'} \quad (12.28)$$

The diffusivity of the dyes in water is on the order of $10^{-9} \text{ m}^2/\text{s}$ and for Iodide it is $4 \cdot 10^{-9} \text{ m}^2/\text{s}$ (Skagius, 1986). Other data are taken from Tables 12-12 and 12-19. The channel widths, $2d$, may be estimated with these data and are summarized in Table 12-20.

Table 12-20. Estimated equivalent channel widths $2d$.

Tracer	ϵ_f flow porosity $\cdot 10^5$	a' (central value) l/m	$D_e \epsilon_p$ $\cdot 10^{16}$ m^2/s	Channel width ($2d$) m	Sum of apertures ($\Sigma\delta$) m
Eosin B	3.4	20	0.1	0.034	0.154
Uranine	2.0	8	0.1	0.050	0.064
Elbenyl	15.5	17	0.1	0.182	0.060
Eosin Y	6.9	6	0.1	0.023	0.567
Iodide	3.0	0.8	2	0.335	0.019

The channel widths obtained are smaller or, at most, of the same magnitude as the penetration depths into the stagnant water for one year contact time (Equation 12.19). Therefore, the assumption that the concentration over the channel width is evened out is thus not grossly violated.

The above analysis gives no indications of how large the apertures of the channels are. An estimate of the sum of the apertures of the channels, assuming that they all have the same widths, can be made in the following way. The sum of all the cross section areas of the channels is denoted as $2d \cdot (\Sigma\delta)$, see Figure 12-14. The total area of rock, A_0 , that these channels intersect at the face of the drift was utilized to evaluate the flow porosity, ϵ_f , see Table 12-12. The porosity is the ratio of the cross section of the channels to the cross section of the area containing the channels

$$\epsilon_f = (\Sigma\delta) \cdot 2d / A_0$$

From the above expression the sum of the channel aperture ($\Sigma\delta$) can be obtained. The values range from 19 mm to 567 mm and are given in Table 12-20.

The tracers arrived in many of the sheets. If every sheet on the average had a few channels, several tens of channels would determine the sum of apertures ($\Sigma\delta$). So for 50 channels this would mean a 3 mm aperture for Eosin B, slightly more than 1 mm for Uranine and Elbenyl, more than 10 mm for Eosin Y, and a 0.4 mm aperture for Iodide. However, most of these values are considerably larger than what the visual observations indicated.

Therefore the diffusion into stagnant pools of water cannot alone explain the loss of tracer. Also the diffusion into the rock matrix is also not solely the cause for the loss of tracer if the matrix diffusivity values obtained in the laboratory are representative of the rock adjacent to the channels in contact with the water. Some other cause(s) of the incomplete tracer recovery must be sought.

12.5.4 Discussion

Eosin Y was found to have migrated in substantial quantities to a gallery about 150 m away from the injection point although the drift was located only 18 m away. This indicates that the assumption that all the injected tracer mass moves towards the experimental drift may not be true. In that case the analysis based on this assumption may determine too large specific surfaces and channel widths.

If most of the tracer moved in the direction of the drift the results of the calculations indicate that both matrix diffusion and diffusion into stagnant pools of water may play a role. There are probably other mechanisms which could cause the recovery to be small. One such possible cause is that the injection, although small, compared to the total flowrate may be large when viewed on a local scale. A dipole type of flow may then develop where some of the flow moves away from the drift for some distance before returning to the drift. This would produce a lengthening of the concentration curve tails and a lowering of the tracer recovery during a certain observation time.

12.6 DETERMINATION OF HYDRAULIC CONDUCTIVITY

12.6.1 Overview

The hydraulic conductivity of the rock adjacent to the drift is evaluated based on the assumption that the rock mass may be described, at least, as a homogeneous porous medium and that Darcy's law is valid. Some simplifying assumptions needed to be introduced because the head boundary conditions are not known exactly due to the presence of drifts and tunnels in the old mine. For a homogeneous porous medium the simplifying assumptions would introduce only minor errors and are generally accepted in most other cases which study the properties of fractured rocks.

The hydraulic conductivity can then be obtained from the following expression which is derived by applying Darcy's law to flow to an infinitely long cylinder located in an infinite medium with a constant head far from the cylinder

$$K_p = \frac{Q \ln(r_2/r_1)}{2\pi L \Delta h f} \quad (12.29)$$

where Q is the flowrate to an L m long part of the drift where the water flowrate is measured over a fraction f of the area (the sheets cover 50 % of the area of the drift. The term Δh is the hydraulic head difference between the drift and at points at a distance r_2 from the center of the drift. The radius of the drift is r_1 . The hydraulic head was measured in the three vertical injection holes. Flowrates were measured in about 375 sheets in the upper half of the drift. In addition, ventilation experiments were conducted to measure the inflow to the lower half of the drift and to the access drift.

Hydraulic head measurements

In each of the three vertical 70 m long injection holes, the hydraulic heads were measured prior to the injection of the tracers and after the end of the injection. The measurements were made at the injection points and in the section above the uppermost injection point. Table 12-21 summarizes the obtained heads.

Table 12-21. Hydraulic heads measured in the three injection holes. The expression "head1" indicates measurements when no injection was taking place and "head2" when injection was taking place.

Hole I			Hole II			Hole III			
dist-	head1	head2	dist-	head1	head2	dist-	head1	head2	
ance			ance			ance			
m		m	m	m	m	m	m	m	m
18		135	145	10	120	125	13	195	216
32		180	193	34	172	176	19	205	218
70	200	205	56	204	204	29	202	228	
			70	210	210	37	202	205	
						50	202	203	

Figures 12-15 to 12-18 show a plot of the heads versus the logarithm of the radial distance for each injection hole. For radial flow to an infinite cylindrical hole in a homogeneous medium, the points should lie on a straight line which should intersect the drift at head zero at a distance equal to the radius.

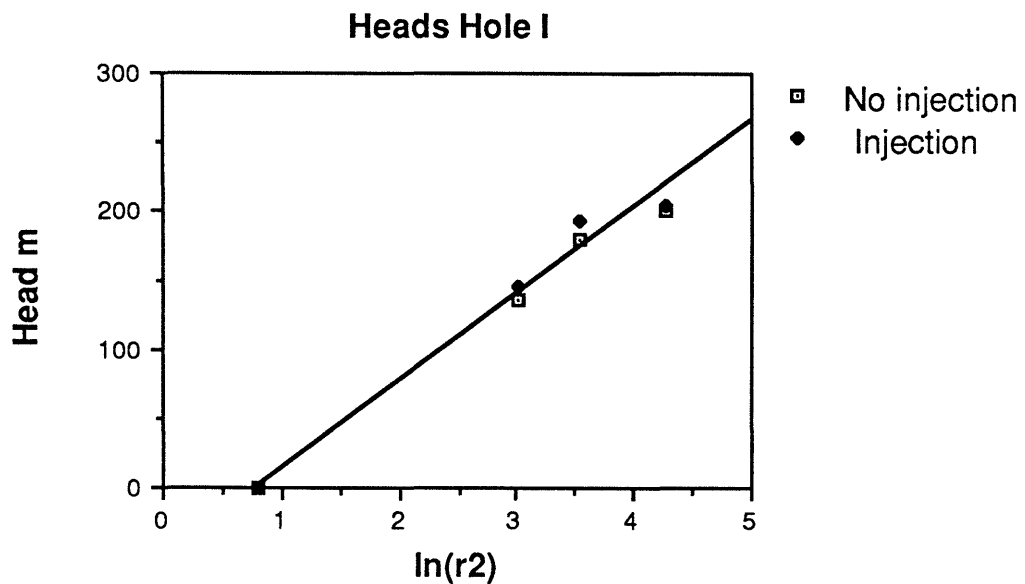


Figure 12-15. Hydraulic heads in hole I.

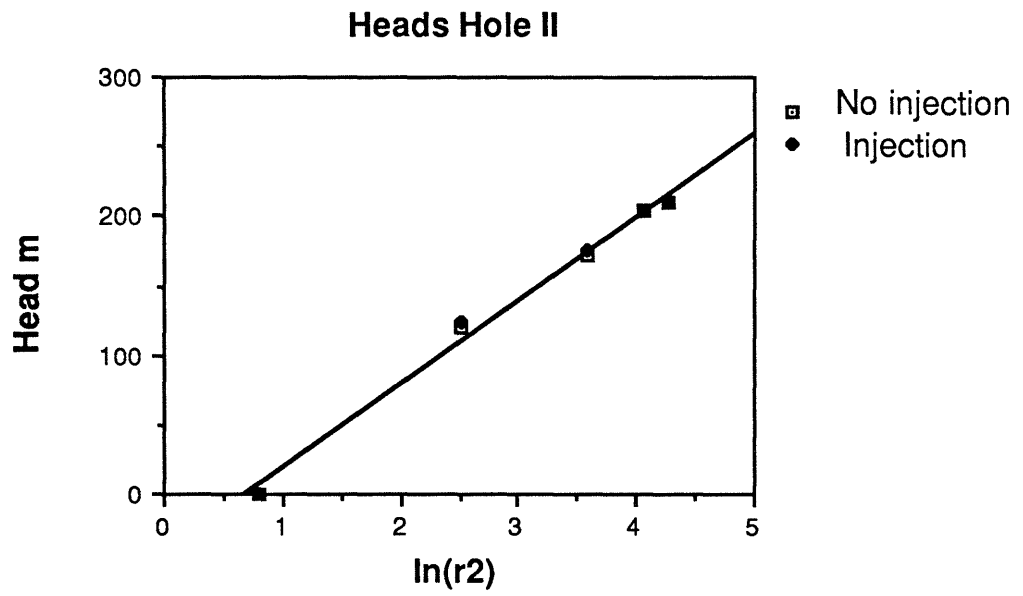


Figure 12-16. Hydraulic heads in hole II.

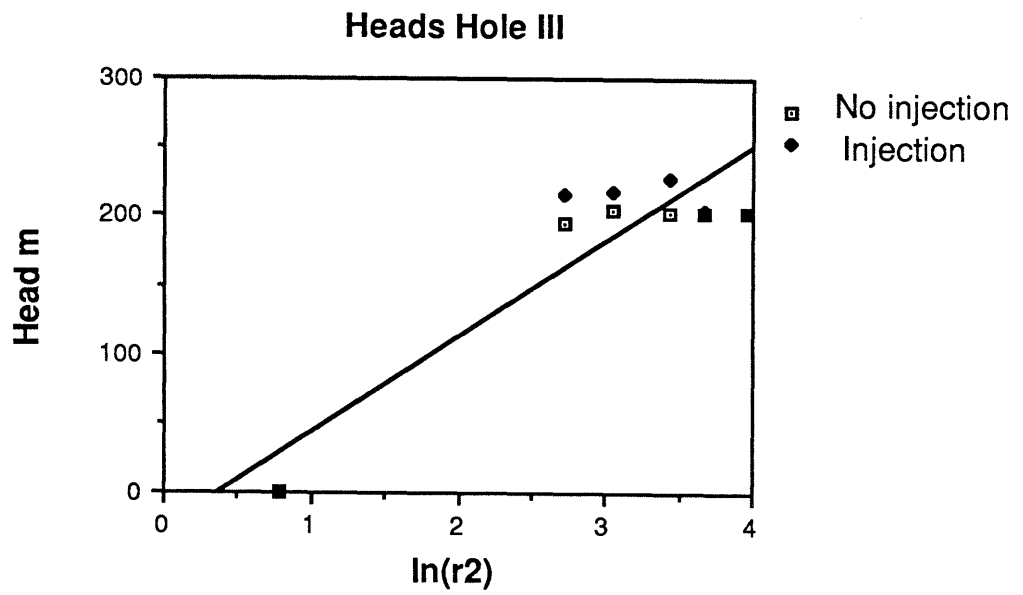


Figure 12-17. Hydraulic heads in hole III.

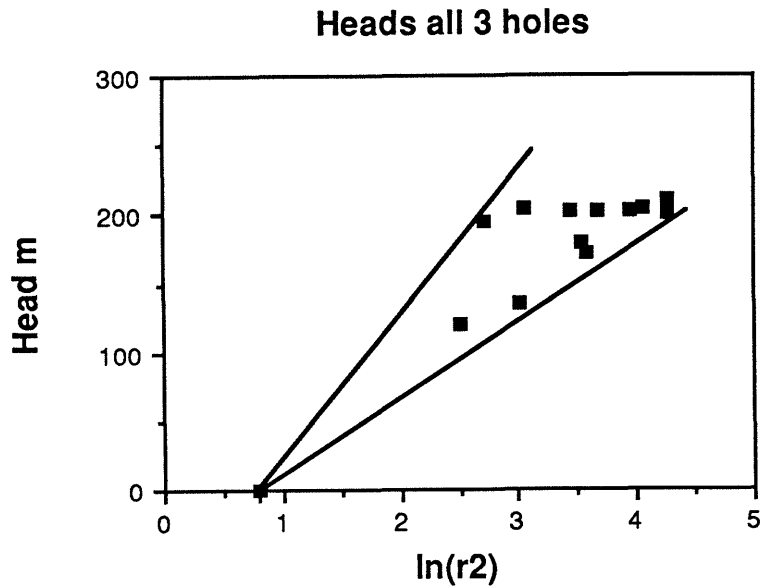


Figure 12-18. Compilation of hydraulic heads in the different injection holes.

In Figures 12-15 and 12-16 all the points are well aligned on the straight line which has been fitted by a least squares fit. In Figure 12-17 the points deviate considerably from the expected straight line indicating that the medium is not homogeneous along hole III. Figure 12-18 shows all the heads in all the holes.

The lines in Figure 12-18 show the upper and lower bounds of the hydraulic head gradients in the three holes.

12.6.2 Flowrate measurements

The flowrates in the individual sheets were measured over a period of more than 2 years. Figure 12-19 shows the variation of the flowrates in the sheets over the monitoring period. During this time two ventilation test series were also performed. In the ventilation test, the test site was sealed off by a wall and the flowrate and humidities of the in and outgoing ventilation air were measured. The moisture contained in the air was found to be equal to the sum of the water flowrate from the lower half of the drift, which was not covered by plastic sheets, and the rate of water loss through the sheets by molecular diffusion. Figure 12-20 shows the measured moisture flowrates.

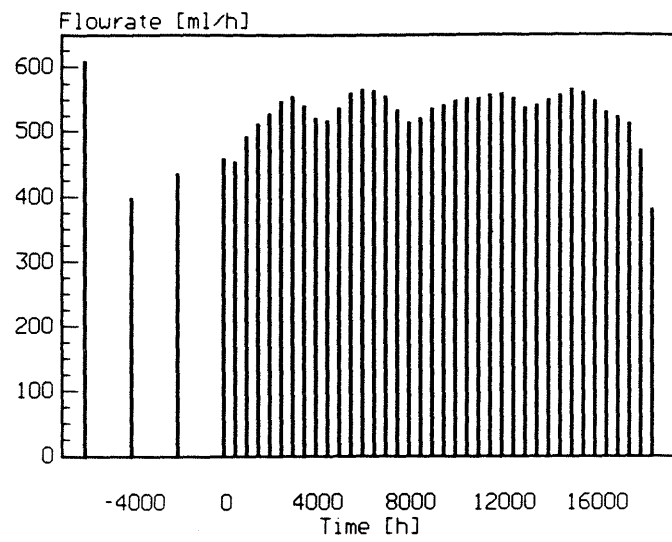


Figure 12-19. Flowrates in the plastic sheets during the measurement period. Average values are for 500 hours.

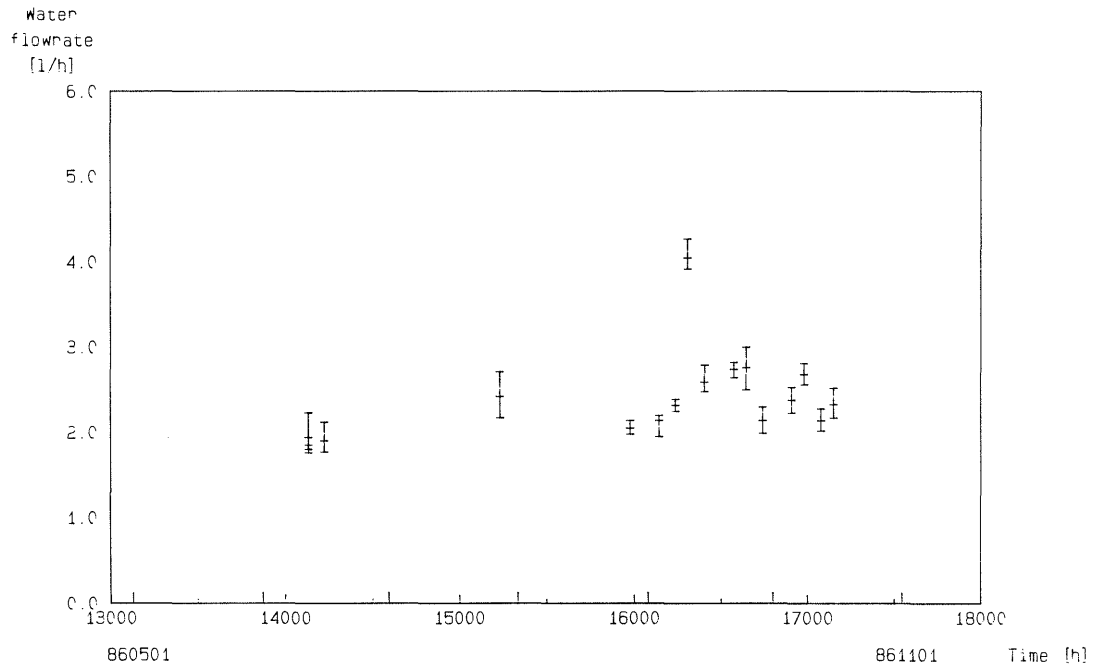


Figure 12-20. Flowrate of the water from the uncovered part of the experimental drift.

The access drift was sealed off in a similar way. The air leaving the experimental site passed through the access drift where more moisture was picked up. The sum of water picked up in the two drifts is shown in Figure 12-21.

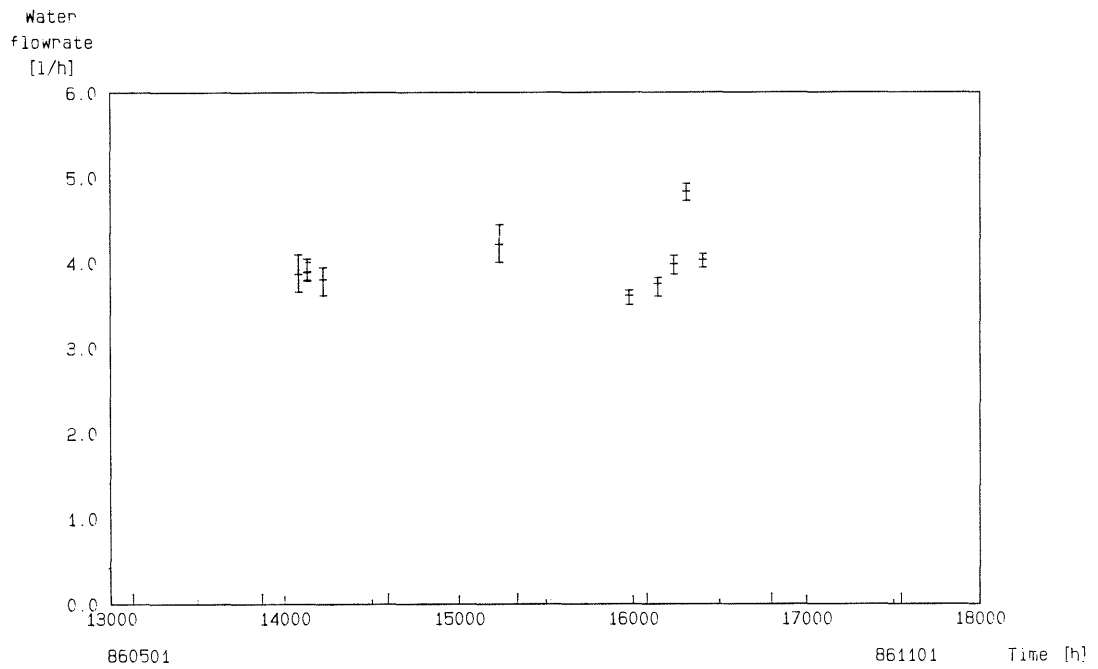


Figure 12-21. Sum of the water flowrates of from the uncovered part of the experimental drift and from the access drift.

Table 12-22 gives the flowrates in the different parts of the drifts.

Table 12-22. Flowrates in the different parts of the drifts.

Part of drift	Flowrate l/h	Length of drift m
Plastic sheets	0.7	100
Bottom part	2.4*	100
Access drift	2	115

* Covered parts of floor + ventilation

12.6.3 Results

Using the above flowrate and head data in Equation 12.29 the hydraulic conductivities of the different parts of drifts are obtained. These values are summarized in Table 12-23.

Table 12-23. Hydraulic conductivities in the Stripa 3-D drifts.

Location	Conductivity $\cdot 10^{11}$ m/s	
	Steep gradient	Low gradient
Experimental drift		
Ceiling + upper sides	0.56	1.07
Floor + lower sides	1.9	3.6
Average	1.3	2.3
Access drift	0.7	1.3

The flowrates varied considerably over the length of the drift and so did the hydraulic conductivities. The data in Table 12-23 were averaged over more than 100 m of drift. The variations within the experimental drift are shown in Figure 12-22 where 10 m averages are shown. It is observed that on a 10 m scale the hydraulic properties of the rock are far from constant. The difference of the hydraulic conductivity between the access drift and the experimental drift is a factor of 2. This may indicate that the 100 m scale is not sufficient enough to obtain reasonably constant average values.

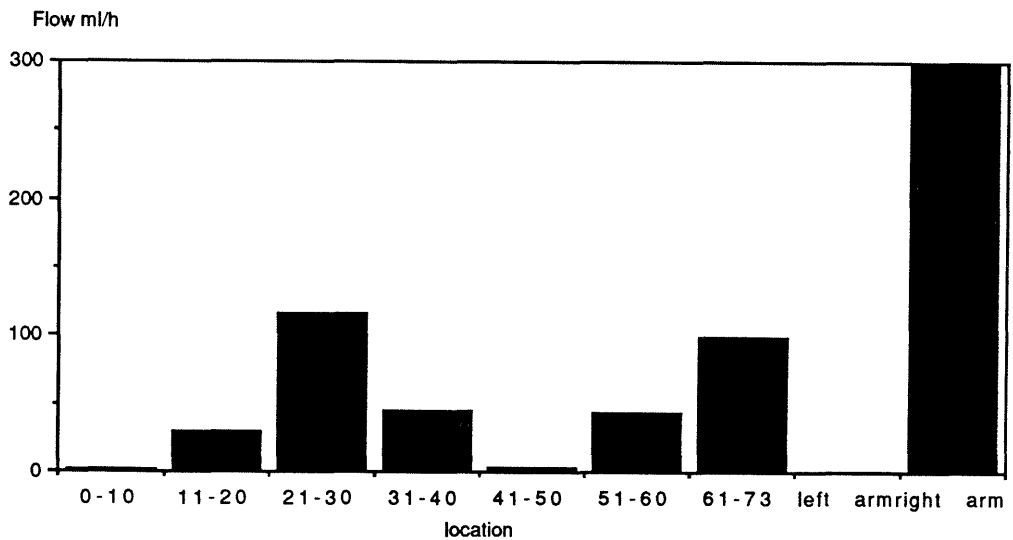


Figure 12-22. Flowrate in the experimental drift averaged over 10 m.

12.6.4 Discussion

A difference exists between the hydraulic conductivities of the upper and the lower parts of the drift. This may be caused by the hydraulic head difference, between the top and bottom of the drift, that drives

the water down and thus collects at the bottom of the drift. If the very steep hydraulic head gradient near the drift is considered (see Figure 12-18), the head difference over the 3 m radial distance is about 60 m. Since the height of the drift is about 3 m, the radial gradient is 20 times larger than the tangential gradient. Therefore, the down flow of water should be negligible in comparison to the inflow provided the conductivity ratio in these directions do not compensate the gradient ratio. At present there is no information available which would indicate such a large conductivity ratio around the drift.

The inflow to the pilot hole in the section that coincided with the drift was 3.0 l/h. This is the same value as was found for the total value from the experimental drift. Thus, the hydraulic conductivity estimated from the flow data to the drift and those from the hole are thus practically identical.

One noteworthy result of the inflow measurements is the large variations along the drift which indicate that even larger areas are needed to reach the size of a REV (Representative Elementary Volume).

12.7 FLOWRATE AND TRACER DISTRIBUTION

12.7.1 Overview

The measurements of flowrates and tracer concentration in every sheet which carries waters make it possible to develop a very detailed assessment of the flowrate and tracer flow distribution. The sheets are 2 m² although there are a few smaller and irregular sheets which were put up after the main covering in spots where there was visual water or tracer seepage. The 375 sheets cover an area of about 700 m². Of these sheets 266 carried no measurable amounts of water. In this section the flowrates of water and tracers from the point of view of "channeling" or uneven distribution over the observation area are analyzed.

12.7.2 Flowrate distribution

The flowrates to the individual sheets varied by about $\pm 10\%$ over the more than two years of monitoring. The variation over 10 m sections along the drift is shown in Figure 12-22. It is observed that the 10 m sections were not large enough to attain the size of a REV at this site.

In Table 12-24 the flowrates in the different sheets, which are grouped in intervals, are shown at a particular point.

Table 12-24. The distribution of flowrates in the Stripa 3-D drift among the 375 sheets.

Flowrate/sheet ml/h	Number of sheets	Flowrate total ml/h	Cumulative % area % flowrate
<0.1	266	0	100.0
0.1- <0.2	13	1.3	29.1
0.2- <0.4	7	1.6	25.6
0.4- <0.8	10	5.6	23.7
0.8- <1.6	20	22.6	21.1
1.6- <3.2	19	46.1	15.7
3.2- <6.4	14	63.0	10.7
6.4- <12.8	12	108.5	6.9
12.8- <25.6	7	124.0	3.7
25.6- <51.2	6	215.0	1.9
>=51.2	1	60.0	0.3
Total	375	647.7	

It can be seen in Table 12-24 that 50 % of flow takes place in about 3 % of all the covered area and that 90 % of the flow comes in about 10 % of the sheets

The number of sheets which carry a certain flowrate are shown in Figure 12-23 below. Note that the flowrate intervals follow a geometric progression with a difference of a factor of 2 between them.

In Figure 12-24 the same data have been plotted to show the flowrate in different flowrate ranges.

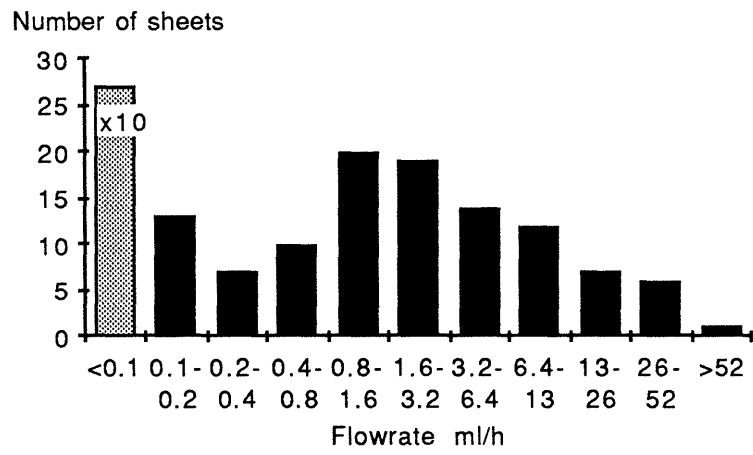


Figure 12-23. The distribution of flowrates among the 375 sheets in the Stripa 3-D drift.

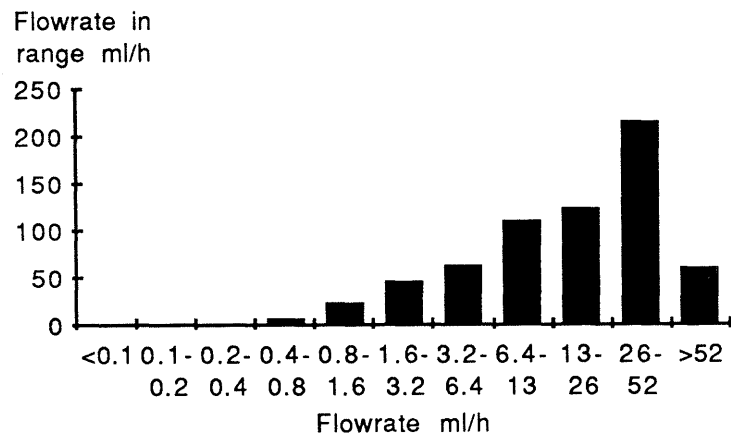


Figure 12-24. Sum of the flowrates in the different flowrate ranges in the Stripa 3-D drift.

12.7.3 Tracer distribution

The tracers arrived in very varying rates in concentration and in water flow to the different sheets. The mass flowrate to a sheet is determined by the product of the flowrate and concentration. The differences in mass flowrates to the different sheets show if any preferential paths may exist. Figures 12-25 - 12-29 show how the tracer recovery is divided among different sheets for the five tracers Eosin B, Uranine, Elbenyl, Eosin Y, and Iodide. The bars in the histograms show how much of a tracer was recovered in a given range of mass recovery. The right hand bar in Figure 12-25 shows that there were four sheets (the figure above the bar) which had a tracer recovery in the range 400-800 mg. The sum of the tracer that arrived to these four sheets is given by the height of the bar.

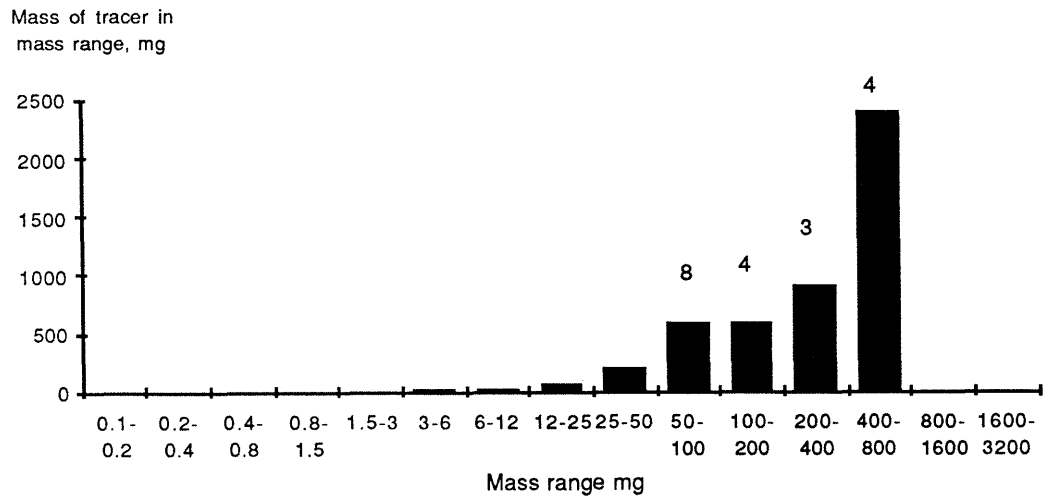


Figure 12-25. Histogram over the recovery of Eosin B in different mass ranges. 43 sheets carried this tracer in measurable quantities.

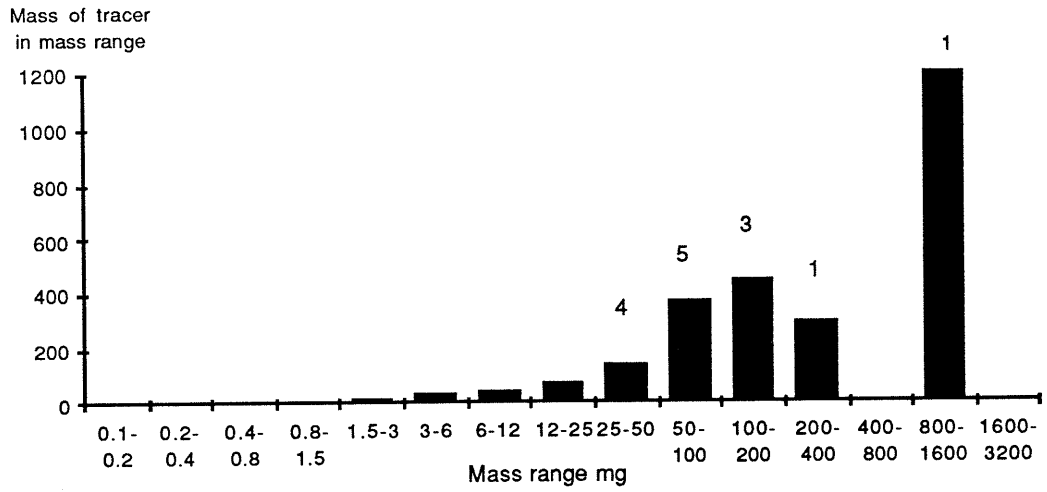


Figure 12-26. Histogram over the recovery of Uranine in different mass ranges. 45 sheets carried this tracer in measurable quantities.

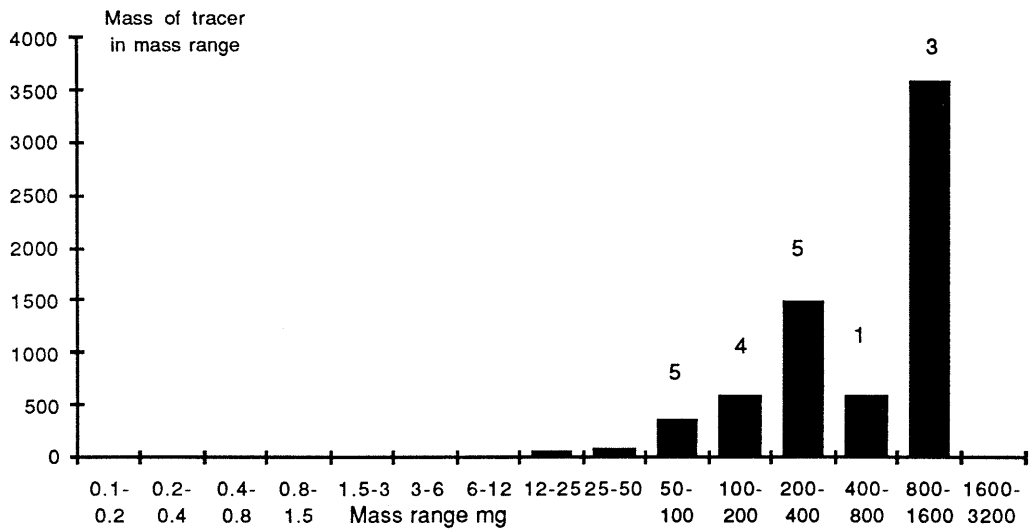


Figure 12-27. Histogram over the recovery of Elbenyl in different mass ranges. 27 sheets carried this tracer in measurable quantities.

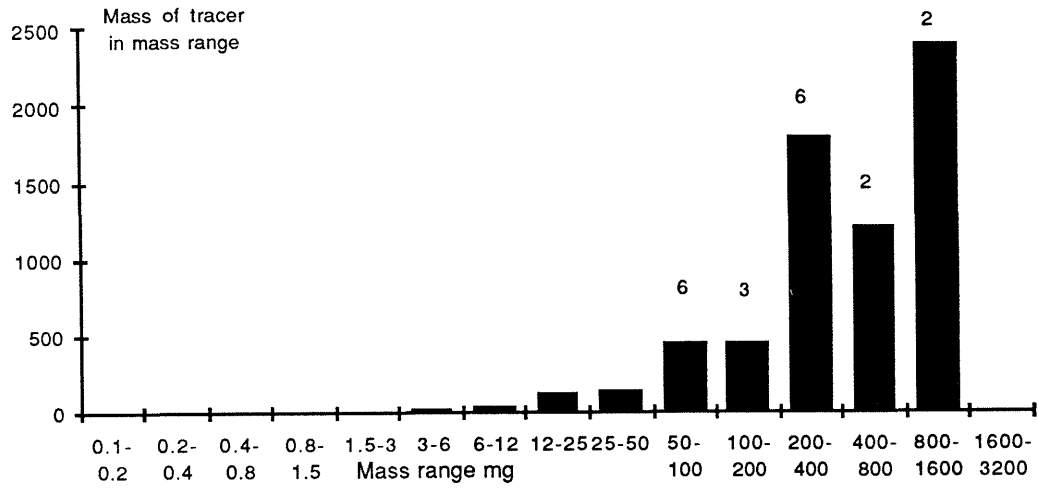


Figure 12-28. Histogram over the recovery of Eosin Y in different mass ranges. 46 sheets carried this tracer in measurable quantities.

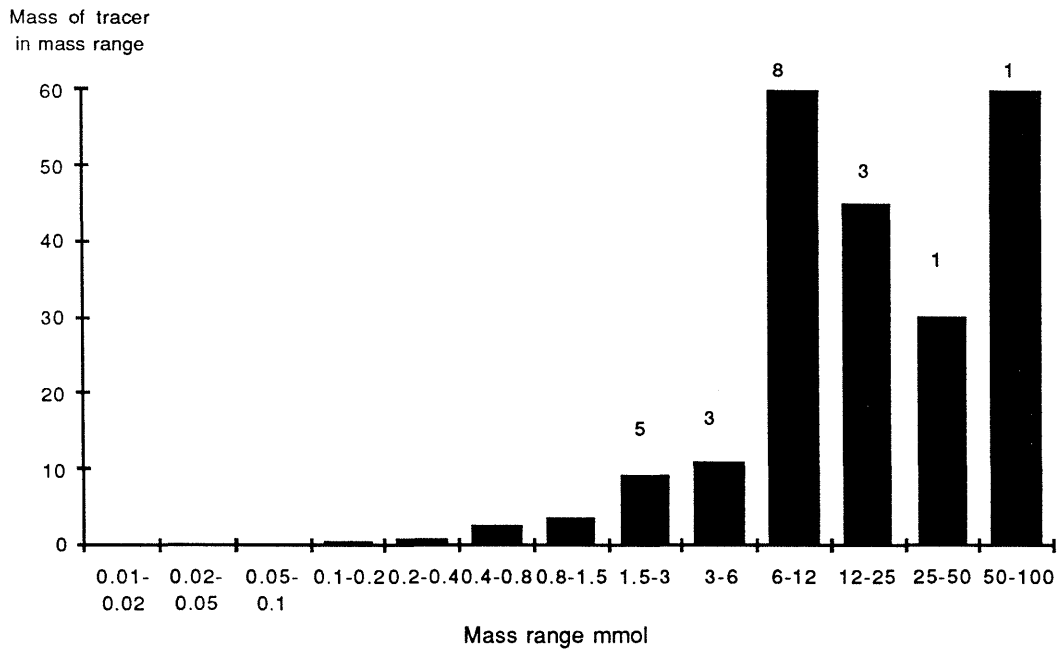
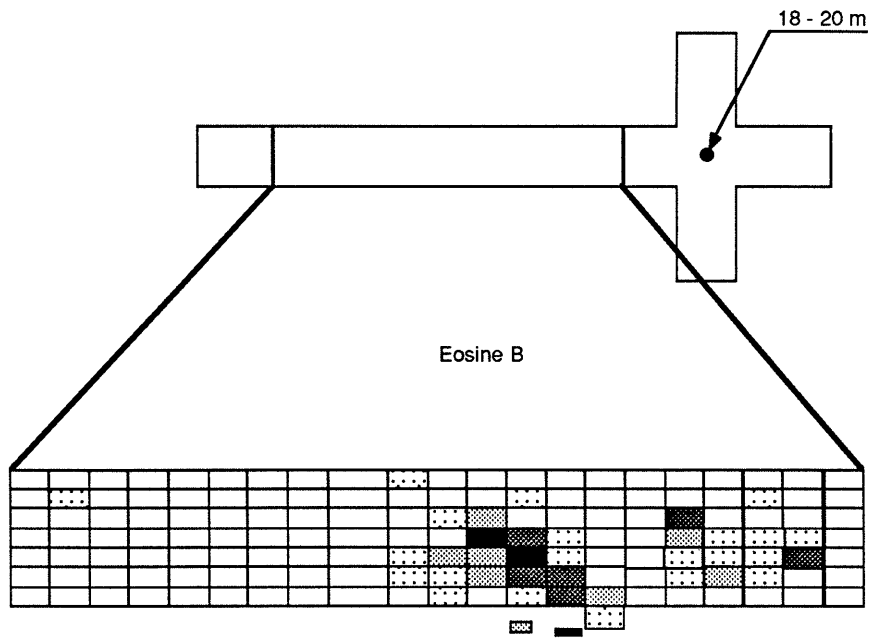


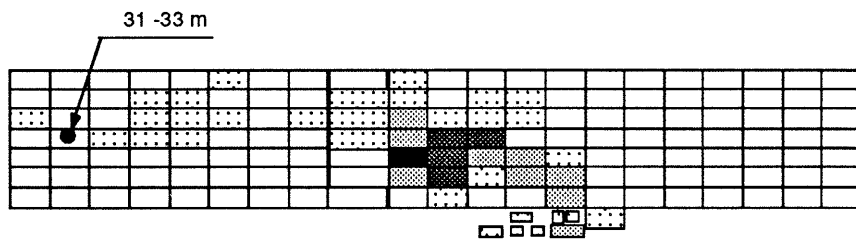
Figure 12-29. Histogram over the recovery of Iodide in different mass ranges. 52 sheets carried this tracer in measurable quantities.

It is seen that for all the tracers 3 to 5 sheets out of 27 to 52 sheets carried more than half the tracer.

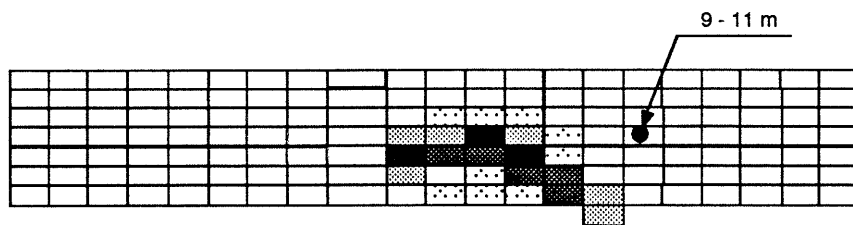
It is shown in Figures 12-30 - 12-34 how the sheets, which carried different mass flows (recoveries) of the tracers, are located in the drift. Figures 7-7 - 7-13 in Chapter 7 show the location of the maximum concentrations.



Uranine

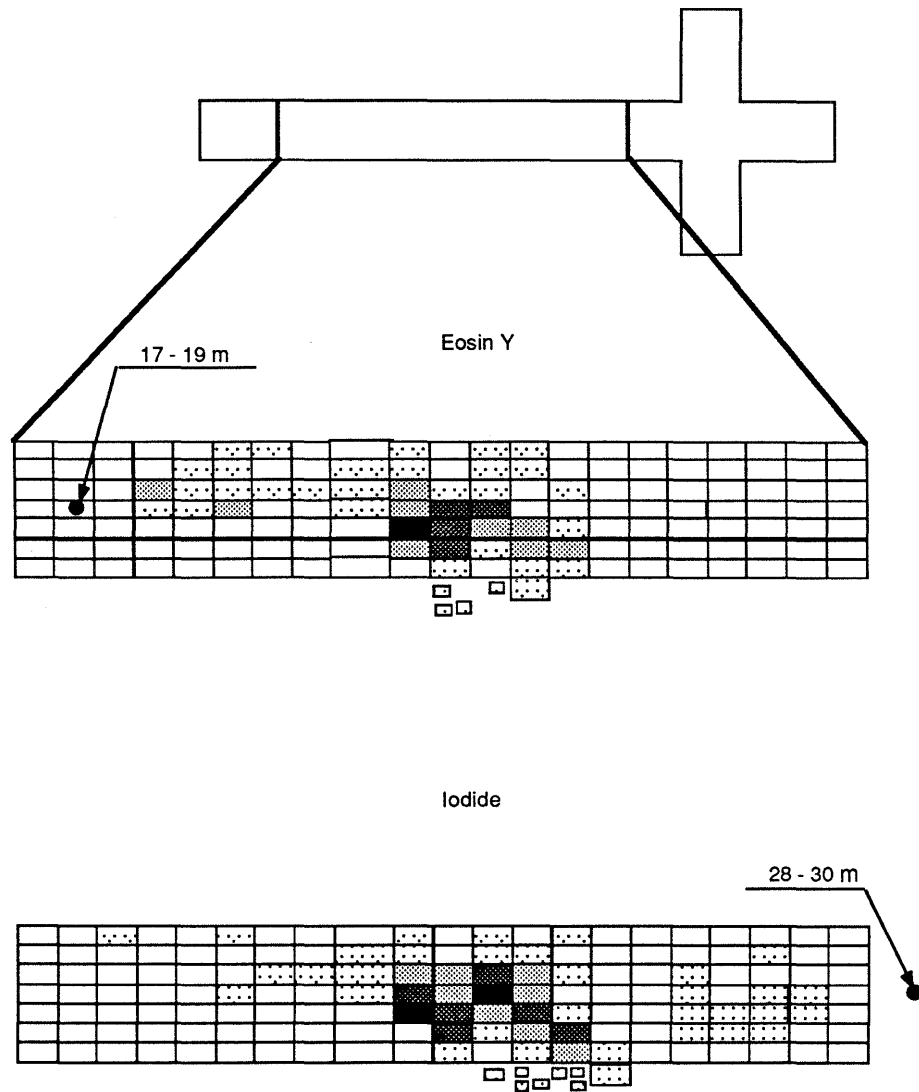


Elbenyl



Figures 12-30 - 12-32.

Location of the sheets where the tracers have been recovered. The darker the sheets are the larger the recovery.



Figures 12-33 - 12-34.

Location of the sheets where the tracers have been recovered. The darker the sheets are the larger the recovery.

12.7.4 Discussion

The distribution of flowrates in the different sheets show that a few spots carried most of the water. This is an indication of channeling. The dimensions of the channels are not known from these observations but Figures 5-2 and 10-2 indicate that the larger flowrates are observed in those parts of the drift where many fracture intersections exist. This may be an indication that the water flows along fracture intersections where the channels are very narrow.

The tracers were spread out among many sheets. It is clear that the tracers were not confined entirely to one or a few channels but spread considerably. However, a small fraction of the sheets carried a large fraction of the tracer.

12.8 SOME OTHER INDICATIONS AND OBSERVATIONS

There are both some indirect observations of channeling and some more direct indications.

The flowrate distribution over the experimental drift as seen in Figure 6-2 shows clearly that adjacent sheets may carry very varying flowrates. One of the 375 sheets carried 10 % of the water. Often the sheets adjacent to a sheet that carried a considerable flowrate was dry or nearly dry. The size of the channels in the fractures were not measured in the experimental drift but observations in other tunnels and drifts in Sweden indicate that channels widths vary from a few centimeters to many tens of centimeters or even a meter or more (Neretnieks, 1987).

The distribution of tracers over the different sheets showed a similar behavior as the flowrate distribution. One tracer Duasyn, which was injected in hole III at 37 m distance from the drift, was first detected in a sheet at the opposite end of the drift. The water where it was found contained very little or none of the other tracers. One conclusion is that Duasyn must have passed over the main area of sheets, where the other tracers were found, without being drawn down into those sheets, see Figures 7-3 and 7-7. The sheets where this tracer was subsequently found had another pattern of travel than that of the other tracers. Duasyn must have traveled in a pathway(s) which bypassed the system of pathways that the other tracers traveled.

Eosin Y which was injected in hole I at 18 m from the drift had a recovery of 34 %. Neither this tracer nor any other tracers were found in any other waters in the mine area that were sampled at intervals during the experimental time. After the sampling was finished in December 1986 and the mining operations were starting for the next phase of the Stripa program, Eosin Y was found in a newly excavated gallery about 150 m away from the injection point. The amounts found were estimated to be on the order of several tens of percent of the total injected mass of this tracer. There were no indications either in the hydraulic head measurements or by any other observations that the tracer should travel in this direction.

Tritium was found in two sheets out of six sheets sampled. Tritium was only found in a few places previously in the water filtrating into the mine. The presence of Tritium indicated that there were paths which carried surface water down to the drift in less than 30 years

time. These paths could be isolated over a distance of several hundred meters from the other paths where there was no detectable concentration of Tritium.

An estimate of the average travel time from the surface can be made by proportioning the travel time for the tracers. The travel time should increase approximately with the square of the distance (for cylindrical symmetry). The travel times for injection distances around 30 m were 5500 and 7000 hours (0.6 to 0.8 years). For a distance of 300 m in the same medium the expected average travel time would be 60 - 80 years. Considering that the rock has a higher conductivity nearer the surface and that an ideal cylindrical symmetry for flow does not exist, a variation of the velocities which would permit a less than 30 year travel time in some paths seems to be reasonable.

In the stand alone appendix "Flowrate curves and tracer breakthrough curves for individual sheets - smoothed data" the tracer concentrations in the different sheets are presented. It is seen that the forms of the concentration curves vary considerably between adjacent sheets. In a medium with frequent mixing of the waters in different paths this would not be the case. This is expected, however, in a medium where there are few opportunities for mixing such as in a medium with separate channels.

Except for the tracer Iodide, where the fitting to theoretical curves indicated a low dispersion, the dispersion of the tracer pulses was large. This is to be expected if there are a few channels with different velocities. If the flow and transport properties of the individual channels and the mixing frequencies are known, the average velocity and dispersion are readily determined (Rasmuson, 1985). A velocity difference of a factor of two in a two channel pathway may cause a dispersion of the magnitude that was observed. It is to be expected that the fewer the channels and the less mixing between the channels the larger will be the differences between the form of different concentration curves. This is clearly noticeable when comparing different curves for the same tracer.

Simulations with fracture network models (Schwartz and Smith, 1987) show that dispersion in networks of channels have quite considerable tailing which would be interpreted as large dispersion. It was noted earlier that dispersion increased when fewer channels participated in the transport and that preferential paths may develop even in systems with many fractures but where the hydraulic properties vary between the fractures.

Tsang et al. (1987a, 1987b) and Moreno et al. (1987a, 1987b) have made a series of simulations of flow and tracer transport in individual fractures which are modeled as having a stochastic variable aperture in the whole plane of the fracture. The simulations show that the water flows in a few major preferred paths which sometimes divide into and sometimes combine into new paths but always show a distinct channel pattern. The tracer simulations show long tailing and a large variability between different simulations even in cases where the statistical properties of the generated fractures are the same.

Rasmuson (1985) has used analytical moment methods to study the impact of mixing between different pathways on the average travel times and on the dispersion in the ensemble of channels. The analysis shows that when the differences in conductivity between channels

increases an increasingly larger number of mixings must take place before the dispersivity becomes constant in the medium.

In the present experiments the properties of the concentration curves resemble those of the simulated curves described above in the sense that very variable results are obtained in nearby locations and that the dispersion is large.

SUMMARY OF MAIN RESULTS, DISCUSSION, AND CONCLUSIONS

The results of the investigation will be discussed in relation to the aims that were stated at the outset of the project. They were:

1. Develop techniques for large scale tracer experiments in low permeability fractured rock
2. Determine flow porosity
3. Obtain information on longitudinal and transverse dispersion
4. Obtain information on channeling
5. Obtain data and other information for validation and/or modification of models.

13.1

DEVELOPMENT OF TECHNIQUES FOR TRACER TESTS

The single most prominent feature of the present investigation was the use of a multitude of plastic sheets in a long underground drift. The use of a drift located well below the water table ensured that the water flow would mainly be directed towards the drift from practically all the tracer injection points. The use of a 100 m long drift with about 375 plastic sheets made it possible to monitor the flowrate and tracer transport in detail which cannot be done by other known techniques such as "between hole tracer tests." Most of the information obtained with the present technique, e.g. variability of conductivity and channeling, is difficult, if at all possible, to obtain with other methods.

There are some drawbacks with using a drift. One is that the presence of the drift itself influences and changes the rock stresses in the vicinity of the drift. The influence is estimated to extend between 1 and 2 tunnel diameters. Most of the distance covered by the tracers is thus in the "undisturbed" rock. The water velocity in a porous medium increases inversely proportional to the square of the radial distance to the drift. The residence time of the tracers in the disturbed zone is thus expected to be a very small fraction of the total residence time. The tracers will have traveled mostly in the undisturbed rock.

The situation is somewhat different for the flowrate distribution over the covered drift surface. It is known that the rock stresses will influence the conductivity of the fractures. Some may become less and some more permeable depending on how they are located in the stress field. There are at present no methods to determine how an individual fracture in a drift may have changed its conductivity. Our concepts of how water flows in fractured rock is that the water flow takes place in individual channels in the plane of fracture. The channels are widely spaced and most of the fracture is closed. It is in the closed sections of the fracture that the rock stresses are transmitted. The open sections of the fracture are not in contact with each other. An increase or decrease in the rock stress is anticipated to close or open

the already open channels to some extent but not to radically redistribute the channels within the fracture plane or to drastically change the number of channels. The general picture of the water flowrate (and conductivity) distribution over a large section of the rock may well be maintained. This must, however, be investigated further.

Several of the the details of the experimental techniques were developed within the experiment. The packers used to seal off the injection holes everywhere except at the injection point were made of swelling bentonite. This ensured that there could be no bypassing of water along the injection holes and that there could be no packer failure due to loss of inflation pressure or failure of rubber elements. The tracer pathways are definitely known to be in the rock mass.

A multitude of potential tracers (>100), mostly organic dyes, were tested for stability, detectability, sorption properties, etc. Several new tracers were synthesized to obtain special large molecular weight tracers with low diffusivities. Only a few of the tested dyes had properties which permitted their use as tracers in this type of investigation. In all 11 tracers were found to be usable and were used. Most of them have not been used previously in tracer tests.

Ventilation tests were performed in the drift at two constructed wooden frame walls that were covered with plastic sheets and sealed with foamed plastic. These walls were quick and cheap to build and gave valuable information on water flowrates in the uncovered part of the drift.

Samples were taken for Tritium analysis in several sheets and at other locations on two occasions. Tritium was found to be present in two of the six sampled sheets. Had the samples instead been taken from the mixed water of the sheets, the Tritium concentration would have been below the detection limit. The presence of Tritium in the waters indicate the presence of fast nearly isolated channels of small extent. Probably such channels would have gone unnoticed had not the plastic sheeting technique been used.

Fracture mapping in the drift was made visually and by stereo photography. The latter technique proved to be fast and is readily computerized.

13.2

FLOW POROSITY

The flow porosity was determined for 6 different tracers using information on flowrates, residence times of tracers, and flow distribution.

Because of the large variations in flowrate in different sheets and over different sections of the drift it was not obvious how the averaging of the data was to be done. The entity "flow porosity" is by nature an averaged property. The averaging volume must be large enough for the property to become reasonably constant for it to have a well defined meaning. The flowrate variations were too large and too irregular in the drift for it to make up a large enough rock volume. Still we wish to assess this entity in some well defined way. Two approaches were explored. In the first it was assumed that all the water flowrate to all of the drift was the representative flux. The residence time for this water would be represented by the residence times of the different

tracers from the different injection distances. This approach would assume that the drift as a whole makes up a representative volume. It is known, however, that most of the water to the drift (end and right arm) carried no tracer. The residence time of this water is thus not known. In the second approach we chose not to include this water flowrate in the evaluations. Only that section (length) of the drift where the traced water was collected was used as a representative rock area. The water flowrate in that section and the residence time of that water was used in the calculations.

Even so, there still remained some uncertainties in the porosity values. The length section of drift used in the calculations contained some dry areas which were included. Other dry areas of rock are located immediately adjacent to sections used. The unresolved question is how large a portion of the adjacent dry rock belongs to the section of wet rock. The porosity values may be representative for the wet part of the rock but then there is an unknown mass of "dry" rock which has a porosity equal to zero.

The porosity was found to decrease with distance from the drift. The values for the rock far from the drift were found to be on the order of $2 \cdot 10^{-5}$ - $7 \cdot 10^{-5}$, the porosity in the 10 m nearest the drift was found to be $15.5 \cdot 10^{-5}$ which indicates that the presence of the drift has increased the porosity.

The water residence times which were used to estimate the porosity varied considerably between sheets. Also the residence times for major flow paths and averaged flow paths were quite variable. These and other observations indicate the presence of channeling. This adds further the need to use the average properties with considerable caution. The presence of Tritium in some sheets, for example, indicates that there is some part of the porosity which is not well connected to other parts of the rock porosity.

13.3 LONGITUDINAL AND TRANSVERSE DISPERSION AND CHANNELING

Three mechanisms for "dispersion" have been modeled: hydrodynamic dispersion, channeling, and matrix diffusion effects. Hydrodynamic dispersion is modeled as Fickian diffusion. It can be quantified as a Peclet number, Pe , a dispersion length, α , or as dispersivity, D_L . Channeling has been modeled as if flow were to take place in a multitude of independent channels with a known property distribution. The distribution of channel apertures is modeled as being lognormal and the cubic law is assumed to be valid. The channeling can be quantified by a single entity, the standard deviation in the lognormal distribution of apertures. Other ways of describing channeling are known, e.g. by assuming a given number of channels, 2, 3, 4, or more, each having known characteristics. In the latter approach at least one parameter value must be assigned to each channel and it is our experience that such values seldom can be uniquely chosen. If no independent information is known for the channels this approach gives dubious results.

When the channels are few the first approach is not good either because it implicitly assumes that the statistics apply to large number of channels. It does, however, not over interpret the available information.

The evaluated Peclet numbers range from very low values, less than 4 to about 35. Values less than 4 indicate that the transport to a large extent is dominated by dispersion. For values of $Pe < 1$, as was found in many of the fitted curves, the hydrodynamic dispersion description is very dubious. In molecular diffusion situations it would imply that the molecular diffusion in the mobile water dominates the transport of the tracer over that induced by advection. In the present case the dispersion is induced by the advection and it is not easily conceived how advection can be neglected in comparison to the dispersion if the latter is induced by the former. Seemingly very low Peclet numbers (high dispersion) are easily attained when there are channels which have different velocities and which do not mix their waters much over the travel distance. It may be illustrated by the following: A system of two channels which have the same flowrate, no dispersion, but where the velocity in one channel is two times that in the other, would have a $Pe=2.5$ if evaluated by the method of moments.

The models used do not describe some of the important causes of dispersion and attempt to force the parameter values to account for processes which they cannot do. This is clearly seen in the fitted concentration curves. The model results cannot describe the several ups and downs in the experimental curves. Furthermore the experimental curves in adjacent sheets with the same tracer in many cases are quite dissimilar. This indicates that there either must be very large differences in the values of the dispersivities and velocities in the different pathways to the different sheets or that there are mechanisms which cause these variations that have not been modeled. If the former is true then there are strong differences between adjacent pathways, which would be termed channeling. If there are unmodelled processes, then one of them may be the transport in several pathways. This is supported by other information such as the presence of Tritium in some sheets and the very large variations in the ratios between tracers in adjacent sheets. If there was a regular mixing constantly occurring then this is the basis for the concept of hydrodynamic dispersion the curve forms and the ratios in adjacent sheets would behave in a much more regular way.

The transverse spreading of the tracers to many different sheets which most often contain different fractures indicates that the tracers have spread to several channels in one fracture and that they have spread from the channels in one fracture to channels in other fractures. This would be called transverse dispersion in a homogeneous porous medium and could be quantified by a transverse dispersivity. In this case where the flowrates are so very variable between the sheets we have found no meaningful way to evaluate an equivalent transverse dispersivity. The tracers will follow the water and will of course not be found in the dry areas of the rock. Most of the tracers have spread to a very large part of the sheets in the center of the drift where there is water flow. A visual inspection of the spread of the tracers can be observed in Figures 12.30–12.34. The tracers have spread out over the entire covered width of the drift (7 m) and for 10 to 20 m along the drift. This has taken place over travel distances which vary between 10 m and more than 30 m. The spreading may have occurred gradually along the travel path but it may also be argued that it may have taken place mostly near the drift where the porosity has increased due to the presence of the drift. The latter case is not probable because

there are large variations in the curve forms and in the ratios of tracer concentrations between very nearby sheets. Also the tracer concentration ratios do not seem to vary in a regular fashion.

The rock matrix is known to be porous and to contain stagnant water. It seems also probable that there are stagnant or near stagnant pools of water in the fractures themselves. The tracers may migrate in and out of these stagnant waters by molecular diffusion. This will cause a pulse to spread in a way similar to that caused by hydrodynamic dispersion. It will also withdraw the tracer from the mobile water and cause less than a full recovery of the tracer to be attained.

Measurements of the matrix diffusion properties of the used tracers in Stripa granite have been performed. Models including the matrix diffusion effects have been used to fit the tracer curves. The fits improved only marginally. A more sensitive approach was also taken, namely to try to attribute the loss of tracer to the diffusion into stagnant pools of water. Five tracers, (four dyes and Iodide) were used for this analysis. A fourth dye only arrived in so few sheets and in such small quantities that it was not used. Bromide could not be used because its recovery could not be determined with sufficient accuracy due to interference from Iodide.

The results show that for the tracer to have been taken up by the rock matrix, fracture spacings (equivalent water carrying fractures) for the dyes of between 7 to 40 cm and for Iodide between 50 and 100 cm are needed. These values are probably much too small considering that about 100 fractures are visible in the whole drift of 100 m. The diffusivity data used were for intact rock. It is known from other measurements that the rock and fracture coating or alteration materials adjacent to water conducting fractures may be much more porous and have much higher diffusivities. If this is the case then the matrix diffusion effects may still have played an important role in these experiments.

It was attempted to experimentally investigate this by simultaneously injecting a small readily mobile molecule, Flouride, together with a large molecular weight molecule, STR-7, which was specifically synthesized for the purpose. STR-7 is based on a polyethylene-glycol of molecular weight 15,000. Both molecules were injected simultaneously at the injection zone where Uranine was previously injected. The injection of Uranine was also continued during the same time. Neither Flouride nor STR-7 could be found in the sheets where Uranine was found. The reason for this is not known but it is suspected that at about the time when the two new tracers were injected a new pathway leading not to the drift but to some other tunnel may have opened. The reason for this suspicion is that the Uranine curves behave as if the Uranine injection also was discontinued.

The diffusion into stagnant water in the fracture was also explored. For Uranine, Elbenyl, and Iodide this effect may contribute noticeably but it probably has a small effect for Eosin B and Eosin Y. This latter effect is more speculative than the matrix diffusion because many assumptions must be made regarding the geometry and quantity of the stagnant water zones.

Similar effects may be caused by the slow flow into semi-stagnant pools of water. There is even less information available for speculations on this process.

13.4

OBSERVATIONS TO MODIFY CONCEPTS AND MODELS

The water flow is very unevenly distributed over the investigated portion of the rock. There are large dry areas extending over many tens of meters. If the Stripa rock is representative for low permeability granites, then the use of porous medium models with essentially constant properties may give results with unknown and probably large errors for water flow and especially for tracer transport.

The results of the tracer experiments and the Tritium measurements give strong support to the notion that a non-negligible portion of the flow takes place in channels which have little contact with other main channels. This cannot be treated by the models which have been applied in the analysis of the experiment. A probably fruitful avenue would be to try to incorporate the variability in the models. So called stochastic models are available for porous media and some attempts to apply them to this type of rock have been made recently (Gelhar, 1987). These models need considerable amounts of data to obtain the statistic properties. They also must be made to incorporate the correct processes.

The mechanisms of diffusion into stagnant pools of water, matrix diffusion, and the frequency of mixing and especially that of the non-mixing of channels will have to be studied more.

NOTATION

a, a'	specific surface	m^{-1}
A	parameter defined in eq. 12.8	$s^{1/2}$
A	surface area	m^2
B	parameter defined in eq. 12.10	$m/s^{1/2}$
C	concentration in mobile fluid	mol/m^3
C_p	concentration in pore fluid	mol/m^3
C_o	concentration at inlet boundary	mol/m^3
DF	dilution factor	—
d_p	particle diameter	m
D_e	effective diffusivity	m^2/s
D_L	dispersion coefficient	m^2/s
D_p	pore diffusivity	m^2/s
D_w	diffusivity in bulk liquid	m^2/s
E	parameter defined in eq. 12.26	
G	parameter defined in eq. 12.25	
h	hydraulic head	m
k	constant	—
K	volumetric distribution coefficient	—
K_a	distribution coefficient for surface sorption	m
K_d	distribution coefficient for volume sorption	m^3/kg
k_p	hydraulic conductivity	m/s
L	slab thickness	m
M	amount of diffusing component	mol
N	flowrate of diffusing component	mol/s
Pe	Peclet number vz/D_L	—
q	concentration in solid phase	mol/kg
Q	flowrate of water	m^3/s
r	radial direction	m
R	retardation factor in general	—
R_a	retardation factor due to surface sorption	—
R_d	retardation factor due to volume sorption	—

S	fracture spacing	m
t	time	s
t_0	residence time for tracer	s
t_R	relative residence time	—
t_w	residence time for water	s
v	water velocity	m/s
V_s	volume of rock	m^3
x	distance into rock	m
z	distance in flow direction	m
α	capacity factor	—
δ	fracture aperture	m
δ_c	fracture aperture determined by "cubic law"	m
δ_f	fracture aperture from residence time	m
δ_l	fracture aperture from laminar velocity	m
ϵ_f	porosity of mobile fluid	—
ϵ_p	porosity of rock matrix	—
ϵ_t	"transport porosity" of matrix	—
λ	decay constant	s^{-1}
η	penetration depth	m
ρ_p	density of rock matrix	kg/m^3
ρ_s	density of solid proper	kg/m^3
ξ	integration parameter	—
σ_ℓ	logarithmic standard deviation of fracture widths	—
σ_z	standard deviation of water travel distance	m
σ_t	standard deviation of water residence time	s
ℓ	parameter defined in eq. 12.8	—

LITERATURE

Abelin, H., I. Neretnieks., S. Tunbrant, and L. Moreno, Final report of the migration in a single fracture – Experimental results and evaluation. Stripa Project Technical Report 85-03, Stockholm 1985.

Bear, J., Hydrodynamic dispersion, in flow through porous media, edited by R.J.M. de Wiest, Academic, New York, 1969.

Bird, R.B., Stewart, W.E., Lightfoot, E.N., Transport Phenomena, Wiley, 1960.

Birgersson, L., and I. Neretnieks, Diffusion in the matrix of granitic rock. Field test in the Stripa mine. Scientific Basis for Nuclear Waste Management V, Berlin, June 1982, Elsevier, 1982, p. 519.

Birgersson, L., and I. Neretnieks, Diffusion in the matrix of granitic rock. Field test in the Stripa mine. Scientific Basis for Nuclear Waste Management VII, Boston, Nov. 1983, Elsevier 1984, p. 247.

Bourke, P.J., Durrance, E.M., Heath, M.J., and Hodgkinson, D.P., Fracture hydrology relevant to radionuclide transport, Atomic Energy Research Establishment, Harwell, England, AERE-R 11414, January 1985.

Brace, W.F., Walsh, J.B., and Frangos, W.I., Permeability of granite under high pressure, J. Geophys. Res. 73, 1968, p. 2225.

Bradbury, M.H., Lever, D., and Kinsey, D., Aqueous phase diffusion in crystalline rock, In: Scientific basis for nuclear waste management V, Berlin 1982, Elsevier, 1982, p. 569-578.

Carlsson, L., Winberg, A., and Grundfelt, B., Model calculations of the groundwater flow at Finnsjön, Fjällveden, Gideå and Kamlunge, KBS TR 83-45, May 1983.

Crank, J., The mathematics of diffusion, 2nd Ed., Oxford University Press, New York, 1975.

Carslaw, H.S., Jaeger, J.C., Conduction of heat in solids, 2nd Ed., Oxford University Press, New York, 1959.

de Josselin de Jong, G., Longitudinal and transverse diffusion in granular deposits, Eos. Trans. AGU, 39, 1958, p. 68.

Gelhar, L.W., Applications of stochastic models to solute transport in fractured rocks. Report, Massachusetts Institute of Technology, January 1987.

KBS – technical reports can be obtained from INIS CLEARING HOUSE, International Atomic Energy Agency, P.O. Box 100, A-1400 VIENNA, Austria.

Gelhar, L.W., and Axness, C.L., Three-dimensional stochastic analysis of macro dispersion in aquifers, *Water Resources Res.* 19, 1983, p. 161-180.

Gustavsson, E., and Klockars, C-E., Studies on groundwater transport in fractured crystalline rock under controlled conditions using non-radioactive tracers, KBS TR 81-07, 1981.

Landström, O., Klockars, C-E., Persson, O., Andersson, K., Torstenfelt, B., Allard, B., Larsson, S.Å., and Tullborg, E.L., A comparison of in situ radionuclide migration studies in the Studsvik area and laboratory measurements, In: *Scientific basis for nuclear waste management V*, Berlin, June 1982, Elsevier 1982, p. 697-706.

Lapidus, L., and Amundsen, N.R., Mathematics of adsorption in beds, *J. Phys. Chem.* 56, 1952, p. 984.

Maloszewski, P. and Zuber, A., On the theory of tracer experiments in fissured rock with a porous matrix, Rapport 1244/17P, Institute of Nuclear Physics, Cracow, 1984.

Matheron, G., and de Marsily, G., Is transport in porous media always diffusive? A counterexample, *Water Resources Res.* 6, 1980, p. 901.

Mercado, A., The spreading pattern of injected water in a permeability stratified aquifer, Symposium of Haifa: Artificial Recharge and Management of Aquifers, March 19-20, IAHS-AISH Publ. 72, 1967, p. 23.

Moreno, L., I. Neretnieks, and C-E. Klockars, Evaluation of some tracer tests in the granitic rock at Finnsjön. KBS Technical Report 83-38, Stockholm 1983.

Moreno, L., I. Neretnieks, and T. Eriksen, Analysis of some laboratory tracer runs in natural fissures, *Water Resources Res.* 21, 1985, p. 951-958.

Moreno, L., Y.W. Tsang, C.F. Tsang, F.V. Hale, and I. Neretnieks, Flow and tracer transport in a single fracture. A stochastic model and its relation to some field observations. Manuscript submitted to publication 1987.

Moreno, L., Y.W. Tsang, C.F. Tsang, and I. Neretnieks, Flow and solute transport in a single fracture. A two-dimensional statistical model. Nuclear Fuel Safety Project, Technical report, Stockholm, 1987.

Neretnieks, I., Diffusion in the rock matrix: An important factor in radionuclide retardation? *J. Geophys. Res.* vol 85, p 4379-4397, 1980.

Neretnieks, I., A note on fracture flow mechanisms in the ground, *Water Resources Res.* 19, 1983, p. 364-370.

Neretnieks, I., Transport in fractured rock. Paper at the IAH 17th International Congress on the Hydrology of Rocks of Low Permeability, Tucson, Arizona, Jan 1985, Proceedings.

Neretnieks, I., Channeling effects in flow and transport in fractured rocks - Some recent observations and models. Paper presented at GEOVAL symposium, Stockholm, April 1987. Proceedings in print.

Neretnieks, I., Eriksen, T., and Tähtinen, P., Tracer movement in a single fissure in granitic rock: Some experimental results and their interpretation, *Water Resources Res.* 18, 1982, p. 849.

Neretnieks, I., and A. Rasmuson, An approach to modelling radionuclide migration in a medium with strongly varying velocity and block sizes along the flow path. *Water Resources Res.* vol 20, 1984, p. 1823.

Nordström, D.K., Hydrogeological and hydrogeochemical investigations in boreholes – Final report of the phase I geochemical investigations of the Stripa groundwaters, Stripa Project Report 85-06, 1985.

Rasmuson, A., and Neretnieks, I., Exact solution of a model for diffusion in particles and longitudinal dispersion in packed beds, *AIChE J.* 26, 1980, p. 686-690.

Rasmuson, A., Analysis of hydrodynamic dispersion in discrete fracture networks using the method of moments, *Water Resources Res.*, 21, 1985, p. 1677-1683.

Sauty, J.P., An analysis of hydrodispersive transfer in aquifers, *Water Resources Res.* 16, 1980, p. 145.

Schwartz, F.W., Macroscopic dispersion in porous media: The controlling factors, *Water Resources Res.* 13, 1977, p. 743.

Schwartz, F.W., Smith, L., An overview of the stochastic modelling of dispersion in fractured media. In *Advances in transport phenomena in porous media*. Nato ASI series E, Applied Sciences no 128, Ed. J. Bear and M.Y. Corapcioglu, Martinus Nijhoff publ. 1987, p. 727-750.

Skagius, K., and I. Neretnieks, Measurements of cesium and strontium diffusion in biotite gneiss, SKB Technical Report 85-15, Stockholm 1985.

Skagius, K., and I. Neretnieks, Porosities and diffusivities of some nonsorbing species in crystalline rocks. *Water Resources Res.* vol 22, p. 389, 1986a.

Skagius, K., and I. Neretnieks, Diffusivity measurements and electrical resistivity measurements in rock samples under mechanical stress. *IBID* 22, p. 570, 1986b.

Skagius, K., Diffusion of dissolved species in the matrix of some Swedish crystalline rocks. Ph.D. Thesis, Dept. Chemical Engineering, Royal Institute of Technology, May 1986.

Snow, D.T., Rock fracture spacings, openings and porosities, *J. Soil Mech. Found. Div. Am. Soc. Civ. Eng.*, 94, 1968, p. 73.

Tang, G.H., E.O. Frind, E.A. Sudicky, Contaminant transport in fractured porous media. An analytical solution for a single fracture, *Water Resources Res.* 17, 1981, p. 555.

Tsang, Y.W. and C.F. Tsang, Channel model of flow through fracture media, *Water Resources Res.*, Vol, 23, No. 3, pp. 467-479, 1987a.

Tsang, Y.W., C.F. Tsang, and I. Neretnieks, Some properties of a channeling model of fracture flow, *Sven. Kärnbränsleförsörjning Technical Report, Nuclear Fuel Safety Project, Stockholm, in press, 1987b.*

ACKNOWLEDGEMENTS

This work was performed within the OECD/NEA International Stripa Project managed by the Swedish Nuclear Fuel and Waste Management Co. We gratefully acknowledge the financial support and the never failing encouragement and help from the initiator of the project Lars B. Nilsson and the project manager Hans Carlsson. Great thanks are due to the chairmen of the technical subgroups, Rudi Beck and Paul Gnirk, and the members of TSG1 for their support and constructive advice.

We would also like to thank Clarissa Villalobos for performing the analysis in an accurate and well documented manner and Margareta Lundberg for preparing the reports.

LIST OF ILLUSTRATIONS

- Figure 3-1. Overview of the mine adjacent to the 3-D test site.
- Figure 3-2. Dimensions of the 3-D test site.
- Figure 3-3. Location of the injection points and the tracer injected at each point.
- Figure 4-1. 3-D test site with surroundings.
- Figure 5-1. Orientation of the 100 most prominent fractures.
- Figure 5-2. Actual fracture map over 3-D migration test site.
- Figure 5-3. Number of individual fractures and zones in the different fracture sets.
- Figure 5-4. Dip and directions for individual fractures and fracture zones.
- Figure 5-5. Fracture coating and filling materials for individual fractures and fracture zones.
- Figure 5-6. Extrapolation of "wet" fractures based on stereo photos.
- Figure 5-7. Extrapolations of "wet" fractures based on stereo photos.
- Figure 6-1. Results from inflow measurements in the pilot hole.
- Figure 6-2. Water inflow rates into the test site before drilling of the injection holes.
- Figure 6-3. Water inflow rates along the two main axes of the test site.
- Figure 6-4. Comparison of the water in flowrates to the pilot hole and later measurements at the test site.
- Figure 6-5. Total flowrate as function of time. Integral over whole test site (main drift, and arm). Time zero is when the injection started.
- Figure 6-6. Water inflow rates into 2 m sections of the injection holes.
- Figure 6-7. Location of the two walls used for the ventilation experiment.
- Figure 7-1. Location of the injection zones and injected tracers.

- Figure 7-2. Time schedule for tracer injection.
- Figure 7-3. Example of different breakthrough curves.
- Figure 7-4. The injection flowrate at injection point II:2 (Eosin B).
- Figure 7-5. Areas in the test site where the different tracers have emerged.
- Figure 7-6. Areas where tracers have been found in the test site.
- Figure 7-7. Tracer occurrence in the main drift for the individual tracers.
- Figure 7-8. Number of sampling areas into which individual tracers have emerged as function of time. Time of appearance is the first arrival of the tracer with a concentration above the detection limit.
- Figure 7-9. Detailed breakthrough curve for one sampling before data processing.
- Figure 7-10. Breakthrough curves in sampling area 27+1 which is located in the central part of the main drift.
- Figure 7-11. Breakthrough curve after sorting out analysis errors.
- Figure 7-12. Breakthrough curve after second smoothing.
- Figure 7-13. Location of Tritium sampling.
- Figure 8-1. Principle layout of diffusion cell used in matrix diffusion measurements.
- Figure 8-2. Typical concentration - time curve from a matrix diffusion experiment.
- Figure 9-1. Average water flowrate from fracture 1 and fracture 2 in Stripa.
- Figure 9-2. Concentration at the outlet of a medium with parallel fractures which has been injected with a tracer pulse.
- Figure 9-3. Predicted curves using the hydrodynamic dispersion model and the channeling dispersion model. For nonsorbing tracer for a longer distance (10 times) and a lower flow ($Pe = 100$, $\sigma = 0.208$).
- Figure 9-4. Experimentally determined dispersion lengths in fractured crystalline rock.
- Figure 10-1. Division of test site into two different drifts, and the cross-section of the drifts showing the parts used in the compilation of fracture data.

- Figure 10-2. Fracture length, fracture zone length, and number of single fracture intersections per m^2 for main drift and arm.
- Figure 10-3. Water flowrates for main drift and arm before drilling of the injection holes.
- Figure 10-4. Water flowrates in main drift at 6000 h after start of tracer injection.
- Figure 10-5. Tracer mass flowrates at 6000 h after start of injection.
- Figure 11-1. The 360 m level around the 3-D test site.
- Figure 11-2. Disturbances and their occurrence and duration in time.
- Figure 11-3. Total flowrate as function of time. Integral over whole test site, main drift and arm.
- Figure 11-4. Flowrate variations in time for 3 different sampling sheets.
- Figure 11-5. Water inflow rates into the test site divided into sheets where tracers were later found and those where no tracers emerged.
- Figure 11-6. Natural water pressure at the top zone in injection hole II (70 m depth). N2,N3,N4,W1, and W2 refer to the drilling of the investigation holes for Stripa Project III.
- Figure 11-7. Pressure decrease in hole III zone 2 when drilling hole W2 (Stripa Phase III).
- Figure 11-8. Injection pressure and injection flowrate versus time for zone 1 in injection hole II (56 m depth).
- Figure 11-9. 3-D test site with injection holes.
- Figures 12-1 to 12-5. Eosin B breakthrough curve from sheets 57, 60, 66, 108, and 120. The full line gives a fitted curve by the AD model and the crosses show selected experimental points.
- Figure 12-6. Uranine breakthrough curve in sheet 108. The full line gives a fitted curve by the AD model and crosses show selected experimental points
- Figures 12-7, 12-8, 12-9. Elbenyl, Eosin Y, and Iodide breakthrough curves in sheet 108. The full line gives a fitted curve by the AD model and the crosses show selected experimental points.
- Figure 12-10. Porosity versus distance from drift.
- Figure 12-11. Recovered tracer/total injected tracer versus time.

- Figure 12-12. Recovery of Eosin Y as a function of time with the specific surface a' as a parameter.
 $D_e = 2 \cdot 10^{-14}$, $\epsilon_p = 5 \cdot 10^{-4}$, $t_w = 6000$ h,
 $Q = 198$ ml/h, $L_p = 27$ m, $r_1 = 2.23$, $r_2 = 20.2$ m, $\epsilon_f = 6.9 \cdot 10^{-5}$.
- Figure 12-13. Recovery of Iodide as a function of time with the specific surface a' as a parameter.
 $D_e = 2 \cdot 10^{-13}$, $\epsilon_p = 1 \cdot 10^{-3}$, $t_w = 7000$ h,
 $Q = 200$ ml/h, $L_p = 31$ m, $r_1 = 2.23$, $r_2 = 31.2$, $\epsilon_f = 3.0 \cdot 10^{-5}$.
- Figure 12-14. A fracture cross section with a channel containing flowing water is shown. In contact with the flowing water are stagnant volumes of water into which the tracer is carried by diffusion.
- Figure 12-15. Hydraulic heads in hole I.
- Figure 12-16. Hydraulic heads in hole II.
- Figure 12-17. Hydraulic heads in hole III.
- Figure 12-18. Compilation of hydraulic heads in the different injection holes.
- Figure 12-19. Flowrates in the plastic sheets during the measurement period. Average values are for 500 hours.
- Figure 12-20. Flowrate of the water from the uncovered part of the experimental drift.
- Figure 12-21. Sum of the water flowrates of from the uncovered part of the experimental drift and from the access drift.
- Figure 12-22. Flowrate in the experimental drift averaged over 10 m.
- Figure 12-23. The distribution of flowrates in the Stripa 3-D drift among the 375 sheets in the Stripa 3-D drift.
- Figure 12-24. Sum of the flowrates in the different flowrate ranges in the Stripa 3-D drift.
- Figure 12-25. Histogram over the recovery of Eosin B in different mass ranges. All 43 sheets carried this tracer in measurable quantities.
- Figure 12-26. Histogram over the recovery of Uranine in different mass ranges. All 45 sheets carried this tracer in measurable quantities.
- Figure 12-27. Histogram over the recovery of Elbenyl in different mass ranges. All 27 sheets carried this tracer in measurable quantities.

- Figure 12-28. Histogram over the recovery of Eosin Y in different mass ranges. All 46 sheets carried this tracer in measurable quantities.
- Figure 12-29. Histogram over the recovery of Iodide in different mass ranges. All 52 sheets carried this tracer in measurable quantities.
- Figure 12-30. Eosin B
- Figure 12-31. Uranine
- Figure 12-32. Elbenyl
- Figure 12-33. Eosin Y
- Figure 12-34. Iodide
-
- Figure A2-1. Injection pressures and injection flowrates at 5000 - 10,000 h for Hole I, zone 1 (32 m).
- Figure A2-2. Injection pressures and injection flowrates at 5000 - 10,000 h for Hole I, zone 2 (18 m).
- Figure A2-3. Injection pressures and injection flowrates at 5000 - 10,000 h for Hole II, zone 1 (56 m).
- Figure A2-4. Injection pressures and injection flowrates at 5000 - 10,000 h for Hole II, zone 2 (10 m).
- Figure A2-5. Injection pressures and injection flowrates at 5000 - 10,000 h for Hole II, zone 3 (10 m).
- Figure A2-6. Injection pressures and injection flowrates at 5000 - 10,000 h for Hole III, zone 1 (37 m).
- Figure A2-7. Injection pressures and injection flowrates at 5000 - 10,000 h for Hole III, zone 2 (29 m).
- Figure A2-8. Injection pressures and injection flowrates at 5000 - 10,000 h for Hole III, zone 3 (19 m).
- Figure A2-9. Injection pressures and injection flowrates at 5000 - 10,000 h for Hole III, zone 4 (13 m). Injection is by membrane pump.
-
- Figure A3-1. Monitored pressures at Hole I, top (70 m).
- Figure A3-2. Monitored pressures at Hole I, zone 1 (32 m).
- Figure A3-3. Monitored pressures at Hole I, zone 2 (18 m).
- Figure A3-4. Monitored pressures at Hole II, top (70 m).
- Figure A3-5. Monitored pressures at Hole II, zone 1 (56 m).
- Figure A3-6. Monitored pressures at Hole II, zone 2 (34 m).

- Figure A3-7. Monitored pressures at Hole II, zone 3 (10 m).
- Figure A3-8. Monitored pressures at Hole III, top (50 m).
- Figure A3-9. Monitored pressures at Hole III, zone 1 (37 m).
- Figure A3-10. Monitored pressures at Hole III, zone 2 (29 m).
- Figure A3-11. Monitored pressures at Hole III, zone 3 (19 m).
- Figure A3-12. Monitored pressures at Hole III, zone 4 (13 m).
- Figure A4-1. Individual fracture length per m^2 for the different fracture sets (main drift and arm).
- Figure A4-2. Zone length per m^2 for the different fracture sets (main drift and arm).
- Figure A4-3. Fracture coating/filling materials per m^2 for individual fractures (main drift and arm).
- Figure A4-4. Coating/filling materials per m^2 for zones (main drift and arm).
- Figure A5-1. Inflow rates for 8 different 2 m sections as a function of time.
- Figure A5-2. Inflow rates into the main drift and arm at different times.
- Figure A6-1. Location of the two walls for the ventilation experiment.
- Figure A6-2. Measuring points.
- Figure A6-3. Water flowrate to the 3-D drift.
- Figure A6-4. Water flowrate to the 3-D drift and access drift combined.
- Figure A7-1. Injection of Eosin B.
- Figure A7-2. Injection of Uranine.
- Figure A7-3. Injection of Elbenyl.
- Figure A7-4. Injection of Eosin Y.
- Figure A7-5. Injection of Iodide.
- Figure A7-6. Injection of Fluoride.
- Figure A7-7. Real injection curve, hole 1 zone 1. Tracer Uranine 0-16000 h. Tracer Uranine+STR-7+F⁻ 5000-12500 h.
- Figure A7-8. Real injection curve, hole 1 zone 2. Tracer Eosin Y.
- Figure A7-9. Real injection curve, hole 2 zone 1. Tracer Phloxine.

- Figure A7-10. Real injection curve, hole 2 zone 2. Tracer Rose Bengal.
- Figure A7-11. Real injection curve, hole 2 zone 3. Tracer Elbenyl.
- Figure A7-12. Real injection curve, hole 3 zone 1. Tracer Duasyn.
- Figure A7-13. Real injection curve, hole 3 zone 2. Tracer Iodide.
- Figure A7-14. Real injection curve, hole 3 zone 3. Tracer Eosin B.
- Figure A7-15. Real injection curve, hole 3 zone 4. Tracer Bromide.
- Figure A8-1. Principle of concentration-time curve at the low concentration side.
- Figure A8-2. The diffusion cell.
- Figure A8-3. Concentration versus time for Iodide diffusion.
- Figure A8-4. Concentration versus time for Uranine diffusion.
- Figure A8-5. Concentration-time curves from the diffusion experiment.
(a) - (u)
- Figure A9-1. Water flowrates into main drift and arm at -6000 h.
- Figure A9-2. Fracture length per area for individual fractures, divided into 4 fracture sets.
- Figure A9-3. Water flowrates into main drift and arm at -6000 h.
- Figure A9-4. Fracture length per area for fracture zones, divided into 4 fracture sets.
- Figure A9-5. Water flowrates into main drift and arm at -6000 h.
- Figure A9-6. Fracture length per area for individual fractures, presented for the different fracture fillings.
- Figure A9-7. Water flowrates into main drift and arm at -6000 h.
- Figure A9-8. Fracture length per area for individual fractures, presented for the different fracture fillings.
- Figure A9-9. Water flowrates into main drift and arm at -6000 h.
- Figure A9-10. Fracture length per area for fracture zones, presented for the different fracture fillings.
- Figure A9-11. Water flowrates into main drift and arm at -6000 h.

- Figure A9-12. Fracture length per area for fracture zones, presented for the different fracture fillings.
- Figure A11-1. Model fits with AD-model.
- Figure A11-2. Model fits with AC-model.
- Figure A11-3. Model fits with ADD-model.
- Figure A11-4. Model fits with AD-model, grouped sheets.
- Figure A11-5. Model fits with ADD-model, grouped sheets.
- Figure A11-6. Model fits with AD-model for Uranine with truncated injection curve.
- Figure A17-1. Naming of individual sheets within the test site.

STRIPA PROJECT
3-D MIGRATION EXPERIMENT

REPORT 3
PERFORMED EXPERIMENTS, RESULTS AND EVALUATION

Appendix 1 - 14

Harald Abelin, Lars Birgersson, Jard Gidlund, Luis Moreno,
Ivars Neretnieks, Hans Widén, Thomas Ågren

STORAGE MEDIUM FOR THE OBTAINED DATA

The data from the experiment can be divided into seven groups:

1. Water flowrates
2. Tracer concentration in water to test site
3. Rock characteristics and fracture data
4. Water chemistry
5. Injection pressures and flowrates
6. Hydrostatic pressures
7. Daily logs.

1 WATER FLOWRATES

Detailed information on water flowrates is stored in binders, 5¼" disks on the HP80 series computers, and presented in plots. Compiled and smoothed data for the inflow to the plastic sheets (see Stand Alone Appendix, "Flowrate Curves and Tracer Breakthrough Curves for Individual Sheets - Smoothed Data") are available on 5¼" disks on the IBM PC system as ordinary ASCII files produced by DATAFLEX (database manager). Data from the ventilation experiment is stored in binders.

2 TRACER CONCENTRATION IN WATER TO TEST SITE

Detailed information on tracer breakthrough is stored on 5¼" disks to the HP80 series computers and is presented in plots. Compiled and smoothed data are available on the 5¼" disks on the IBM PC system as ordinary ASCII files produced by DATAFLEX.

3 ROCK CHARACTERISTICS AND FRACTURE DATA

Detailed data on fracture mapping of the test site are stored in binders, and a magnetic tape on the HP9000 series computers (VIAK AB, Falun, Sweden). Compiled data are also available on 5¼" disks on the IBM PC system as ASCII files produced by DATAFLEX.

Core logging has been performed by SGAB (Swedish Geological) and the data are stored in binders and in the case of the three injection holes also available on 5¼" disks on the ABC 800 system computers.

Deviation measurements have been performed by Reflex AB, Stockholm, Sweden, and the data are stored in binders.

A1.2

TV logging of the pilot hole was performed by Undervattensfoto Ingenjörfirma, Stockholm, Sweden. Injection holes were logged by the former Kontrollteknik AB, Dals Långed, Sweden. All TV logs are stored on VHS video tapes.

Radar measurements were performed by SGAB. These data are stored in binders and 5¼" disks on the ABC 800 system computers.

4 **WATER CHEMISTRY**

The water analysis were performed by IMAB, Linköping, Sweden, and in the case of the Tritium analysis Naturhistoriska Museet, Stockholm, Sweden. All the data are stored in binders.

5 **INJECTION PRESSURES AND INJECTION FLOWRATES**

These data are stored in binders and 5¼" disks on the HP80 series computers.

6 **HYDROSTATIC PRESSURES**

These data are stored on 5¼" disks on the HP80 series computers for which various plots can be produced.

7 **DAILY LOGS**

Field notebooks and binders.

INJECTION FLOWRATES COMPARED WITH INJECTION PRESSURES

To illustrate the effects on injection flowrates and injection pressures of a varying surrounding pressure at the injection points, plots with pressures and flowrates measured between 5000 to 10,000 h are presented. It was observed that a decrease in injection pressure and an increase in injection flowrate coincided with the opening of the adjacent bore hole N1 at approximately 7500 h and 8000 h. For further discussions on disturbances see Report 3, "Performed Experiments, Results and Evaluation."

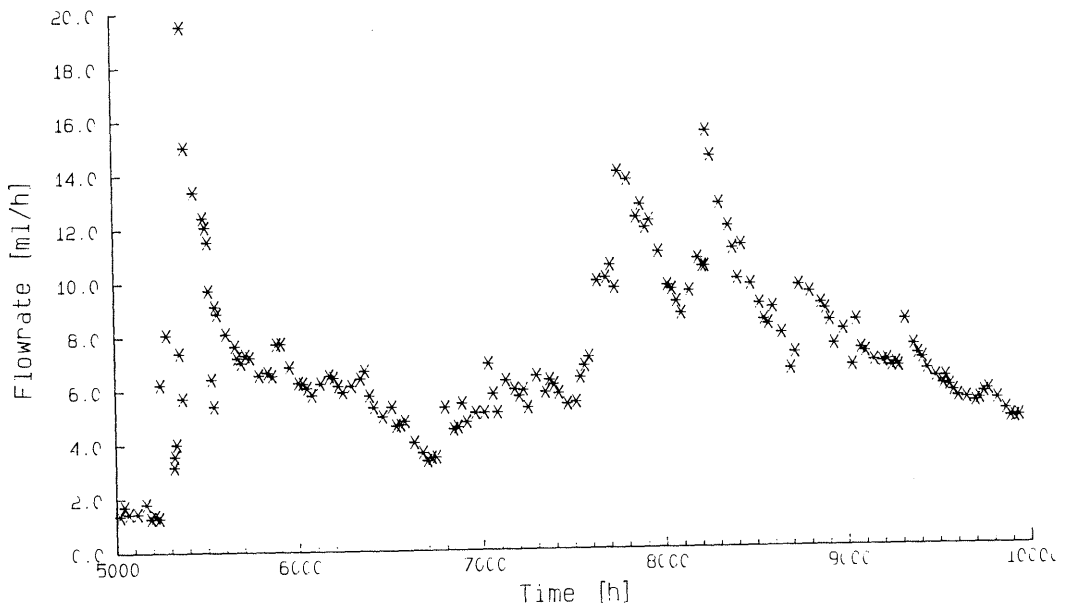
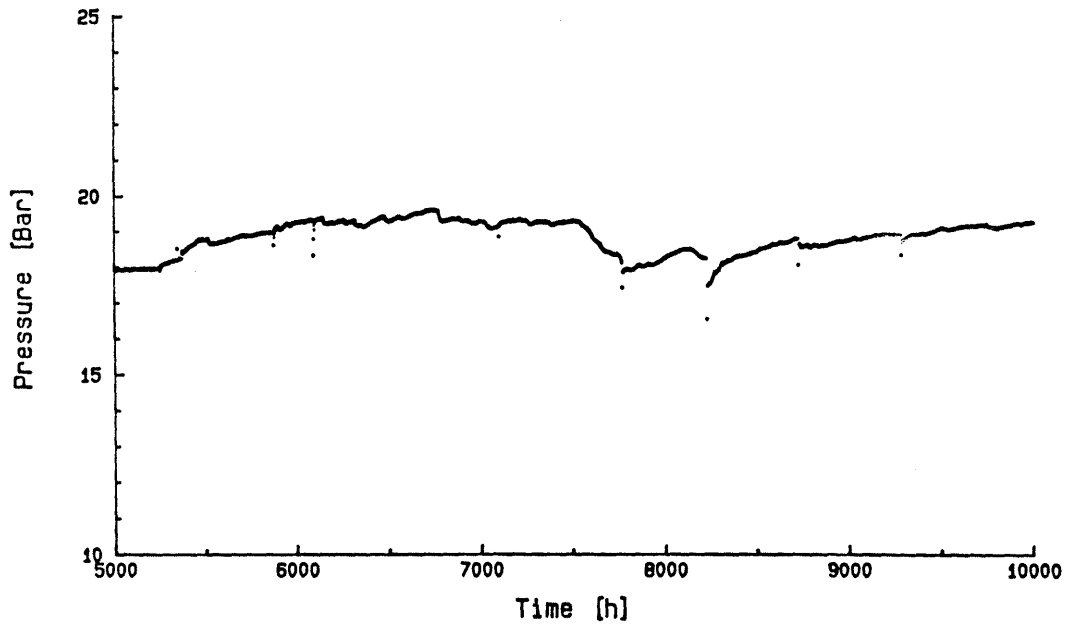


Figure A2-1. Injection pressures and injection flowrates at 5000 - 10,000 h for Hole I, zone 1 (32 m).

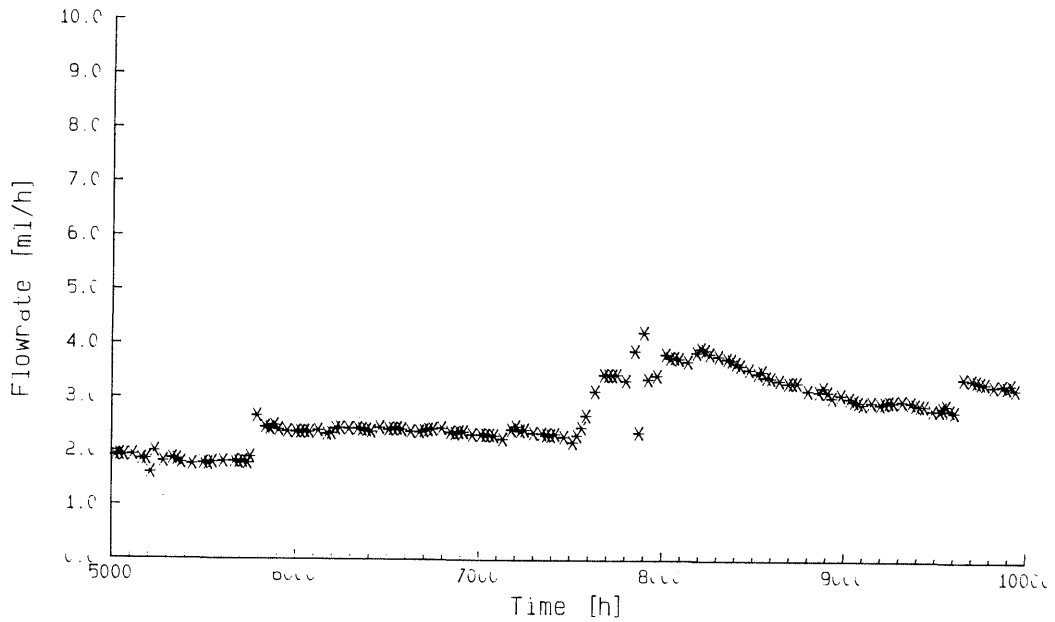
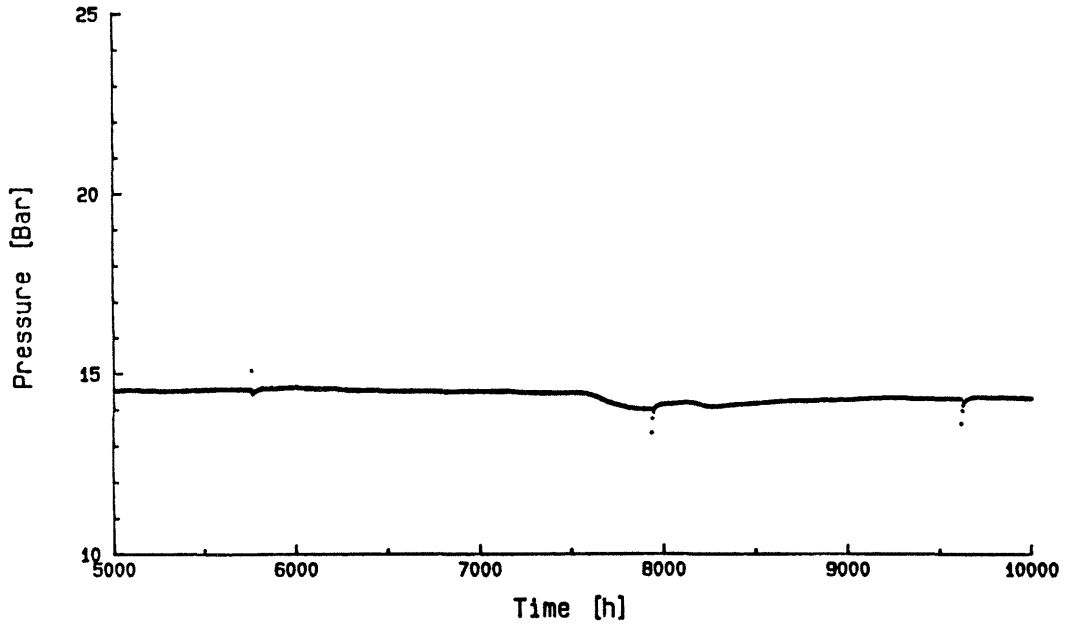


Figure A2-2. Injection pressures and injection flowrates at 5000 - 10,000 h for Hole I, zone 2 (18 m).

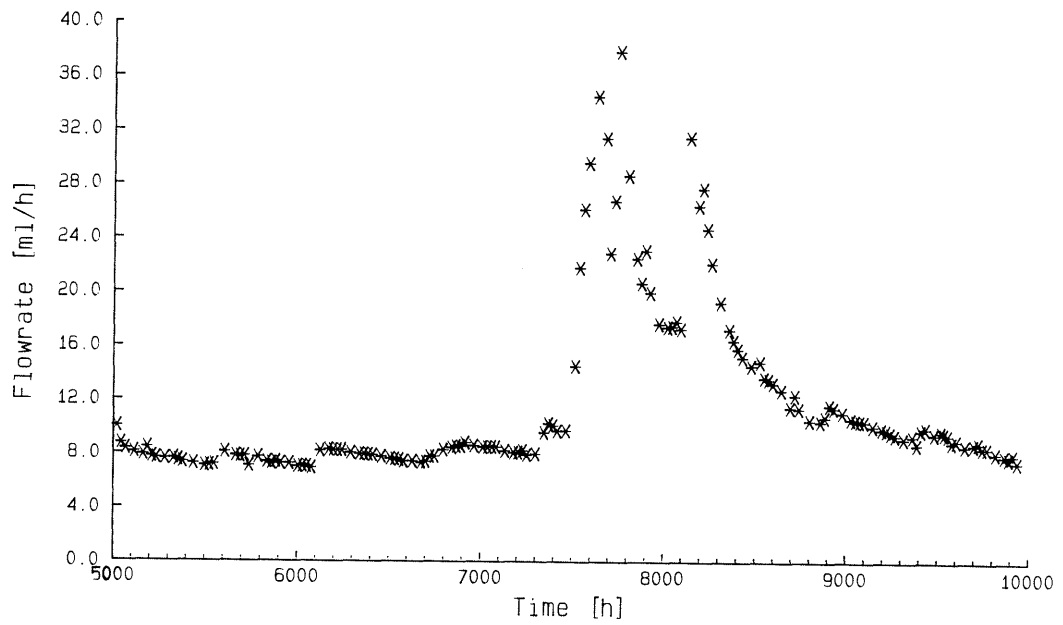
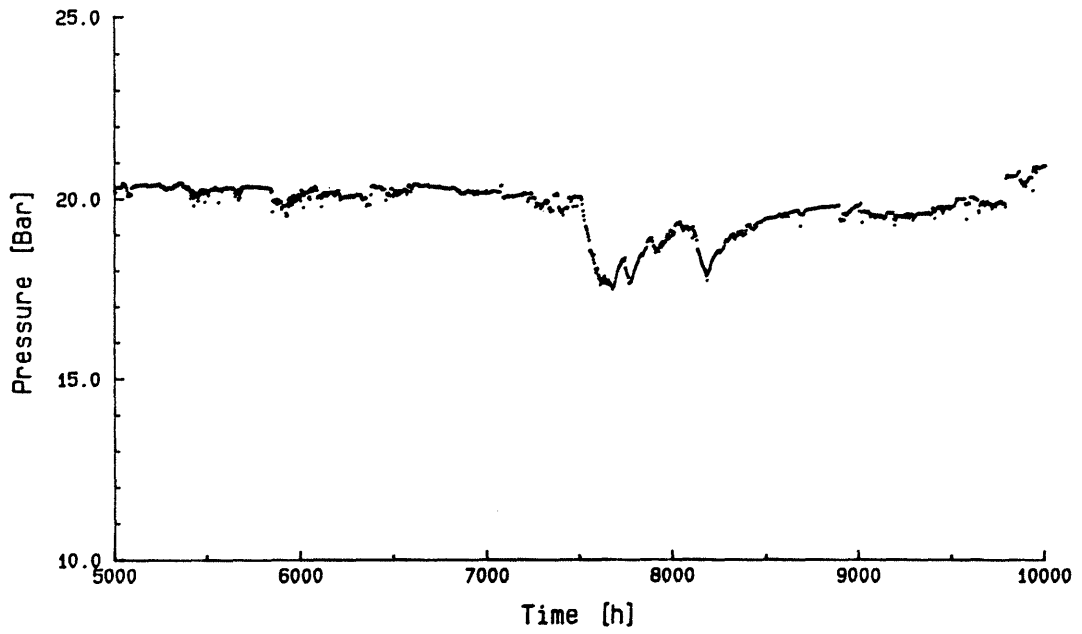


Figure A2-3. Injection pressures and injection flowrates at 5000 - 10,000 h for Hole II, zone 1 (56 m).

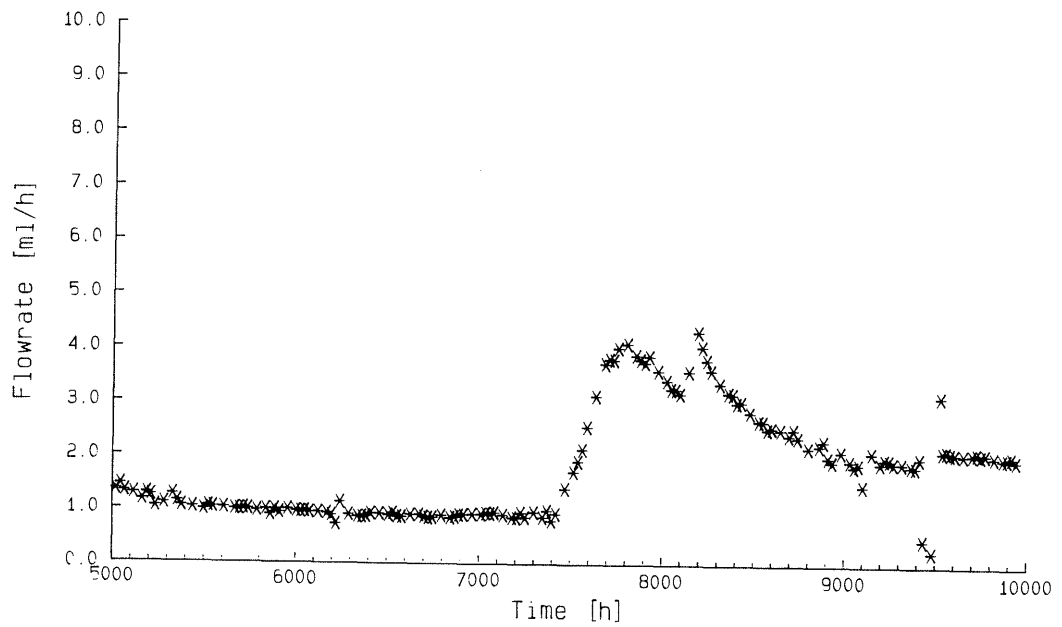
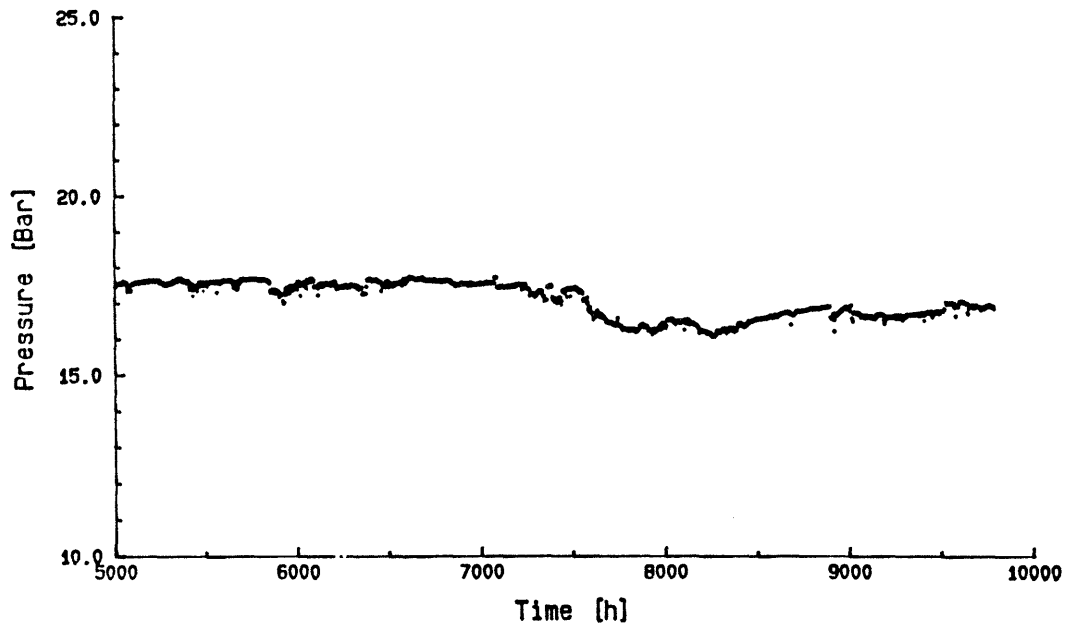


Figure A2-4. Injection pressures and injection flowrates at 5000 - 10,000 h for Hole II, zone 2 (34 m).

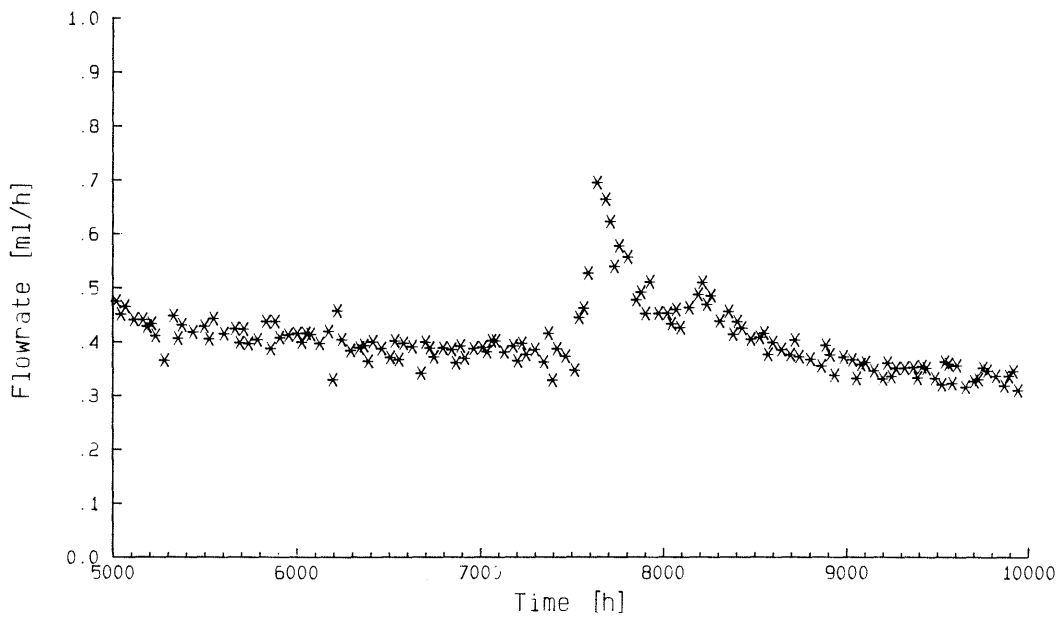
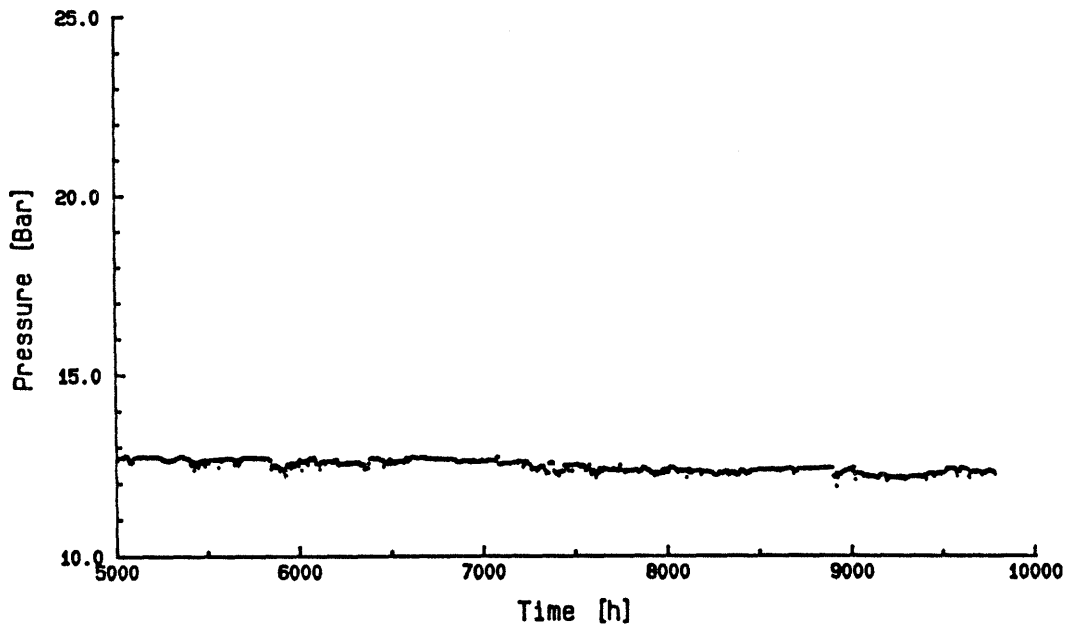


Figure A2-5. Injection pressures and injection flowrates at 5000 - 10,000 h for Hole II, zone 3 (10 m).

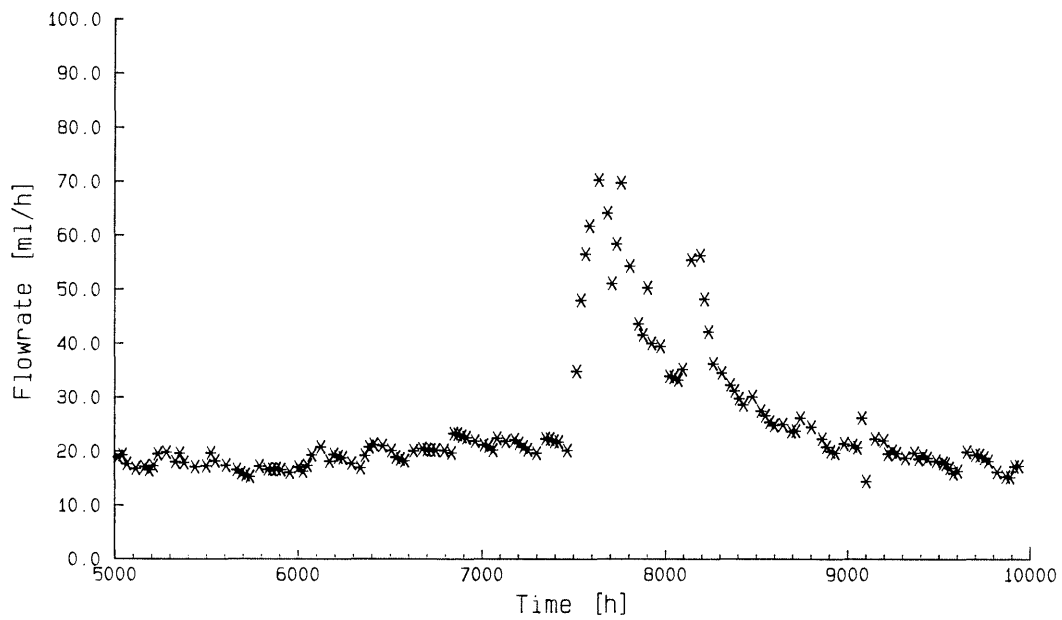
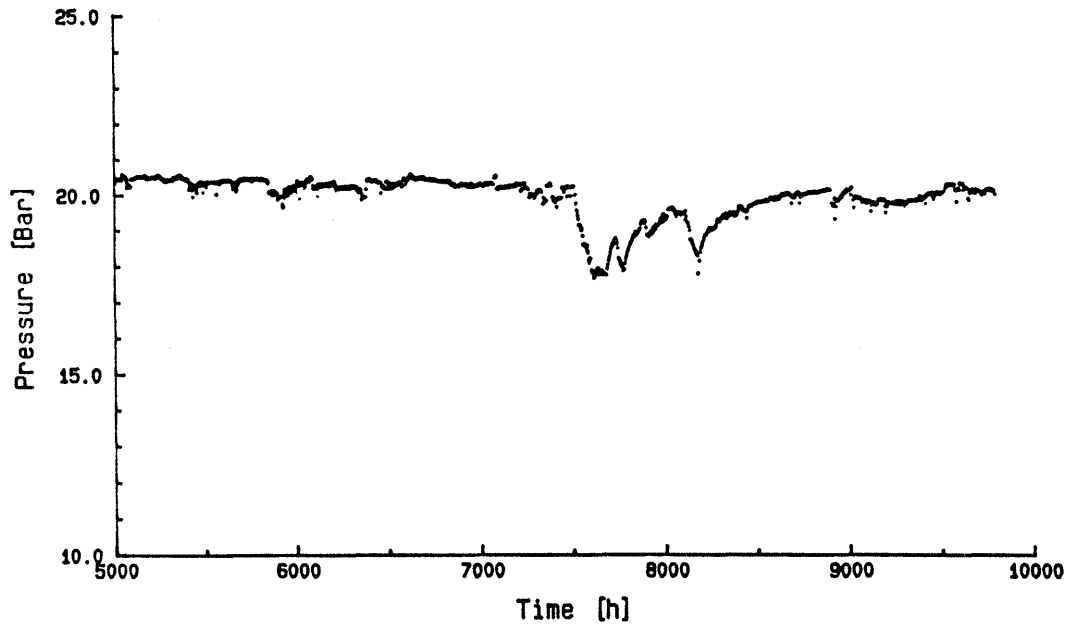


Figure A2-6. Injection pressures and injection flowrates at 5000 - 10,000 h for Hole III, zone 1 (37 m).

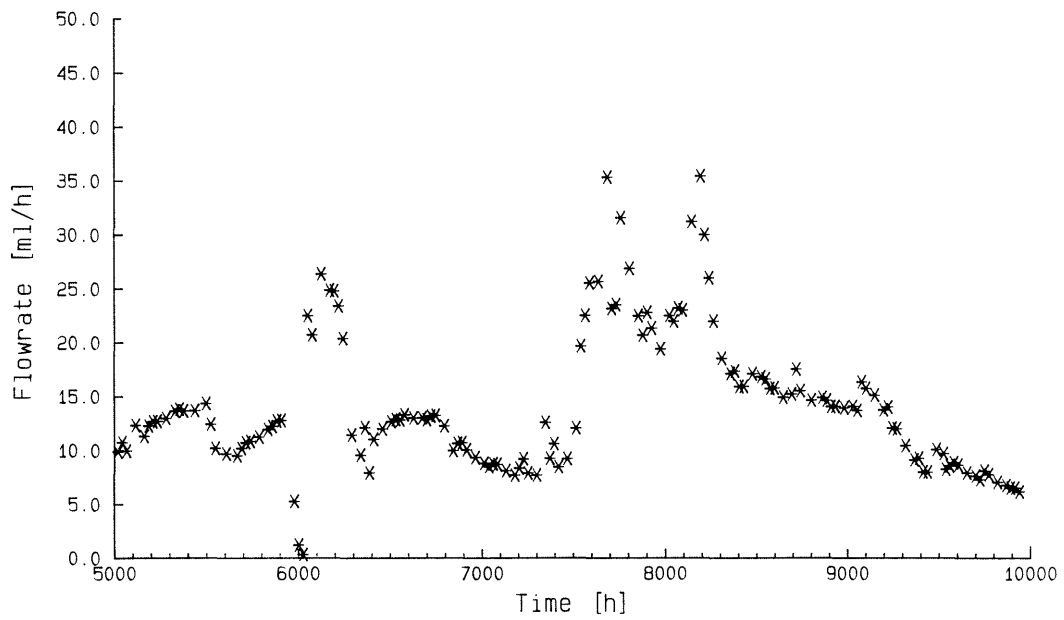
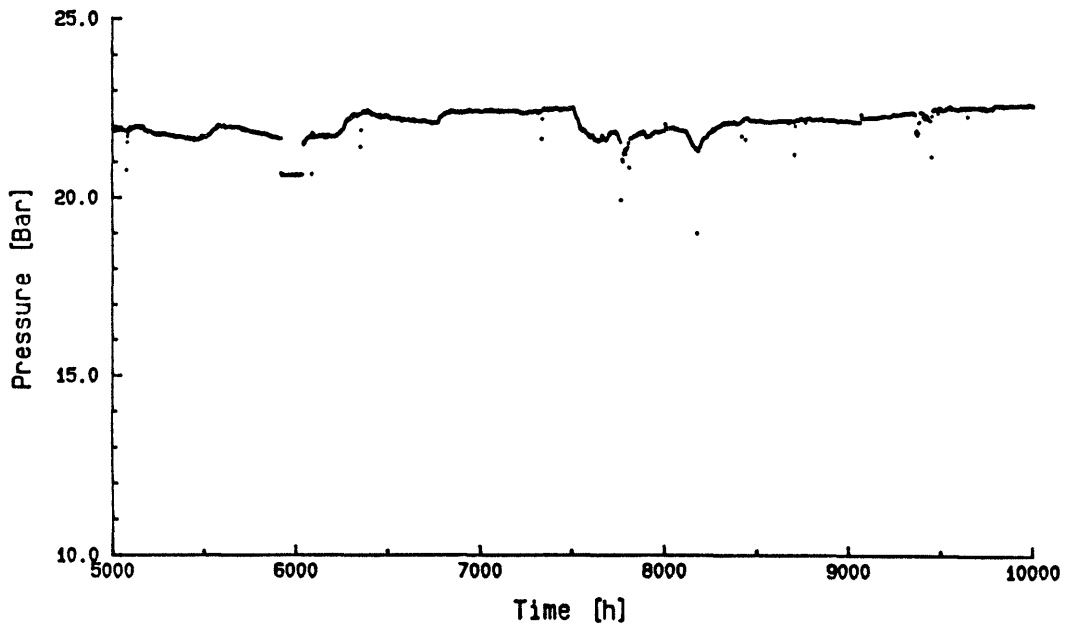


Figure A2-7. Injection pressures and injection flowrates at 5000 - 10,000 h for Hole III, zone 2 (29 m).

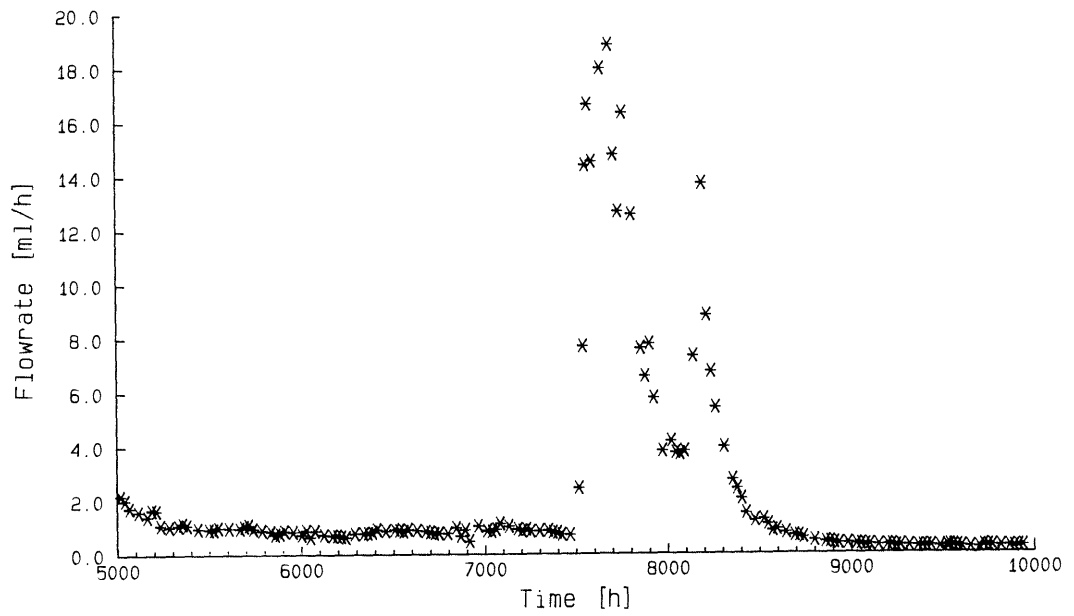
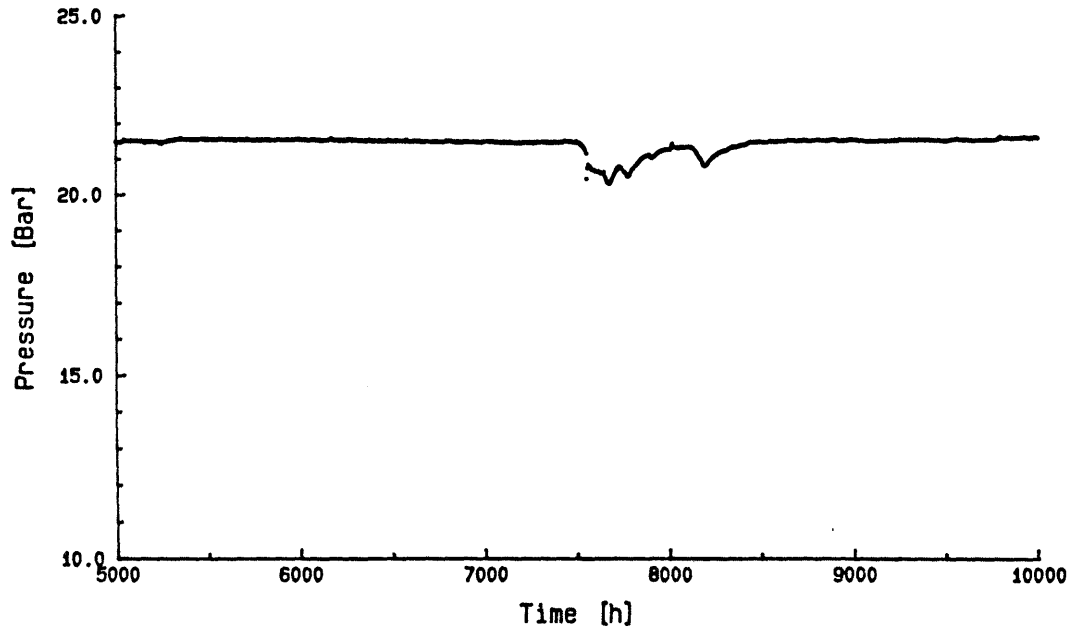


Figure A2-8.

Injection pressures and injection flowrates at 5000 - 10,000 h for Hole III, zone 3 (19 m).

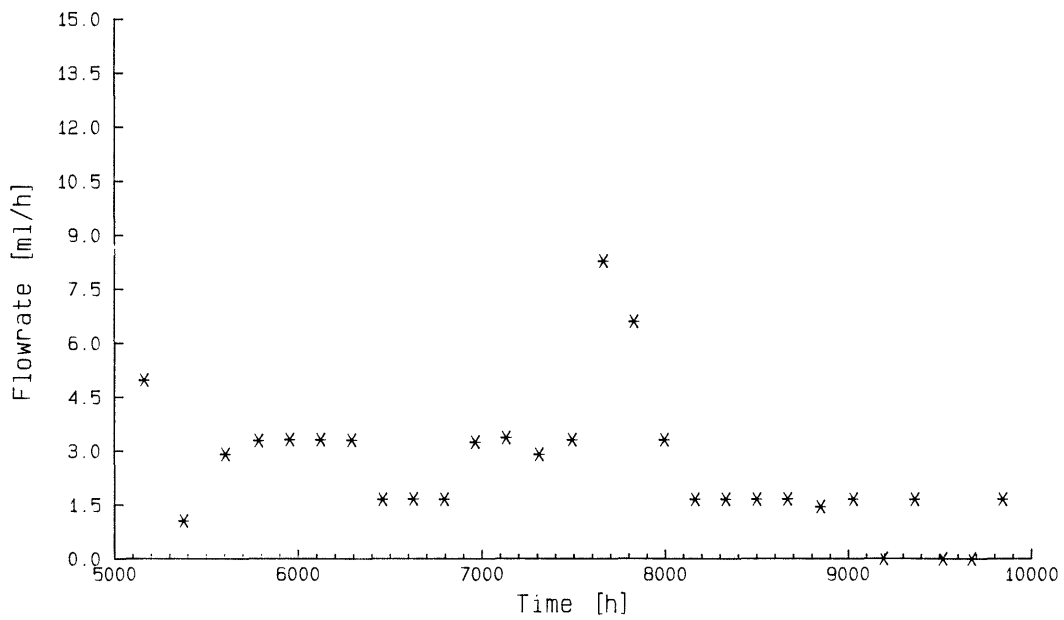
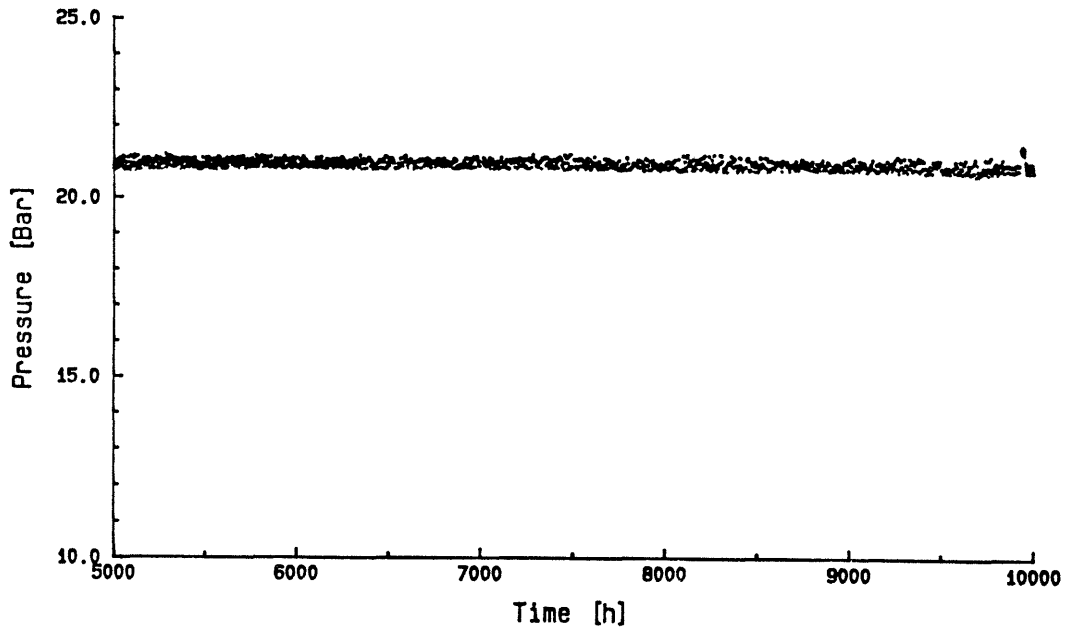


Figure A2-9. Injection pressures and injection flowrates at 5000 - 10,000 h for Hole III, zone 4 (13 m). Injection is by membrane pump.

MONITORED PRESSURES AS A FUNCTION OF TIME

The pressures in 12 zones were monitored for 18,500 hours. Of these 12 zones, 3 were top zones where no injection occurred so that the natural pressure at these points could be measured. For the rest of the 9 zones the pressures were the injection pressures used. The pressures are presented in two time intervals, -2000 - 20,000 and 15,500 - 18,500. The latter time interval shows the effect of drilling of the investigation holes (N4, N3, N2, W1, and W2) for Stripa Project Phase III. In Figures A3-1 to A3-12, the first part of the bar is when the hole was drilled and the second part shows the time period when the hole was left open for measurements.

The pressures seems to be more noisy for injection point III:4. This is due to that a membrane pump was used for injection and not the usual system of a pressurized long tube.

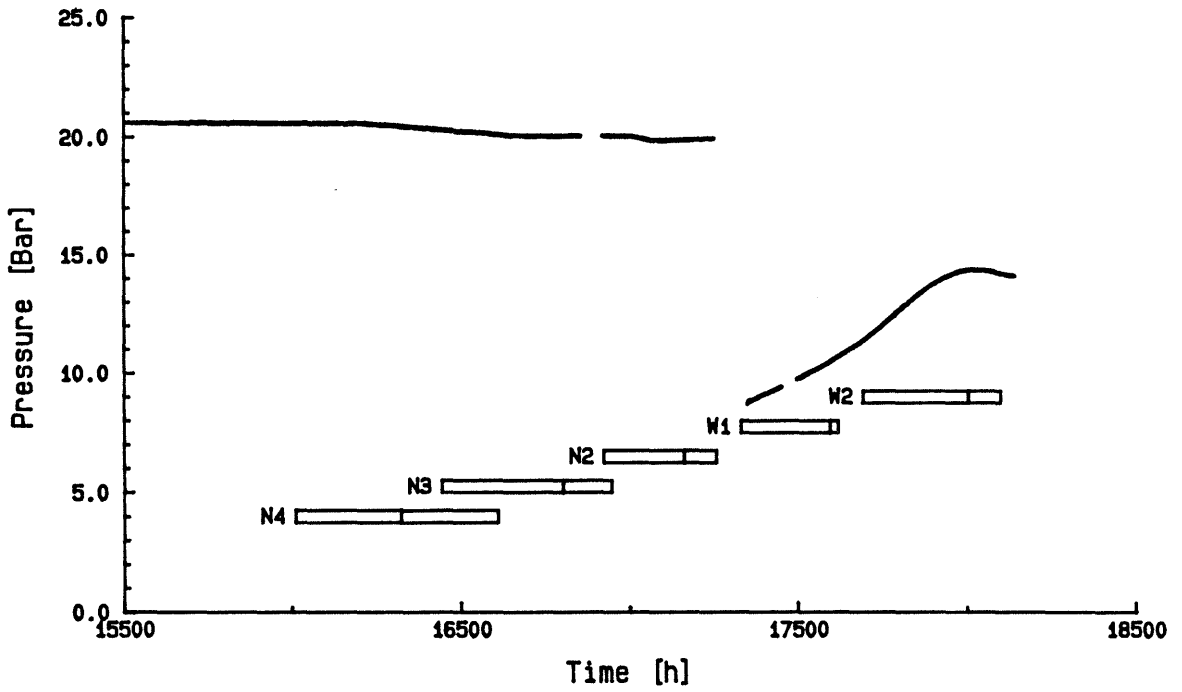
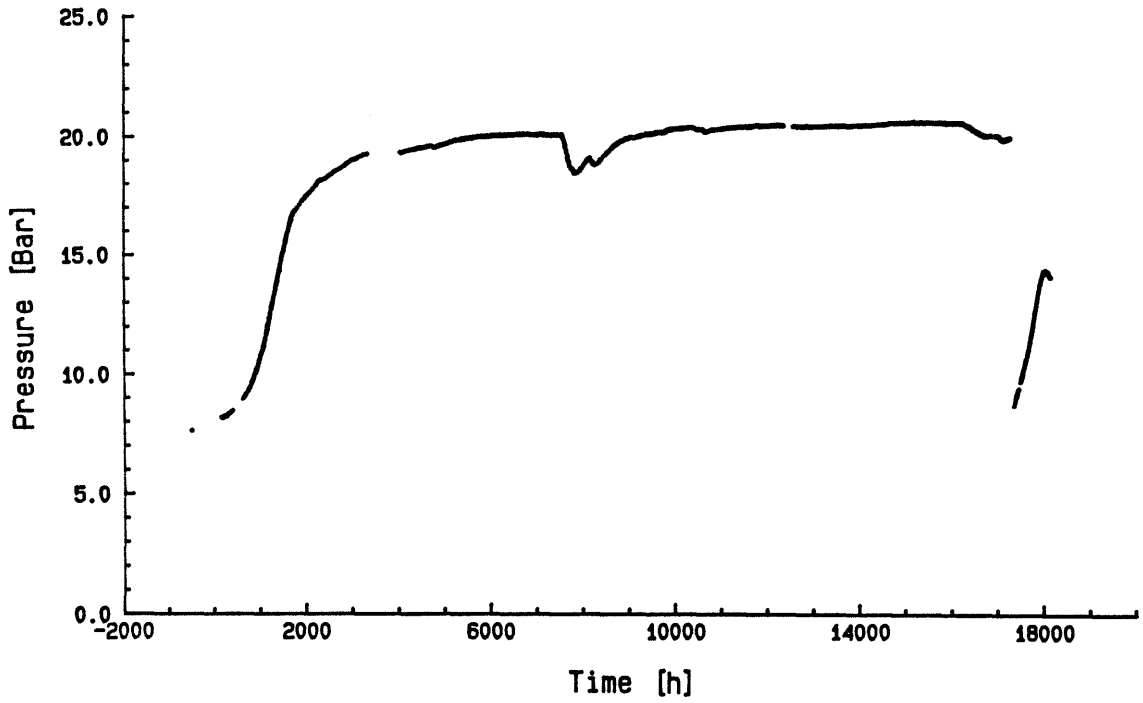


Figure A3-1. Monitored pressures at Hole I, top (70 m).

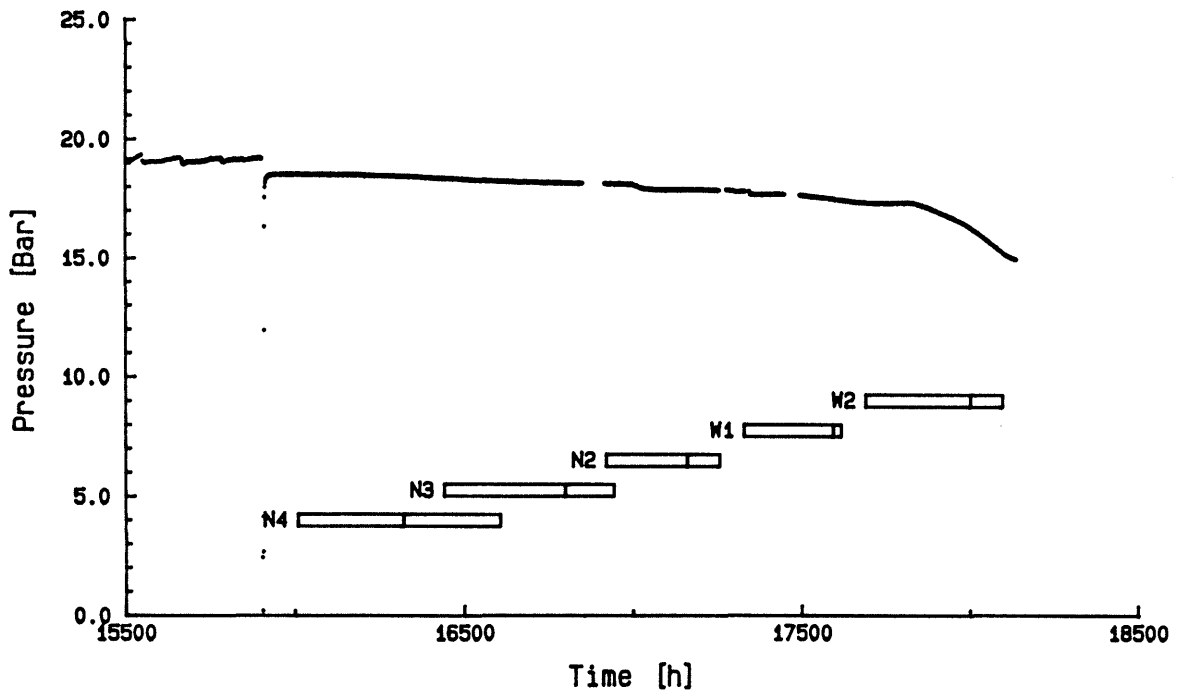
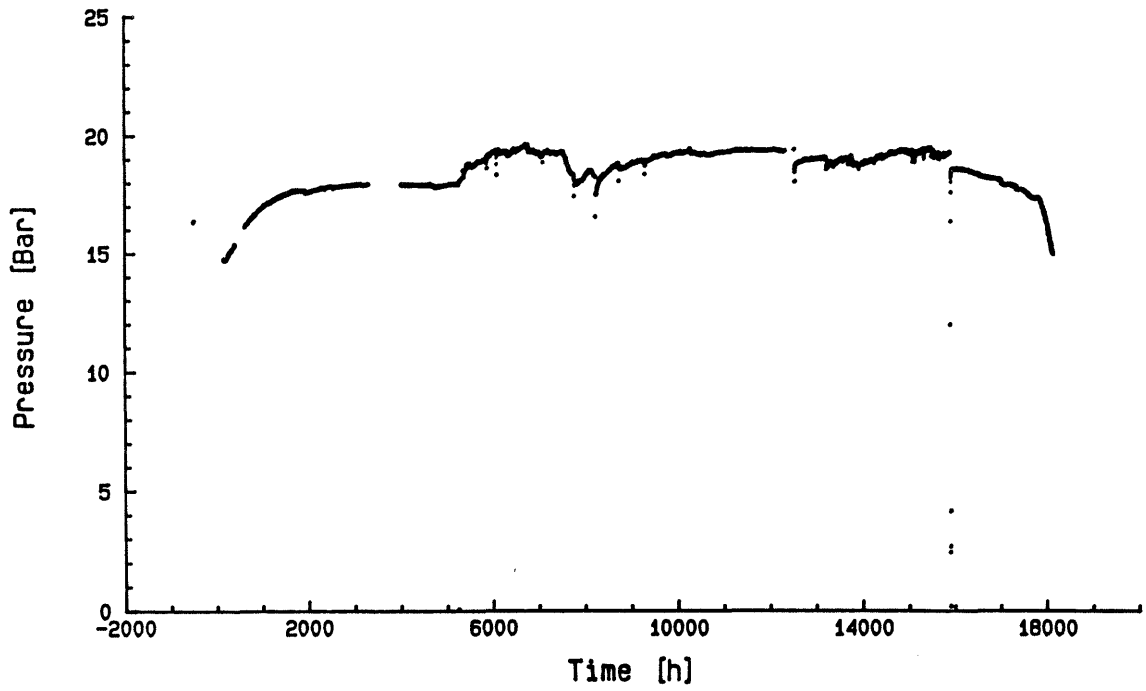


Figure A3-2. Monitored pressures at Hole I, zone 1 (32-m).

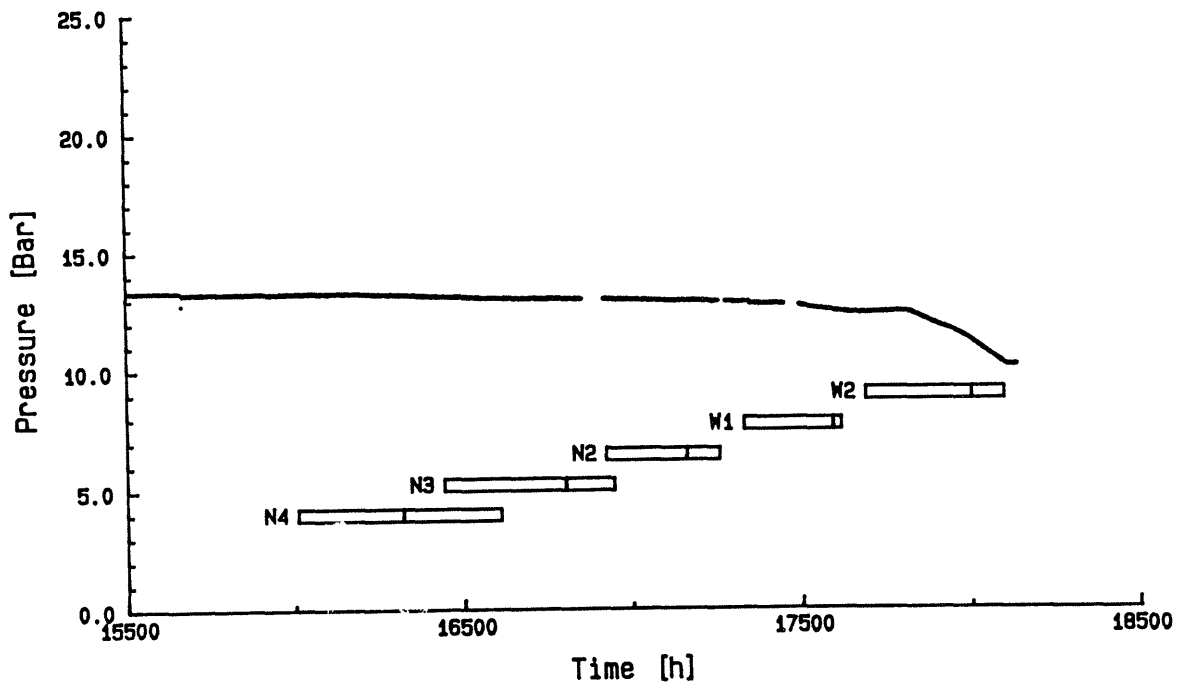
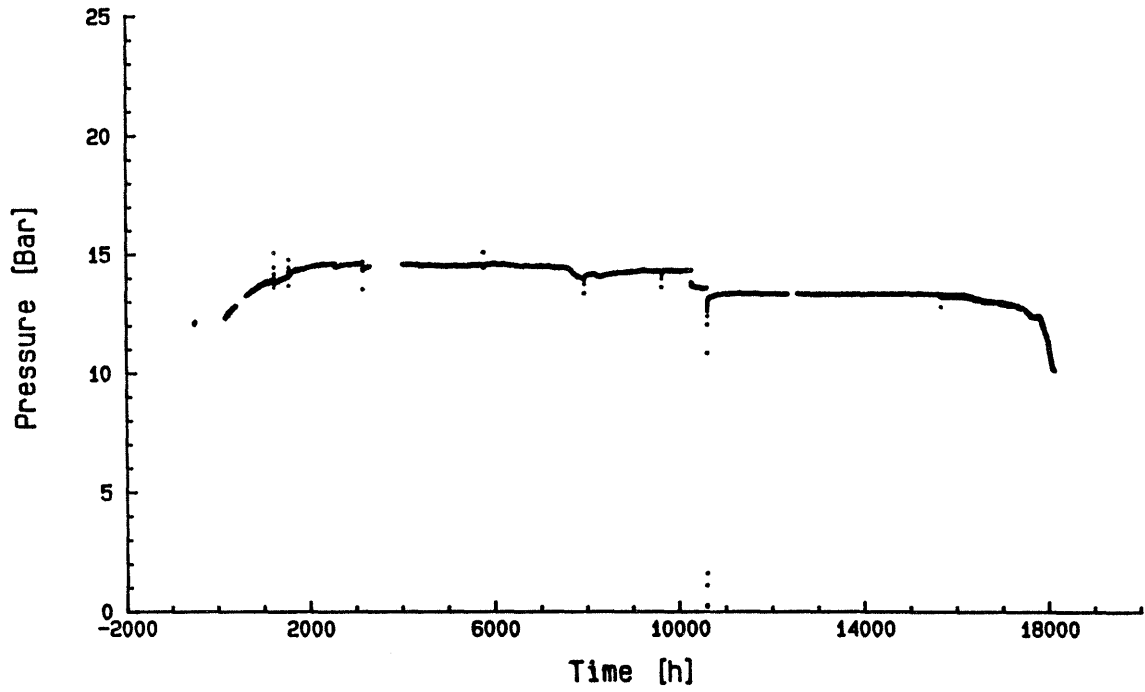


Figure A3-3. Monitored pressures at Hole I, zone 2 (18 m).

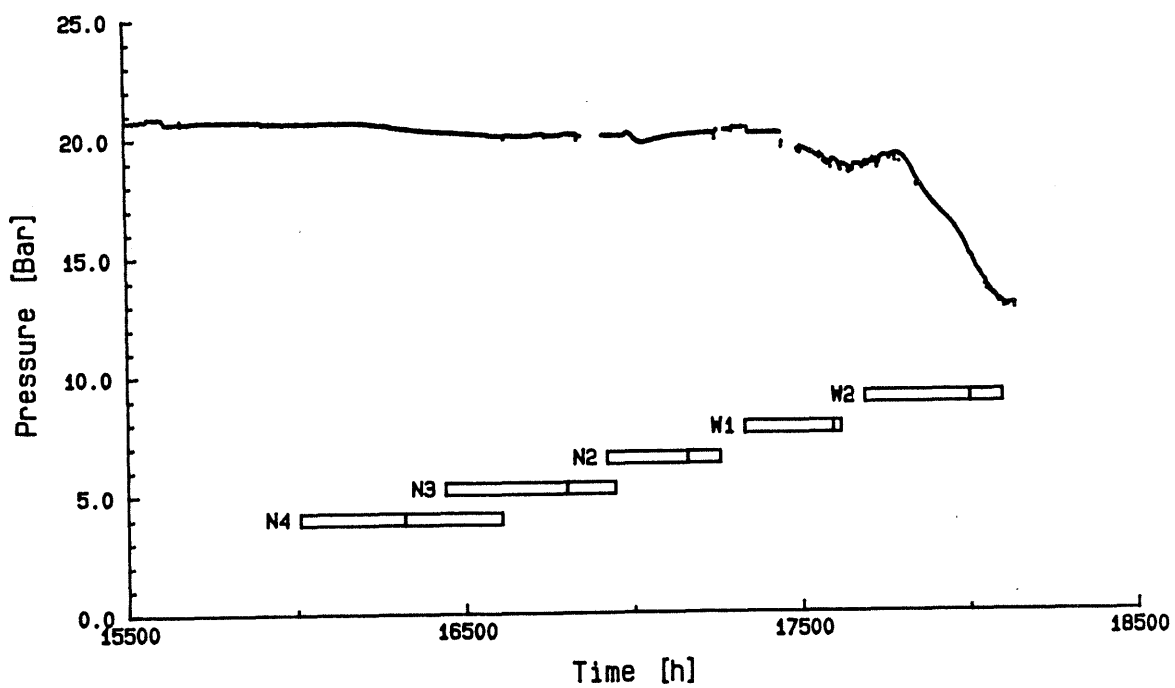
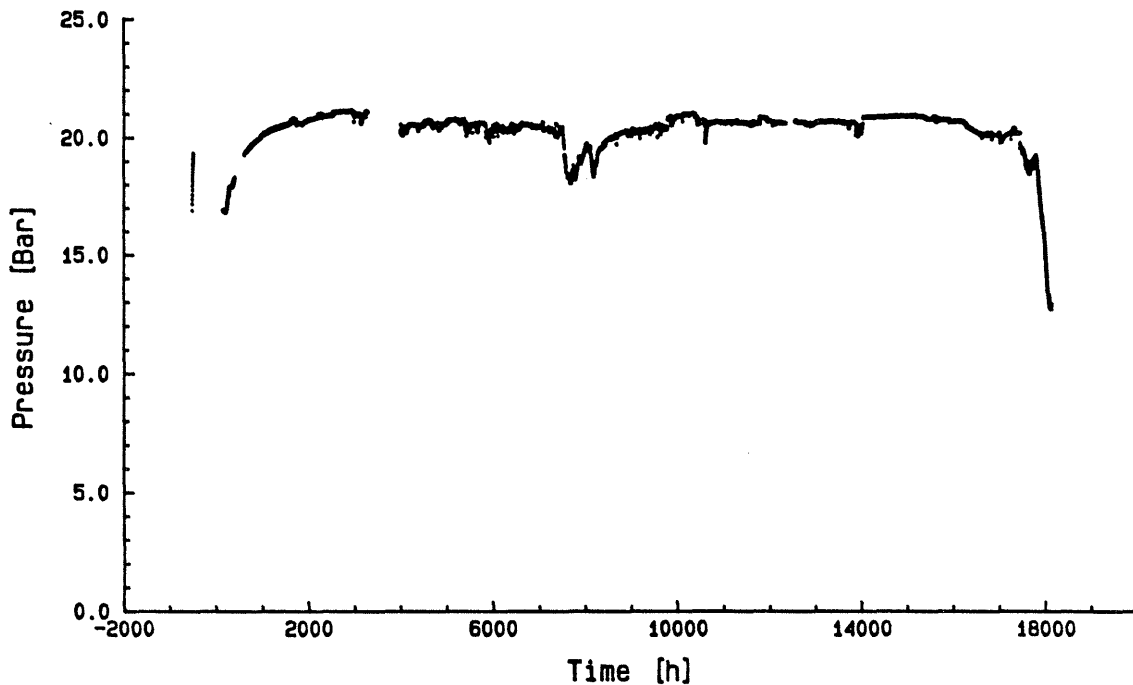


Figure A3-4. Monitored pressures at Hole II, top (70 m).

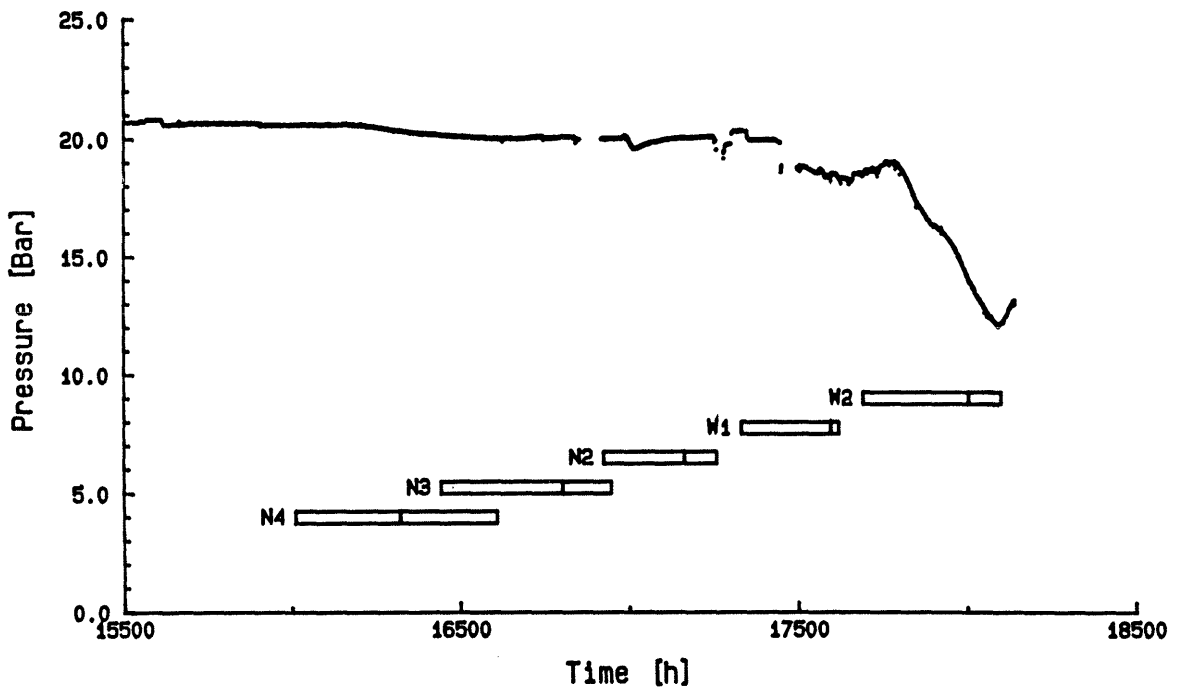
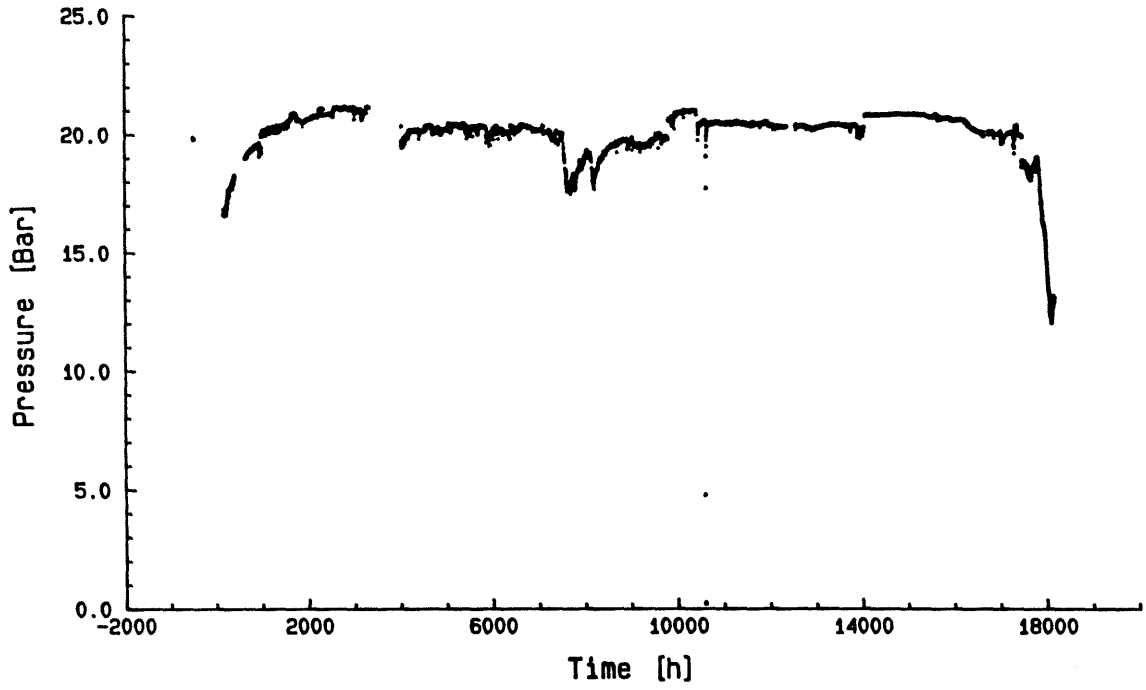


Figure A3-5. Monitored pressures at Hole II, zone 1 (56 m).

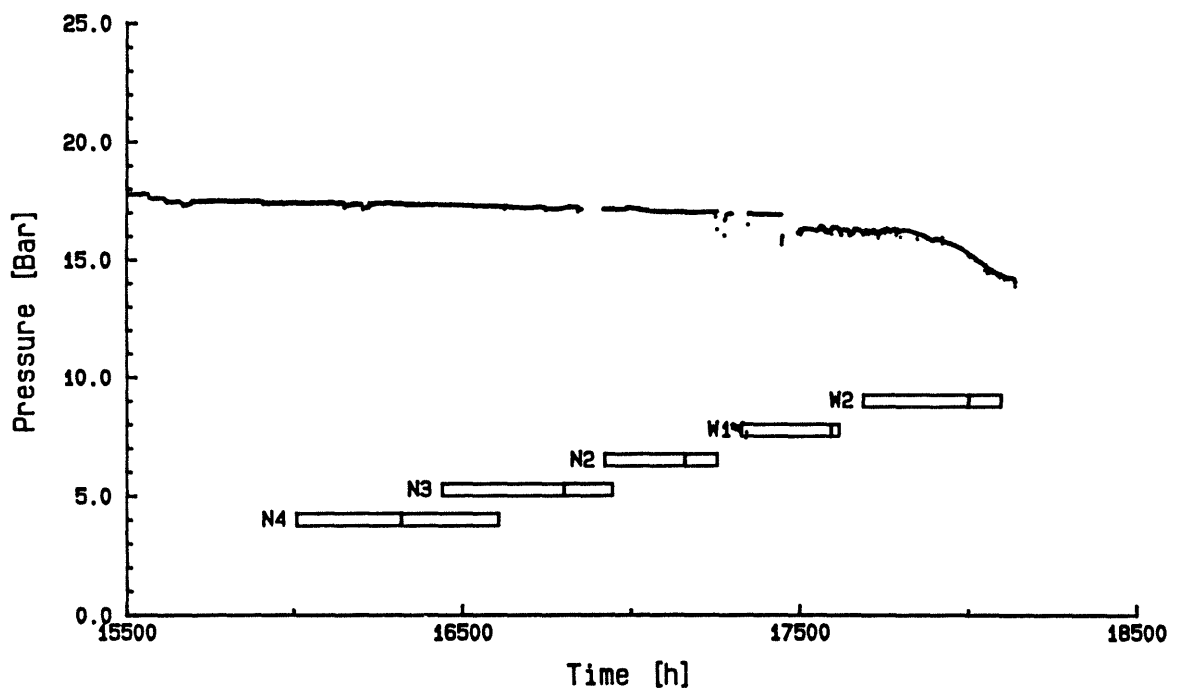
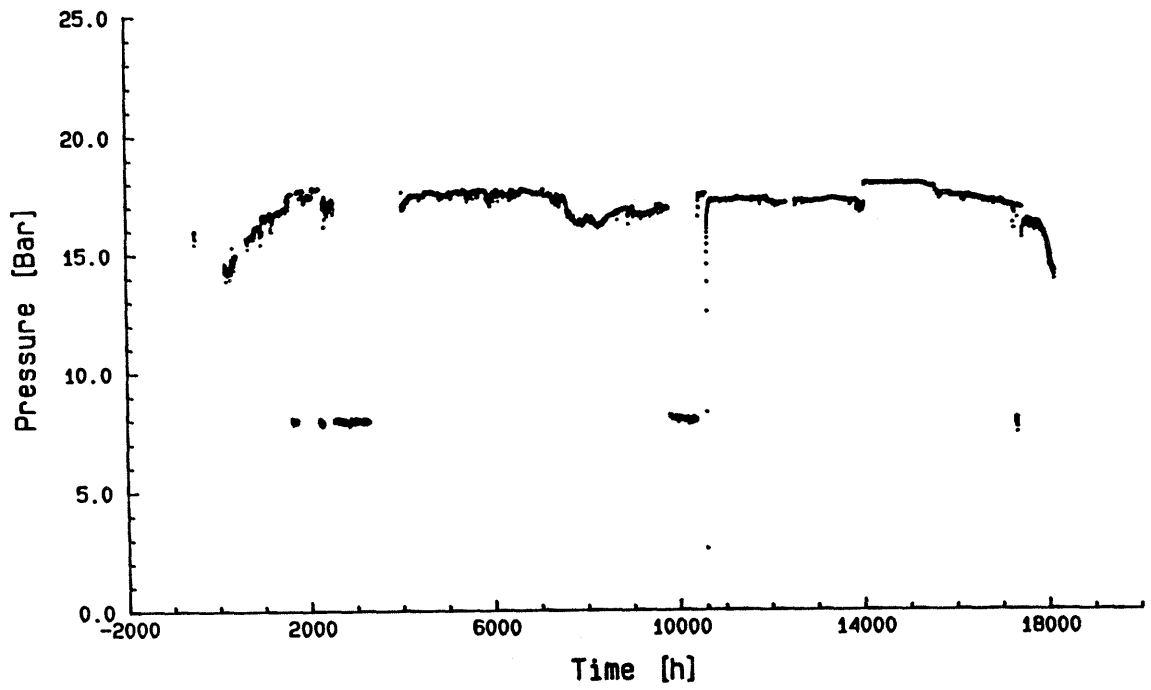


Figure A3-6. Monitored pressures at Hole II, zone 2 (34 m).

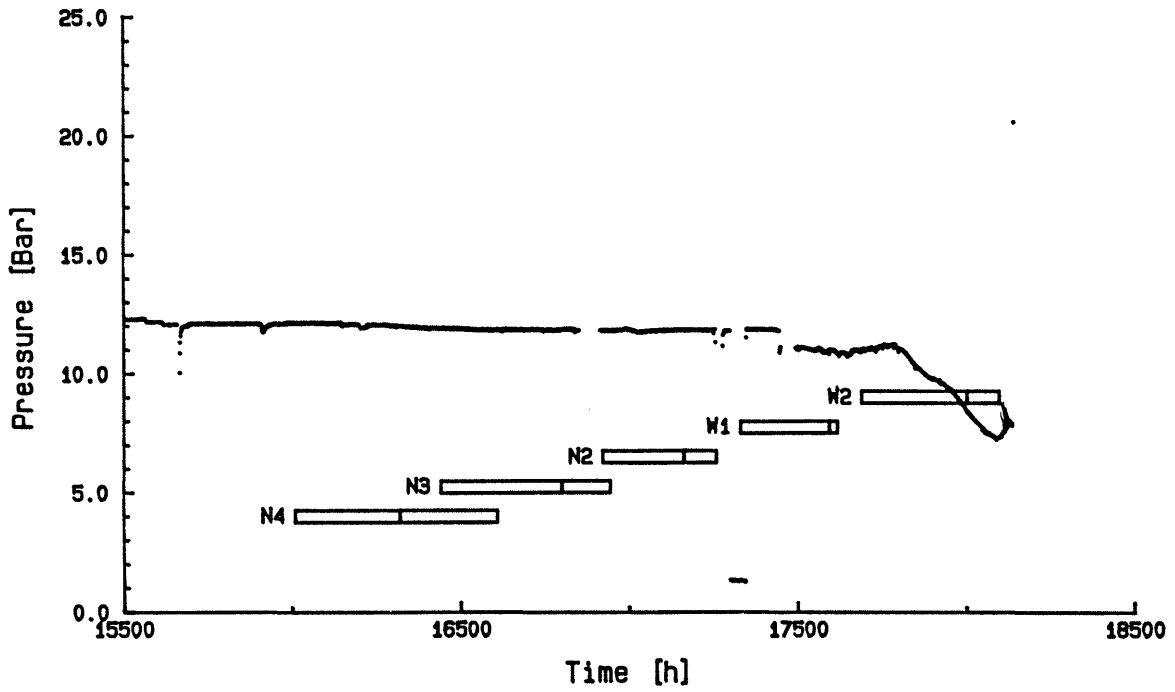
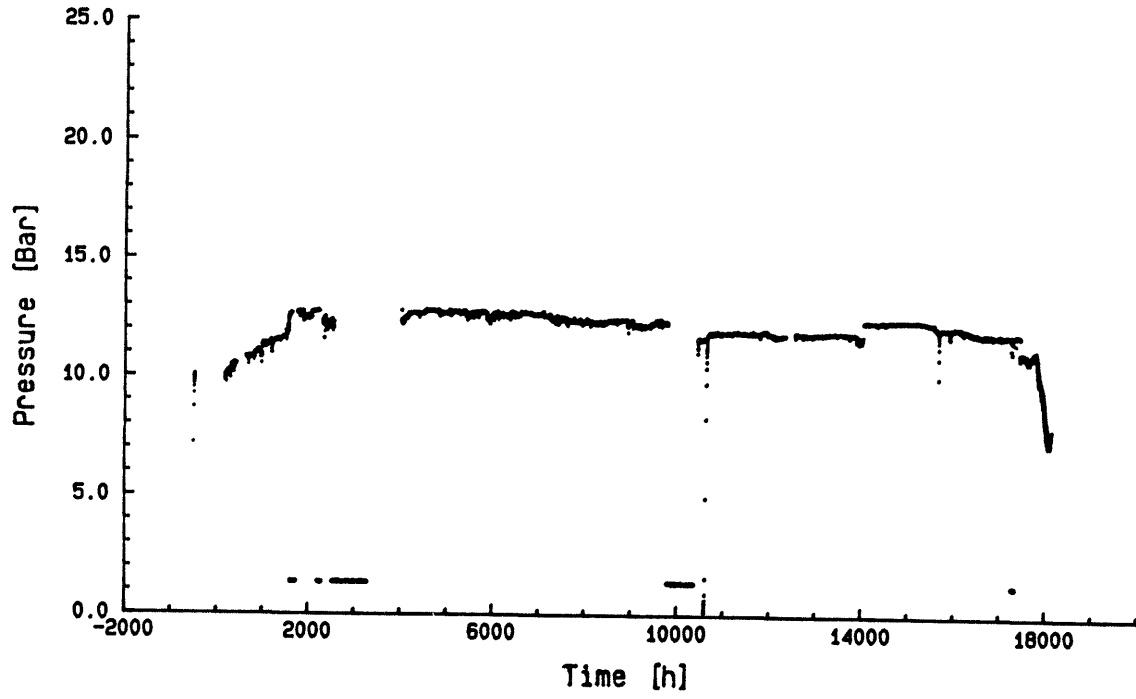


Figure A3-7. Monitored pressures at Hole II, zone 3 (10 m).

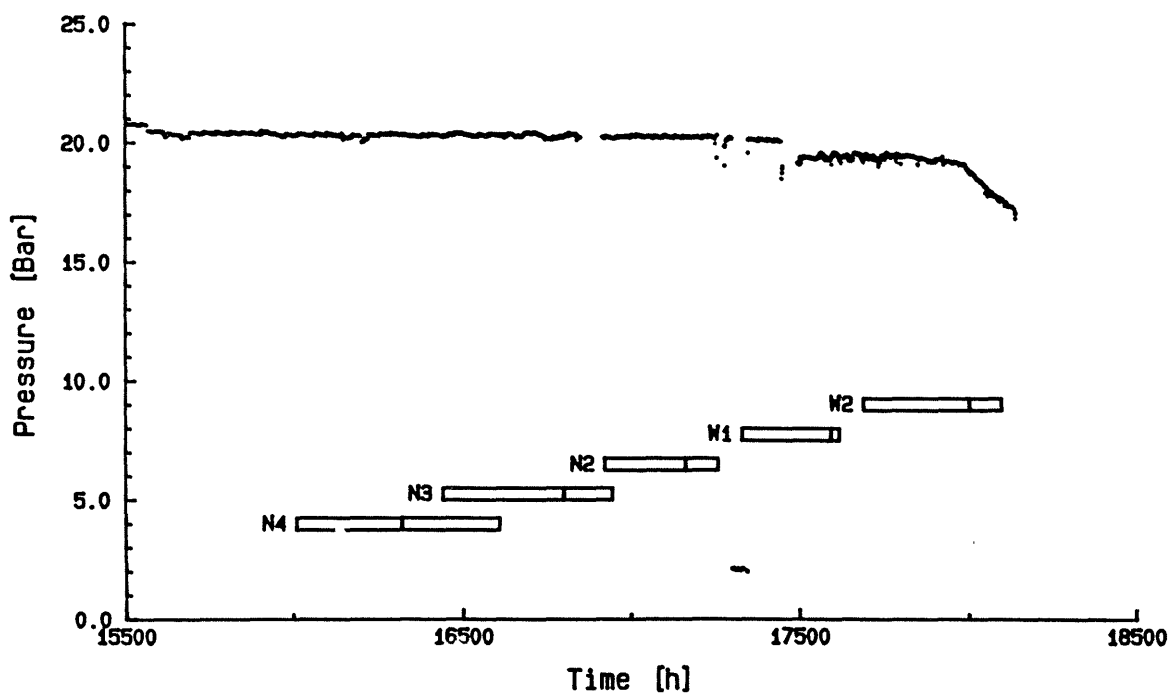
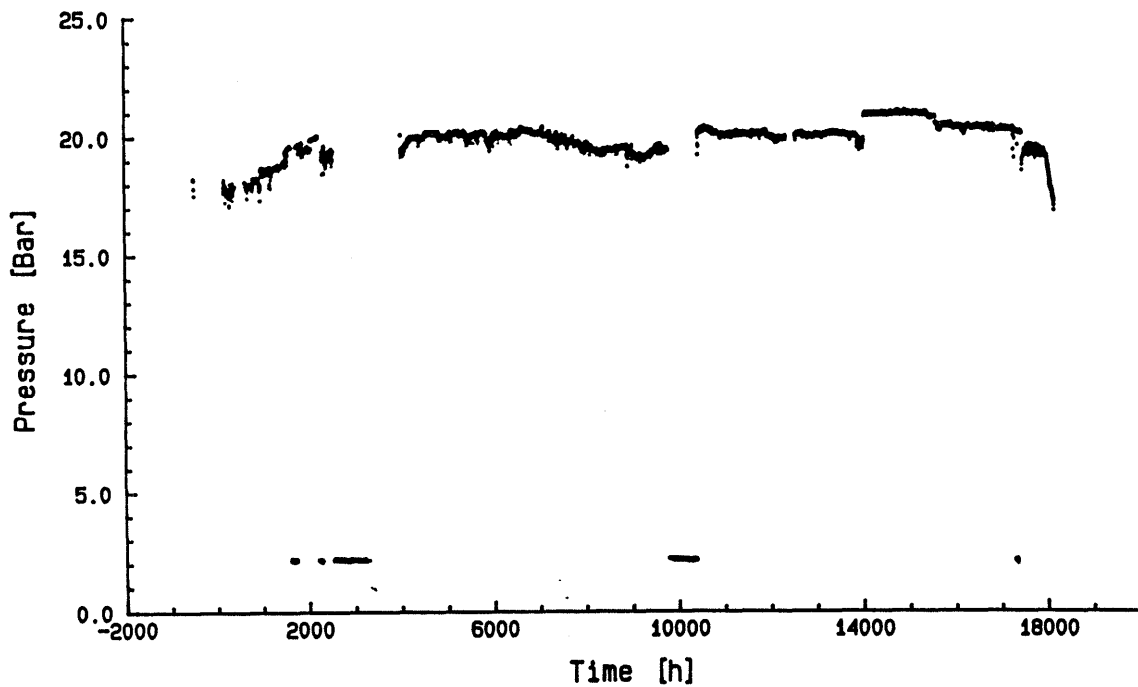


Figure A3-8. Monitored pressures at Hole III, top (50 m).

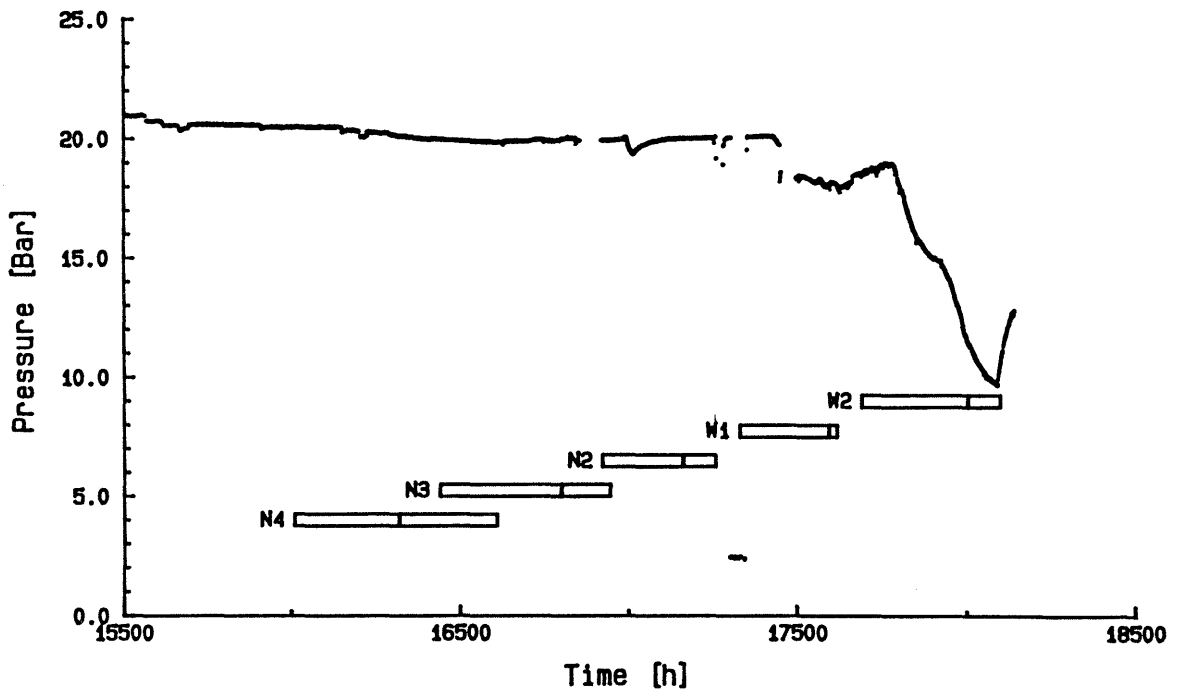
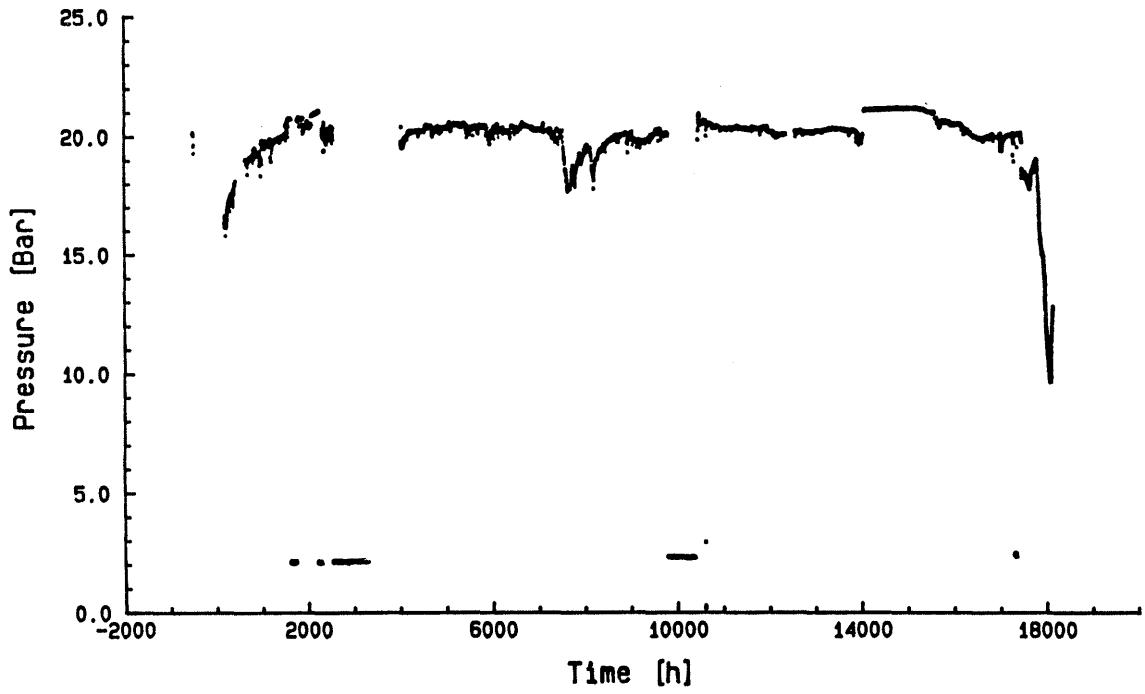


Figure A3-9. Monitored pressures at Hole III, zone 1 (37 m).

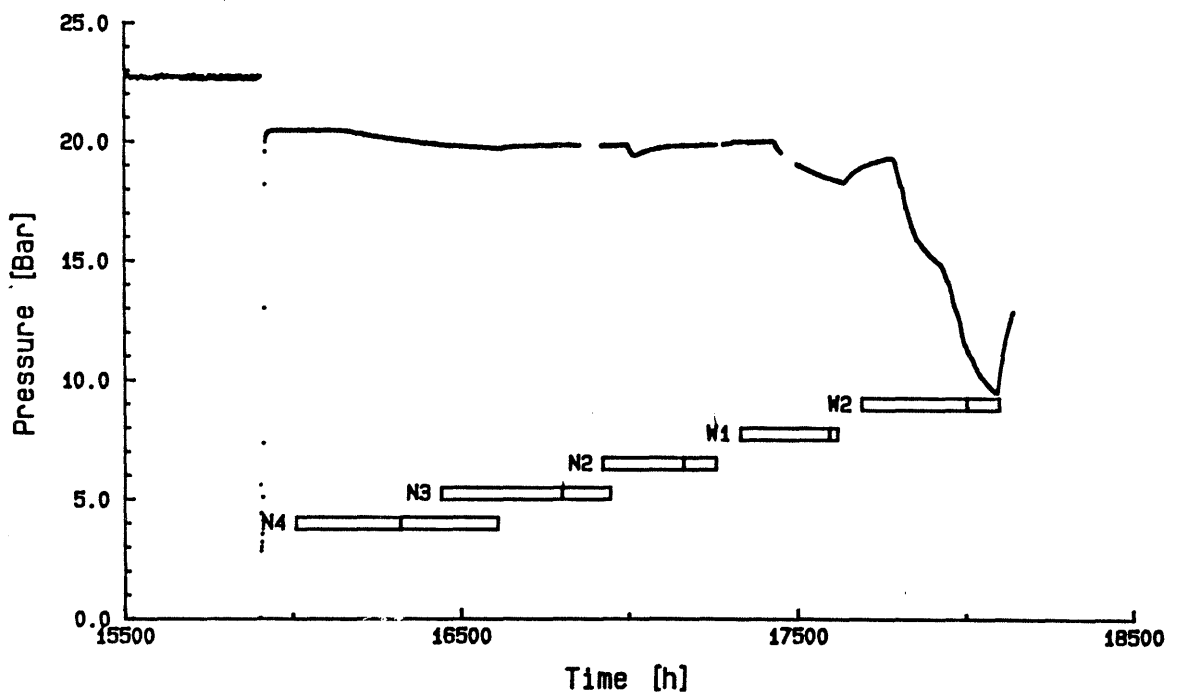
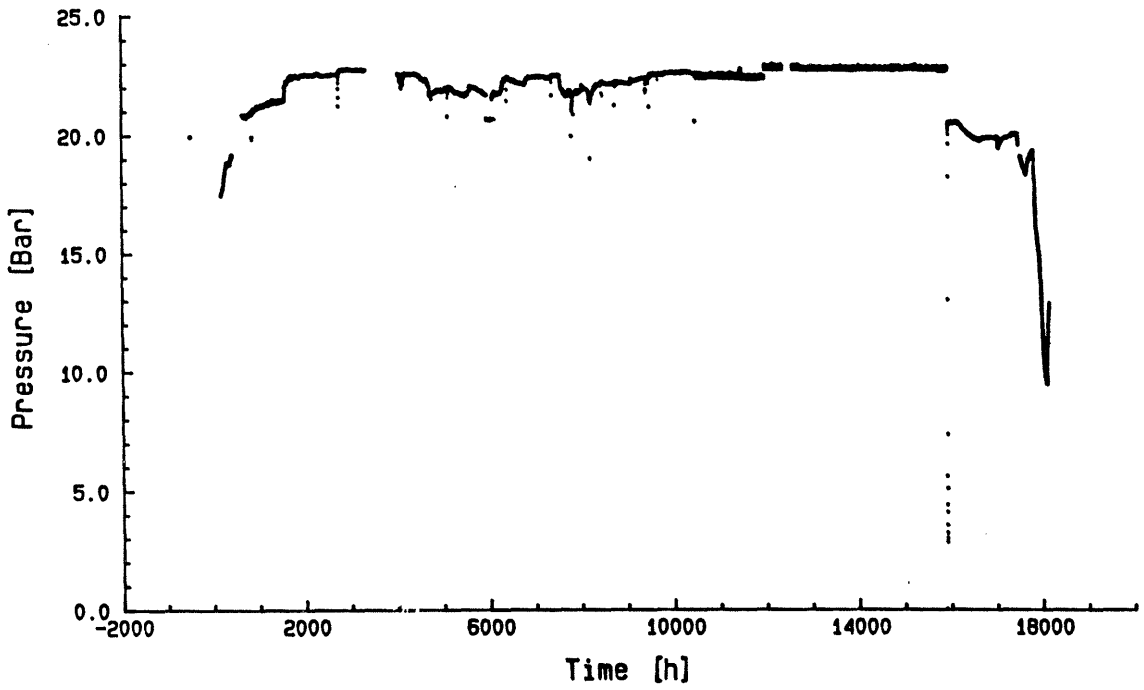


Figure A3-10. Monitored pressures at Hole III, zone 2 (29 m).

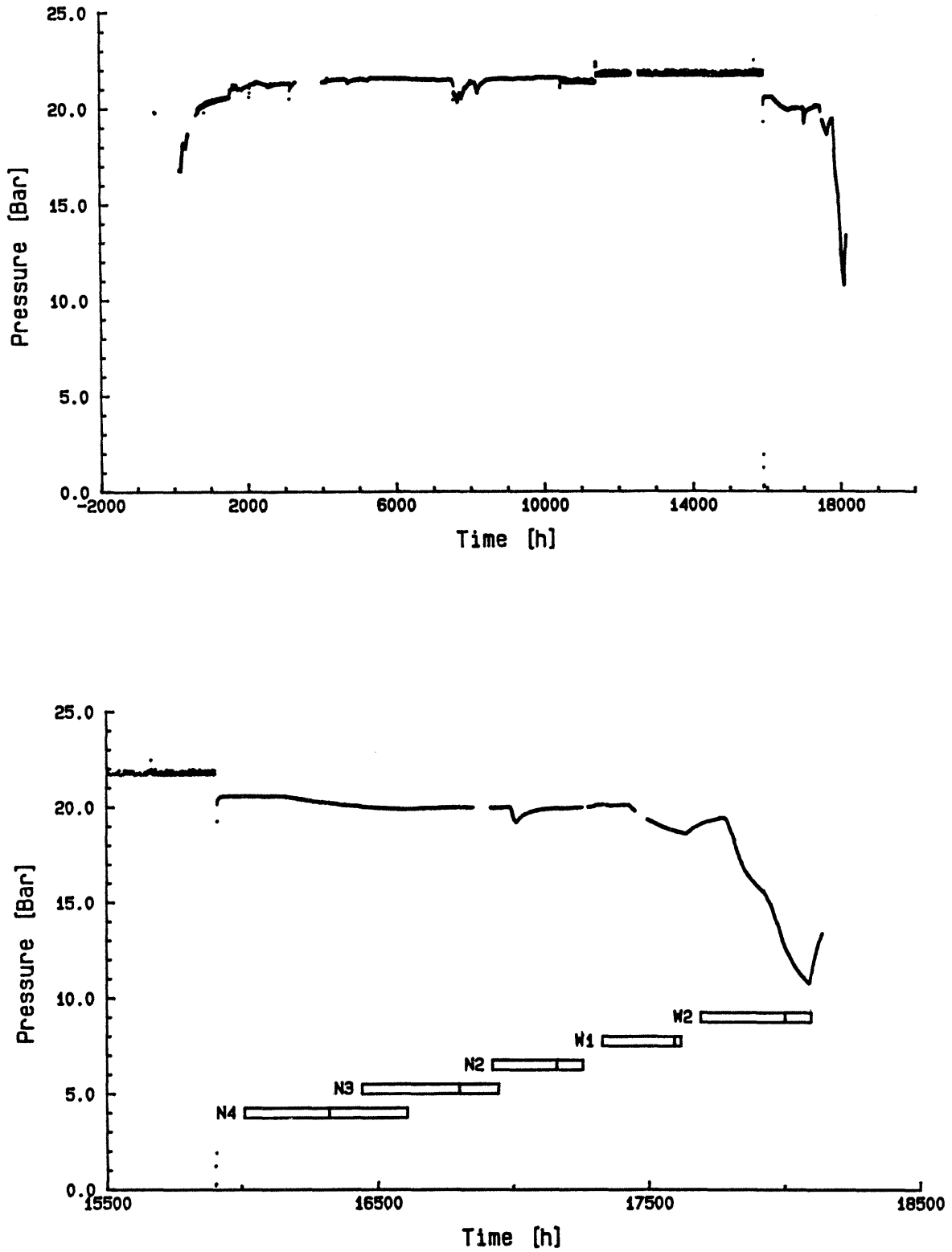


Figure A3-11. Monitored pressures at Hole III, zone 3 (19 m).

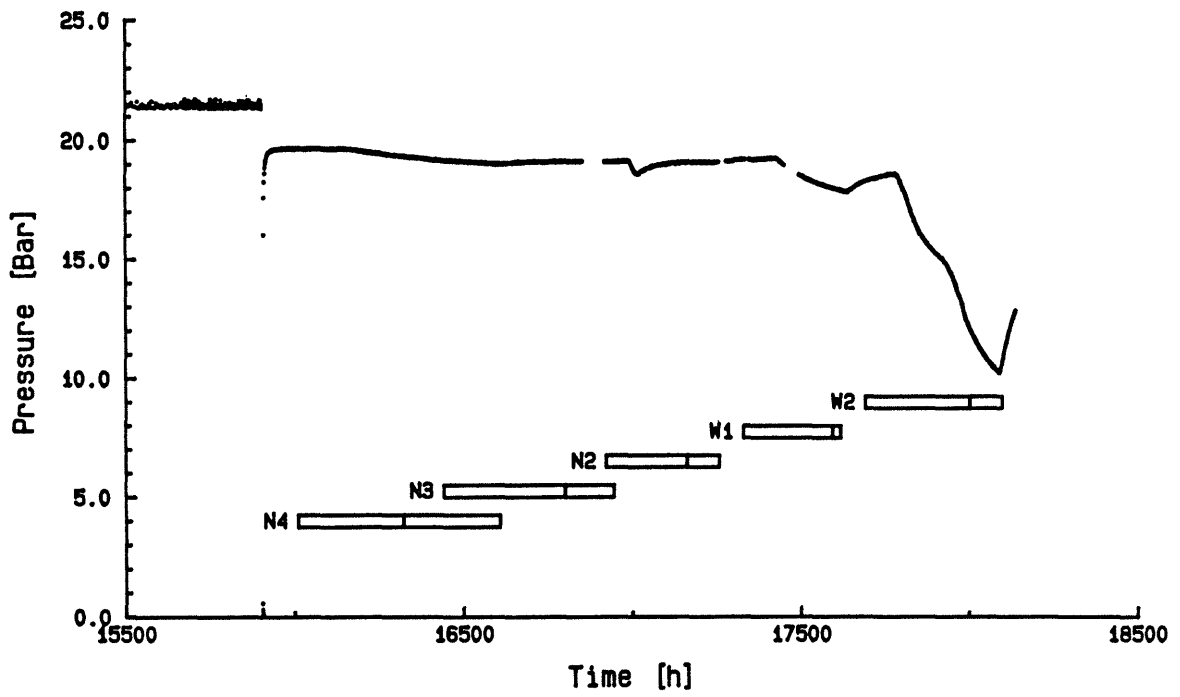
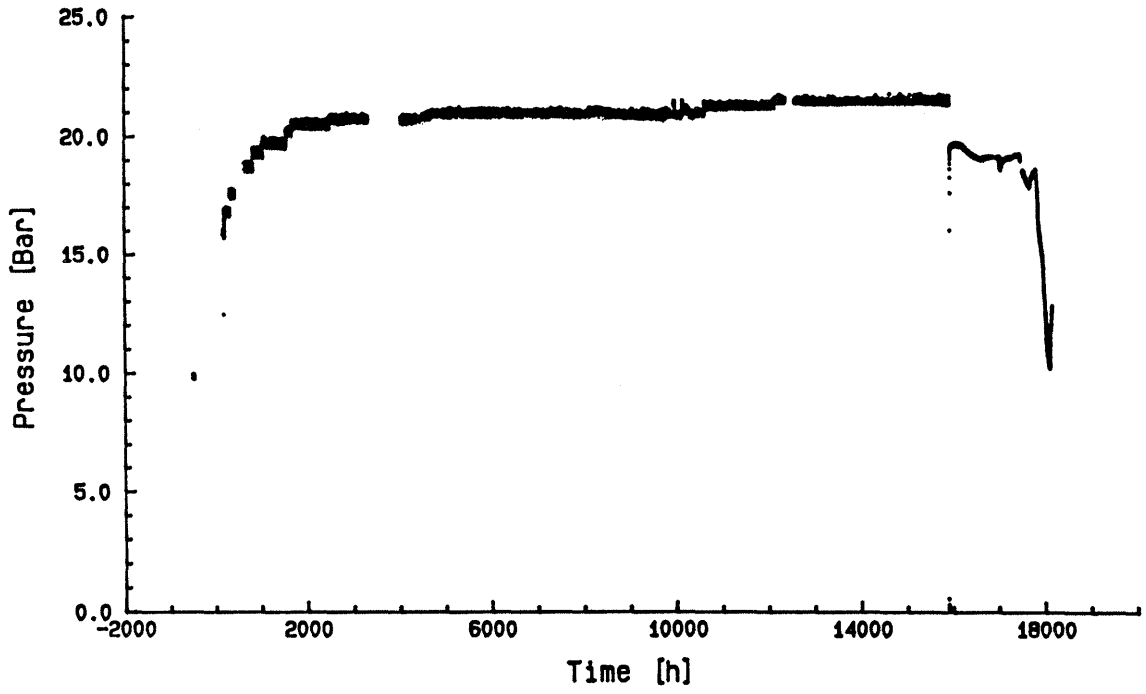


Figure A3-12. Monitored pressures at Hole III, zone 4 (13 m).

COMPILATION OF FRACTURE CHARACTERISTICS

The mapped fractures have been separated into two major groups: individual fractures and fracture zones. For each of the two major groups the fracture length per area for the 4 different fracture sets and for the mineral coating/filling materials are presented.

A4.2

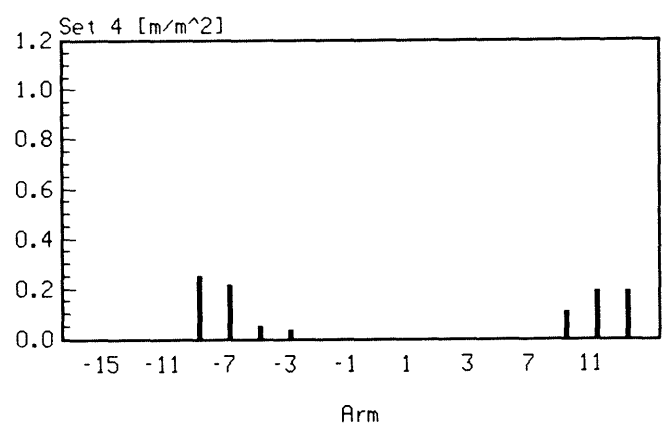
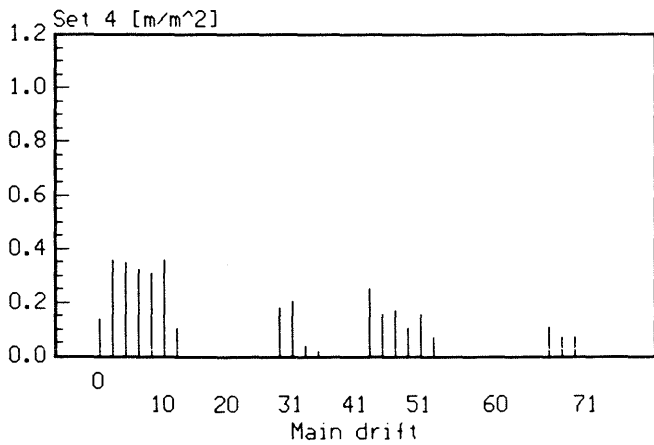
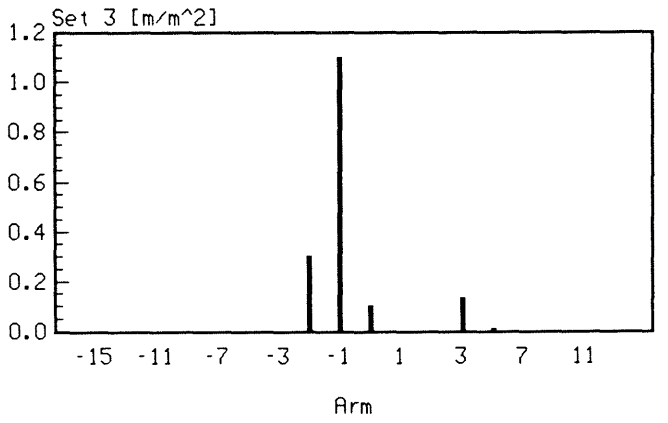
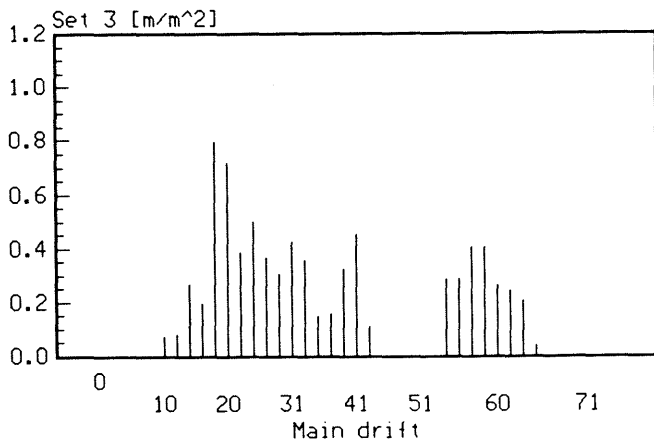
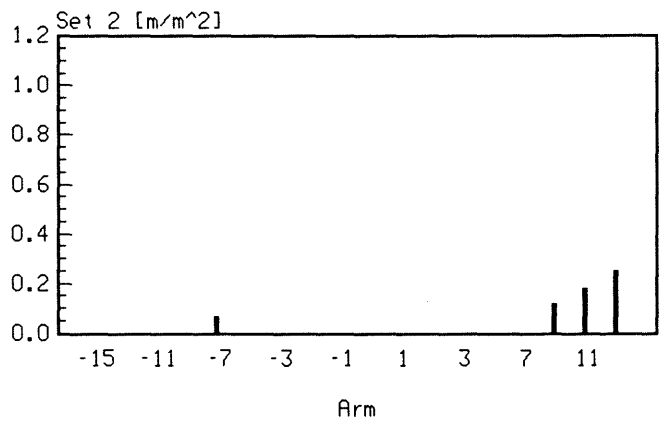
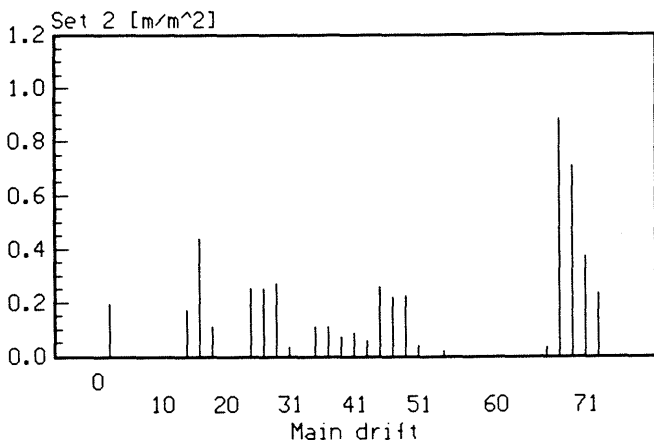
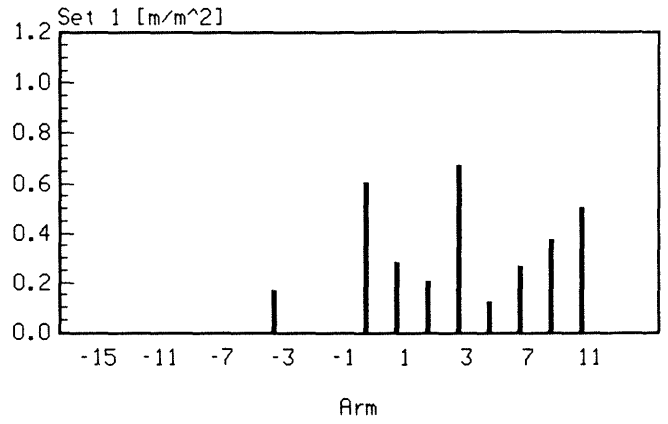
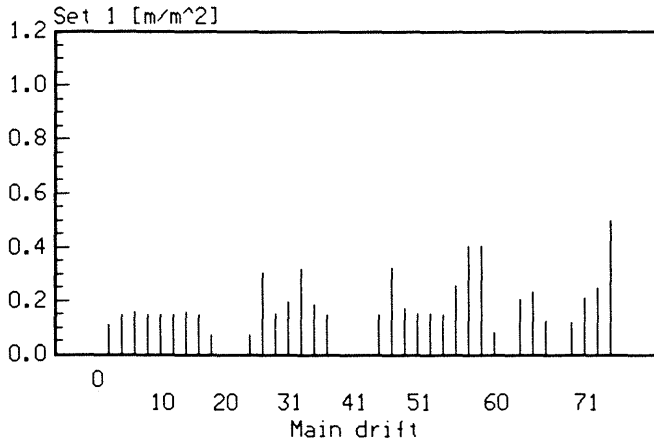


Figure A4-1.

Individual fracture length per m^2 for the different fracture sets (main drift and arm).

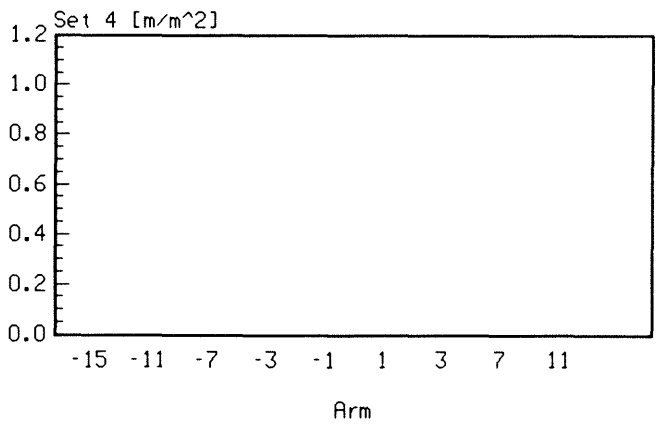
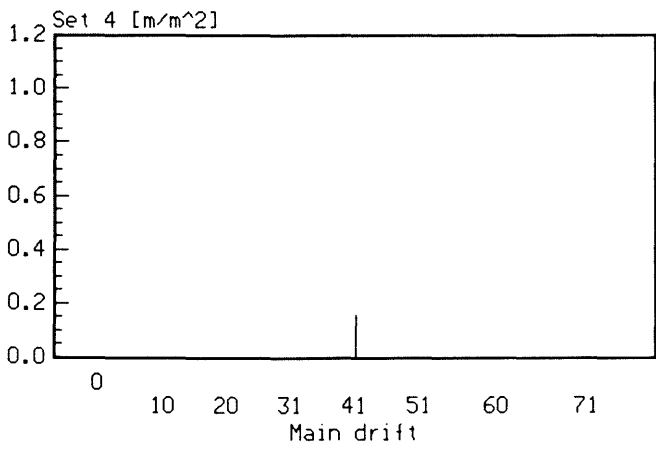
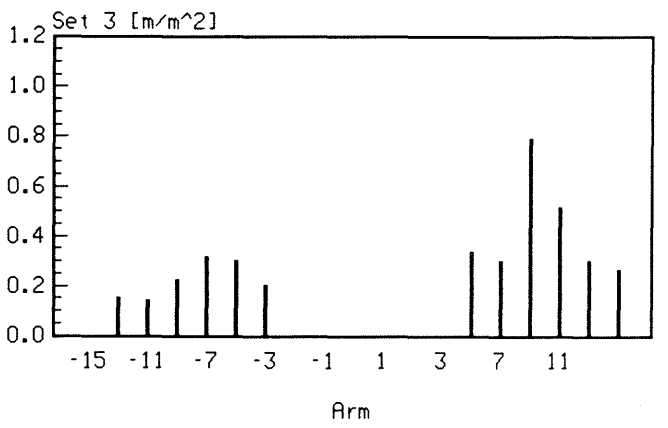
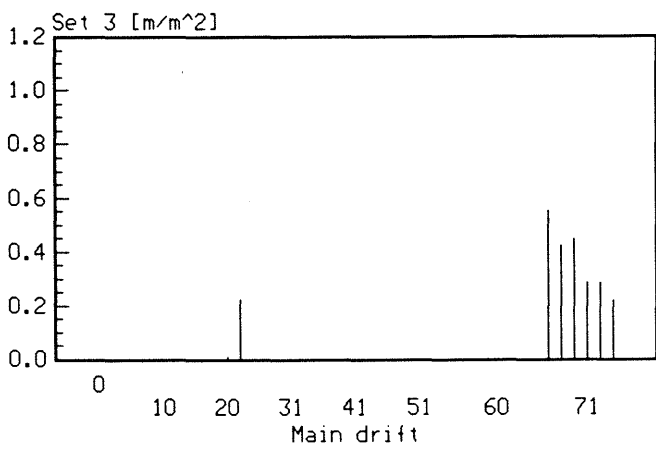
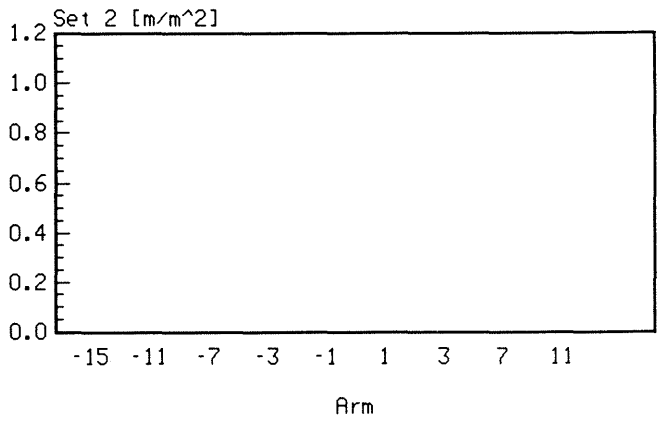
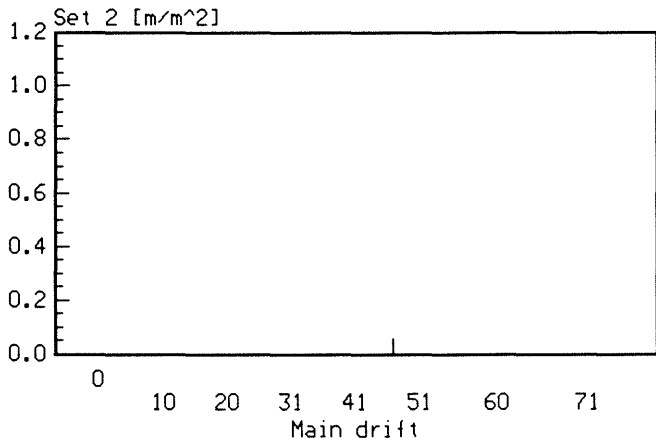
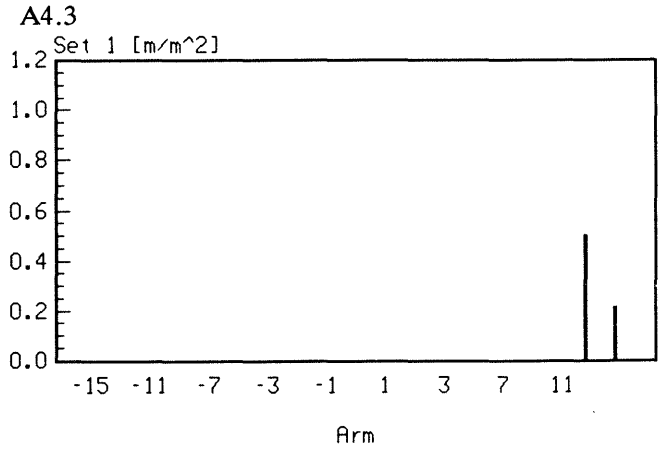
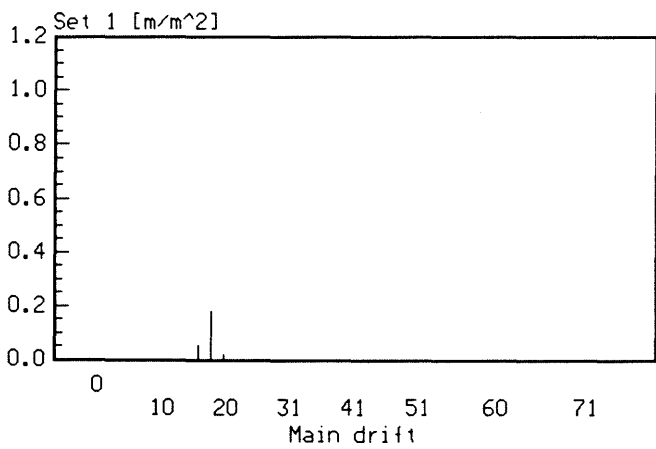


Figure A4-2. Zone length per m^2 for the different fracture sets (main drift and arm).

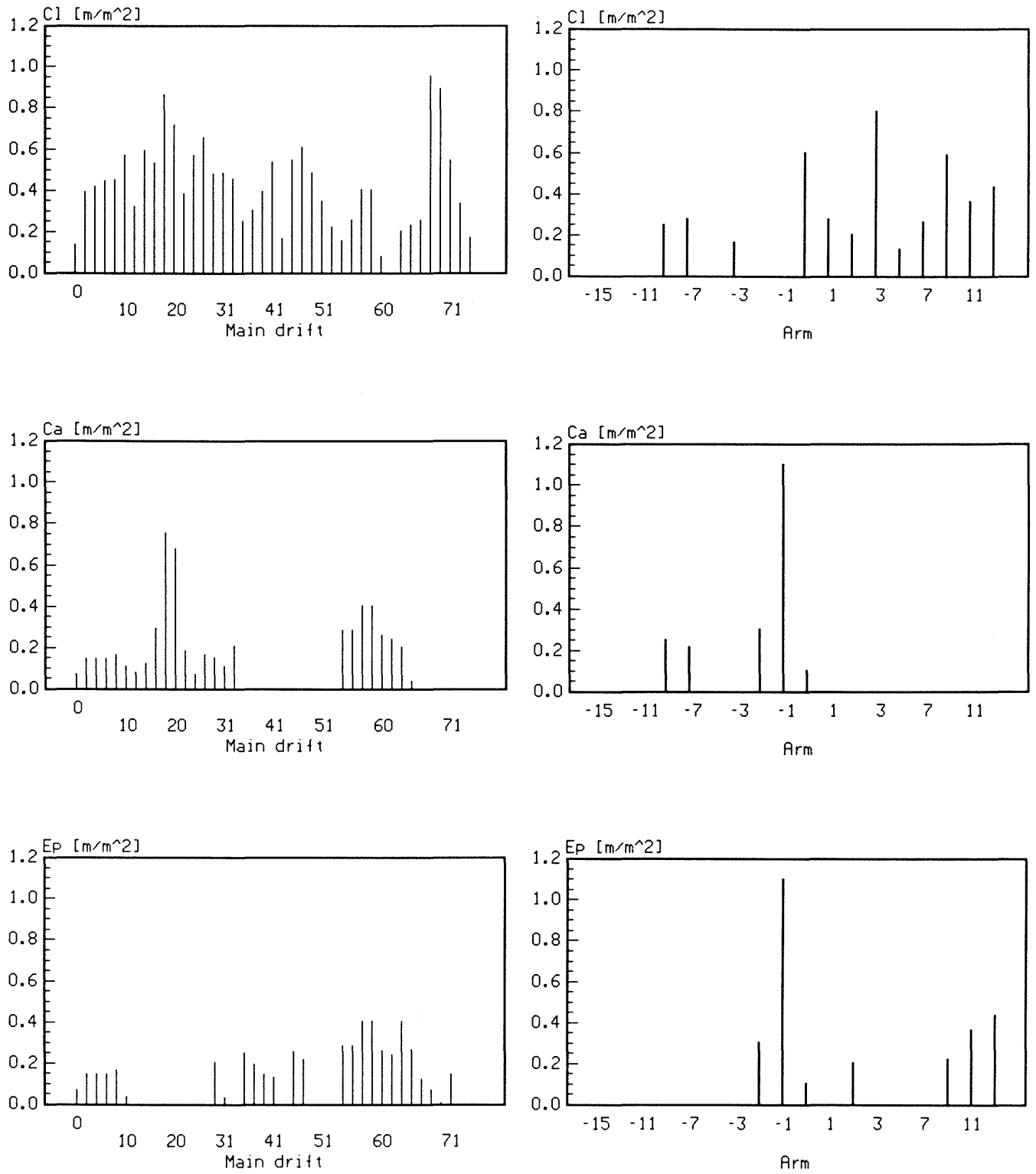


Figure A4-3.

Fracture coating/filling materials per m² for individual fractures (main drift and arm).

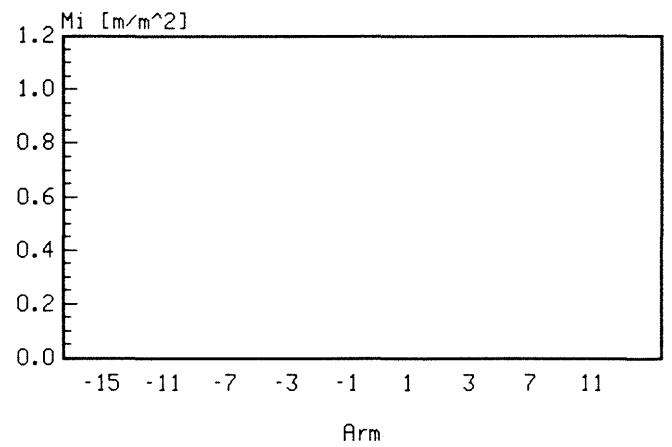
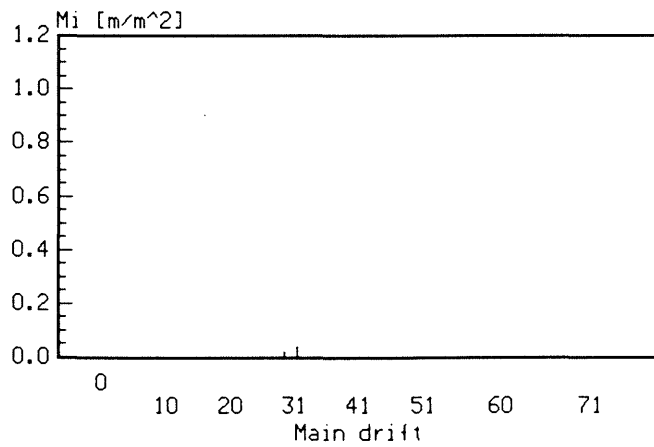
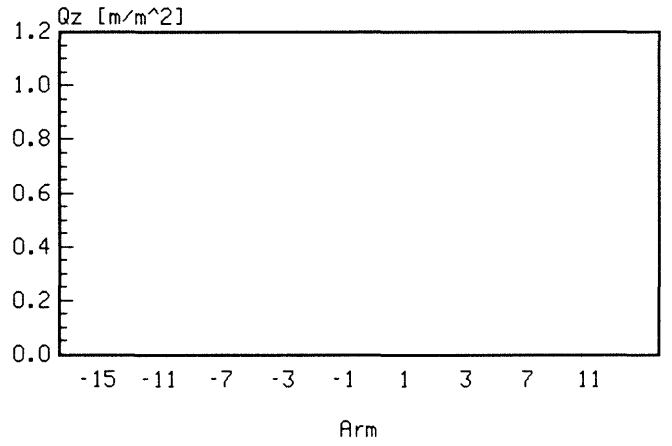
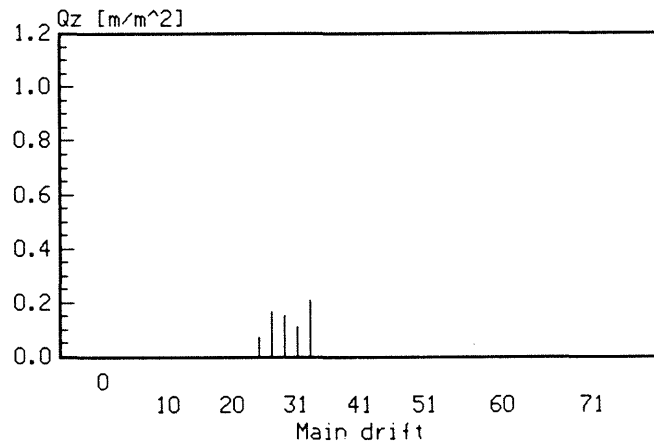
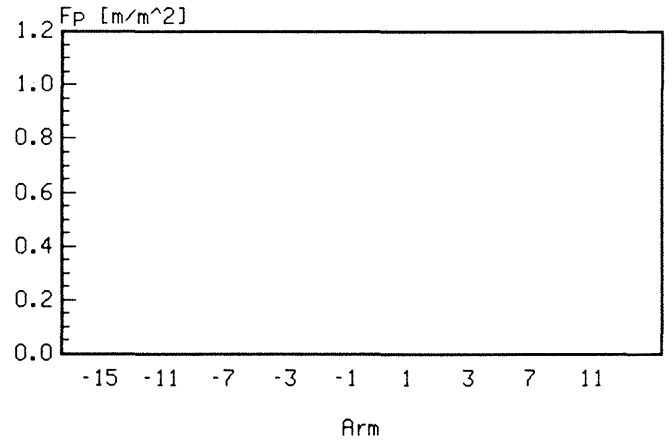
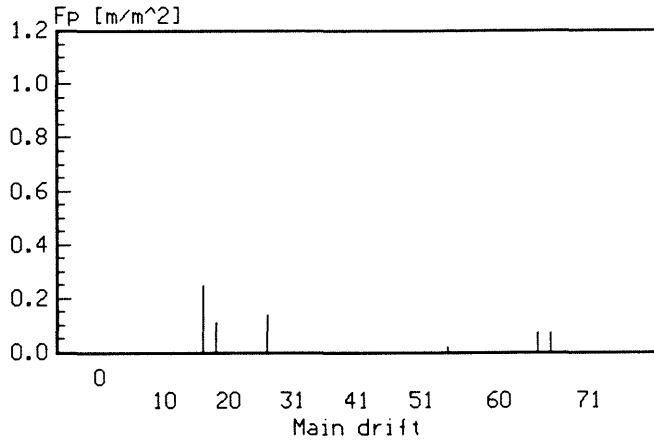


Figure A4-3.

Continued.

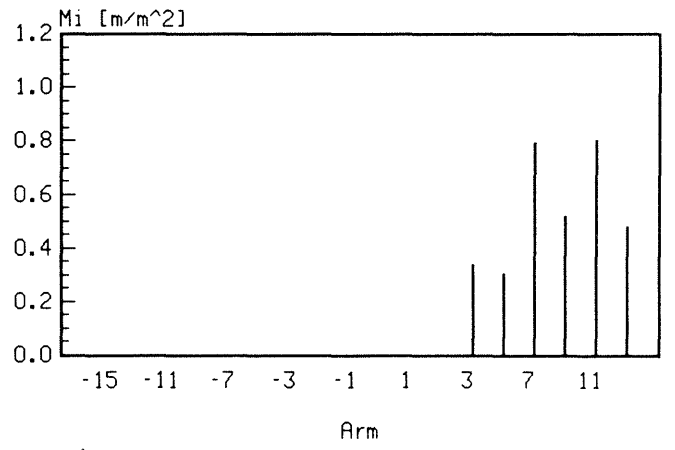
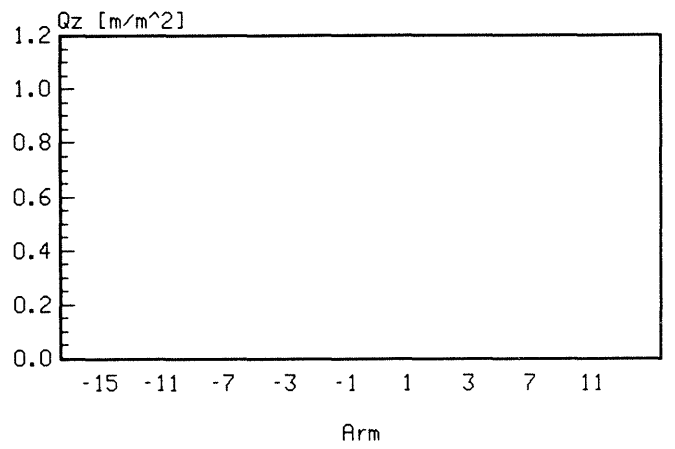
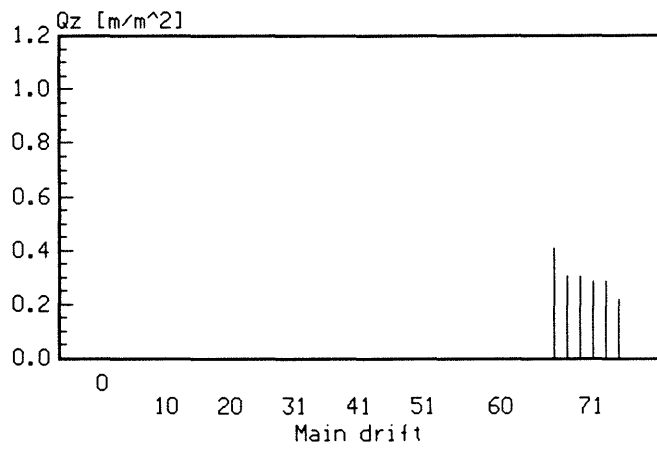
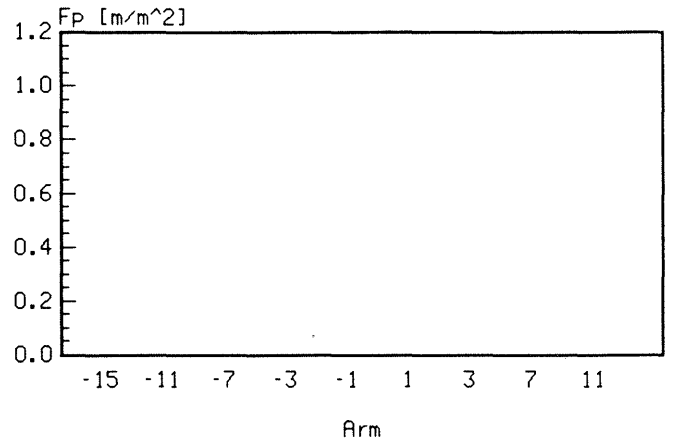
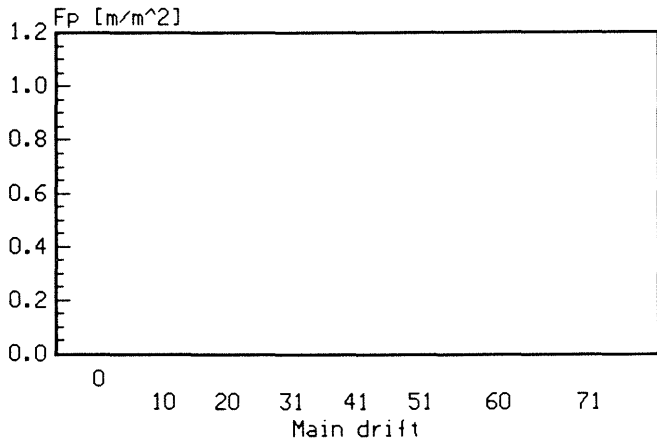


Figure A4-4. Continued.

FLOW VARIATIONS WITH TIME AT SOME SELECTED LOCATIONS IN THE TEST SITE

The flowrates for some 2 m sections of the drifts are presented. In one case at location 60 only the inflow to a single sheet is presented. This location was dry prior to the drilling but afterwards gave considerable amounts of water. Four plots are from the main drift (12, 25, 33, and 73 - the figures correspond to the distance in meters from the entrance of the main drift according to the local coordinate system), one from a single sheet of interest (60) and three from the right part of the arm (+9, +11, and +13 - the figures correspond to distance from the axis of the main drift).

The inflow rates for the main drift and arm at different times are presented in Figure A5-2.

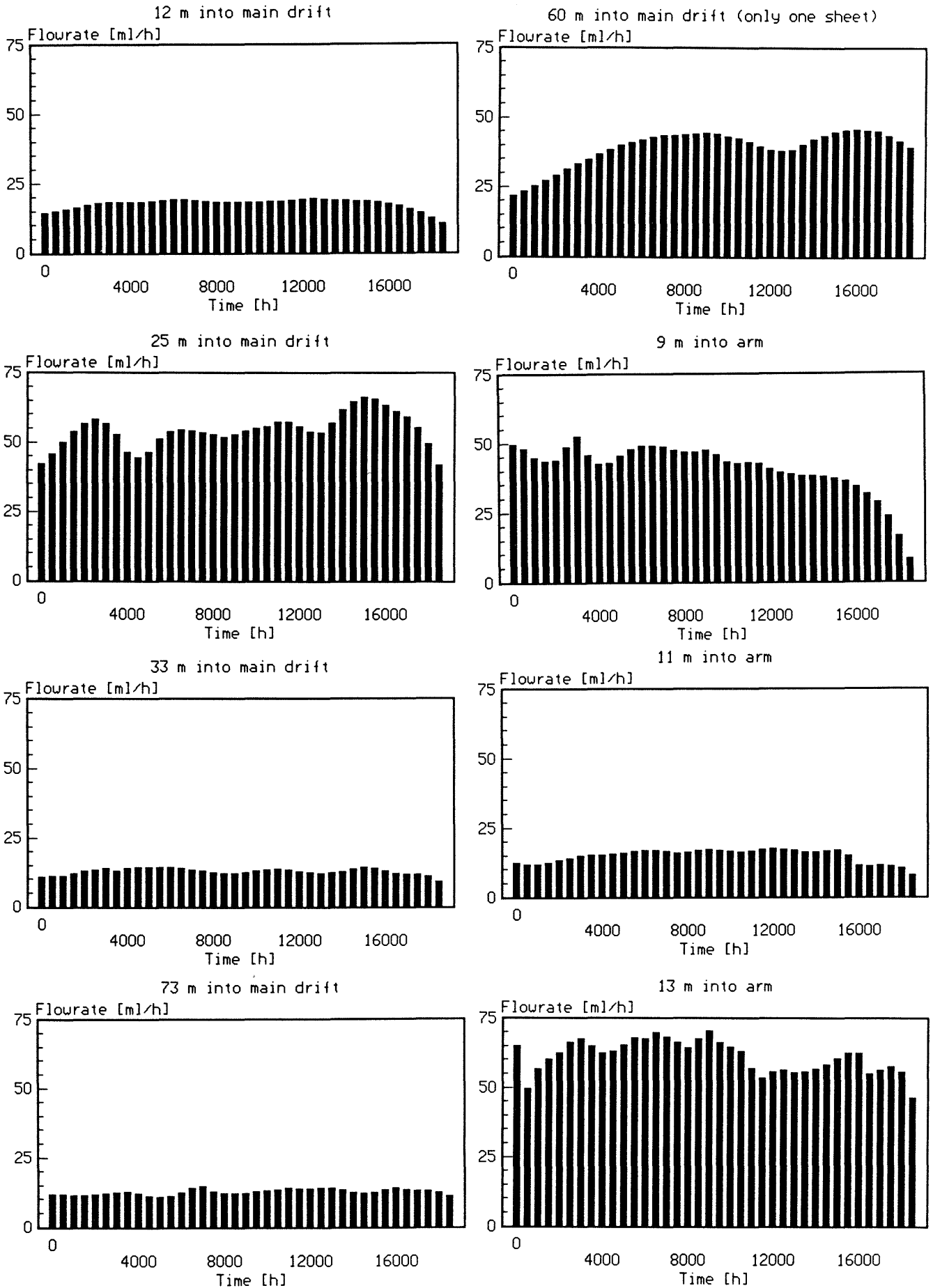


Figure A5-1. Inflow rates for 8 different 2 m sections as a function of time.

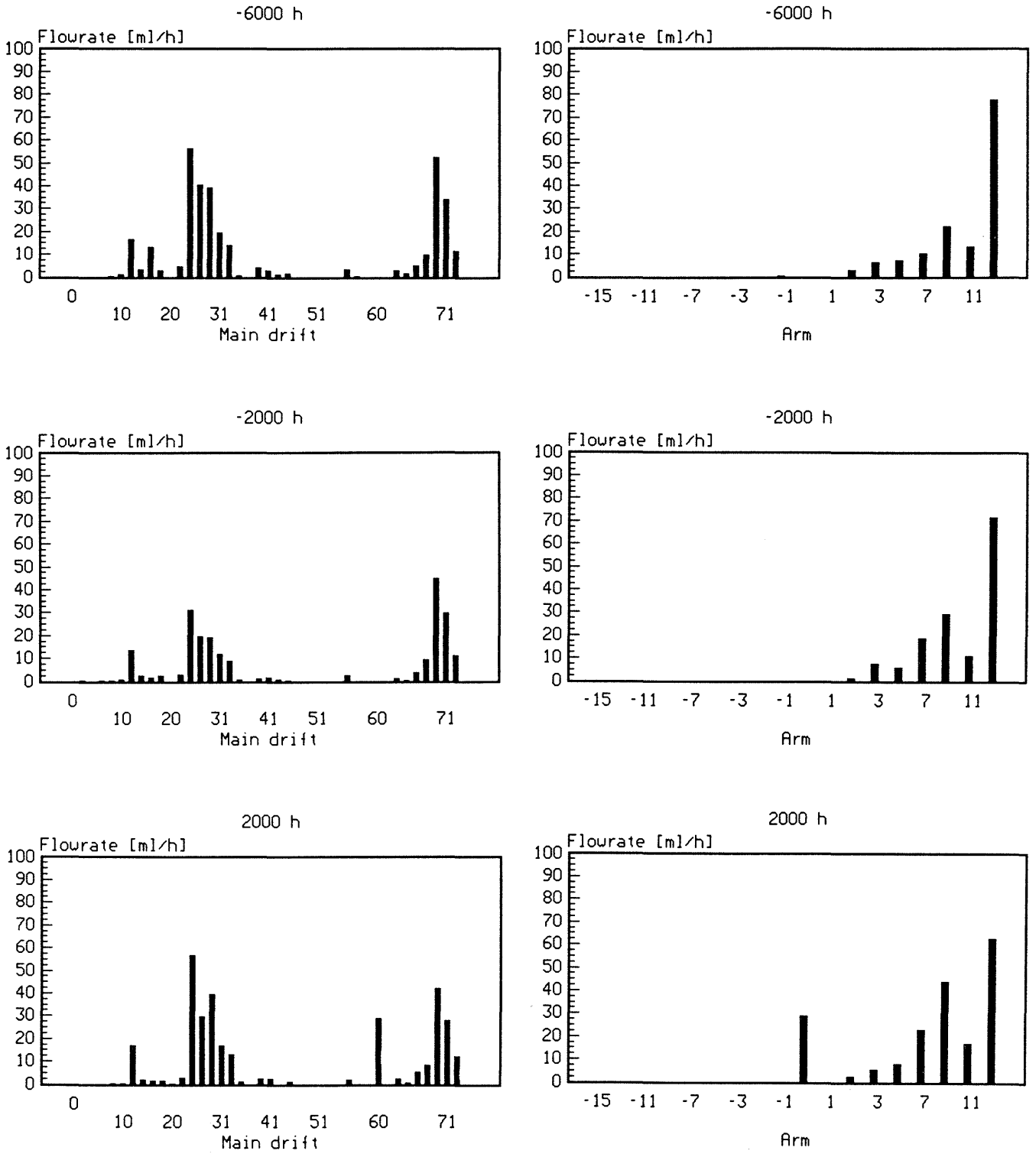


Figure A5-2. Inflow rates into the main drift and arm at different times.

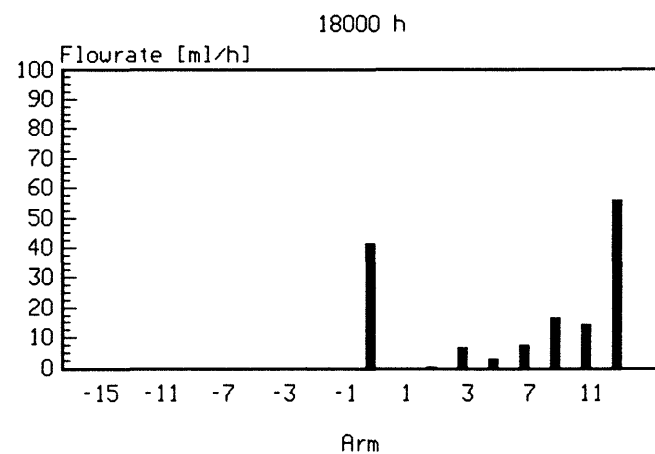
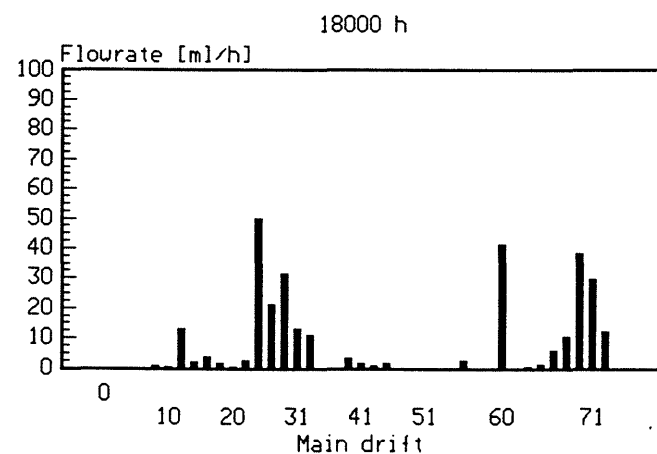
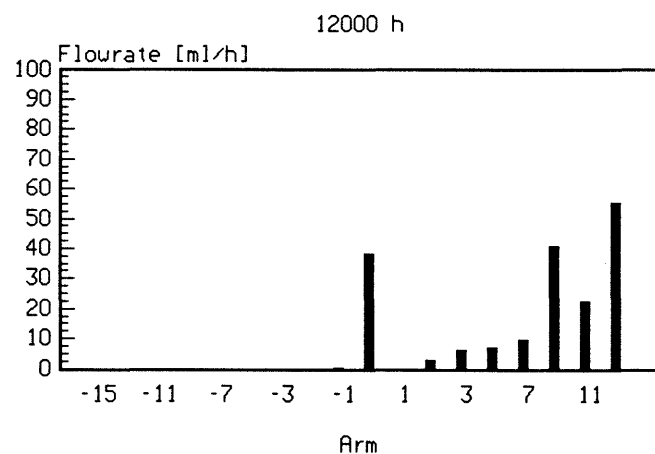
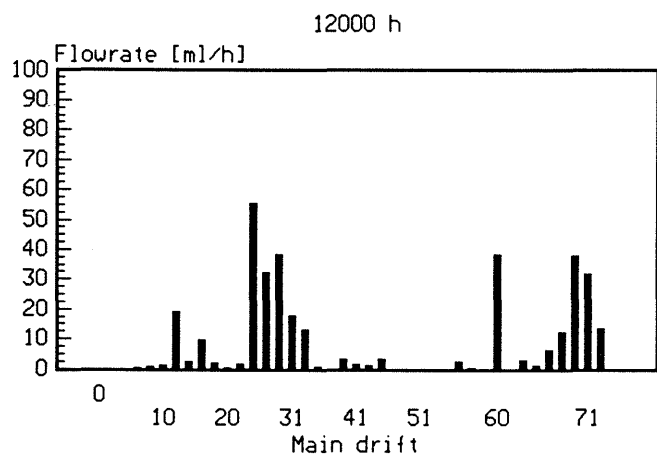
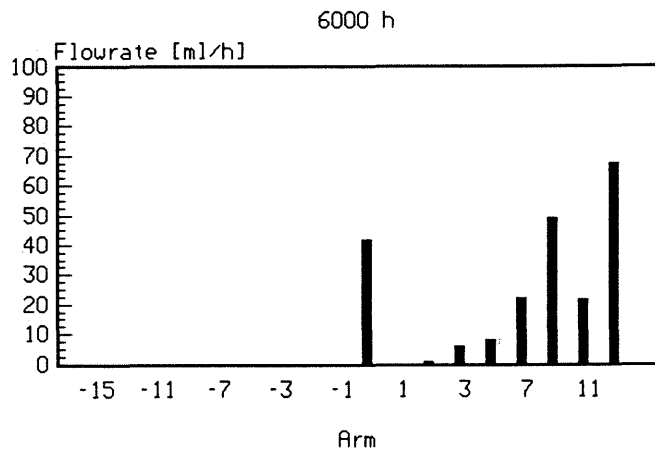
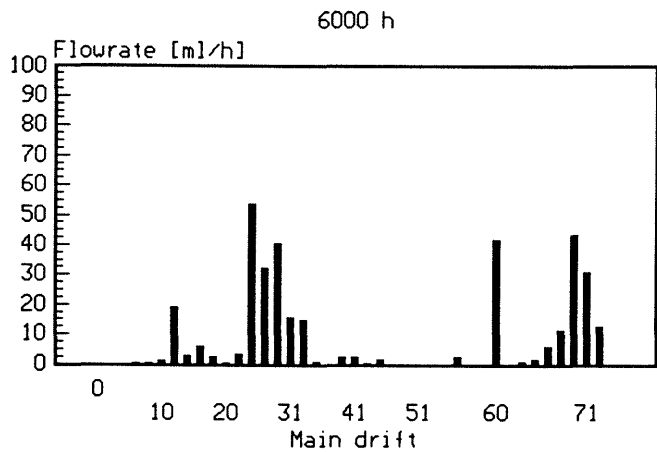


Figure A5-2.

Continued.

VENTILATION EXPERIMENT

SUMMARY

Measurements of the water inflow from the 3-D drift area below and after the excavation of the 3-D test site area showed that there were some differences between the measured values.

One possible reason for the difference could have been the outward transport of water by the ventilation air. Another reason may be that the excavation at the 3-D drift changed the water flow in the 3-D drift test site area.

To determine the total inflow into the test site, a ventilation experiment was performed.

This difference before and after the excavation of the 3-D drift can be explained by the ventilation air transporting water from the 3-D drift.

INTRODUCTION

The ventilation experiment is an extension to the 3-Dimensional (3-D) experiment.

Water inflow from the 3-D drift area was measured before and after the excavation of the 3-D drift test site area. Before the excavation, measurements of water inflow were obtained from a pilot hole drilled into the future drift area location. Water inflow measurements after excavation were measured in the excavated 3-D drift area. It was assumed that the inflows would be equivalent to each other, but a discrepancy was found to exist between the inflows measurements. The sources which may have introduced the difference in the water inflow from the 3-D drift could have been either the ventilation air or the excavation of the access drift and the 3-D drift. Reasons to suspect the circulating ventilation air was that it could transport out water from the excavation site. If this did not cause the discrepancy, then the excavation of the test site may have altered the water flow path in the surrounding rock.

To investigate if the ventilating air caused the water inflow difference, the ventilation experiment was devised. It was designed to evaluate the amount of water present in the air leaving the 3-D and access drift areas. This water amount was determined by measuring the air velocity, air temperature, and Rh-humidity at specific locations in the test site area.

BACKGROUND

Before the 3-D experiment was conducted, a suitable test site area for the 3-D drift was located. A pilot hole, known as the 3D-Pilot Hole No. 1 (3D-P1), was drilled horizontally from the main

A6.2

drift extending into the area of rock to determine if the rock area was granite or leptite. This is shown in Figure A6-1. Determining that the rock was granite, the area was chosen for the 3-D drift. Then measurements of the total water inflow into the pilot hole were taken. Along the total 150 m length the water inflow was measured to be approximately 6.5 l/hr and in that part of the pilot hole where the 3-D drift was later excavated it was about 3.0 l/hr.

Once these measurements were completed, the access drift and the 3-D drift were excavated horizontally to the main drift (Figure A6-1). The upper part of the 3-D drift was covered completely with plastic sheets so that the water flow could be measured. In the plastic sheets, emerging water from the rock was collected and then drained through tubing leading from the plastic sheets. From this procedure, the water flow measured for the covered upper part of the drift was about 0.7 l/hr. The water flow coming out into the floor of the 3-D drift was also measured and was found to be about 0.4 l/hr. Thus the total water flow found was 1.1 l/hr, compared to 3 l/hr obtained in the pilot hole in the same area.

One possible reason for the difference could have been the outward transport of water by the ventilation air present in the test site. Another reason maybe that the excavation of the 3-D drift changed the water flow in the area surrounding the drift. In order to investigate this difference, the ventilation experiment was initiated and carried out in the excavated area.

The ventilation experiment procedure was to measure the water content present in the ventilation air coming from the 3-D drift and passing through the access drift. By knowing the amount of water in the air, the amount of water possibly transported out from the excavation site could be determined.

VENTILATION EXPERIMENT

The ventilation experiment set-up consists of two walls, one wall built at the access drift's entrance and the other wall at the 3-D drift's entrance, where the measurements were conducted to determine the water content of the ventilation air leaving the 3-D drift and passing out through the access drift. See Figure A6-1 for the location of the walls. The values measured in the experiment were the relative humidity, air temperature, and air velocity.

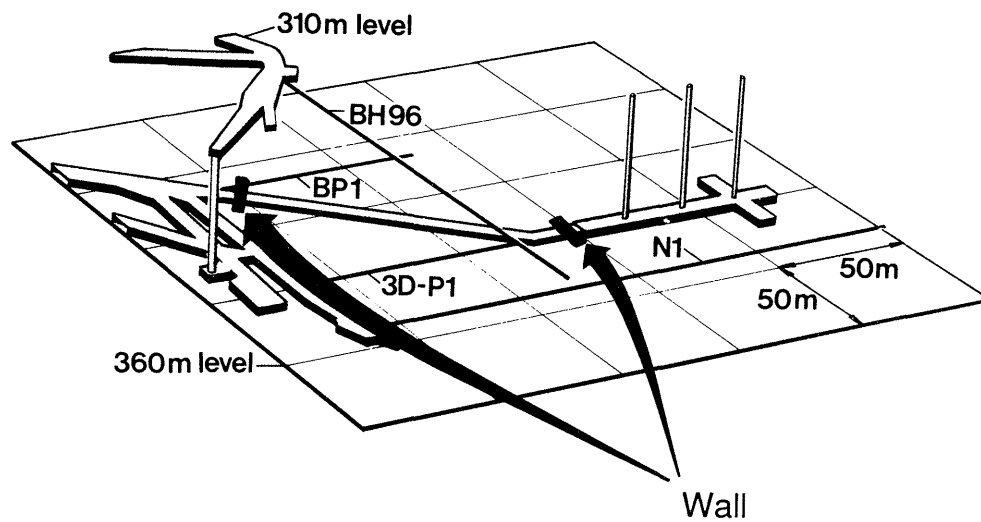
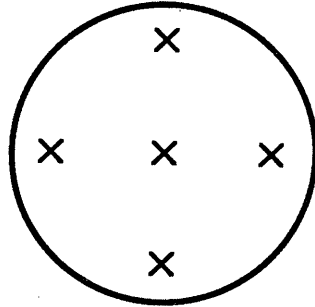


Figure A6-1. Location of the two walls for the ventilation experiment.

The walls were built of wood and sealed completely with a plastic film. The ventilation tube for the incoming air started in the main drift, continued through the access drift thus going through the two walls, extending into the 3-D drift, and ending at the cross in the 3-D drift. This layout is illustrated in Figure A6-1. The air exiting the excavated site passed through a 5 m long ventilation tube, one in each wall.



The air velocity was only measured in the ventilation tube. Air leaks in the existing space between the doors of the walls at the access and 3-D drift entrances and the floor introduced errors in the air velocity traveling through the exit tubes. At each wall, the air velocity was measured at five points inside the ventilation tube. One point was located in the center and the other four positioned inward one tenth of a diameter from the ventilation's tube inner diameter. Figure A6-2 shows the location of the five measuring points.

Figure A6-2. Measuring points.

The air velocity was measured over a 20 second time period and one mean value was calculated from this time period. A final mean value from the five mean value points was used in the calculations. To determine if the velocity varied between the 20 seconds measurements, ten 20 seconds measurements were taken at the same point inside the ventilation tube and each measurement resulted in reproducing the same final value.

The air temperature and relative humidity were measured four times at both center points in the ventilation tube and exiting tubes. The measurements were conducted over a half year time period to give an indication of the variance in the measured results.

The measurements for the ventilation experiment were made during the time period of March 1986 and October 1986. The first set of measurements was performed to develop measuring techniques to achieve good reproducible results, and they showed little variances in the measured values. Some of the guide lines that were developed and followed are listed:

- o Measure the air velocity consistently at the same points in the ventilation tube
- o Measure the air velocity probe at a fixed position in the ventilation tube, not hand held
- o Repeat the measurements for the temperature and the relative humidity
- o Measure at steady state conditions in the access drift.

RESULTS AND DISCUSSION

Figures A6-3 and A6-4 show the water flowrates to the 3-D drift and the flowrates from the 3-D drift and access drift combined. The water quantity present in the ventilation air coming from the 3-D drift was found to be on the average 2 l/h. The combined water quantity in the air from the 3-D and access drift was found to be

A6.5

about 4 l/h. The flowrate of water in the ventilation air from the 3-D drift was 2 l/h. The combined total water flow to the 3-D drift thus is 2 l/h (from ventilation) + 0.7 l/h (from sheets) + 0.4 l/h (from covered areas on the floor) making a total of 3.1 l/h. This compares well with the flowrate found in the pilot hole, 3 l/h, in that section of rock where subsequently the 3-D drift was excavated.

The air velocity was measured in five points located in the ventilation tube at both walls in the access drift over a time period of 20 seconds. A mean value for each point was calculated. One overall mean value was determined from the five mean values and was used in the subsequent calculations. Checking the variation of the air velocity, ten 20 seconds measurements were all taken at the same point in the ventilation tube at both walls. The results from the ten measurements gave the same reading ten times. Since the velocity indicated no sign of varying during the ten 20 seconds measurements, it was then concluded that the flow variations were small.

The quantity of water contained in the air was determined by the air temperature and relative humidity measurements. These values were read four times at the centers of the ventilation tube and exit tubes. The measurements were conducted over a time period of one half year so that variation in the results could be observed.

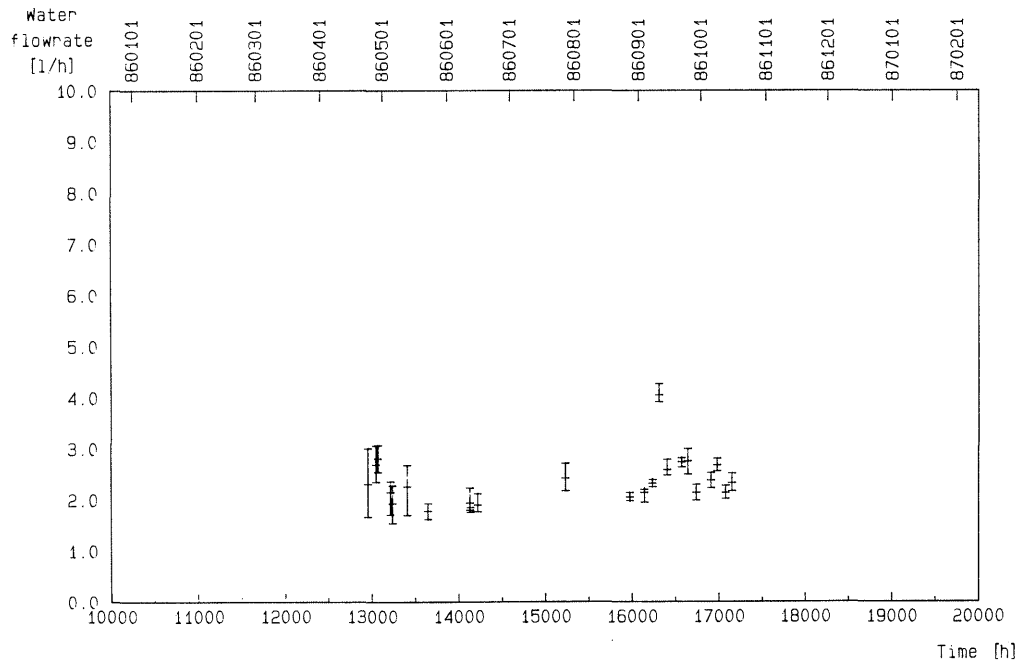


Figure A6-3. Water flowrate to the 3-D drift.

A6.6

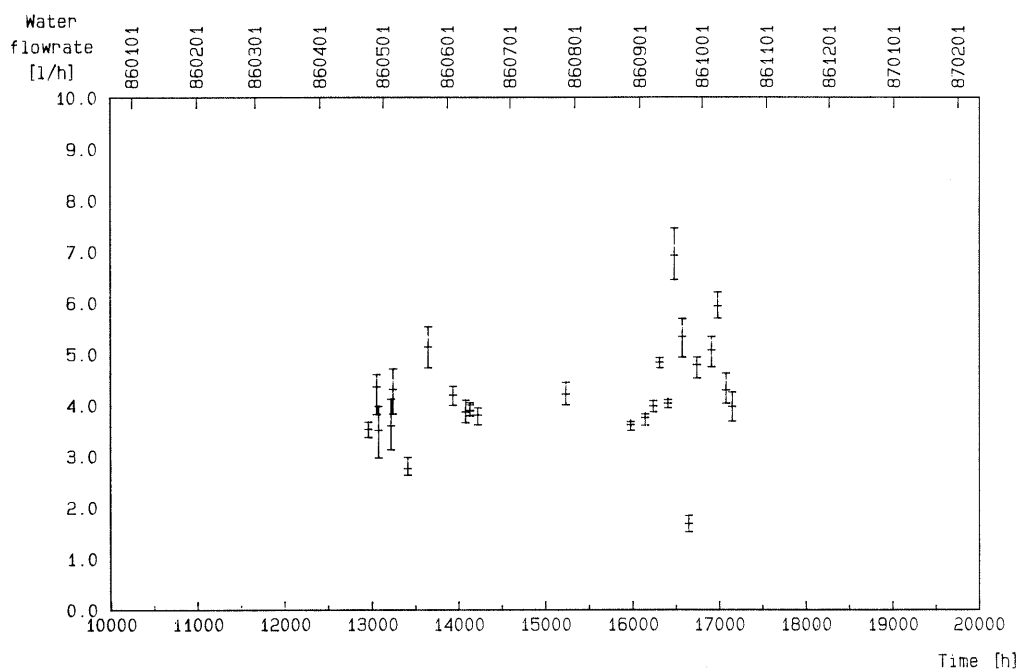


Figure A6-4. Water flowrate to the 3-D drift and access drift combined.

Observations made from Figures A6-3 and A6-4 show that a big variance is present at the beginning of the measurements. This occurs because the methods used in measuring were not fully developed. Therefore many sources of error were introduced into the calculated values. From these experiences, corrections were made in the measuring techniques. After 14,000 hours the velocity measurements were performed with a fixed probe inserted into the ventilation tube and all experimental values were measured outside both walls. At 16,450 hours one wall inside the access drift was cleaned with water which introduced additional water into the area. This caused error in all the future 3-D drift and access drift measurements and thus are not considered as representative values for the experiment, see Figure A6-4.

CONCLUSIONS

The difference observed between the water inflow in the pilot hole and the measured water inflow to the 3-D drift in the covered parts is caused by the ventilation air transporting away humidity from the uncovered parts of the drift. The ventilation air was responsible for transporting out about 2.0 l/hr of water from the 3-D drift. The water inflow from the covered upper part and the covered part of the floor of the 3-D drift was approximately 0.7 l/hr and 0.4 l/hr, respectively. Adding all the water amounts gives a total water measurement of about 3.1 l/hr. This is in good agreement with the pilot hole water inflow measurement of about 3.0 l/hr. Therefore, it can be concluded from these observations that the water inflow measurement difference between the before and after excavations of the 3-D drift was caused by the ventilation air transporting out water from the 3-D drift. In addition to this, these measurements gave no indication that the conductivity of the surrounding rock was altered during the excavation of the 3-D drift.

INJECTION CURVES: REAL AND IDEALIZED**INTRODUCTION**

This appendix shows the injection curves for the different tracers. In Table A7-1 the idealized curves, consisting of between three and five different step injections, are shown. These same curves are shown in Figures A7-1 to A7-6 and are plotted with the flowrate as a function of time. The real injection curves are plotted in Figures A7-7 to A7-15.

Table A7-1 Injection curves used in the fitting process.

Tracer 1		EOSIN B
Time for injection (h)		Injection flow (ml/h)
3 434		8.87
4 032		1.90
936		8.37
2 043		0.24
5 217		3.36
Time delay	141 h	
Total time	15 662 h	
Total injection	63.98 l	
Total mass	95.98 g	
Tracer 2		URANINE
Time for injection (h)		Injection flow (ml/h)
277		8.80
747		4.27
4 215		1.99
5 550		6.90
5 030		4.90
Time delay	1 h	
Total time	15 819 h	
Total injection	76.96 l	
Total mass	76.96 g	

Table A7-1 continued.

Tracer 3		ELBENYL
Time for injection (h)		Injection flow (ml/h)
278		1.99
240		0.91
264		0.23
744		0.03
8 664		0.44
Time delay	0 h	
Total time	10 190 h	
Total injection	4.65 l	
Total mass	9.29 g	
Tracer 6		EOSIN Y
Time for injection (h)		Injection flow (ml/h)
349		6.40
7 151		2.34
2 690		3.38
Time delay	1 h	
Total time	10 190 h	
Total injection	28.06 l	
Total mass	28.06 g	
Tracer 8		IODIDE
Time for injection (h)		Injection flow (ml/h)
2 006		8.31
2 606		2.79
2 730		11.72
4 776		14.10
3 544		4.63
Time delay	141 h	
Total time	15 662 h	
Total injection	139.67 l	
Total mass	1.82 mol	

A7-1 continued.

Tracer 9		BROMIDE
Time for injection (h)	Injection flow (ml/h)	
842	10.56	
10 560	3.55	
4 260	1.05	
Time delay	169 h	
Total time	15 662 h	
Total injection	50.84 l	
Total mass	0.97 mol	

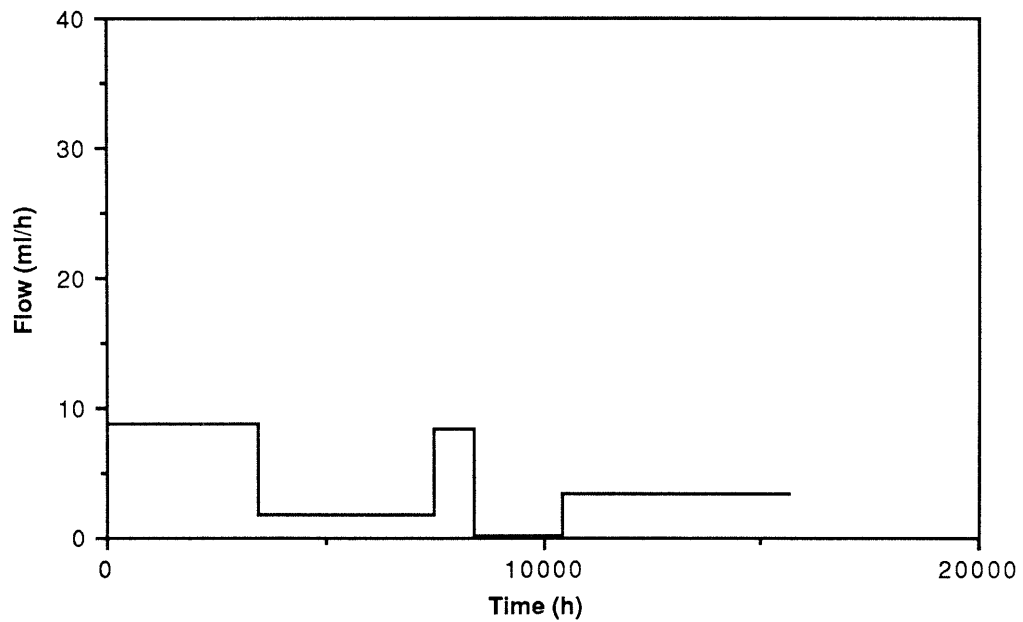


Figure A7-1. Injection of Eosin B.

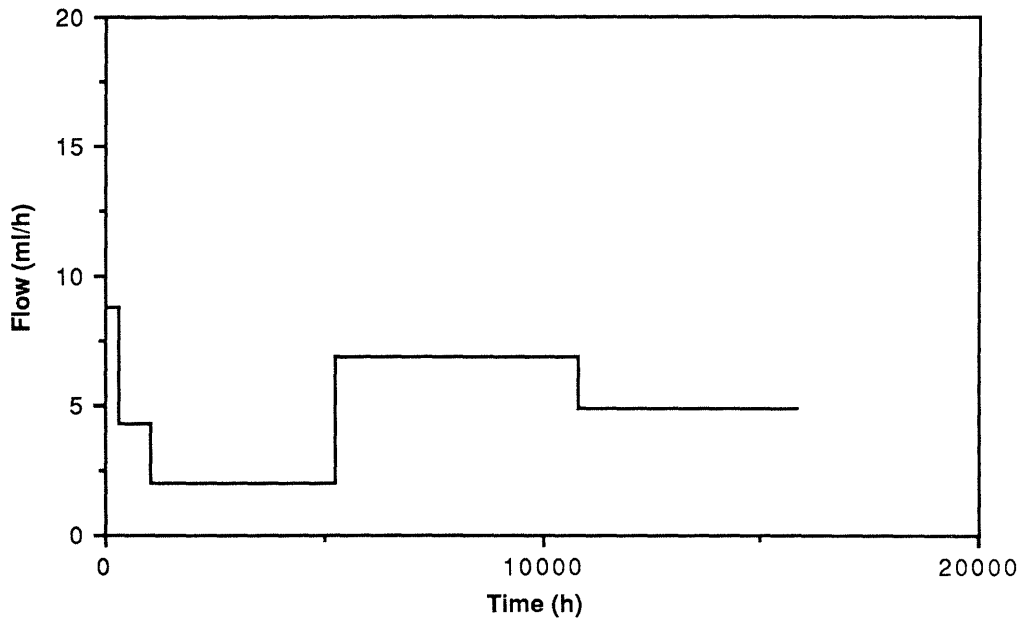


Figure A7-2. Injection of Uranine.

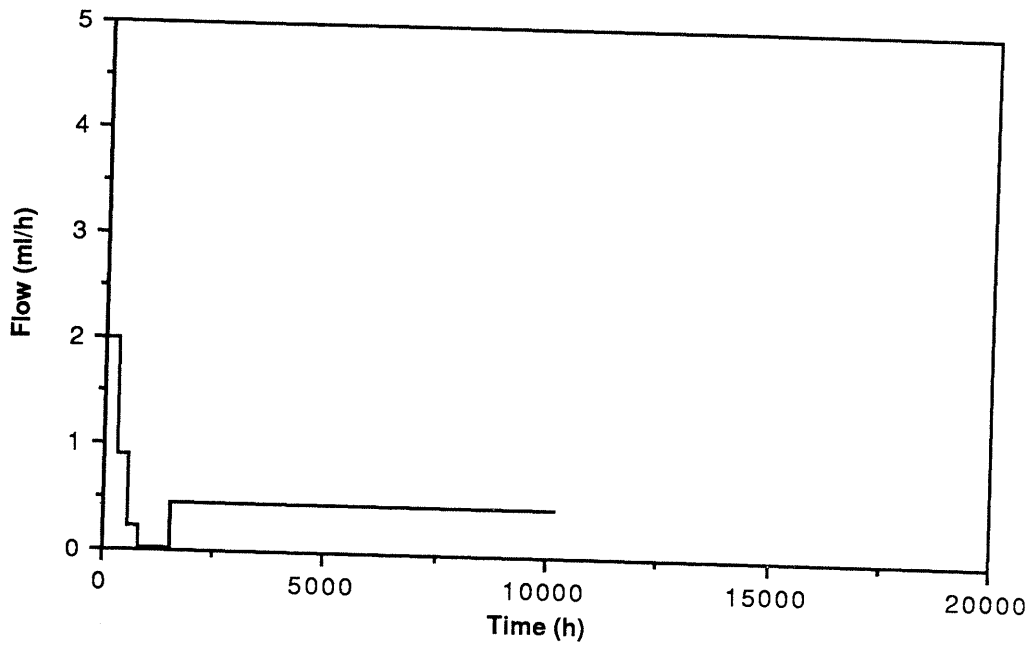


Figure A7-3. Injection of Elbenyl.

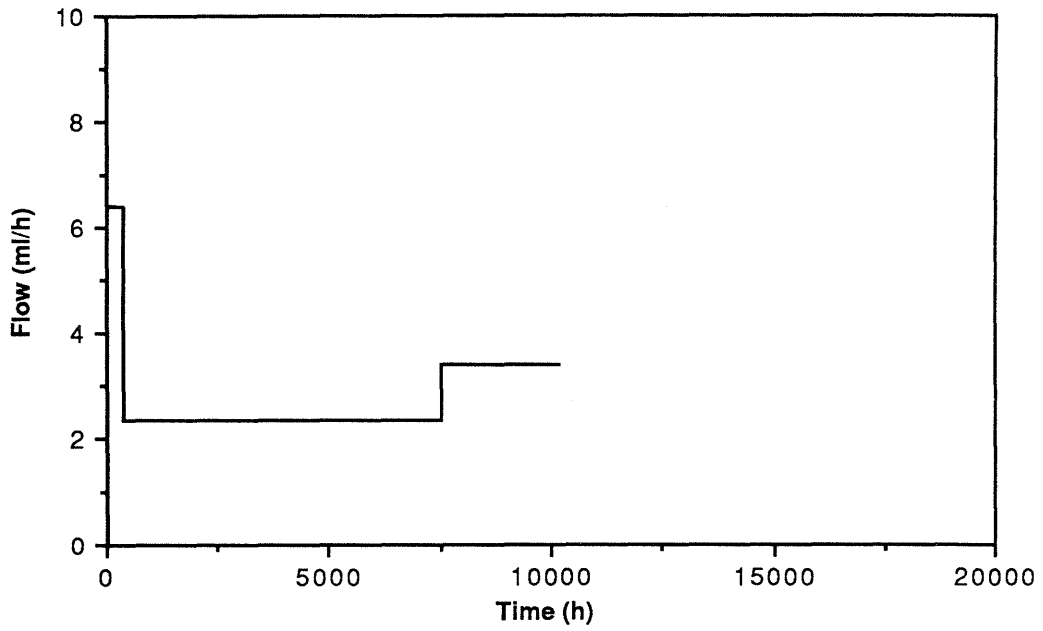


Figure A7-4. Injection of Eosin Y.

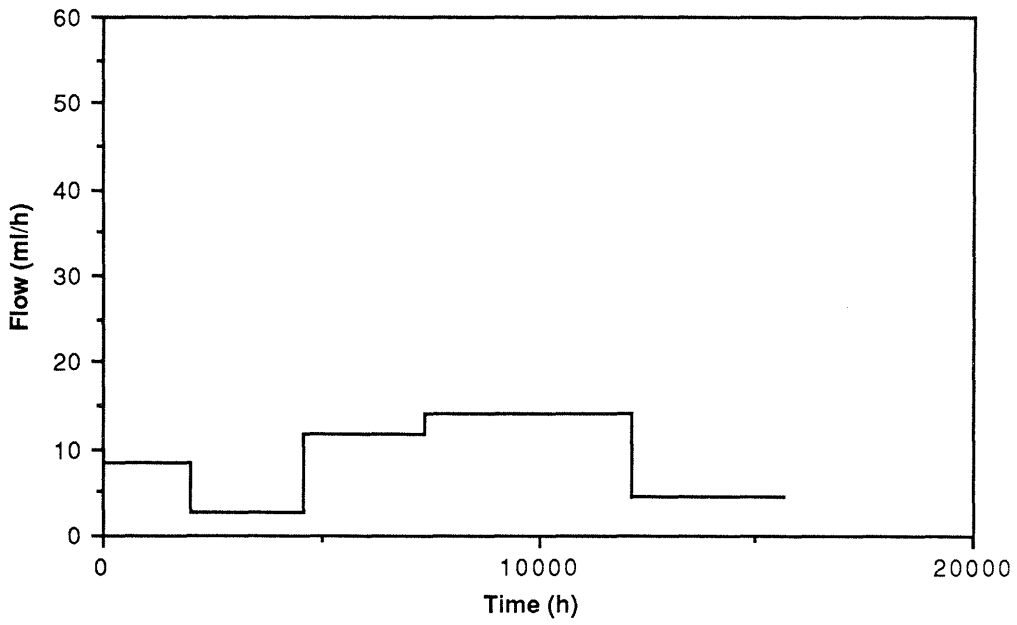


Figure A7-5. Injection of Iodide.

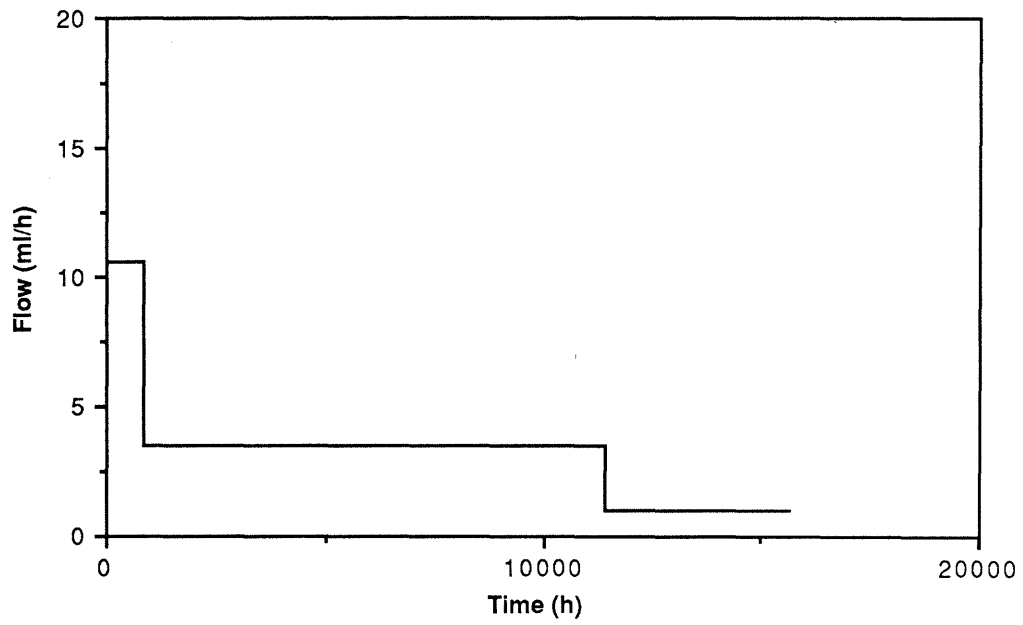


Figure A7-6. Injection of Fluoride.

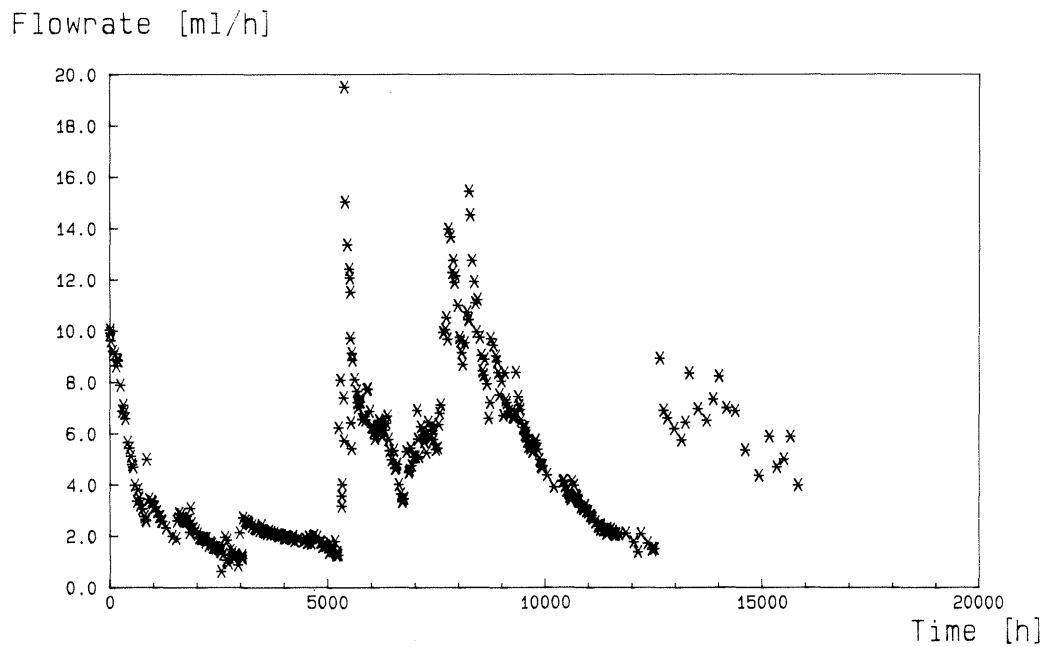


Figure A7-7. Real injection curve, hole 1 zone 1. Tracer Uranine 0-16000 h. Tracer Uranine+STR-7+F⁻ 5000-12500 h.

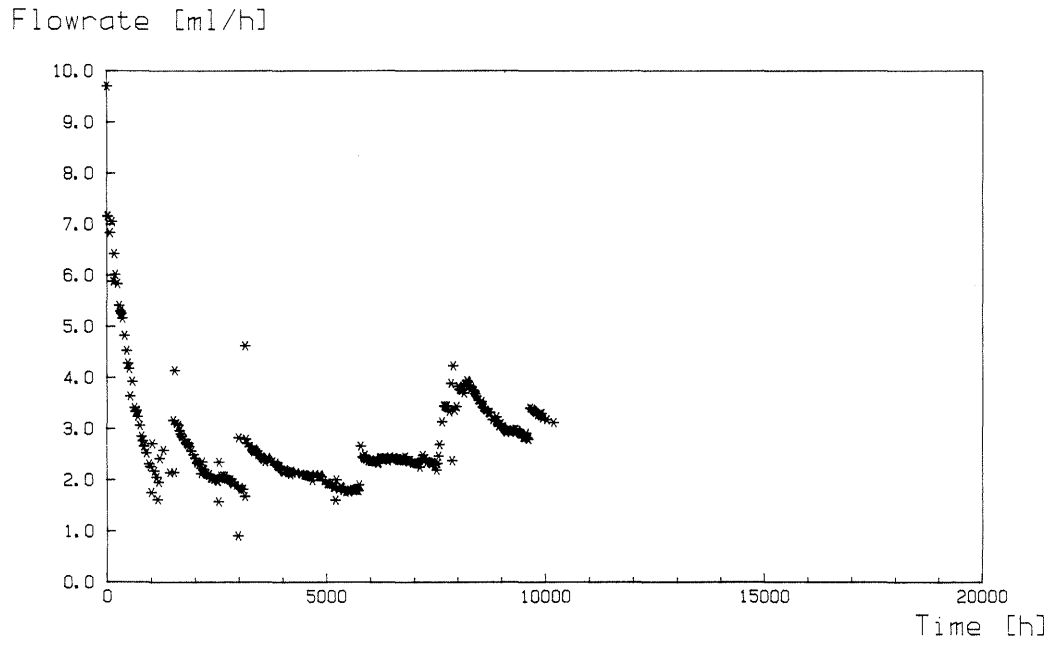


Figure A7-8. Real injection curve, hole 1 zone 2. Tracer Eosin Y.

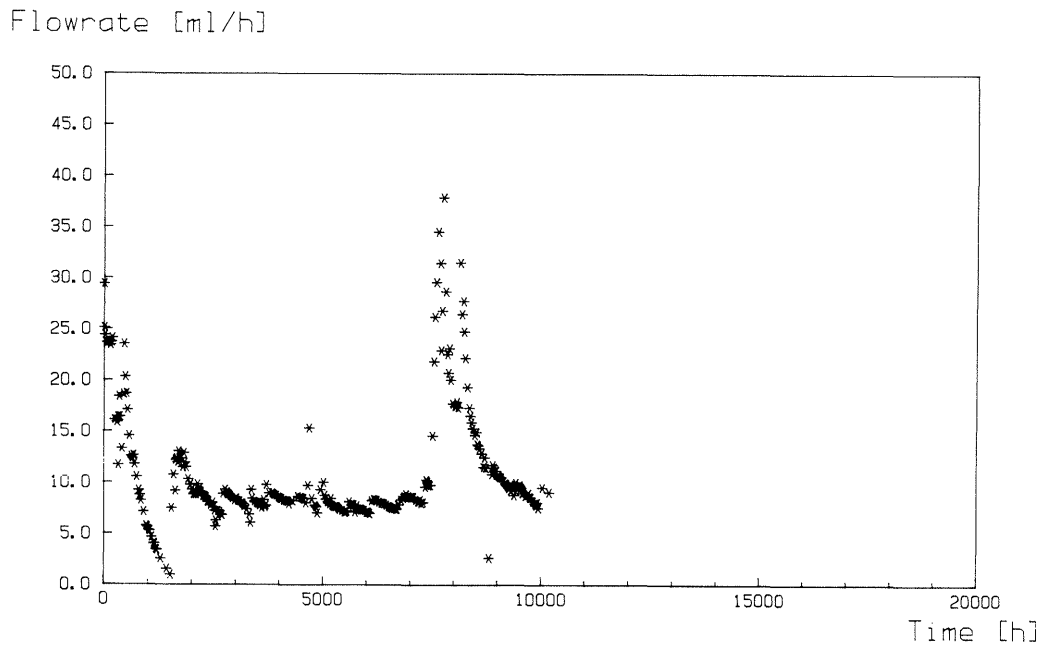


Figure A7-9. Real injection curve, hole 2 zone 1. Tracer Phloxine.

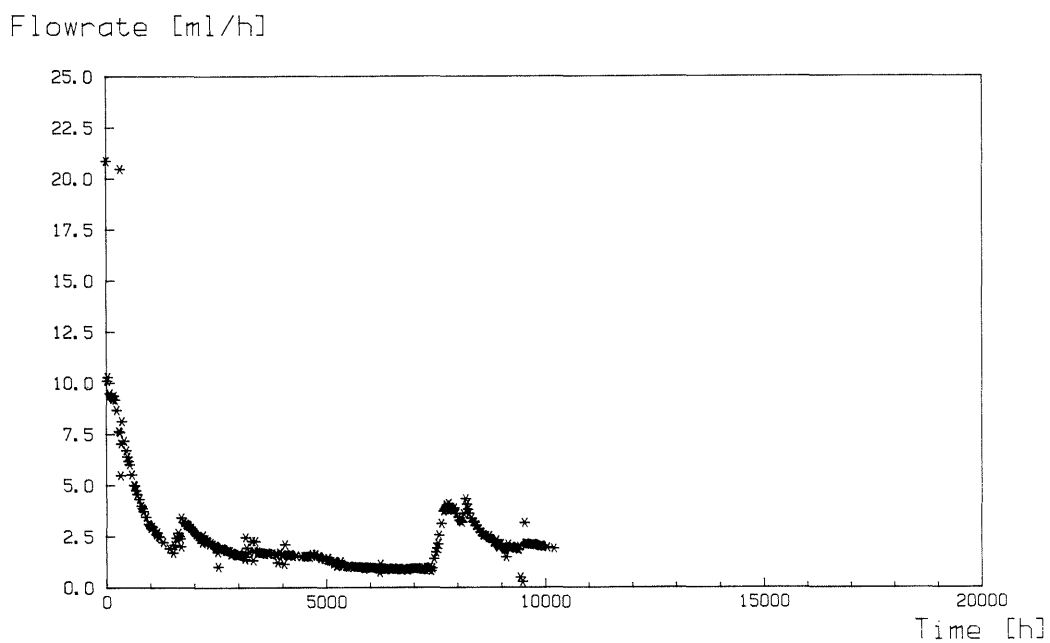


Figure A7-10. Real injection curve, hole 2 zone 2. Tracer Rose Bengal.

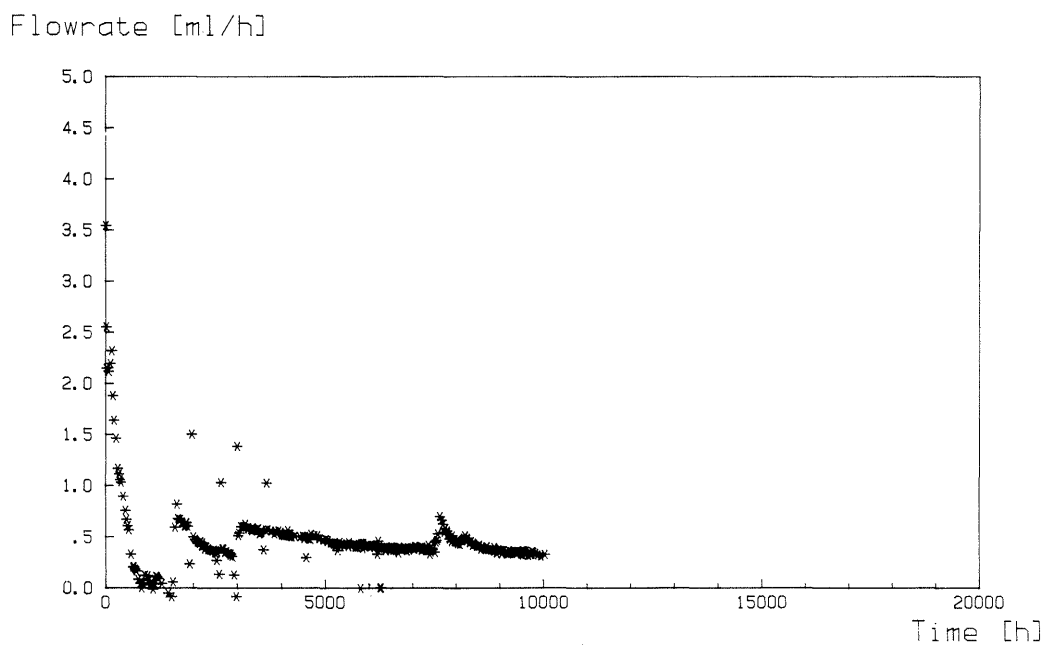


Figure A7-11. Real injection curve, hole 2 zone 3. Tracer Elbenyl.

Flowrate [ml/h]

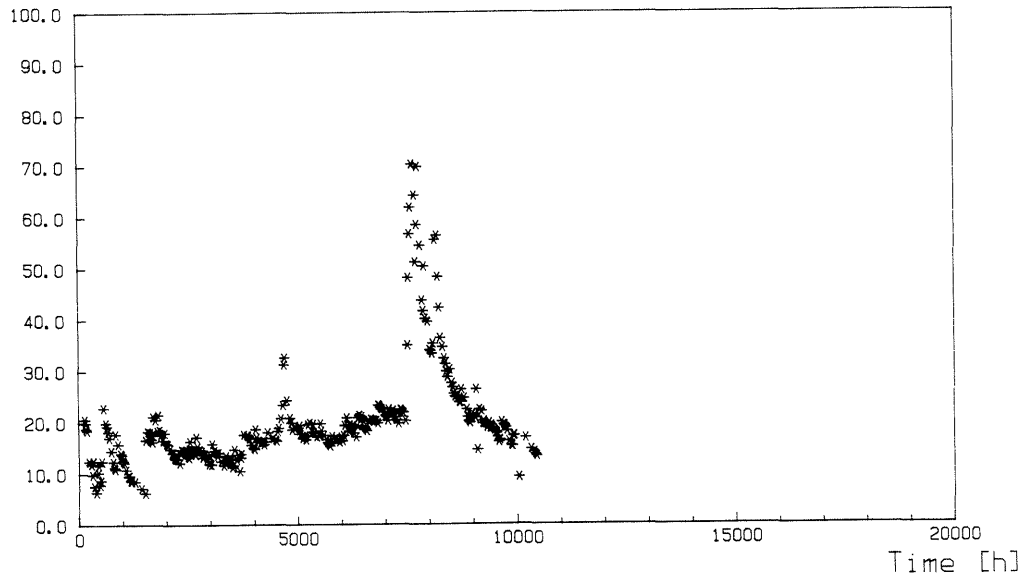


Figure A7-12. Real injection curve, hole 3 zone 1. Tracer Duasyn.

Flowrate [ml/h]

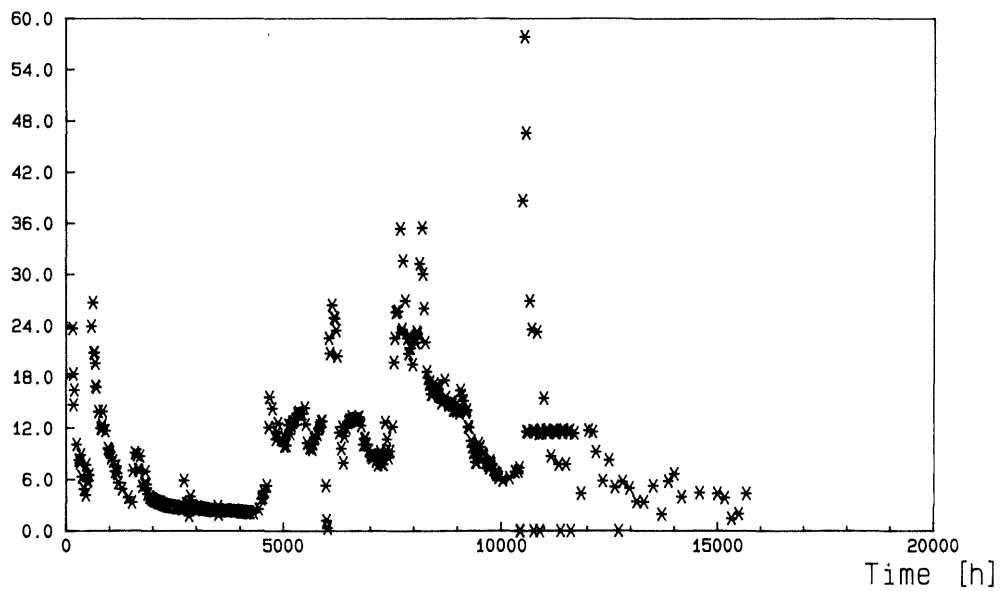


Figure A7-13. Real injection curve, hole 3 zone 2. Tracer Iodide.

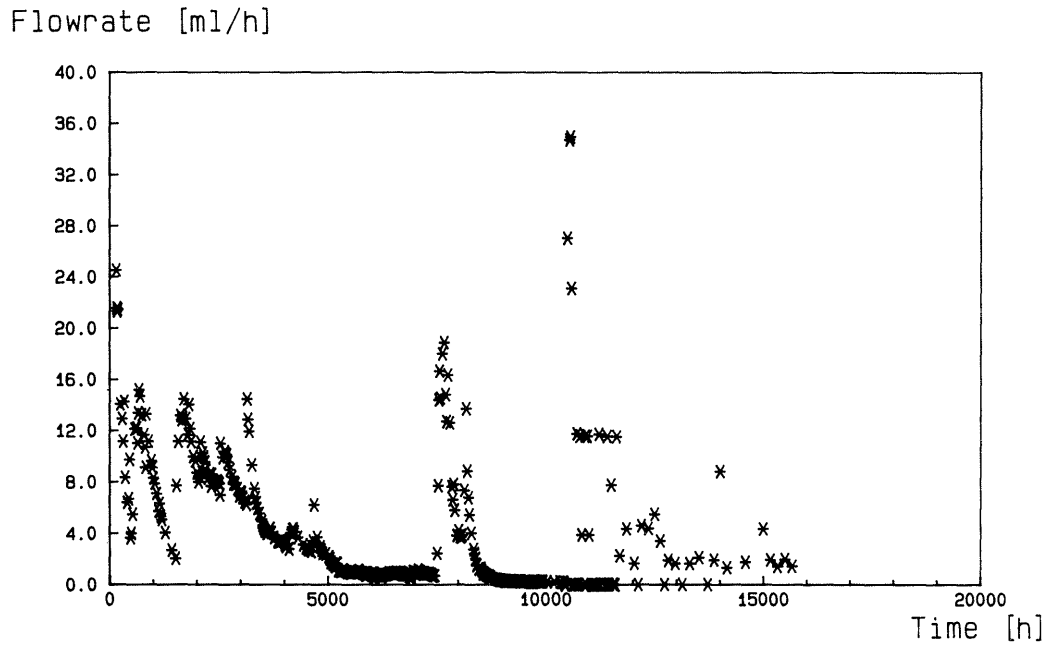


Figure A7-14. Real injection curve, hole 3 zone 3. Tracer Eosin B.

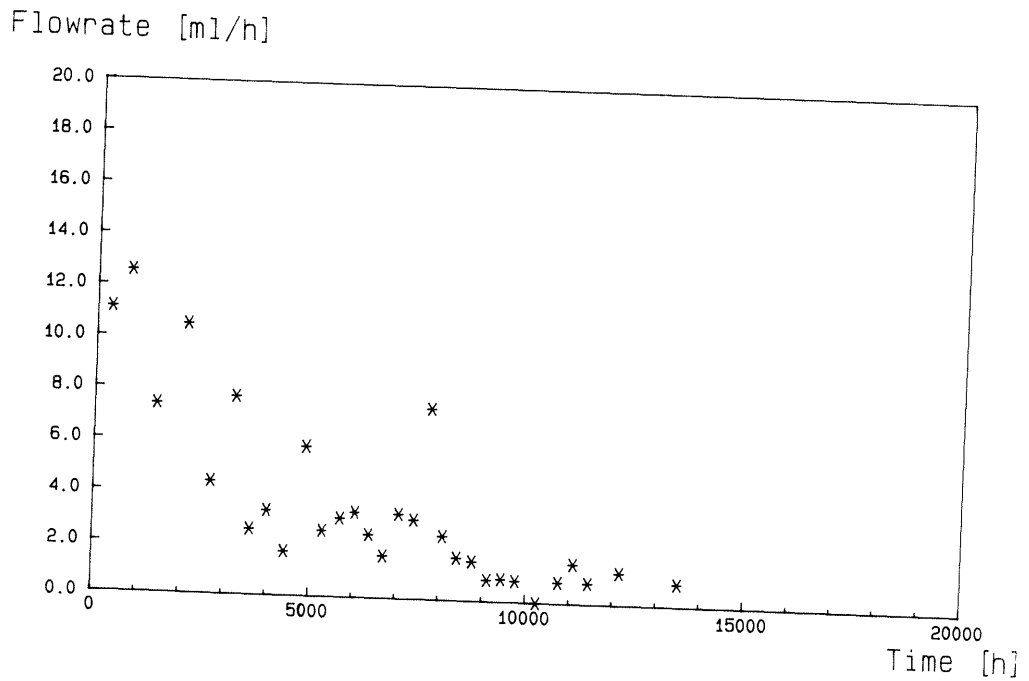


Figure A7-15. Real injection curve, hole 3 zone 4. Tracer Bromide.

DIFFUSION MEASUREMENTS

SUMMARY

Several different tracers were used in the 3-D experiment in the Stripa mine. The tracers were of two types: dyes and salts. The diffusion experiments show how the different dyes and salts diffused through granite. The dyes have a lower diffusivity than the salts.

INTRODUCTION

Diffusion measurements of tracers used in the Stripa 3-D experiment.

Eight tracers of the eleven different tracers used in the 3-D experiment are used in the diffusion experiment. The eight tracers are four dyes (Uranine, Elbenyl, Eosin Bluish, Eosin Yellowish), three salts (Iodide, Bromide, Flouride), and one large molecular weight tracer (STR-7).

Theory

Fick's second law gives the rate of change of the concentration in a homogeneous medium. For one dimensional transport, the diffusion equation is written:

$$\frac{\partial C}{\partial t} = D \frac{\partial^2 C}{\partial x^2} \quad (\text{A8.1})$$

The diffusion coefficient D is assumed to be constant.

In a porous medium the effects of the pores must be taken into consideration. This is accounted for by the total porosity which is the sum of "transport" porosity and "storage" porosity. The transport porosity is defined as those pores that allow the unhampered transport of species from one side to the other side of the sample. The pores characterized with a dead end are denoted by "storage" porosity. These pores will contribute to the capacity of the pore system to hold the dissolved species, but will contribute nothing or very little to the transport within the sample. Equation (A8.1) can be written as

$$(\epsilon_p + K_d \rho_p) \frac{\partial C}{\partial t} = D_p \epsilon_t \frac{\partial^2 C}{\partial x^2} \quad (\text{A8.2})$$

ϵ_p = total porosity

ϵ_t = "transport porosity"

K_d = sorption coefficient

A8.2

ρ_p = density of the solid material

D_p = pore diffusion coefficient

Assuming that the porous system may be approximated by a homogeneous system, a combination of Equations (A8.1) and (A8.2) gives

$$D = \frac{D_p \epsilon_t}{\epsilon_p + K_d \rho_p} = \frac{D_e}{\alpha} \quad (\text{A8.3})$$

α = rock capacity factor

D_e = effective diffusion coefficient

The rock capacity factor and the effective diffusion coefficient are defined as follows:

$$\alpha = \epsilon_p + K_d \rho_p$$

$$D_e = D_p \epsilon_t$$

Crank (1975) gives a solution to Equation (A8.2) for the case of diffusion through a porous slab initially at zero concentration. The inlet concentration is C_1 and the outlet concentration at $x=L$ is C_2 , where $C_2 \ll C_1$.

$$\frac{C(x, t)}{C_1} = 1 - \frac{x}{L} - \frac{2}{\pi} \sum_{n=1}^{\infty} \frac{1}{n} \sin \frac{n\pi x}{L} \exp \left(- \frac{D_e n^2 \pi^2 t}{L^2 \alpha} \right) \quad (\text{A8.4})$$

After differentiating Equation (A8.4) the rate of transport, N , out from the slab at $x=L$ is obtained by evaluating the gradient at $x=L$.

$$N = - D_e \left. \frac{\partial C}{\partial x} \right|_{x=L} \quad (\text{A8.5})$$

By integrating Equation (A8.5) with respect to time t , the total amount of diffusing substance M which had passed through the slab in time t is obtained

$$\frac{M}{LC_1} = \frac{D_e t}{L^2} - \frac{\alpha}{6} - \frac{2\alpha}{\pi^2} \sum_{n=1}^{\infty} \frac{(-1)^n}{n^2} \exp \left(- \frac{D_e n^2 \pi^2 t}{L^2 \alpha} \right) \quad (\text{A8.6})$$

As $t \rightarrow \infty$, Equation (A8.6) approaches the linear relation

$$M = \frac{C_1 D_e}{L} t - \frac{C_1 L \alpha}{6} \quad (\text{A8.7})$$

with the slope $\frac{C_1 D_e}{L}$ and the intercept on the time axis is

$$t = \frac{L_2 \alpha}{6 D_e}$$

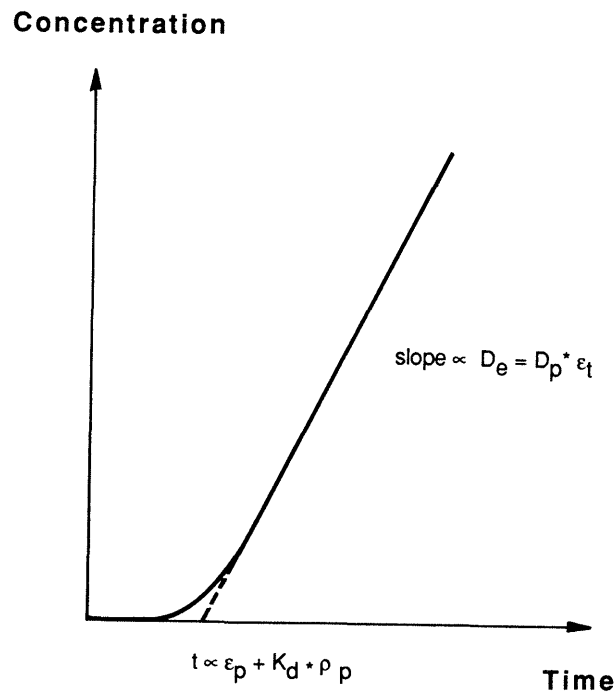


Figure A8-1. Principle of concentration-time curve at the low concentration side.

If there is no sorption then $\alpha = \epsilon_p$, which means that the intercept on the time axis gives the total porosity of the material. In the result tables the porosity determined in this way is called "from time lag." The porosity was determined by weighing the samples wet and dry, which is denoted as "weighing."

EXPERIMENTAL

The experimental procedure in the diffusion experiment is in principle the same which had been used by Skagius (1986). Different tracers used in the diffusion experiment are the same as those used in the 3-D experiment. First a granite sample was obtained from the extensometer drift in the Stripa mine at 360 m level. The drill core from the 76 mm hole was cut into 10 mm long pieces. From these pieces, rock tablets with diameters of 43 mm were drilled out from

the center. The tablets were placed into a hole of a 10 mm thick PVC plate and secured with glue. The hole has the same diameter as the rock tablets of 43 mm. Then two chambers made of transparent PVC were fastened on each side of the PVC plate, see Figure A8-2.

One chamber was filled with 500 ml tracer solution and the other with 500 ml sodium nitrate solution of the same ionic strength to avoid osmotic effects.

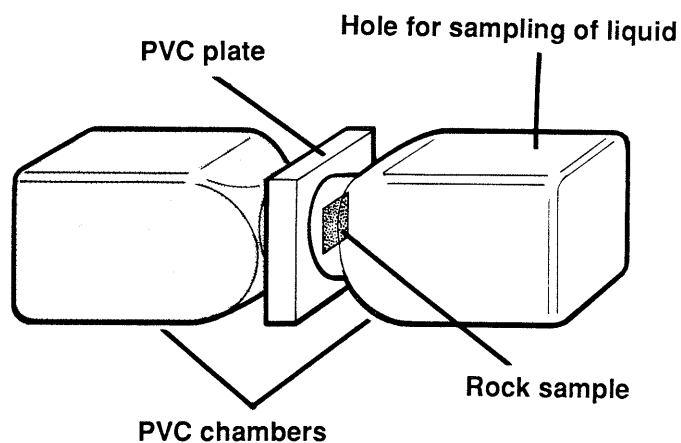


Figure A8-2. The diffusion cell.

A test performed with a cell containing a PVC plate instead of a granite tablet showed that the diffusion through the PVC plate and the glue was negligible.

Eleven different nonsorbing tracers were used in the 3-D experiment: seven dyes (Uranine, Elbenyl Brilliant Flavine, Eosin Blueish, Eosin Yellowish, Duasyn, Phloxine, Rose Bengal), three salts (I^- , Br^- , F^-), and a large molecular weight tracer called STR-7. The tracers that had arrived to the 3-D drift and the two tracers which were injected simultaneously with Uranine were tested. Seven tracers were tested in different mixtures with other tracers. Three tracers were mixed in each cell and a total of eight cells were used. Seven cells contained granite tablets and one a PVC plate. Every tracer was in solution with all of the other tracers in at least one of the cells, see Table A8-1.

Because Elbenyl Brilliant Flavine has a low extension coefficient, it is difficult to analyze the tracer in a mixture with other dyes. Thus new cells, experiments 9 and 11, with Iodide and Elbenyl Brilliant Flavine were started. One binary mixture of STR-7 and I^- was also tested in cell No. 10.

Samples of 10 ml were taken out from the low concentration side of the diffusion cell and the tracer concentrations were measured. The dyes were measured with a spectrophotometer and the I^- , Br^- , and F^- were measured with ion selective electrodes. To keep the volume constant, 10 ml of sodium nitrate solution was added.

Table A8-1. Tracer composition.

Table A8-1 shows the composition of tracers on the high concentration side of the diffusion cell from the different cells.

Experiment No.	Tracers	Concentration
1	Uranine Elbenyl Br ⁻	10 000 ppm 5 000 ppm 0.1 M
2	Eosin blueish Elbenyl I ⁻	10 000 ppm 5 000 ppm 0.1 M
3	Eosin Y Elbenyl F ⁻	10 000 ppm 5 000 ppm 0.1 M
4	Uranin F ⁻ I ⁻	10 000 ppm 0.1 M 0.1 M
5	Uranin Eosin B Eosin Y	10 000 ppm 10 000 ppm 10 000 ppm
6	Eosin Y Br ⁻ I ⁻	10 000 ppm 0.1 M 0.1 M
7	Eosin B Br ⁻ F ⁻	10 000 ppm 0.1 M 0.1 M
8	Same tracers as in cell No.1, but the granite piece was replaced by a PVC-plate.	
9	Elbenyl I ⁻	5 000 ppm 0.1 M
10	STR-7 I ⁻	20 000 ppm 0.1 M
11	Elbenyl I ⁻	5 000 ppm 0.1 M

RESULTS AND DISCUSSION

Problems occurred with some of the tracers. It was difficult to analyze Bromide and Fluoride in low concentrations on the low concentration side of the diffusion cell. In cell No. 6 the Iodide interfered with the Bromide analyses. Because Elbenyl Br. Flavine has a low extension

A8.6

coefficient, it was only possible to dissolve about 5000 ppm of the tracer in water. Figures A8-3 and A8-4 show two examples of the concentration-time curves.

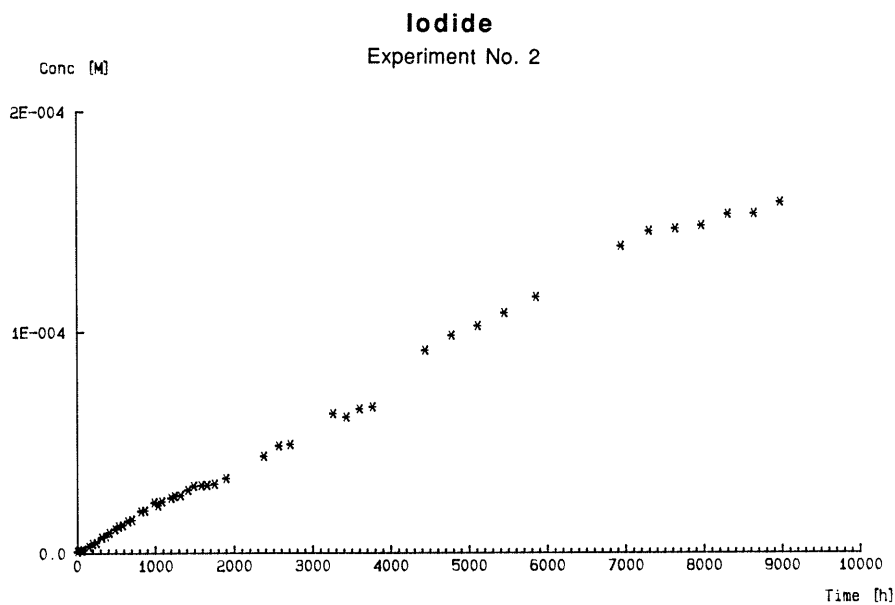


Figure A8-3. Concentration versus time for Iodide diffusion.

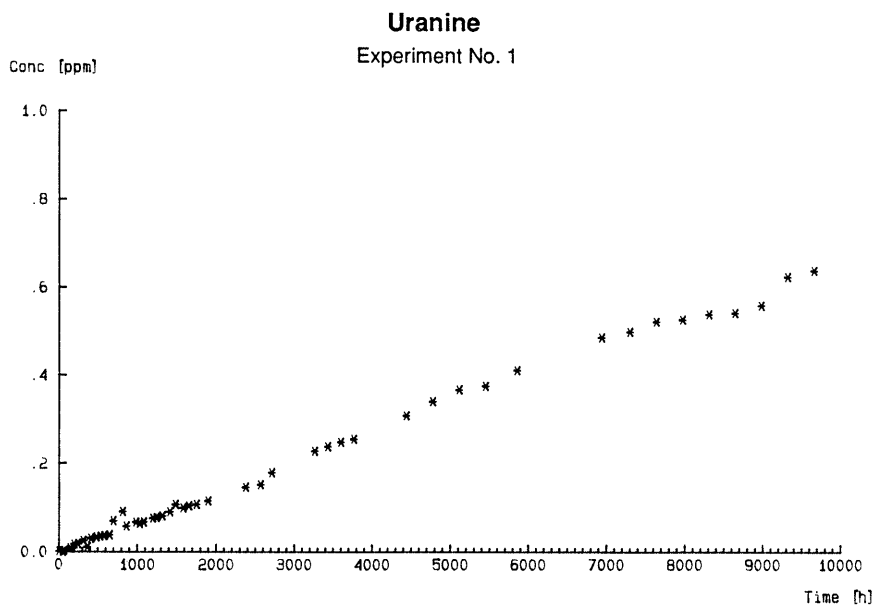


Figure A8-4. Concentration versus time for Uranine diffusion.

A8.7

The measured effective diffusivity for Iodide and Bromide are in the range of $11 \cdot 10^{-14}$ – $31 \cdot 10^{-14}$ m²/s. This is in good agreement with the effective diffusivity value for Iodide obtained by Skagius (1986). The effective diffusivities for the other dyes are in the range of $1 \cdot 10^{-14}$ – $8 \cdot 10^{-14}$ m²/s. Again Skagius' measurements for Uranine are of the same magnitude. The effective diffusivities for the large molecular weight tracer, STR-7, was less than $0.01 \cdot 10^{-14}$ m²/s, see Table A8-2.

The porosities were found to be 0.01 – 0.13 % from the time lag measurements and 0.48 – 0.70 % from weighing. The other concentration–time curves are appended.

The concentration–time curves obtained in the experiments are shown in Figure A8-5 (a)–(u). The numbers refer to the experiment numbers in Table A8-1.

CONCLUSION

The results show that different dyes and salts can diffuse through granite. The effective diffusion coefficient for Iodide and Bromide are in the same range, $11 \cdot 10^{-14}$ – $31 \cdot 10^{-14}$ m²/s. The dyes (Uranine, Elbenyl, Eosin Blueish, Eosin Yellowish) have lower effective diffusivities $1 \cdot 10^{-14}$ – $8 \cdot 10^{-14}$ m²/s.

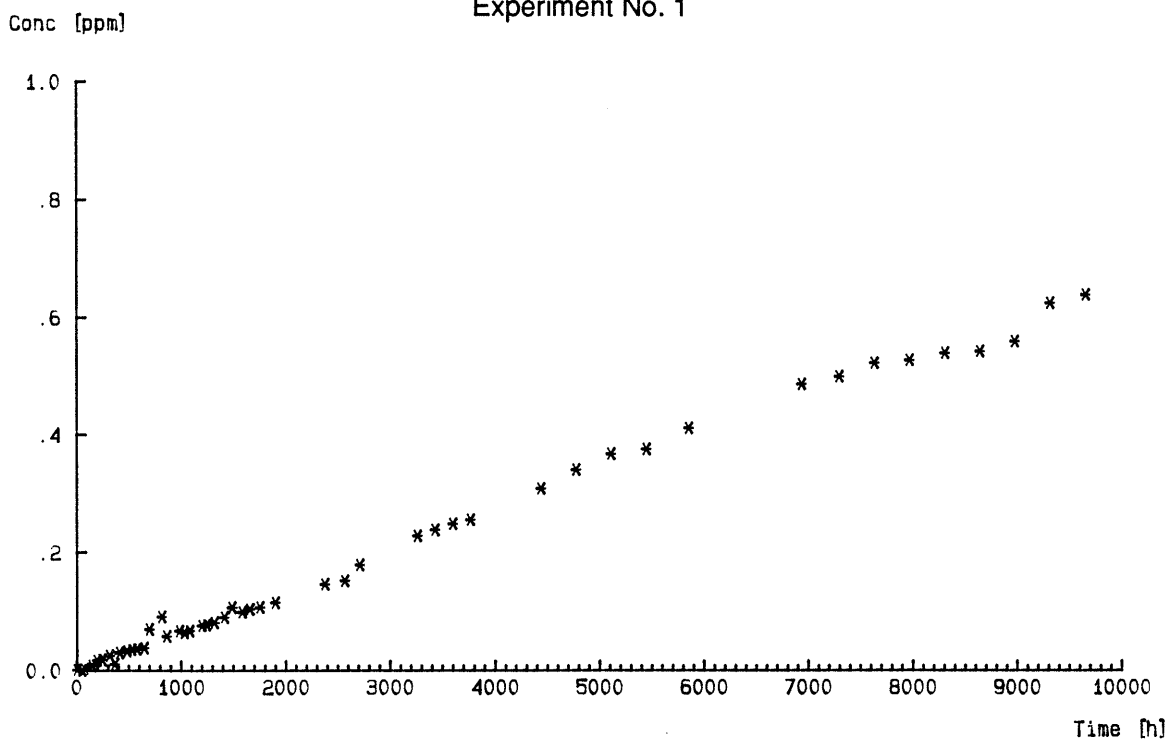
Table A8-2. Obtained results on effective diffusivity and porosity.

Exp No.	Tracers	$D_e \cdot 10^{+14}$	ϵ_p weighing	ϵ_p time lag
1	Uranine Elbenyl Br ⁻	0.9 1.2 31	0.59	0.01
2	Eosin B Elbenyl I ⁻	2 2.3 26	0.51	0.04 0.13
3	Eosin Y Elbenyl F ⁻	1.5 1.2 <5	0.70	0.02
4	Uranine F ⁻ I ⁻	1.6 <5 11	0.63	0.03
5	Uranine Eosin B Eosin Y	1.7 1.2 2.3	0.55	0.03 0.02 0.04
6	Eosin Y Br ⁻ I ⁻	2.9 Interference by I ⁻ 29	0.50	0.06 0.09

Table A8-2 continued.

7	Eosin B Br ⁻ F ⁻	0.3 - <5	0.69	0.05
8	Same tracers as in cell No. 1, but the granite piece was replaced by a PVC plate.			
9	Elbenyl I ⁻	7.8 14	0.63	0.03
10	STR-7 I ⁻	<0.01 22	0.49	0.05
11	Elbenyl I ⁻	3.3 27	0.48	0.06

Uranine
Experiment No. 1



Elbenyl
Experiment No. 1

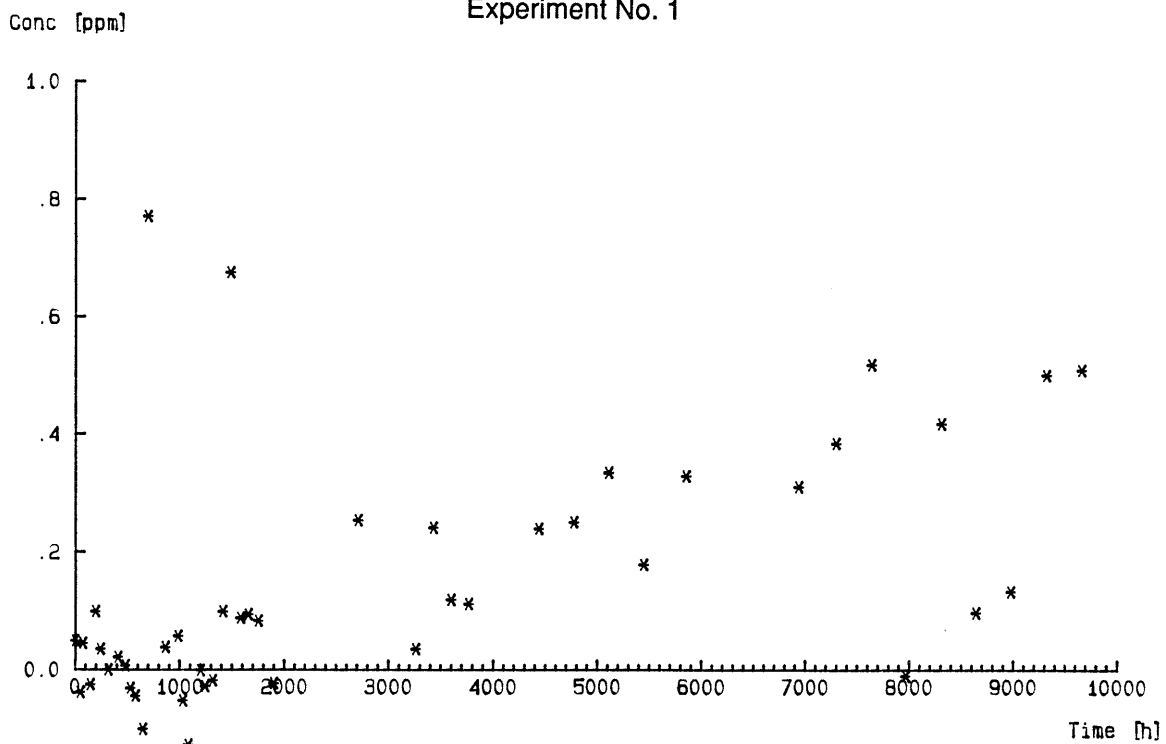


Figure A8-5 (a) - (u).

Concentration-time curves from the diffusion experiment.

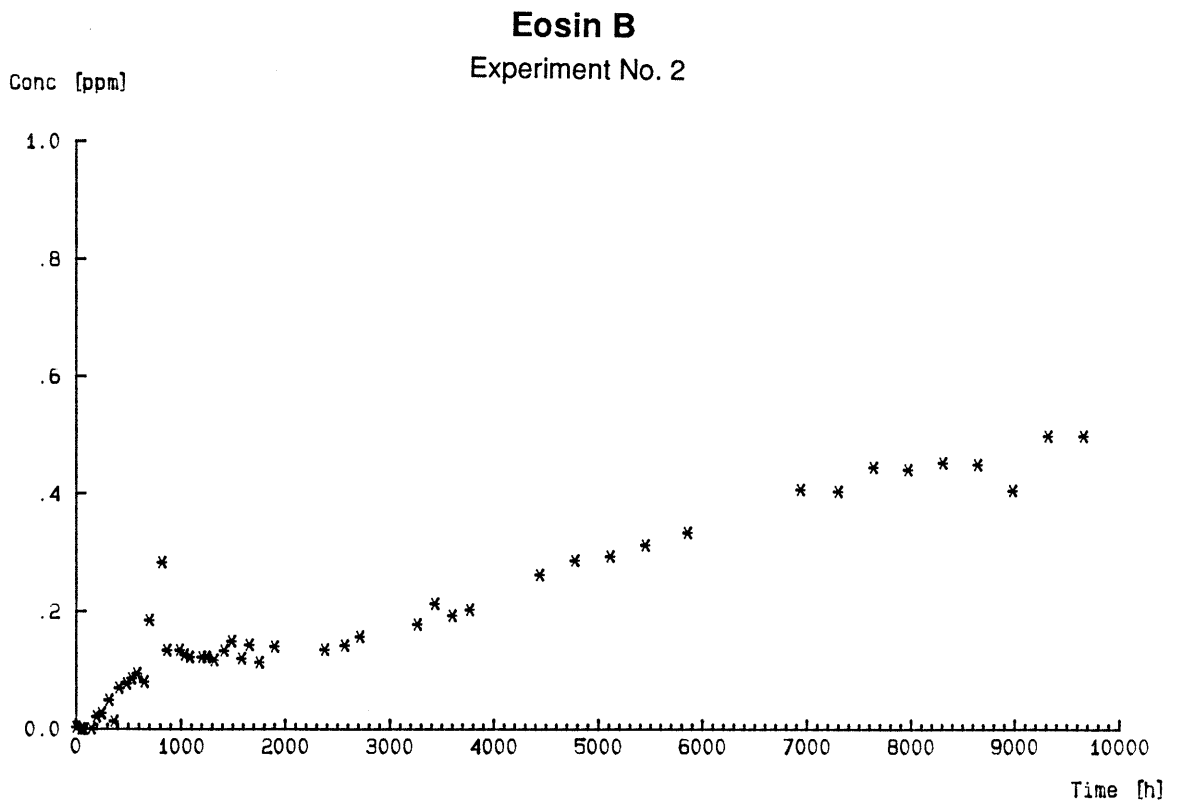
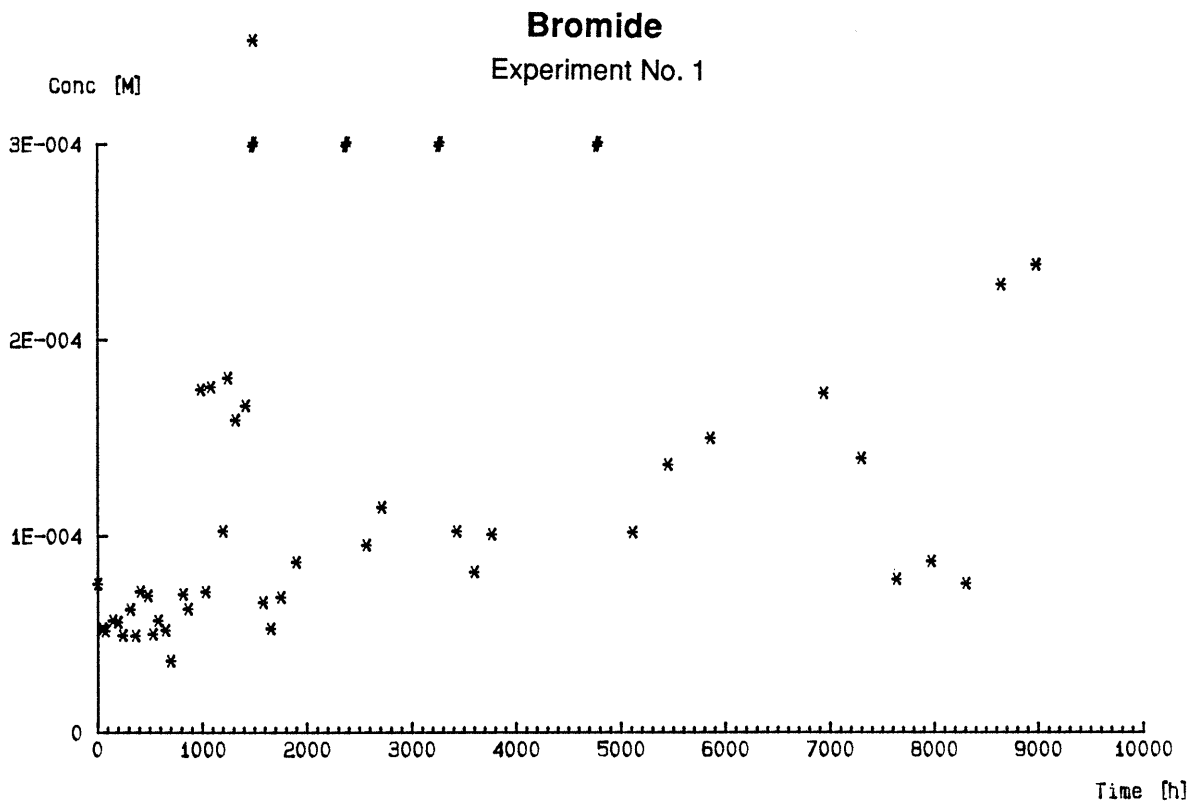


Figure A8-5. Concentration-time curves from the diffusion experiment.

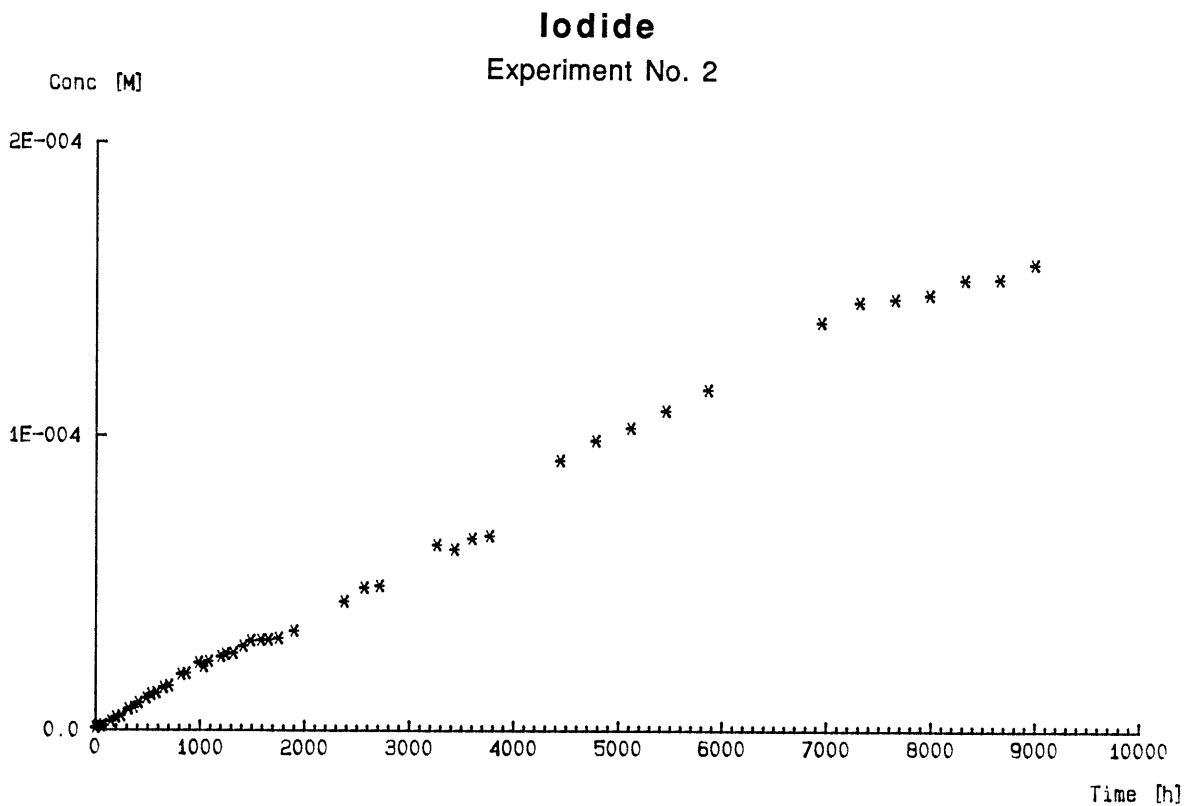
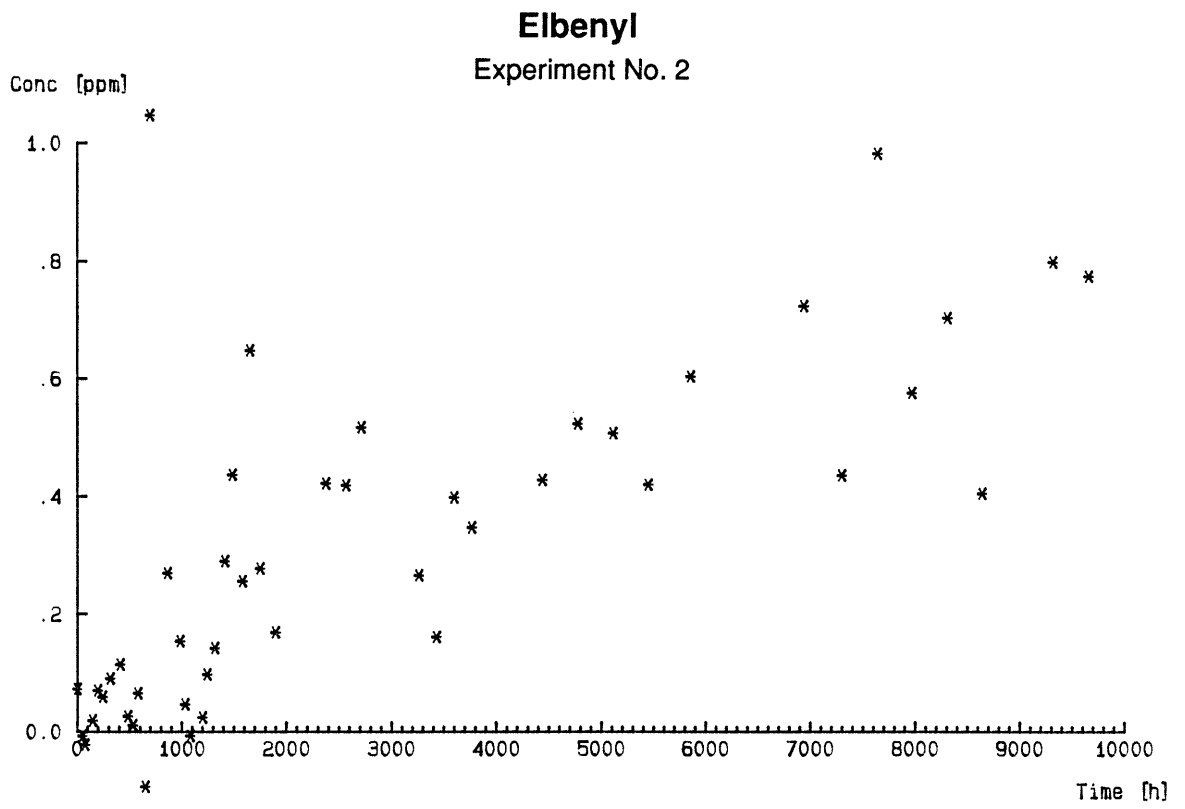
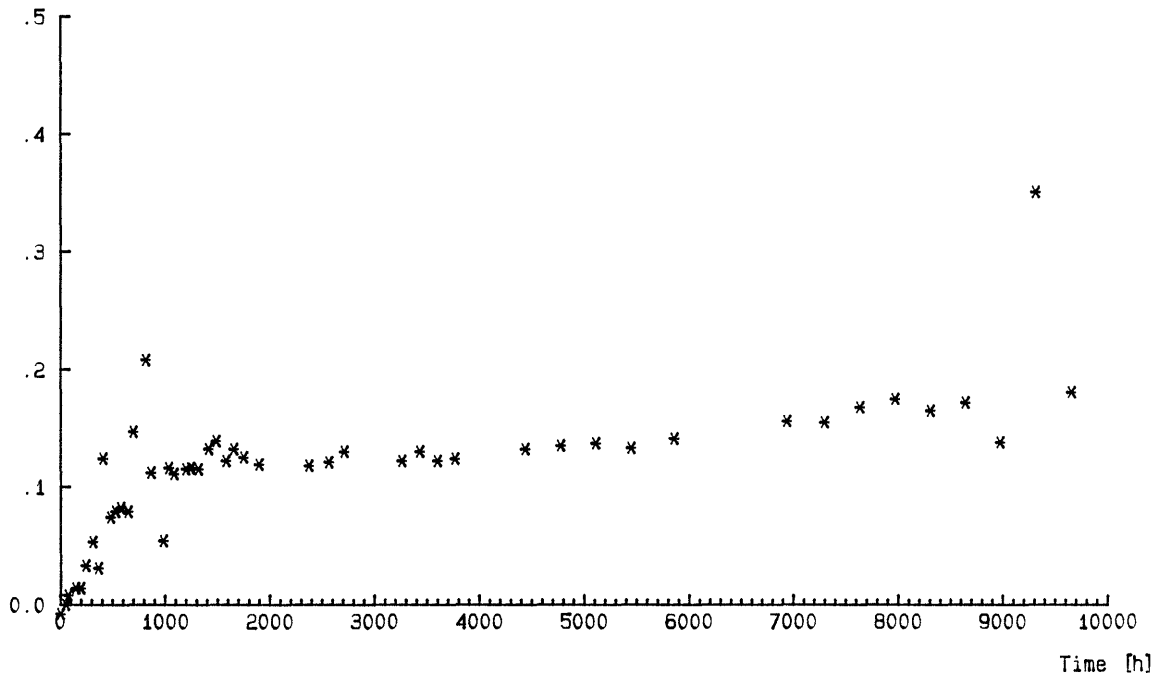


Figure A8-5. Concentration-time curves from the diffusion experiment.

Eosin Y

Experiment No. 3

Conc [ppm]

**Elbenyl**

Experiment No. 3

Conc [ppm]

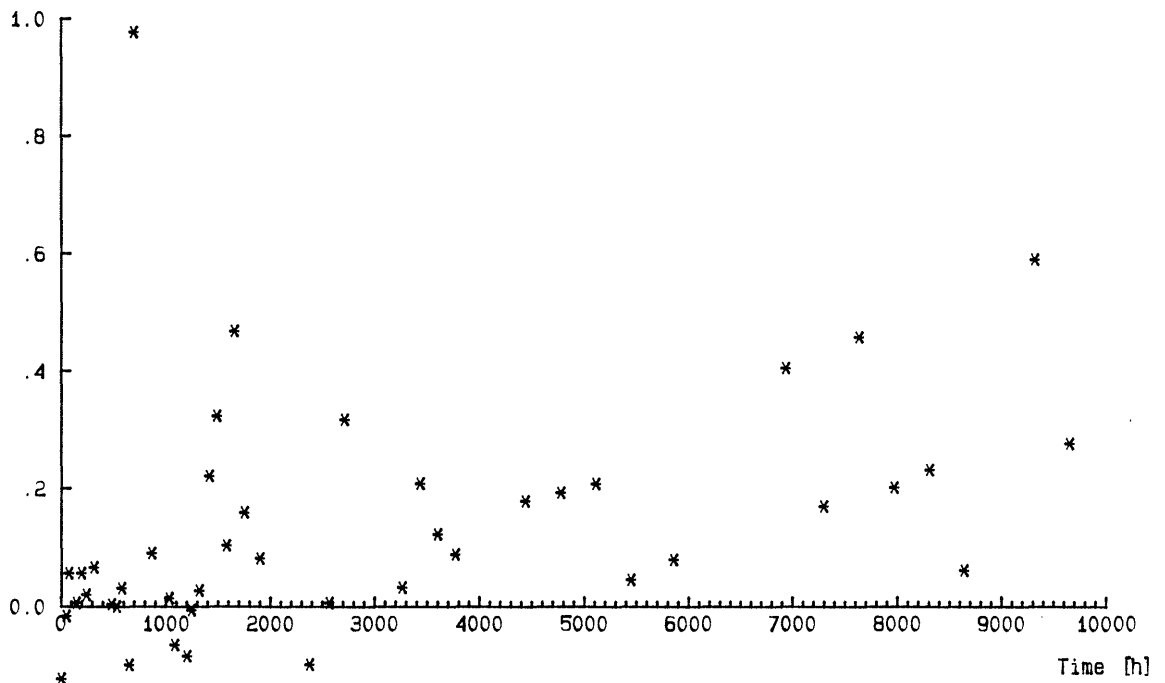


Figure A8-5. Concentration-time curves from the diffusion experiment.

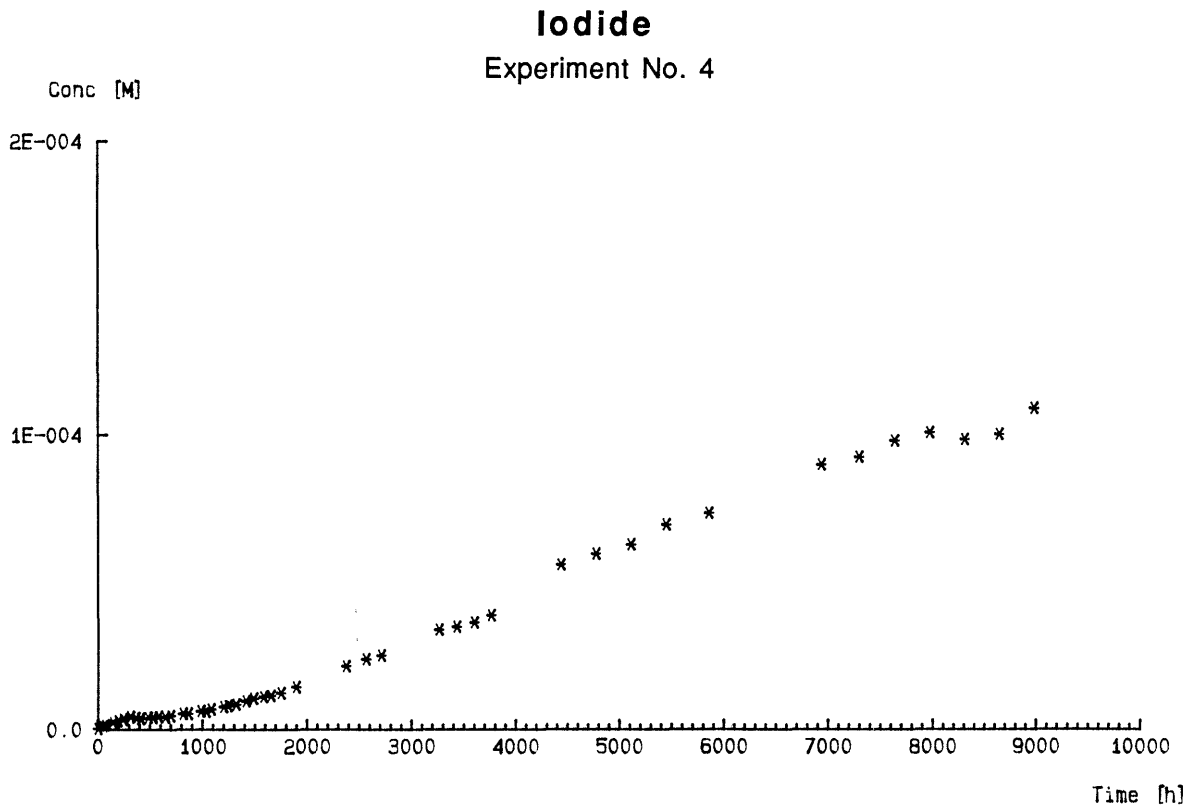
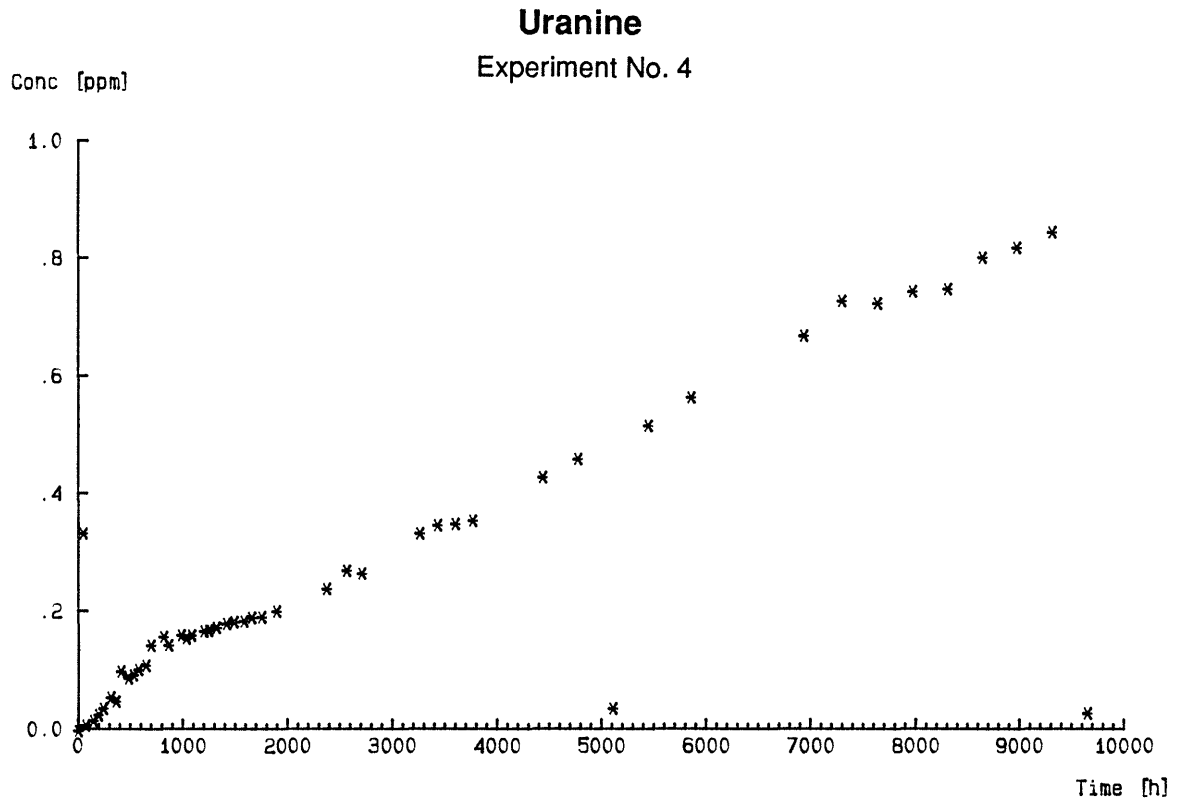
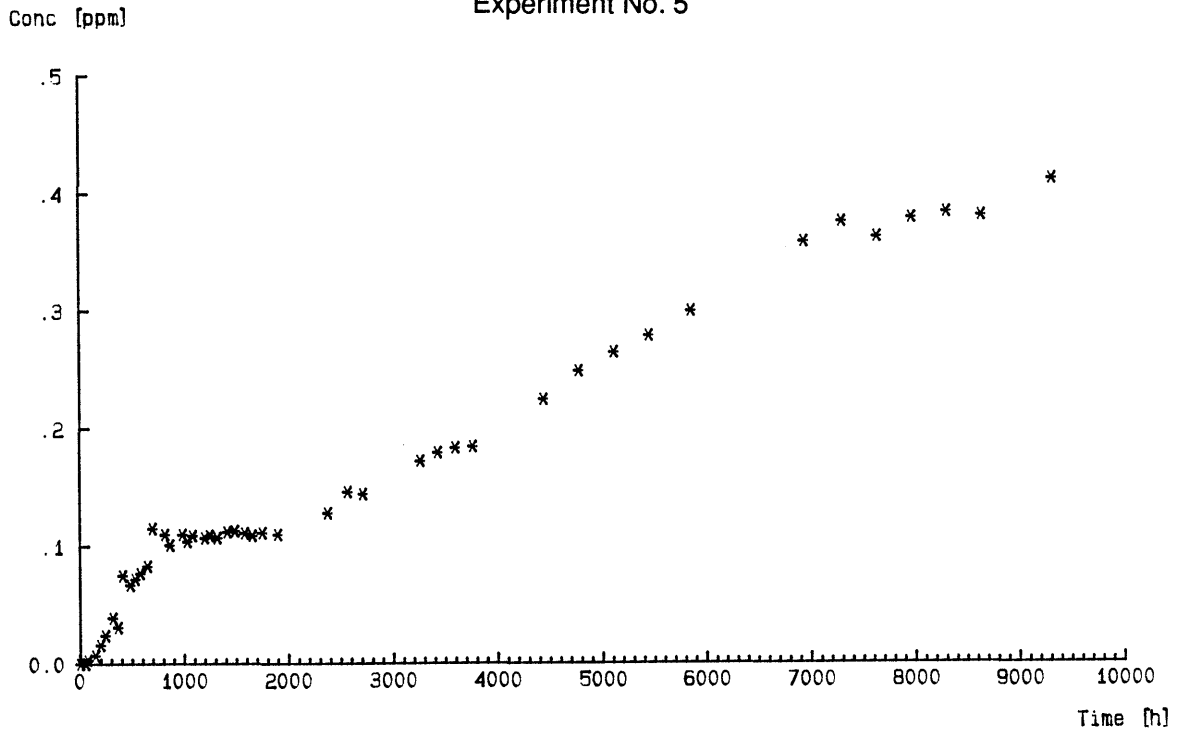


Figure A8-5. Concentration-time curves from the diffusion experiment.

Uranine
Experiment No. 5



Eosin B
Experiment No. 5

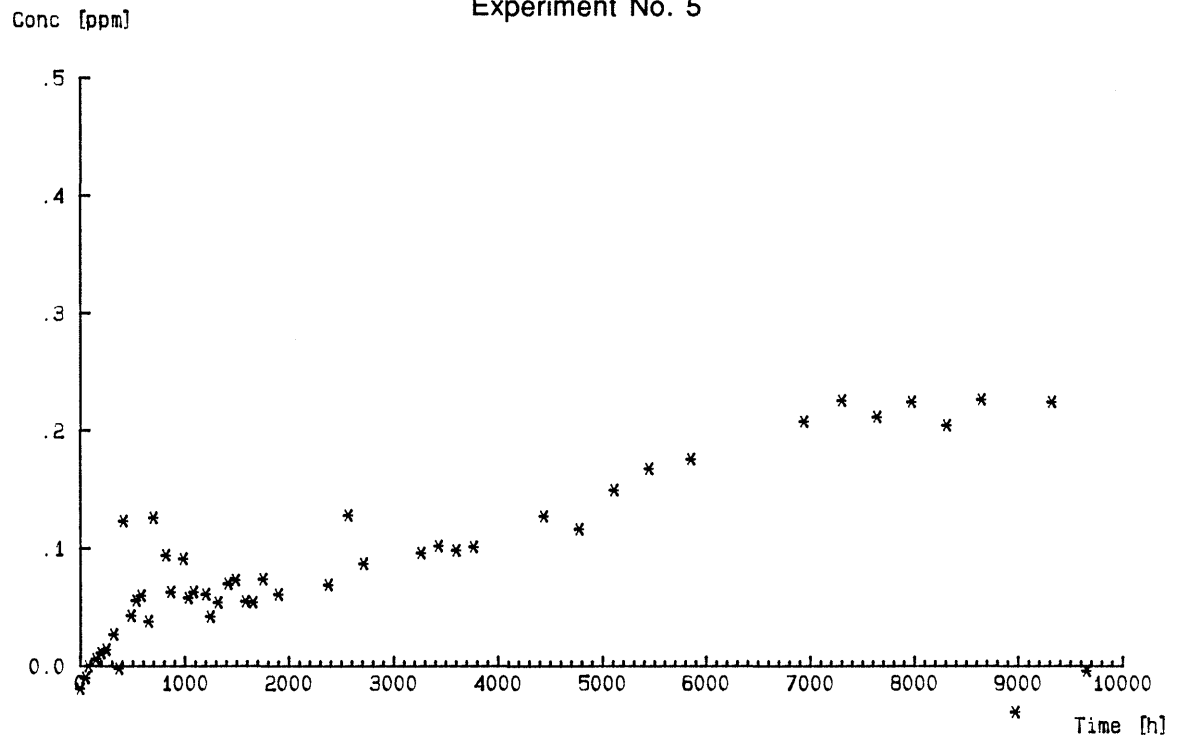
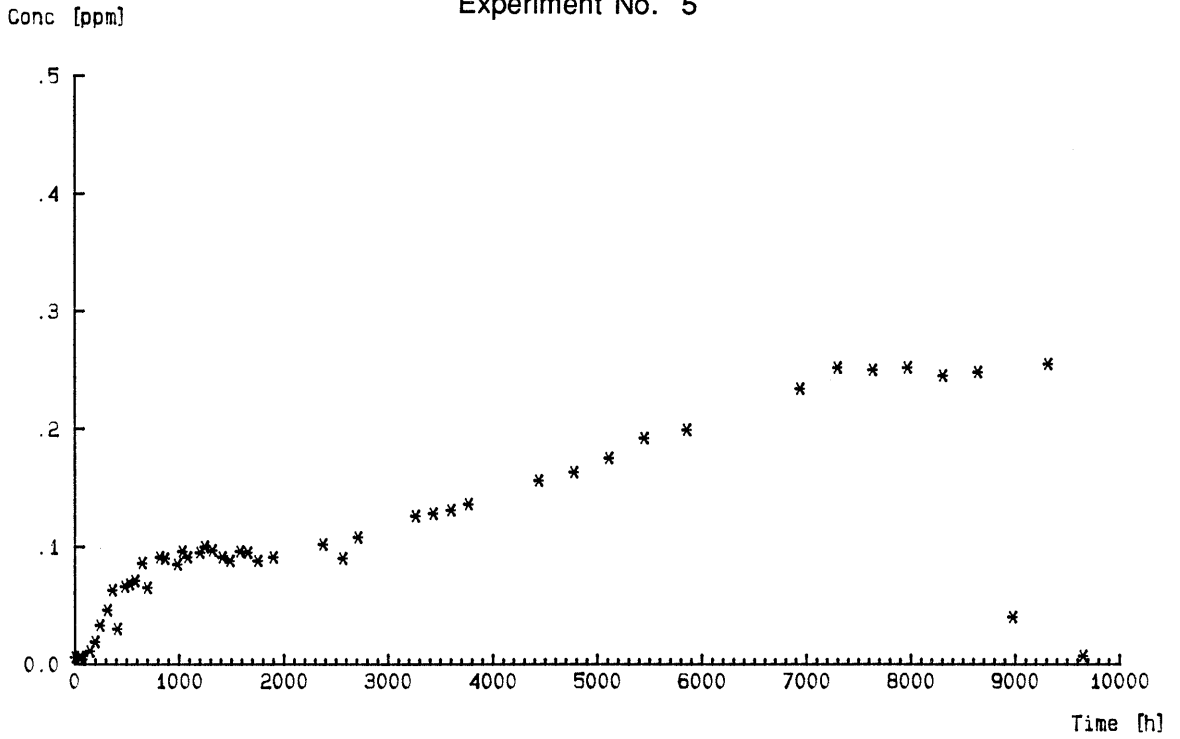


Figure A8-5. Concentration-time curves from the diffusion experiment.

Eosin Y
Experiment No. 5



Eosin Y
Experiment No. 6

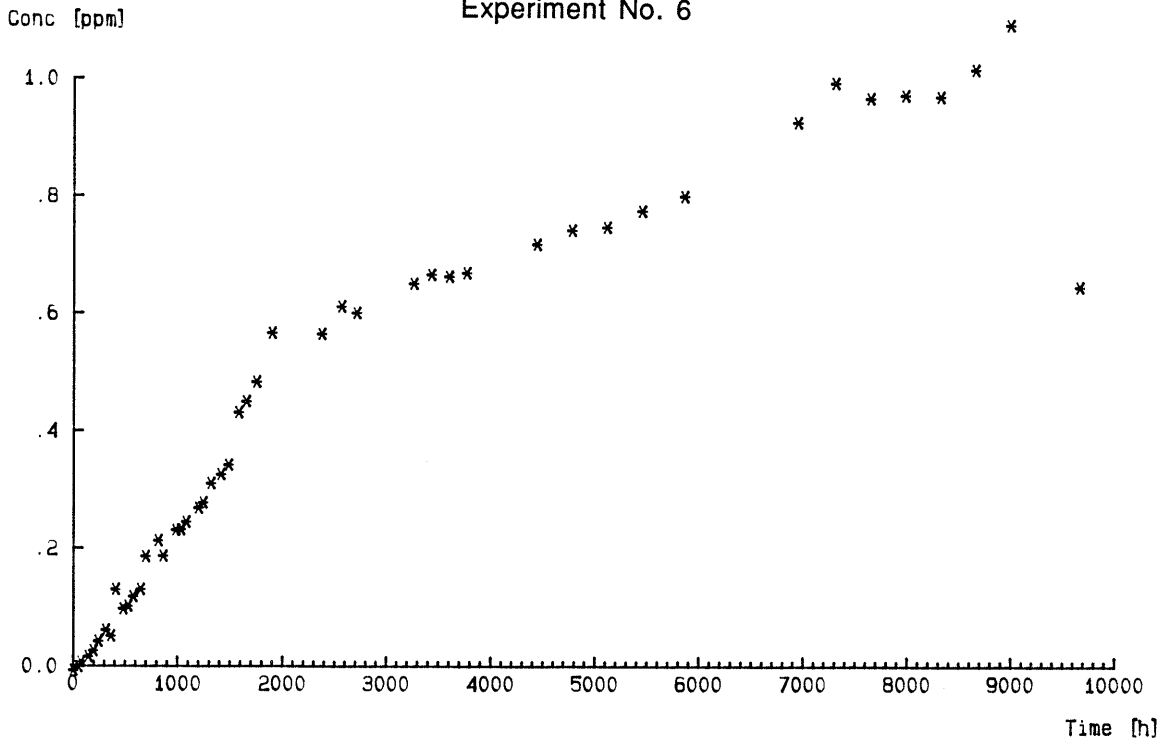
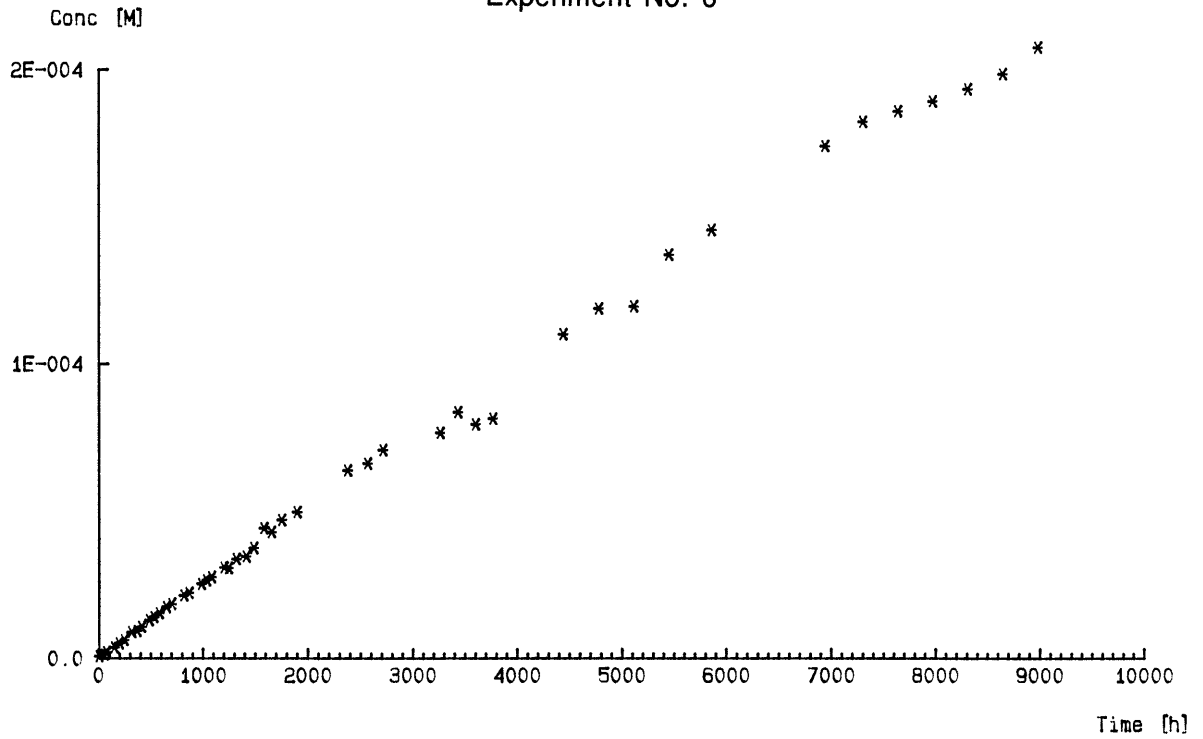


Figure A8-5. Concentration-time curves from the diffusion experiment.

Iodide

Experiment No. 6



Eosin B

Experiment No. 7

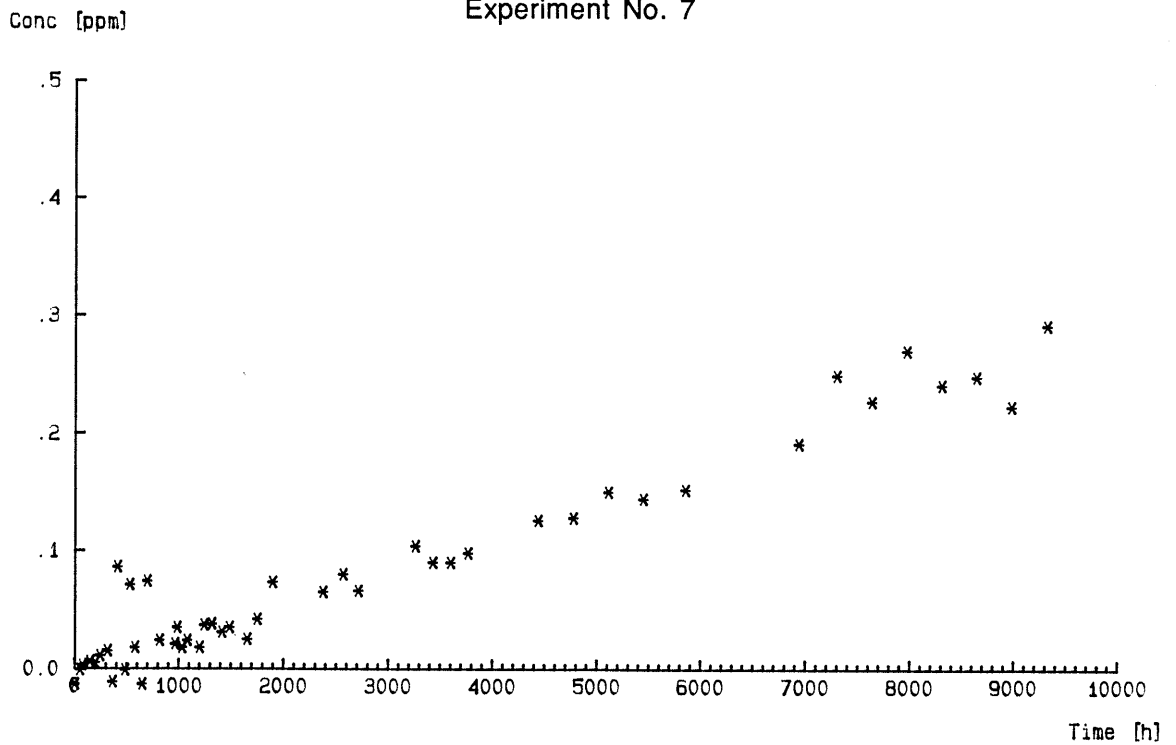


Figure A8-5. Concentration-time curves from the diffusion experiment.

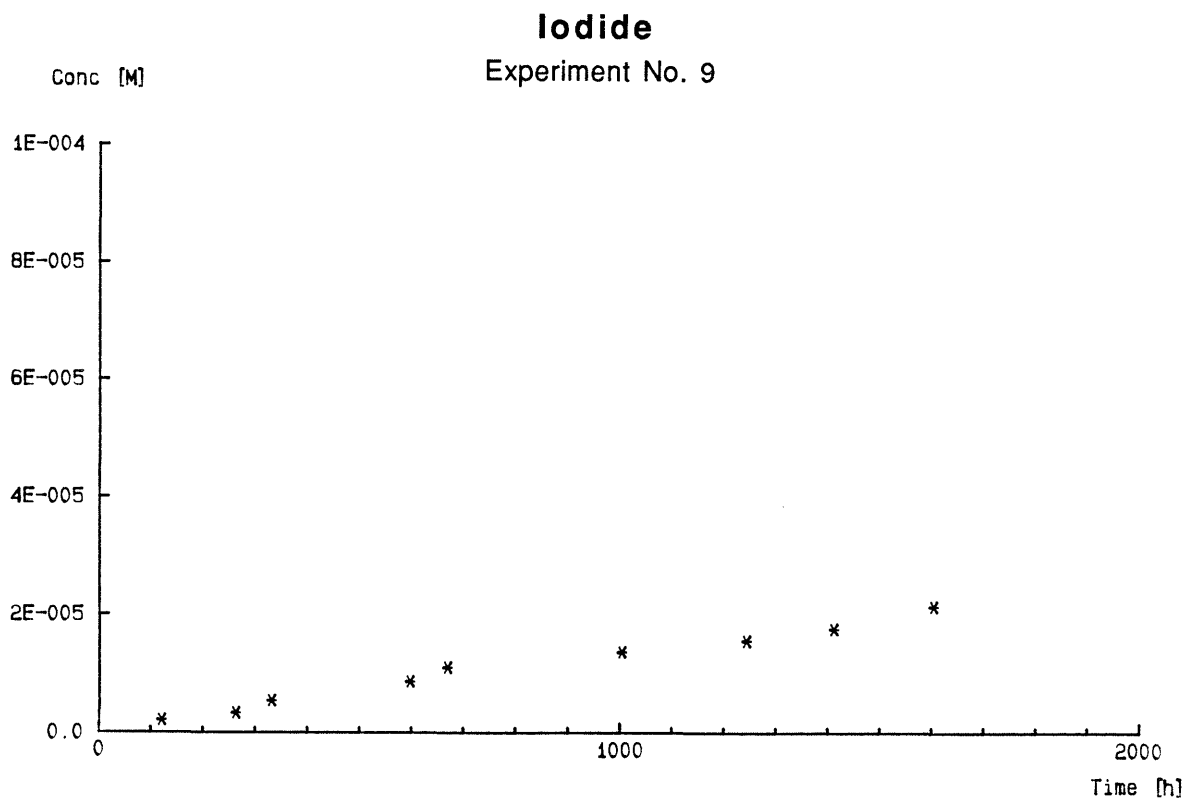
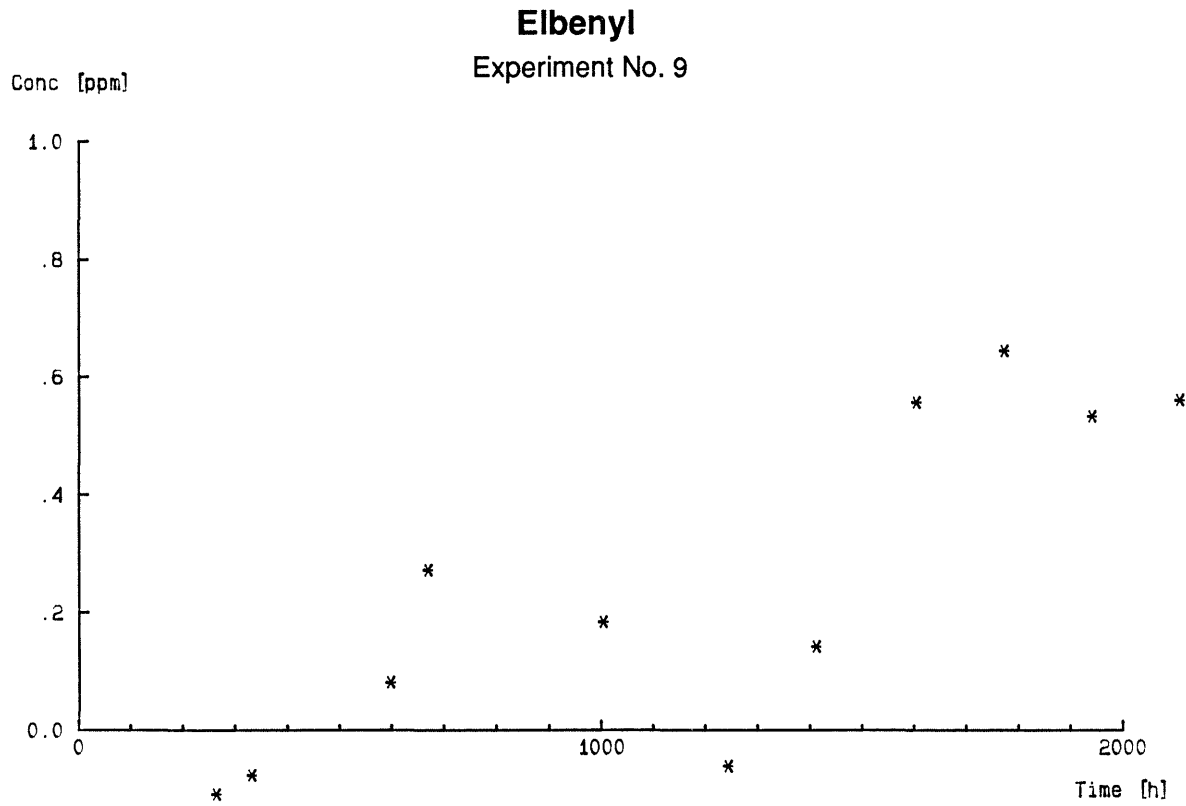
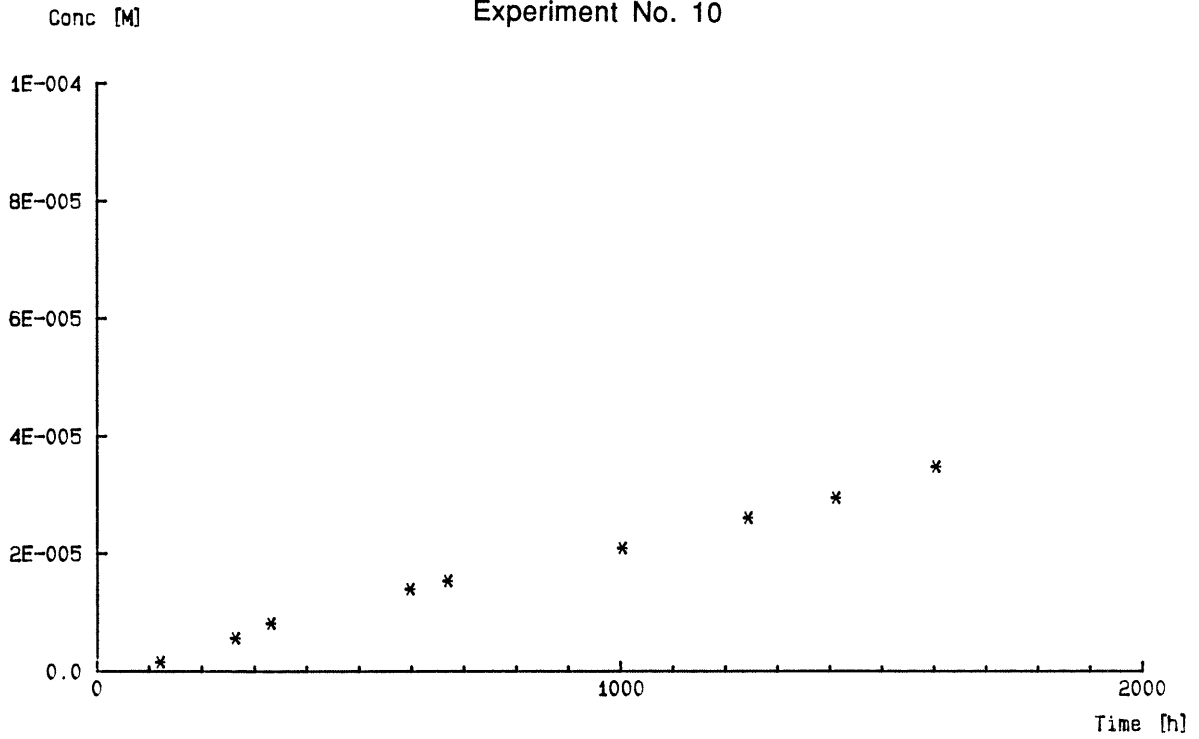


Figure A8-5. Concentration-time curves from the diffusion experiment.

Iodide

Experiment No. 10



Elbenyl

Experiment No. 11

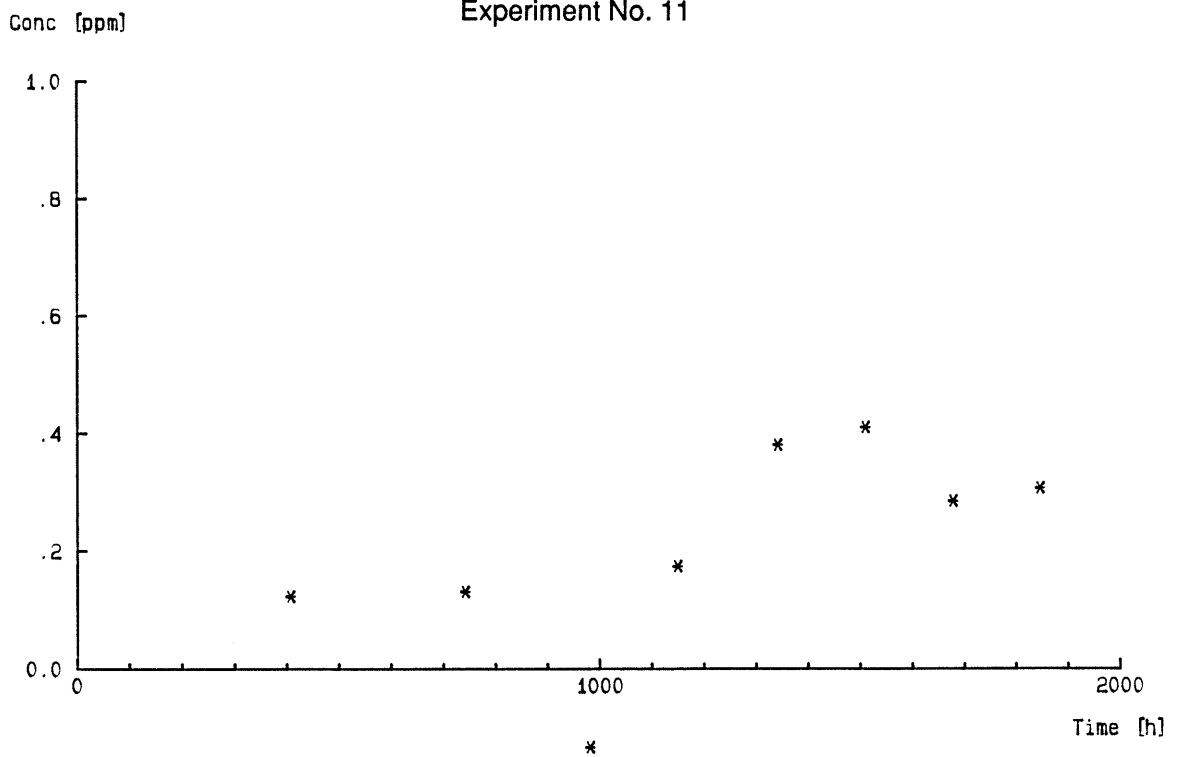


Figure A8-5. Concentration-time curves from the diffusion experiment.

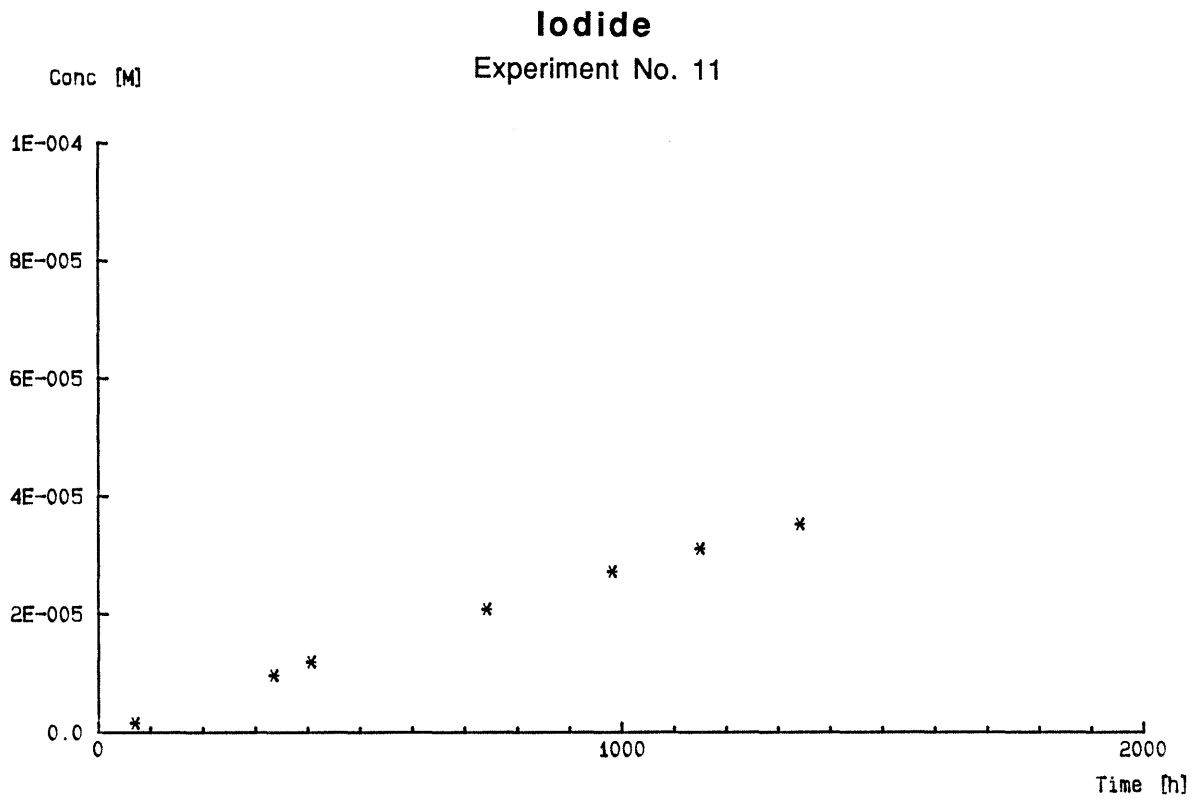


Figure A8-5. Concentration-time curves from the diffusion experiment.

NOTATION

C	concentration in mobile fluid	mol/m ³
C ₁	concentration at the high concentration side	mol/m ³
C ₂	concentration at the low concentration side	mol/m ³
D	diffusivity	m ² /s
D _e	effective diffusivity	m ² /s
D _p	pore diffusivity	m ² /s
K _d	sorption coefficient	m ³ /kg
L	slab thickness	m
M	amount of diffusing component	mol
N	flowrate of diffusing component	mol/s
t	time	s
x	distance into the rock	m
α	rock capacity factor	—
ε _p	total porosity	—
ε _t	"transport porosity" of matrix	—
ρ _p	density of rock matrix	kg/m ³

REFERENCES

Crank J.; The Mathematics of Diffusion, 2nd ed., Oxford University Press, New York, 1975, p 50–51.

Skagius K.; Diffusion of dissolved species in the matrix of some Swedish crystalline rocks, Ph. D. Thesis, Department of Chemical Engineering, Royal Institute of Technology, Stockholm, Sweden (1986).

COMPARISON BETWEEN FRACTURE CHARACTERISTICS AND
WATER FLOWRATES

The fractures used in the comparison are only those that were covered with plastic sheets. The fractures are separated into two major groups, single fractures and fracture zones. For each of the two major groups, the fracture length per area is presented for 4 different fracture sets as well as for mineral coating/filling materials. The presented water flowrates are those obtained before the drilling of the injection holes.

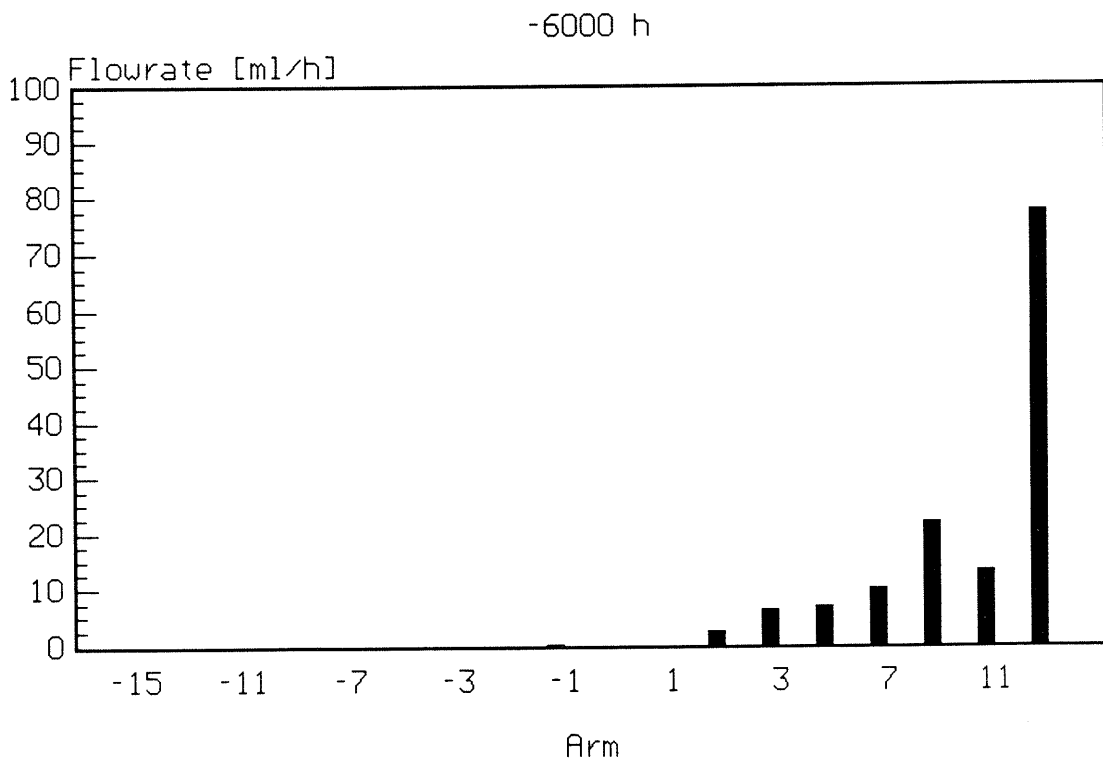
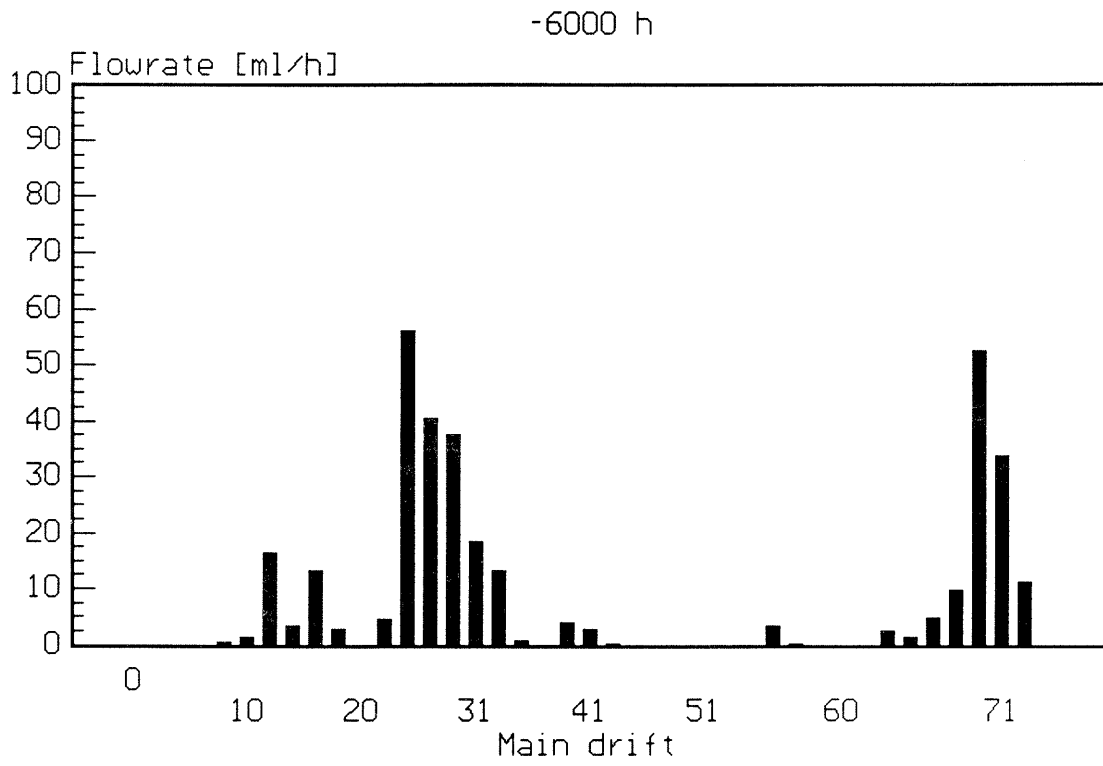


Figure A9-1. Water flowrates into main drift and arm at -6000 h.

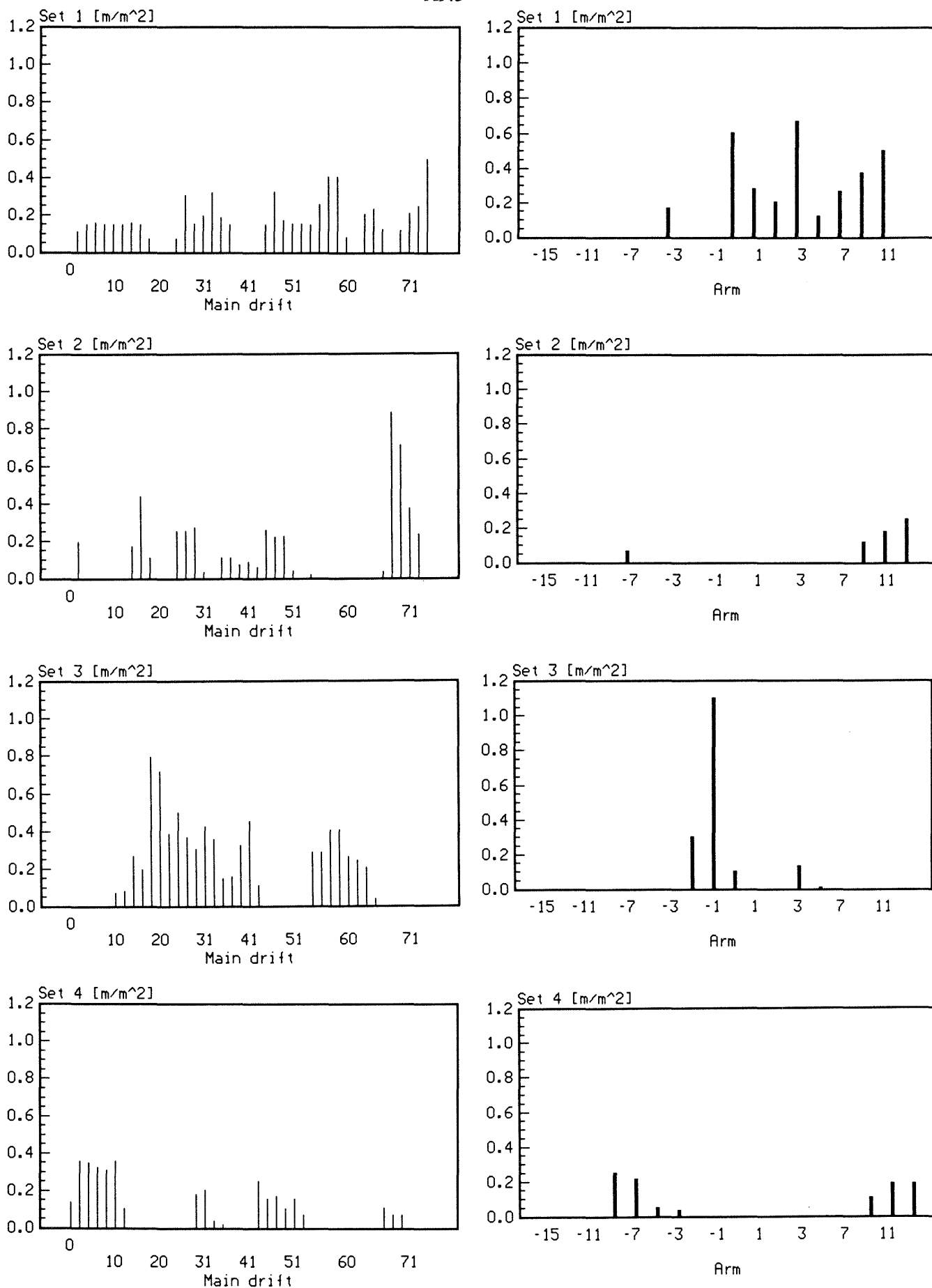
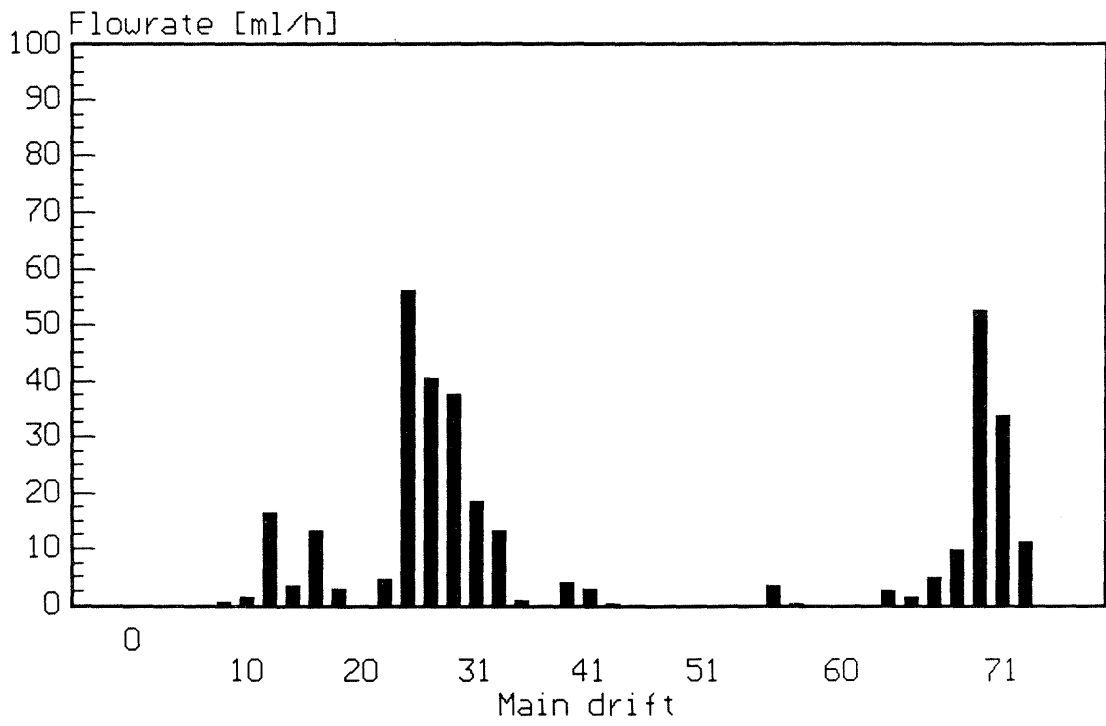


Figure A9-2. Fracture length per area for individual fractures, divided into 4 fracture sets.

A9.4

-6000 h



-6000 h

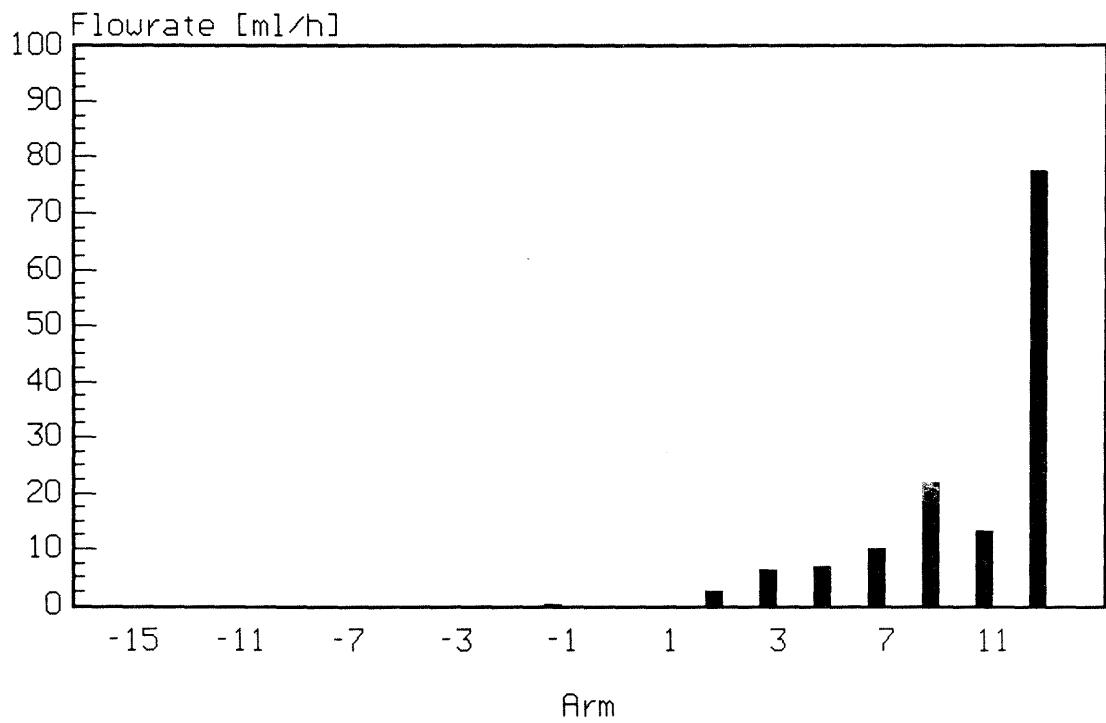


Figure A9-3. Water flowrates into main drift and arm at -6000 h.

A9.5

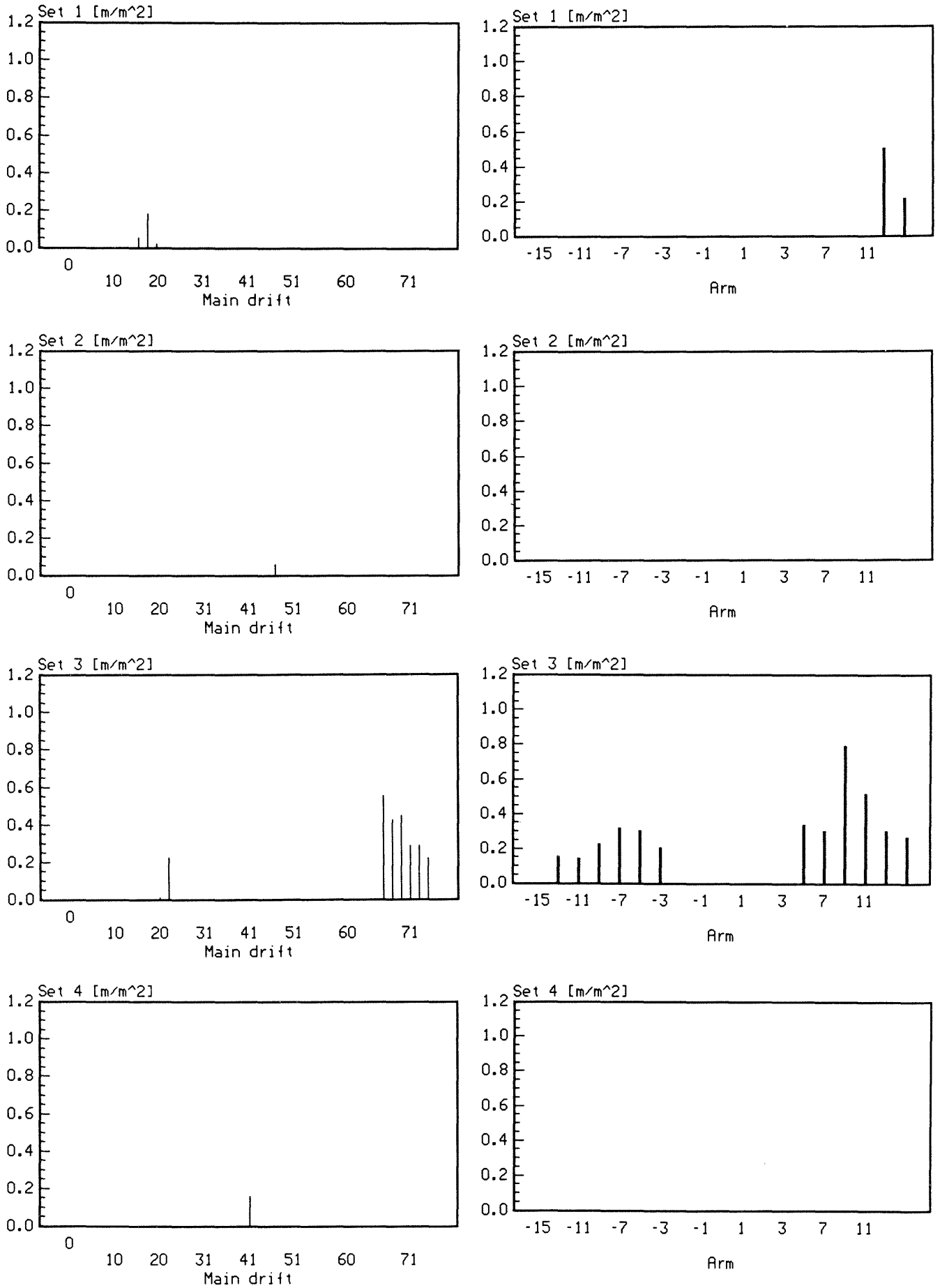


Figure A9-4. Fracture length per area for fracture zones, divided into 4 fracture sets.

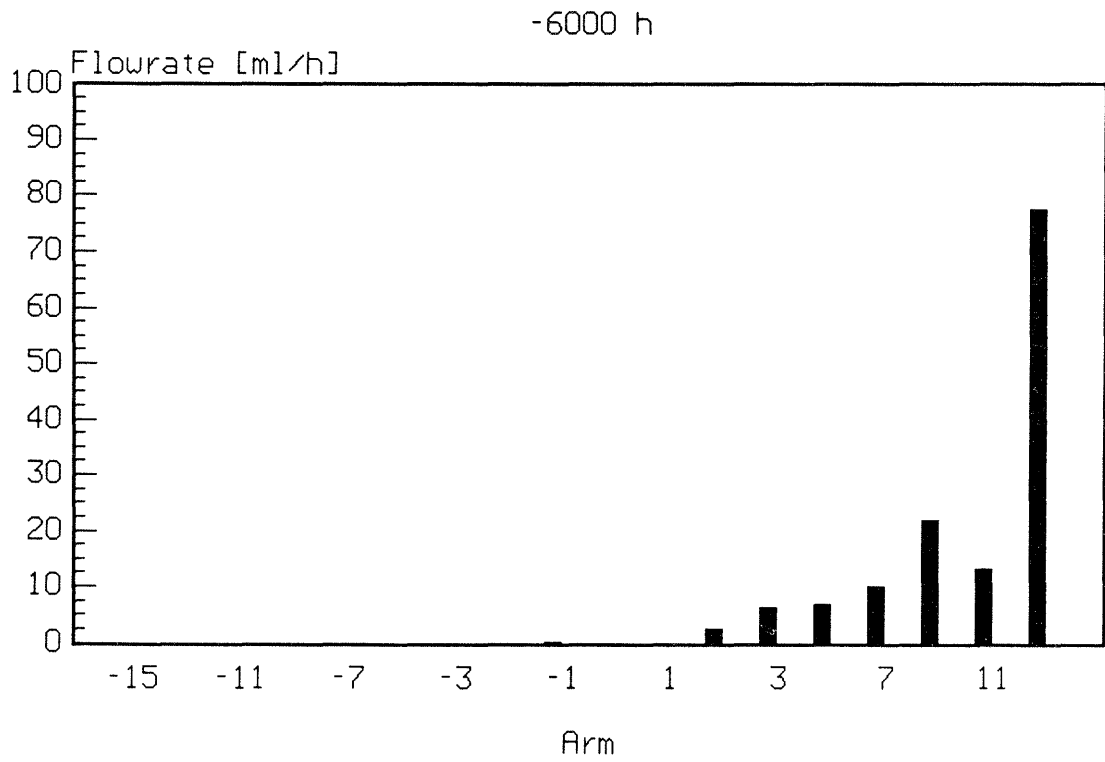
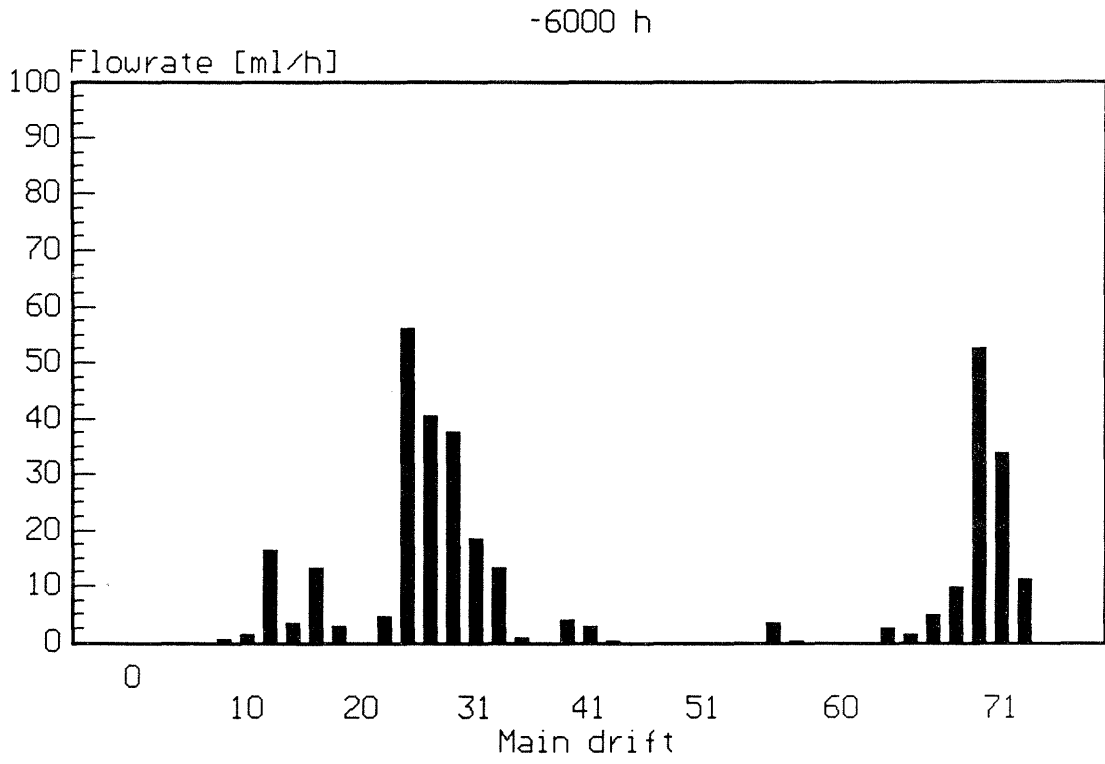


Figure A9-5. Water flowrates into main drift and arm at -6000 h.

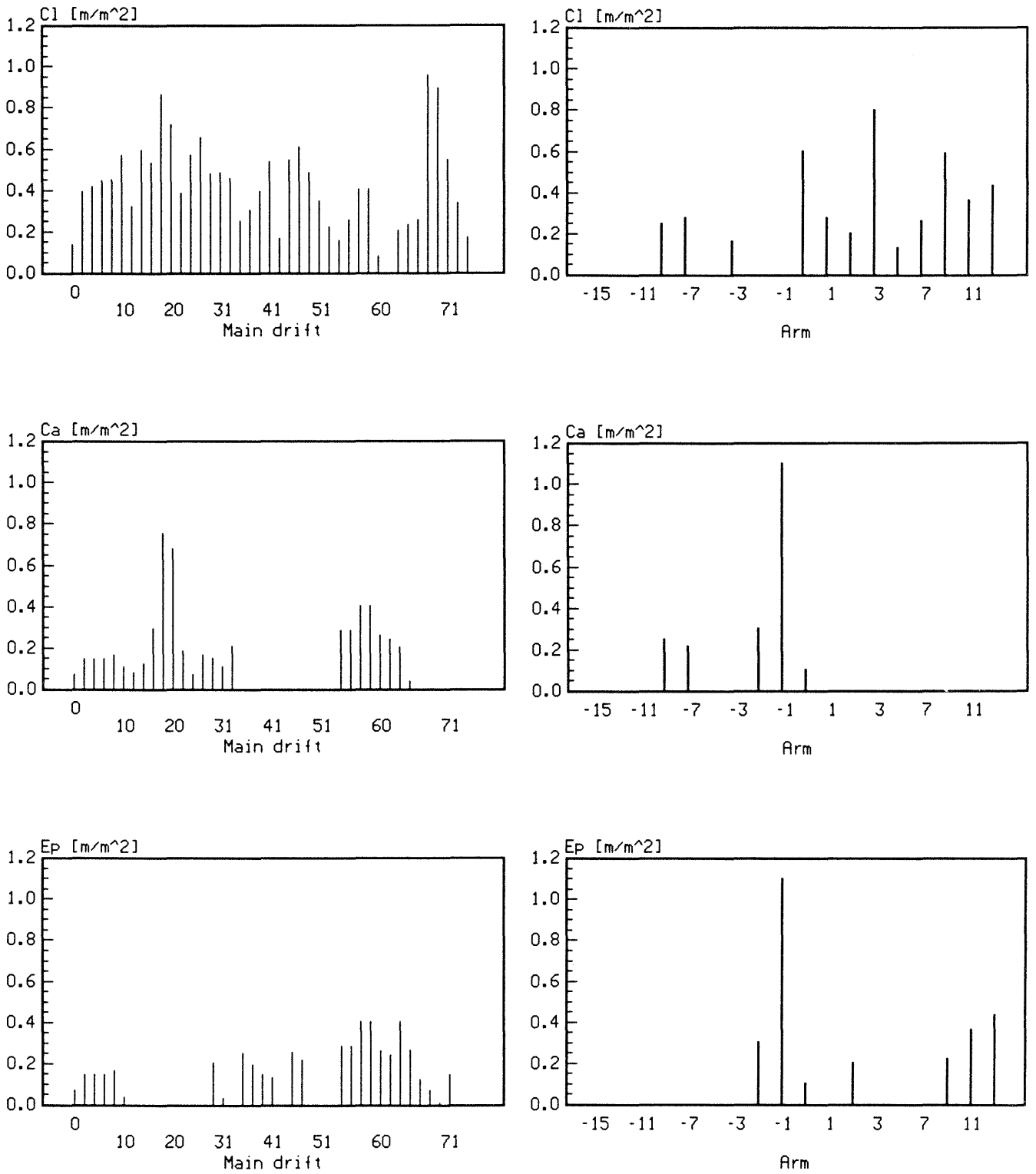


Figure A9-6.

Fracture length per area for individual fractures, presented for the different fracture fillings.

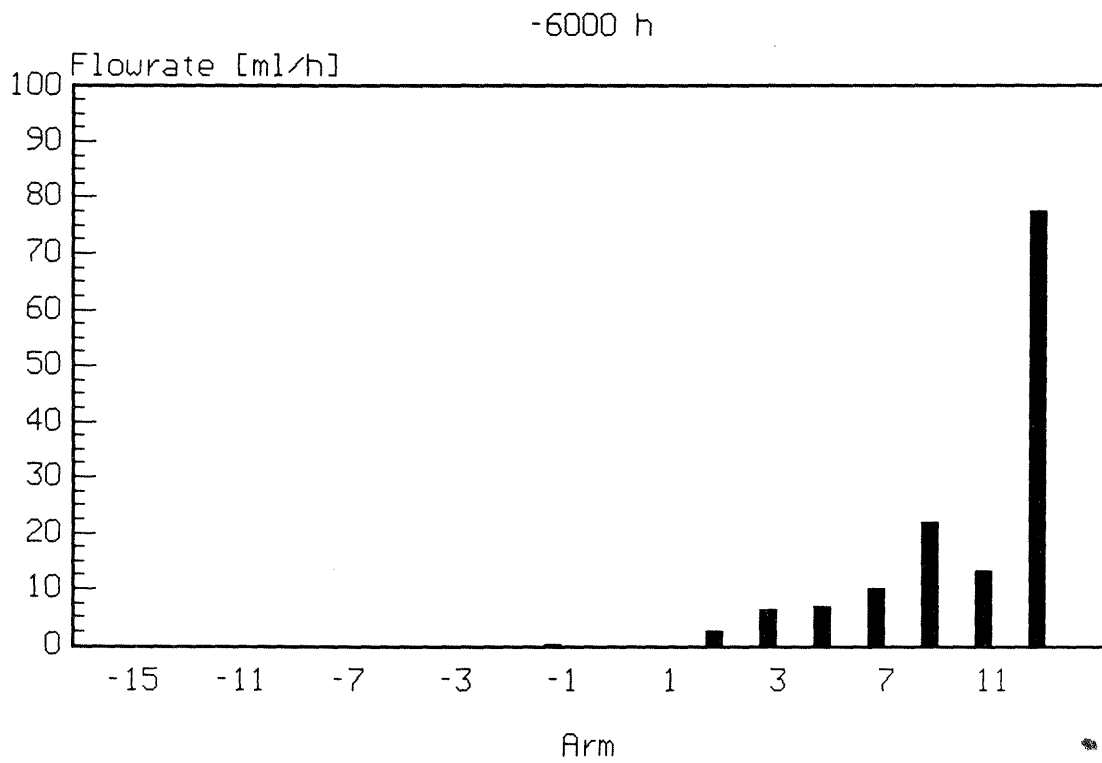
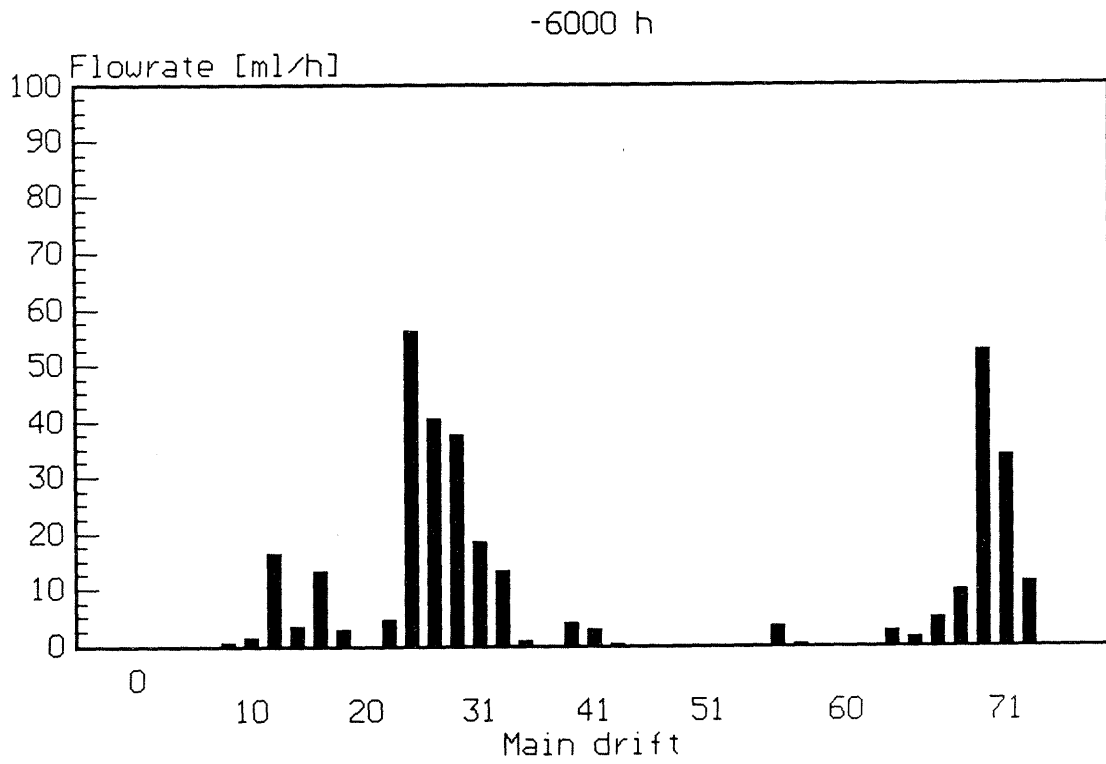


Figure A9-7. Water flowrates into main drift and arm at -6000 h.

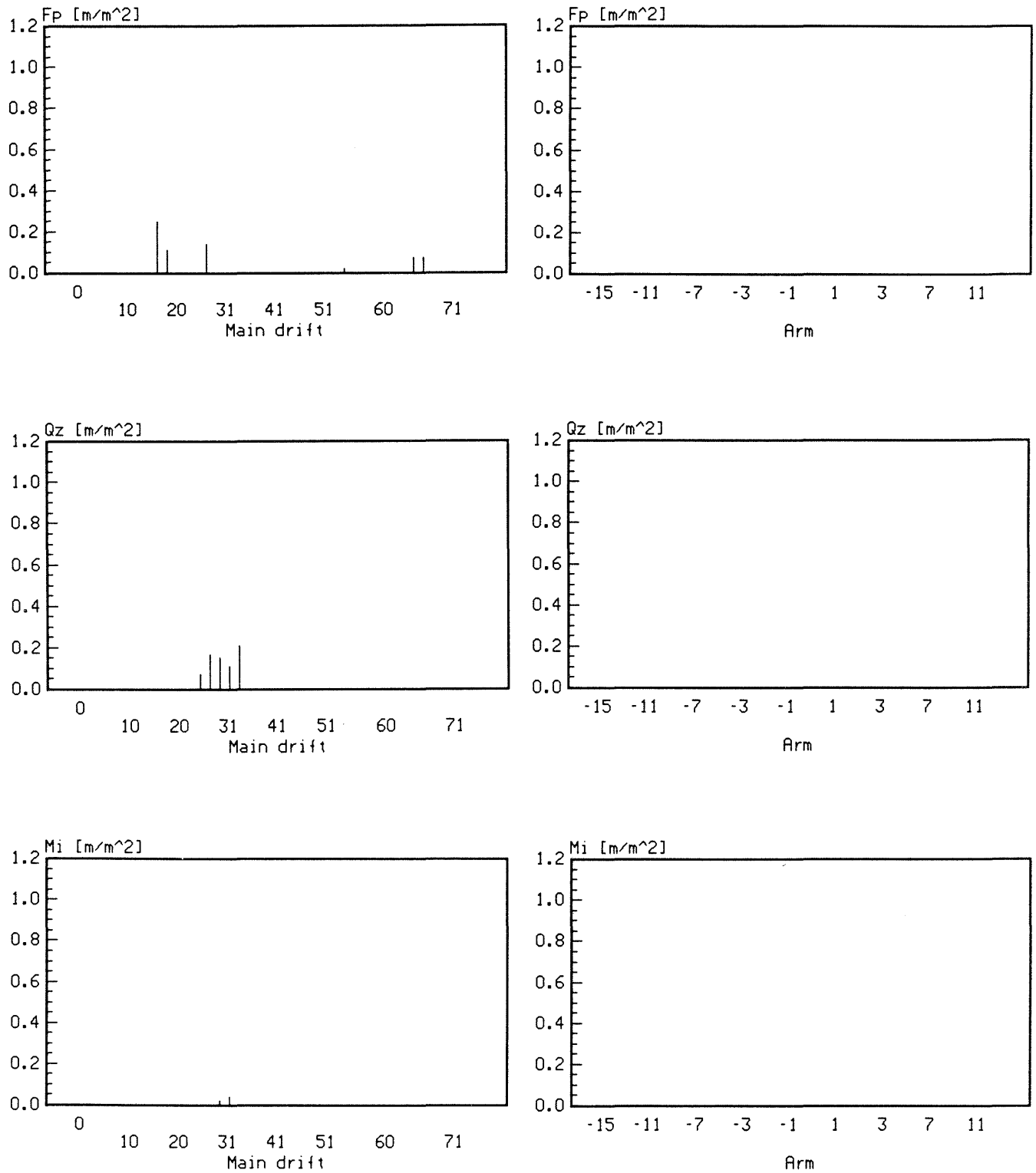


Figure A9-8.

Fracture length per area for individual fractures, presented for the different fracture fillings.

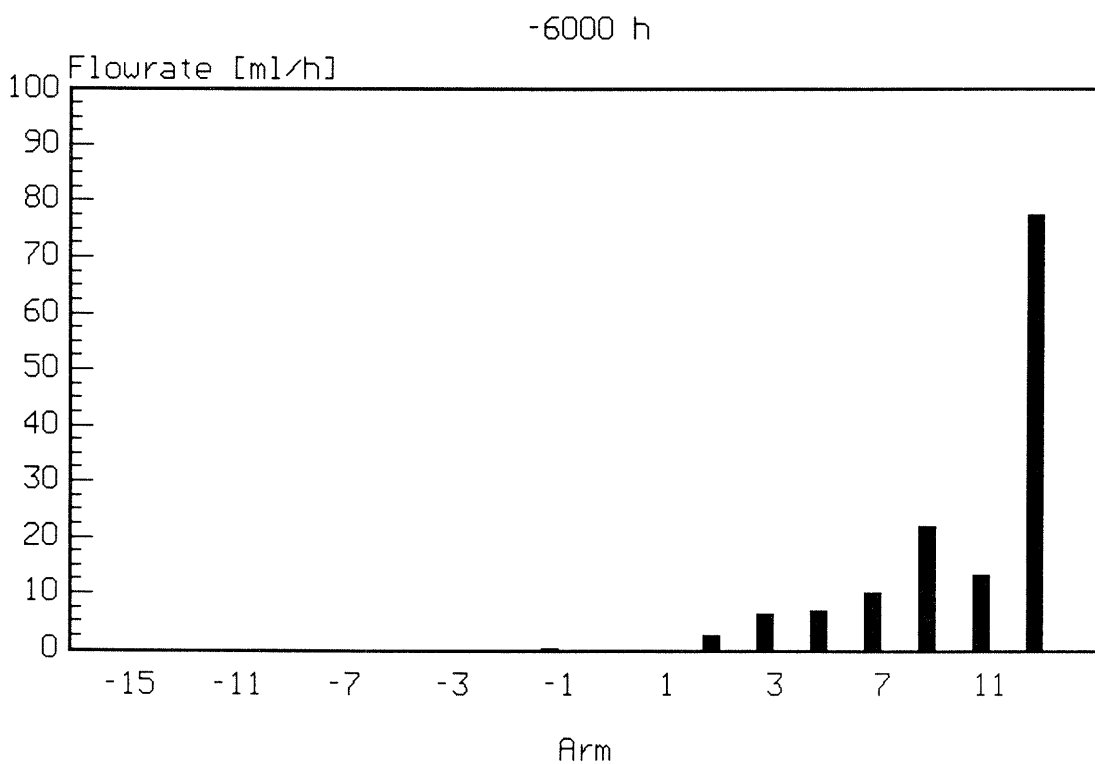
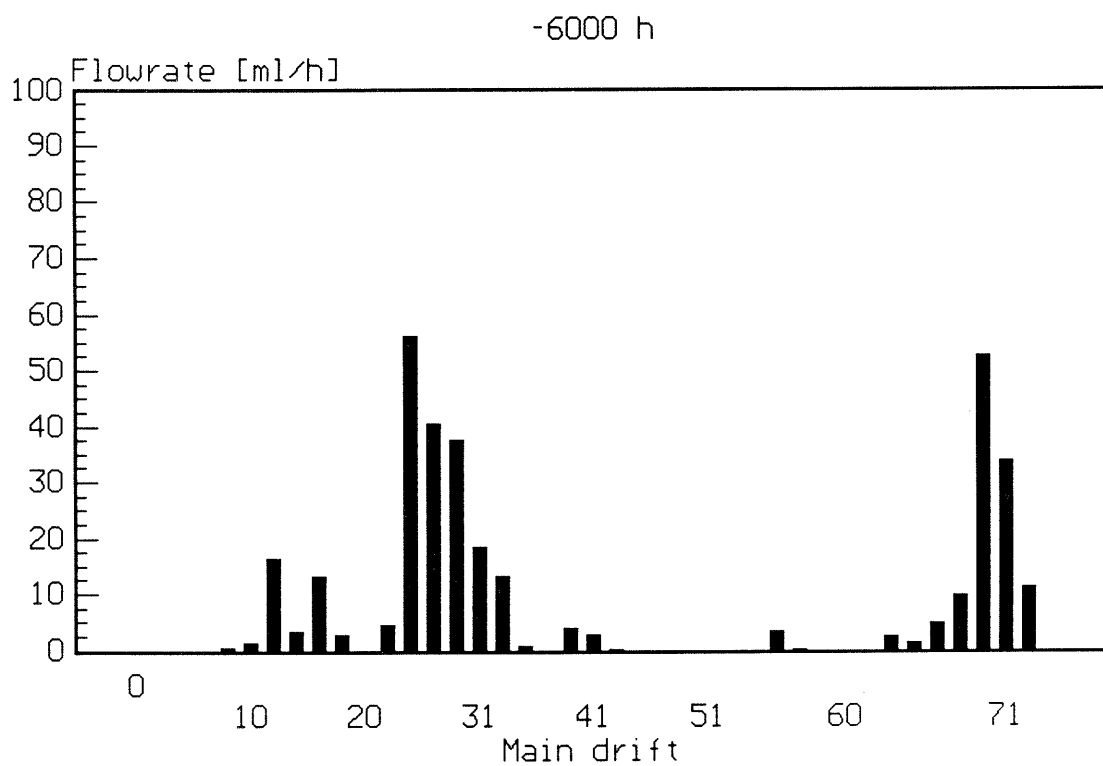


Figure A9-9. Water flowrates into main drift and arm at -6000 h.

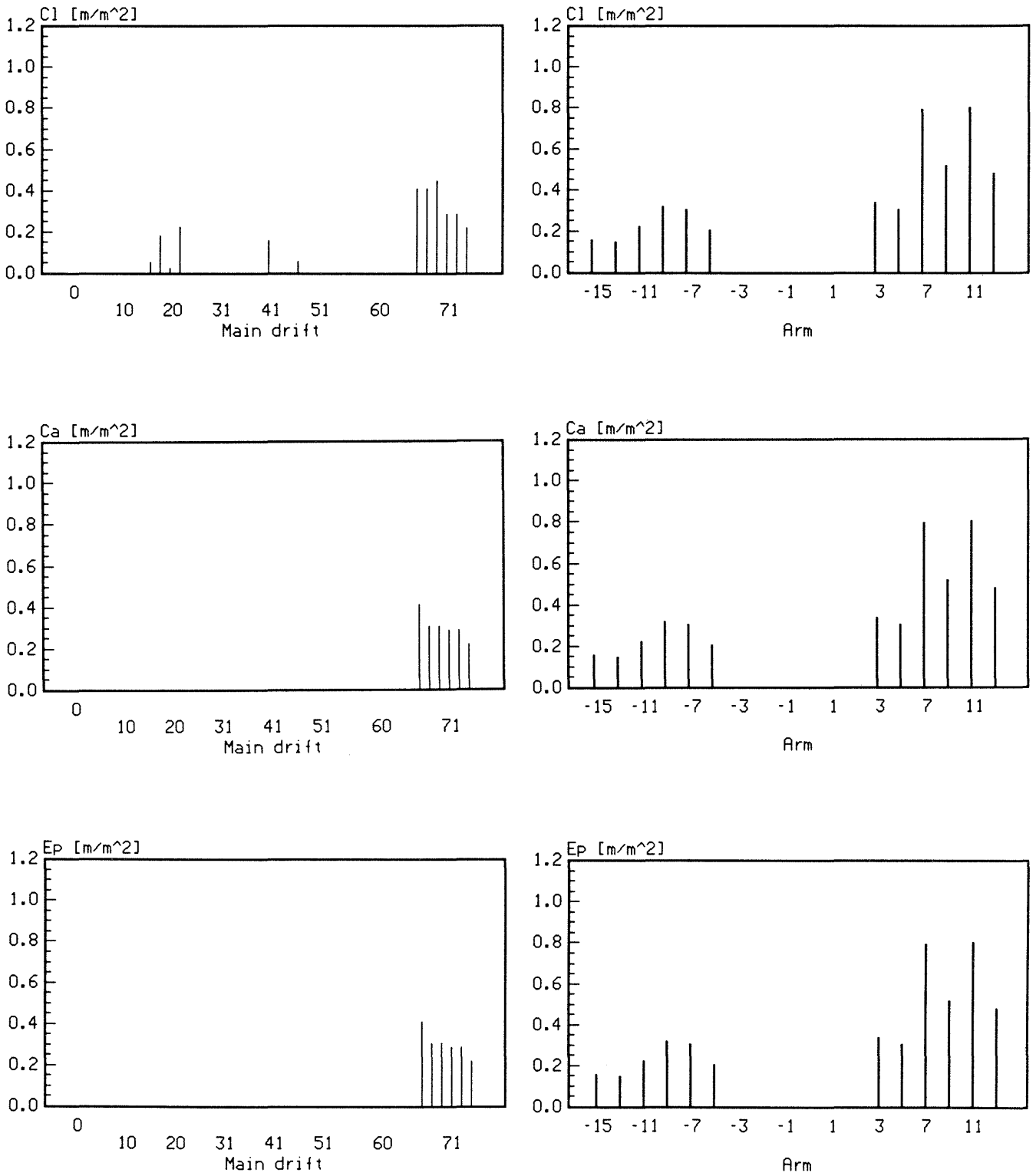


Figure A9-10. Fracture length per area for fracture zones, presented for the different fracture fillings.

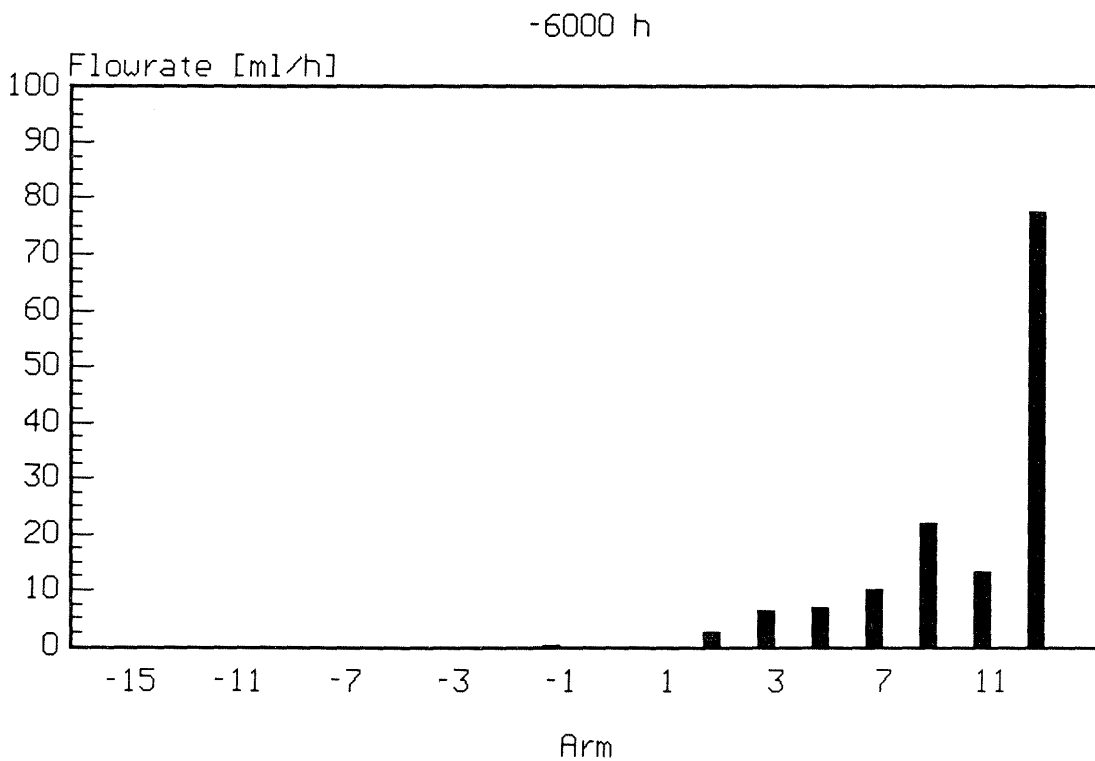
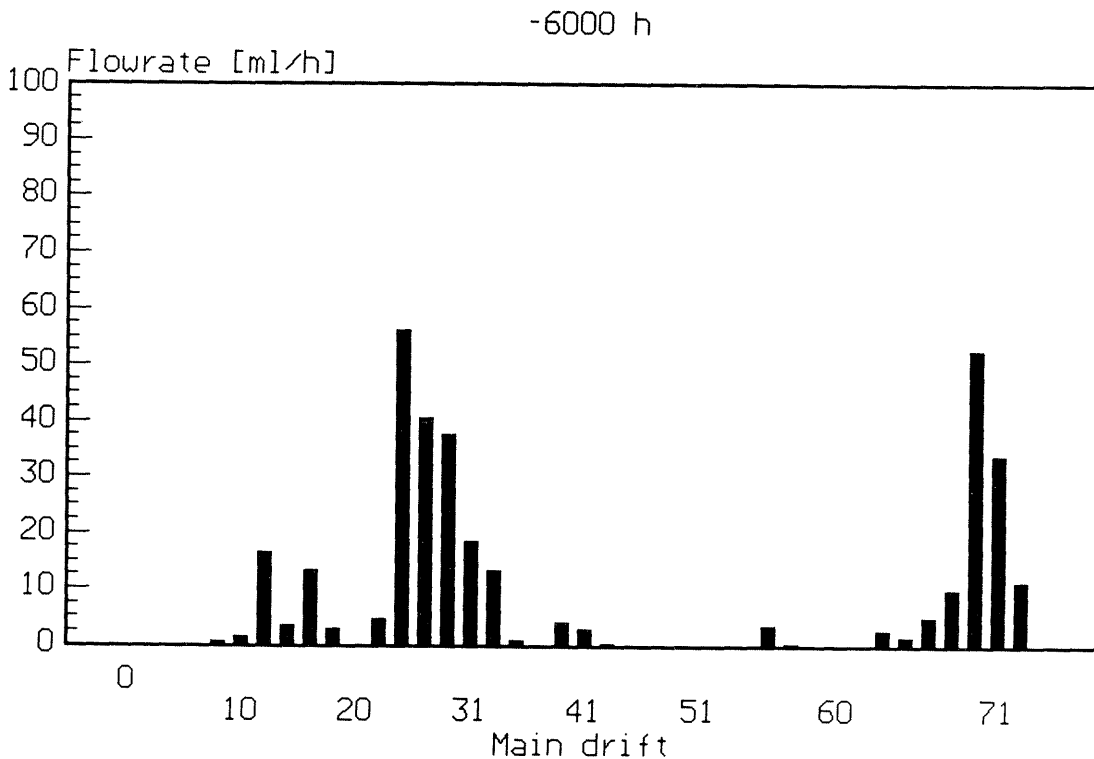


Figure A9-11. Water flowrates into main drift and arm at -6000 h.

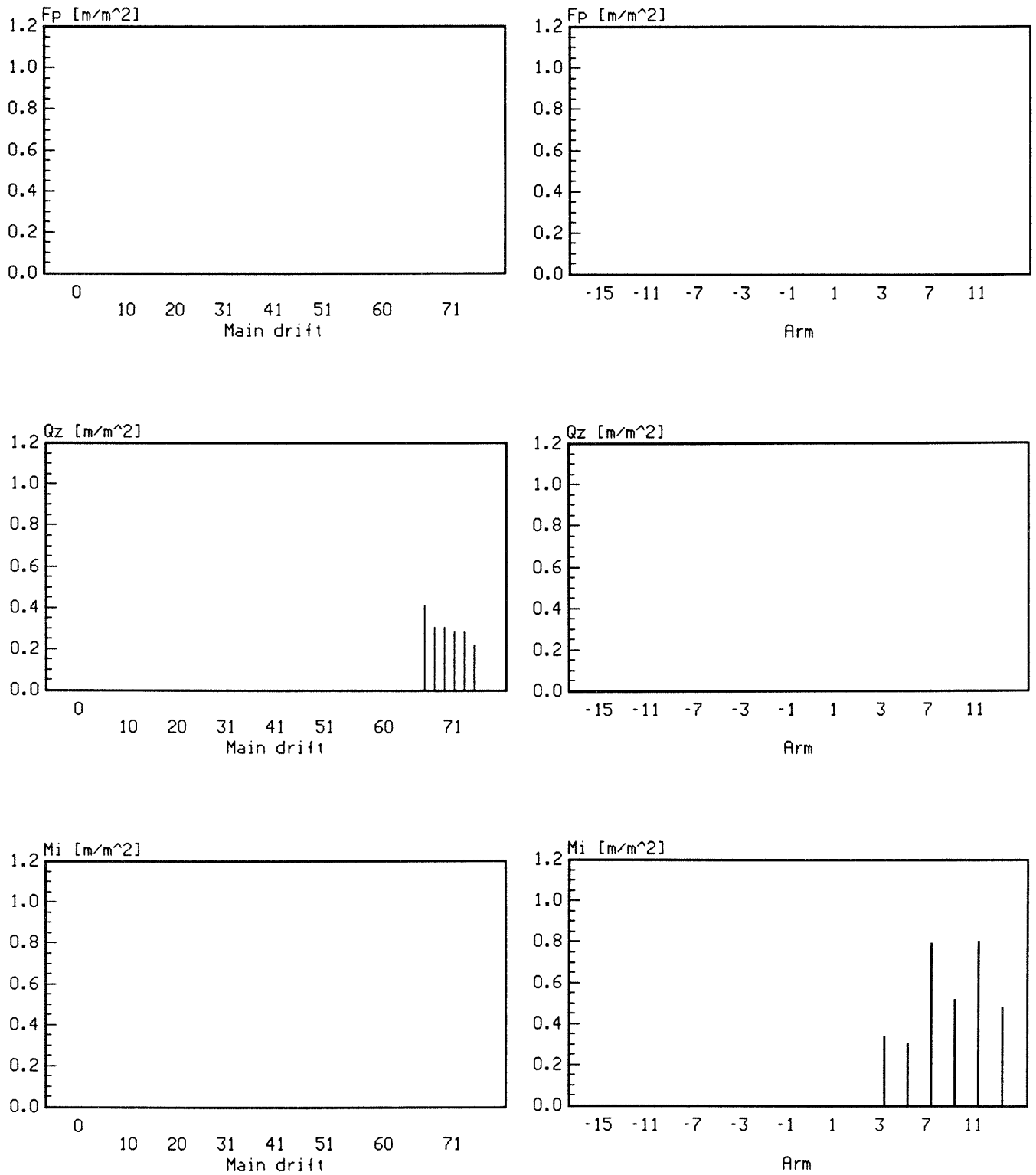


Figure A9-12. Fracture length per area for fracture zones, presented for the different fracture fillings.

AD MODEL FITS TO ALL CURVES

The results from the fitting with the Advection–Dispersion model are given for all the curves that were considered possible to fit. Among these are curves that had very few experimental points and very low concentrations. The plots for the fits are shown in Appendix 16 "Fitted Breakthrough Curves" (stand alone appendix). The breakthrough curves that were selected for more detailed fitting are shown in Appendix 11.

A10.2

Table A10-1. Results of fitting using the AD model.
Condition that the Peclet number greater than 4 is used.

Number	Pe	t_{wh}	Dilution	Standard-deviation
Tracer: Eosin B				
531	6.4	6935	171.9	.078
541	22.6	2772	1079.1	.349
571	5.0	7096	151.1	.145
581	4.0	4514	145.9	.227
591	4.0	3986	200.7	.180
601	4.0	20470	181.7	.112
611	4.0	13690	187.1	.126
621	4.0	6171	289.5	.211
631	4.0	4748	237.9	.206
641	4.0	7906	423.8	.293
651	4.0	4916	687.8	.241
661	4.0	5004	313.3	.219
671	4.0	4807	615.5	.198
681	4.0	1620	2371.9	.218
691	4.0	2292	3068.7	.481
701	145.3	1272	12615.6	.484
721	4.0	1966	6014.4	.244
1061	4.0	9884	766.9	.287
1081	4.0	5331	797.4	.323
1091	4.0	4089	286.0	.129
1101	4.0	15580	436.6	.184
1131	4.0	4548	246.3	.136
1141	4.0	6593	931.7	.144
1151	5.3	3104	264.9	.171
1181	4.0	4471	155.0	.172
1201	4.0	7077	135.5	.086
1211	4.0	9388	345.3	.097
2001	4.2	4438	253.6	.154
Tracer: Uranine				
602	4.0	3163	1177.7	.343
612	4.0	3738	3127.9	.295
622	4.0	2257	1933.9	.413
642	4.7	2273	1151.7	.384
652	4.0	2390	1932.7	.317
662	4.0	2760	1936.1	.359
672	4.0	2723	1447.6	.253
682	4.0	7063	498.5	.277
692	4.0	3971	962.5	.210
702	4.0	8792	1171.1	.240
712	4.0	4223	695.4	.248
722	4.0	4507	920.0	.233
872	4.0	6269	2107.0	.140
892	4.0	1234	4723.7	.374
902	4.0	11680	1041.0	.165
922	4.0	4744	5096.8	.215

A10.3

Table A10-1 continued.

962	4.0	4712	1510.3	.174
972	4.0	9150	971.8	.192
982	4.0	10570	1309.2	.155
992	4.0	5431	1588.1	.334
1022	4.0	7257	2360.7	.144
1032	4.0	4795	2056.3	.181
1042	4.0	3824	5685.0	.399
1062	4.0	3569	2783.2	.255
1072	4.2	3694	656.2	.253
1082	4.0	3634	2194.4	.287
1102	4.1	2671	2691.8	.314
1112	4.0	5164	20395.7	.261
1142	4.1	5209	10463.5	.236
1342	12.0	11810	190.4	.032
1352	414.0	15070	4899.6	.054

Tracer:		Elbenyl		
593	4.0	1698	112.2	.188
603	4.0	2112	285.8	.146
623	4.0	3395	246.7	.234
643	6.1	2014	247.7	.220
653	5.0	1922	337.2	.207
663	4.0	1969	202.3	.201
673	4.0	2423	256.0	.197
683	5.6	1978	382.2	.114
693	9.1	1385	1036.8	.557
703	8.1	1824	1537.3	.313
713	4.4	2667	1445.1	.096
723	6.2	1889	807.4	.105
1033	4.0	3109	1545.6	.048
1063	7.9	2023	1255.5	.131
1083	6.3	1636	583.6	.286
1093	5.5	3266	396.3	.187
1103	8.5	1821	1034.1	.142
1133	4.0	3397	550.5	.350
1153	4.0	2796	531.1	.087

Tracer:		Eosin Y		
606	8.0	5041	152.9	.071
616	8.3	3652	775.8	.247
626	6.0	4522	238.2	.109
646	6.6	5090	130.7	.100
656	6.6	5875	239.5	.083
666	11.8	5121	233.4	.101
676	7.4	6142	189.1	.111
686	5.5	7320	94.9	.074
696	5.3	6625	147.5	.116
706	5.6	7303	331.3	.061
716	5.3	7831	93.5	.066
726	10.5	6601	149.1	.083
856	4.9	8714	224.8	.061
866	8.8	7047	372.0	.077

A10.4

Table A10-1 continued.

876	6.0	8861	90.3	.036
896	27.0	5933	201.6	.045
906	4.7	8933	72.4	.033
916	4.0	25180	1388.7	.087
926	4.0	11590	264.7	.058
946	4.0	10490	106.1	.035
966	25.6	9317	265.9	.037
976	23.8	8752	239.2	.048
986	28.0	9909	351.6	.028
996	114.7	8122	550.4	.169
1026	17.4	9118	418.6	.070
1036	5.8	8078	273.7	.086
1046	11.0	7616	570.5	.109
1066	6.8	6502	314.2	.103
1076	6.4	8034	84.3	.071
1086	6.0	6324	277.6	.085
1106	8.3	5709	345.5	.139
1116	24.7	6794	3659.0	.180
1136	5.1	5849	1200.9	.139
1146	8.2	7292	834.7	.063
<hr/>				
Tracer:	Iodide			
538	4.0	8911	1278.3	.211
558	68.3	4144	1427.0	.527
578	16.0	4875	385.1	.798
588	4.0	4456	406.0	.483
608	21.3	7609	98.0	.047
618	18.6	7209	126.8	.078
628	4.0	11160	40.3	.046
648	23.1	7493	88.0	.050
658	21.5	7596	75.7	.047
668	27.0	7012	69.4	.073
678	16.4	9622	57.5	.023
688	4.0	12410	100.5	.047
698	25.2	7792	187.9	.067
708	15.8	9114	420.4	.097
718	28.8	7385	175.4	.077
728	4.0	15740	114.6	.049
998	32.7	8412	215.6	.058
1028	40.7	8293	124.5	.072
1038	34.0	7558	98.6	.064
1068	44.7	7497	73.9	.074
1078	23.9	8084	164.3	.044
1088	54.5	7113	82.3	.065
1098	4.0	11740	38.4	.056
1108	34.5	7031	76.2	.061
1138	17.7	7607	53.7	.087
1158	4.0	8026	37.1	.172
1188	4.0	3290	560.1	.685
1208	4.0	4378	559.9	.534
1228	4.0	451	1063.8	.590
2008	4.0	5093	382.2	.417

A10.5

Table A10-1 continued.

Tracer:	Bromide			
539	9.0	2904	41.4	.217
549	9.5	1461	24.7	.294
579	4.0	2595	19.9	.180
599	4.0	5240	18.1	.187
609	4.0	6187	24.1	.156
619	4.0	4324	28.3	.218
629	4.0	9209	14.2	.118
649	4.0	7525	24.9	.270
659	4.0	8961	24.5	.184
669	4.0	6416	20.0	.211
679	4.0	10160	19.8	.182
689	4.0	6691	40.0	.208
709	4.0	7594	100.7	.329
719	4.0	10880	45.0	.158
729	4.0	8186	59.9	.170
1069	4.0	10120	22.2	.197
1079	4.0	15840	30.9	.106
1089	4.0	11800	21.0	.183
1099	4.0	4923	15.8	.220
1109	4.0	9238	23.2	.162
1139	4.0	7830	17.4	.313
1149	4.0	10270	21.5	.104
1159	8.4	2735	12.8	.148
1189	11.0	1728	18.0	.230
1209	19.0	2206	16.9	.244

A10.6

Table A10-2. Results of fitting using the AD model. Condition that the Peclet number greater than 1 is used.

Number	Pe	t_{wh}	Dilution	Standard-deviation
Tracer: Eosin B				
581	1.0	9533	113.4	.113
591	1.0	7589	164.4	.084
601	1.0	56030	108.6	.064
611	1.0	34120	122.1	.072
621	1.0	12320	222.4	.105
631	1.0	11020	165.1	.094
641	1.0	14630	327.7	.178
651	1.0	8949	559.5	.134
661	1.0	9548	250.9	.113
671	1.0	9603	489.9	.125
681	2.4	1840	2237.1	.199
691	1.0	4779	2310.9	.298
721	1.0	3632	4840.3	.141
1061	1.0	20080	536.9	.165
1081	1.0	9688	641.6	.203
1091	1.5	6302	248.0	.082
1101	1.0	31960	321.0	.117
1131	2.4	5706	227.8	.119
1141	2.9	7598	876.7	.134
1181	1.1	8564	125.6	.104
1201	1.3	13340	104.4	.040
1211	3.2	10190	329.2	.091
Tracer: Uranine				
602	1.0	3449	1133.7	.310
612	1.0	3795	3154.6	.248
622	1.0	2205	2120.9	.419
642	1.0	2815	1086.1	.341
652	1.0	3302	1833.9	.283
662	1.0	3007	1850.1	.320
672	1.0	3173	1364.6	.225
682	1.0	6186	627.7	.200
692	1.0	5435	882.6	.181
702	1.0	9849	1371.6	.185
712	1.0	5643	633.3	.211
722	1.0	6169	828.5	.194
872	1.0	17040	1338.0	.078
892	1.0	1447	4578.8	.333
902	1.0	17370	1150.6	.123
922	1.0	7348	4340.3	.171
962	1.0	9413	1178.1	.129
972	1.0	11080	1096.9	.105
982	1.0	14990	1467.6	.087
992	1.7	3333	2098.2	.295
1022	1.0	14120	1904.0	.106
1032	1.0	8000	1717.0	.140

A10.7

Table A10-2 continued.

1042	1.0	3009	7122.5	.355
1062	1.0	4530	2554.9	.218
1072	1.0	5262	559.3	.202
1082	1.0	4668	2014.5	.251
1102	1.0	3310	2522.7	.274
1112	1.0	8286	16995.2	.202
1142	1.0	9335	8453.1	.181
<hr/>				
Tracer: Elbenyl				
593	2.2	2038	108.2	.179
603	2.4	2447	275.4	.138
623	1.0	5419	212.8	.174
663	3.9	1963	202.4	.201
673	1.3	3692	230.0	.171
1033	3.6	3244	1517.5	.046
1133	1.0	5163	480.2	.293
<hr/>				
Tracer: Eosin Y				
916	1.0	85430	626.2	.039
926	3.9	11610	264.1	.058
946	3.0	12110	97.0	.031
<hr/>				
Tracer: Iodide				
538	1.0	24060	806.5	.132
588	1.0	8840	323.9	.380
628	3.7	11620	39.2	.045
688	1.2	30410	60.6	.028
728	1.2	41200	62.9	.027
1098	1.4	25630	24.7	.036
1158	1.0	23350	21.9	.101
1188	1.0	5368	480.2	.582
1208	2.0	5735	506.6	.483
1228	2.9	478	1059.5	.587
2008	3.2	5534	369.1	.402
<hr/>				
Tracer: Bromide				
579	2.4	3037	19.2	.168
599	1.0	11360	13.8	.116
609	1.0	12910	18.0	.093
619	1.0	8757	22.9	.168
629	1.0	22760	9.5	.059
649	1.0	17520	17.2	.167
659	1.0	19330	17.9	.115
669	1.0	13100	15.0	.138
679	1.0	22220	13.4	.109
689	1.0	14890	29.3	.133
709	1.0	13140	77.8	.229
719	1.1	26660	29.2	.087
729	1.0	16840	45.0	.108
1069	1.0	22230	15.1	.121

A10.8

Table A10-2 continued.

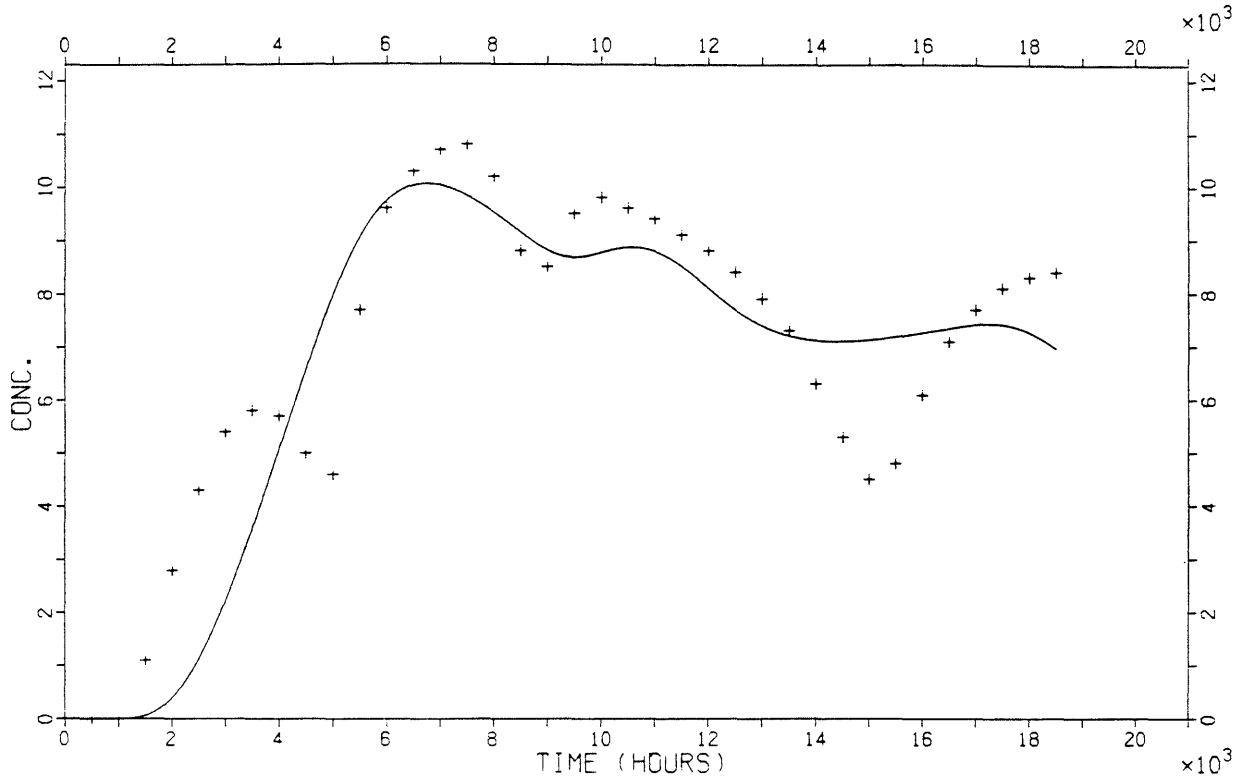
1079	1.0	45550	17.6	.055
1089	1.0	29400	13.6	.105
1099	1.0	9714	12.5	.162
1109	1.0	20130	16.8	.096
1139	1.0	15790	12.7	.210
1149	1.0	26960	13.7	.051

FITS OF ALL SELECTED CURVES

For each of the five tracers Eosin B, Uranine, Elbenyl, Eosine Y and Iodide, five breakthrough curves were selected for more detailed fitting than was performed with the 167 curves shown in Appendix 10. The selection of these curves was based on the amount of tracer that had arrived at the different plastic sheets. The 25 breakthrough curves selected were among those with a high contribution to the total recovery from different sections of the drift, therefore, the five curves chosen for each tracer may not include the five highest breakthrough curves.

Sheet number 57 tracer Eosin B, AD-model

Pe = 5.1 Tw = 7045 Dil = 151.3 SD = .14



Sheet number 60 tracer Eosin B, AD-model

Pe = 4.0 Tw = 20470 Dil = 181.7 SD = .11

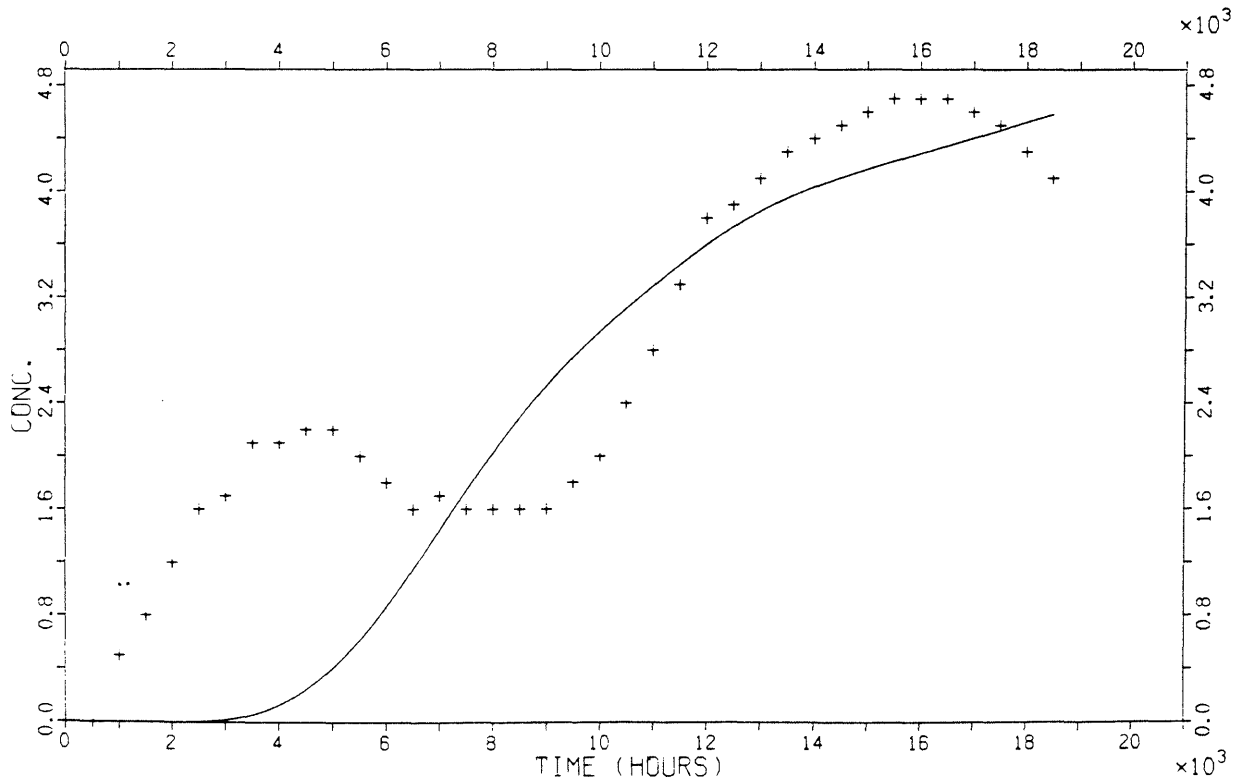
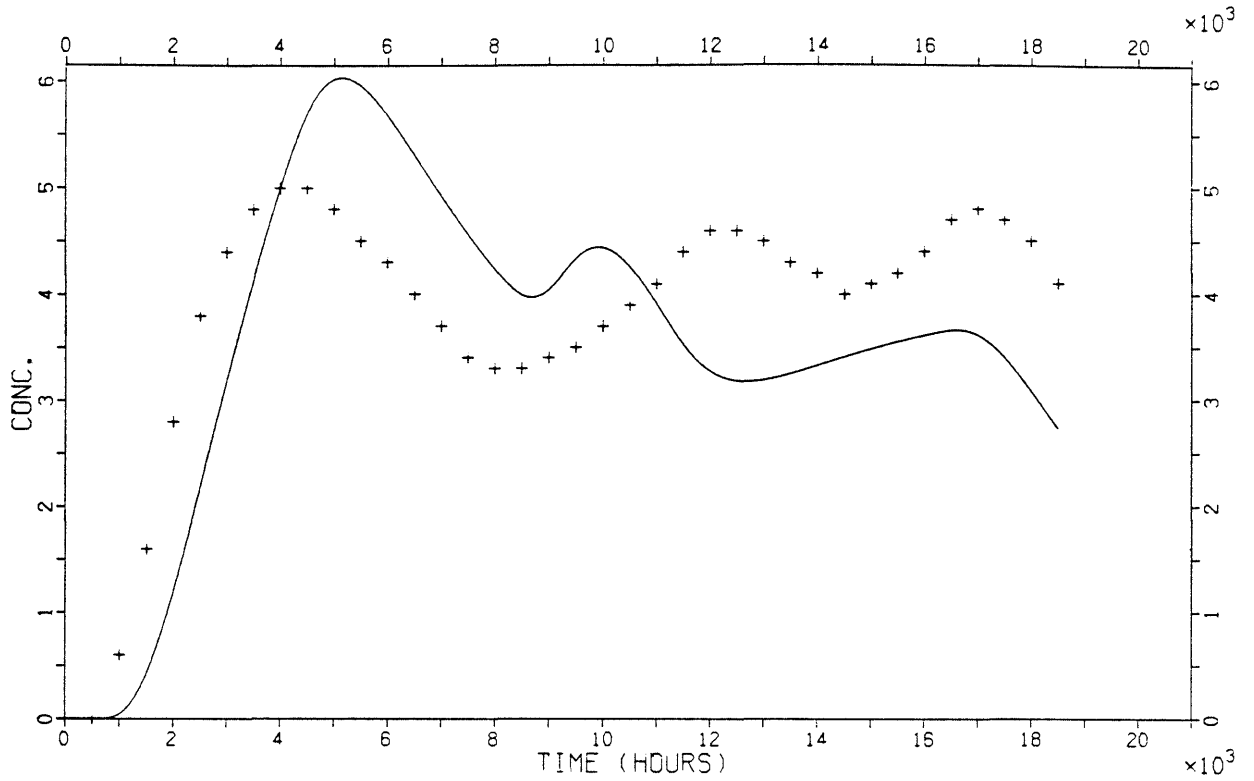


Figure A11-1. Model fits with AD-model.

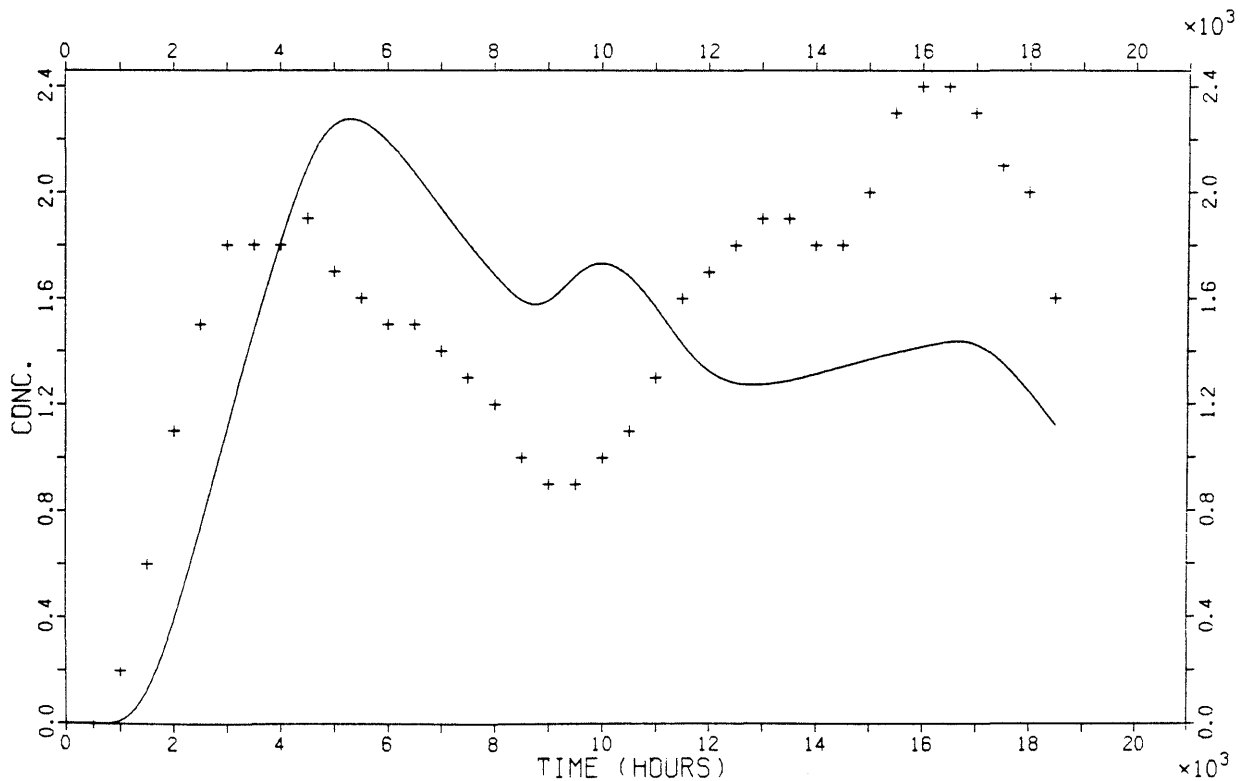
Sheet number 66 tracer Eosin B, AD-model

Pe = 4.0 Tw = 5004 Dil = 313.3 SD = .22



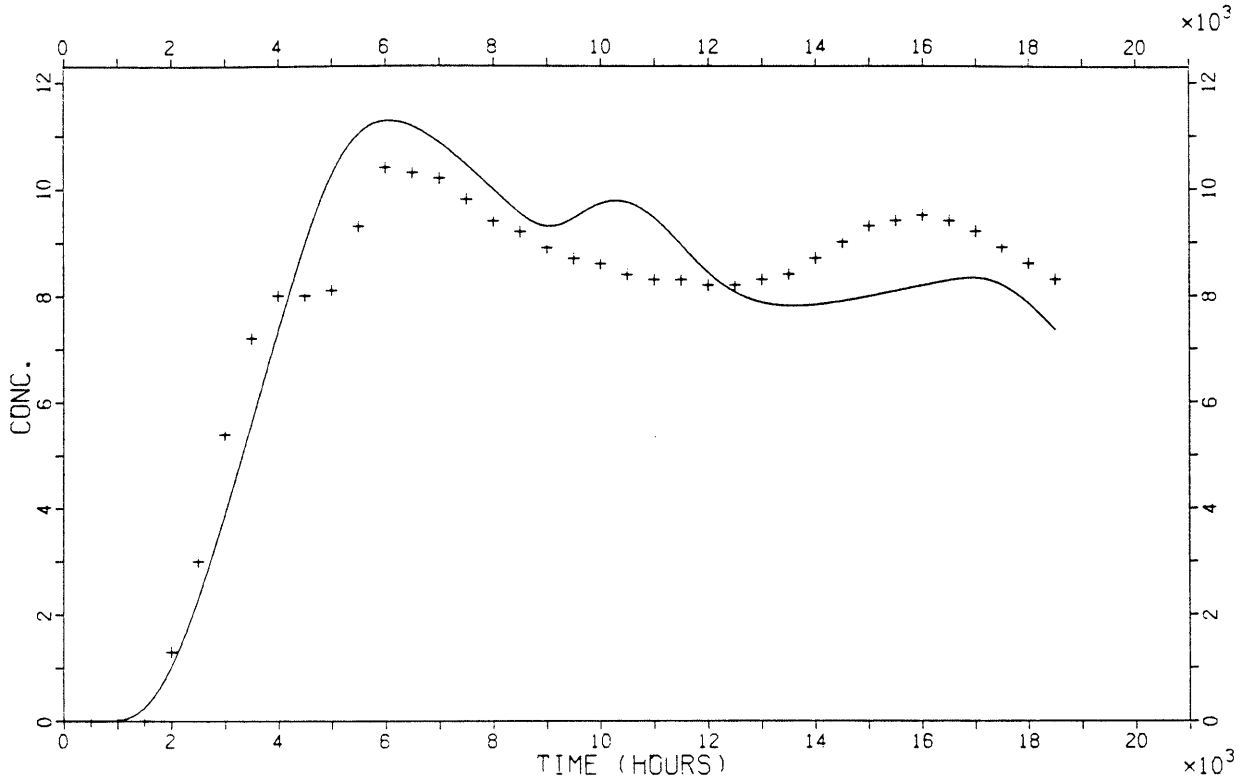
Sheet number 108 tracer Eosin B, AD-model

Pe = 4.0 Tw = 5331 Dil = 797.4 SD = .32



Sheet number 120 tracer Eosin B, AD-model

Pe = 4.0 Tw = 7077 Dil = 135.5 SD = .09



Sheet number 64 tracer Uranine, AD-model

Pe = 4.7 Tw = 2273 Dil = 1152 SD = .38

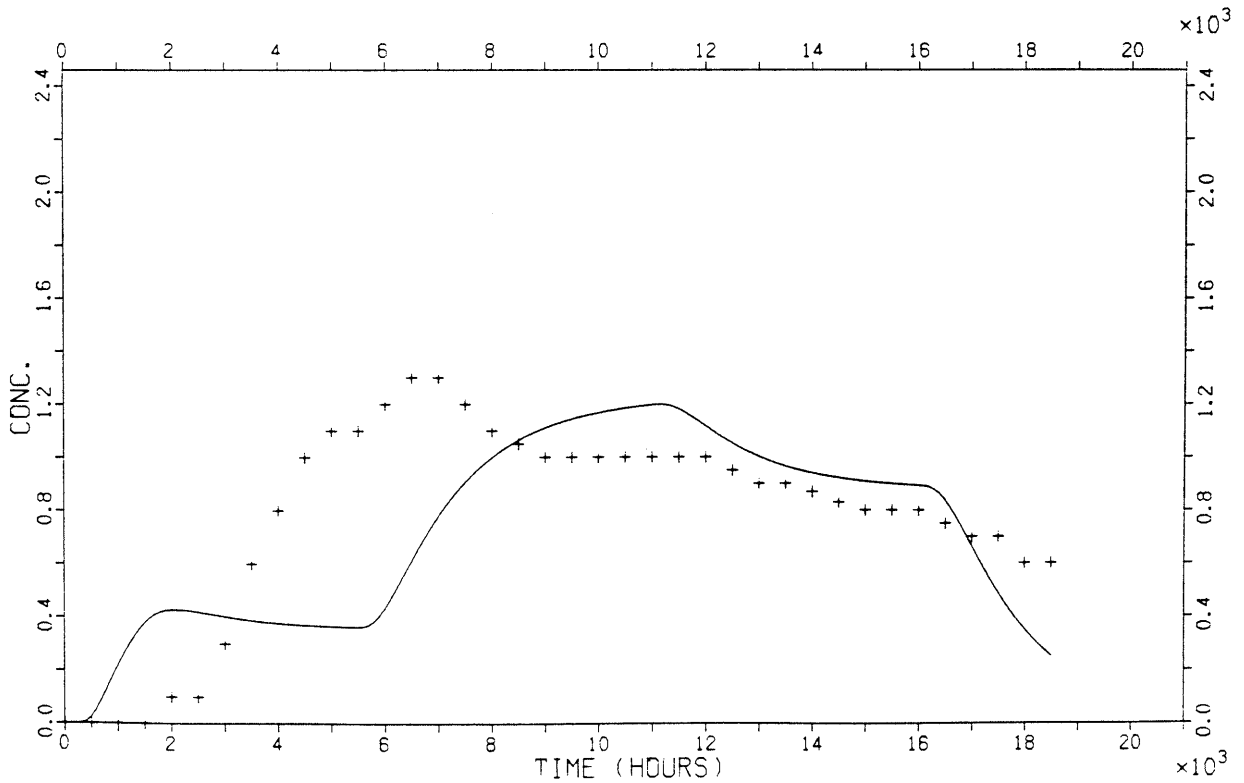
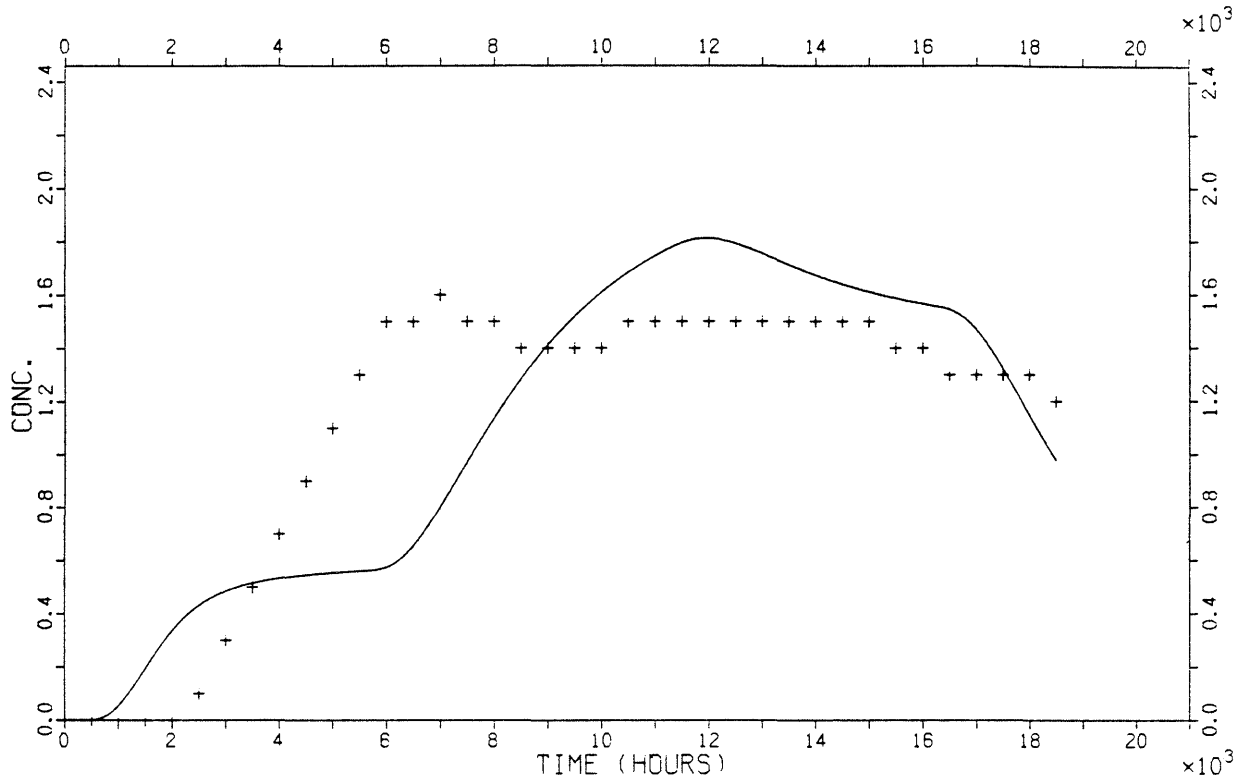


Figure A11-1. Continued.

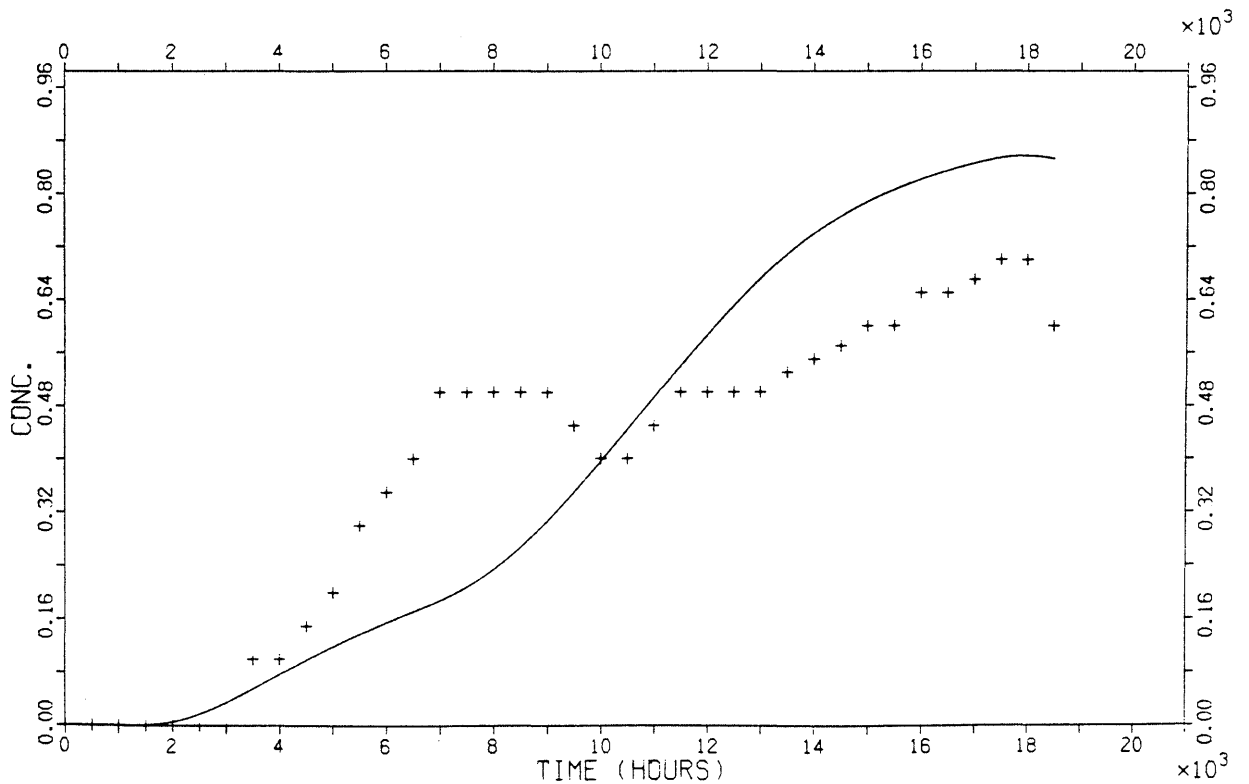
Sheet number 71 tracer Uranine, AD-model

Pe = 4.0 Tw = 4223 Dil = 695 SD = .25



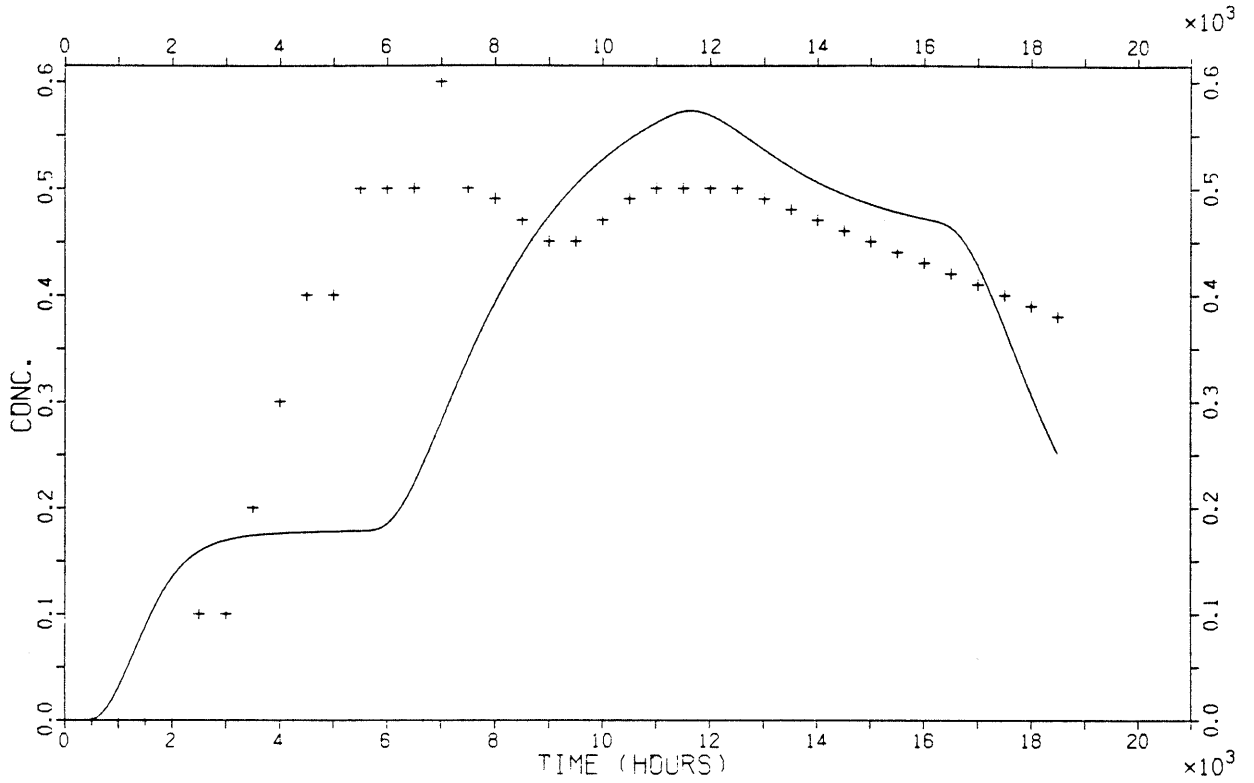
Sheet number 90 tracer Uranine, AD-model

Pe = 4.0 Tw = 7445 Dil = 1670 SD = .19



Sheet number 108 tracer Uranine, AD-model

Pe = 4.0 Tw = 3634 Dil = 2194 SD = .29



Sheet number 134 tracer Uranine, AD-model

Pe = 12.0 Tw = 11810 Dil = 190 SD = .03

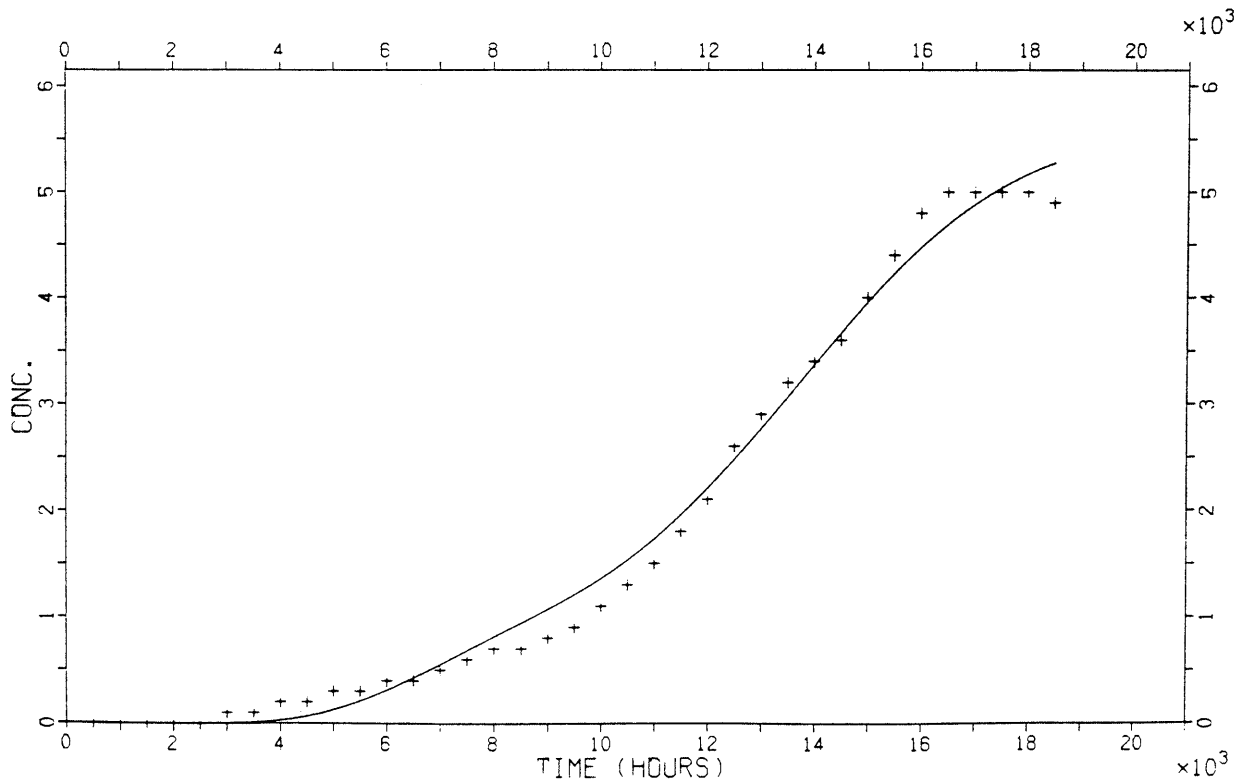
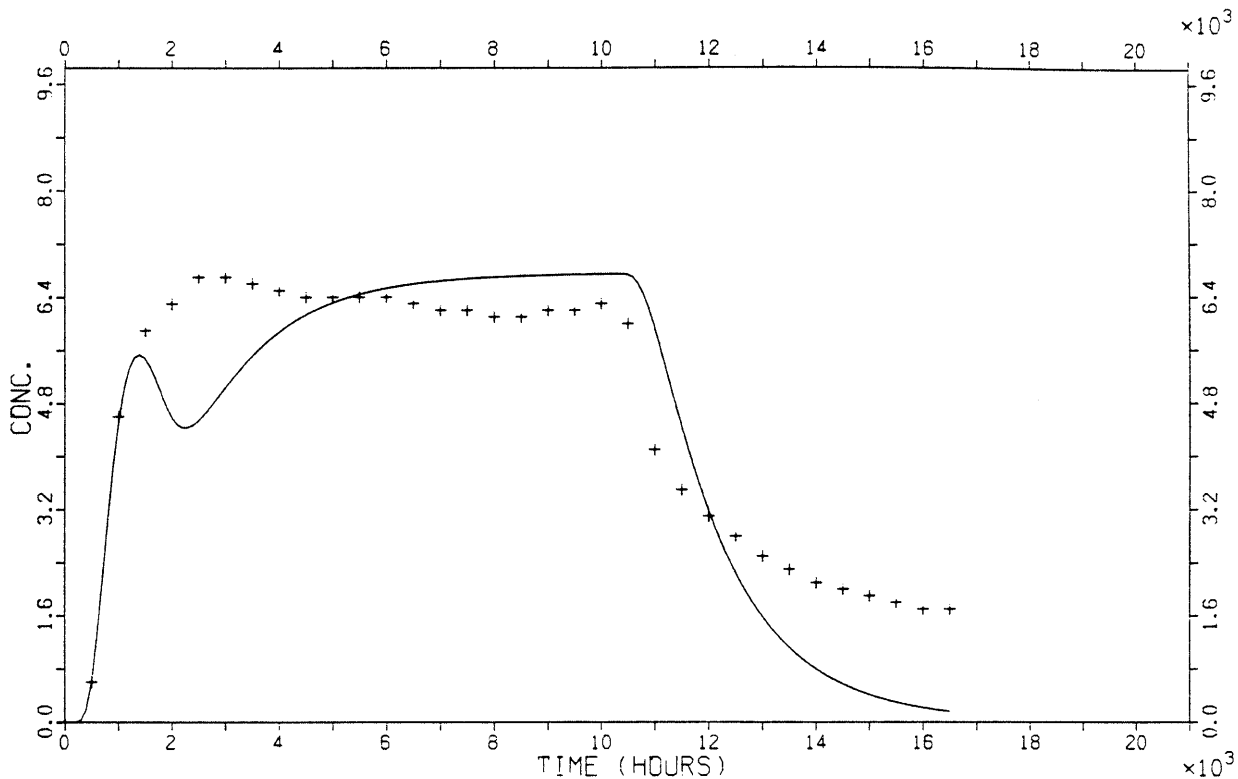


Figure A11-1. Continued.

Sheet number 60 tracer Elbenyl, AD-model

Pe = 4.0 Tw = 2112 Dil = 285.8 SD = .15



Sheet number 64 tracer Elbenyl, AD-model

Pe = 6.1 Tw = 2014 Dil = 247.7 SD = .22

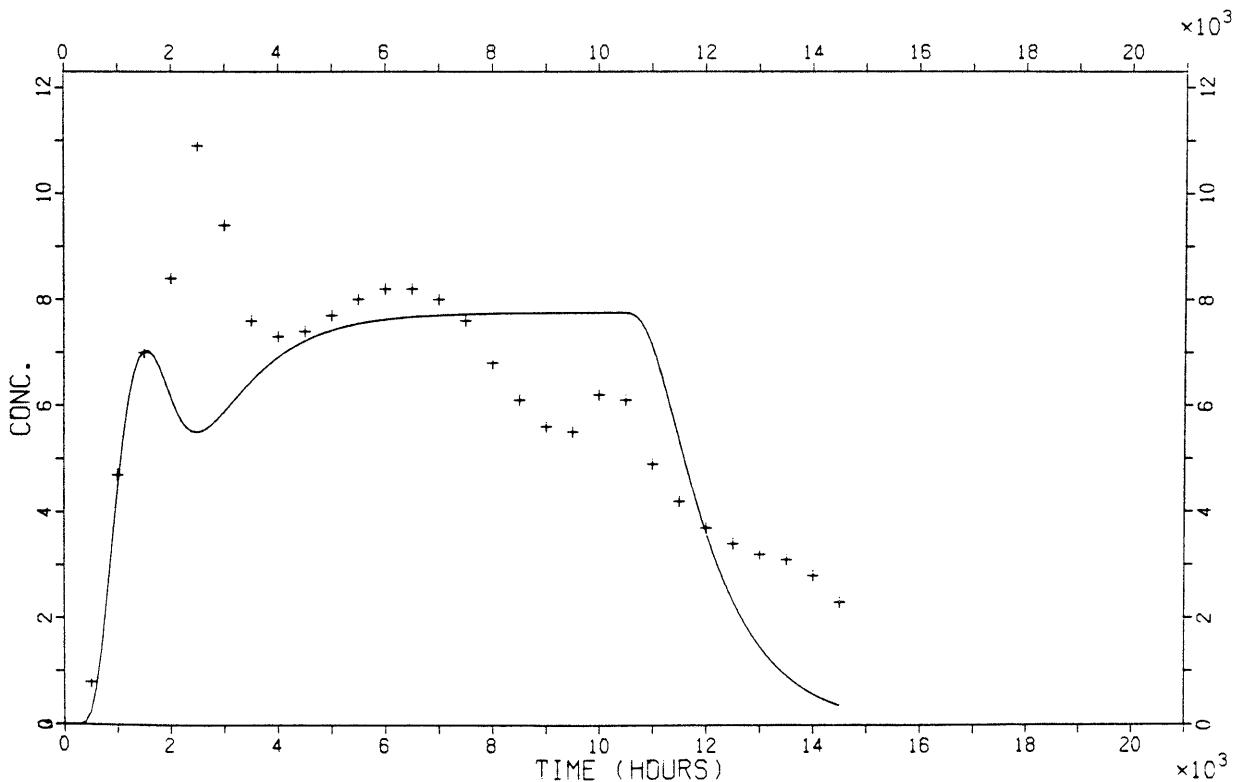
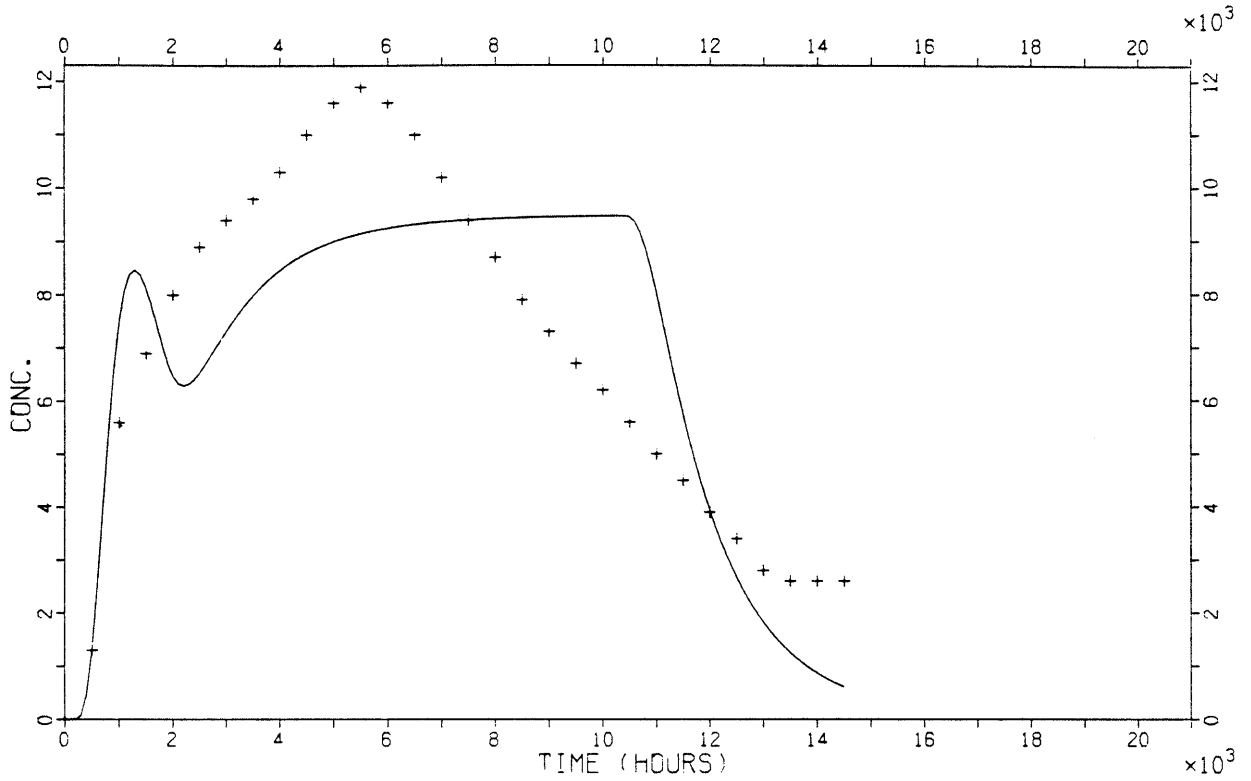


Figure A11-1. Continued.

Sheet number 66 tracer Elbenyl, AD-model

Pe = 4.0 Tw = 1969 Dil = 202.3 SD = .20



Sheet number 68 tracer Elbenyl, AD-model

Pe = 5.6 Tw = 1978 Dil = 382.2 SD = .11

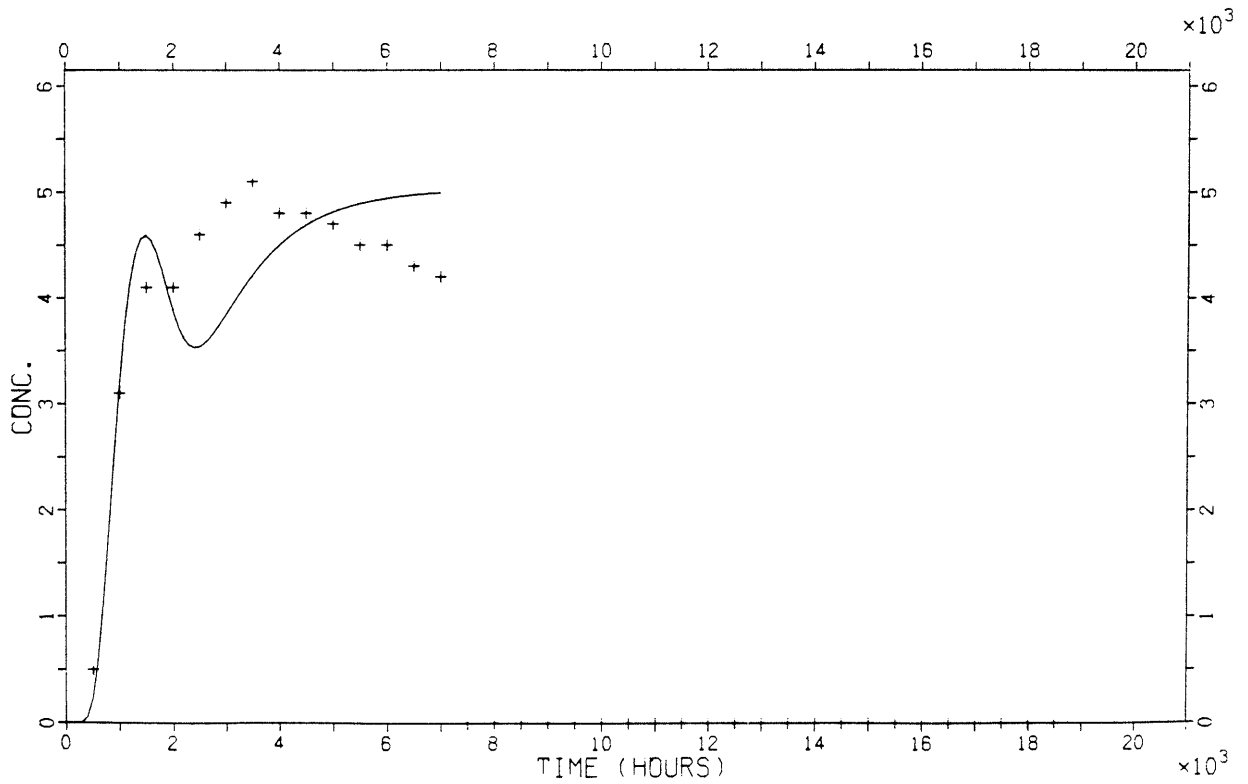
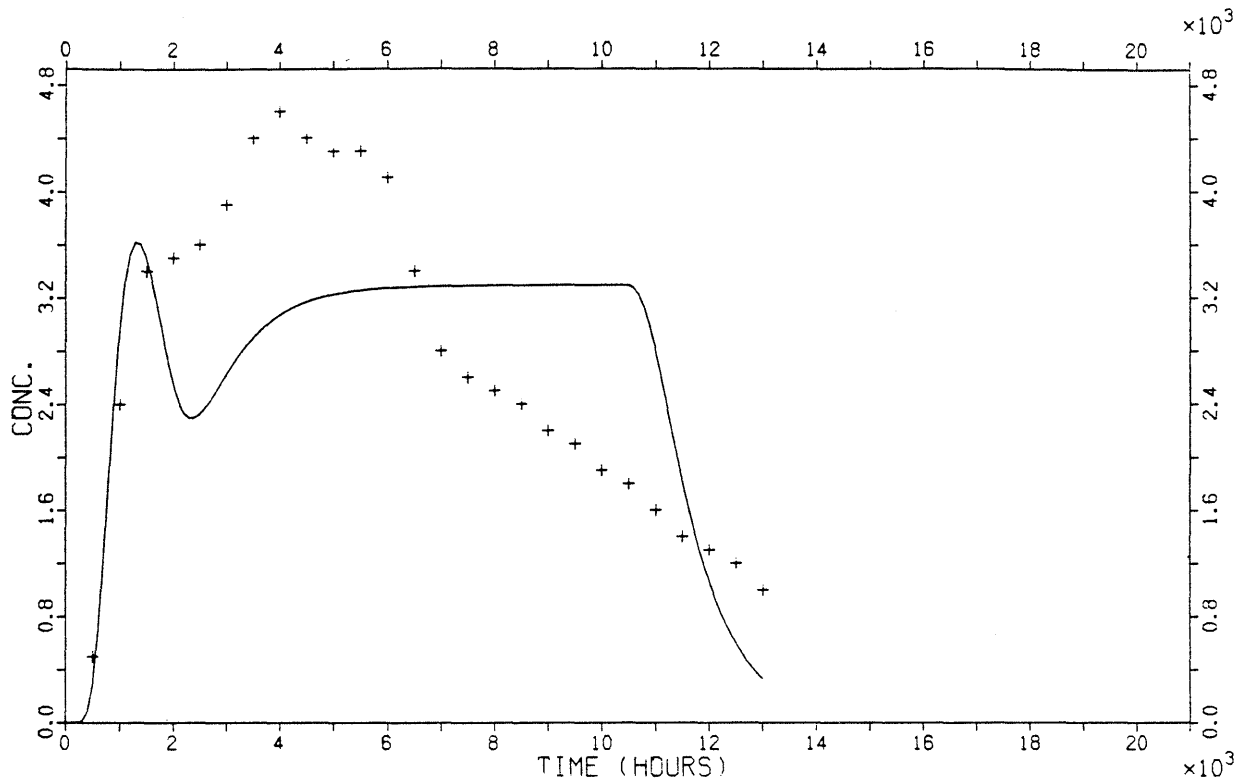


Figure A11-1. Continued.

Sheet number 108 tracer Elbenyl, AD-model

Pe = 6.3 Tw = 1636 Dil = 583.6 SD = .29



Sheet number 64 tracer Eosin Y, AD-model

Pe = 6.6 Tw = 5090 Dil = 130.7 SD = .10

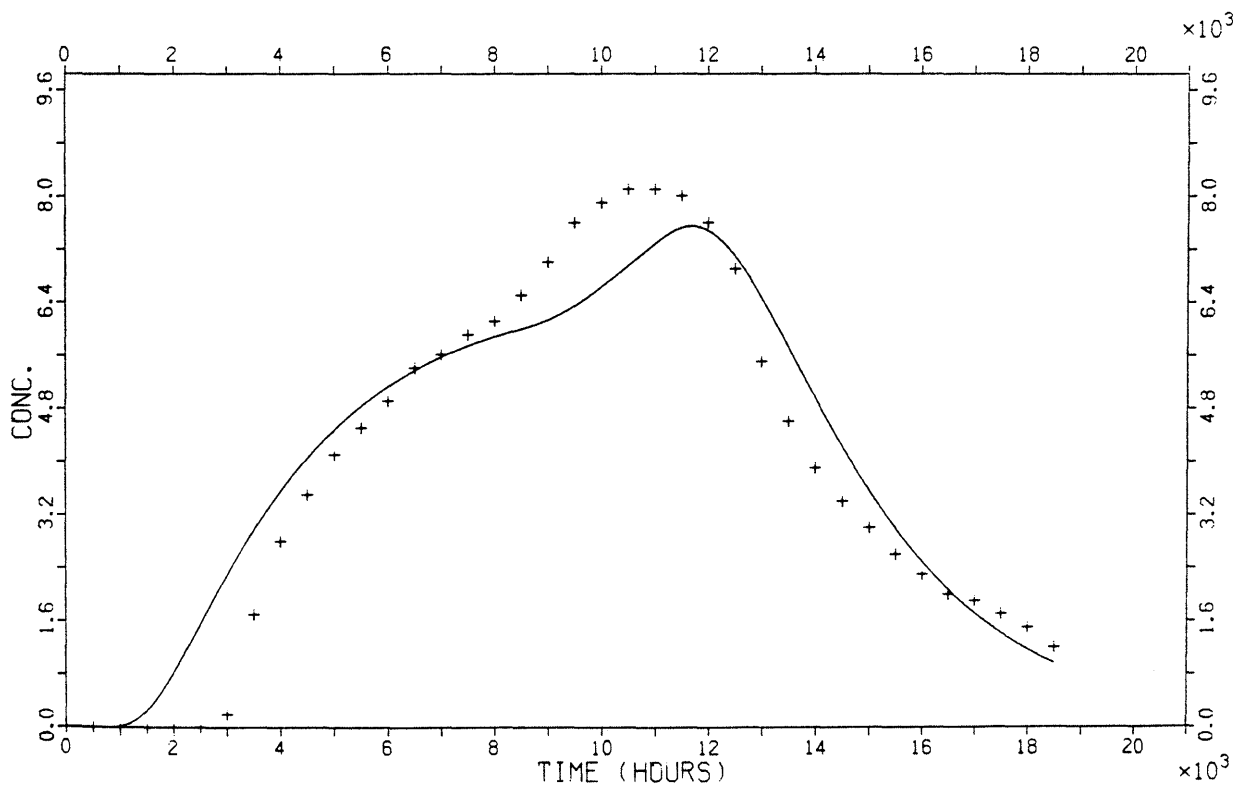
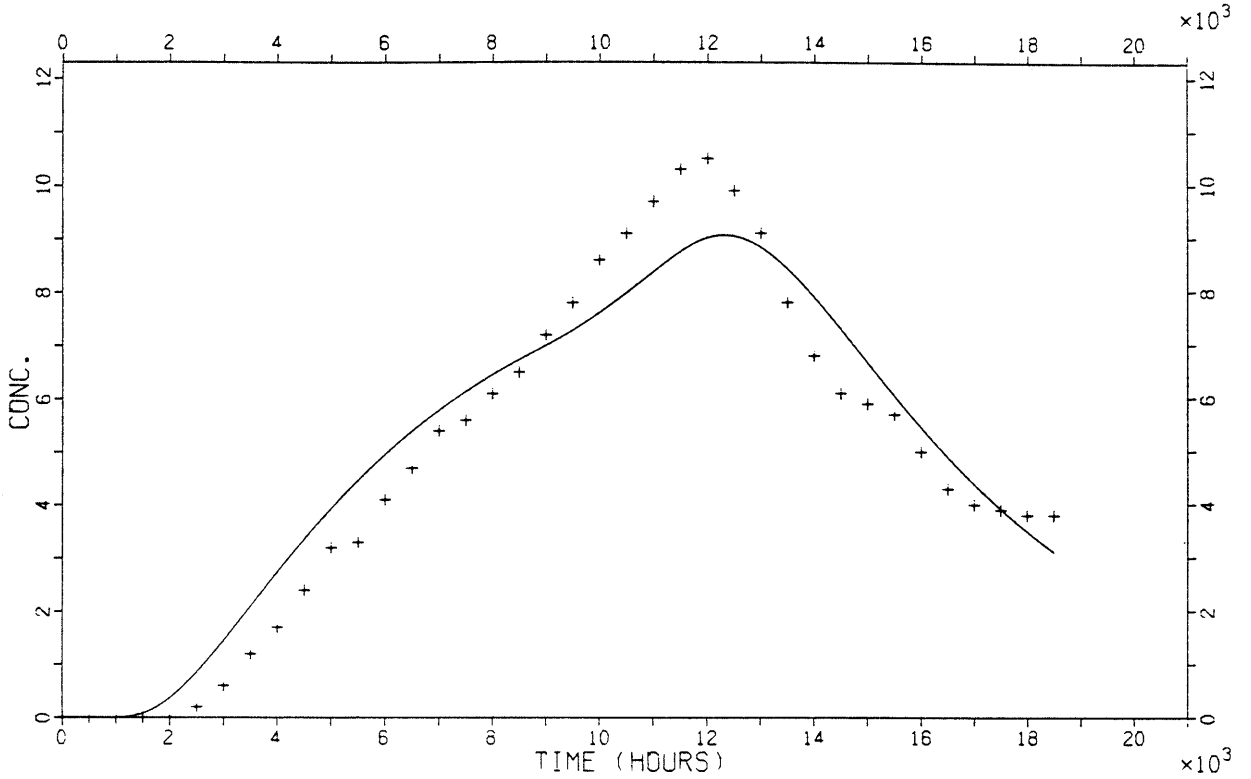


Figure A11-1. Continued.

Sheet number 68 tracer Eosin Y, AD-model

Pe = 5.5 Tw = 7320 Dil = 94.9 SD = .07



Sheet number 71 tracer Eosin Y, AD-model

Pe = 5.3 Tw = 7831 Dil = 93.5 SD = .07

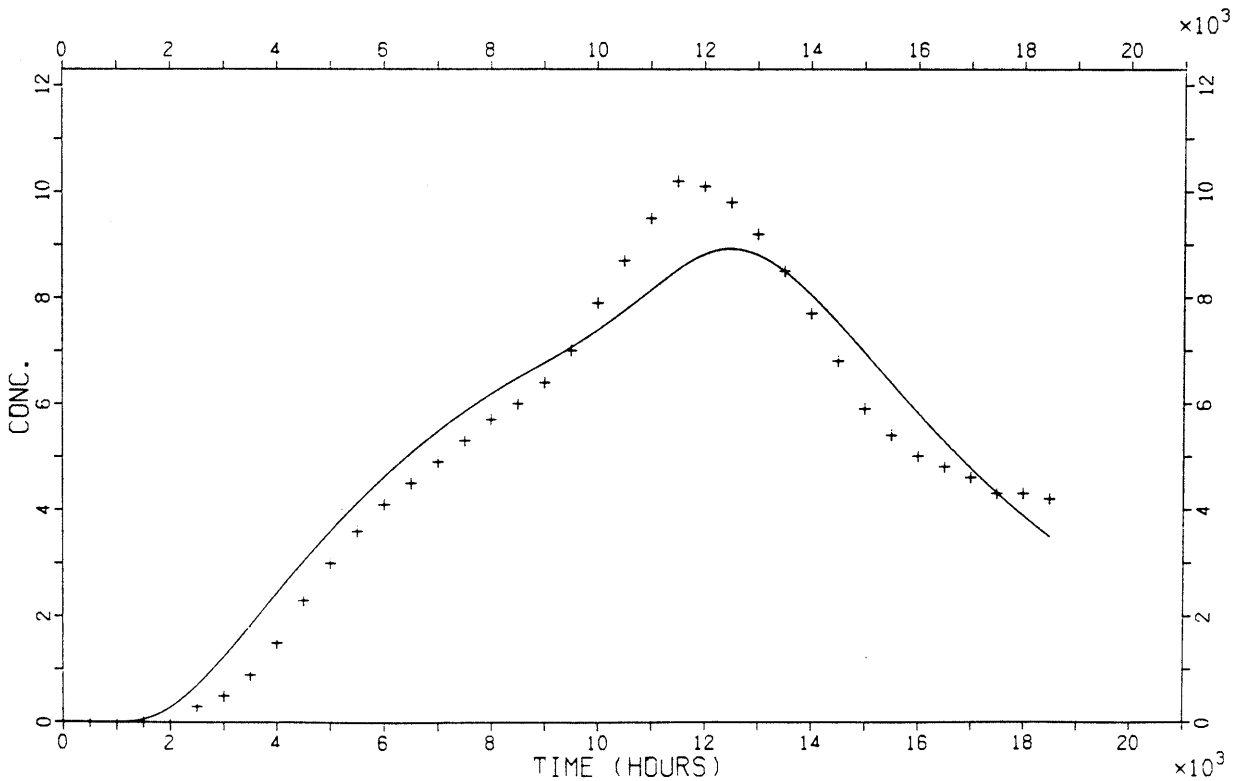
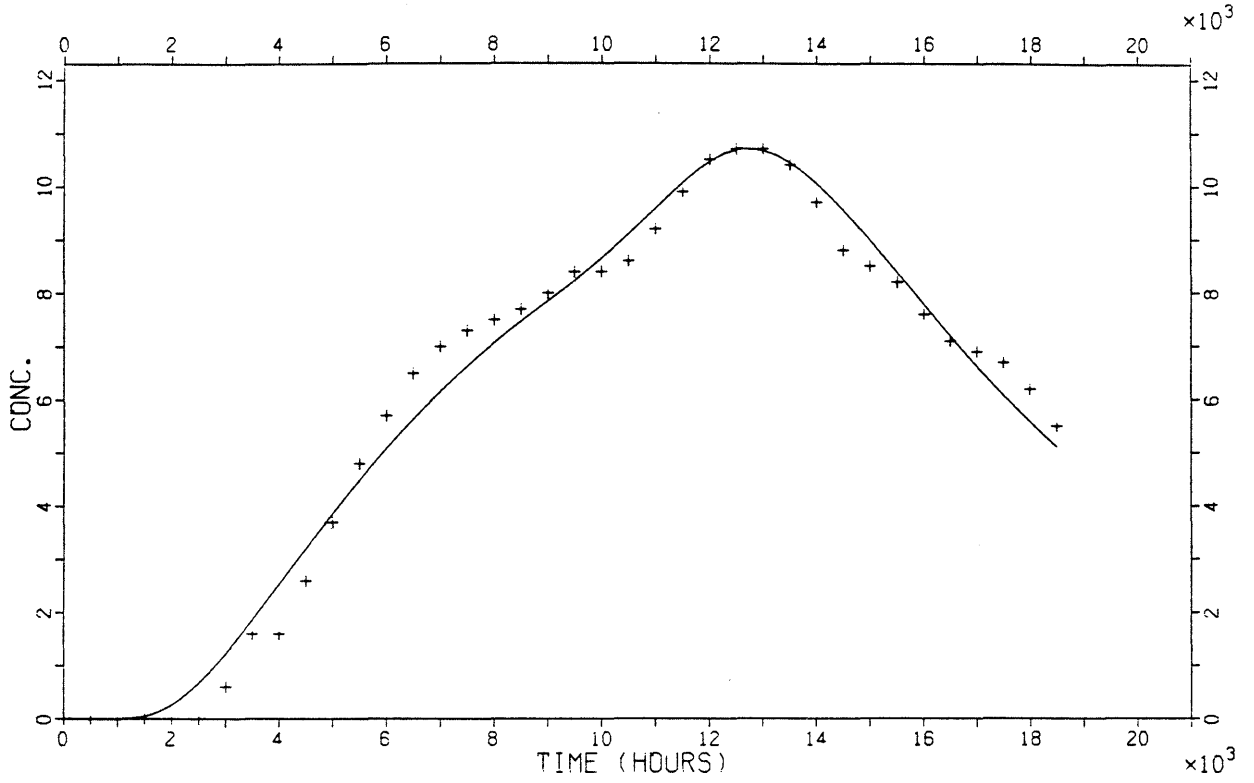


Figure A11-1. Continued.

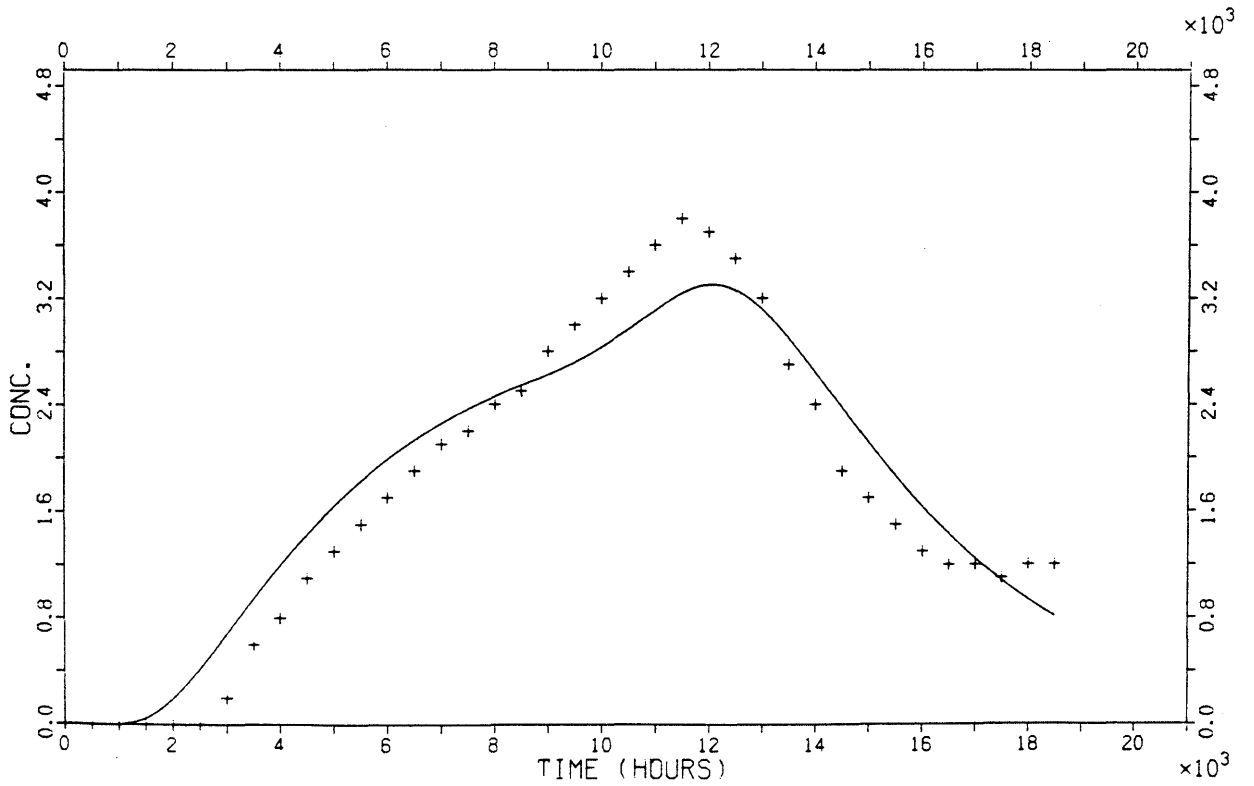
Sheet number 90 tracer Eosin Y, AD-model

Pe = 4.7 Tw = 8933 Dil = 72.4 SD = .03



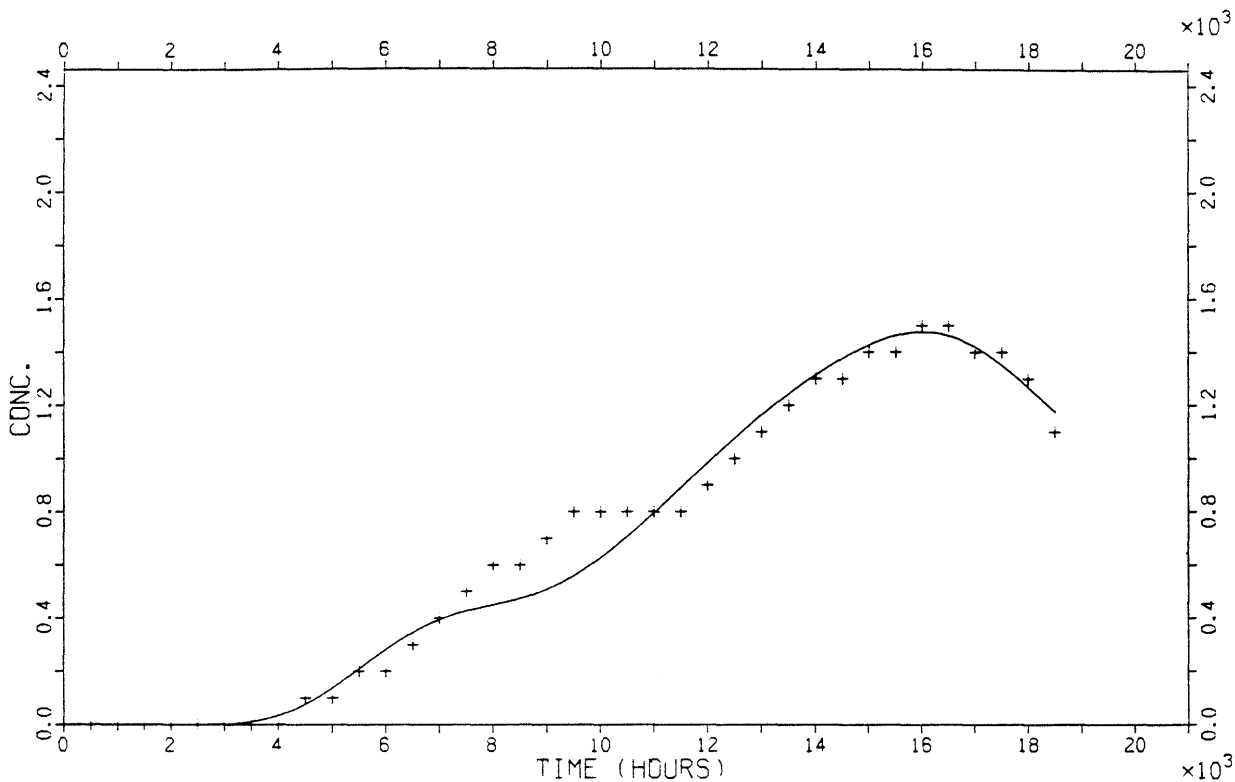
Sheet number 108 tracer Eosin Y, AD-model

Pe = 6.0 Tw = 6324 Dil = 277.6 SD = .08



Sheet number 61 tracer Iodide, AD-model

Pe = 18.6 Tw = 7209 Dil = 126.8 SD = .08



Sheet number 62 tracer Iodide, AD-model

Pe = 4.0 Tw = 11160 Dil = 40.3 SD = .05

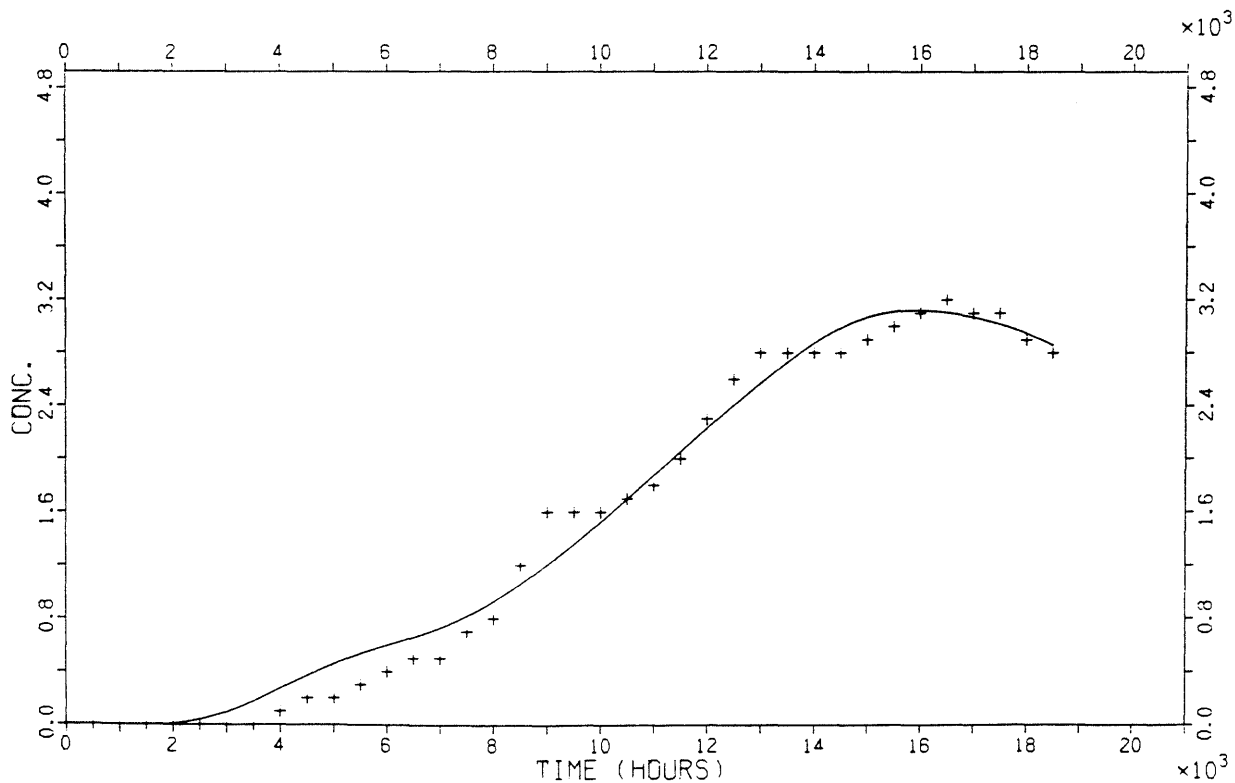
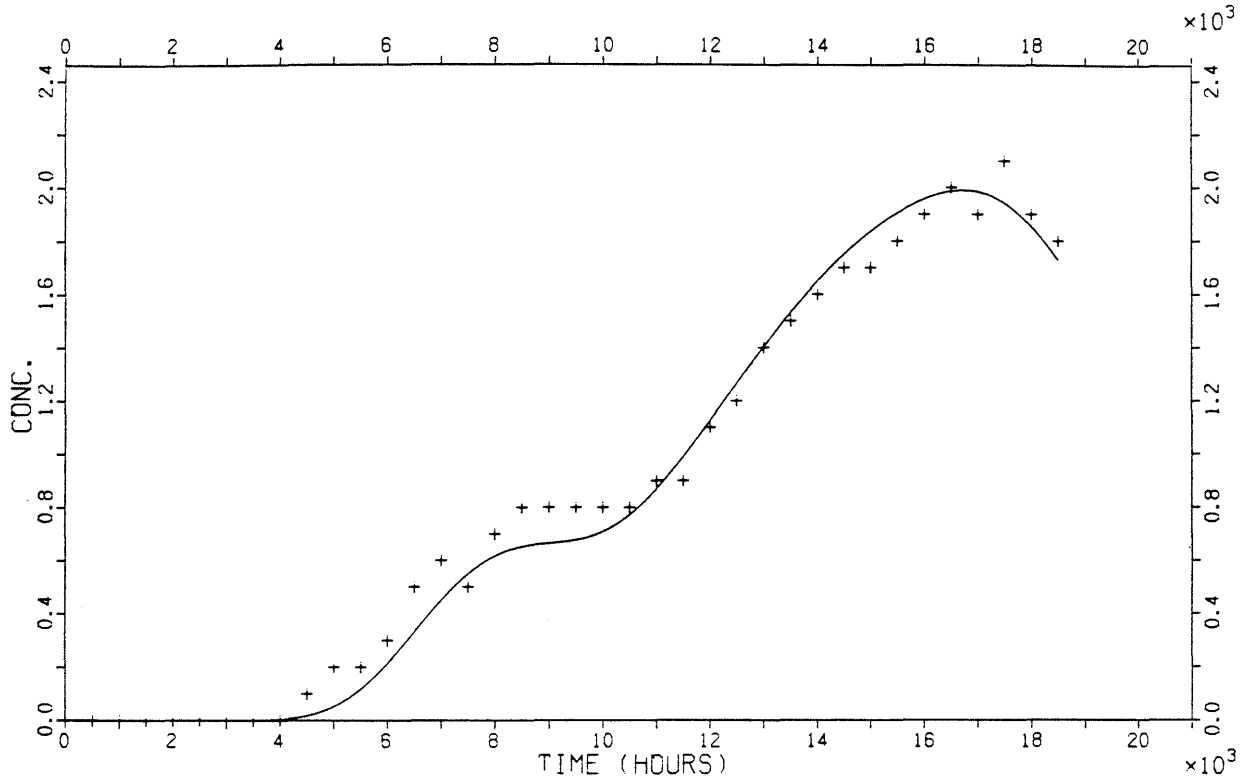


Figure A11-1. Continued.

Sheet number 103 tracer Iodide, AD-model

Pe = 34.0 Tw = 7558 Dil = 98.6 SD = .06



Sheet number 108 tracer Iodide, AD-model

Pe = 54.5 Tw = 7113 Dil = 82.3 SD = .06

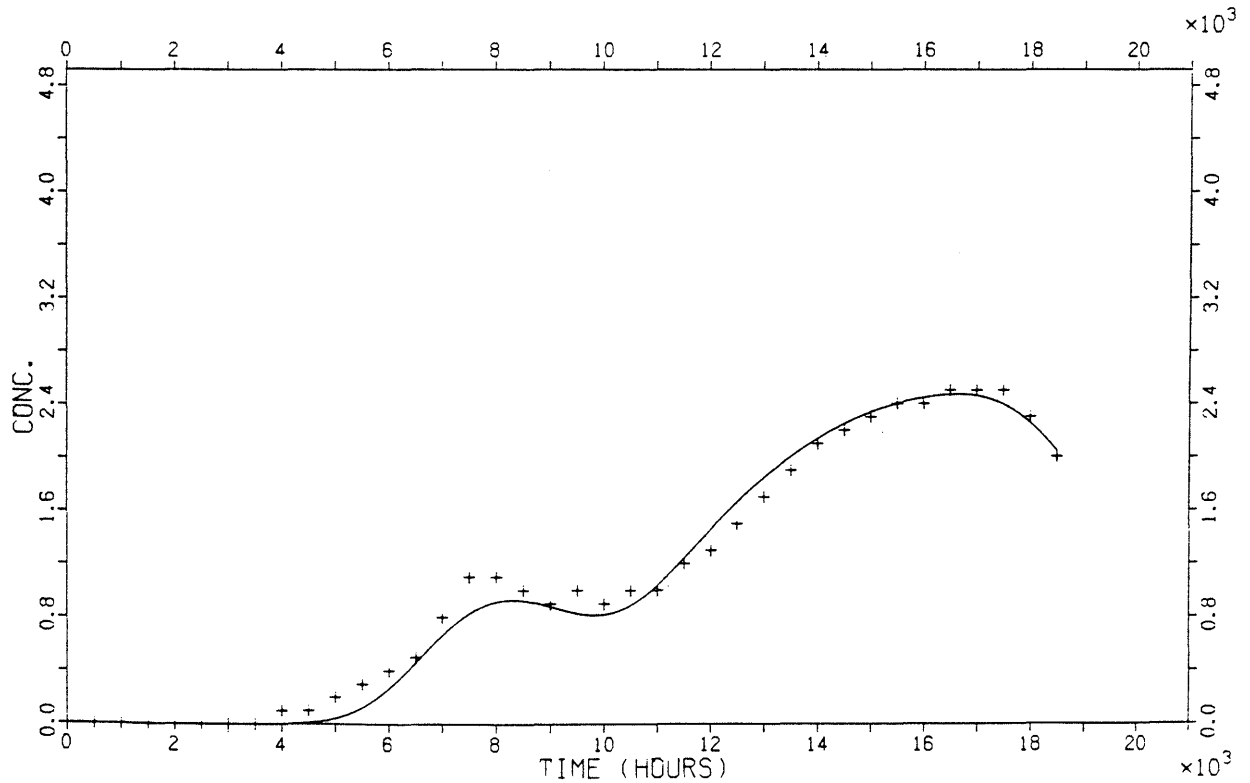


Figure A11-1. Continued.

Sheet number 110 tracer Iodide, AD-model

Pe = 34.5 Tw = 7031 Dil = 76.2 SD = .06

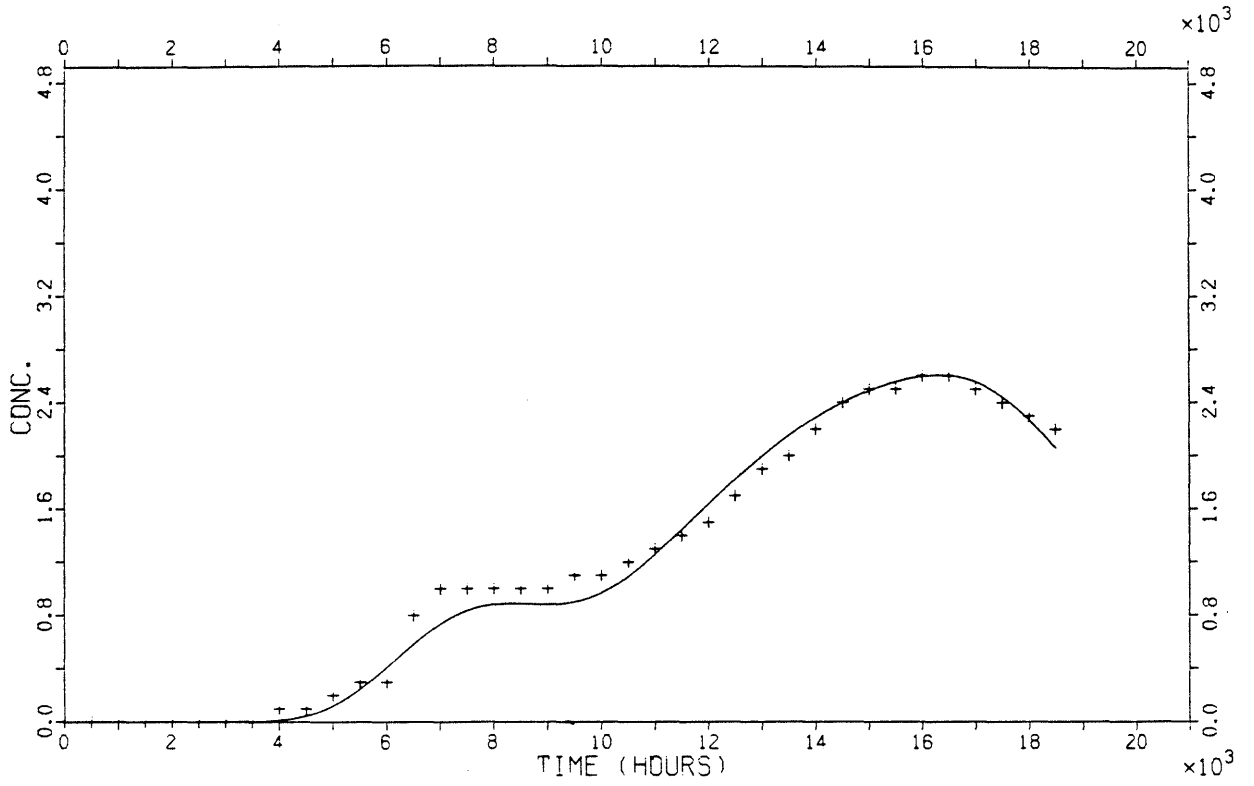
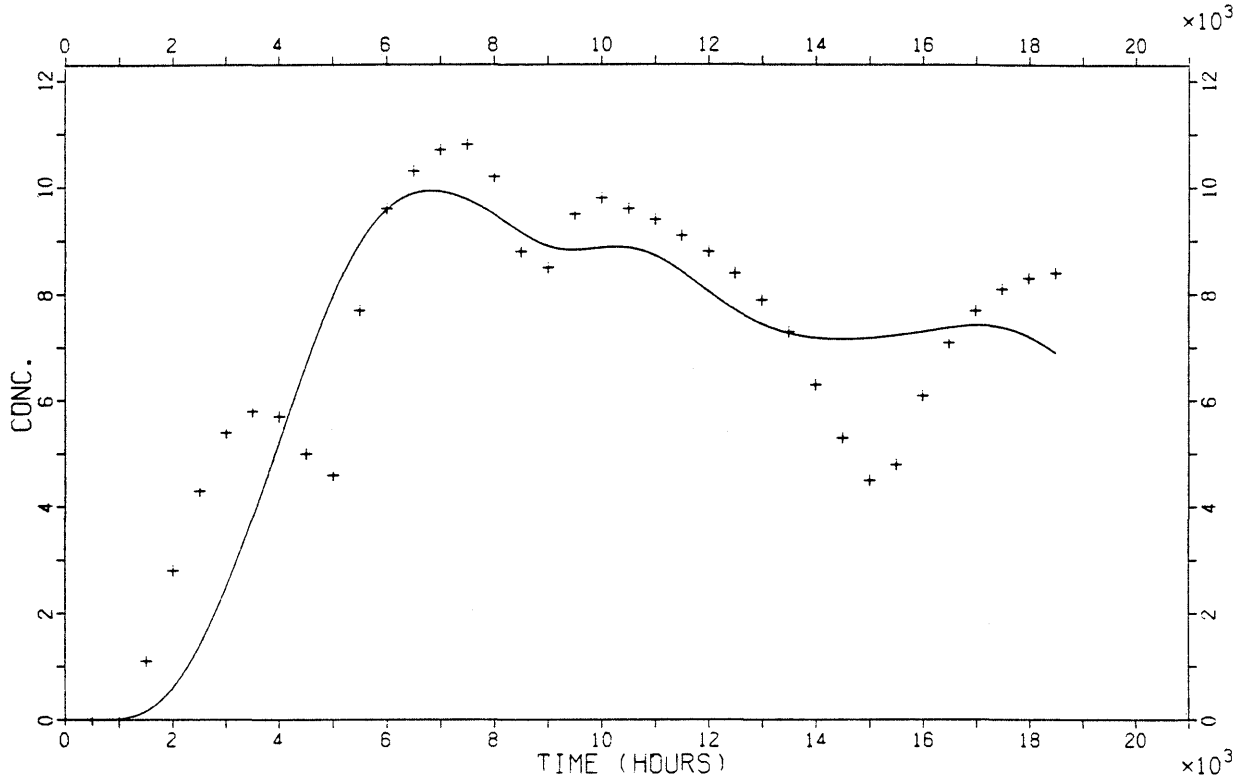


Figure A11-1. Continued.

Sheet number 57 tracer Eosin B, AC-model

Stand. dev = .301 Tw = 7794 Dil = 150.0 SD = .14



Sheet number 60 tracer Eosin B, AC-model

Stand. dev = .318 Tw = 9870 Dil = 201.6 SD = .12

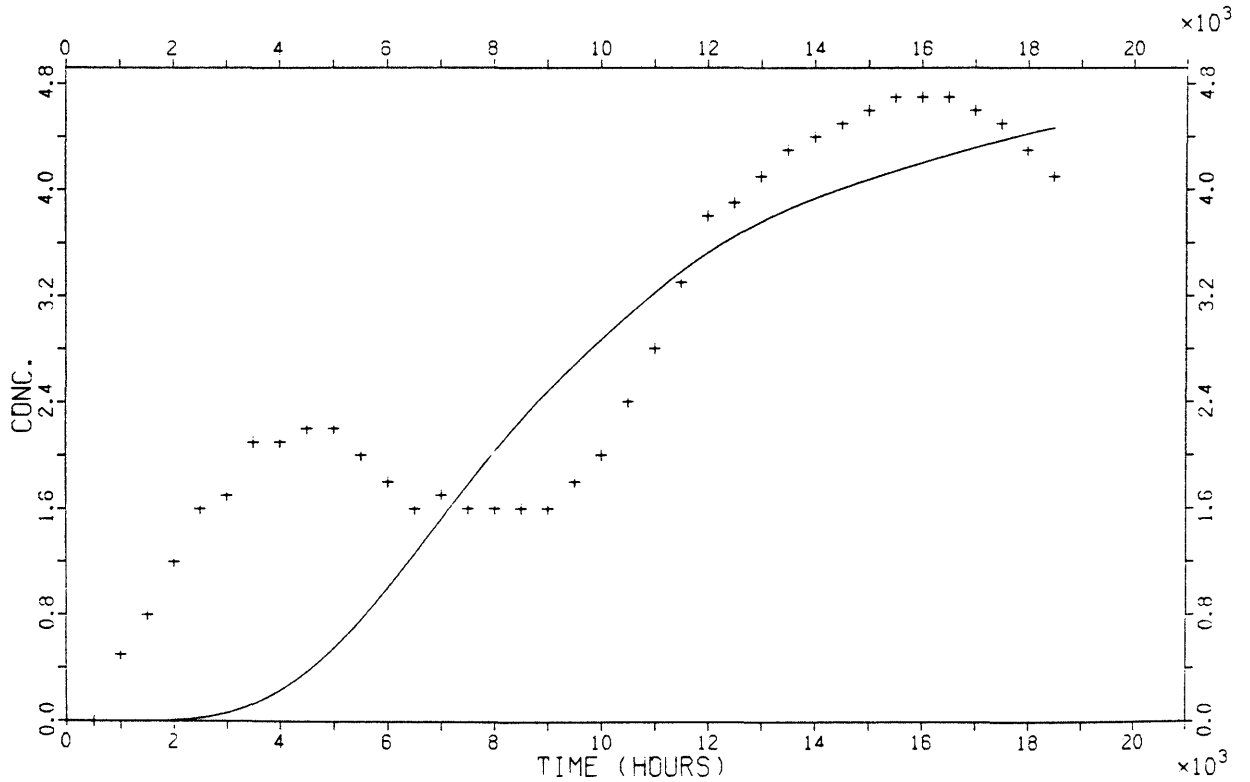
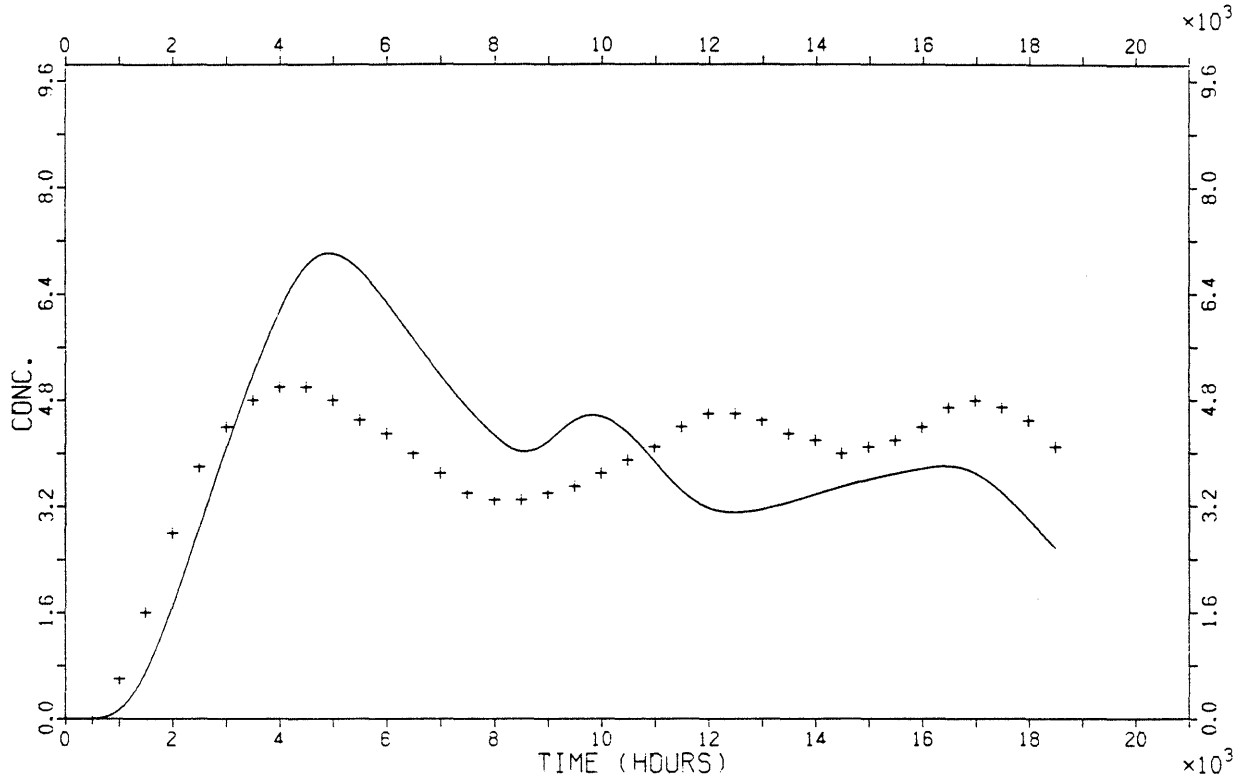


Figure A11-2. Model fits with AC-model.

Sheet number 66 tracer Eosin B, AC-model

Stand. dev = .318 Tw = 4994 Dil = 318.8 SD = .23



Sheet number 108 tracer Eosin B, AC-model

Stand. dev = .318 Tw = 5191 Dil = 800.4 SD = .33

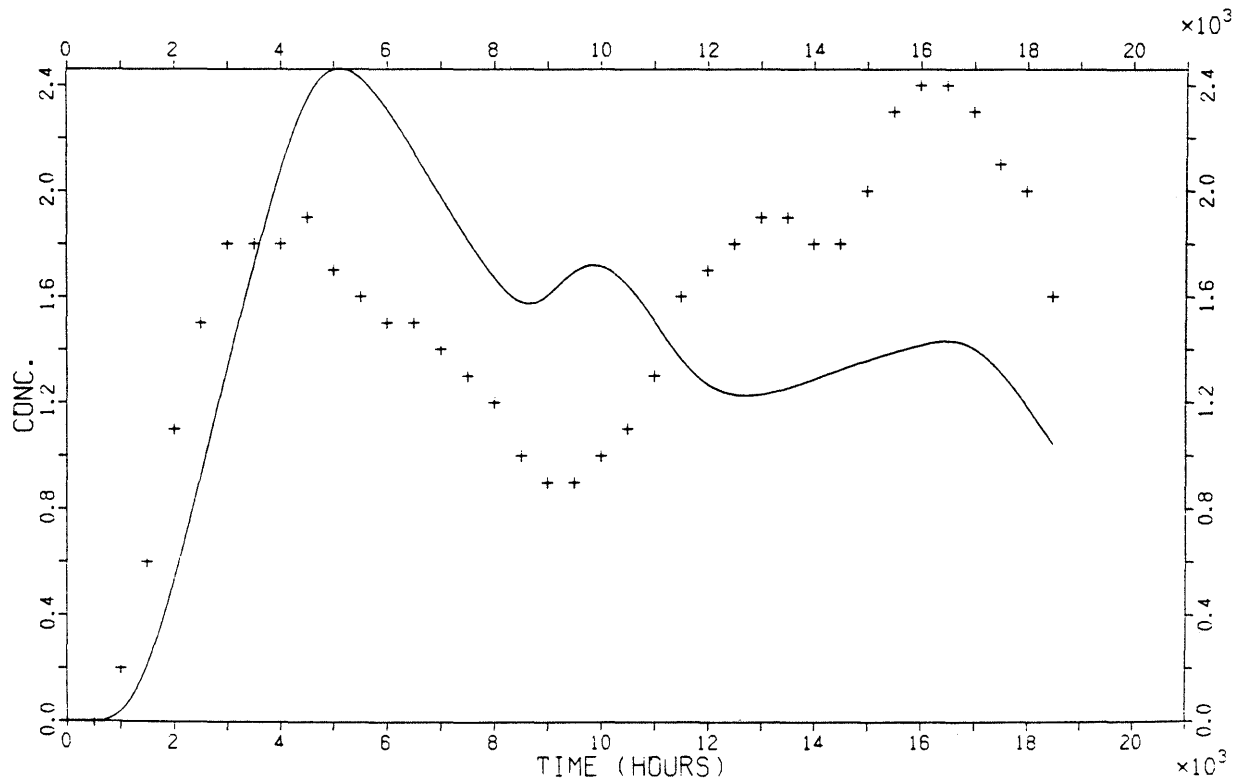
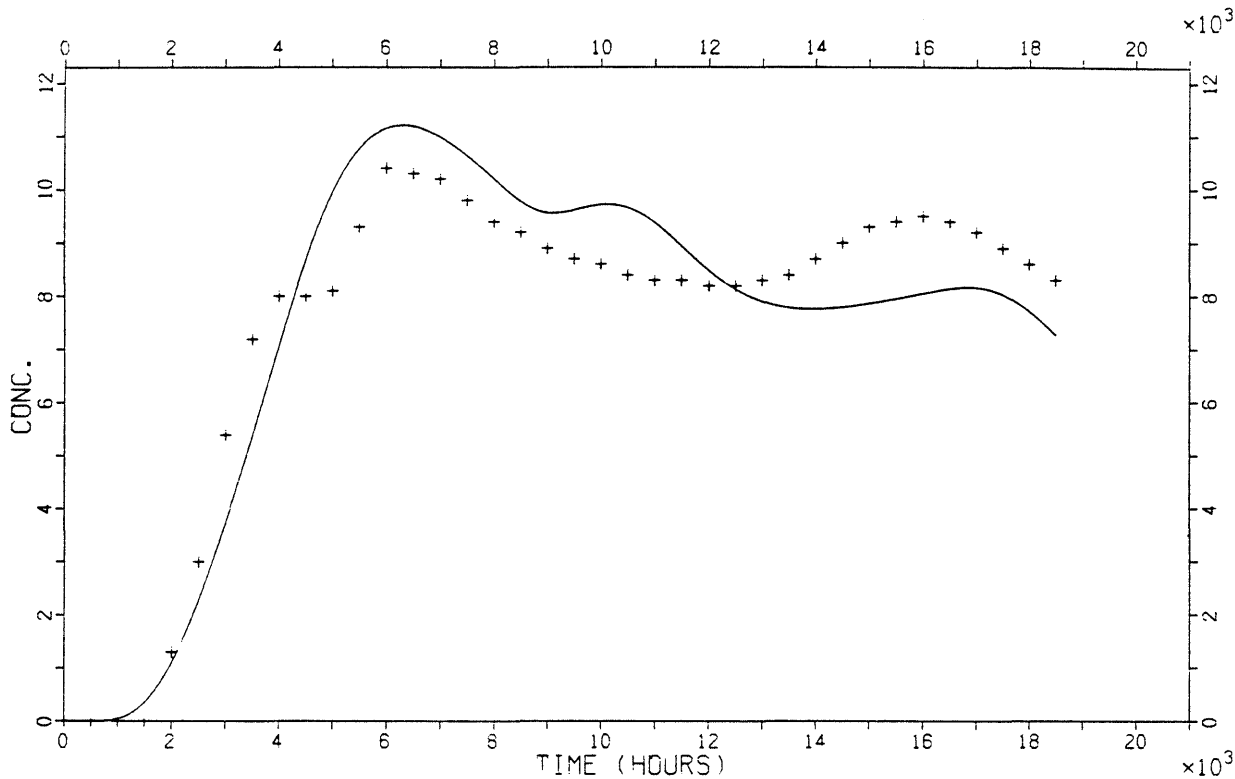


Figure Aii-2. Continued.

Sheet number 120 tracer Eosin B, AC-model

Stand. dev = .318 Tw = 7774 Dil = 135.9 SD = .09



Sheet number 64 tracer Uranine, AC-model

Stand. dev = .318 Tw = 3039 Dil = 1162 SD = .39

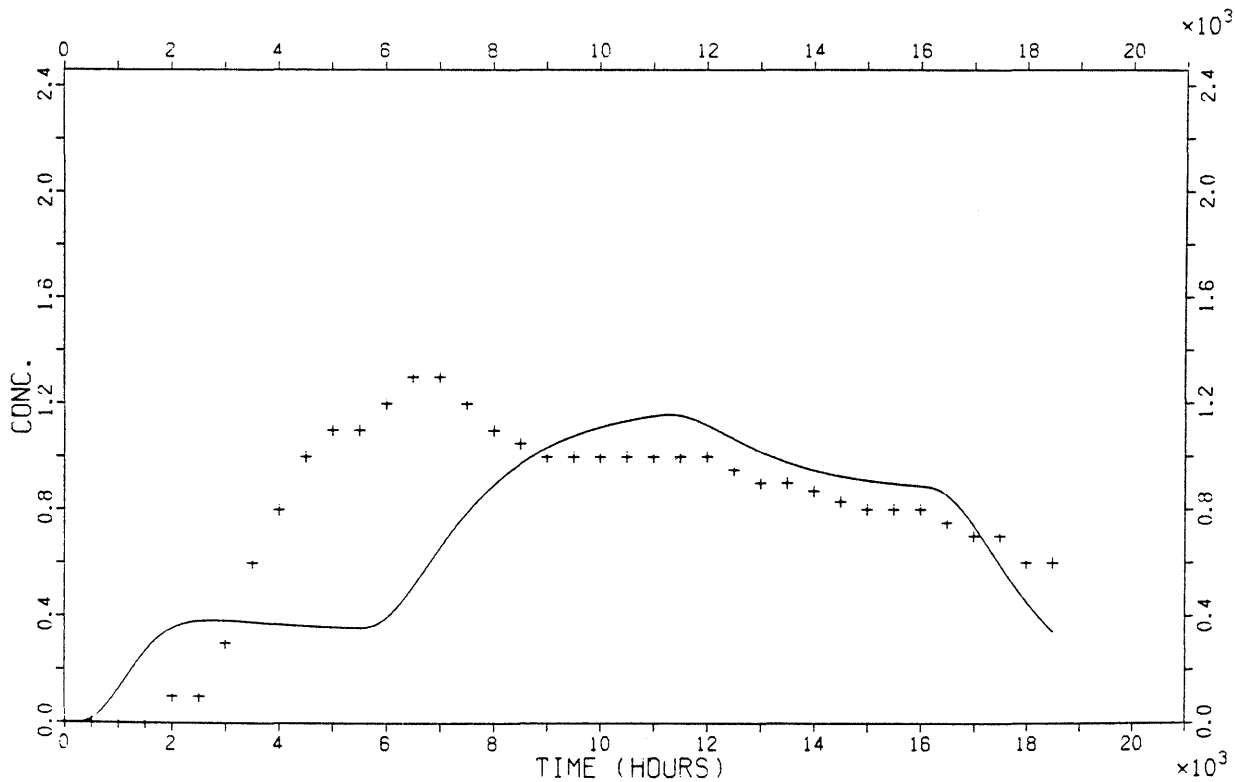
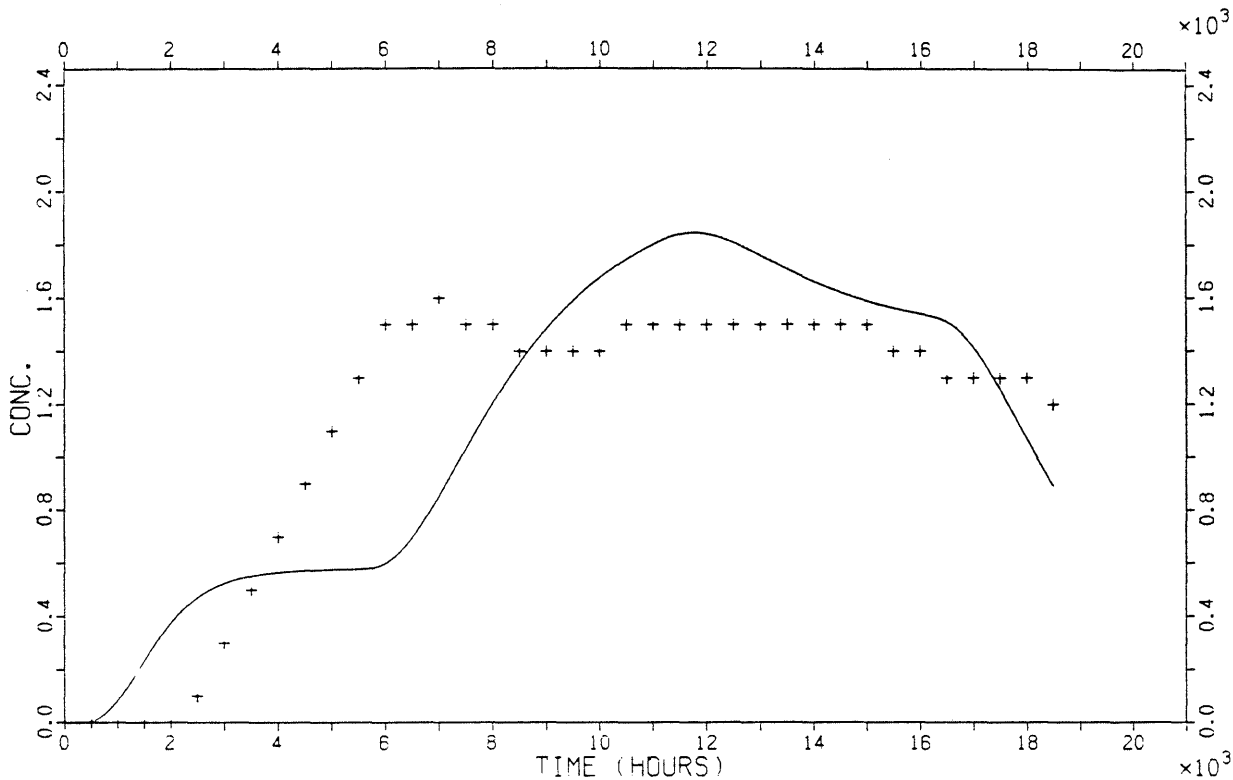


Figure A11-2. Continued.

Sheet number 71 tracer Uranine, AC-model

Stand. dev = .318 Tw = 4225 Dil = 692 SD = .25



Sheet number 90 tracer Uranine, AC-model

Stand. dev = .318 Tw = 7445 Dil = 1666 SD = .19

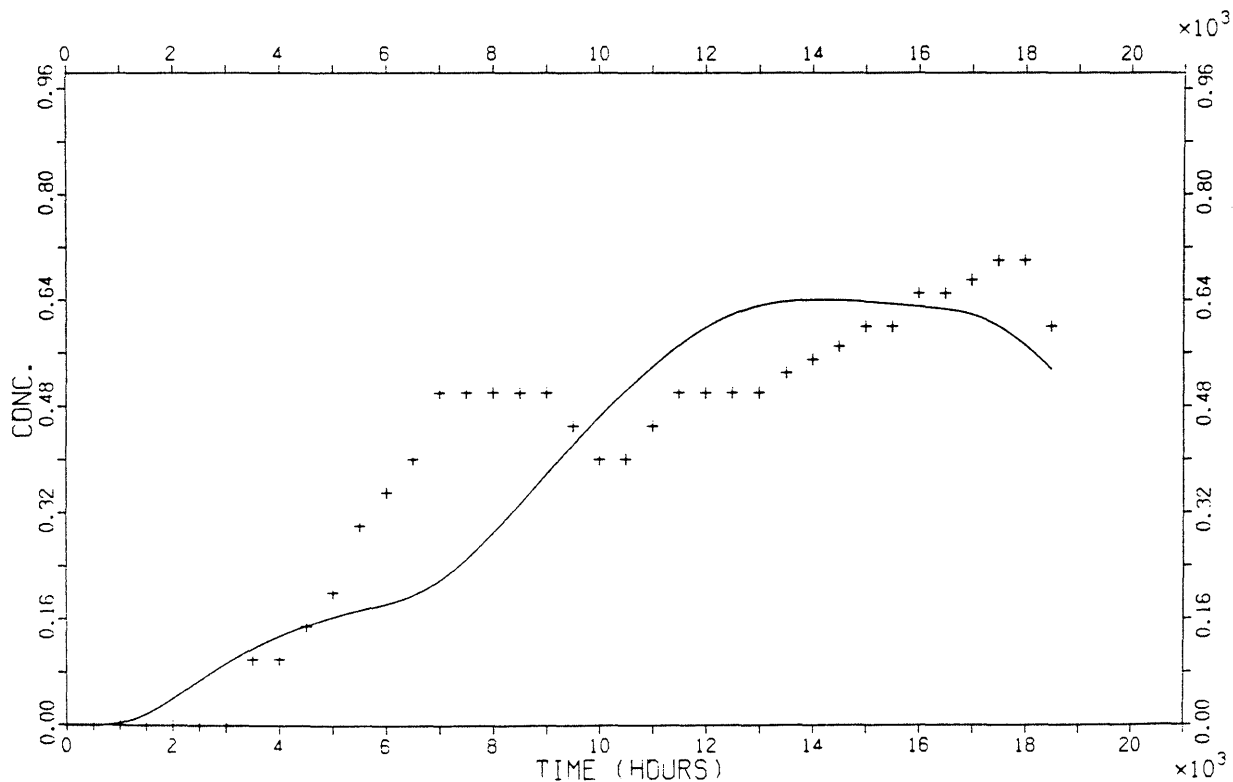
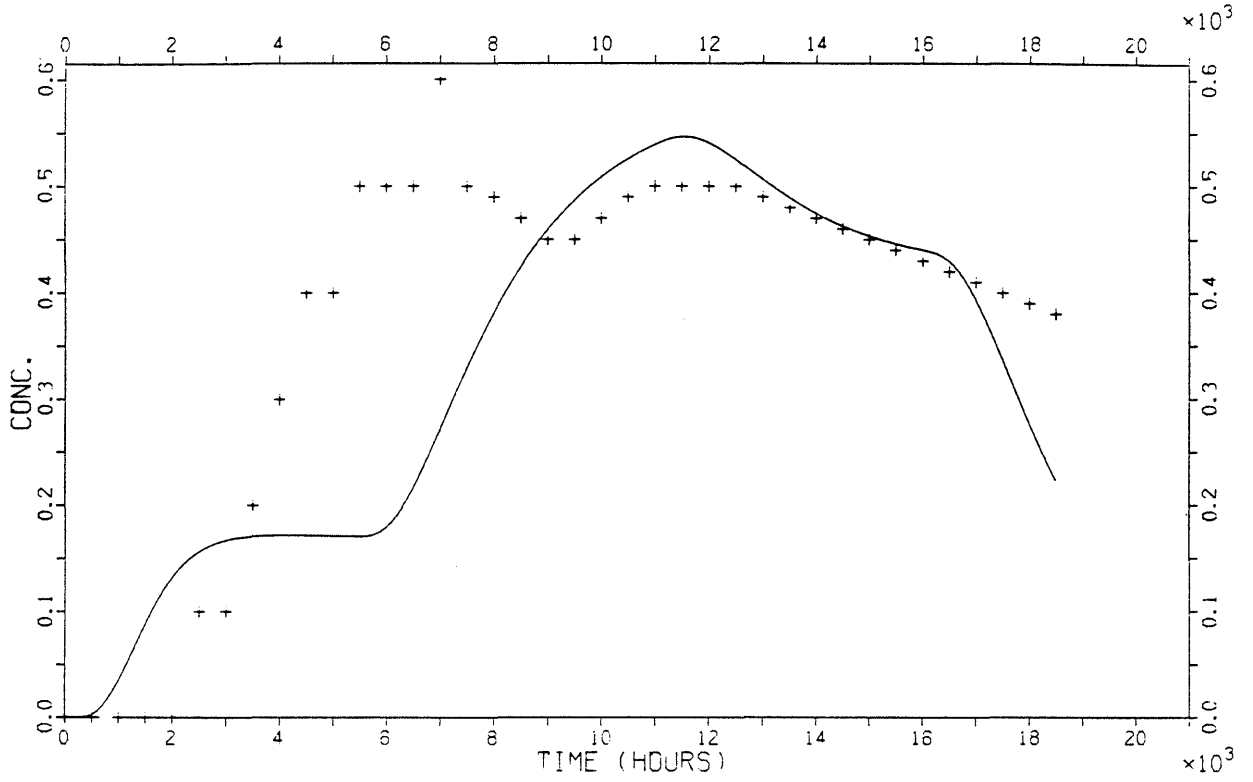


Figure A11-2. Continued.

Sheet number 108 tracer Uranine, AC-model

Stand. dev = .320 Tw = 3555 Dil = 2325 SD = .31



Sheet number 134 tracer Uranine, AC-model

Stand. dev = .194 Tw = 2080 Dil = 193 SD = .03

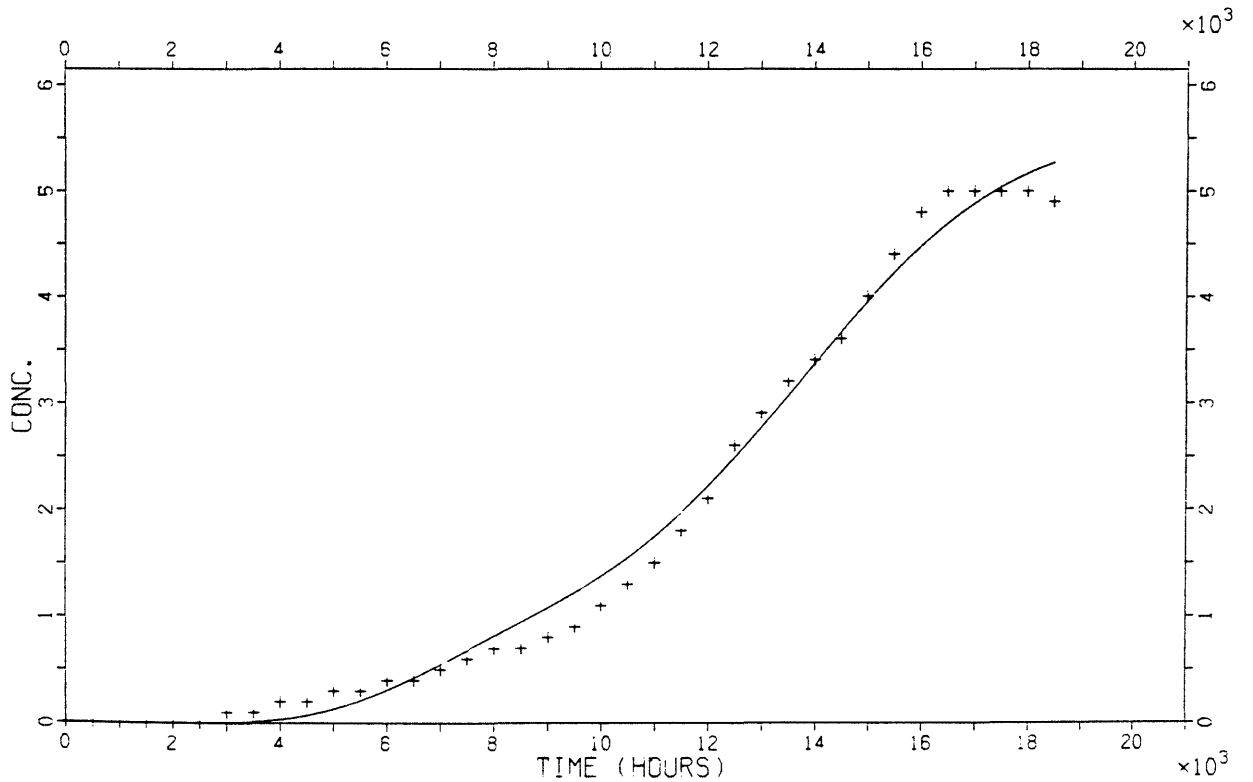
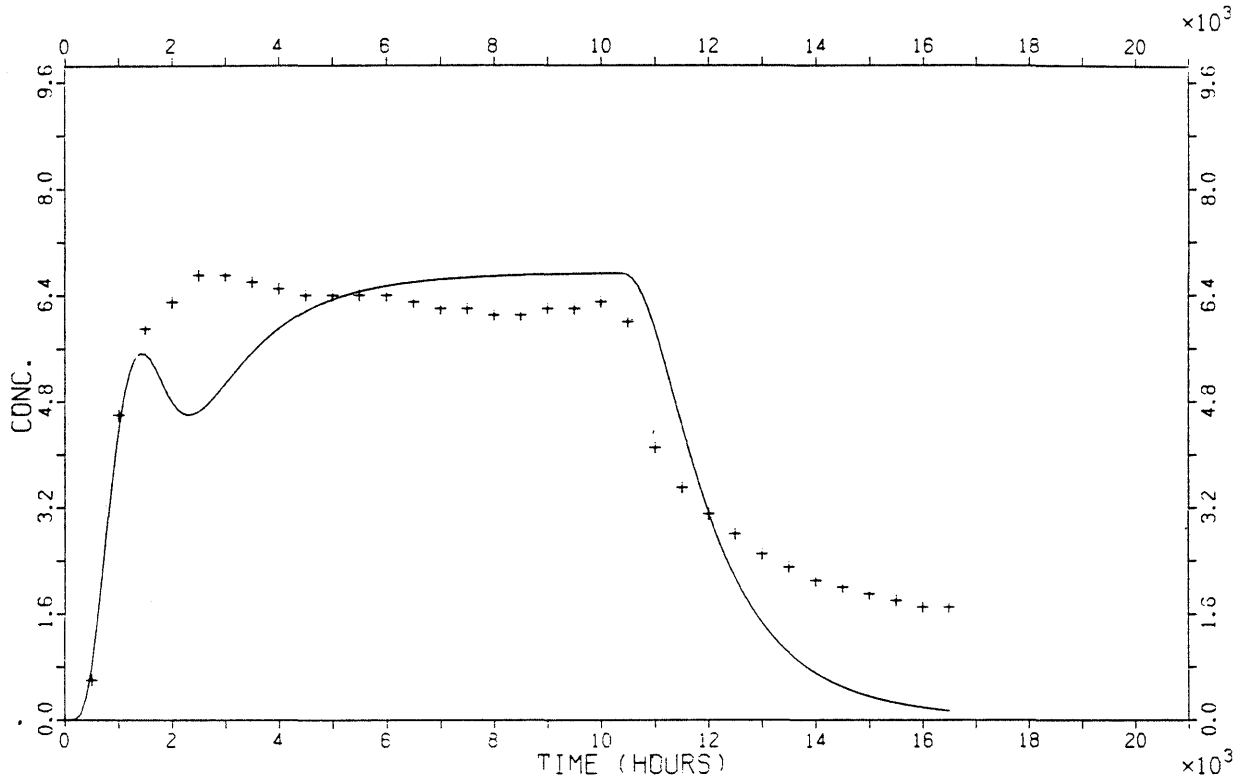


Figure A11-2. Continued.

Sheet number 60 tracer Elbenyl, AC-model

Stand. dev = .318 Tw = 2329 Dil = 284.9 SD = .14



Sheet number 64 tracer Elbenyl, AC-model

Stand. dev = .281 Tw = 2194 Dil = 246.6 SD = .22

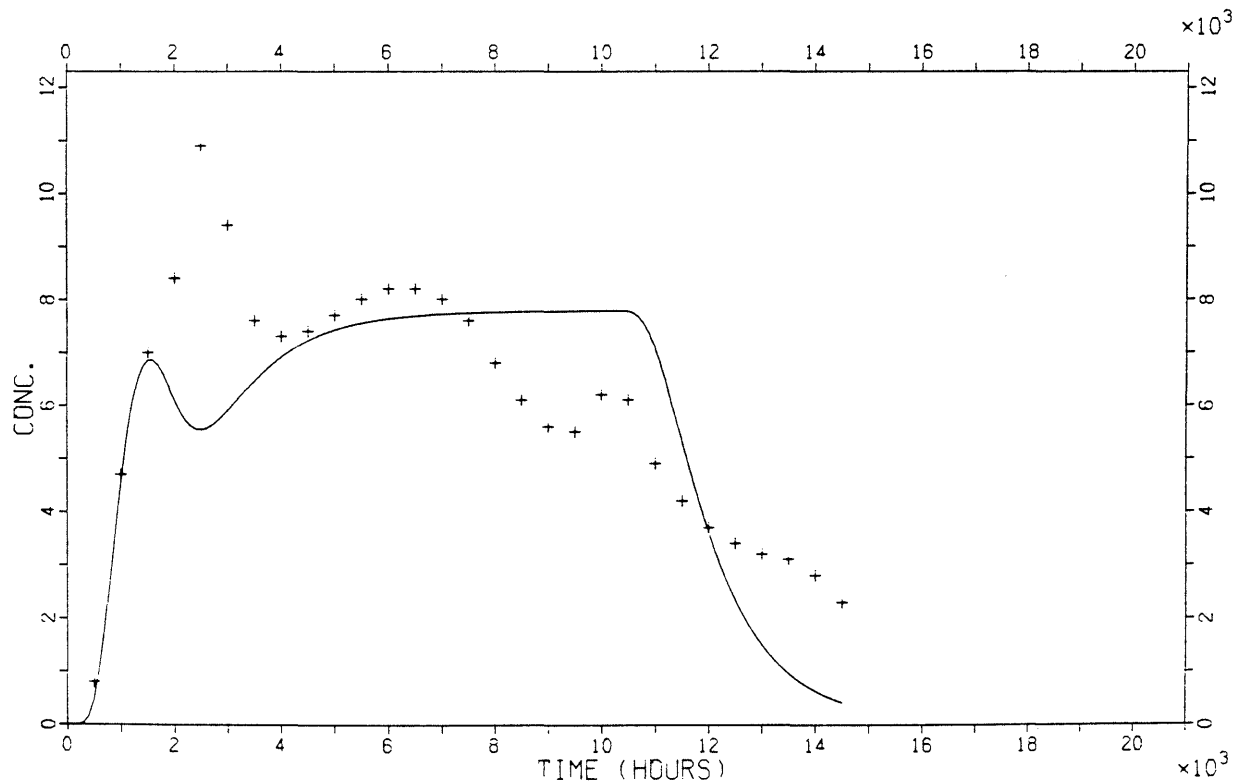
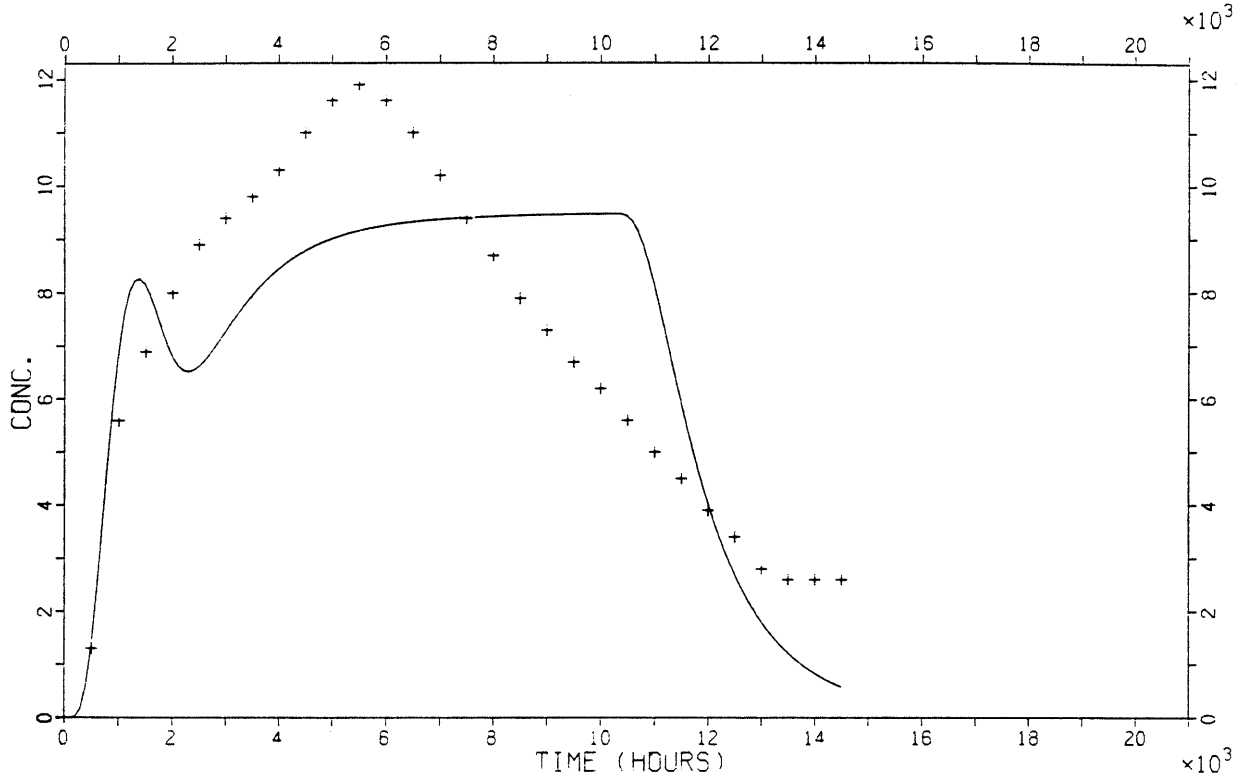


Figure A11-2. Continued.

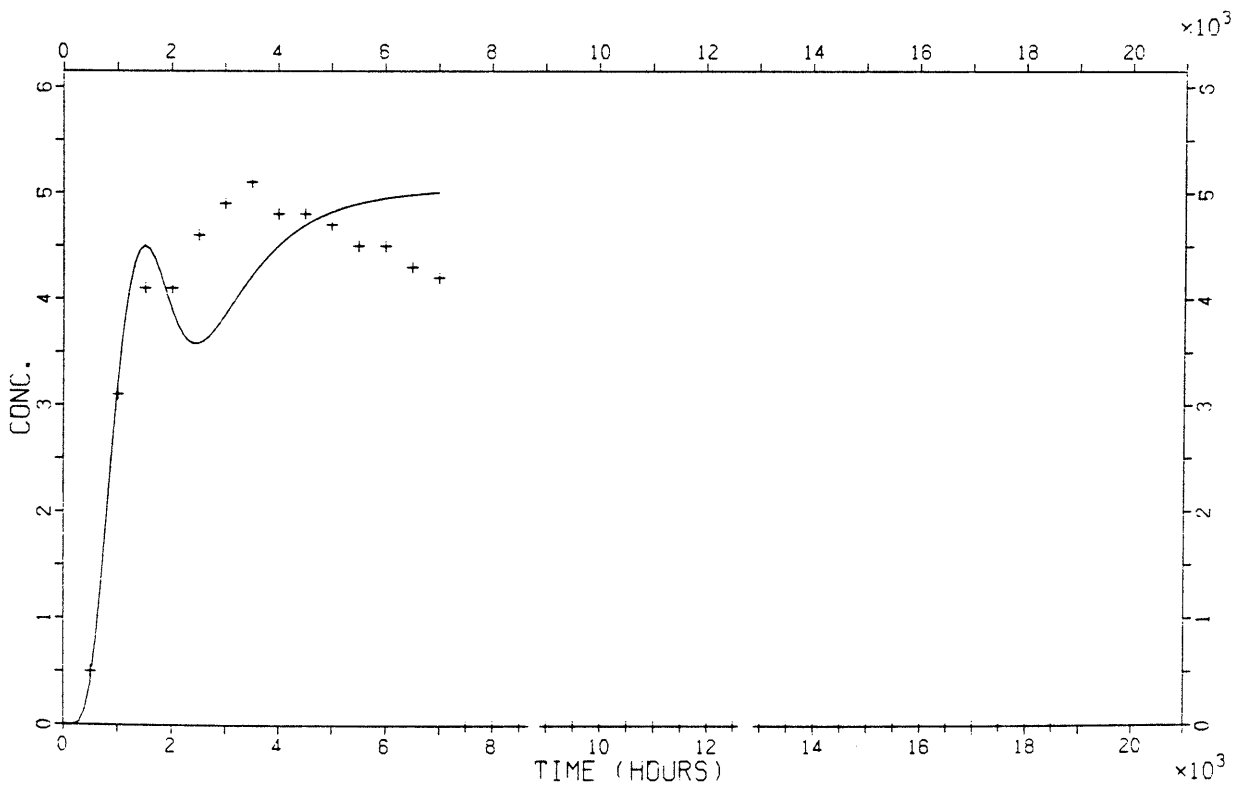
Sheet number 66 tracer Elbenyl, AC-model

Stand. dev = .318 Tw = 2187 Dil = 202.2 SD = .20



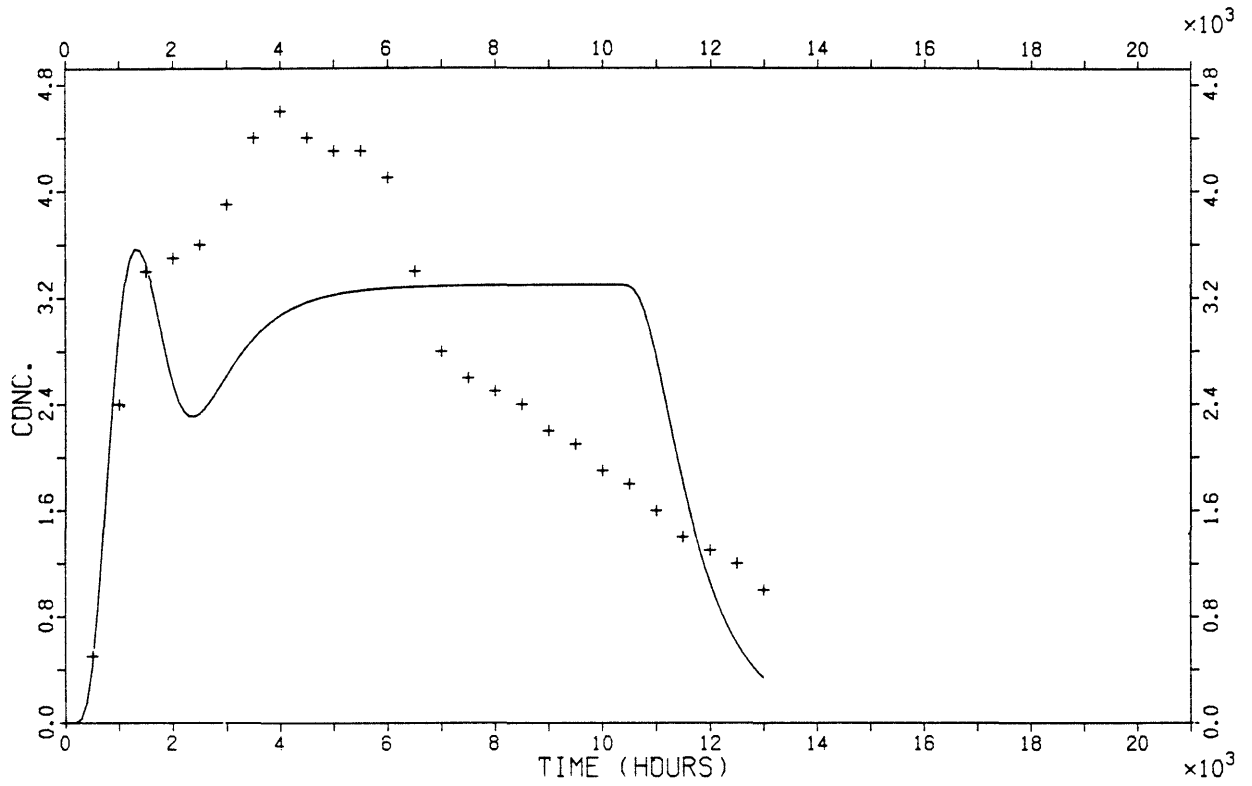
Sheet number 68 tracer Elbenyl, AC-model

Stand. dev = .287 Tw = 2160 Dil = 380.2 SD = .11



Sheet number 108 tracer Elbenyl, AC-model

Stand. dev = .273 Tw = 1762 Dil = 581.4 SD = .28



Sheet number 64 tracer Eosin Y, AC-model

Stand. dev = .267 Tw = 5468 Dil = 130.2 SD = .10

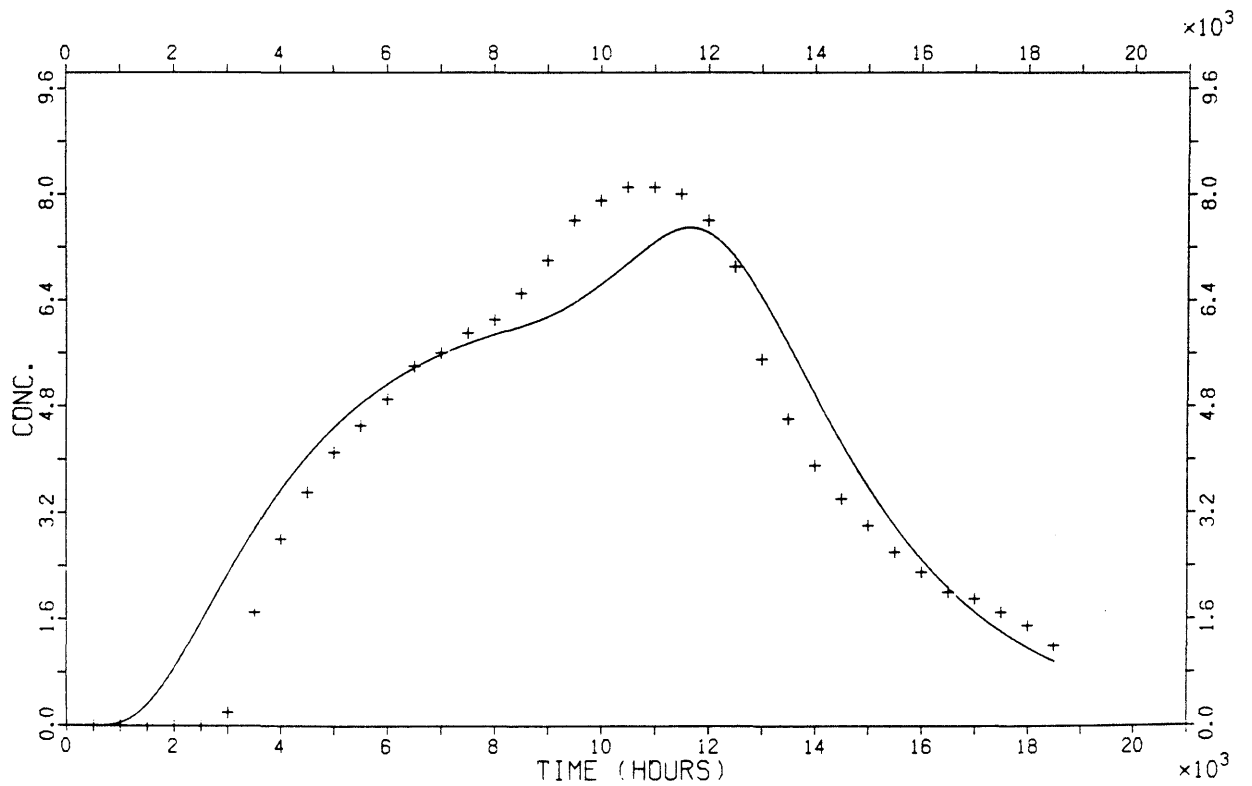
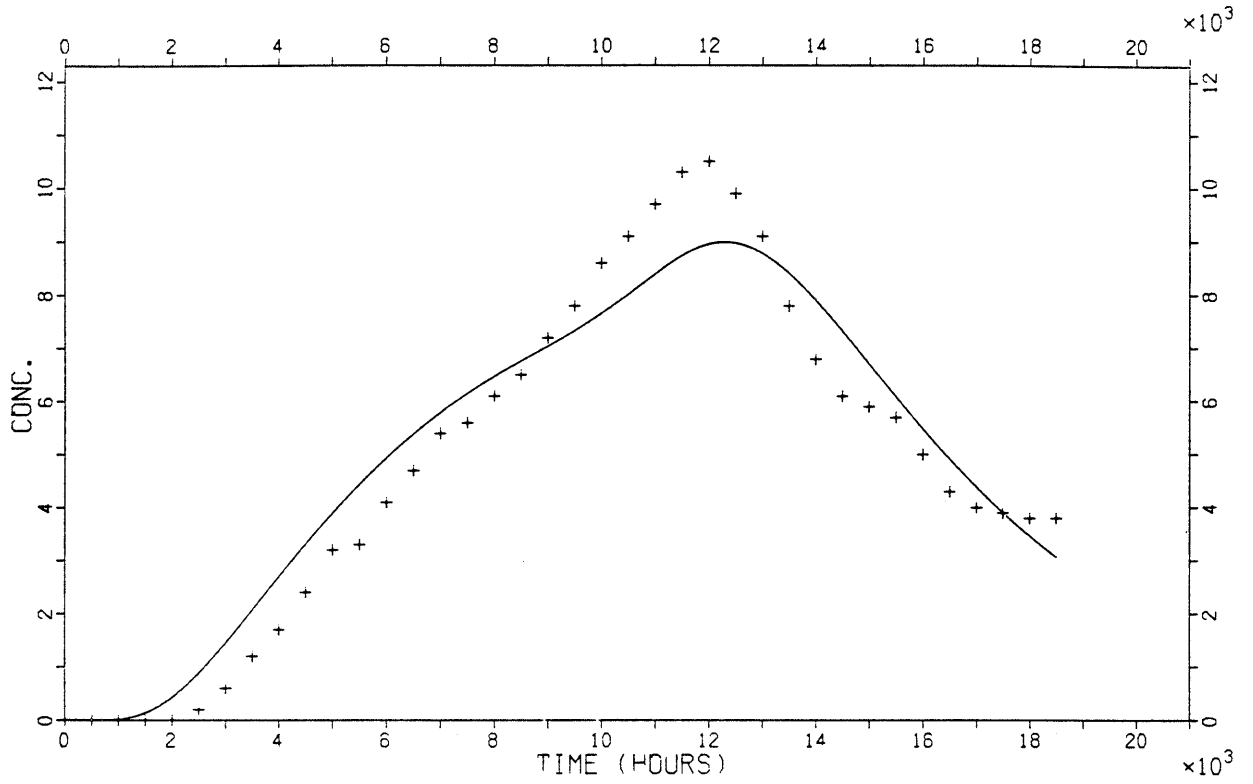


Figure A11-2. Continued.

Sheet number 68 tracer Eosin Y, AC-model

Stand. dev = .285 Tw = 7899 Dil = 95.1 SD = .08



Sheet number 71 tracer Eosin Y, AC-model

Stand. dev = .286 Tw = 8409 Dil = 94.0 SD = .07

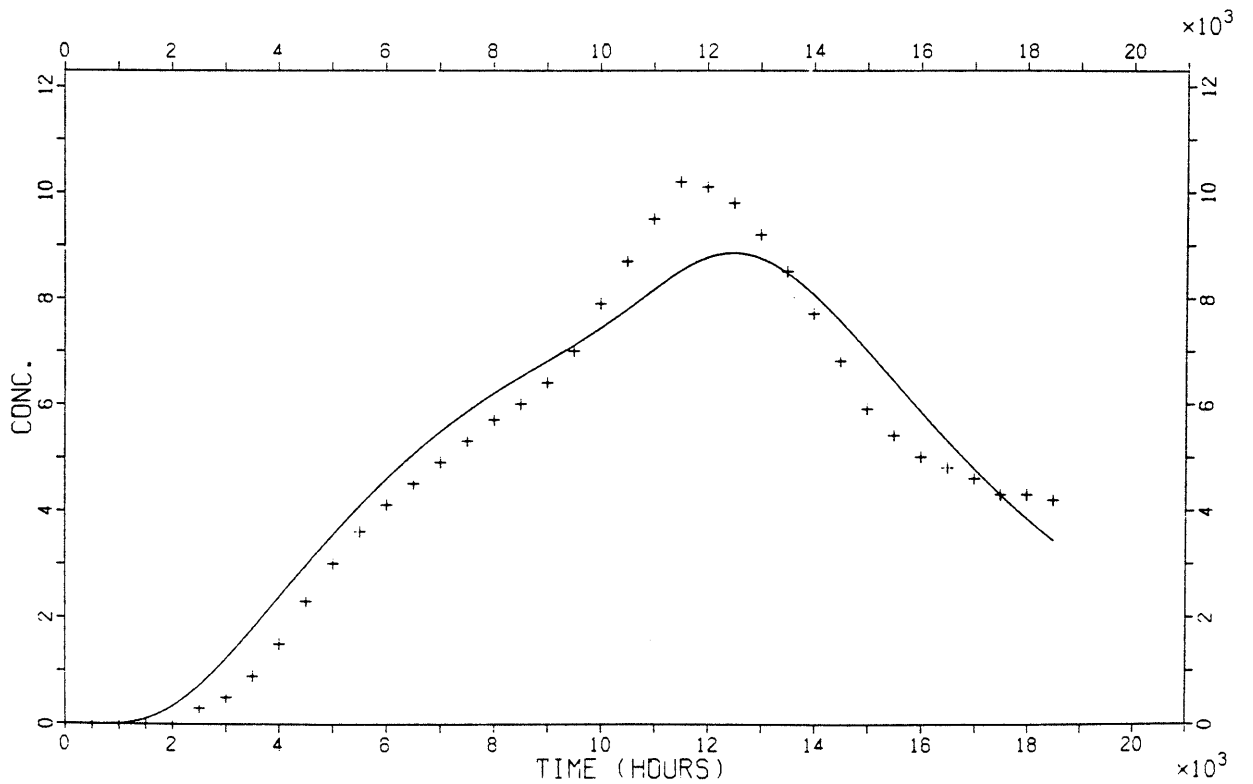
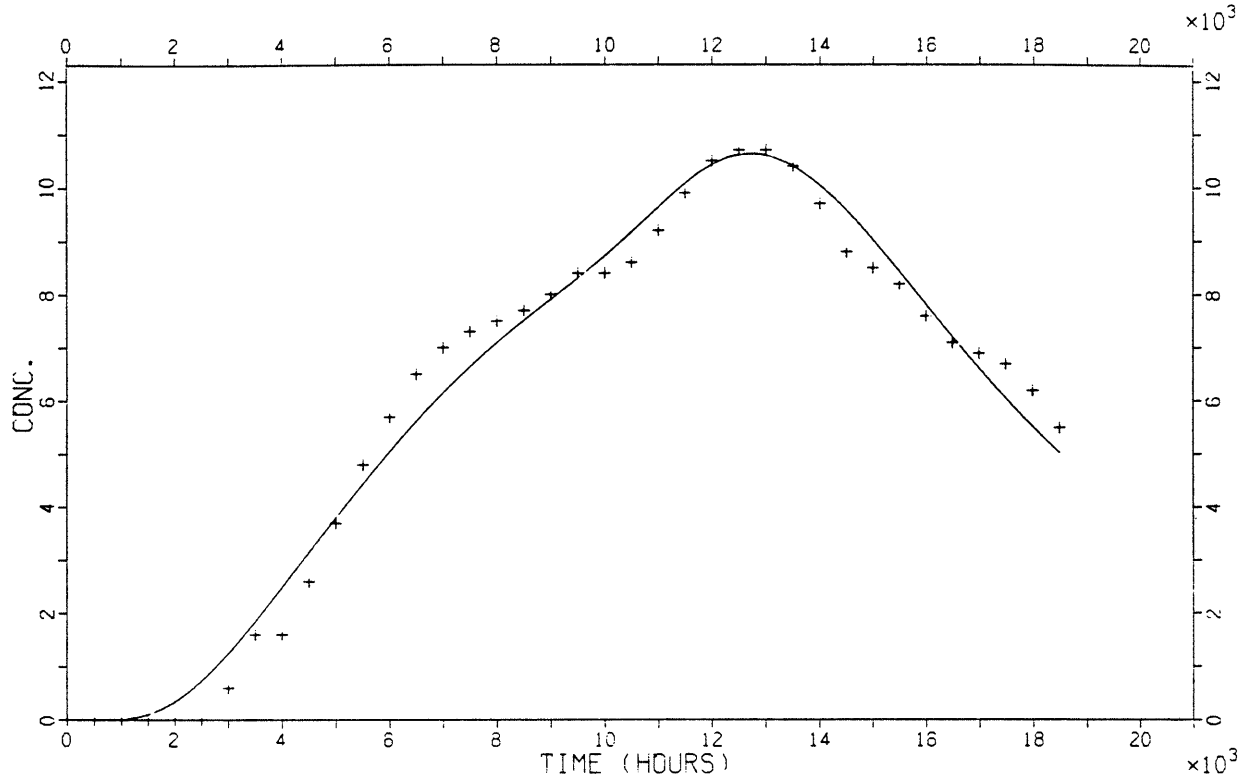


Figure A11-2. Continued.

Sheet number 90 tracer Eosin Y, AC-model

Stand. dev = .296 Tw = 9476 Dil = 73.7 SD = .03



Sheet number 108 tracer Eosin Y, AC-model

Stand. dev = .275 Tw = 6801 Dil = 277.8 SD = .09

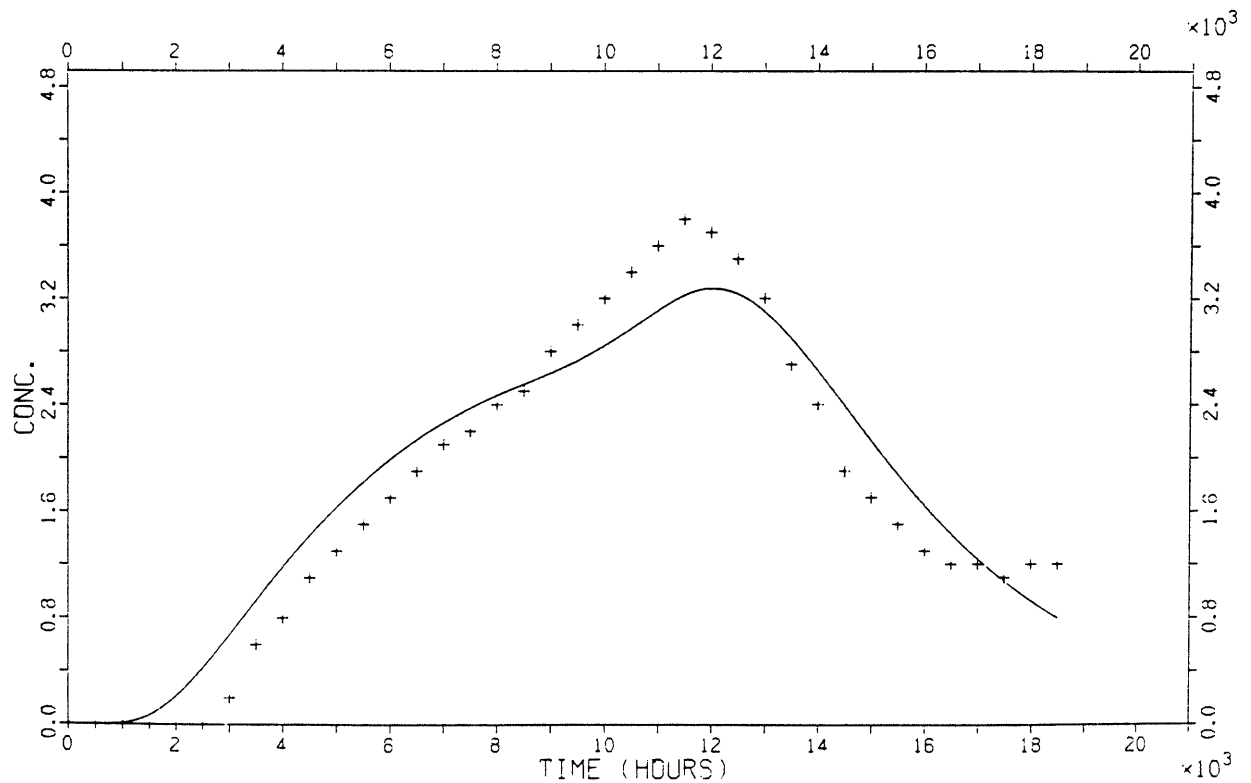
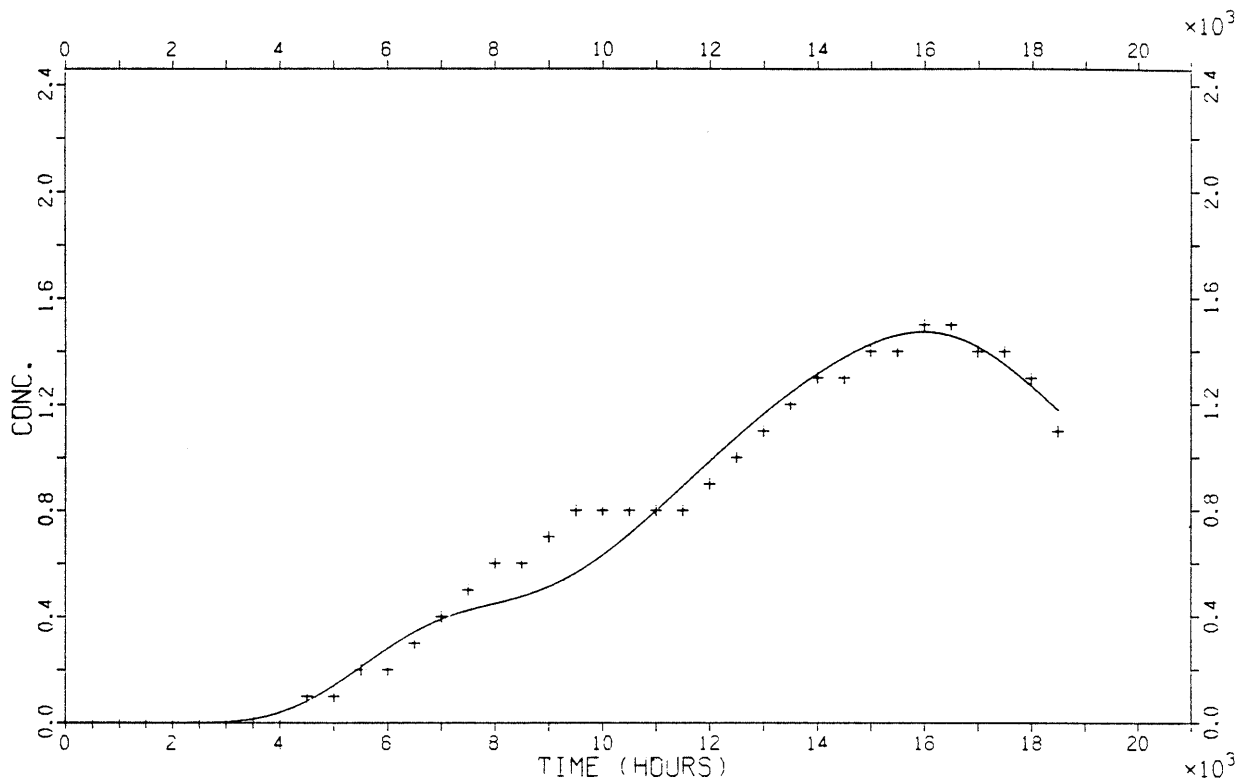


Figure A11-2. Continued.

Sheet number 61 tracer Iodide, AC-model

Stand. dev = .165 Tw = 7450 Dil = 126.2 SD = .08



Sheet number 62 tracer Iodide, AC-model

Stand. dev = .318 Tw = 1970 Dil = 41.1 SD = .05

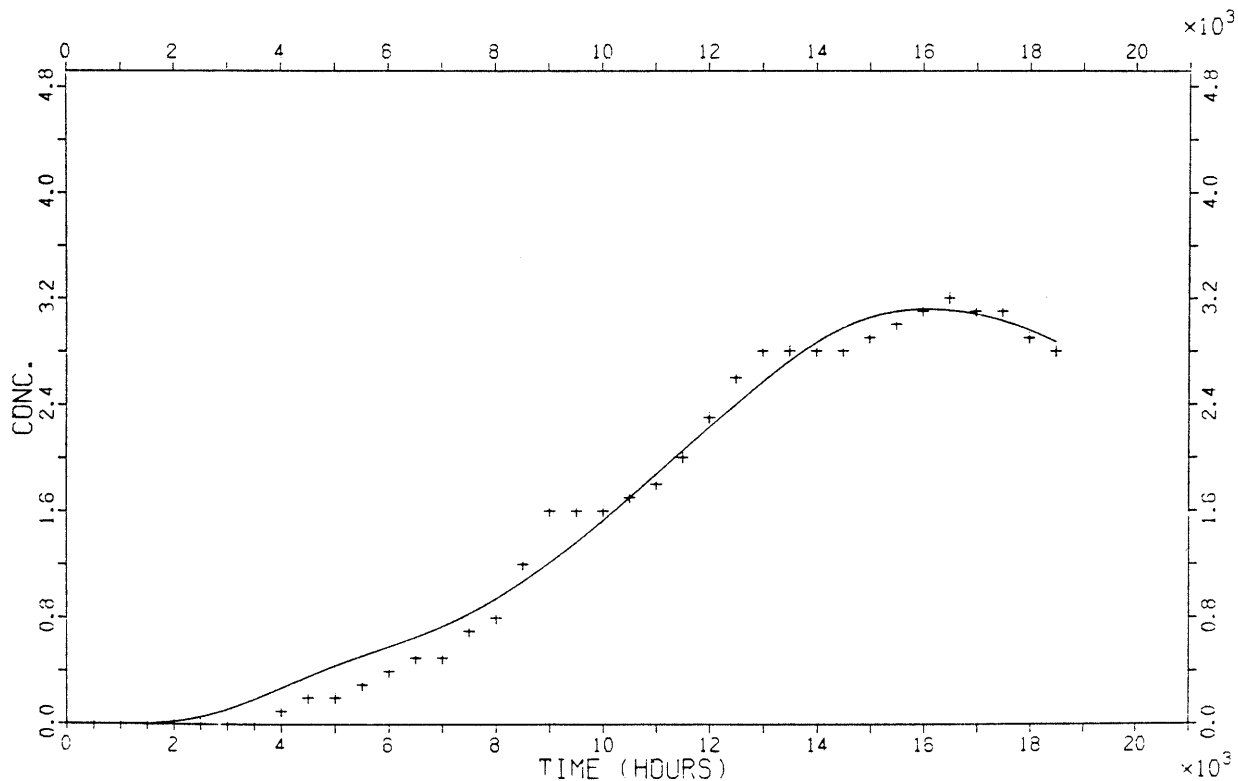
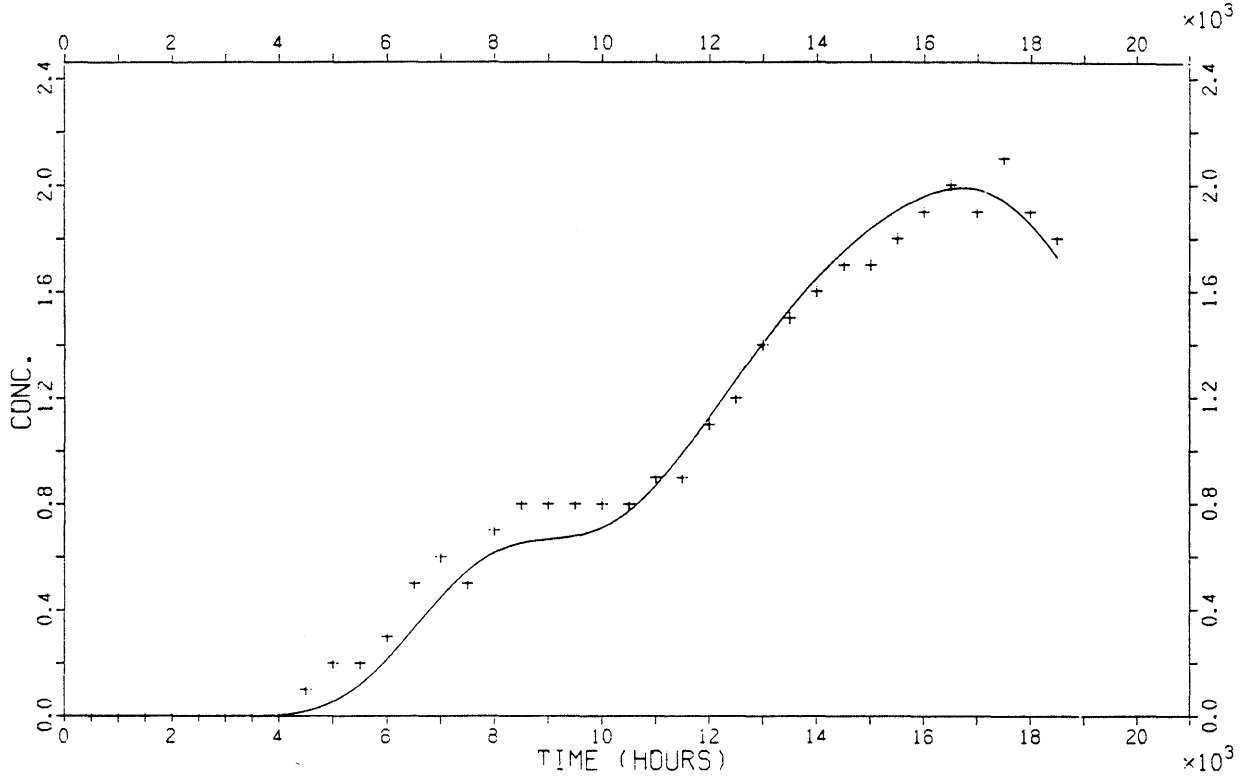


Figure A11-2. Continued.

Sheet number 103 tracer Iodide, AC-model

Stand. dev = .121 Tw = 7677 Dil = 98.5 SD = .06



Sheet number 108 tracer Iodide, AC-model

Stand. dev = .096 Tw = 7180 Dil = 82.3 SD = .06

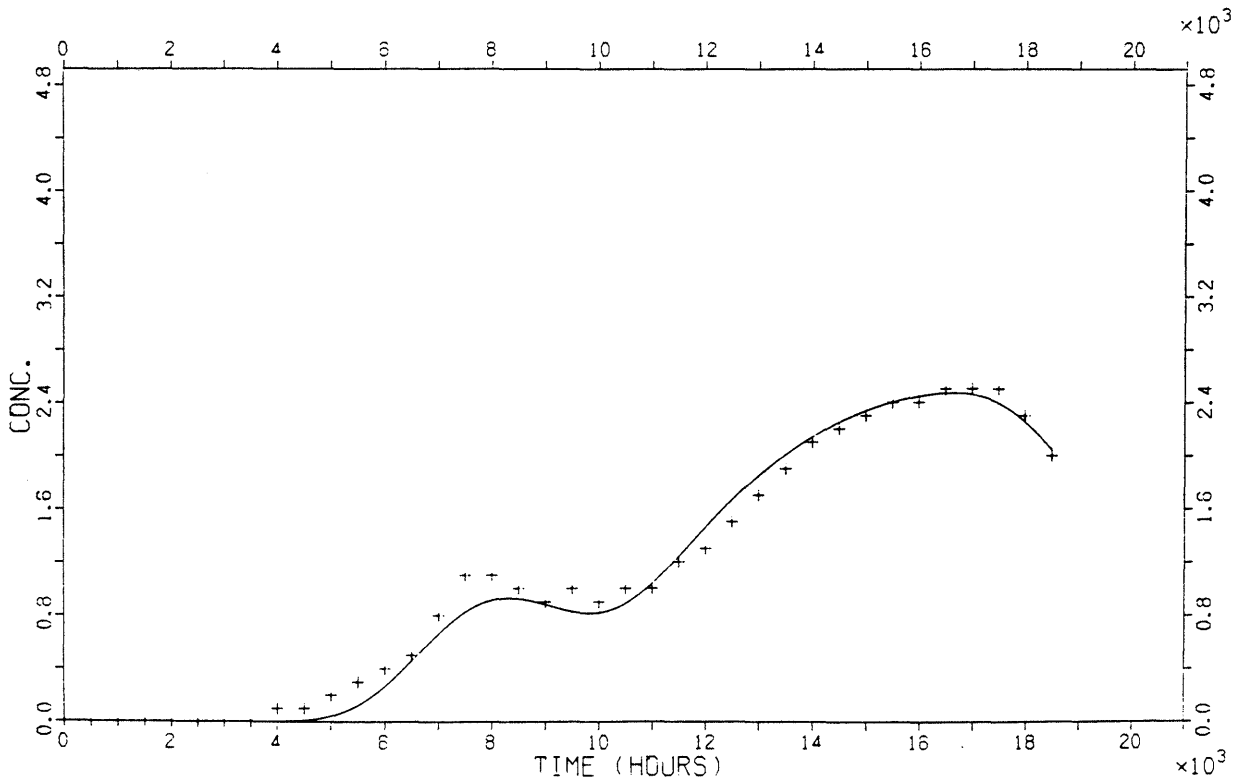


Figure A11-2. Continued.

Sheet number 110 tracer Iodide, AC-model

Stand. dev = .120 Tw = 7136 Dil = 76.0 SD = .06

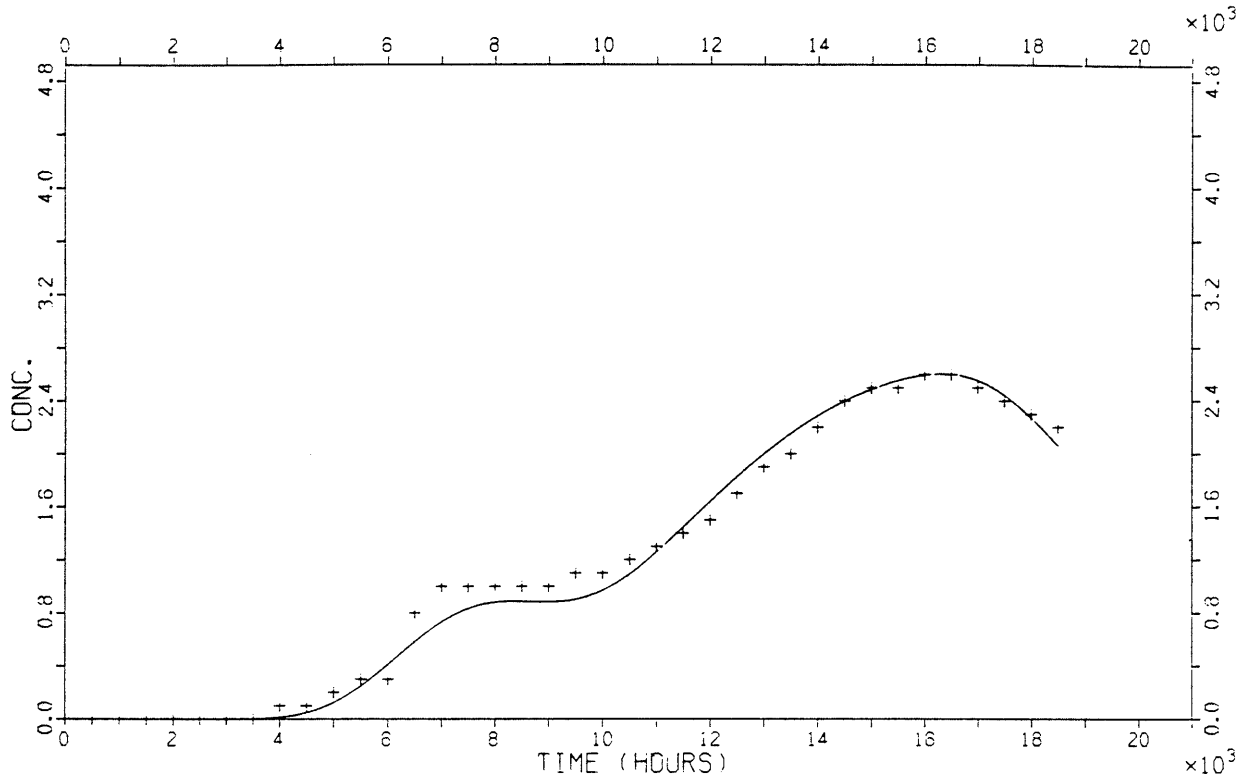
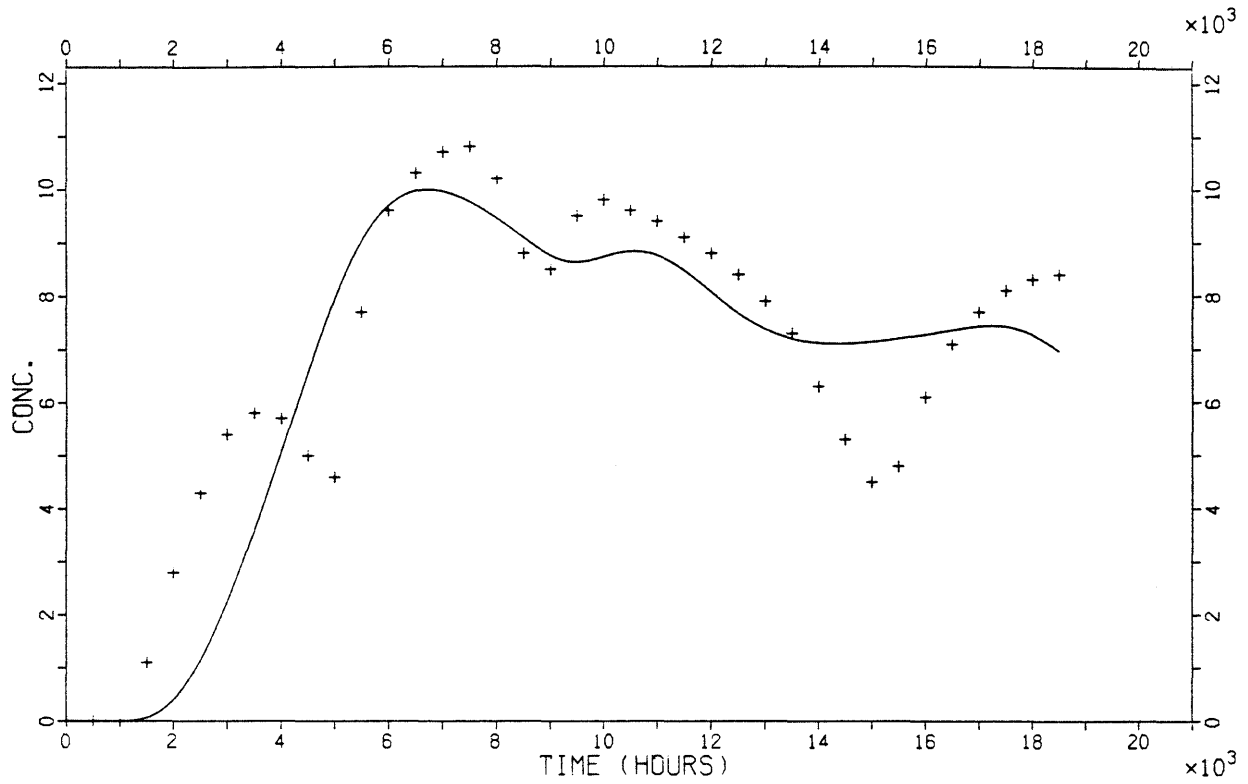


Figure A11-2. Continued.

Sheet number 57 tracer Eosin B, ADD-model

Pe = 5.1 Tw = 7035.0 A = 3.10E+05 Dil = 150.1 SD = .14



Sheet number 60 tracer Eosin B, ADD-model

Pe = 4.0 Tw = 20470.0 A = 2.00E+05 Dil = 181.7 SD = .11

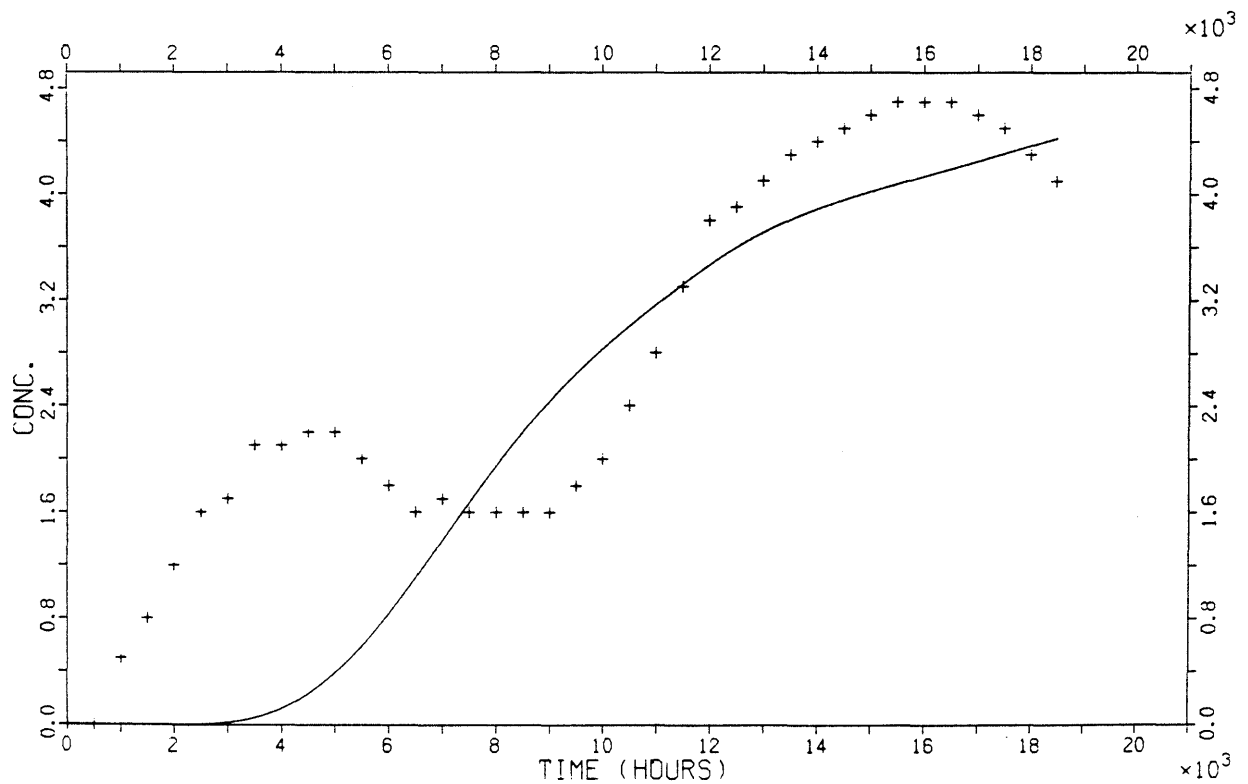
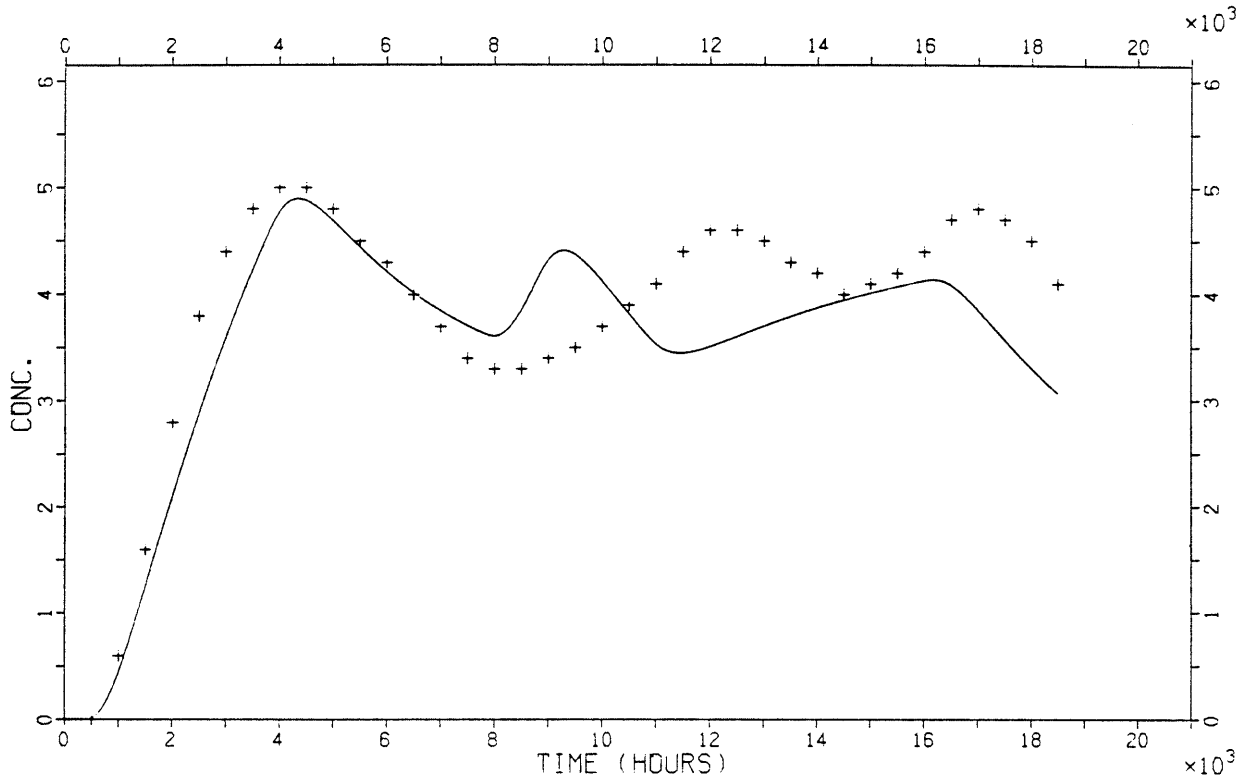


Figure A11-3. Model fits with ADD-model.

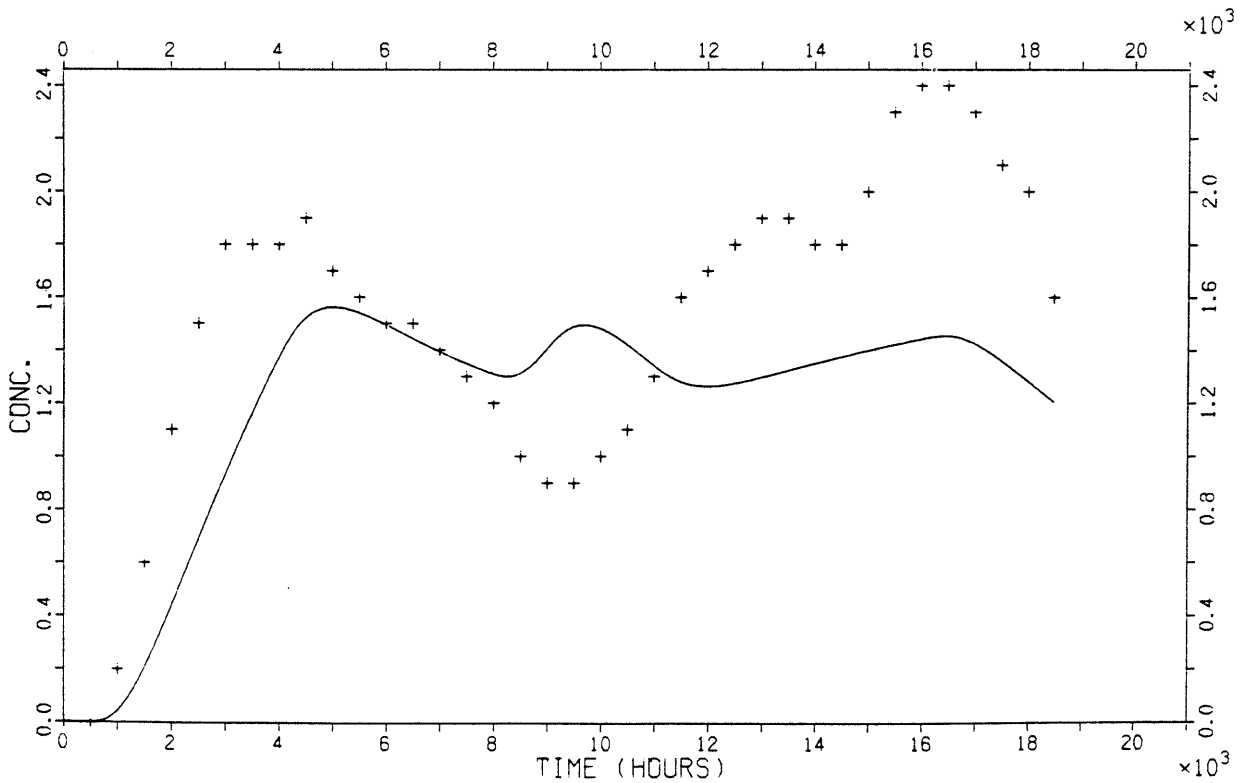
Sheet number 66 tracer Eosin B, ADD-model

Pe = 4.0 Tw = 1944.0 A = 1039.0 Dil = 168.9 SD = .07

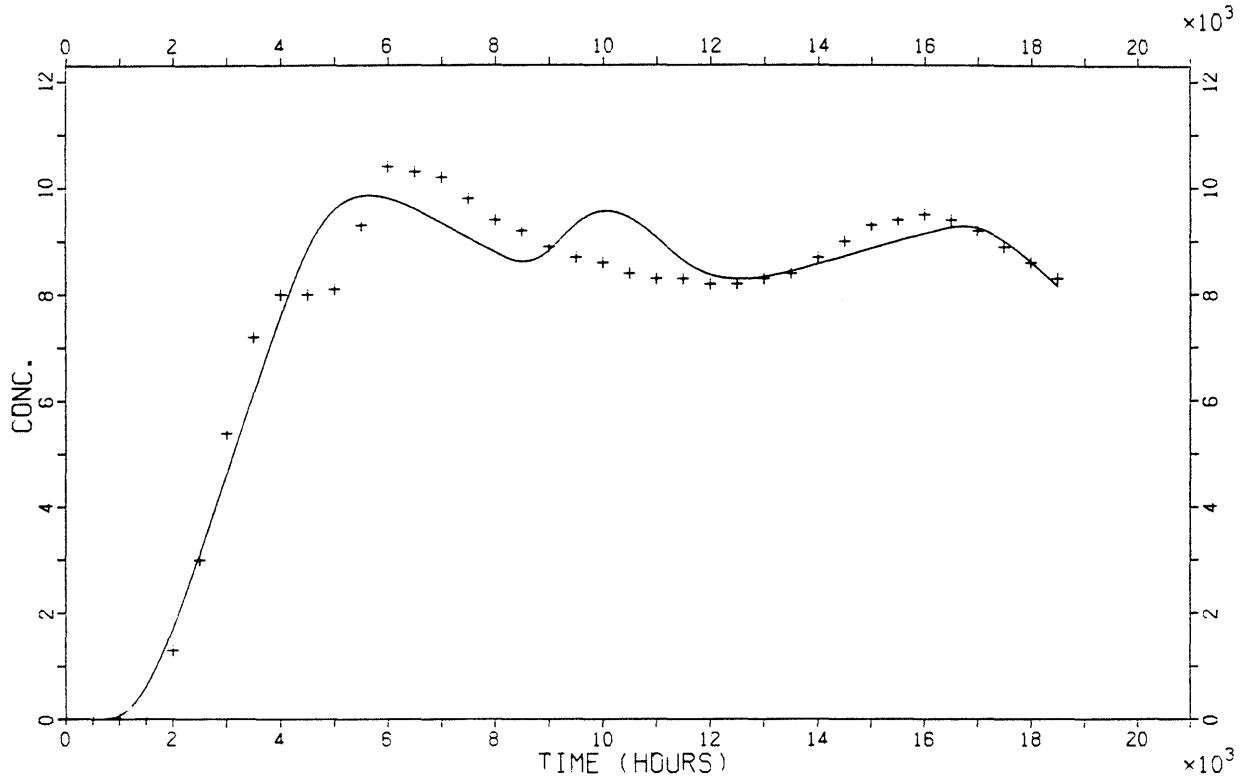


Sheet number 108 tracer Eosin B, ADD-model

Pe = 4.2 Tw = 3118.0 A = 1636.0 Dil = 465.7 SD = .17



A11.30
Sheet number 120 tracer Eosin B, ADD-model
 Pe = 4.0 Tw = 4687.0 A = 2987.0 Dil = 78.2 SD = .03



Sheet number 64 tracer Uranine, ADD-model
 Pe = 19.8 Tw = 15.1 A = 28.9 Dil = 946.1 SD = .29

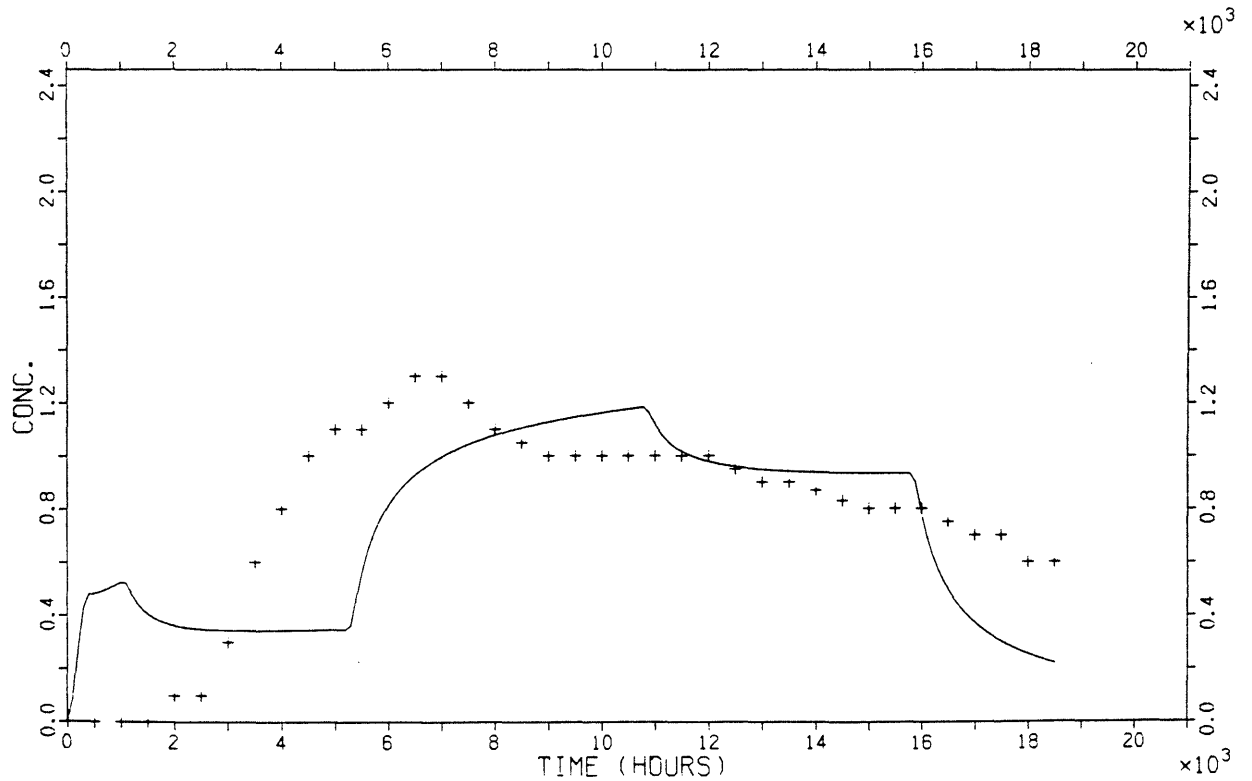
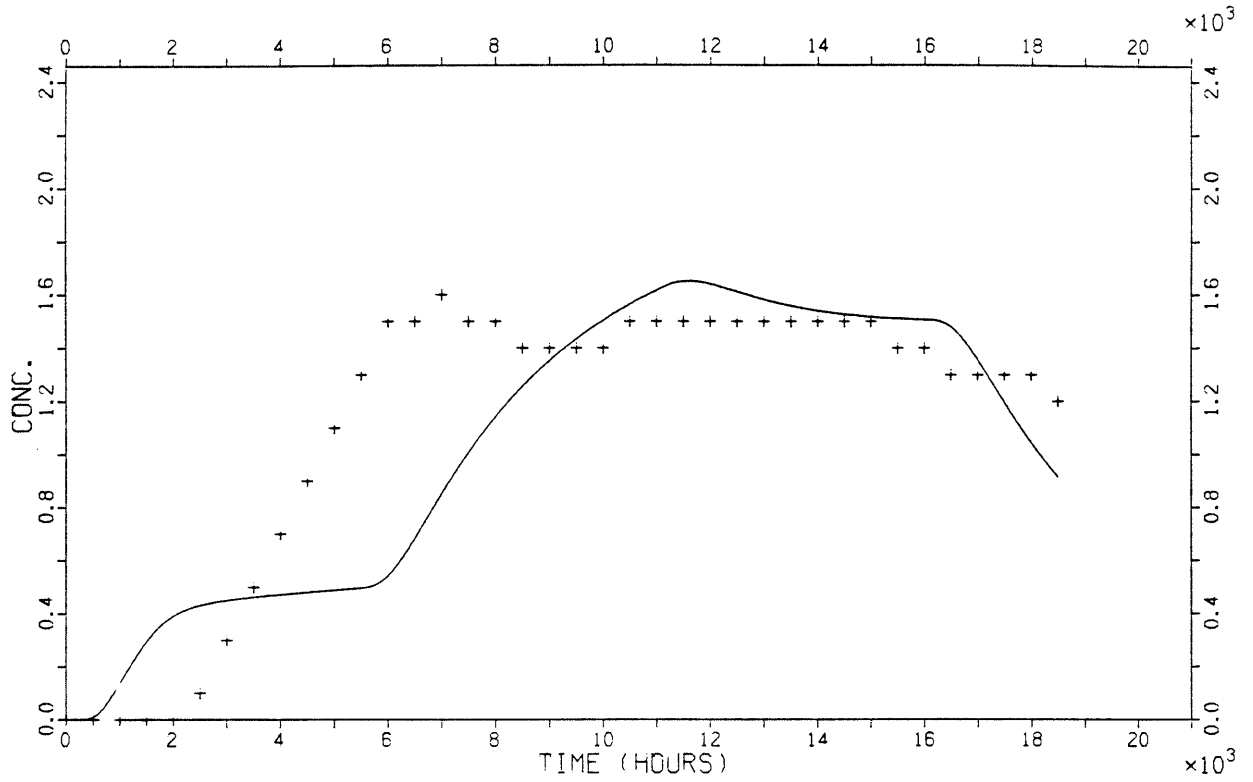


Figure A11-3. Continued.

A11.31
Sheet number 71 tracer Uranine, ADD-model
 Pe = 6.5 Tw = 26.5 A = 22.5 Dil = 470.4 SD = .15



Sheet number 90 tracer Uranine, ADD-model
 Pe = 4.0 Tw = 11170.0 A = 1.18E+05 Dil = 1052.2 SD = .16

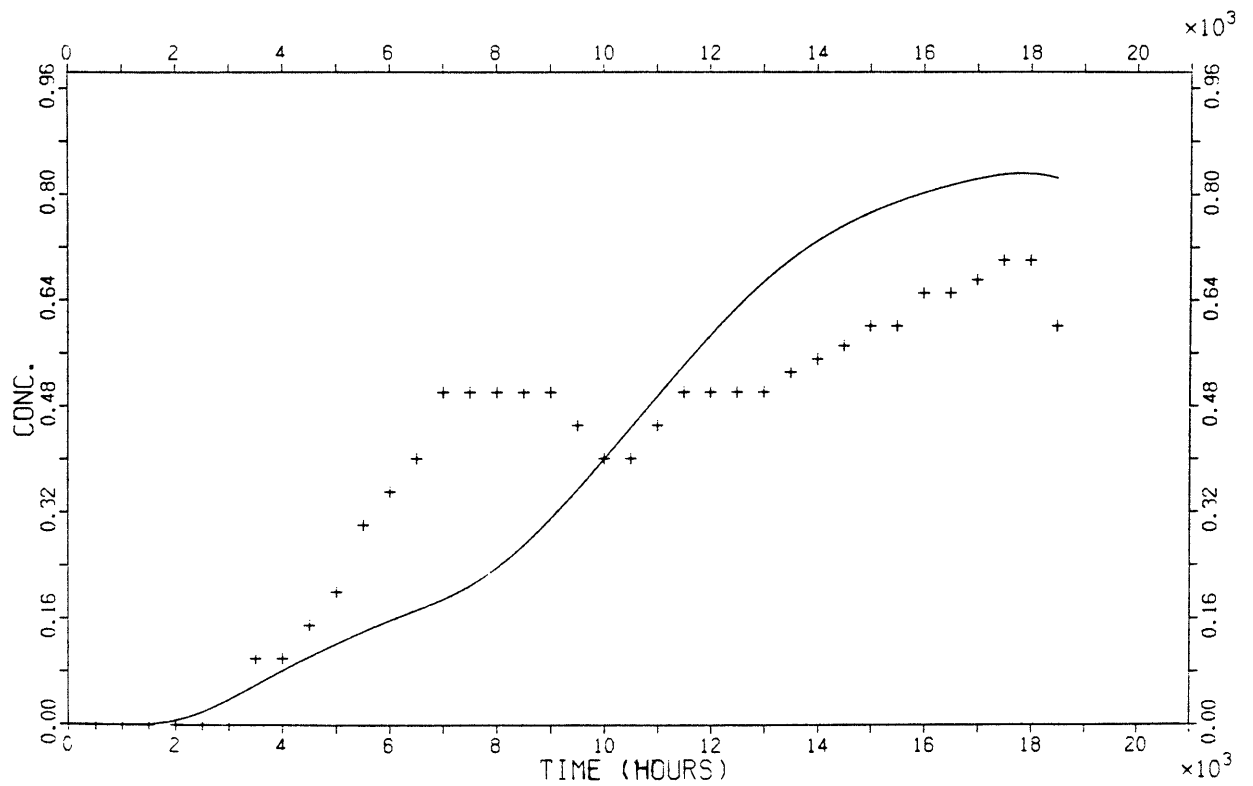
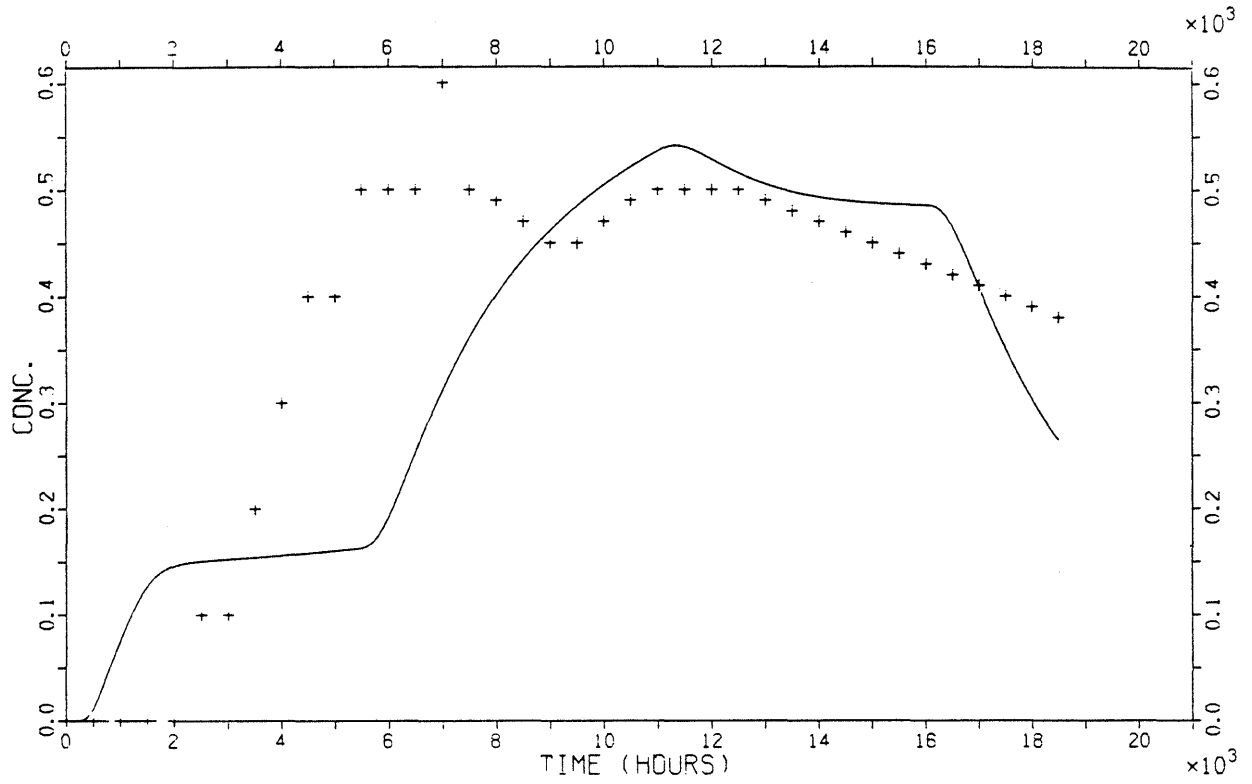


Figure A11-3. Continued.

Sheet number 108 tracer Uranine, ADD-model

Pe = 4.0 Tw = 1979.0 A = 2309.0 Dil = 1645.3 SD = .21



Sheet number 134 tracer Uranine, ADD-model

Pe = 11.7 Tw = 12000.0 A = 9.44E+04 Dil = 173.0 SD = .03

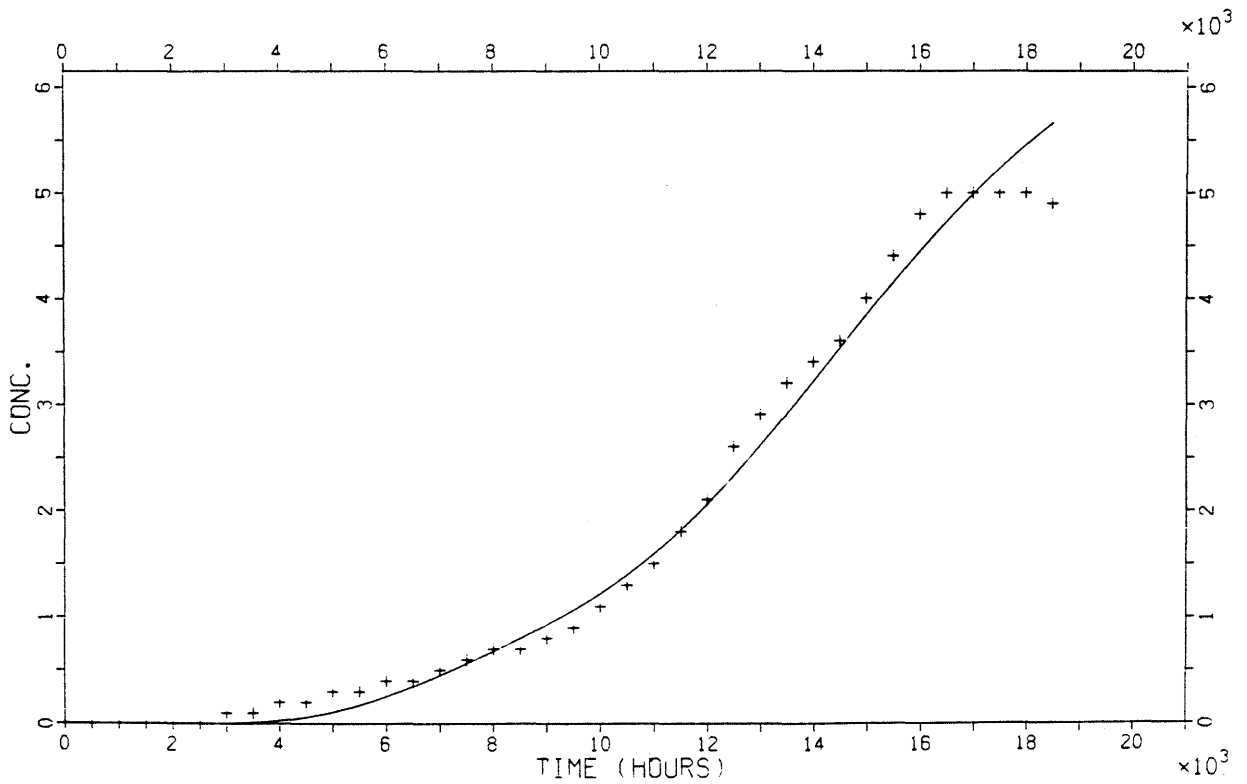
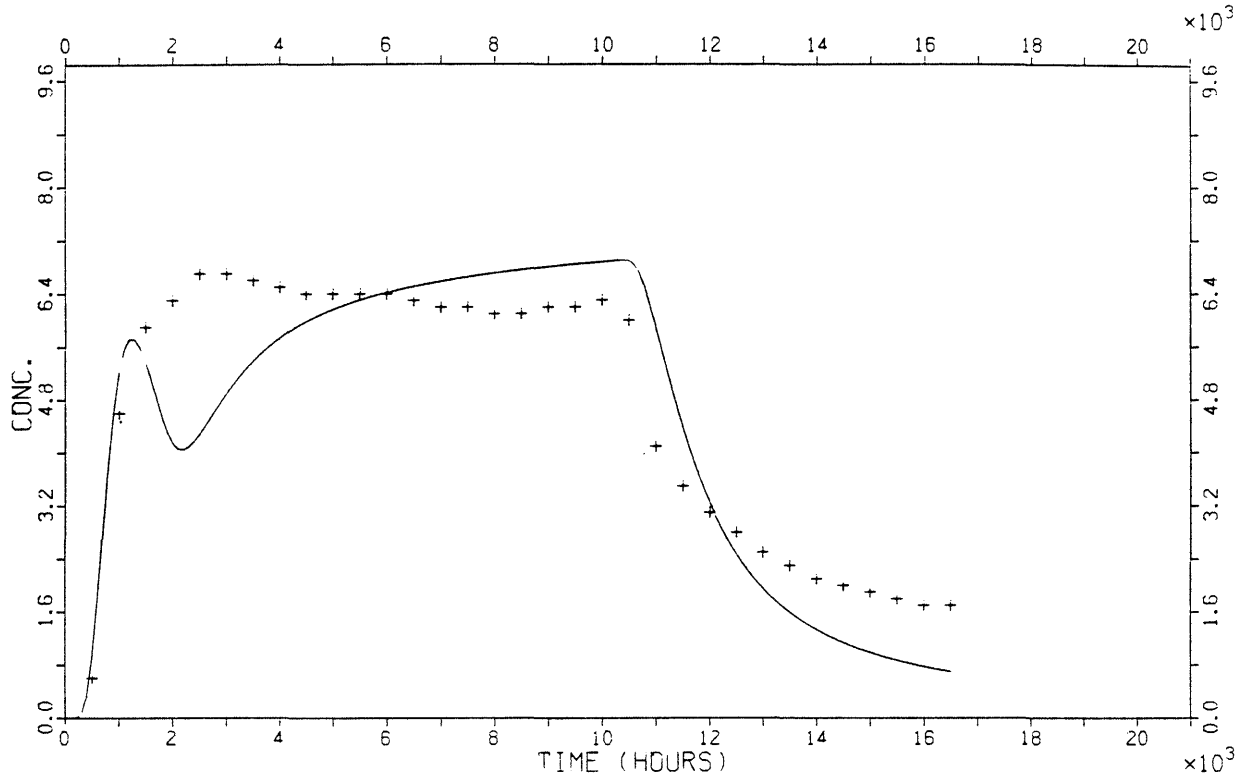


Figure A11-3. Continued.

Sheet number 60 tracer Elbenyl, ADD-model

Pe = 5.8 Tw = 1402.0 A = 3632.0 Dil = 239.9 SD = .11



Sheet number 64 tracer Elbenyl, ADD-model

Pe = 6.1 Tw = 2014.0 A = 7.62E+16 Dil = 247.7 SD = .22

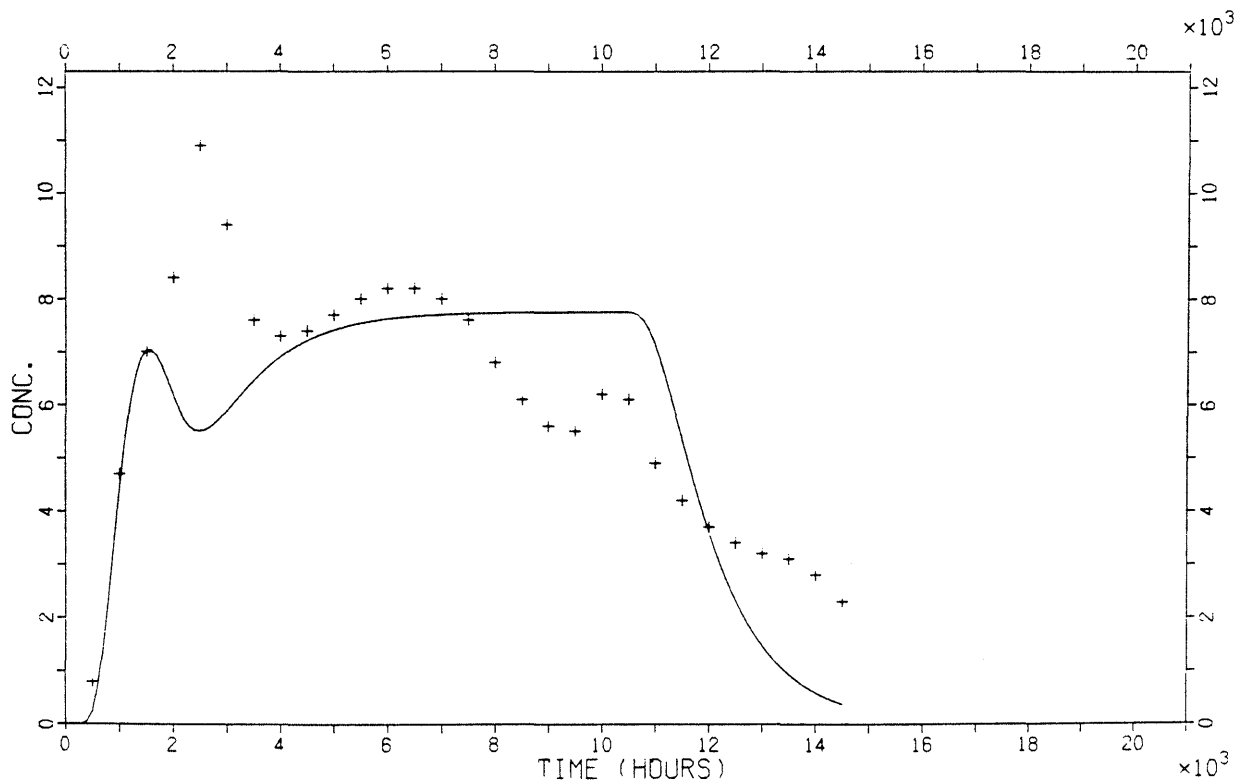
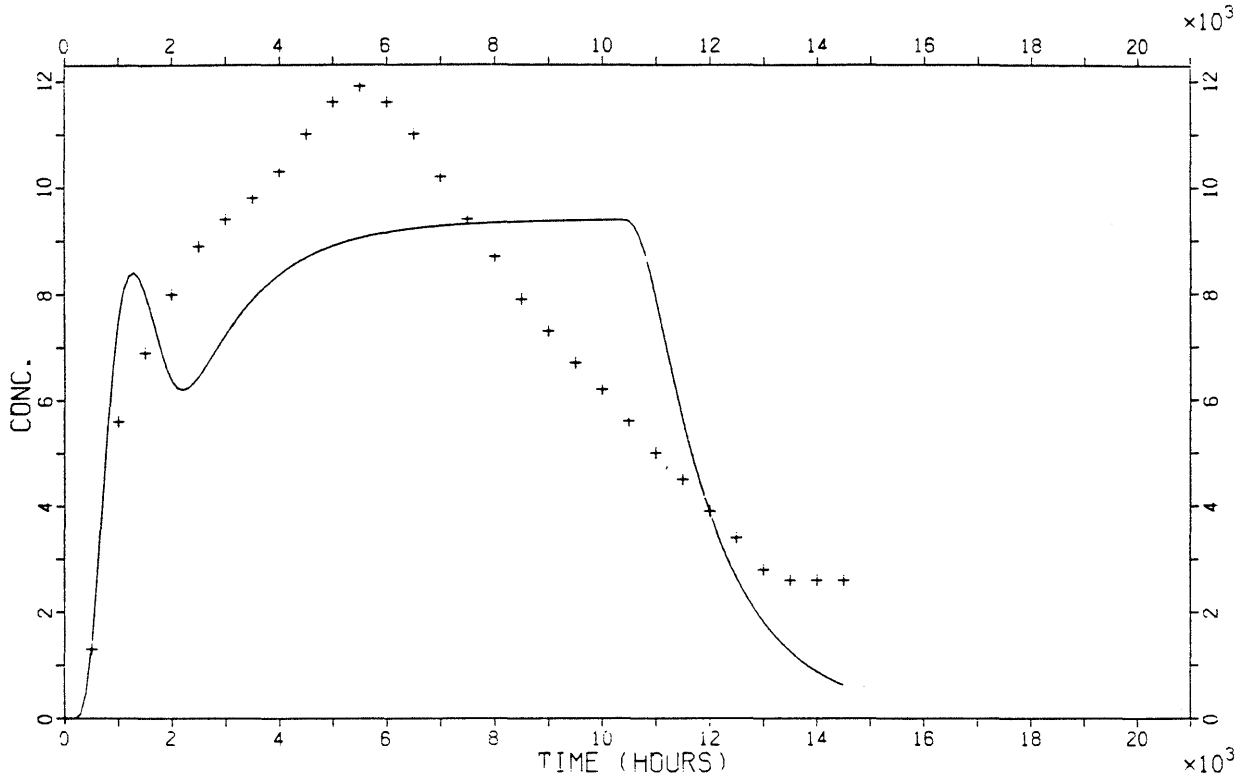


Figure A11-3. Continued.

Sheet number 66 tracer Elbenyl, ADD-model

Pe = 4.0 Tw = 1941.0 A = 2.00E+05 Dil = 203.6 SD = .20



Sheet number 68 tracer Elbenyl, ADD-model

Pe = 5.6 Tw = 1978.0 A = 1.25E+13 Dil = 382.2 SD = .11

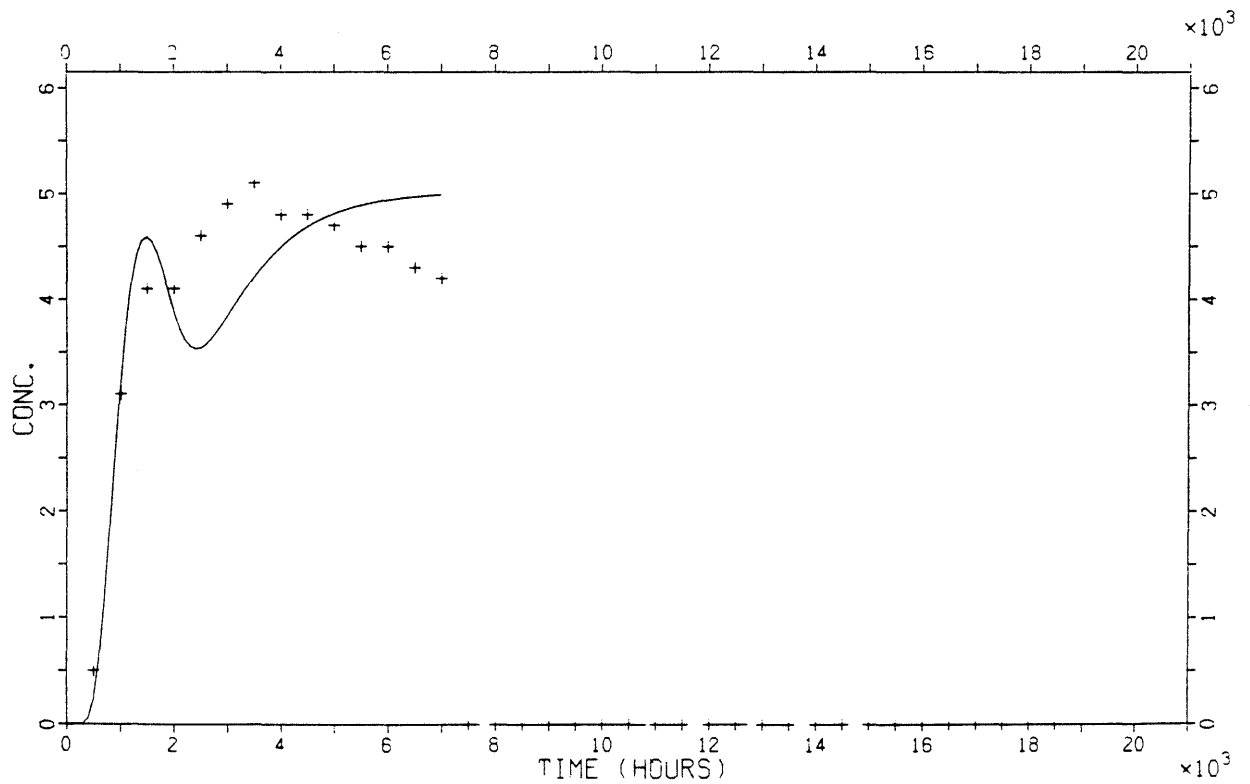
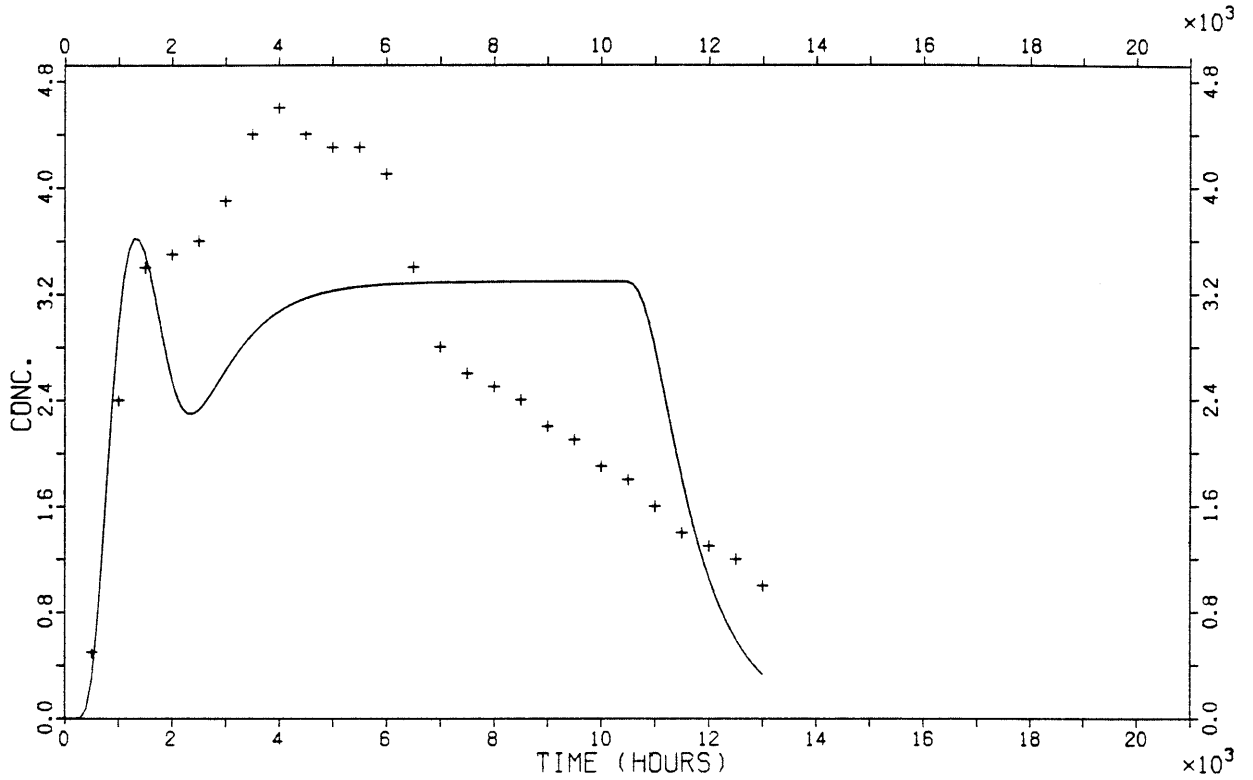


Figure A11-3. Continued.

Sheet number 108 tracer Elbenyl, ADD-model

Pe = 6.3 Tw = 1636.0 A = 4.51E+16 Dil = 583.6 SD = .29



Sheet number 64 tracer Eosin Y, ADD-model

Pe = 5.5 Tw = 7274.0 A = 3.93E+05 Dil = 94.4 SD = .07

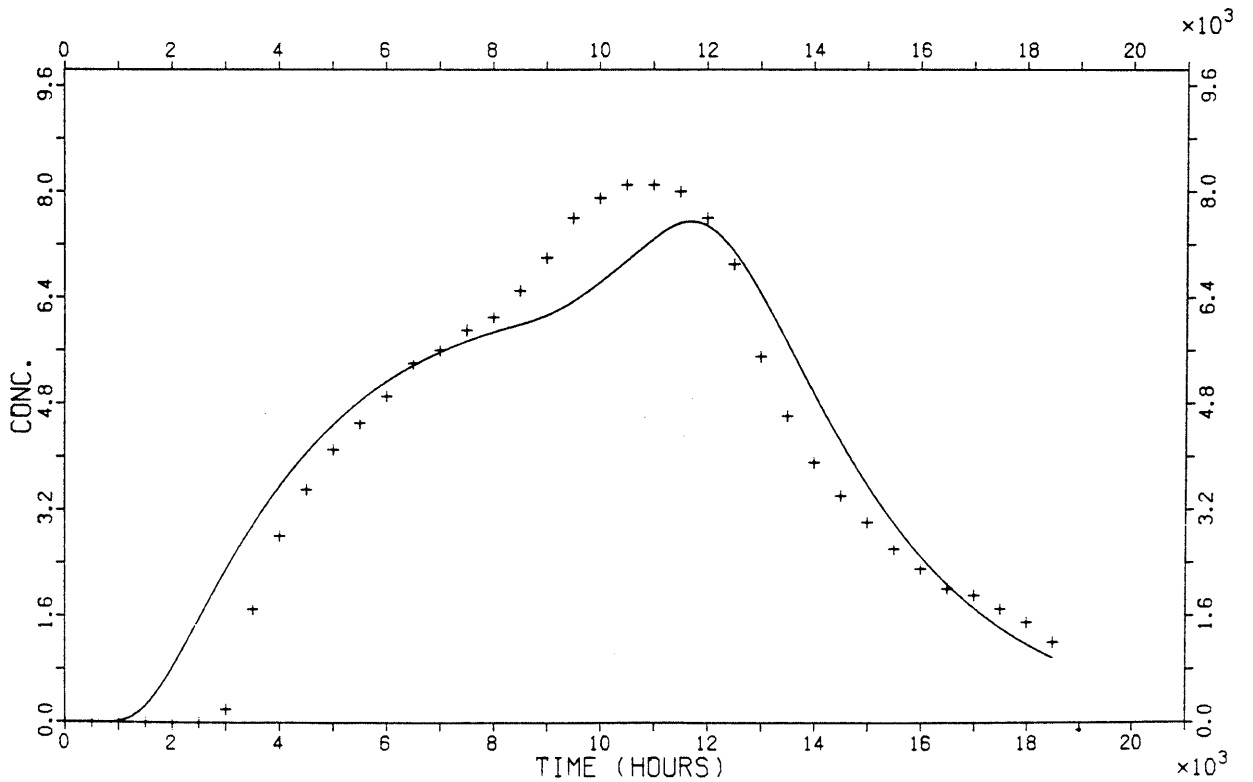
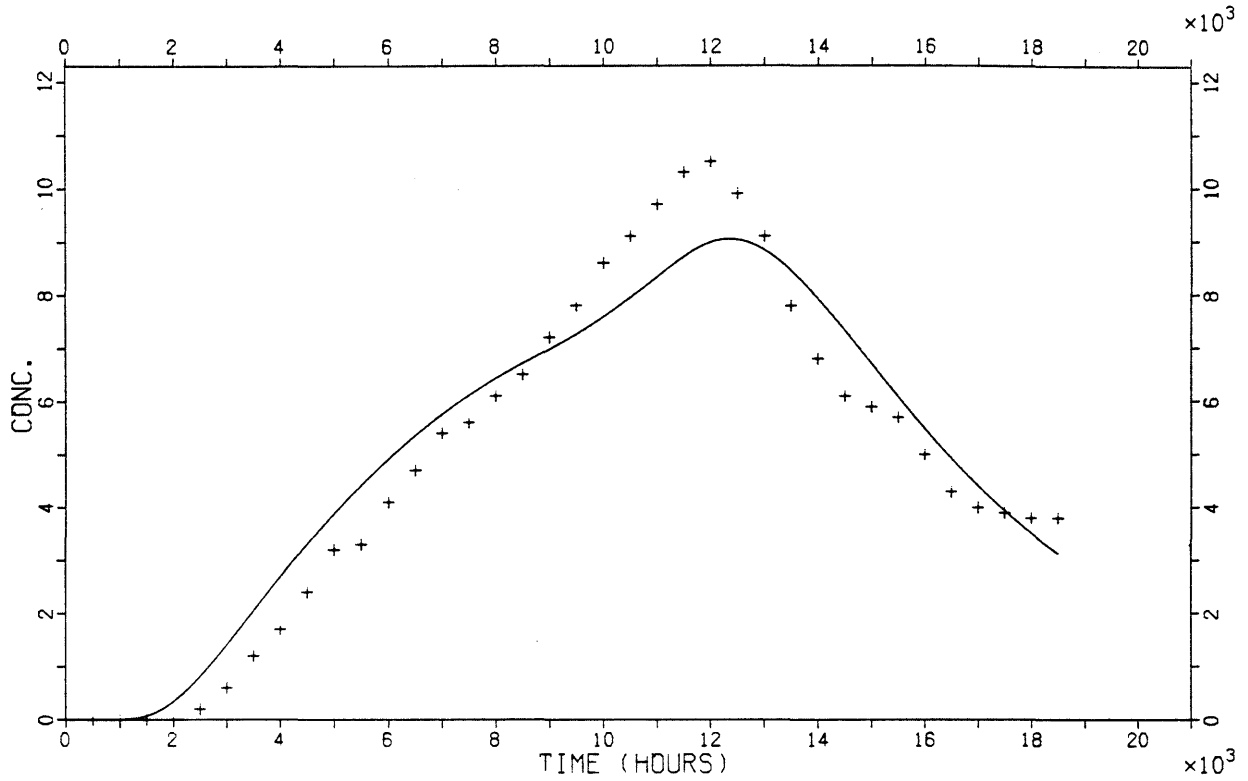


Figure A11-3. Continued.

Sheet number 68 tracer Eosin Y, ADD-model

Pe = 5.4 Tw = 7758.0 A = 2.82E+05 Dil = 92.7 SD = .06



Sheet number 71 tracer Eosin Y, ADD-model

Pe = 34.8 Tw = 2829.0 A = 1669.0 Dil = 43.1 SD = .03

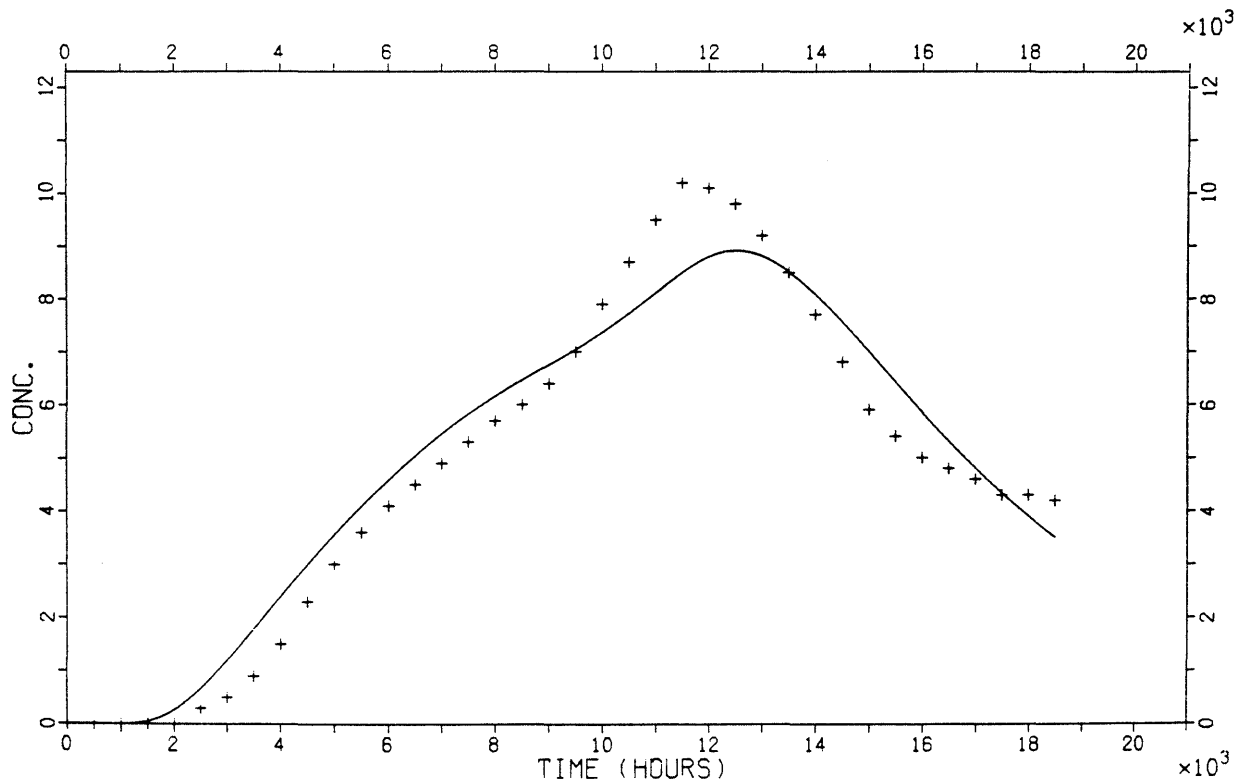
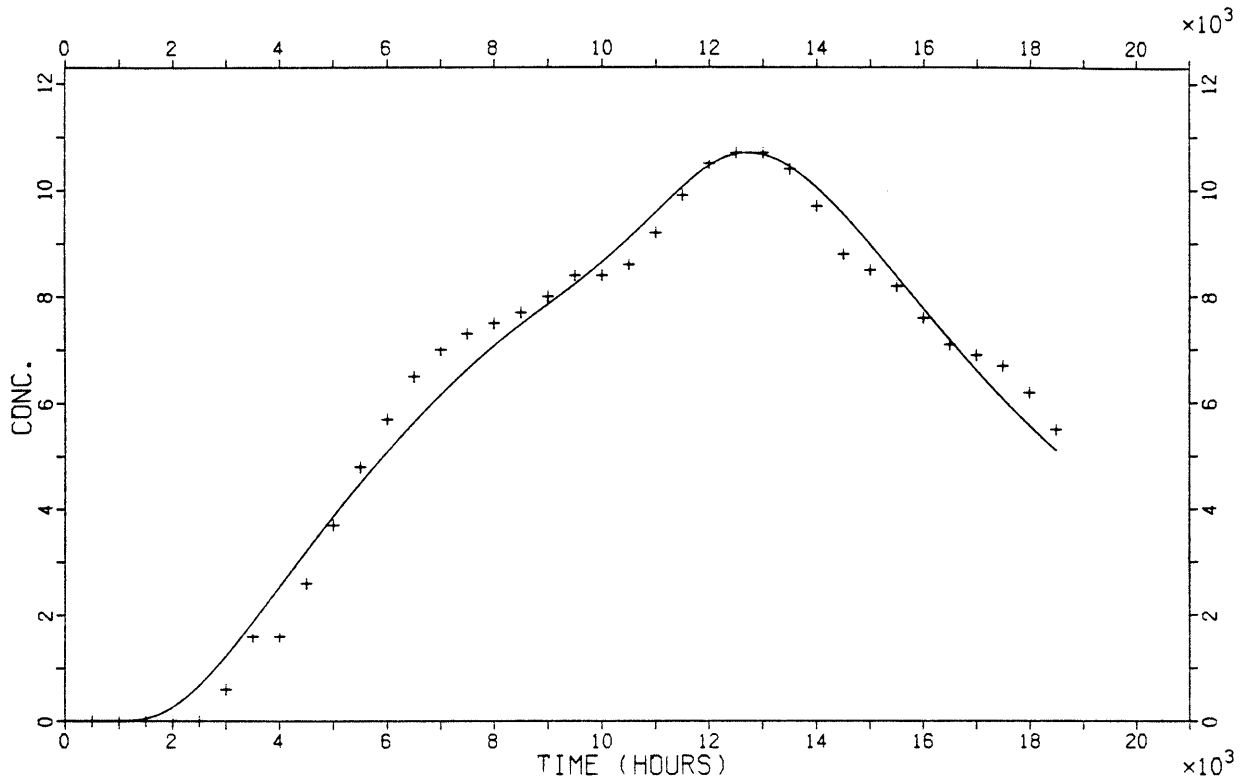


Figure A11-3. Continued.

A11.37
Sheet number 90 tracer Eosin Y, ADD-model

Pe = 6.0 Tw = 6325.0 A = 2.02E+05 Dil = 277.6 SD = .09



Sheet number 108 tracer Eosin Y, ADD-model

Pe = 18.6 Tw = 7206.0 A = 4.94E+07 Dil = 126.8 SD = .08

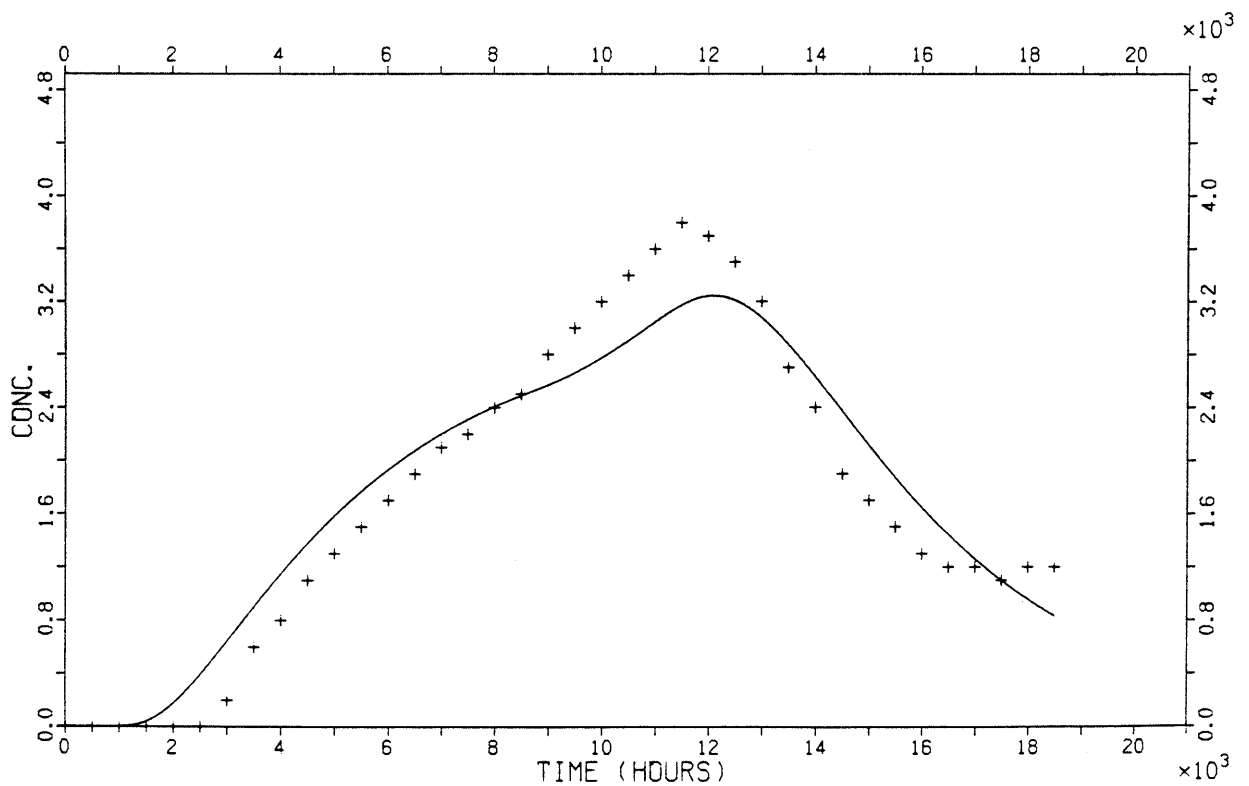
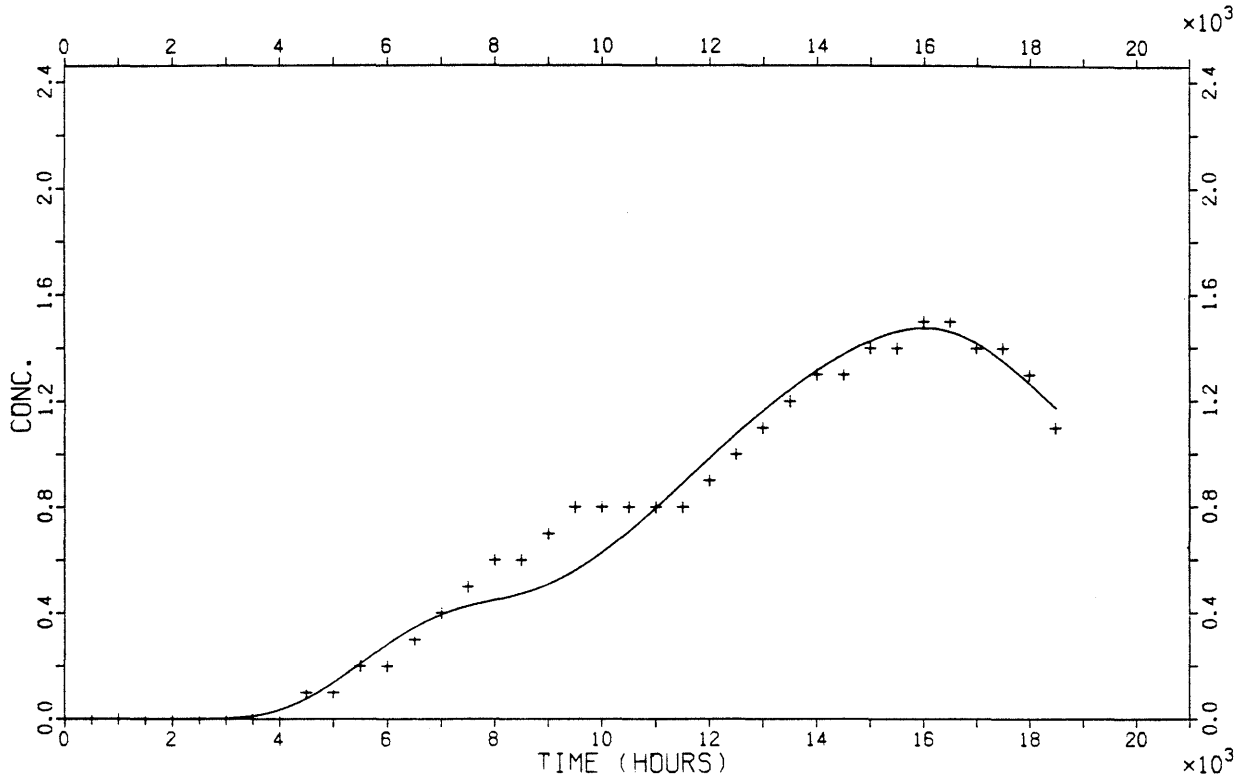


Figure A11-3. Continued.

Sheet number 61 tracer Iodide, ADD-model

Pe = 18.6 Tw = 7206.0 A = 4.94E+07 Dil = 126.8 SD = .08



Sheet number 62 tracer Iodide, ADD-model

Pe = 4.0 Tw = 11090.0 A = 5.00E+05 Dil = 40.2 SD = .05

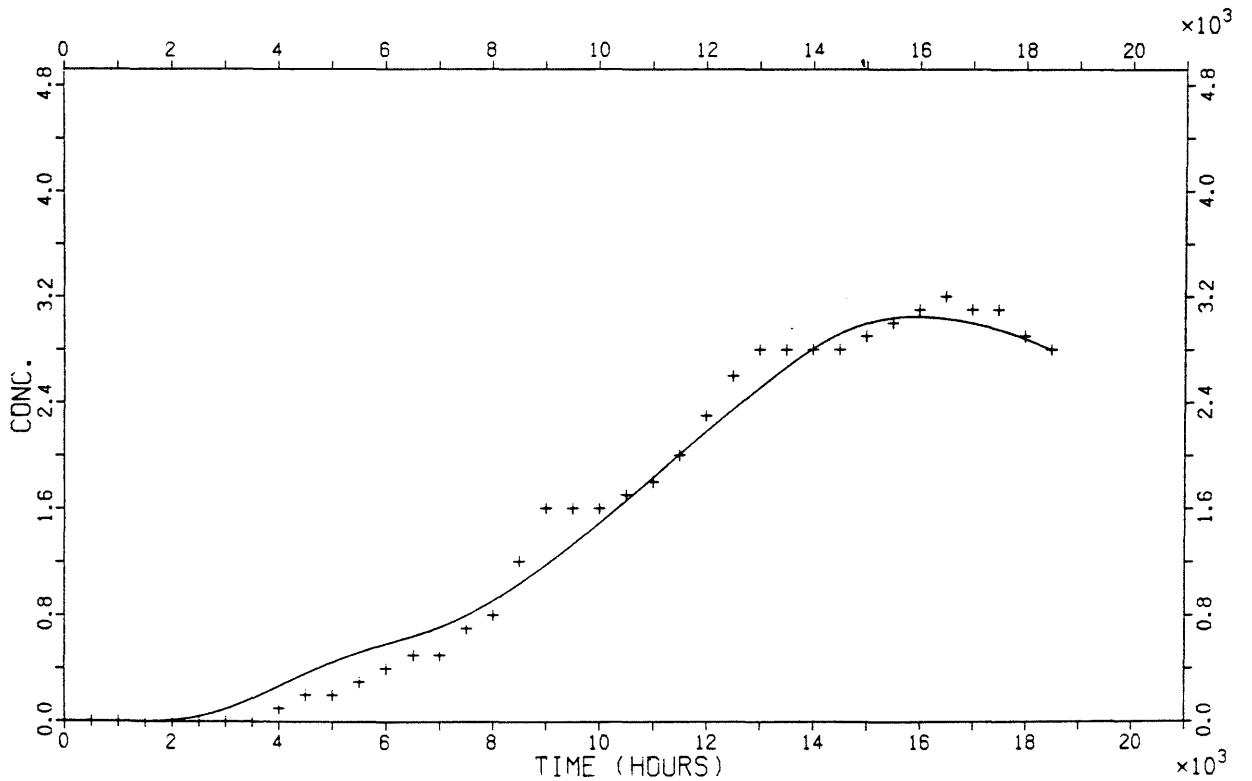
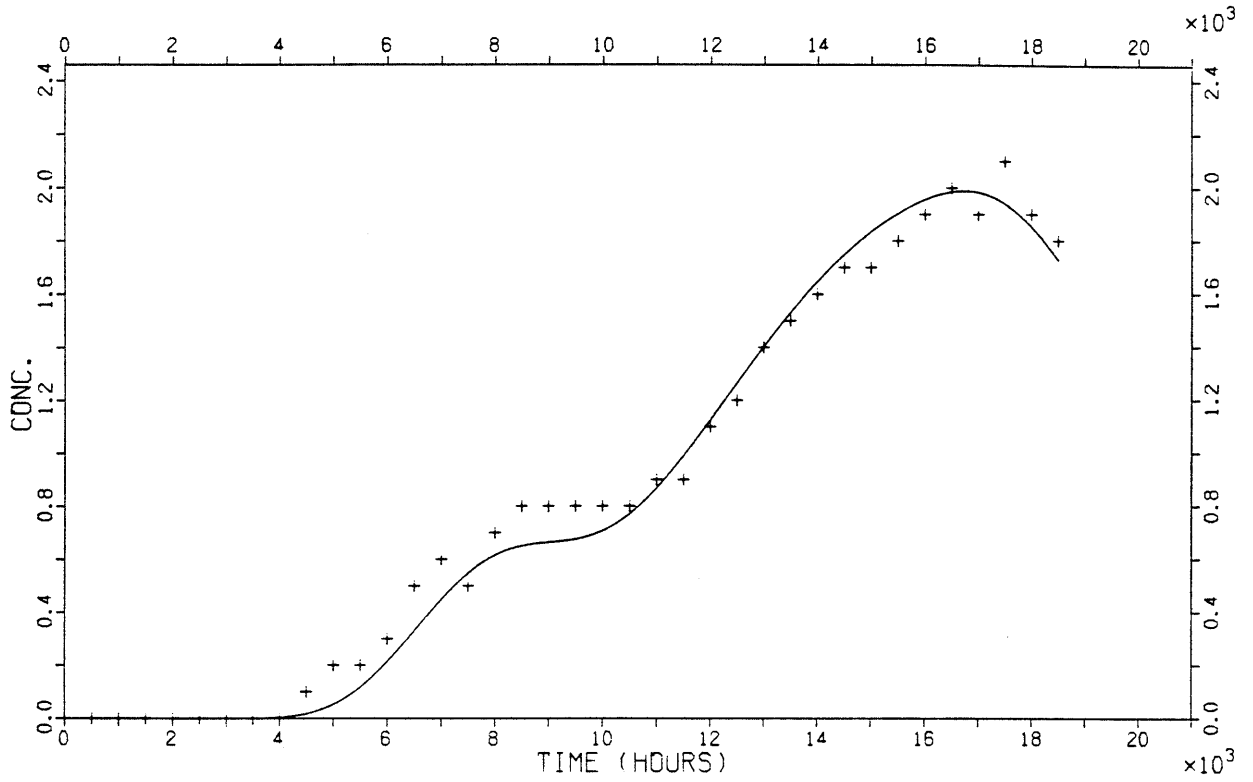


Figure A11-3. Continued.

Sheet number 103 tracer Iodide, ADD-model

Pe = 34.0 Tw = 7557.0 A = 4.49E+06 Dil = 98.6 SD = .06



Sheet number 108 tracer Iodide, ADD-model

Pe = 54.5 Tw = 7113.0 A = 5.28E+08 Dil = 82.8 SD = .06

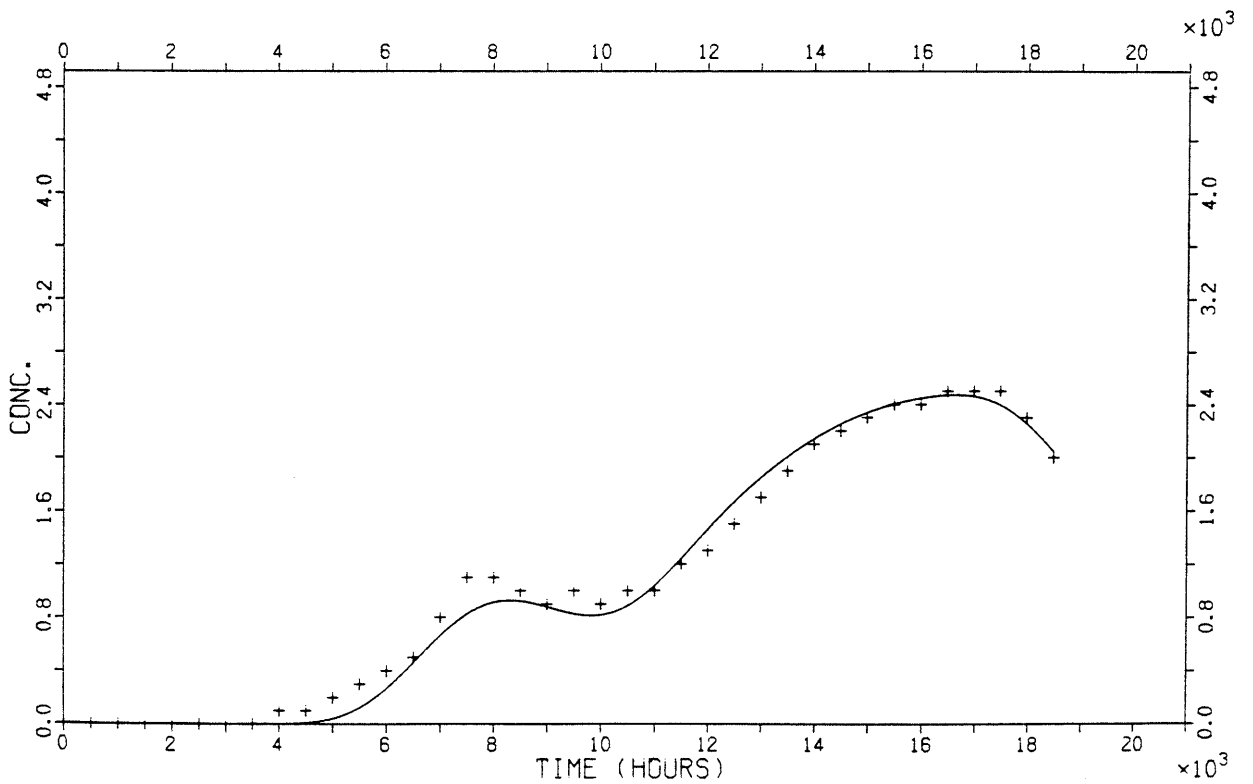
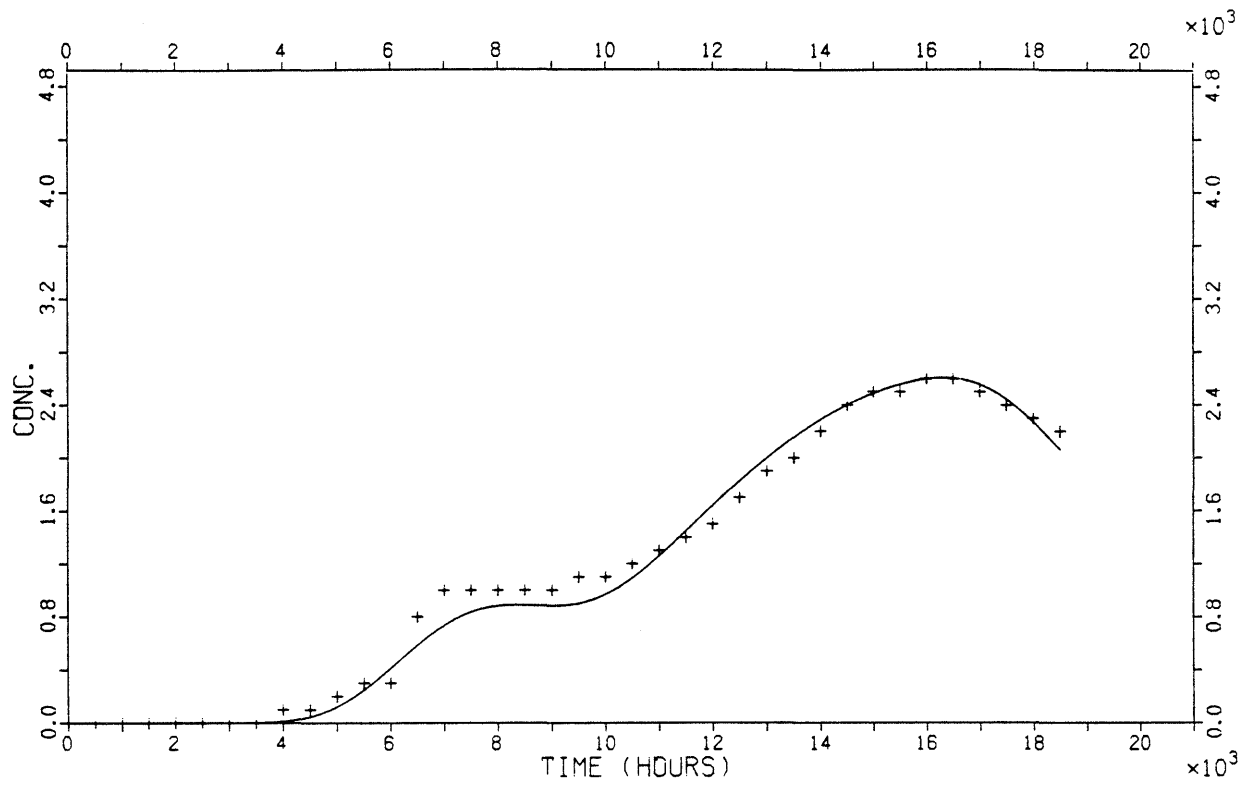


Figure A11-3. Continued.

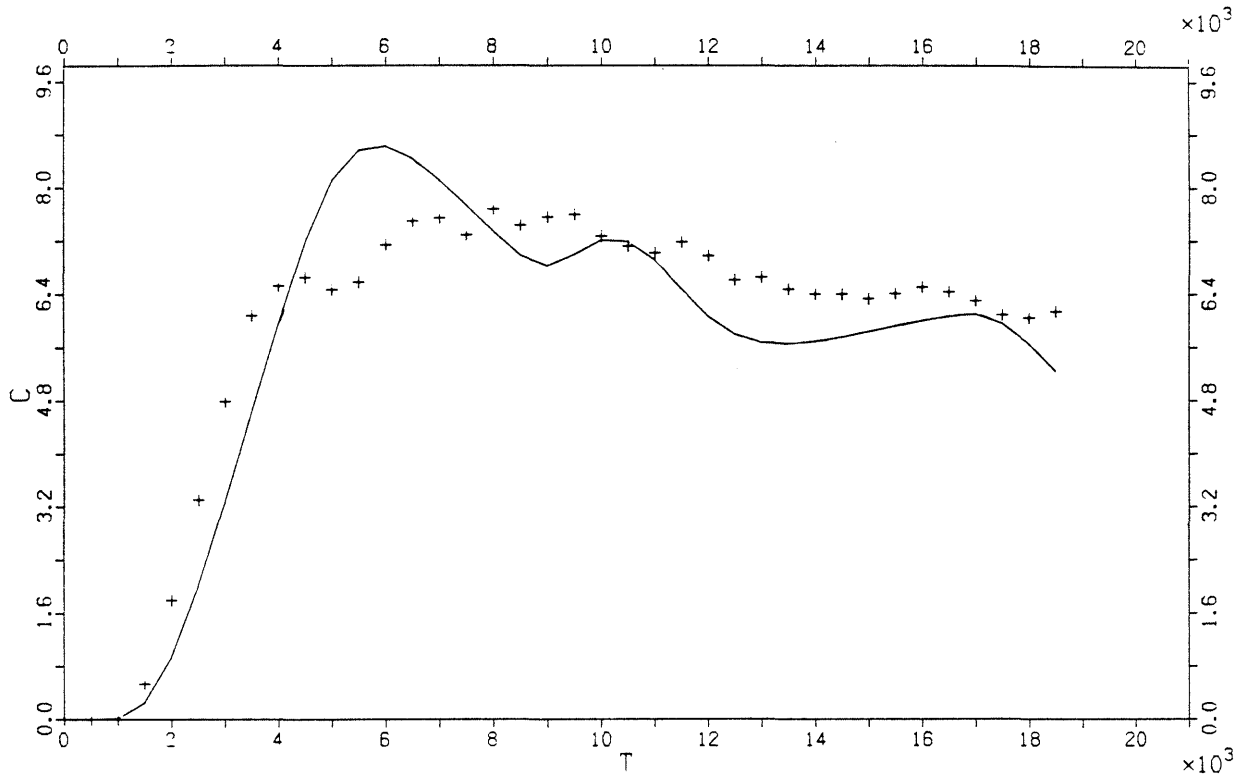
Sheet number 110 tracer Iodide, ADD-model

Pe = 34.5 Tw = 7030.0 A = 2.50E+07 Dil = 76.2 SD = .06



Tracer Eosin B, grouped sheets, AD-model

Pe = 4.0 Tw = 6338.0 DIL = 185.4 SD = .10 Section = 39 - 45



Tracer Eosin B, grouped sheets, AD-model

Pe = 4.0 Tw = 4481.0 DIL = 1067.6 SD = .46 Section = 25 - 35

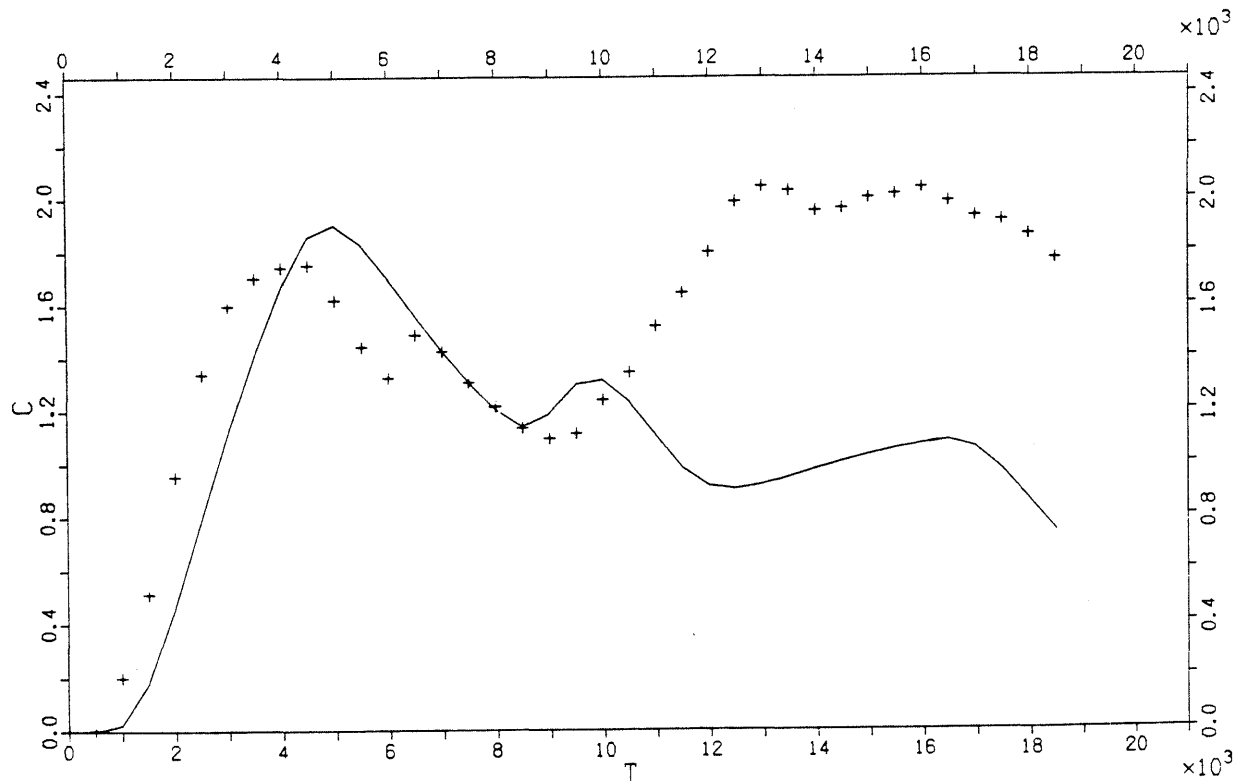
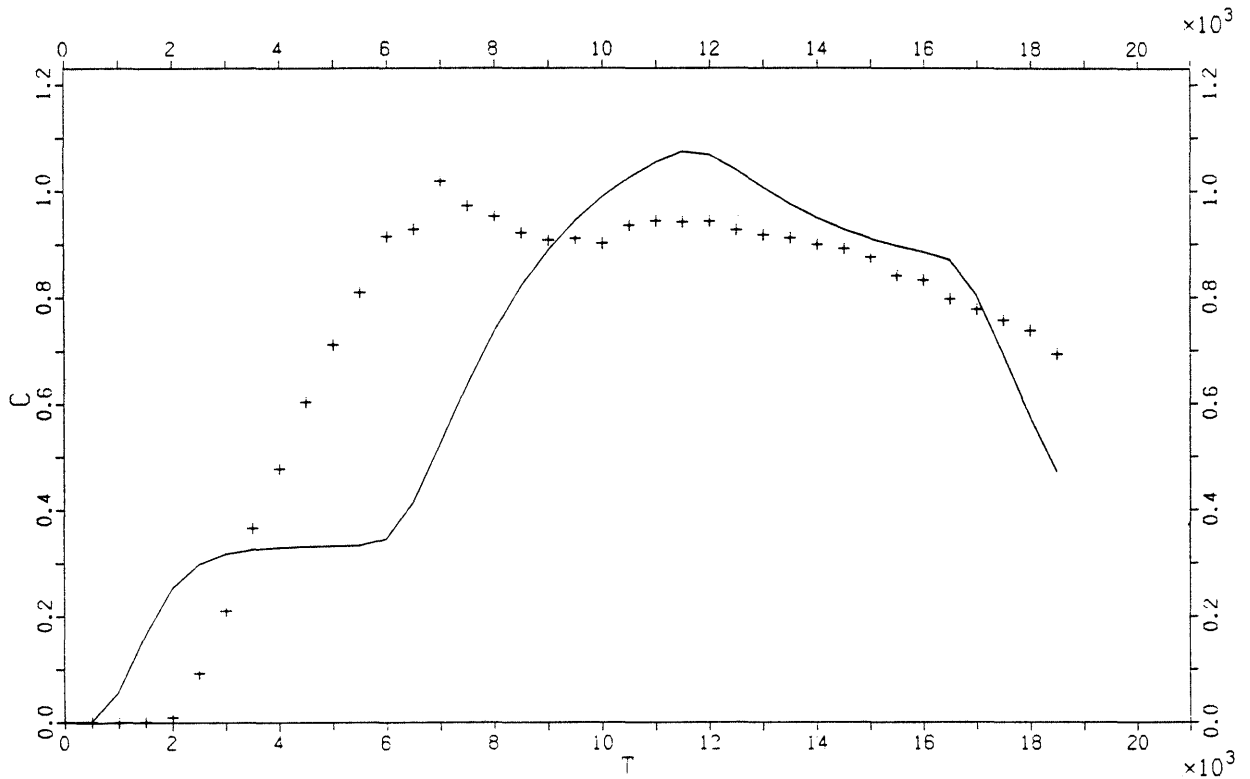


Figure A11-4. Model fits with AD-model, grouped sheets.

Tracer Uranine, grouped sheets, AD-model

Pe = 4.0 Tw = 3583.0 DIL = 1200.3 SD = .26 Section = 25 - 35



Tracer Uranine, grouped sheets, AD-model

Pe = 4.0 Tw = 4932.0 DIL = 2895.2 SD = .20 Section = 12 - 22

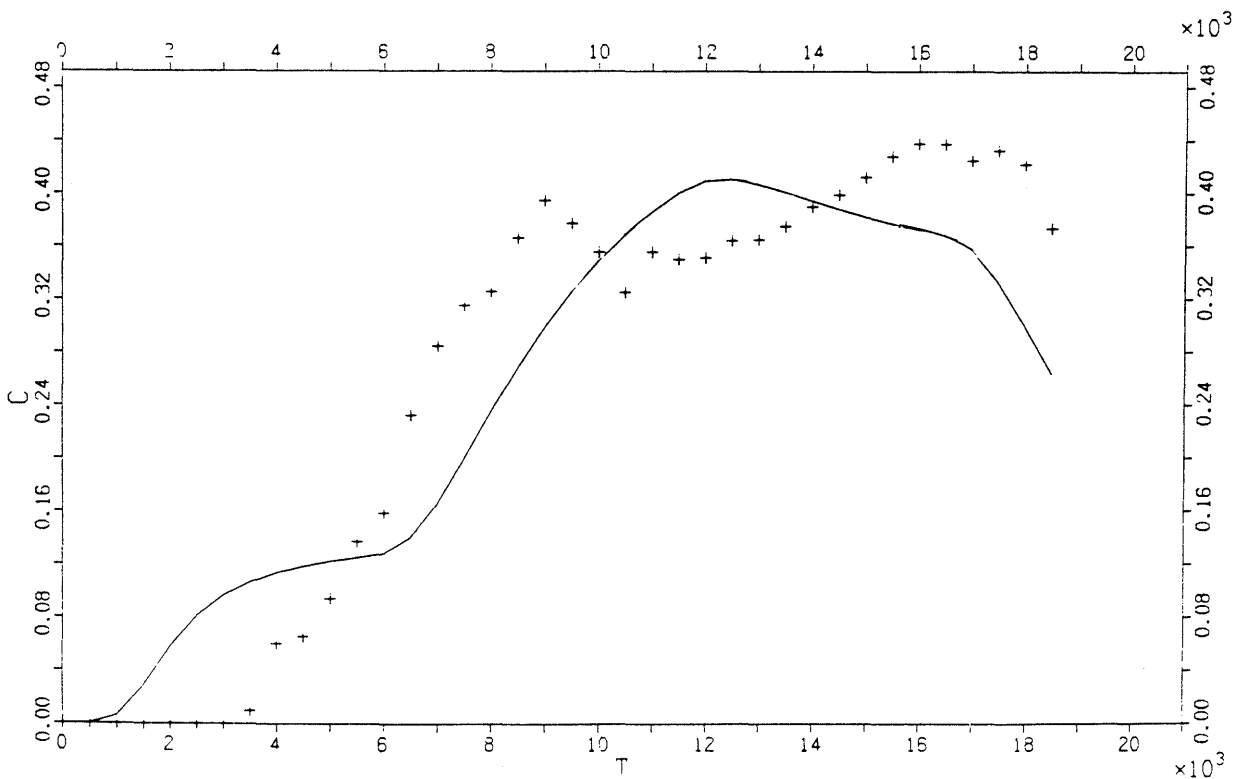
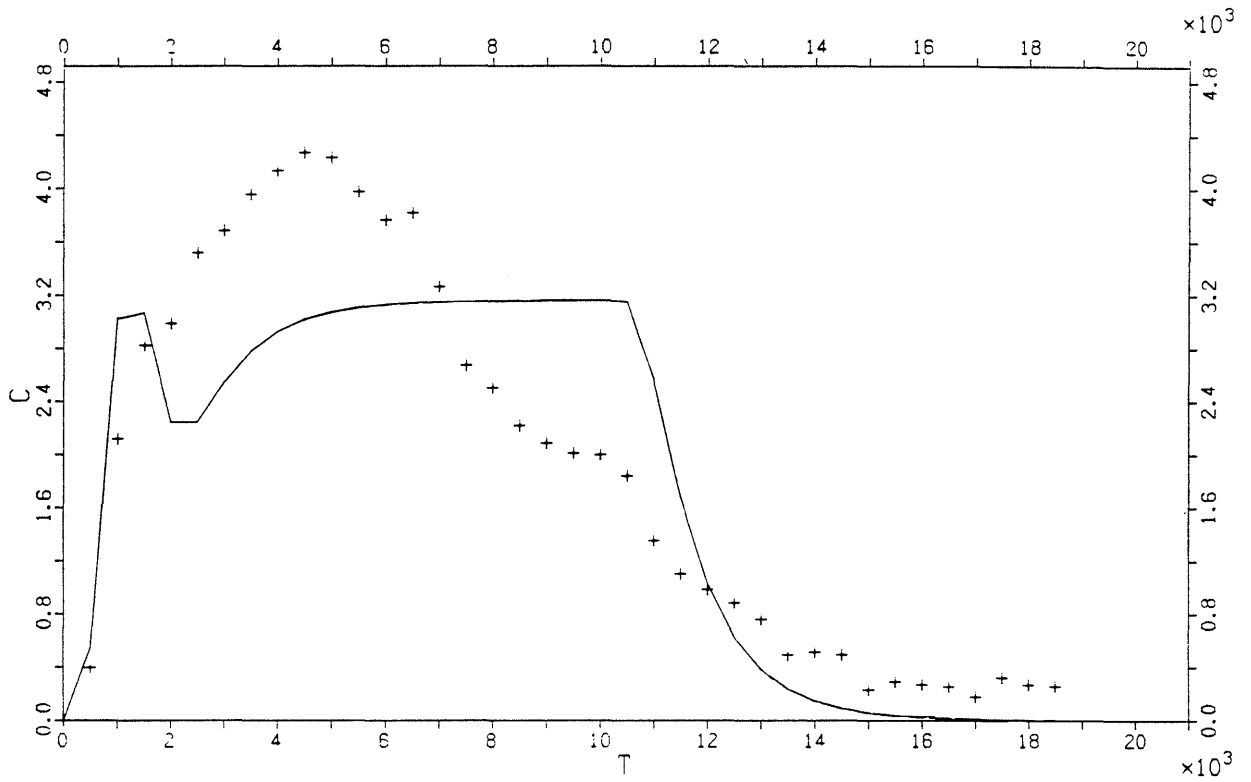


Figure A11-4. Continued.

Tracer Elbenyl, grouped sheets, AD-model

Pe = 4.8 Tw = 1658.0 DIL = 607.2 SD = .23 Section = 25 - 35



Tracer Eosin Y, grouped sheets, AD-model

Pe = 5.9 Tw = 6938.0 DIL = 153.4 SD = .07 Section = 25 - 35

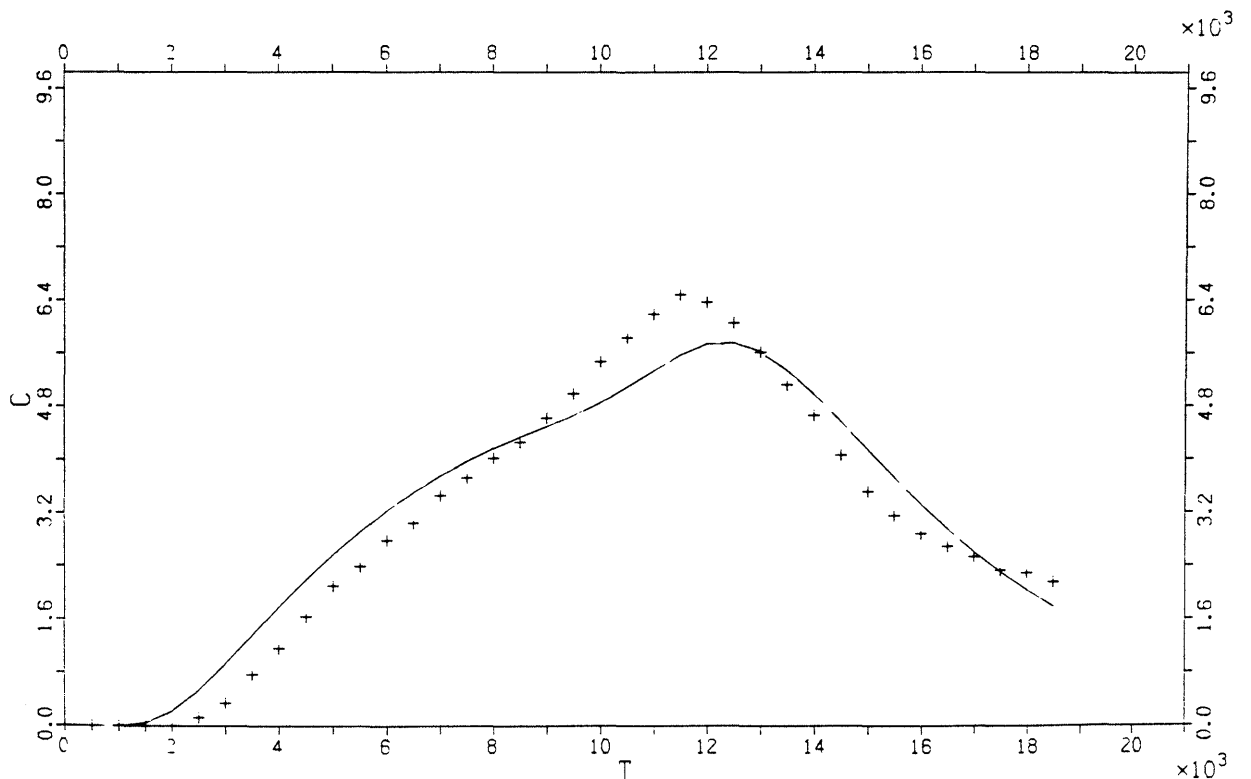
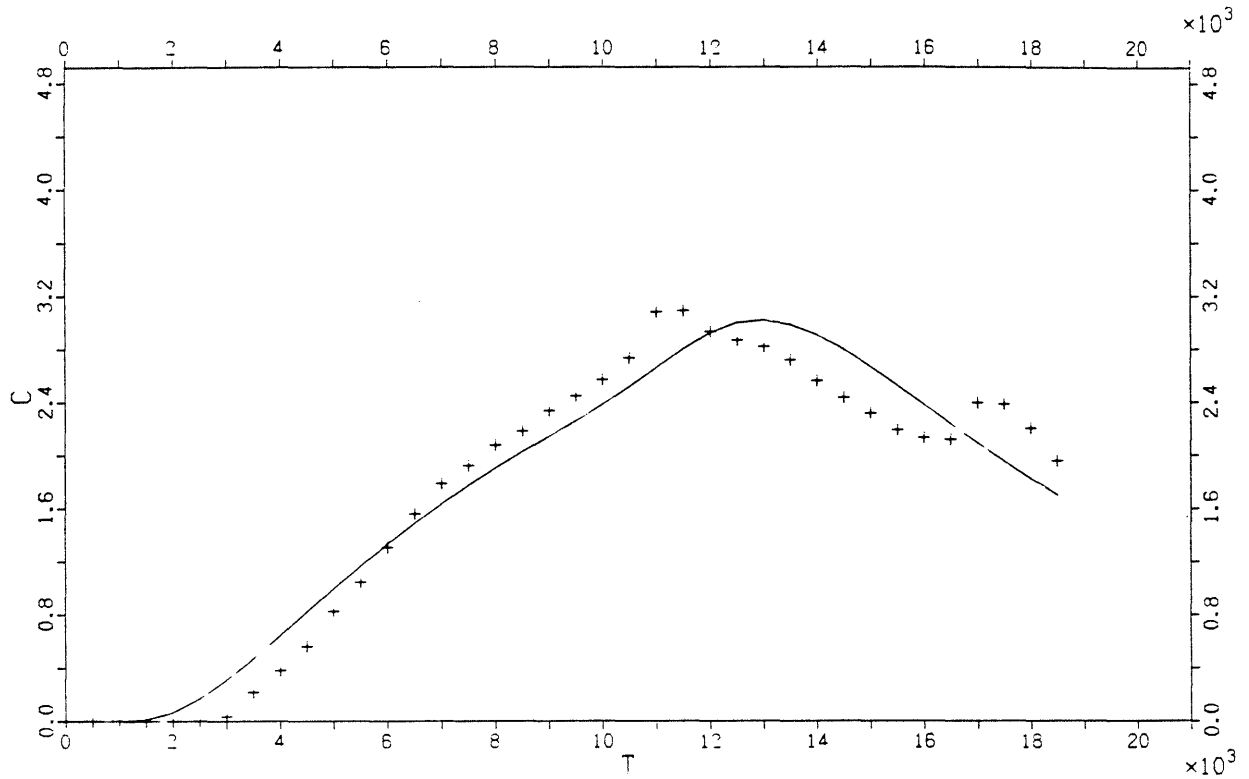


Figure A11-4. Continued.

Tracer Eosin Y, grouped sheets, AD-model

Pe = 4.0 Tw = 10320.0 DIL = 234.0 SD = .06 Section = 12 - 22



Tracer Iodide, grouped sheets, AD-model

Pe = 32.8 Tw = 7262.0 DIL = 118.31 SD = .05 Section = 25 - 35

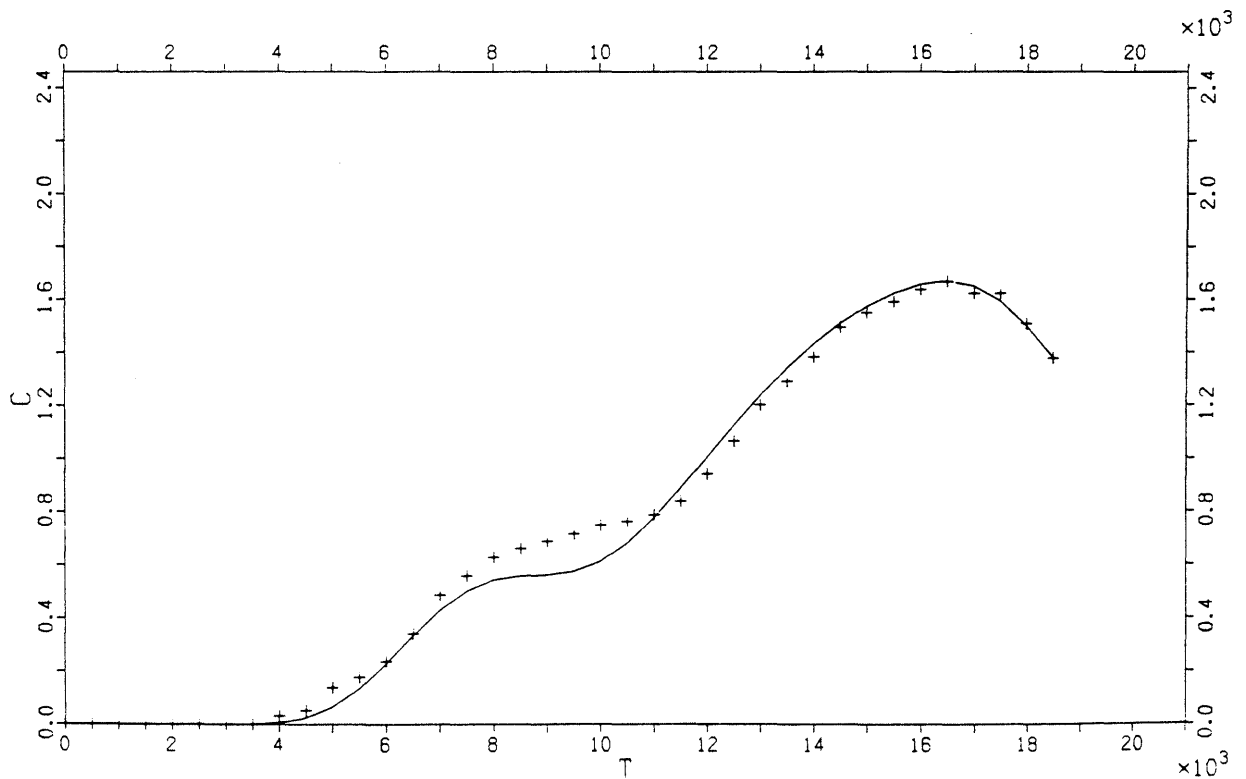


Figure A11-4. Continued.

Tracer Iodide, grouped sheets, AD-model

Pe = 4.0 Tw = 4544.0 DIL = 760.7 SD = .48 Section = 39 - 45

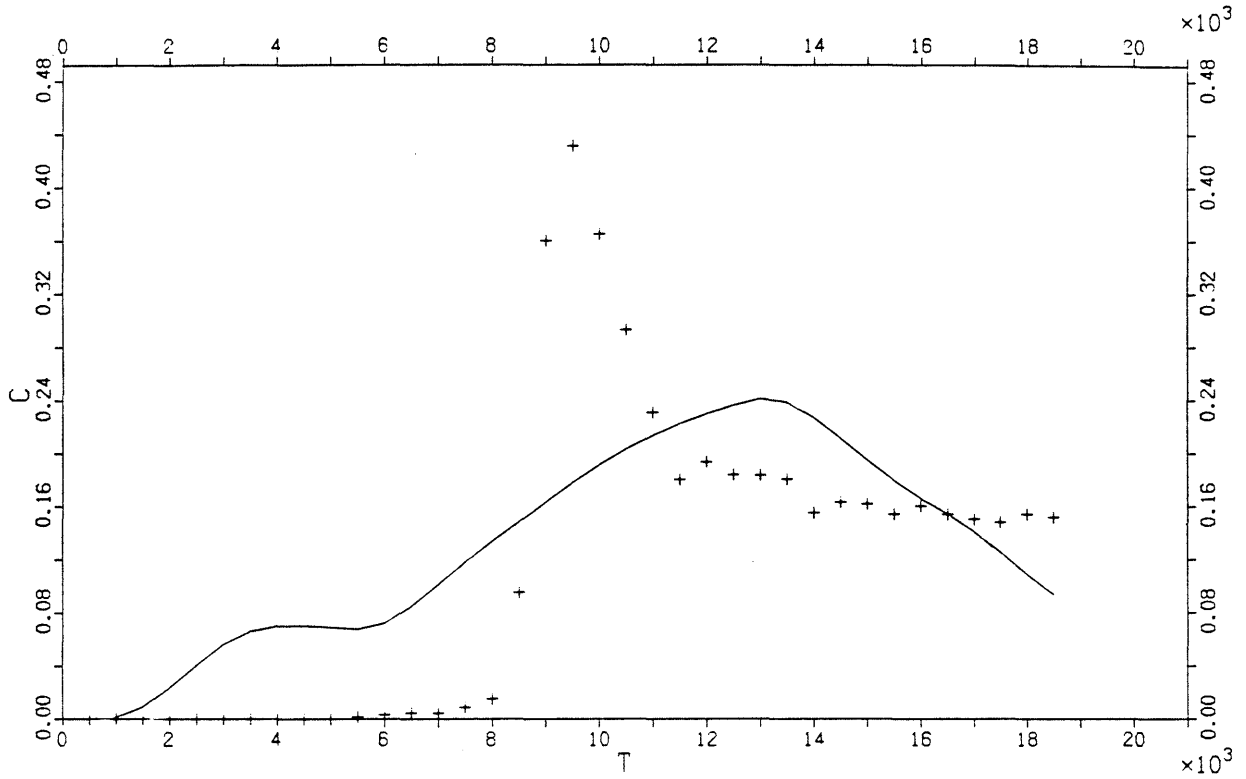
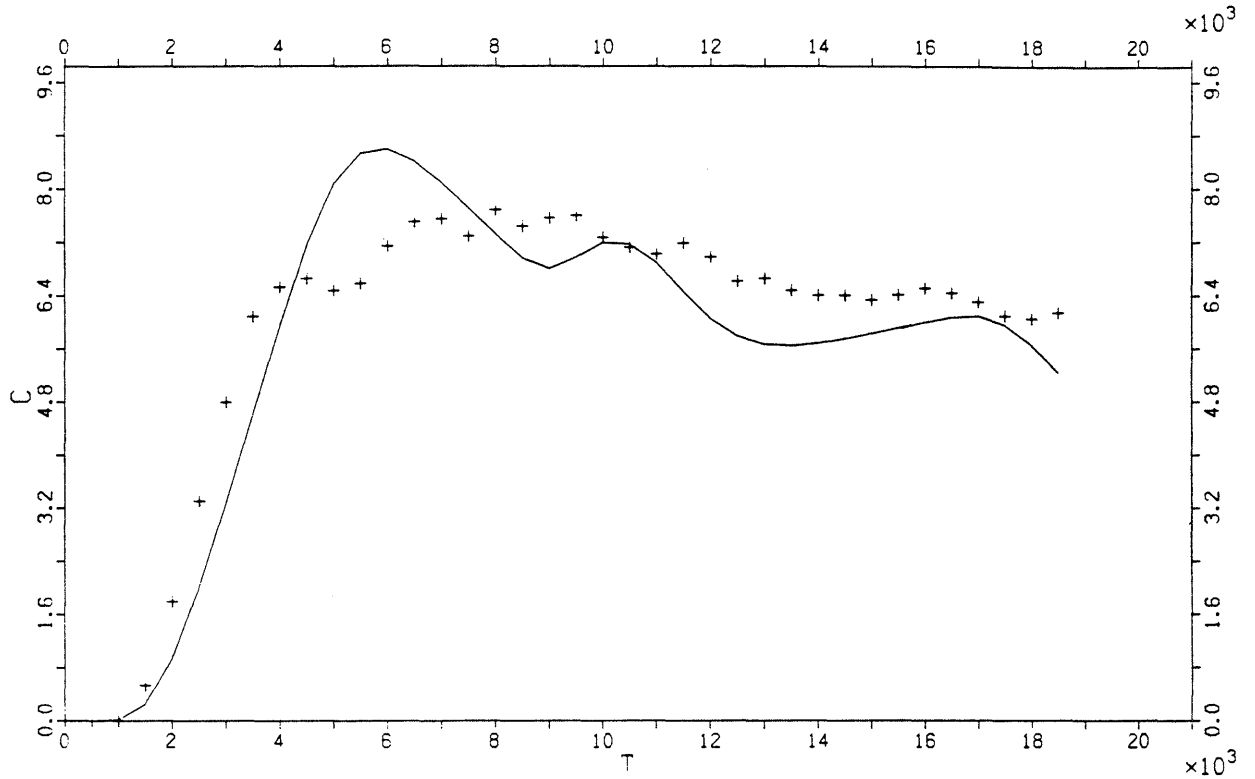


Figure A11-4. Continued.

Tracer Eosin B, grouped sheets, ADD-model

Pe = 4.0 Tw = 6338.0 A = .9917E+06 DIL = 185.37 SD = .10 Section = 39-45



Tracer Eosin B, grouped sheets, ADD-model

Pe = 4.0 Tw = 96.0 A = .1518E+02 DIL 106.46 SD = .03 Section = 25-35

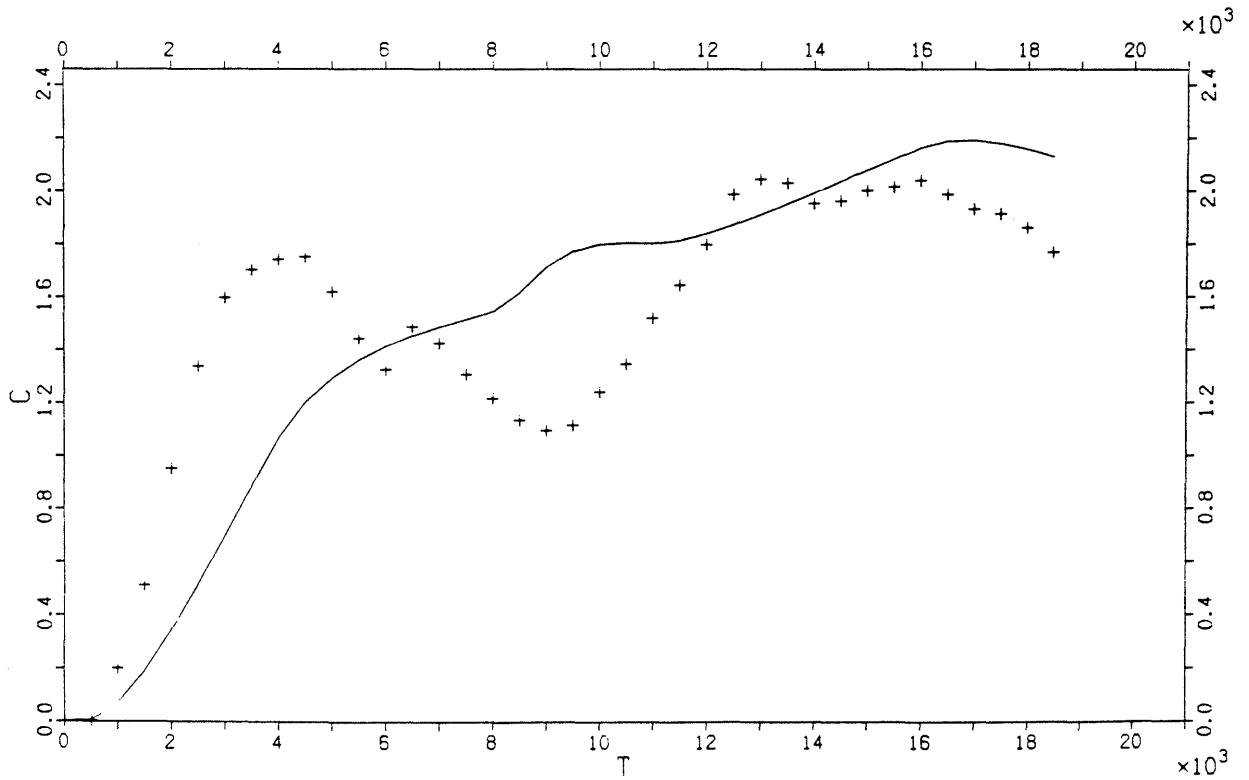
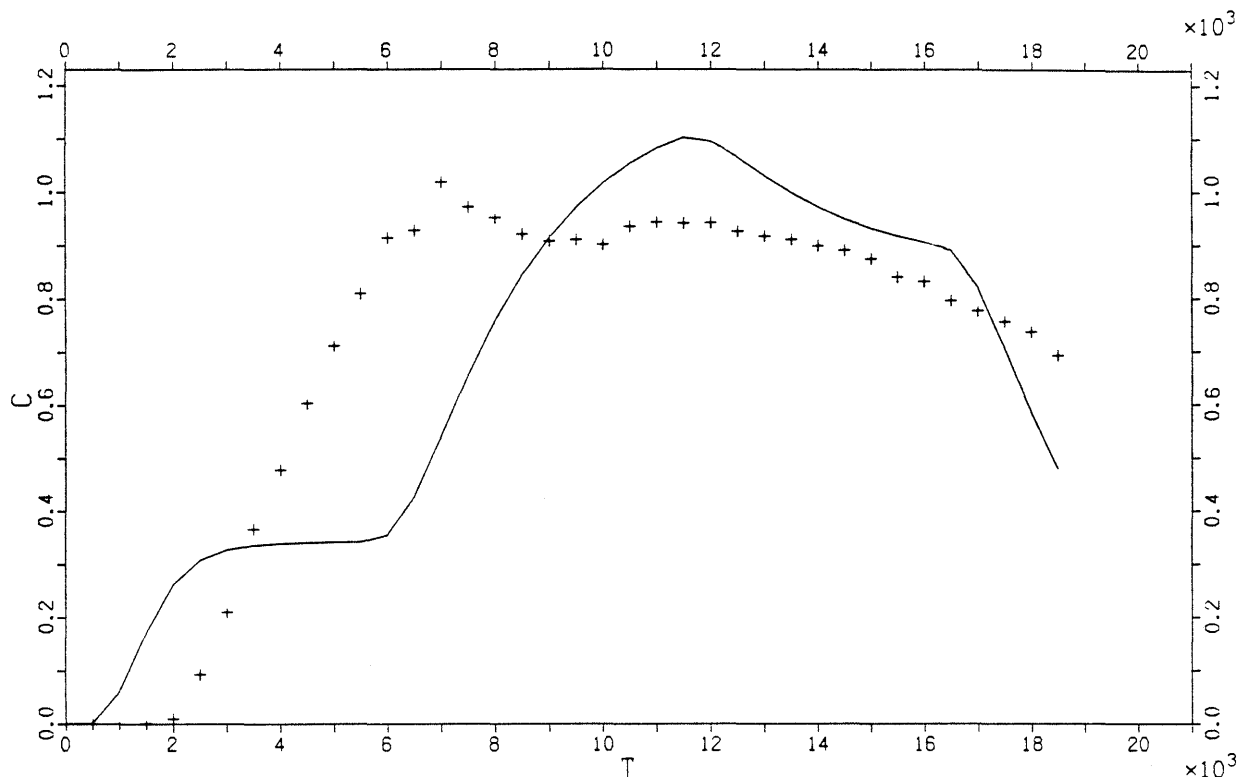


Figure A11-5. Model fits with ADD-model, grouped sheets.

Tracer Uranine, grouped sheets, ADD-model

Pe = 4.0 Tw = 3543.0 A = .4588E+06 DIL = 1168.36 SD = .26 Section = 25-35



Tracer Uranine, grouped sheets, ADD-model

Pe = 4.0 Tw = 4404.0 A = .5967E+04 DIL = 2096.00 SD = .13 Section = 12-22

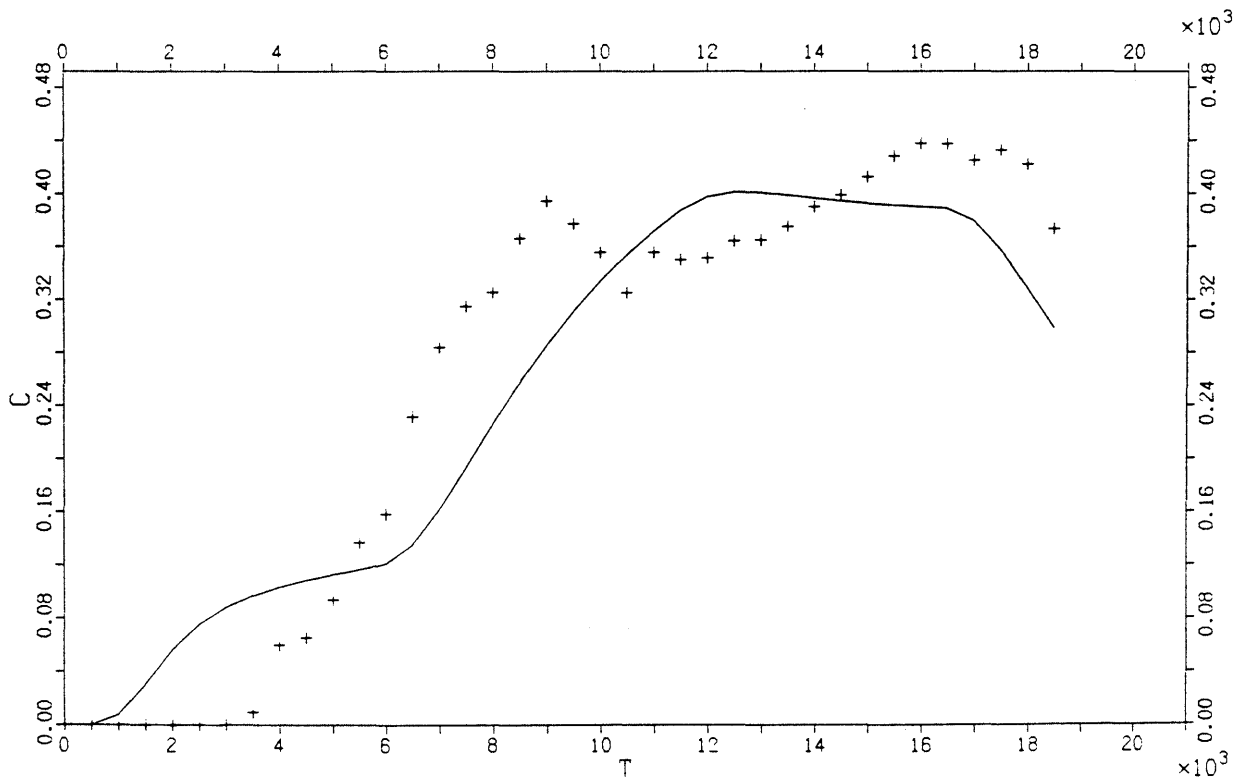
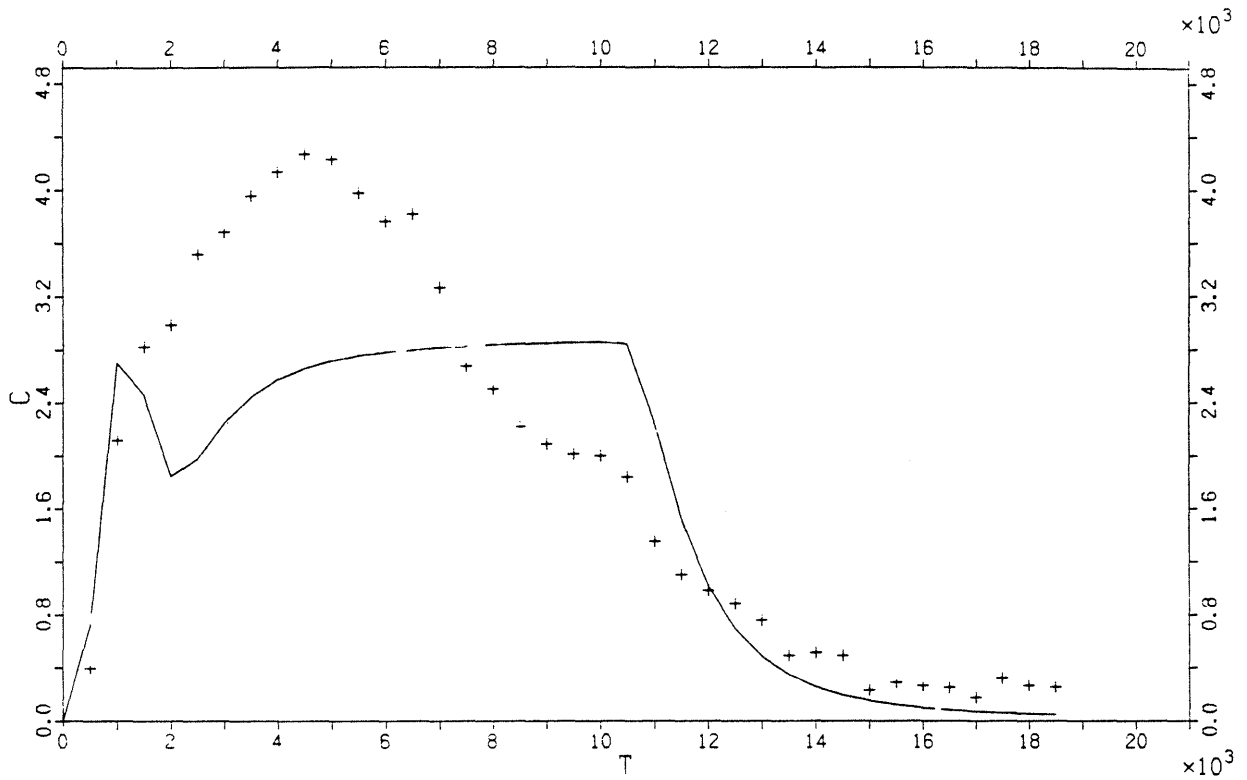


Figure A11-5. Continued.

Tracer Elbenyl, grouped sheets, ADD-model

Pe = 4.8 Tw = 1658.0 A = .4144E+08 DIL = 607.20 SD = .27 Section = 25-35



Tracer Eosin Y, grouped sheets, ADD-model

Pe = 5.9 Tw = 6938.0 A = .4817E+15 DIL = 153.44 SD = .07 Section = 25-35

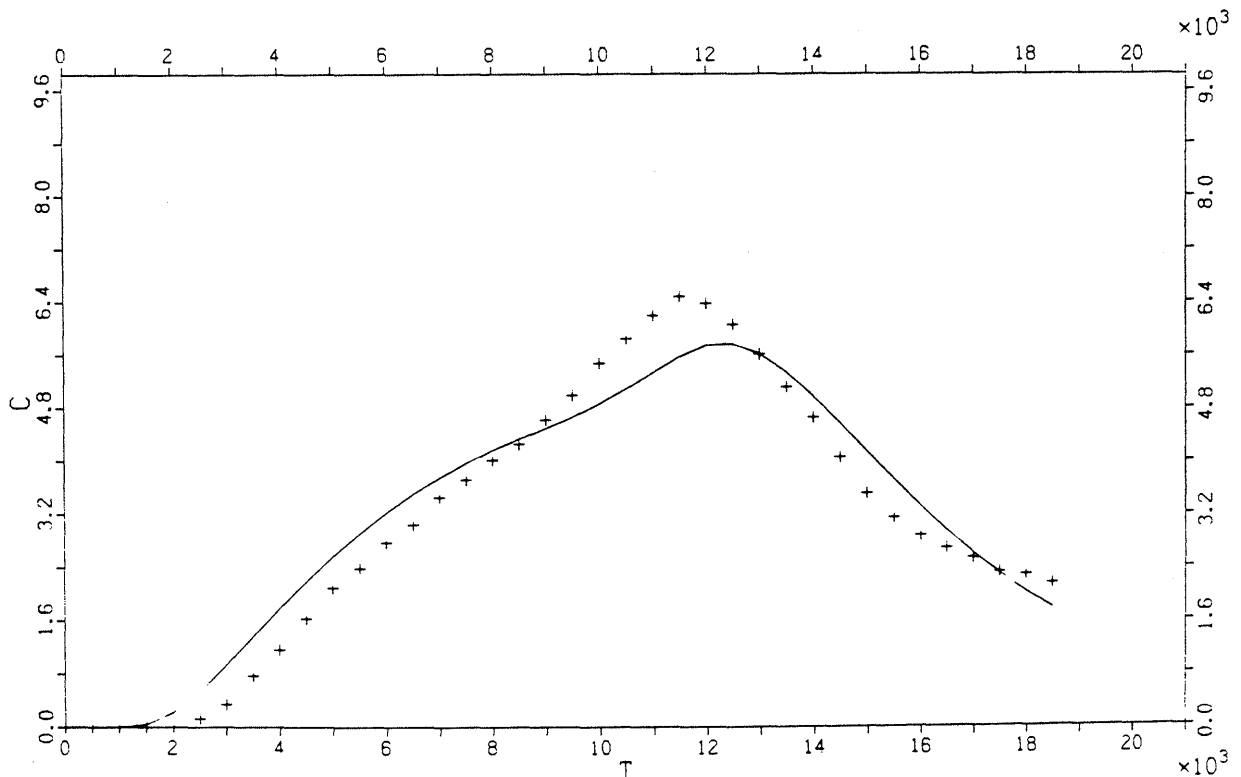
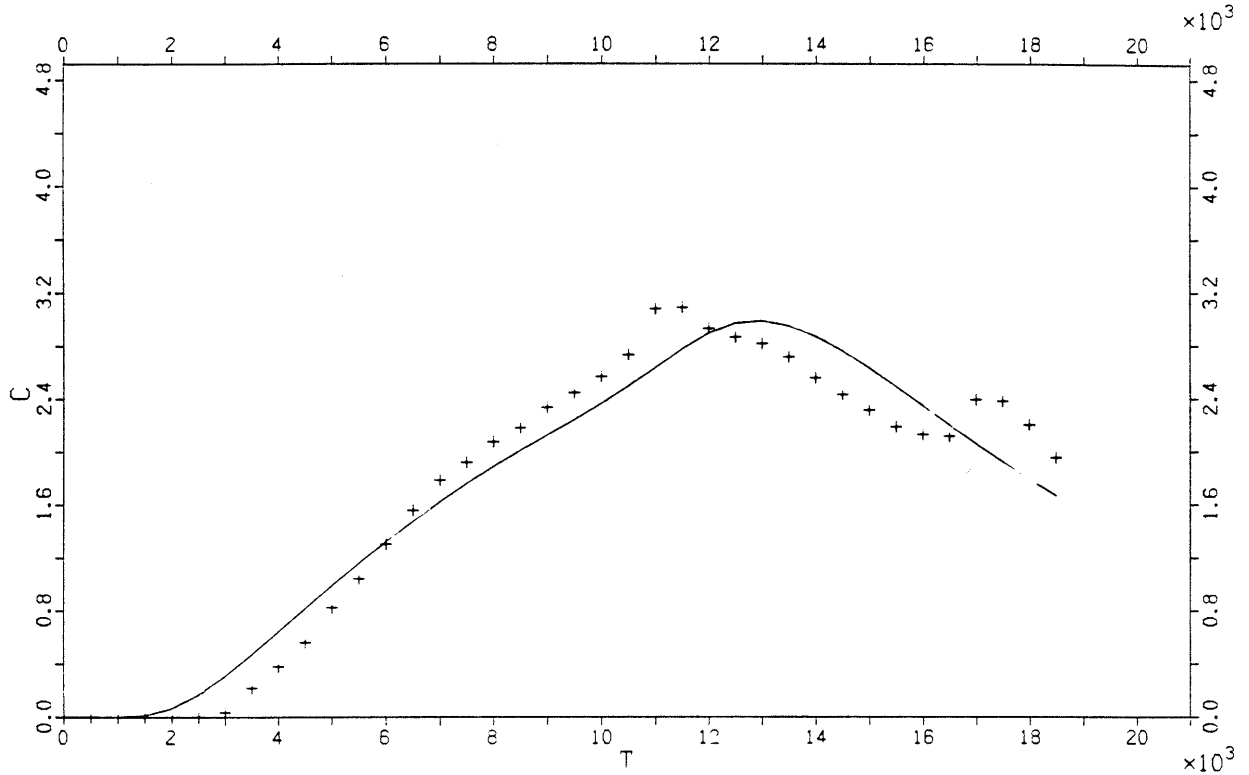


Figure A11-5. Continued.

Tracer Eosin Y, grouped sheets, ADD-model

Pe = 4.0 Tw = 10270.0 A = .2303E+07 DIL = 236.46 SD = .06 Section = 12-22



Tracer Iodide, grouped sheets, ADD-model

Pe = 32.9 Tw = 7262.0 A = .4141E+09 DIL = 118.29 SD = .05 Section = 25-35

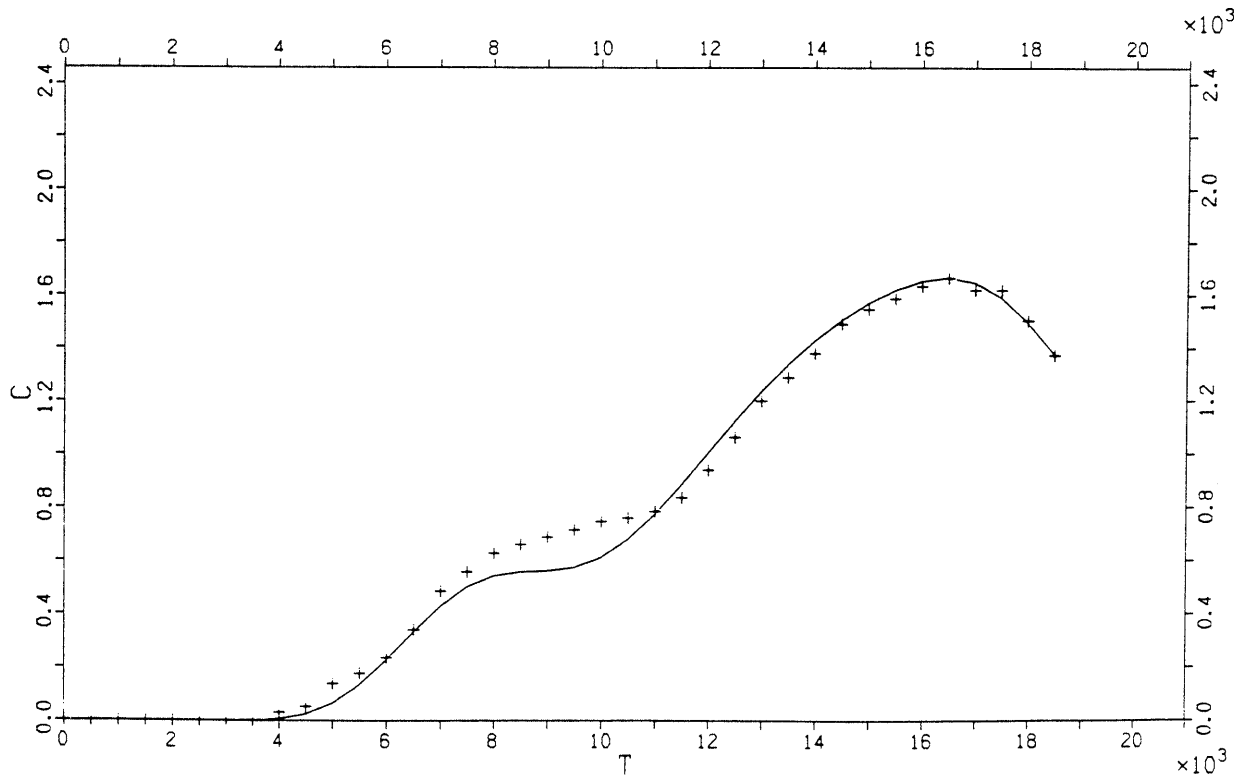


Figure A11-5. Continued.

Tracer Iodide, grouped sheets, ADD-model

Pe = 4.0 Tw = 1243.0 A = .5938E+03 DIL = 379.01 SD = .24 Section = 39-45

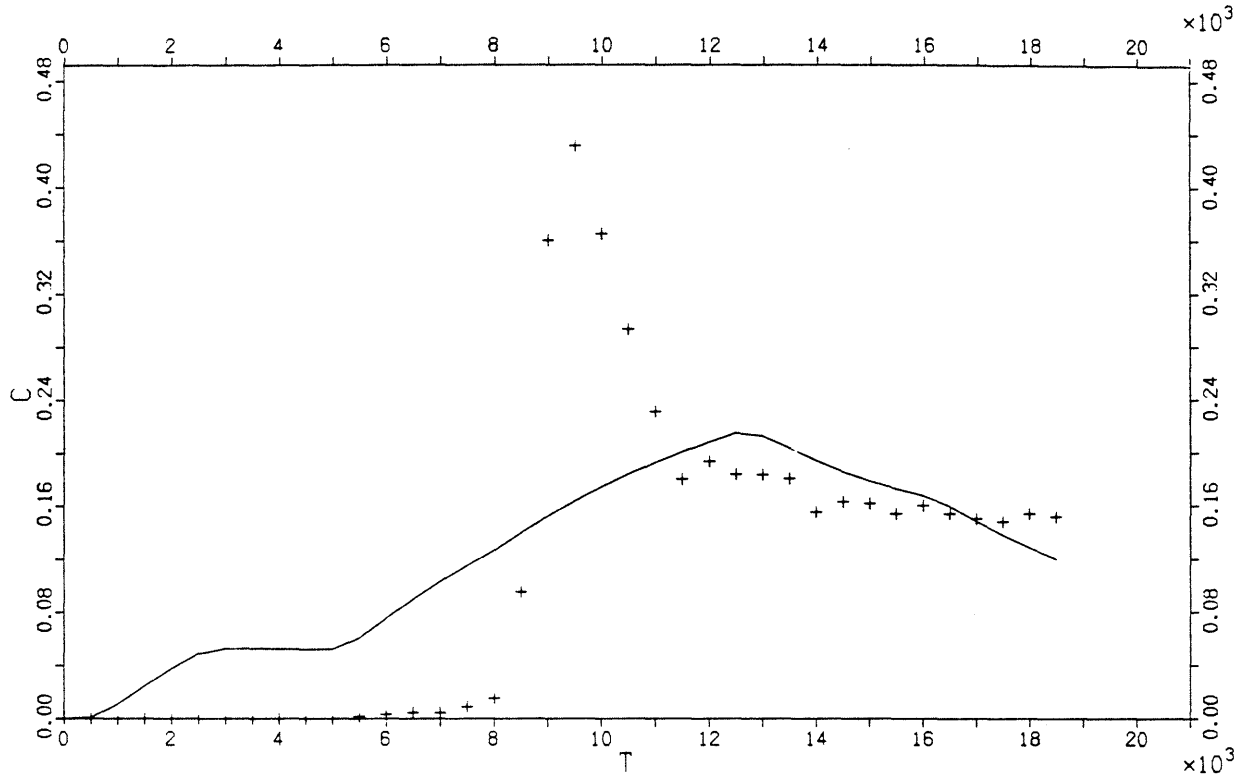
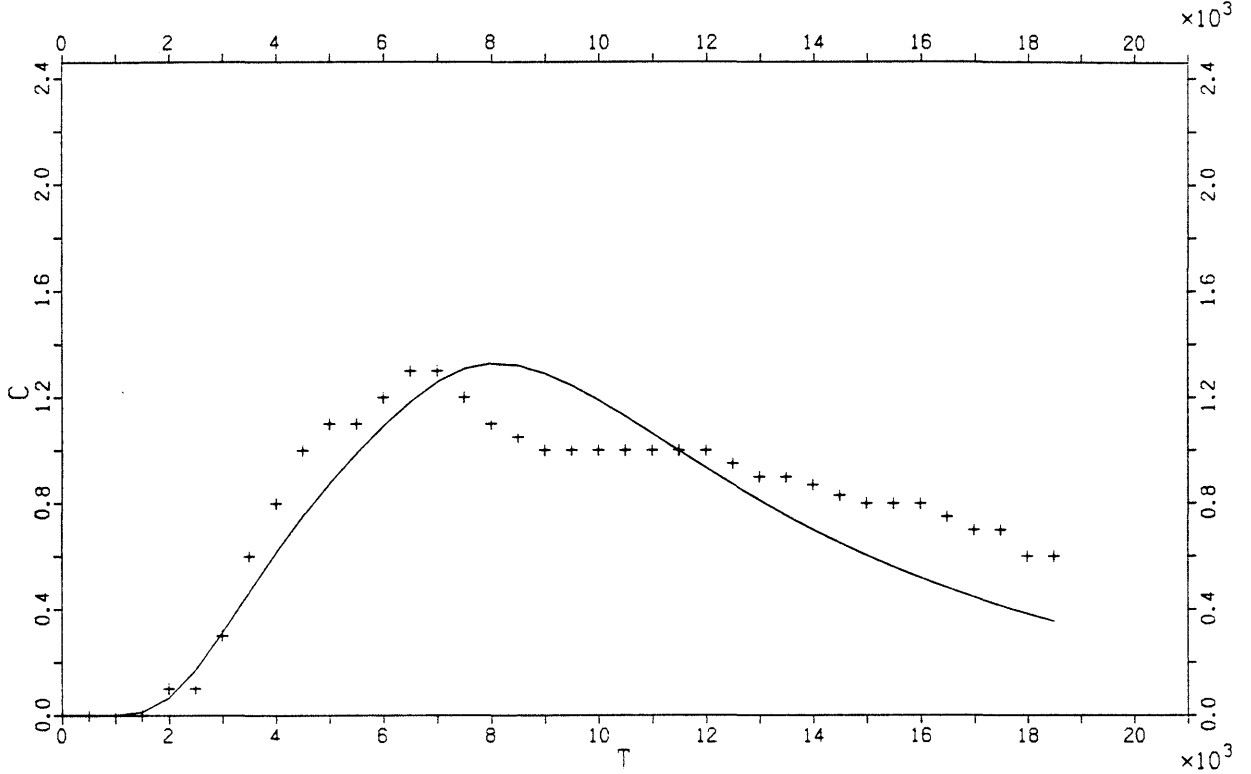


Figure A11-5.

Continued.

Uranine, truncated injection curve, AD-model

Sheet number = 64 Pe = 4.0 Tw = 10250.0 DIL = 328.19 SD = .058



Uranine, truncated injection curve, AD-model

Sheet number = 71 Pe = 4.0 Tw = 14170.0 DIL = 174.34 SD = .044

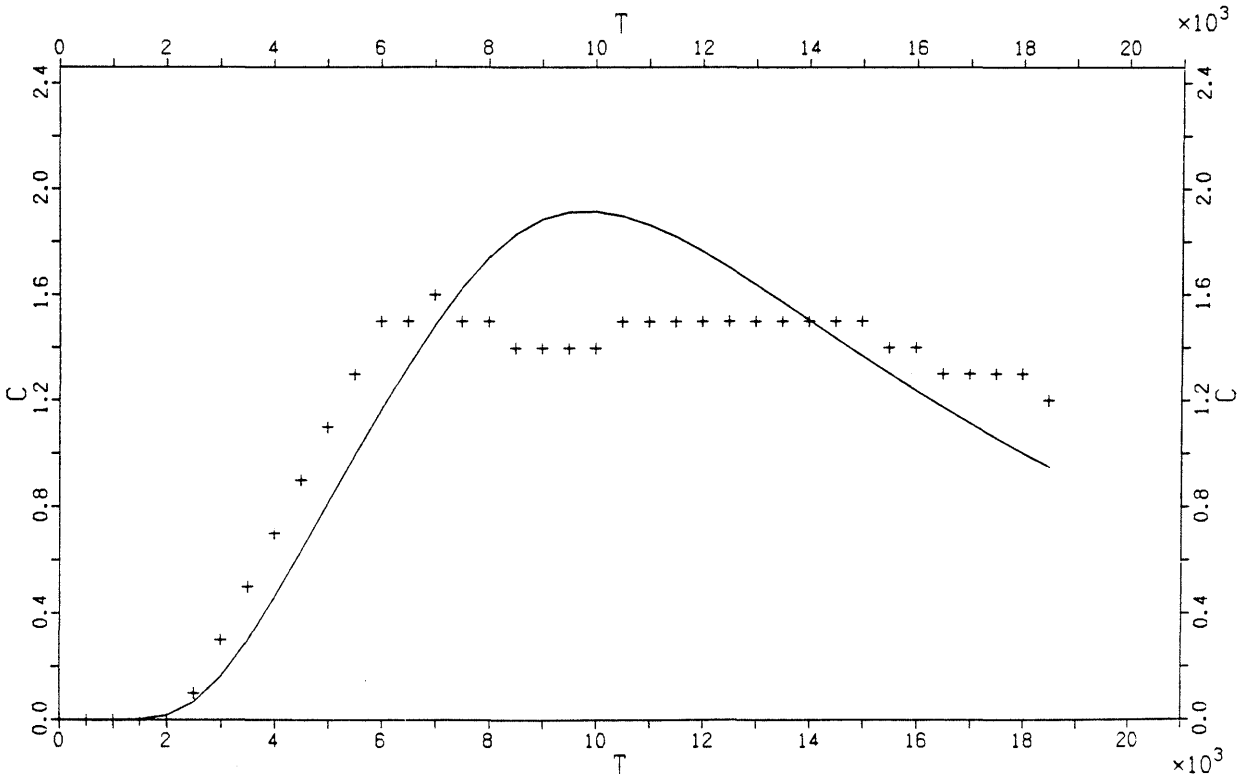
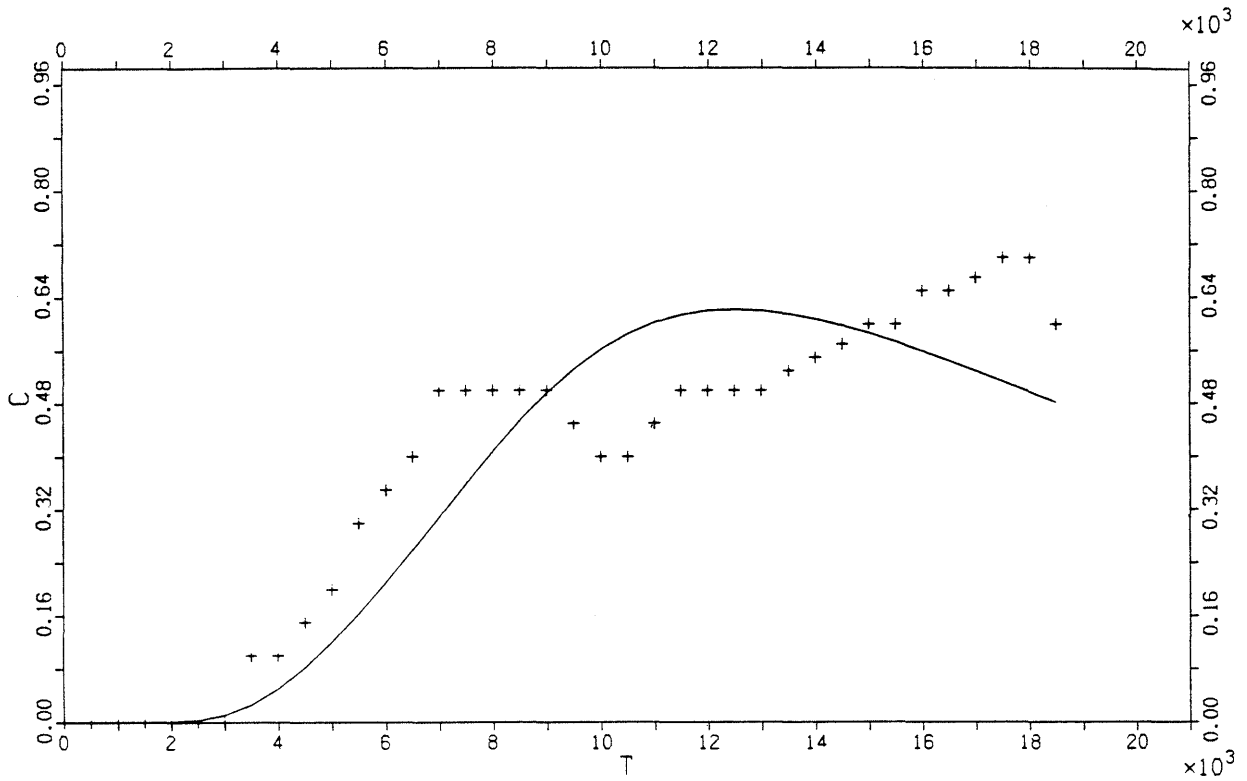


Figure A11-6. Model fits with AD-model for Uranine with truncated injection curve.

Uranine, truncated injection curve, AD-model

Sheet number = 90 Pe = 4.0 Tw = 19920.0 DIL = 395.26 SD = .043



Uranine, truncated injection curve, AD-model

Sheet number = 108 Pe = 4.0 Tw = 12880.0 DIL = 567.21 SD = .052

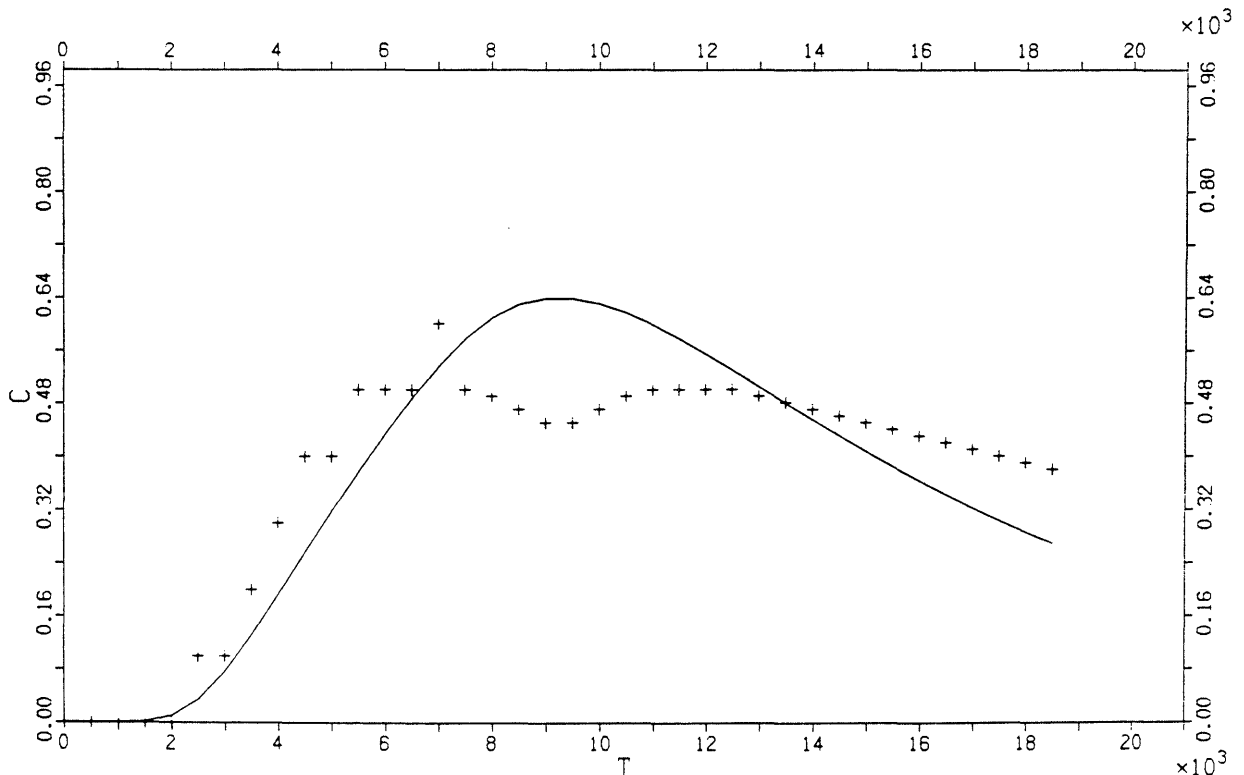


Figure A11-6. Continued.

Uranine, truncated injection curve, AD-model

Sheet number = 134 Pe = 7.1 Tw = 28520.0 DIL = 33.96 SD = .006

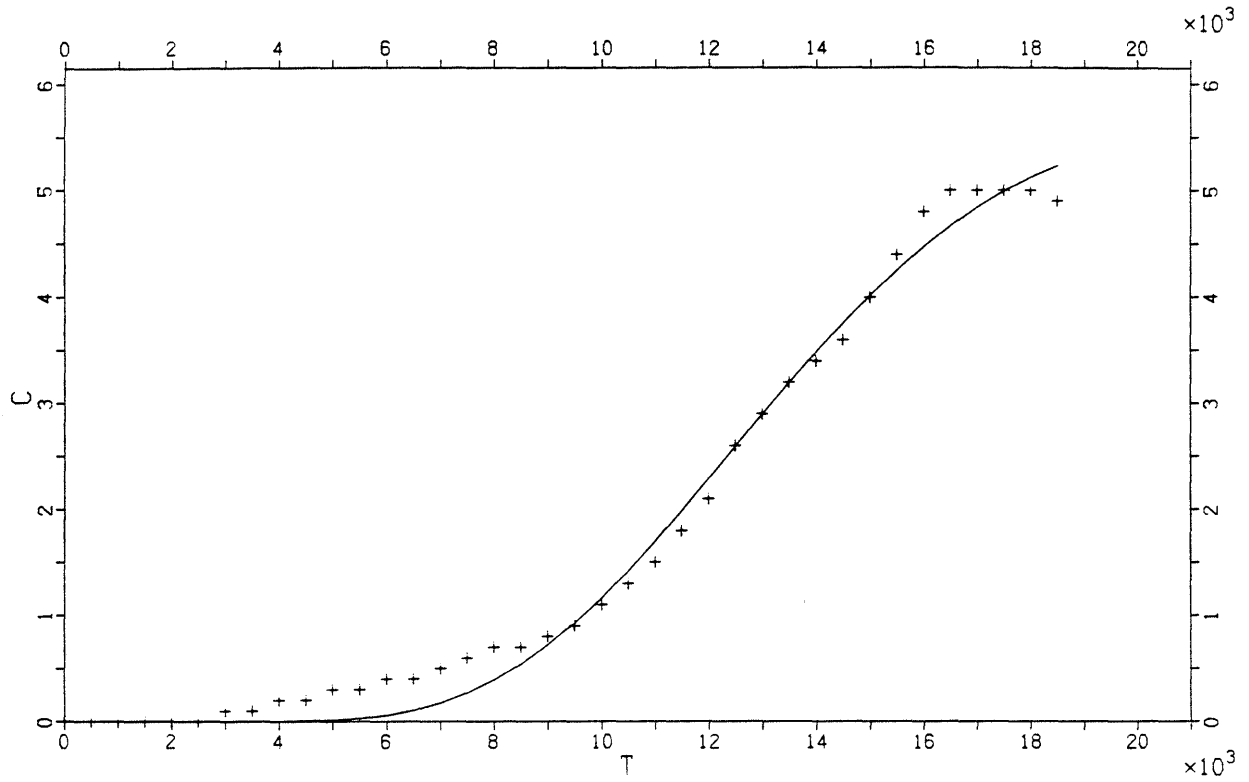


Figure A11-6. Continued.

RECOVERY OF TRACERS

The total amount of tracer which reached a given sheet, during the observation time (about 18,500 hours) was calculated. The results are shown for each tracer in Tables 12-1 - A12-7.

The recovery of the different tracer as a function of time is also shown in Table A12-8.

Table A12-1. TRACER: EOSIN B
Tracer recovered during the observation time, and
part of the total recovery

Number	recovered tracer, mg	Part of recovery
53	197.905	.043
54	18.515	.004
55	1.095	.000
56	.180	.000
57	94.965	.020
58	25.685	.006
59	73.755	.016
60	294.968	.063
61	443.135	.095
62	41.230	.009
63	5.180	.001
64	205.130	.044
65	140.615	.030
66	618.162	.133
67	26.098	.006
68	71.100	.015
69	57.910	.012
70	.800	.000
71	24.050	.005
72	5.160	.001
101	.120	.000
106	22.445	.005
108	756.650	.163
109	181.635	.039
110	72.818	.016
113	111.980	.024
114	5.000	.001
115	6.160	.001
118	79.500	.017
119	.235	.000
120	318.243	.068
121	5.510	.001
122	3.300	.001
174	62.095	.013
180	4.570	.001
181	463.020	.100
182	27.625	.006
184	43.470	.009
185	83.460	.018
186	32.795	.007
187	14.295	.003
200	9.505	.002
202	.018	.000

A12.3

Table A12-1 continued.

RECOVERED TRACER, mg	4650.087
INJECTED TRACER, mg	95 926
RECOVERY, %	4.85

Table A12-2. TRACER: URANINE
Tracer recovered during the observation time, and
part of the total recovery.

Number	recovered tracer, mg	Part of recovery
60	81.145	.038
61	29.185	.014
62	4.413	.002
64	67.641	.031
65	35.989	.017
66	71.268	.033
67	6.187	.003
68	253.670	.118
69	167.385	.078
70	6.418	.003
71	810.400	.377
72	58.360	.027
86	1.620	.001
87	5.418	.003
89	.265	.000
90	6.909	.003
91	.000	.000
92	3.605	.002
94	1.610	.001
95	1.225	.001
96	.872	.000
97	13.310	.006
98	5.215	.002
99	1.725	.001
101	.045	.000
102	22.610	.011
103	52.533	.024
104	.410	.000
106	5.535	.003
107	112.220	.052
108	188.665	.088
110	14.578	.007
111	.776	.000
113	.650	.000
114	.310	.000
134	45.758	.021
135	3.565	.002
174	1.630	.001
180	.285	.000
181	28.815	.013
182	1.835	.001
184	3.710	.002
185	6.545	.003

Table A12-2 continued.

186	11.265	.005
187	2.785	.001
202	.000	.000
205	.395	.000
206	13.355	.006

RECOVERED TRACER, mg	2152.110
INJECTED TRACER, mg	76 963
RECOVERY, %	2.80

A12.6

Table A12-3. TRACER: ELBENYL
Tracer recovered during the observation time, and
part of the total recovery.

Number	recovered tracer, mg	Part of recovery
59	148.455	.024
60	469.080	.077
61	361.680	.059
62	52.133	.009
63	5.540	.001
64	387.853	.063
65	302.153	.049
66	973.335	.159
67	92.510	.015
68	388.000	.063
69	271.438	.044
70	10.883	.002
71	871.200	.143
72	81.835	.013
103	89.298	.015
106	18.185	.003
107	103.660	.017
108	1044.170	.171
109	158.840	.026
110	42.883	.007
113	54.200	.009
115	3.565	.001
174	107.165	.018
180	8.525	.001
184	32.640	.005
186	19.910	.003
187	14.400	.002
RECOVERED TRACER, mg	6113.536	
INJECTED TRACER, mg	9 293	
RECOVERY, %	65.78	

Table A12-4. TRACER: EOSIN Y
Tracer recovered during the observation time, and
part of the total recovery.

Number	recovered tracer, mg	Part of recovery
60	375.348	.039
61	74.402	.008
62	24.045	.003
63	1.655	.000
64	349.320	.036
65	172.860	.018
66	354.303	.037
67	19.349	.002
68	1114.220	.116
69	680.805	.071
70	20.360	.002
71	3536.850	.369
72	237.868	.025
85	277.820	.029
86	33.080	.003
87	84.925	.009
89	3.950	.000
90	107.945	.011
91	10.665	.001
92	34.025	.004
94	43.228	.005
95	16.968	.002
96	3.170	.000
97	50.925	.005
98	19.540	.002
99	5.535	.001
101	.355	.000
102	97.750	.010
103	247.243	.026
104	2.325	.000
106	29.750	.003
107	481.830	.050
108	887.200	.093
110	64.782	.007
111	3.128	.000
112	.705	.000
113	10.100	.001
114	2.785	.000
115	.710	.000
172	.000	.000
174	7.515	.001
180	.760	.000
184	13.320	.001

Table A12-4 continued.

185	9.640	.001
186	51.390	.005
187	13.840	.001
205	4.040	.000

RECOVERED TRACER, mg	9582.329
INJECTED TRACER, mg	28 058
RECOVERY, %	34.15

Table A12-5. TRACER: DUASYN
Tracer recovered during the observation time, and part of the total recovery.

Number	recovered tracer, mg	Part of recovery
69	.618	.093
70	.338	.051
72	1.823	.273
84	.000	.000
85	.000	.000
86	.000	.000
91	1.610	.241
96	.008	.001
97	1.238	.186
103	.533	.080
159	.500	.075
RECOVERED TRACER, mg		6.668
INJECTED TRACER, mg		303 640
RECOVERY, %		0.002

Table A12-6. TRACER: IODIDE
Tracer recovered during the observation time, and
part of the total recovery.

Number	recovered tracer, mMol	Part of recovery
53	.194	.001
54	.033	.000
55	.008	.000
56	.002	.000
57	.216	.001
58	.085	.000
59	1.161	.005
60	9.072	.040
61	7.561	.034
62	1.695	.008
63	.021	.000
64	8.141	.036
65	8.356	.037
66	18.884	.084
67	.216	.001
68	11.205	.050
69	9.055	.040
70	.245	.001
71	35.385	.157
72	2.841	.013
90	.011	.000
91	.423	.002
96	.065	.000
97	.336	.001
98	.527	.002
99	.227	.001
101	.019	.000
102	5.880	.026
103	12.300	.055
104	.110	.000
106	2.158	.010
107	3.801	.017
108	53.445	.237
109	6.691	.030
110	5.839	.026
111	.242	.001
112	.057	.000
113	3.800	.017
114	1.005	.004
115	.198	.001
116	.006	.000
118	.217	.001
120	.688	.003
122	.031	.000
159	.100	.000
174	1.903	.008

A12.11

Table A12-6 continued.

177	.040	.000
178	.025	.000
180	.021	.000
181	6.102	.027
182	.386	.002
184	.937	.004
185	1.651	.007
186	1.316	.006
187	.320	.001
200	.046	.000

RECOVERED TRACER, mMol	225.299
INJECTED TRACER, mMol	1,816
RECOVERY, %	12.39

Table A12-7. TRACER: BROMIDE
Tracer recovered during the observation time, and
part of the total recovery.

Number	recovered tracer, mMol	Part of recovery
53	11.762	.008
54	9.647	.007
55	1.584	.001
56	.171	.000
57	14.117	.010
58	2.809	.002
59	9.859	.007
60	67.084	.045
61	66.819	.045
62	9.531	.006
63	.372	.000
64	46.903	.032
65	41.586	.028
66	117.887	.079
67	6.084	.004
68	82.487	.056
69	56.293	.038
70	2.217	.001
71	186.050	.125
72	15.104	.010
79	.103	.000
80	.657	.000
82	1.126	.001
87	1.506	.001
90	1.399	.001
91	5.621	.004
96	.390	.000
97	2.794	.002
98	3.152	.002
99	.964	.001
101	.118	.000
102	26.951	.018
103	55.711	.038
104	1.141	.001
106	10.165	.007
107	22.766	.015
108	261.183	.176
109	43.050	.029
110	25.451	.017
111	2.967	.002
112	1.646	.001
113	19.384	.013
114	2.544	.002
115	1.913	.001
116	.446	.000
118	9.192	.006
119	.160	.000

Table 12-7 continued.

120	38.671	.026
122	2.534	.002
127	2.836	.002
144	110.400	.074
159	.710	.000
174	13.510	.009
177	1.892	.001
178	1.065	.001
180	.627	.000
181	34.745	.023
182	2.231	.002
184	6.454	.004
185	8.187	.006
186	6.327	.004
187	1.704	.001
200	.560	.000
<hr/>		
RECOVERED TRACER, mMol	1483.319	
INJECTED TRACER, mMol	966	
RECOVERY, %	153.52	
<hr/>		
RECOVERED TRACER CALCULATED SUBTRACTING BACKGROUND VALUE (0.05 mM)	1259.475	
RECOVERY, %	130.33	
<hr/>		

A12.14

Table A12-8. Tracer recovery as a function of time.

Time (h)*	Tracer number							
	1 Eosin B	2 Uranine	3 Elbenyl	6 Eosin Y	7 Duasyn	8 Iodide	9 Bromide	
1	.00	.00	.00	.00	.00	.00	.00	.00
2	.12	.00	12.24	.00	.00	.00	.00	2.73
3	6.64	.00	96.53	.00	.00	.00	.00	6.51
4	31.18	.04	270.95	.00	.00	.00	.00	13.72
5	85.26	.46	484.40	.00	.00	.00	.00	27.09
6	173.25	4.43	727.84	4.89	.00	.00	.00	47.25
7	288.40	16.21	998.35	23.11	.00	.00	.00	73.90
8	417.50	38.13	1280.10	66.31	.00	.00	.00	106.41
9	546.19	68.70	1563.54	138.49	.00	.11	.11	142.66
10	671.72	106.57	1847.26	240.01	.00	.42	.42	181.50
11	796.02	153.40	2139.78	378.54	.00	1.12	1.12	221.80
12	916.71	209.81	2434.82	552.60	.00	2.32	2.32	261.34
13	1033.50	275.85	2723.41	760.45	.00	3.94	3.94	299.87
14	1158.25	349.00	3013.83	1001.67	.00	6.29	6.29	339.90
15	1291.27	428.14	3288.80	1275.36	.00	9.69	9.69	382.75
16	1417.11	508.39	3531.41	1575.13	.00	13.95	13.95	424.76
17	1531.46	584.24	3751.35	1891.36	.00	18.67	18.67	463.25
18	1635.68	656.10	3947.74	2220.61	.00	23.67	23.67	498.82
19	1734.29	725.71	4128.78	2570.86	.00	28.91	28.91	533.89
20	1832.69	795.97	4303.26	2955.37	.00	34.47	34.47	570.85
21	1938.65	867.70	4479.02	3382.62	.00	40.40	40.40	611.03
22	2056.83	942.10	4657.64	3851.94	.00	46.65	46.65	653.75
23	2189.22	1019.83	4821.33	4359.42	.00	53.17	53.17	697.24
24	2339.79	1099.79	4962.99	4902.65	.00	60.16	60.16	741.55
25	2500.39	1180.29	5090.63	5451.47	.00	67.85	67.85	786.76
26	2664.71	1259.90	5207.73	5970.72	.00	76.44	76.44	833.45
27	2831.97	1337.45	5314.22	6444.49	.00	85.95	85.95	881.67
28	3001.43	1414.63	5407.58	6879.09	.00	96.39	96.39	932.62
29	3174.37	1494.70	5498.13	7291.55	.00	108.06	108.06	988.48
30	3352.02	1578.16	5594.36	7676.94	.00	121.16	121.16	1050.10
31	3536.87	1663.35	5682.60	8024.76	.16	135.45	135.45	1116.52
32	3723.27	1746.02	5760.13	8334.10	.70	150.13	150.13	1183.15
33	3904.36	1823.56	5833.57	8605.10	1.49	164.51	164.51	1245.27
34	4075.85	1895.45	5901.67	8844.23	2.33	178.42	178.42	1301.03
35	4236.70	1965.06	5962.89	9062.66	3.16	191.73	191.73	1351.37
36	4389.18	2033.49	6018.91	9260.57	4.06	204.41	204.41	1398.54
37	4530.05	2097.08	6070.35	9435.47	5.31	215.90	215.90	1443.37
38	4650.08	2152.10	6113.53	9582.32	6.66	225.28	225.28	1483.30

* Time = multiply by 500 hours

RESULTS FROM FIT WITH TRUNCATED INJECTION CURVES
FOR URANINE

The injection of Uranine was changed after approximately 5000 h to a mixture of Uranine, Fluoride, and the large molecular tracer STR-7. The Fluoride and STR-7 were not detected during the time of the experiment. A possible explanation for this is, that by some reason, the flowpaths changed in such a way that the tracers were transported in another direction than before the change of the composition of the injection flow. This is indicated by the fact that if the injection of Uranine that was made after 5240 hours is not accounted for, the fittings are much better than if all the injection is used. The results are shown in Tables A13-1 and A13-2. These tables should be compared with Tables 12-2a and A12-8a.

Table A13-1. Results obtained using the Advection-Dispersion model. The condition that the Peclet number greater than 4.0 is imposed and only the tracer injected before 5240 h is taken into account.

Tracer: Uranine

Number	Peclet number	Residence time hours	Dilution factor	Standard deviation
642	4.0	10250.0	328.19	.058
712	4.0	14170.0	174.34	.044
902	4.0	19920.0	395.26	.043
1082	4.0	12880.0	567.21	.052
1342	7.1	28520.0	33.96	.006

Table 13-2. Results obtained using the Advection-Dispersion model. The condition that the Peclet number greater than 4.0 is imposed and only the tracer injected before 5240 h is taken into account.

Tracer	Peclet number	Residence time hours	Dilution factor	Standard-deviation	Section of drift
Uranine	4.0	13090.0	308.74	.043	25-35 m
Uranine	4.0	18520.0	582.75	.030	12-22 m

TABLE OF SHEET NUMBERING

Table 14-1. Table to convert the coordinates of the sheet to an Identification number.

ID number: Method of notation for data storage in computer.
 Sheet coordinate: Location in drift: the first digit located before the + or - sign is the location in x-direction (the drift's longitudinal direction) and the last digits are the side locations in relation to the x-direction (+ is right side and - is left side of the drift).

Sheet	ID number
-12+2.75	157
-10+2.5	135
-5+0	134
-5+1	206
0+1	78
2+1	77
2+2	76
6-1	79
8-2	80
8-1	202
8+1	75
10-2.75* (10-2.75, 12-2.75)	159
10-2	82
10-1	81
12-2.5	83
12-2	84
12-1	85
12+0	205
12+2.75	154
14-2.75	160
14-2.5	88
14-2	86
14-1	89
14+0	87
14+1	74
16-2.75	161
16-2.5	91
16-2	94
16-1	95
16+0	90
18-2.75	162
18-2.5	92
18-2	93
20-2.75	153
20-1* (20-1, 18-1)	96
22-2.75	163

A14.2

Table A14-1 continued.

22-2.5	100
22-2	98
22-1	99
22+0	97
23.5-2.75	164
24.2+2.75	165
25-2.75	156
25-2.5	101
25-2	104
25-1	102
25+0	103
25+1	71
25+2	72
25+2.5	73
25+2.75	166
27-2	105
27-1	106
27+0	107
27+1	68
27+2	69
27+2.5	70
27+2.75	189
29-2.5	112
29-2	111
29-1	110
29+0	108
29+1	65
29+2	175
29+2* (29+2, 29+2.5)	67
29+2.5	176
29+2.75	190
29+2.75 G	186
31-2.75	167
31-2	114
31-1	113
31+0	109
31+1	66
31+2	64
31+2.5	63
31+2.75	191
31+2.75 F	185
31+2.75 H	187
33-2.5	116
33+0	115
33+1	62
33+2	60
33+2.5	61
33+2.75	192
33+2.75 A	180
33+2.75 B	181
33+2.75 C* (33+2.75, 31+2.75)	182
33+2.75 D* (33+2.75, 31+2.75)	183
33+2.75 E* (33+2.75, 31+2.75)	184
35-2.5	117
35+2.5	59
35+2.75	174
37+1	172

Figure A14-1 continued.

37+2.75	193
39-2	171
39-1	120
39+0	118
39+1	58
39+2	200
39+2.5	201
41-1	123
41+0	119
41+1	54
41+2	57
43-2* (43-2, 45+0)	121
43-2	177
43-1	124
43+0	122
43+1	56
43+2	55
45+0	178
45+1	53
45+2	52
47-1	204
47+0	125
51-2.75	168
55-2.5	126
57-2.75	188
57-2.5	130
57-1	127
57.5+11	50
57.5+13	47
58-1	129
58+11	49
59+11* (59+11, 60+11)	48
60+0	128
60+3	25
60+13	46
61+2	21
61+3	24
61+5	26
61+11	35
61+13	44
62+2	18
62+3	20
62+5	27
62+7	28
62+9	34
62+11	36
62+13	43
62+15.25	42
62.5+3	23
62.5+5	29
62.5+7	30
62.5+9	33
62.5+11	37
62.5+13	45
62.75+7	31
62.75+9	32
62.75+10	38

Figure A14-1 continued.

62.75+11	39
62.75+13	41
62.75+15.25	194
62.8+11	40
63-2.75	169
63+1	22
63+2	17
65+1	170
65+2	19
65+2.5	16
67+1	14
67+2	12
67+2.5	13
67+2.75	15
69+1	203
69+2	9
69+2.5	10
69+2.75	8
71-2* (71-2, 73-2)	1
71-1	5
71+0	2
71+1	11
71+2	6
73-2.5	179
73-1	3
73+0	4
73+1	7
Access drift 1	136
Access drift 2	137
Access drift 3	138
Access drift 4	139
G 10-2 (Floor)	152
G 12-2 (Floor)	155
G 27-1 (Floor)	149
G 51-1 (Floor)	150
G 58+11 (Floor)	143
G 59+13 (Floor)	142
G 59+9 (Floor)	144
G 60+9 (Floor)	147
G 61+9 (Floor)	141
G 61+9* (G 61+9, G 61+11, G 62+11, G 62+13) (Floor)	151
G 61+11 (Floor)	145
G 62+11* (G 62+11, G 62+13) (Floor)	146
G 62+13 (Floor)	140
G 69+0 (Floor)	148
G Access drift (Floor)	158
3D Pilot Hole 1 (beginning 3D drift)	131
3D Pilot Hole 1 (Start)	132
Hole N1	133
Hole N2	240
Hole N3	241
Hole N4	242

Figure A14-1 continued.

Hole R3	222
Hole V3	245
Hole W1	243
Hole W2	244
Hole 1 310 m level	230
Hole 2 310 m level	231
Hole BMT lower	220
Hole BMT upper	221

A14.6

Table A14-2. Table to convert Identification number to sheet co-ordinates.

ID number: Method of notation for data storage in computer.

Sheet co-ordinate: Location in drift: the first digit located before the + or - sign is the location in x-direction (the drift's longitudinal direction) and the last digits are the side locations in relation to the x-direction (+ is right side and - is left side of the drift).

ID number	Sheet
1	71-2* (71-2, 73-2)
2	71+0
3	73-1
4	73+0
5	71-1
6	71+2
7	73+1
8	69+2.75
9	69+2
10	69+2.5
11	71+1
12	67+2
13	67+2.5
14	67+1
15	67+2.75
16	65+2.5
17	63+2
18	62+2
19	65+2
20	62+3
21	61+2
22	63+1
23	62.5+3
24	61+3
25	60+3
26	61+5
27	62+5
28	62+7
29	62.5+5
30	62.5+7
31	62.75+7
32	62.75+9
33	62.5+9
34	62+9
35	61+11
36	62+11
37	62.5+11
38	62.75+10
39	62.75+11
40	62.8+11
41	62.75+13

A14.7

Table A14-2 continued.

42	62+15.25
43	62+13
44	61+13
45	62.5+13
46	60+13
47	57.5+13
48	59+11* (59+11, 60+11)
49	58+11
50	57.5+11
52	45+2
53	45+1
54	41+1
55	43+2
56	43+1
57	41+2
58	39+1
59	35+2.5
60	33+2
61	33+2.5
62	33+1
63	31+2.5
64	31+2
65	29+1
66	31+1
67	29+2* (29+2, 29+2.5)
68	27+1
69	27+2
70	27+2.5
71	25+1
72	25+2
73	25+2.5
74	14+1
75	8+1
76	2+2
77	2+1
78	0+1
79	6-1
80	8-2
81	10-1
82	10-2
83	12-2.5
84	12-2
85	12-1
86	14-2
87	14+0
88	14-2.5
89	14-1
90	16+0
91	16-2.5
92	18-2.5
93	18-2
94	16-2
95	16-1
96	20+1* (18-1, 20-1)
96	20-1
97	22+0

Table A14-2 continued.

98	22-2
99	22-1
100	22-2.5
101	25-2.5
102	25-1
103	25+0
104	25-2
105	27-2
106	27-1
107	27+0
108	29+0
109	31+0
110	29-1
111	29-2
112	29-2.5
113	31-1
114	31-2
115	33+0
116	33-2.5
117	35-2.5
118	39+0
119	41+0
120	39-1
121	43-2* (43-2, 45+0)
122	43+0
123	41-1
124	43-1
125	47+0
126	55-2.5
127	57-1
128	60+0
129	58-1
130	57-2.5
131	3D Pilot hole 1 (Beginning 3D drift)
132	3D Pilot hole 1 (Start)
133	Hole N1
134	-5+0
135	-10+2.5
136	Access drift 1
137	Access drift 2
138	Access drift 3
139	Access drift 4
140	G 62+13 (Floor)
141	G 61+9 (Floor)
142	G 59+13 (Floor)
143	G 58+11 (Floor)
144	G 59+9 (Floor)
145	G 61+11 (Floor)
146	G 62+11* (G 62+11, 62+13) (Floor)
147	G 60+9 (Floor)
148	G 69+0 (Floor)
149	G 27-1 (Floor)
150	G 51-1 (Floor)
151	G 61+9* (G 61+9, 61+11, 62+11, 62+13) (Floor)

Table A14-2 continued.

152	G 10-2 (Floor)
153	20-2.75
154	12+2.75
155	G 12-2 (Floor)
156	25-2.75
157	-12+2.75
158	G Access drift (Floor)
159	10-2.75* (10-2.75, 12-2.75)
160	14-2.75
161	16-2.75
162	18-2.75
163	22-2.75
164	23.5-2.75
165	24.2+2.75
166	25+2.75
167	31-2.75
168	51-2.75
169	63-2.75
170	65+1
171	39-2
172	37+1
174	35+2.75
175	29+2
176	29+2.5
177	43-2
178	45+0
179	73-2.5
180	33+2.75 A
181	33+2.75 B
182	33+2.75 C
182	31+2.75 C
183	33+2.75 D
183	31+2.75 D
184	33+2.75 E
184	31+2.75 E
185	31+2.75 F
186	29+2.75 G
187	31+2.75 H
188	57-2.75
189	27+2.75
190	29+2.75
191	31+2.75
192	33+2.75
193	37+2.75
194	62.75+15.25
200	39+2
201	39+2.5
202	8-1
203	69+1
204	47-1
205	12+0
206	-5+1
220	Hole BMT lower
221	Hole BMT upper

Figure A14-2 continued.

222	Hole R3
230	Hole 1 310 m level
231	Hole 2 310 m level
240	Hole N2
241	Hole N3
242	Hole N4
243	Hole W1
244	Hole W2
245	Hole V3
